frontiers | Research Topics

Novel targets for chronic inflammatory diseases: Focus on therapeutic drugs and natural compounds

Edited by
Yan Huang, Zhigang Xiong, Songyan Liao, Feng Li and Li Wu

Published in
Frontiers in Pharmacology

ISSN 1664-8714
ISBN 978-2-8325-3170-9
DOI 10.3389/978-2-8325-3170-9

About Frontiers

Frontiers is more than just an open access publisher of scholarly articles: it is a pioneering approach to the world of academia, radically improving the way scholarly research is managed. The grand vision of Frontiers is a world where all people have an equal opportunity to seek, share and generate knowledge. Frontiers provides immediate and permanent online open access to all its publications, but this alone is not enough to realize our grand goals.

Frontiers journal series

The Frontiers journal series is a multi-tier and interdisciplinary set of open-access, online journals, promising a paradigm shift from the current review, selection and dissemination processes in academic publishing. All Frontiers journals are driven by researchers for researchers; therefore, they constitute a service to the scholarly community. At the same time, the *Frontiers journal series* operates on a revolutionary invention, the tiered publishing system, initially addressing specific communities of scholars, and gradually climbing up to broader public understanding, thus serving the interests of the lay society, too.

Dedication to quality

Each Frontiers article is a landmark of the highest quality, thanks to genuinely collaborative interactions between authors and review editors, who include some of the world's best academicians. Research must be certified by peers before entering a stream of knowledge that may eventually reach the public - and shape society; therefore, Frontiers only applies the most rigorous and unbiased reviews. Frontiers revolutionizes research publishing by freely delivering the most outstanding research, evaluated with no bias from both the academic and social point of view. By applying the most advanced information technologies, Frontiers is catapulting scholarly publishing into a new generation.

What are Frontiers Research Topics?

Frontiers Research Topics are very popular trademarks of the *Frontiers journals series*: they are collections of at least ten articles, all centered on a particular subject. With their unique mix of varied contributions from Original Research to Review Articles, Frontiers Research Topics unify the most influential researchers, the latest key findings and historical advances in a hot research area.

Find out more on how to host your own Frontiers Research Topic or contribute to one as an author by contacting the Frontiers editorial office: frontiersin.org/about/contact

Novel targets for chronic inflammatory diseases: Focus on therapeutic drugs and natural compounds

Topic editors

Yan Huang — Anhui Medical University, China
Zhigang Xiong — Morehouse School of Medicine, United States
Songyan Liao — The University of Hong Kong, Hong Kong, SAR China
Feng Li — Shanghai Jiao Tong University, China
Li Wu — Nanjing University of Chinese Medicine, China

Citation

Huang, Y., Xiong, Z., Liao, S., Li, F., Wu, L., eds. (2023). *Novel targets for chronic inflammatory diseases: Focus on therapeutic drugs and natural compounds*. Lausanne: Frontiers Media SA. doi: 10.3389/978-2-8325-3170-9

Table of contents

frontiers | Frontiers in Pharmacology

TYPE Original Research
PUBLISHED 16 August 2022
DOI 10.3389/fphar.2022.979939

OPEN ACCESS

EDITED BY
Yan Huang,
Anhui Medical University, China

REVIEWED BY
Mei Zeng,
Affiliated Hospital of North Sichuan Medical College, China
Lindi Jiang,
Fudan University, China

*CORRESPONDENCE
Jinhui Tao,
taojinhui@ustc.edu.cn

SPECIALTY SECTION
This article was submitted to Inflammation Pharmacology, a section of the journal Frontiers in Pharmacology

RECEIVED 28 June 2022
ACCEPTED 28 July 2022
PUBLISHED 16 August 2022

CITATION
Li X, Liu Y, Luo C and Tao J (2022), Z1456467176 alleviates gouty arthritis by allosterically modulating P2X7R to inhibit NLRP3 inflammasome activation. *Front. Pharmacol.* 13:979939. doi: 10.3389/fphar.2022.979939

Z1456467176 alleviates gouty arthritis by allosterically modulating P2X7R to inhibit NLRP3 inflammasome activation

Xiaoling Li, Yiming Liu, Chengyu Luo and Jinhui Tao*

Department of Rheumatology and Immunology, The First Affiliated Hospital of USTC, Division of Life Sciences and Medicine, University of Science and Technology of China, Hefei, China

NLRP3 inflammasome activation is a central process in initiating gout flares. The unique conformational rearrangement of the P2X7 receptor (P2X7R) upon ATP binding is critical for the activation of the NLRP3 inflammasome. However, studies on allosteric modulation of P2X7R in gout treatment are limited. Here, we aimed to investigate the therapeutic implications of targeting P2X7R in gout by designing a P2X7R allosteric inhibitor and validating the inhibitory function on NLRP3 inflammasome activation. Through virtual screening, we identified Z1456467176 (N-{3-[(2-aminoethyl) sulfamoyl] phenyl}-2-methyl-3-[3-(trifluoromethyl) phenyl] propanamide hydrochloride) bound to the drug-binding pocket as a potential antagonist of P2X7R. In functional assays, ATP- or BzATP-induced P2X7R function was assessed *in vitro* in HEK-293T cells overexpressing hP2X7R (dye uptake assay) and macrophages (IL-1β release assay). Z1456467176 exhibited a stable and significant P2X7R inhibitory effect. Importantly, in MSU crystal-induced gout, the presence and involvement of ATP were confirmed. Z1456467176 blocked ATP-induced activation of the NLRP3-caspase-1-IL-1β pathway and exerted promising effects in reducing gouty joint inflammation in rats. In addition, molecular docking and molecular dynamics simulation studies showed that the P27XR protein conformation was remodeled by Z1456467176 binding. Collectively, our results provide a potent P2X7R allosteric inhibitor that facilitates the remission of MSU crystal-induced gout inflammation by inhibiting NLRP3 inflammasome activation, suggesting that allosteric inhibition of P2X7R represents a new direction in gout treatment.

KEYWORDS

gout, P2X7 receptor, allosteric regulation, nod-like receptor protein 3, interleukin-1beta

Introduction

Gout is a common cyclical, recurrent and transient "autoinflammatory" disease in adults, characterized by rapidly developing monoarticular synovitis of peripheral joints, manifesting as joint redness, swelling, pain, and restricted movement (Dalbeth et al., 2019). For the occurrence of gout flares, monosodium urate (MSU) crystal-

induced nod-like receptor protein 3 (NLRP3) inflammasome activation is the central link in initiating the inflammatory response (Martinon et al., 2006). However, this is not sufficient to explain the absence of gout flares in individuals with MSU crystal deposition (Carr et al., 2016; Petsch et al., 2016; Zhu et al., 2017). In addition to MSU crystals, it has been shown that metabolic substances in the body, including adenosine triphosphate (ATP), cholesterol, and glucose, contribute to the activation of the NLRP3 inflammasome (Di Virgilio et al., 2017; Hughes and O'Neill, 2018).

Purinergic receptor P2X7 (P2X7R) is an ATP-gated ion channel receptor that regulates NLRP3 inflammasome activation by inducing intracellular and extracellular ion flux (Murakami et al., 2012; Gong et al., 2018). The association between human *P2X7R (hP2X7R)* gene polymorphisms and gout susceptibility was confirmed in our previous study (Tao et al., 2017). In addition, colchicine, a traditional gout therapeutic agent, has been reported to exert anti-inflammatory effects by inhibiting P2X7R activation-induced pore formation (Marques-da-Silva et al., 2011), suggesting that P2X7R would be an attractive therapeutic target for gout. The P2X7R protein is a trimeric complex with each P2X7 subunit consisting of an extracellular ligand-binding region, two transmembrane structural domains (TM), and intracellular N and C termini (Karasawa and Kawate, 2016). As an allosteric protein, a comparison of the structures in the closed and open states of P2X7R shows that the upper body domain remains relatively quiescent (Jiang et al., 2013). However, ATP binding brings about a narrowing of the turrets and a widening of the lower body domain (Karasawa and Kawate, 2016), and P2X7R antagonist binding precludes these constrictions, efficiently blocking receptor activation (Jiang et al., 2013). This conformational rearrangement is required for P2X7R channel opening (Karasawa and Kawate, 2016; McCarthy et al., 2019), which is essential for NLRP3 inflammasome activation. Therefore, allosteric modulation of P2X7R may be an effective strategy to block NLRP3 inflammasome activation for the treatment of gout.

Although the involvement of ATP-P2X7R in the pathogenesis of gout is gradually being recognized, the evaluation of P2X7R for the treatment of gout is still limited. In the present study, we demonstrated that allosteric regulation of P2X7R to inhibit the NLRP3 inflammasome effectively alleviates gout inflammation, providing theoretical and data support for P2X7R as a therapeutic target for gout.

Materials and methods

Z1456467176

Docking studies were performed using the Glide module of Schrodinger software to initiate virtual screening of P2X7R antagonists in a commercial compound library (TSBiochem, China). The crystal of PDB number 5u1x was identified as the docking model. A small-molecule Z1456467176 (N-{3-[(2-aminoethyl) sulfamoyl] phenyl}-2-methyl-3-[3-(trifluoromethyl) phenyl] propanamide hydrochloride) was obtained that binds to the drug antagonist pocket. The purity of the compound was verified by mass spectrometry to be over 90% (Supplementary Data).

Dye uptake assay

HEK-293T cells were maintained in DMEM (Thermo 11965118) supplemented with 10% fetal bovine serum (FBS, HyClone SV30087.03) and incubated at 37°C under a 5% CO_2 atmosphere for 24 h (2×10^5 cells/ml). Transfection was performed with a lentivirus overexpressing hP2X7R (Hanheng Biotechnology Co (China)) or empty lentivirus in the presence of polybrene. On the following day, Z1456467176 (10 μM) or equivalent amounts of DMSO were incubated with HEK-293T cells overexpressing hP2X7R for 30 min. Cells were suspended in 0.5 ml of HEPES buffered medium followed by the addition of 25 μM ethidium bromide (EB, Sigma 1,239-45-8) and 1 mM ATP (Sigma A6559). Cells were collected using a CytoFLEX flow cytometer, counting 1,000 cells each time. The average fluorescence intensity of each sample was read using CytExpert. The IC_{50} value of Z1456467176 (concentrations ranging from 1 nM to 100 μM) was obtained from concentration-response curves for the EB uptake assay (Supplementary Figure S1).

Cell culture and stimulation

THP-1 cells (2×10^5 cells/ml) were cultured in RPMI 1640 medium (HyClone AG29775810) containing 10% FBS and stimulated overnight with 100 ng/ml phorbol 12-myristate 13-acetate (PMA, Sigma P1585) to obtain THP-1-derived macrophages. Bone marrow cells were isolated and collected from bilateral femurs and tibiae of 6-week-old C57BL/6J mice. Mouse bone marrow-derived macrophages (BMDMs) were obtained by culturing for 1 week in DMEM (2×10^6 cells/ml) supplemented with 10% FBS, 20% L929 cell supernatant, and penicillin/streptomycin. Peripheral blood mononuclear cells (PBMCs) from stable gout patients were isolated with lymphocyte isolate and erythrocyte lysate (Haoyang LTS1077, NH4CL 2009) and inoculated in RPMI 1640 medium (2×10^6 cells/ml) and cultured overnight. The supernatant was removed the next day to obtain crude extracted macrophages.

The above cells were then activated with 50 ng/ml LPS (Invitrogen LPS-EK) for 3 h. Furthermore, Z1456467176 at different concentrations was incubated for 30 min before 100 μM BzATP (Sigma B6396) treatment for 15–20 min 10 μM pyroptosis inhibitor (VX-765, MCE HY-13205) was

incubated for 30 min before 100 μg/ml MSU crystal treatment for 4 h. MSU crystals were obtained by dissolving uric acid (2 g, Sigma U0881) in 500 ml of double-distilled water containing NaOH (0.01 M) at 70°C, and the pH was maintained at 8.9. The solution was filtered through a 0.22 μM filter and stored overnight at room temperature with continuous stirring. After centrifugation, the supernatant was discarded, and the precipitate was obtained and dried. The crystals were autoclaved and resuspended in sterile PBS (Chen et al., 2019).

ELISA

ELISA was performed to measure IL-1β, IL-6, and TNF-α levels in cell culture supernatants and IL-1β levels in rat serum according to the manufacturer's instructions (NOVUS Biological VAL101, VAL102, VAL105; Multi Sciences A301BH10152). Rat liver and kidney functions were detected by Jian Cheng C0009-2-1, C0010-2-1, C011-2-1, and C013-2-1 kits (China).

Quantitative PCR

qPCR was performed to detect the gene expression of *IL-1β* and *Actβ* in the peripheral whole blood cells of rats. Samples were processed with a total RNA extraction kit (Solarbio R4161-02) and a cDNA synthesis kit (BIOER BSB40M1) according to the manufacturer's instructions. qPCR was conducted using SYBR Green PCR Master Mix (Muma A4004M). The primer sequences for the rat *IL-1β* gene were F-seq (5′-3′): TGGCAACTGTCC CTGAACTC and R-seq (5′-3′): AAGGGCTTGGAAGCAATC CTTA. The primer sequences for the rat *Actβ* gene were F-seq (5′-3′): ACCCGCCACCAGTTCGC and R-seq (5′-3′): CACGATGGAGGGGAAGACG.

Western blotting

Western blotting was performed to detect protein levels in PBMC lysates from gout patients and in joint grinds from rat gout models. Segmented constant voltage was chosen for electrophoresis, and the concentrated gel was run at a constant voltage of 80 V. After running out of the concentrated gel, the voltage was increased to 120 V until bromophenol blue reached the bottom of the gel. The membrane was rotated at a constant flow of 200 mA in an ice bath and then blocked with 5% skim milk powder for 1 h. The membrane was incubated overnight at 4°C with the following primary antibodies: IL-1β (CST D3A3Z, 1: 1,000), caspase-1 (CST D7F10, 1:1,000), NLRP3 (CST D4D8T, 1:1,000), N-GSDMD (Abcam Ab215203, 1:1,000) and β-actin (CST 8H10D10, 1:1,000). HRP, goat anti-rabbit IgG, and goat anti-mouse IgG (Abbkine A21020, A21010, 1: 5,000) were incubated for 1 h at room temperature and then developed.

Monosodium urate crystal-induced gouty arthritis in rats

Sprague–Dawley (SD) male rats weighing 200 g were purchased from the Laboratory Animal Center of the First Hospital of USTC and housed in a clean environment free of pathogens. A rat model of gout was established according to the classical modeling method (Coderre method (Coderre and Wall, 1987)) and randomly divided into four groups. Each group was treated as follows: 1) Rats in the control group were injected with 100 μl of sterile saline in the right ankle joint cavity. 2) Rats in the MSU group were injected with 100 μl of MSU crystal suspension (0.1 g/ml) in the right ankle joint cavity. 3) Rats in the MSU + ATP group were injected intraperitoneally with 500 μl of ATP solution (10 mM; Solarbio A8270) 30 min before intra-articular injection of MSU crystal suspension. 4) Rats in the MSU + Z1456467176 group were injected intraperitoneally with 500 μl of Z1456467176 solution (40 mg/kg) 30 min before intra-articular injection of MSU crystal suspension. The clinical inflammatory manifestations of rats were evaluated by measuring the ankle joint circumference and calculating the joint swelling index. Rat ankle joint swelling index = (treated circumference - initial circumference)/initial circumference. Rat ankle joints were obtained from each group and tissue homogenates were prepared according to the manufacturer's instructions. The activity of myeloperoxidase (MPO, Jiancheng A044-1-1) was assayed as a quantitative assay for tissue neutrophil infiltration.

LDH and ATP assay

Serum was collected from gout model rats as well as from patients with acute phase gout and normal population. LDH levels were quantified using the LDH Cytotoxicity Assay Kit (Jian Cheng A020-2) according to the manufacturer's instructions. Patients with acute-phase gout were defined as positive joint redness, swelling, and pressure pain in the metatarsophalangeal or ankle or knee joint; elevated joint skin temperature; history of hyperuricemia or gout; and duration of this joint symptom for 2 days and less. The people in the control group were age- and sex-matched to the gout group and had no local or systemic inflammatory symptoms.

ATP (%) values in cell cultures of PBMCs from rats with MSU crystal-induced gouty arthritis and patients with stable gout stimulated with MSU crystals (100 μg/ml) were determined using a luminescent ATP assay kit (Abcam ab113849) according to the manufacturer's instructions.

Magnetic resonance imaging

Rats were anesthetized with intraperitoneal injection of chloral hydrate (0.3 ml/100 g, Maclean C804539) in a gouty arthritis model, and magnetic resonance imaging (MRI) examination was performed after the rats had decreased muscle strength and stabilized respiration. MRI of the ankle joint was performed using a 3.0T MR scanner (GE Discover 750 W) and an eight-channel mouse coil (Medciol MS80-3T) with the following sequence parameters: T2 FLAIR; TE: 101/Ef; TR: 3,800 ms; EC:1/1 50 Hz; slice thickness: 2 mm; FoV = 12*12 cm; matrix size = 256*256.

Immunohistochemistry

The isolated rat ankles were fixed in tissue fixative (containing 10% neutral formalin) for 24 h, and subsequently placed in decalcification solution (containing formalin and EDTA) with shaking for 4-6 weeks to ensure adequate decalcification. The endpoint of decalcification is indeed considered smooth penetration of the needle through the entire bone tissue. After the washing, dehydration, and decalcification steps, the ankle tissue was fixed in paraffin and sectioned for HE staining. Cell count quantification was performed using ImageJ software (NIH).

Molecular dynamics analysis and molecular docking

The trimeric conformation of 5u1x was used as the target protein. Molecular docking was performed using AutoDock 4.2 software. The structure of Z1456467176 was downloaded from the database (https://pubchem.ncbi.nlm.nih.gov), and Chem3D16 was applied for structure optimization. Global docking was used, with the docking box wrapping the entire 5u1x protein and other parameters kept as default. Molecular dynamics simulations of 100 ns were performed, and the binding free energy of the protein and ligand was calculated using g_mmpbsa. The conformation with the lowest energy in the molecular docking results was selected as the initial structure for molecular dynamics. Molecular dynamics (MD) simulations were performed using Gromacs 2019.4 software at constant temperature and pressure as well as periodic boundary conditions. The Amber99sb-ildn force field, TIP3P water model, was applied. The force field parameters for small molecules were generated by the acpype.py script in AmberTools. During the MD simulations, the hydrogen bonds involved were constrained using the LINCS algorithm with an integration step of 2 fs. The electrostatic interactions were calculated using the particle–mesh Ewald (PME) method with the cutoff value set to 1.2 nm. The nonbonded interaction cutoff value was set to 10 Å. The simulation temperature was controlled to 300 K using the V-rescale temperature coupling method, and the NVT and NPT equilibrium simulations were performed at 300 K for 100 ps. Finally, 100 ns of finished MD simulations were performed for the protein and protein-ligand complex systems, and the pure protein system was used as a control group for the experiments. The GROMACS embedded program and PyMOL 2.4 were used to visualize the simulation results.

Ethics

Our protocols for the collection and processing of animal and human samples were approved by the Animal Ethics Committee (2021-N(A)-041) and Medical Research Ethics Committee(2021 KY No.162) of the First Hospital of the University of Science and Technology of China (Anhui Provincial Hospital), respectively. All persons gave their informed consent before their inclusion in the study.

Statistical analyses

Data were analyzed using IBM SPSS Statistics for Windows, version 17.0 (IBM). Quantitative data were tested for normality. Independent sample *t* tests and one-way analysis of variance (ANOVA) were used to compare differences between two groups and multiple groups, respectively. Significant differences revealed by one-way ANOVA were validated by Dunnett's *t* test. Statistical significance was set at $p < 0.05$. All bar graphs were plotted using GraphPad Prism 8.0 software (GraphPad Software).

Results

Z1456467176 inhibits ATP-induced P2X7R pore formation

P2X7R is an ATP-gated channel receptor. Pore formation upon sustained stimulation of ATP allows the influx of extracellular macromolecules. To investigate the inhibitory effect of Z1456467176 on ATP-induced P2X7R pore formation, we constructed a lentivirus overexpressing hP2X7R to transfect HEK-293T cells. ATP-induced uptake of EB by HEK-293T cells was assayed in the presence or absence of Z1456467176. Flow cytometric analysis showed that the uptake of EB by HEK-293T cells overexpressing hP2X7R was significantly increased upon ATP stimulation, whereas Z1456467176 treatment inhibited the uptake of EB by

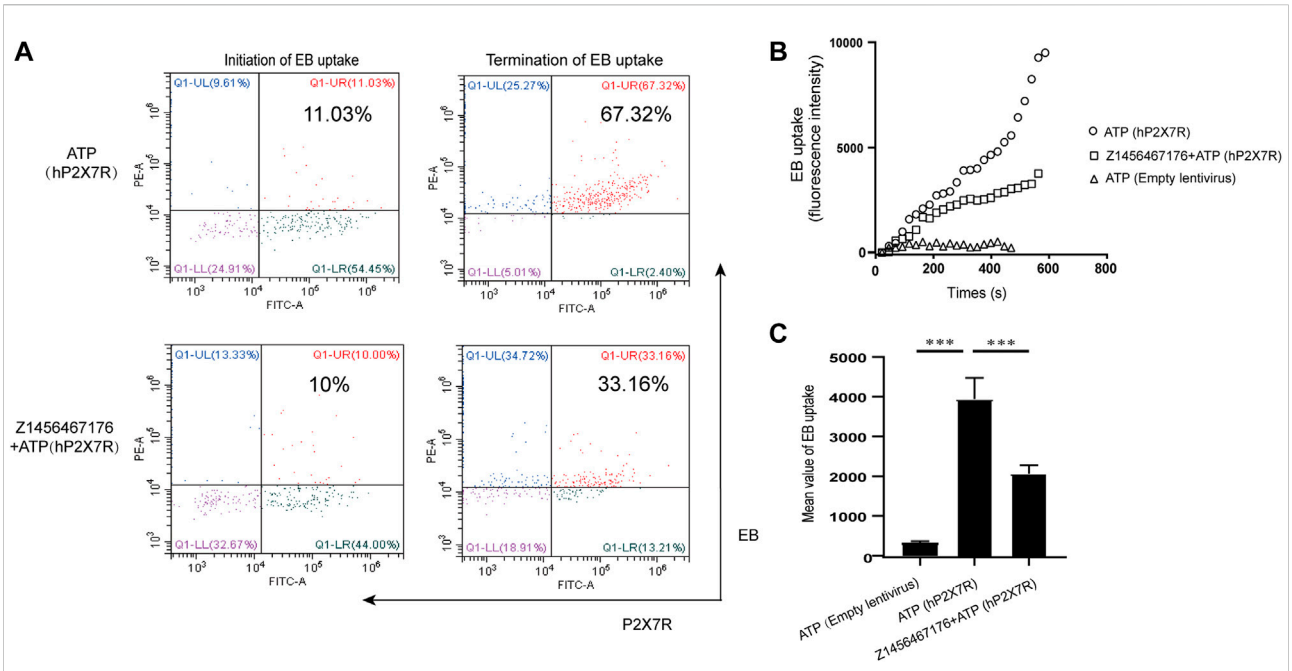

FIGURE. 1
Z1456467176 inhibits ATP-induced P2X7R pore formation. **(A)** Representative flow diagram of EB uptake by HEK-293T cells overexpressing hP2X7R in response to ATP. The red Q1-UR region reflects double-positive staining for EB and hP2X7R. FACS analysis of the intracellular fluorescence intensity **(B)** and mean value analysis of quantified intracellular fluorescence intensity **(C)**. Data are presented as the means ± S.E.M.s. Statistics were analyzed using Dunnett's *t*-test. ***$p < 0.001$.

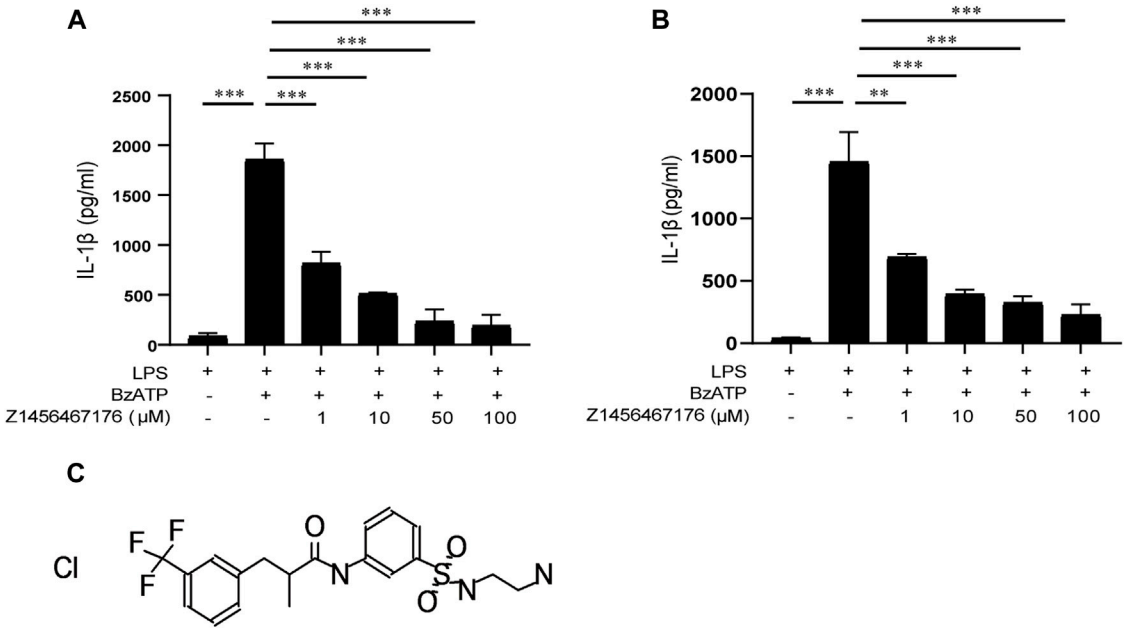

FIGURE. 2
Z1456467176 inhibits BzATP-induced IL-1β secretion in macrophages. ELISA of IL-1β in supernatants from LPS (50 ng/ml)-primed THP-1 cells **(A)** and BMDMs **(B)** treated with various doses of Z1456467176 (1/10/50/100 μM) for 30 min and then stimulated with BzATP (100 μM). **(C)** Chemical structure of Z1456467176. Data are presented as means ± S.E.M. Statistics were analyzed using Dunnett's *t*-test. $n = 3$. **$p < 0.01$; ***$p < 0.001$.

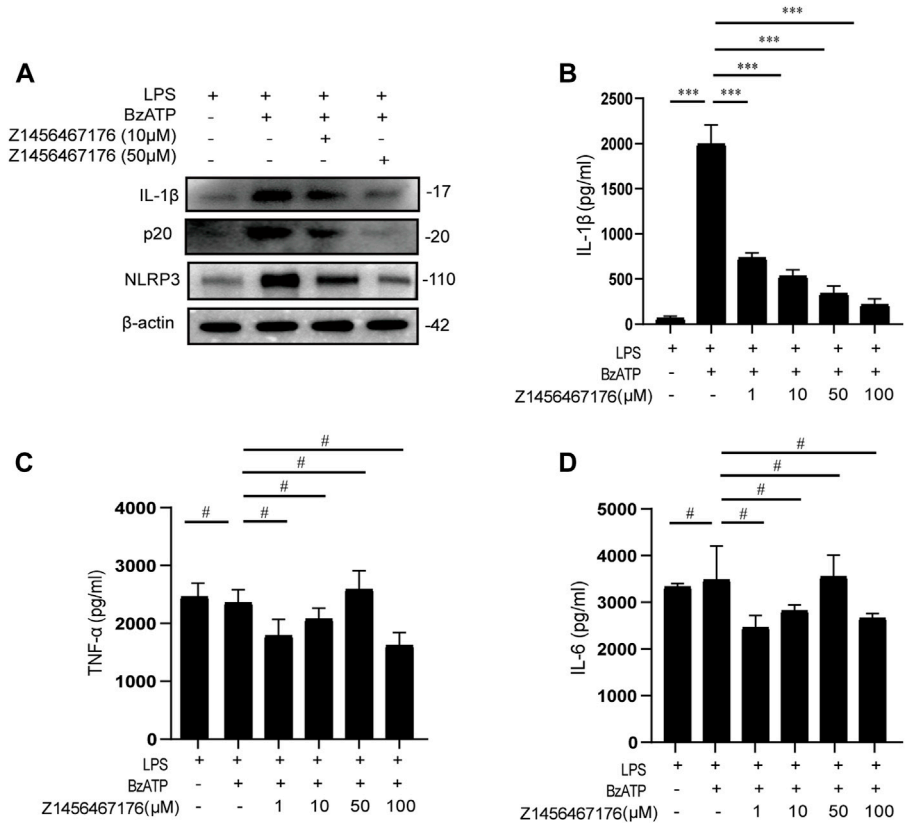

FIGURE. 3
Z1456467176 inhibits the P2X7R-NLRP3-IL-1β pathway *in vitro*. **(A)** WB of NLRP3, caspase-1 (p20), and IL-1β in lysates from LPS-primed PBMCs of gout patients treated with Z1456467176 (10, 50 μM) for 30 min and stimulated with BzATP (100 μM). **(B–D)** ELISA of IL-1β, TNF-α, and IL-6 in culture supernatants from LPS-primed PBMCs of gout patients treated with Z1456467176 for 30 min and stimulated with BzATP. Data are presented as the means ± S.E.M.s. Statistics were analyzed using Dunnett's *t* test. $n = 3$. ***$p < 0.001$.

the cells (Figure 1). This finding indicates that Z1456467176 (EB uptake IC_{50}: 3.416 μM) was able to inhibit ATP-induced P2X7R pore formation, exhibiting a potential P2X7R inhibitory effect.

Z1456467176 inhibits BzATP-induced IL-1β secretion in macrophages

P2X7R has attracted widespread interest as a therapeutic target for gout, as it mediates IL-1β release in response toATP. The release of biologically active IL-1β in gout requires two steps: initiation and activation, a biological process that occurs mainly in macrophages. We next investigated the effect of Z1456467176 on P2X7R activation-induced IL-1β release in an *in vitro* macrophage system including THP-1 cells and BMDMs. BzATP is a synthetic ATP analog that acts only on P2X1R and P2X7R in the P2XR family and exhibits a more potent and specific induction of P2X7R activation than ATP (Gicquel et al., 2017). Thus, BzATP was used to stimulate P2X7R activation in macrophages. As shown in Figure 2, we observed that in LPS-primed THP-1 cells and BMDMs, Z1456467176 was able to inhibit BzATP-induced IL-1β secretion in a dose-dependent manner to varying degrees, suggesting that it functions as a P2X7R antagonist.

With the validation of effectiveness in inhibiting P2X7R pore formation and IL-1β secretion in macrophages of different species *in vitro*, Z1456467176 was identified as a P2X7R antagonist that inhibits ATP- or BzATP-induced P2X7R activation.

Z1456467176 inhibits P2X7R-NLRP3-IL-1β pathway activation *in vitro*

To provide a basis for Z1456467176 in the treatment of gout, we evaluated the inhibitory effect of Z1456467176 on the P2X7R-NLRP3-IL-1β pathway in cultures of PBMCs of gout patients. First, we investigated whether Z1456467176 affected

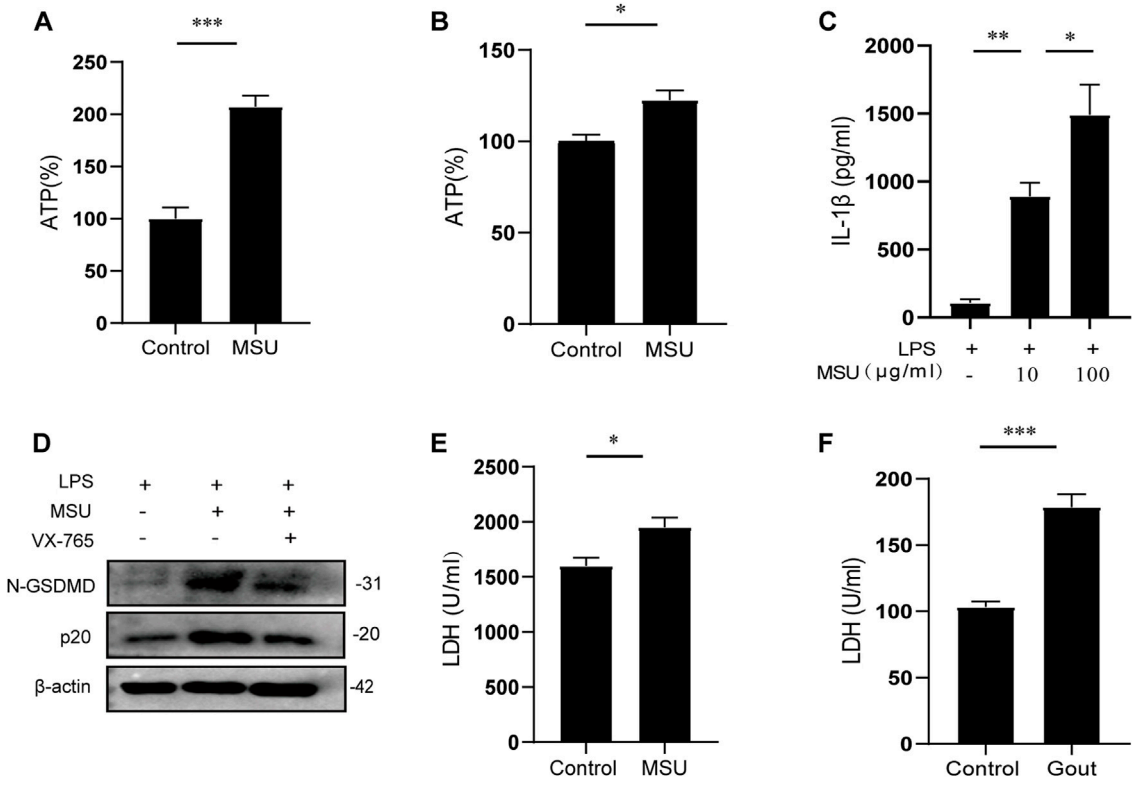

FIGURE. 4
MSU crystal stimulation induces ATP production and release. ATP (%) of cell cultures of PBMCs from MSU crystal (0.1 g/ml)-induced gouty arthritis rats **(A)** and LPS (50 ng/ml)-initiated, MSU crystal (100 μg/ml)-stimulated stable gout patients **(B)**. Control groups were treated with equal amounts of sterile saline or PBS. The ATP (%) values of **(A)** and **(B)** are expressed as a percentage of the MSU group relative to the control group. **(C)** ELISA of IL-1β in culture supernatants from LPS-primed PBMCs of gout patients treated with MSU (10/100 μg/ml) for 4 h **(D)** WB of N-GSDMD and p20 expression in lysates from LPS-primed PBMCs of gout patients treated with VX-765 (pyroptosis inhibitor; 10 μM) for 30 min and then stimulated with MSU (100 μg/ml). LDH levels in the serum of MSU crystal-induced gout rats **(E)** and in acute-phase gout patients **(F)**. Data are presented as the means ± S.E.M.s. Statistics were analyzed using the independent samples *t* test or Dunnett's *t* test. **(A,B)** $n = 3$-4; **(C)** $n = 4$; **(E)** $n = 5$; **(F)** $n = 19$. $^{*}p < 0.05$; $^{**}p < 0.01$; $^{***}p < 0.001$.

P2X7R-induced NLRP3 inflammasome activation in gout. As expected, western blot results showed that BzATP-induced expression of NLRP3, caspase-1 and IL-1β was inhibited in the presence of Z1456467176 (Figure 3A). Since IL-1β secretion is mainly mediated by activated NLRP3 inflammasome, we then examined inflammasome-dependent IL-1β secretion in culture supernatants of PBMCs from gout patients. The results showed that Z1456467176 inhibited BzATP-induced IL-1β secretion in cell culture supernatants in a dose-dependent manner, whereas NLRP3 inflammasome-independent TNF-α and IL-6 levels were unaffected (Figures 3B–D). In addition, we excluded the effect of Z1456467176 on LPS-primed and nigericin-induced NLRP3 inflammasome activation (Supplementary Figure S2). Taken together, these data suggest that Z1456467176 blocks the NLRP3-IL-1β pathway by inhibiting BzATP-induced P2X7R activation in gout patients *in vitro*.

Z1456467176 alleviates gouty arthritis in rats

To investigate the therapeutic effect of Z1456467176 on gout *in vivo*, we first evaluated inflammatory manifestations in a traditional gout model rat. In this model, MSU crystals were injected into the ankle joint cavity of rats to construct gouty arthritis (Coderre and Wall, 1987). Interestingly, ATP did not seem to be involved in this process. However, elevated levels of ATP were detected in the cell cultures of PBMCs from MSU crystal-induced gout rats (Figure 4A). Similarly, the effect of MSU crystal stimulation on ATP release was also observed in cell cultures of PBMCs from gout patients (Figure 4B). These data suggest that MSU crystal stimulation promotes ATP production in gout.

Pyroptosis-induced cell membrane rupture is the main mechanism for the rapid release of cellular contents. To determine whether MSU crystal-induced ATP is released by

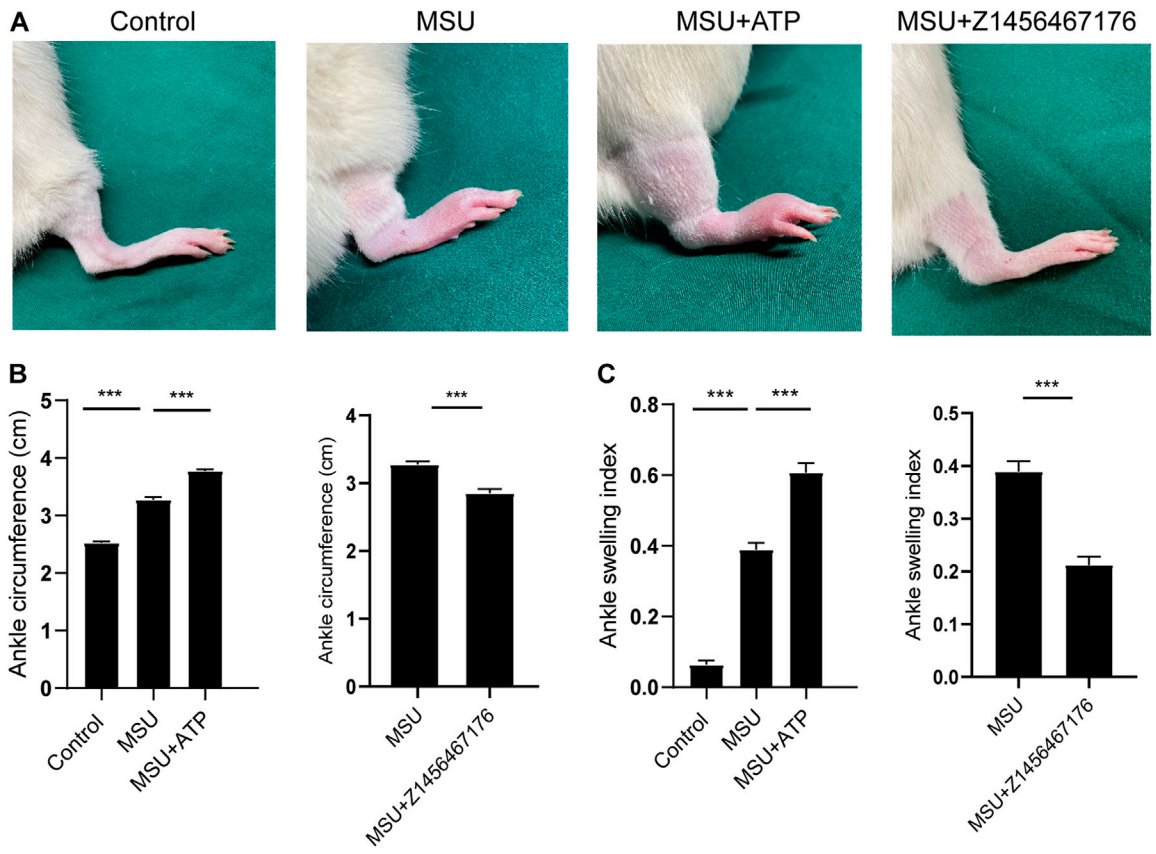

FIGURE. 5
Z1456467176 alleviates gouty arthritis in rats. The rat model of gout was divided into four groups: the control group, MSU group, MSU + ATP group, and MSU + Z1456467176 group. **(A)** Representative diagram of the right ankle joint of rats. **(B,C)** Ankle joint circumference and joint swelling index of the four groups of rats. Data are presented as the means ± S.E.M.s. Statistics were analyzed using the independent samples *t* test or Dunnett's *t* test. $n = 4$. ***$p < 0.001$.

pyroptosis, the levels of pyroptotic markers in gout were tested. The results showed that extracellular IL-1β and LDH release were increased and intracellular caspase-1 and N-GSDMD expressions were up-regulated after MSU crystal stimulation (Figures 4C–F). Collectively, these data suggest that MSU crystal stimulation promotes ATP production, which is released extracellularly through pyroptosis to function as a signaling molecule, confirming the involvement of ATP signaling in MSU crystal-induced gout pathogenesis.

Based on this, we established a rat model of MSU crystal-induced gout to validate the therapeutic effect of Z1456467176 on ATP-P2X7R-associated gout. As expected, in the MSU crystal-induced gout rat model, ATP treatment exacerbated the inflammatory manifestations of arthritis, while intraperitoneal injection of Z1456467176 attenuated the symptoms (Figure 5). Similar to the clinical manifestations, ankle MRI showed that ATP exacerbated MSU crystal-induced inflammation in the soft tissues of the rat ankle joint, while Z1456467176 attenuated it (Figure 6A). In addition, histopathology of the ankle joint showed increased inflammatory cell infiltration in the synovial tissue of the ankle joint of rats in the MSU group compared to the control group. ATP injection exacerbated the MSU crystal-induced inflammatory cell infiltration, while Z1456467176 treatment attenuated it (Figures 6B–D). These results suggest that Z1456467176 effectively relieves MSU-induced gouty joint inflammation.

Z1456467176 inhibits NLRP3 inflammasome activation in rat model of gout

To further elucidate the mechanism by which Z1456467176 alleviates gout inflammation, we examined the expression of the NLRP3 inflammasome pathway in rats. Consistent with the clinical presentation, ATP treatment

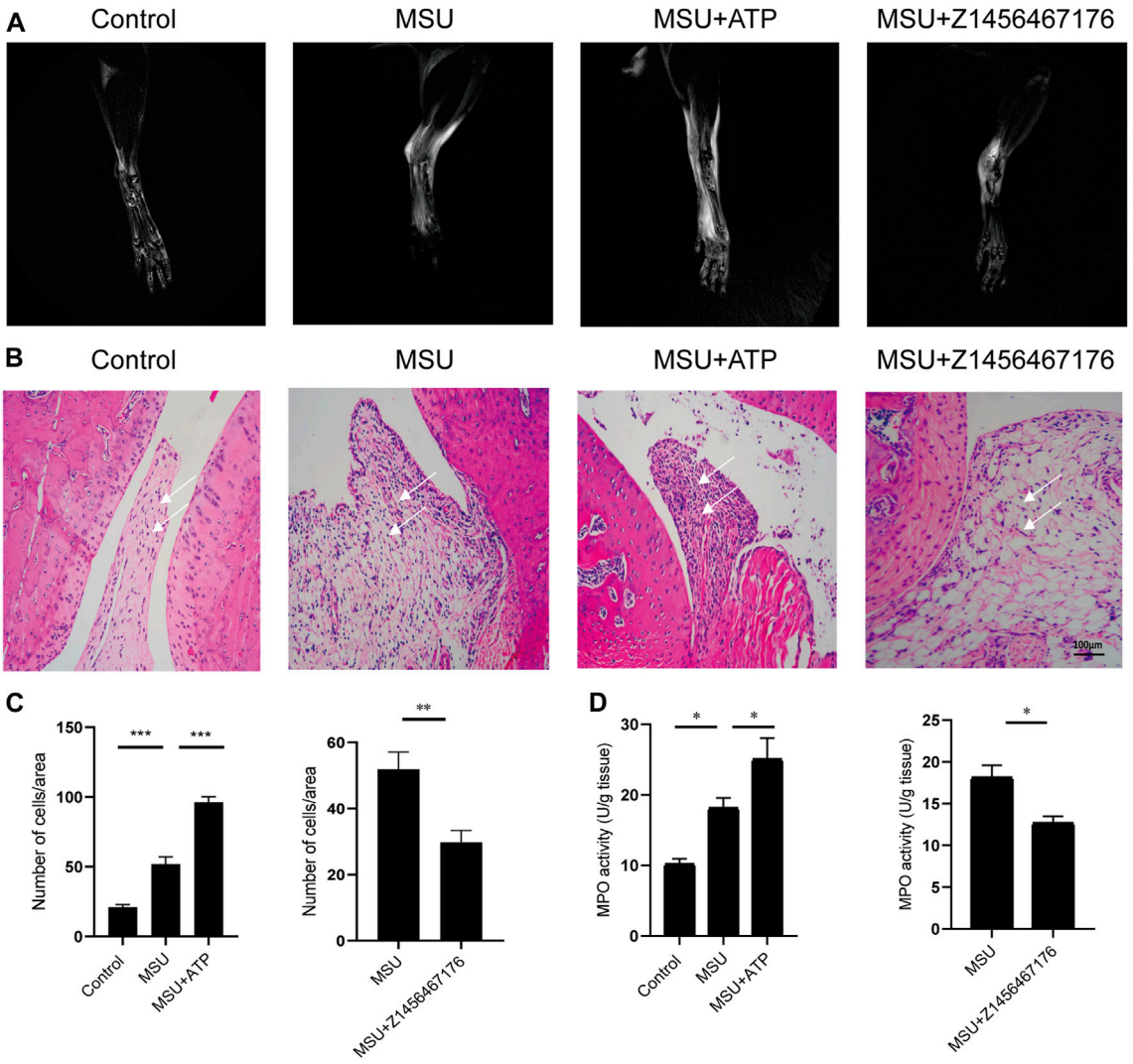

FIGURE. 6
Z1456467176 alleviates gouty arthritis in rats. **(A)** Representative MRI images of the right ankle joint of rats. The white portion reflects the degree of inflammatory edema. **(B)** Representative images of pathological H&E staining of the right ankle joint of rats (×200). The white arrow points to inflammatory cell infiltration in the synovial tissue of the ankle joint. **(C)** Equal-sized areas were taken from each group in **(B)** for quantification of inflammatory cells. **(D)** MPO activity of ankle joint homogenates. Data are presented as the means ± S.E.M.s. Statistics were analyzed using the independent samples *t* test or Dunnett's *t* test. $*p < 0.05$; $**p < 0.01$; $***p < 0.001$.

resulted in an upregulation of IL-1β levels following MSU crystal stimulation in rats, which was inhibited by Z1456467176 (Figures 7A,B). Western blot results of rat joints showed that NLRP3, caspase-1, and IL-1β expression were upregulated by MSU crystal stimulation. Intraperitoneal injection of ATP exacerbated and Z1456467176 inhibited MSU crystal-induced activation of the NLRP3 inflammasome pathway (Figure 7C). Based on the release of extracellular ATP after MSU crystal stimulation, these data suggest that Z1456467176 effectively alleviates the symptoms of gouty arthritis by acting on P2X7R to inhibit ATP-induced activation of the NLRP3 inflammasome.

To further evaluate the safety of Z1456467176 treatment *in vivo*, we next examined the liver and kidney function levels of rats in each group. The results showed no significant impairment of liver and kidney function in rats treated with Z1456467176 compared to other groups (Table 1).

The binding of Z1456467176 rearranges the P2X7R protein conformation

Molecular dynamics simulation was performed to analyze the binding of the protein (P2X7R)–ligand (Z1456467176),

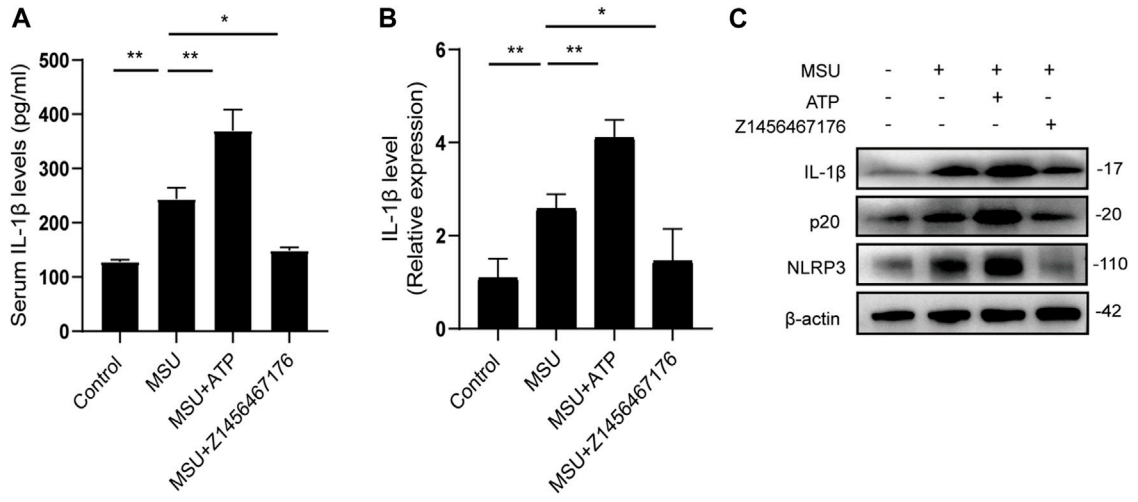

FIGURE. 7
Z1456467176 inhibits NLRP3 inflammasome activation in rat model of gout. **(A)** ELISA of serum IL-1β levels in the four groups. **(B)** qPCR of *IL-1β* gene levels in the peripheral whole blood cells of rats in each group. **(C)** WB of NLRP3, p20, and IL-1β expression in the joints and surrounding synovial tissues of rats in each group. Data are presented as the means ± S.E.M.s. Statistics were analyzed using Dunnett's *t* test. $n = 4$. $^{*}p < 0.05$; $^{**}p < 0.01$.

TABLE 1 Biochemical parameters of rats in gout model.

Biochemical index	Control group	MSU group	MSU + ATP group	MSU + Z1456467176 group	*p* Value
AST (U/L)	15.52 ± 1.89	24.41 ± 7.50	17.79 ± 7.21	20.42 ± 9.07	>0.05
ALT (U/L)	19.99 ± 6.34	32.86 ± 10.39	26.47 ± 10.28	28.81 ± 6.48	>0.05
Bun (mmol/L)	1.40 ± 0.17	1.26 ± 0.44	1.33 ± 0.22	2.16 ± 1.69	>0.05
Cr (μmol/L)	28.33 ± 10.07	34.86 ± 29.03	21.2 ± 9.99	34.35 ± 13.86	>0.05

p value represents the comparison of MSU + Z1456467176 group and other groups in each index.
AST, aspartate transaminase; ALT, alanine transaminase; Bun, blood urea nitrogen; Cr, creatinine.

providing data on receptor and ligand affinity. During the 100 ns kinetic simulations, the RMSD values of the protein–ligand systems were kept in equilibrium, with mean values of 0.3664 ± 0.0137 nm and 0.3413 ± 0.016 nm, respectively, suggesting that the systems reached stability (Figure 8A). The radius of gyration (Rg) values of the protein–ligand system were larger than those of the pure protein system throughout the simulation time (Figure 8B), suggesting that the system swelled due to local conformational changes after ligand binding. The solvent accessible surface area (SASA) of the protein after ligand binding was reduced in the 80-100 ns equilibrium period compared to the protein, 463.3 ± 4.7 and 472.4 ± 5.9, respectively, probably due to the reduced contact area of hydrophobic amino acid residues in the ligand-binding region with the solvent (Figure 8C). During the equilibrium period, the mean values of hydrogen bond formation between protein and protein–ligand were 1968 ± 23.5 and 1947 ± 25.5, respectively, indicating the presence of more hydrogen bonds between water molecules and protein (Figure 8D).

To determine whether Z1456467176 binding resulted in structural rearrangement of the P2X7R protein, we compared the secondary structures of the P2X7R protein and protein–ligand. The results showed that the open region at the upper end and the TM region at the lower end of P2X7R expanded outwards after ligand binding compared with the pure protein, leading to a change in secondary structure (Figure 9), which was consistent with the change in Rg value. Specifically, Figure 9E shows the conformational transition of the secondary structure after protein–ligand binding from α-helix to loop. This indicated that the binding of Z1456467176 significantly changed the conformation of the P2X7R protein.

On this basis, we further analyzed the protein–ligand binding data. The total binding free energy of the protein–ligand is -60.493 kJ/mol, of which the van der Waal energy is

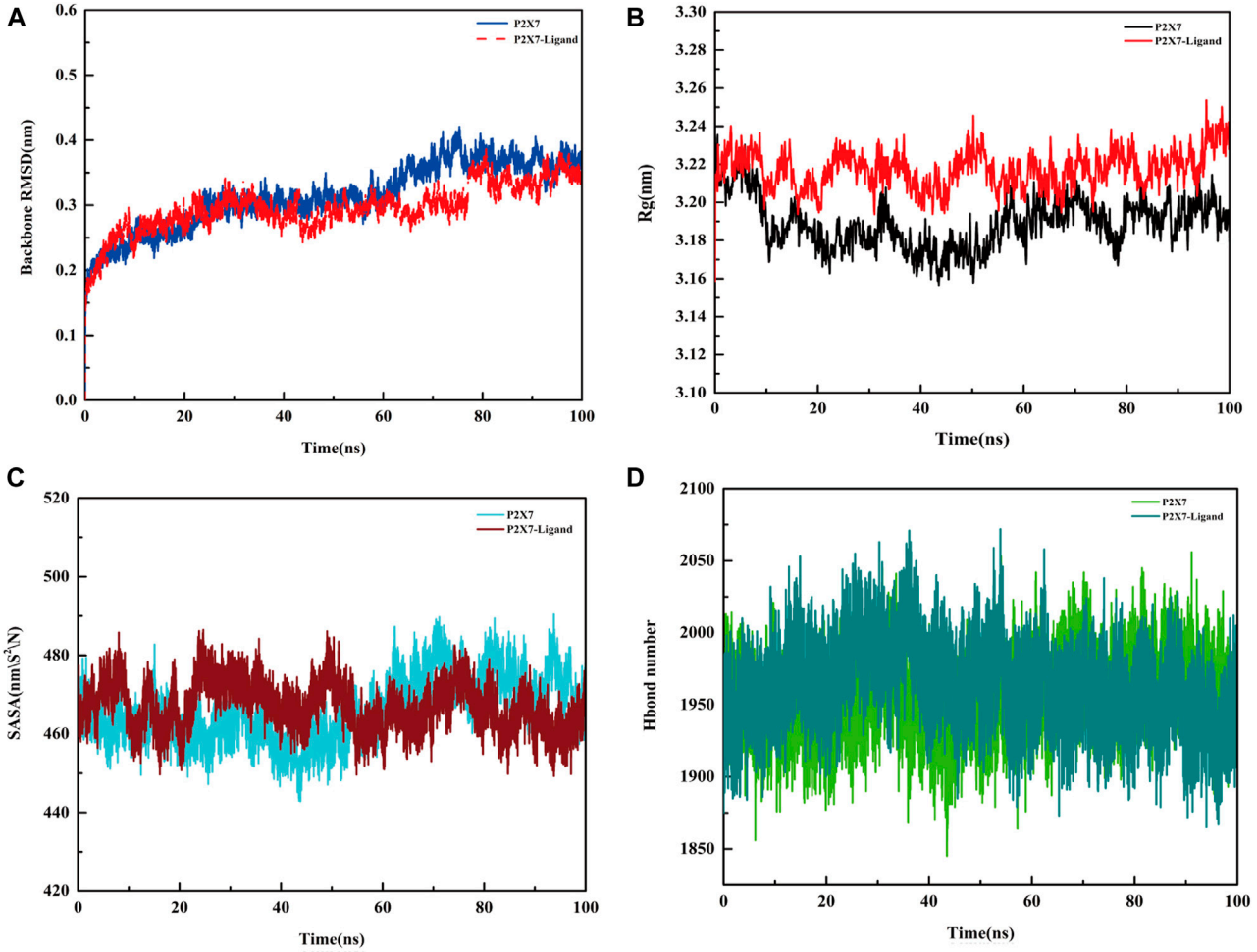

FIGURE. 8
Molecular dynamics simulation of the P2X7R protein and protein–ligand. **(A)** Variation in RMSD values of the protein (P2X7R, blue line) and protein–ligand (Z1456467176, red line) systems with time. **(B)** Rg values of the protein (black line) and protein–ligand (red line) systems with time. **(C)** SASA area of the protein (blue line) and protein–ligand (red line) systems over time. **(D)** The hydrogen bond formed between the protein (light green line), protein–ligand (dark green line) system and water.

-196.508 kJ/mol; the electrostatic energy is -56.783 kJ/mol; the polar solvation energy is 214.035 kJ/mol; and the SASA energy is -21.236 kJ/mol. The binding free energy of the two shows that the van der Waals force and the electrostatic force are dominant, which is beneficial to the combination. The contribution of amino acid residues at different positions to the binding free energy was obtained by decomposing the binding free energy (Supplementary Table S1).

Protein–ligand binding pattern analysis showed that the pi-cation electrostatic interaction exists between the amino groups of Arg316 (C), Asn100 (A), Asn100 (B), Asn100 (C) and the ligand, and the interaction distance is 5.0 Å, 4.7 Å, 4.8 Å, 5.5 Å. In addition, there is an pi-anion electrostatic interaction between the F atom of the ligand and Phe102 (A) with a distance of 5.2 Å. Pi-alkyl hydrophobic interactions exist between Val61 (B), Ile319 (A), Leu320 (B) and the ligand, with distances of 4.0 Å, 6.0 Å, and 3.6 Å, respectively. Hydrogen bonds are formed between Asn100 (A) and the ligand at distances of 1.8 Å and 2.0 Å, respectively (Figure 10).

Discussion

In this study, we identified a potent P2X7R antagonist through virtual screening and functional validation. In *vivo and in vitro* studies, Z1456467176 inhibited ATP- or BzATP-induced P2X7R activation to block the NLRP3-caspase-1-IL-1β pathway, alleviating the clinical manifestations of gouty arthritis and confirming P2X7R as an effective therapeutic target. Importantly, we herein found that the binding of

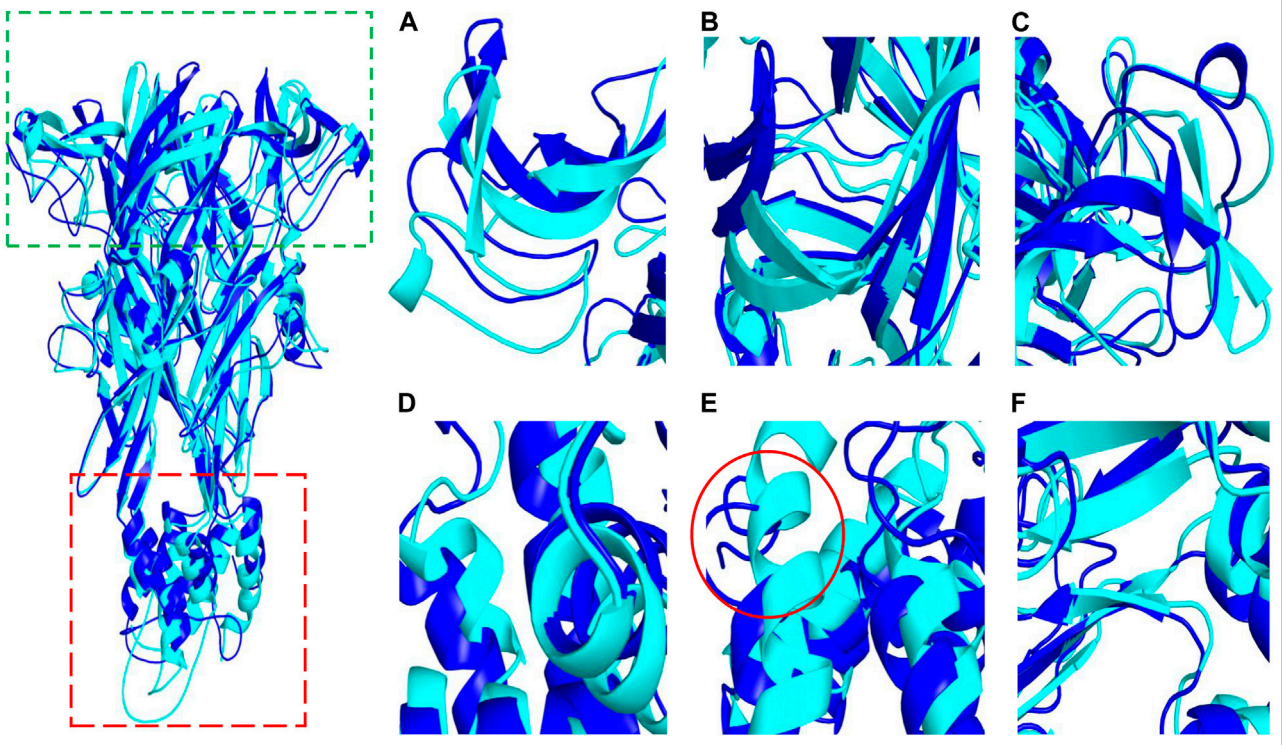

FIGURE. 9
The conformational difference between P2X7R and P2X7R-ligand. The diagram on the left shows conformational differences between the pure protein (P2X7R, blue) and the protein–ligand (Z1456467176, cyan). The green and red boxes indicate the approximate locations of the domains shown in **(A–C)** and **(D–F)**, respectively. **(A–C)** The conformation of the open region at the upper end of P2X7R. **(D–F)** The conformation of the helical region of P2X7R.

Z1456467176 induces a conformational change in the P2X7R protein, suggesting that allosteric inhibition of P2X7R is a promising strategy for gout treatment.

In the past, several competitive and noncompetitive antagonists against P2X7R have been developed. Oxidized ATP is an irreversible competitive P2X7R antagonist but simultaneously exhibits nonspecific modulation of NF-κB signaling pathway expression (Di Virgilio, 2003). Notably, our study showed that Z1456467176 specifically inhibited P2X7R-mediated IL-1β release without affecting IL-6 and TNF-α expression. BBG is a conventional P2X7R antagonist but also affects P2X4R (North, 2002), which is functionally similar to P2X7R (Kanellopoulos et al., 2021), implying a nonselective inhibitory function on P2XRs. Despite the functional similarity, the two receptors are structurally different, with the drug-binding pocket of P2X4R being narrower than that of P2X7R (Sluyter, 2017). Therefore, the antagonists screened by molecular docking based on the P2X7R drug-binding pocket theoretically have higher specificity. In addition, the selectivity of BBG for hP2X7R is lower than that for rats, leading to a limited clinical application (Jiang et al., 2000). KN-62 is an isoquinoline derivative that inhibits human and mouse P2X7R activation, but evidence of inhibition in rats is lacking (Humphreys et al., 1998). Furthermore, KN-62 acts as a complete antagonist to ATP stimulation yet exerts a partial antagonistic effect on the stimulation of the P2X7R-specific agonist BzATP (Humphreys et al., 1998). In the present study, we determined that Z1456467176 responded to different species and exerted effective inhibition of both ATP- and BzATP-induced P2X7R activation.

Currently, we have witnessed the clinical application of several P2X7R antagonists. However, the expected therapeutic effect has not been achieved in the treatment of inflammation-associated diseases (Keystone et al., 2012; Stock et al., 2012; Eser et al., 2015), suggesting that a better understanding of the mechanisms involved in P2X7R-mediated disease pathogenesis is warranted. Gout is characterized by an inflammatory response caused by the deposition of MSU crystals in the joints, cartilage, and surrounding synovial tissue. Gout flares are usually accompanied by triggers including exercise, alcohol intake, overeating, and late nights. Collating these triggers we found that they all cause fluctuations in ATP levels in the body (Lowell and Spiegelman, 2000; Sauer et al., 2000; Mashimo et al., 2015; Alghannam et al., 2021), which points to the possibility that ATP is an important predisposing factor for the development of gout. In this study, we demonstrate that stimulation of MSU crystals induces an increase in ATP production, which is released extracellularly through pyroptosis. Extracellular ATP is a signaling molecule that acts on P2X7R to activate the NLRP3-

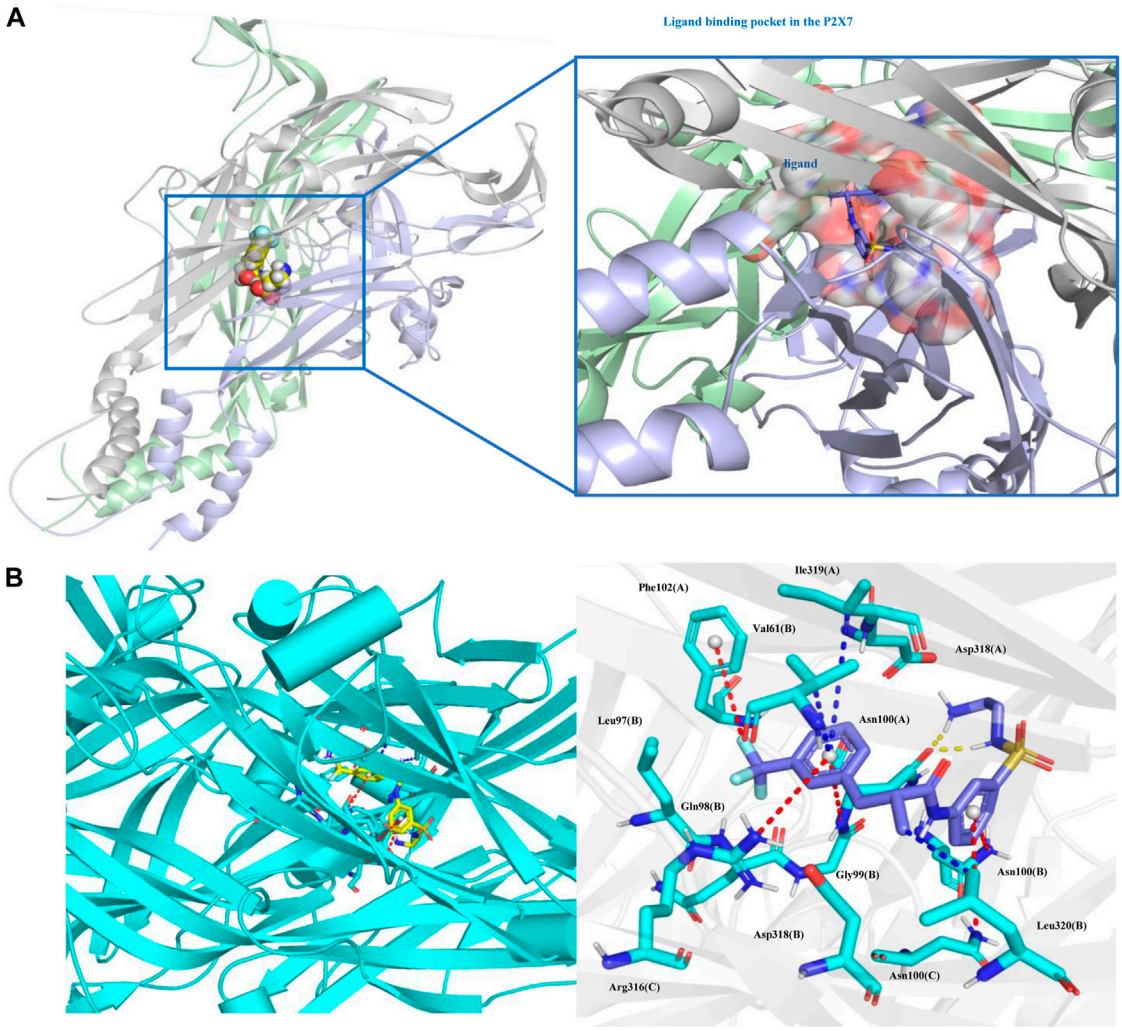

FIGURE. 10
Protein–ligand binding pattern. **(A)** Protein–ligand binding site. **(B)** Interacting amino acid residues and interaction force; the red dotted line represents the electrostatic force, the yellow dotted line represents the hydrogen bond, and the blue dotted line represents the hydrophobic force. Ligand (Z1456467176, blue) and P2X7R residues (green) are represented as stick models.

caspase-1-IL-1β signaling pathway, aggravating MSU crystal-induced gout pathogenesis. Therefore, these results suggest that ATP-P2X7R is involved in the pathogenesis of gout, which is corroborated by a study of *P2X7R* gene polymorphisms and gout susceptibility (Gong and Chen, 2015; Tao et al., 2017). Functionally enhanced *P2X7R* gene polymorphisms in gout patients imply a more sensitive ATP response in these populations, as evidenced by the rapid opening function of P2X7R channels and the massive release of IL-1β (Sorge et al., 2012; Jindrichova et al., 2015). As illustrated by Jiang (Jiang et al., 2013), NS-SNPs characterization of specific residues in P2X7R reveals unique molecular mechanisms that determine differences in P2X7R function, providing new insights into disease mechanisms. P2X7R is a trimeric protein and the conformational changes induced by ATP binding contribute to channel formation (Karasawa and Kawate, 2016). Therefore, screening for allosteric inhibitors that block this process from occurring is a promising direction for gout. The results of molecular docking and kinetic analyses show a greater structural difference in the secondary structure after protein-Z1456467176 binding compared to the pure protein system, exhibiting an outward expansion of the open region at the upper end of P2X7R and the TM region at the lower end. Notably, the closure of the turret located at the upper end of the protein during P2X7R activation is a characteristic conformational change after ATP binding (Karasawa and Kawate, 2016). Thus, structural remodeling leading to the restriction of P2X7R protein response to ATP is responsible for the therapeutic effect of

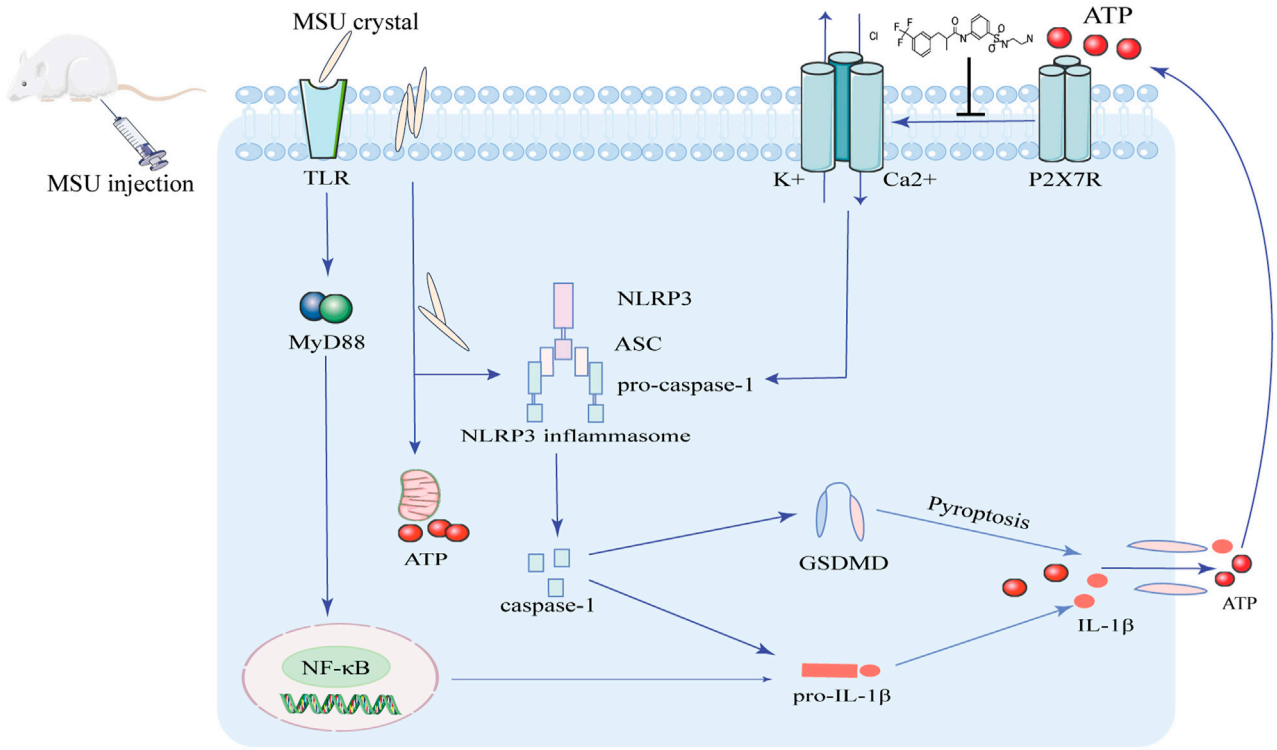

FIGURE. 11
Schematic diagram of the mechanism of Z1456467176 in the treatment of MSU crystal-induced acute gouty arthritis. MSU crystal stimulation promotes ATP production, which is released through caspase-1-dependent pyroptosis. The interaction of extracellular ATP with P2X7R alters the structure of the protein and induces ion flow. Together with MSU crystals, it activates the NLRP3 inflammasome and promotes the release of sufficient IL-1β to trigger the gout inflammatory response. Z1456467176 inhibits ATP-induced channel opening and P2X7R-NLPR3-IL-1β pathway activation by remodeling the structure of P2X7R protein. Thus, acute gouty arthritis induced by MSU crystals was relieved.

Z1456467176 in gout. A growing understanding of the structure–function relationship of P2X7R will facilitate continued efforts to optimize the treatment of gout disease.

Z1456467176 achieved significant therapeutic effects in gout rats *in vivo*, although it did not completely inhibit BzATP-induced IL-1β secretion *in vitro*. IL-1β is the main proinflammatory cytokine in initiating gout; however, the IL-1β-mediated inflammatory response is also critical in resolving infections to some extent, contributing to the body's timely response to danger and self-recovery. In tissue recovery after injury, low levels of IL-1β and TNF-α promote wound healing by increasing growth factor production (Brauchle et al., 1994). In influenza-induced tissue damage, IL-1β and TNF-α are induced to be expressed in type II alveolar epithelial cells and contribute to alveolar regeneration by acting directly on alveolar epithelial cells via surface receptors and NF-κB signaling pathways (Katsura et al., 2019). In addition, mice deficient in IL-1β have been found to have an increased incidence of cysts exposed to UV light, which was shown to be associated with a reduction in skin inflammation (Kulkarni et al., 2017). Thus, the release of moderate amounts of IL-1β following the action of the danger signal ATP in gout contributes to the induction of self-resolution of inflammation in the organism. Similarly, P2X7R has a physiological function to maintain the body's metabolic balance, and excessive inhibition interferes with normal physiological functions. Studies have found that deficiency or inhibition of P2X7R results in impaired pancreatic β-cell function, imbalance in fat distribution, decreased systemic energy expenditure and fatty acid oxidation, and increased metabolic syndrome (Glas et al., 2009; Beaucage et al., 2014; Giacovazzo et al., 2018). Therefore, moderate rather than complete inhibition of P2X7R function contributes to the timely response of the immune system and is more appropriate for disease treatment.

In conclusion, the study identified a potential P2X7R antagonist, Z1456467176, that can inhibit ATP-induced NLRP3-caspase-1-IL-1β pathway activation by allosterically modulating P2X7R, effectively alleviating MSU crystal-induced gouty joint inflammation in rats (Figure 11). These data provide direct experimental evidence for the involvement of P2X7R in gout

pathogenesis, establishing that allosteric inhibition of P2X7R is an effective strategy for gout treatment.

Data availability statement

The datasets presented in this study can be found in online repositories. The names of the repository/repositories and accession number(s) can be found in the article/ Supplementary Material.

Ethics statement

The studies involving human participants were reviewed and approved by the Medical Research Ethics Committee of the First Hospital of University of Science and Technology of China (Anhui Provincial Hospital). The patients/participants provided their written informed consent to participate in this study. The animal study was reviewed and approved by The Animal Ethics Committee of the First Hospital of the University of Science and Technology of China (Anhui Provincial Hospital).

Author contributions

JT and XL contributed to the conception and design of the study. XL, YL, and CL conducted the experiments and analyzed the data. XL drafted the manuscript. All authors contributed to manuscript revision and approved the submitted version.

Funding

This work was supported by the National Natural Science Foundation of China (81771774) and the Anhui Provincial Key Research and Development Plan (201904a07020103).

Conflict of interest

The authors declare that the research was conducted in the absence of any commercial or financial relationships that could be construed as a potential conflict of interest.

Publisher's note

Supplementary material

The Supplementary Material for this article can be found online at: https://www.frontiersin.org/articles/10.3389/fphar.2022.979939/full#supplementary-material

References

Alghannam, A. F., Ghaith, M. M., and Alhussain, M. H. (2021). Regulation of energy substrate metabolism in endurance exercise. *Int. J. Environ. Res. Public Health* 18, 4963. doi:10.3390/ijerph18094963

Beaucage, K. L., Xiao, A., Pollmann, S. I., Grol, M. W., Beach, R. J., Holdsworth, D. W., et al. (2014). Loss of P2X7 nucleotide receptor function leads to abnormal fat distribution in mice. *Purinergic Signal.* 10, 291–304. doi:10.1007/s11302-013-9388-x

Brauchle, M., Angermeyer, K., Hubner, G., and Werner, S. (1994). Large induction of keratinocyte growth factor expression by serum growth factors and pro-inflammatory cytokines in cultured fibroblasts. *Oncogene* 9, 3199–3204.

Carr, A., Doyle, A. J., Dalbeth, N., Aati, O., and McQueen, F. M. (2016). Dual-energy CT of urate deposits in costal cartilage and intervertebral disks of patients with tophaceous gout and age-matched controls. *AJR. Am. J. Roentgenol.* 206, 1063–1067. doi:10.2214/AJR.15.15356

Chen, B., Li, H., Ou, G., Ren, L., Yang, X., and Zeng, M. (2019). Curcumin attenuates MSU crystal-induced inflammation by inhibiting the degradation of IκBα and blocking mitochondrial damage. *Arthritis Res. Ther.* 21, 193. doi:10.1186/s13075-019-1974-z

Coderre, T. J., and Wall, P. D. (1987). Ankle joint urate arthritis (AJUA) in rats: an alternative animal model of arthritis to that produced by freund's adjuvant. *Pain* 28, 379–393. doi:10.1016/0304-3959(87)90072-8

Dalbeth, N., Choi, H. K., Joosten, L. A. B., Khanna, P. P., Matsuo, H., Perez-Ruiz, F., et al. (2019). Gout. *Nat. Rev. Dis. Prim.* 5, 69. doi:10.1038/s41572-019-0115-y

Di Virgilio, F., Dal Ben, D., Sarti, A. C., Giuliani, A. L., and Falzoni, S. (2017). The P2X7 receptor in infection and inflammation. *Immunity* 47, 15–31. doi:10.1016/j.immuni.2017.06.020

Di Virgilio, F. (2003). Novel data point to a broader mechanism of action of oxidized ATP: the P2X7 receptor is not the only target. *Br. J. Pharmacol.* 140, 441–443. doi:10.1038/sj.bjp.0705469

Eser, A., Colombel, J. F., Rutgeerts, P., Vermeire, S., Vogelsang, H., Braddock, M., et al. (2015). Safety and efficacy of an oral inhibitor of the purinergic receptor P2X7 in adult patients with moderately to severely active crohn's disease: A randomized placebo-controlled, double-blind, phase IIa study. *Inflamm. Bowel Dis.* 21, 2247–2253. doi:10.1097/MIB.0000000000000514

Giacovazzo, G., Apolloni, S., and Coccurello, R. (2018). Loss of P2X7 receptor function dampens whole body energy expenditure and fatty acid oxidation. *Purinergic Signal.* 14, 299–305. doi:10.1007/s11302-018-9610-y

Gicquel, T., Le Dare, B., Boichot, E., and Lagente, V. (2017). Purinergic receptors: new targets for the treatment of gout and fibrosis. *Fundam. Clin. Pharmacol.* 31, 136–146. doi:10.1111/fcp.12256

Glas, R., Sauter, N. S., Schulthess, F. T., Shu, L., Oberholzer, J., and Maedler, K. (2009). Purinergic P2X7 receptors regulate secretion of interleukin-1 receptor antagonist and beta cell function and survival. *Diabetologia* 52, 1579–1588. doi:10.1007/s00125-009-1349-0

Gong, Q. Y., and Chen, Y. (2015). Correlation between P2X7 receptor gene polymorphisms and gout. *Rheumatol. Int.* 35, 1307–1310. doi:10.1007/s00296-015-3258-5

Gong, T., Yang, Y., Jin, T., Jiang, W., and Zhou, R. (2018). Orchestration of NLRP3 inflammasome activation by ion fluxes. *Trends Immunol.* 39, 393–406. doi:10.1016/j.it.2018.01.009

Hughes, M. M., and O'Neill, L. A. J. (2018). Metabolic regulation of NLRP3. *Immunol. Rev.* 281, 88–98. doi:10.1111/imr.12608

Humphreys, B. D., Virginio, C., Surprenant, A., Rice, J., and Dubyak, G. R. (1998). Isoquinolines as antagonists of the P2X7 nucleotide receptor: High selectivity for the human versus rat receptor homologues. *Mol. Pharmacol.* 54, 22–32. doi:10.1124/mol.54.1.22

Jiang, L. H., Mackenzie, A. B., North, R. A., and Surprenant, A. (2000). Brilliant blue G selectively blocks ATP-gated rat P2X(7) receptors. *Mol. Pharmacol.* 58, 82–88. doi:10.1124/mol.58.1.82

Jiang, L. H., Baldwin, J. M., Roger, S., and Baldwin, S. A. (2013). Insights into the molecular mechanisms underlying mammalian P2X7 receptor functions and contributions in diseases, revealed by structural modeling and single nucleotide polymorphisms. *Front. Pharmacol.* 4, 55. doi:10.3389/fphar.2013.00055

Jindrichova, M., Bhattacharya, A., Rupert, M., Skopek, P., Obsil, T., and Zemkova, H. (2015). Functional characterization of mutants in the transmembrane domains of the rat P2X7 receptor that regulate pore conductivity and agonist sensitivity. *J. Neurochem.* 133, 815–827. doi:10.1111/jnc.13078

Kanellopoulos, J. M., Almeida-da-Silva, C. L. C., Ruutel Boudinot, S., and Ojcius, D. M. (2021). Structural and functional features of the P2X4 receptor: An immunological perspective. *Front. Immunol.* 12, 645834. doi:10.3389/fimmu.2021.645834

Karasawa, A., and Kawate, T. (2016). Structural basis for subtype-specific inhibition of the P2X7 receptor. *Elife* 5, e22153. doi:10.7554/eLife.22153

Katsura, H., Kobayashi, Y., Tata, P. R., and Hogan, B. L. M. (2019). IL-1 and TNF alpha contribute to the inflammatory niche to enhance alveolar regeneration. *Stem Cell Rep.* 12, 657–666. doi:10.1016/j.stemcr.2019.02.013

Keystone, E. C., Wang, M. M., Layton, M., Hollis, S., and McInnes, I. B. (2012). Clinical evaluation of the efficacy of the P2X7 purinergic receptor antagonist AZD9056 on the signs and symptoms of rheumatoid arthritis in patients with active disease despite treatment with methotrexate or sulphasalazine. *Ann. Rheum. Dis.* 71, 1630–1635. doi:10.1136/annrheumdis-2011-143578

Kulkarni, N. N., Adase, C. A., Zhang, L. J., Borkowski, A. W., Li, F., Sanford, J. A., et al. (2017). IL-1 receptor-knockout mice develop epidermal cysts and show an altered innate immune response after exposure to UVB radiation. *J. Invest. Dermatol.* 137, 2417–2426. doi:10.1016/j.jid.2017.07.814

Lowell, B. B., and Spiegelman, B. M. (2000). Towards a molecular understanding of adaptive thermogenesis. *Nature* 404, 652–660. doi:10.1038/35007527

Marques-da-Silva, C., Chaves, M. M., Castro, N. G., Coutinho-Silva, R., and Guimaraes, M. Z. (2011). Colchicine inhibits cationic dye uptake induced by ATP in P2X2 and P2X7 receptor-expressing cells: implications for its therapeutic action. *Br. J. Pharmacol.* 163, 912–926. doi:10.1111/j.1476-5381.2011.01254.x

Martinon, F., Petrilli, V., Mayor, A., Tardivel, A., and Tschopp, J. (2006). Gout-associated uric acid crystals activate the NALP3 inflammasome. *Nature* 440, 237–241. doi:10.1038/nature04516

Mashimo, K., Arthur, P. G., and Ohno, Y. (2015). Ethanol dose- and time-dependently increases alpha and beta subunits of mitochondrial ATP synthase of cultured neonatal rat cardiomyocytes. *J. Nippon. Med. Sch.* 82, 237–245. doi:10.1272/jnms.82.237

McCarthy, A. E., Yoshioka, C., and Mansoor, S. E. (2019). Full-length P2X7 structures reveal how palmitoylation prevents channel desensitization. *Cell* 179, 659–670. doi:10.1016/j.cell.2019.09.017

Murakami, T., Ockinger, J., Yu, J., Byles, V., McColl, A., Hofer, A. M., et al. (2012). Critical role for calcium mobilization in activation of the NLRP3 inflammasome. *Proc. Natl. Acad. Sci. U. S. A.* 109, 11282–11287. doi:10.1073/pnas.1117765109

North, R. A. (2002). Molecular physiology of P2X receptors. *Physiol. Rev.* 82, 1013–1067. doi:10.1152/physrev.00015.2002

Petsch, C., Araujo, E. G., Englbrecht, M., Bayat, S., Cavallaro, A., Hueber, A. J., et al. (2016). Prevalence of monosodium urate deposits in a population of rheumatoid arthritis patients with hyperuricemia. *Semin. Arthritis Rheum.* 45, 663–668. doi:10.1016/j.semarthrit.2015.11.014

Sauer, H., Hescheler, J., and Wartenberg, M. (2000). Mechanical strain-induced Ca(2+) waves are propagated via ATP release and purinergic receptor activation. *Am. J. Physiol. Cell Physiol.* 279, C295–C307. doi:10.1152/ajpcell.2000.279.2.C295

Sluyter, R. (2017). The P2X7 receptor. *Adv. Exp. Med. Biol.* 1051, 17–53. doi:10.1007/5584_2017_59

Sorge, R. E., Trang, T., Dorfman, R., Smith, S. B., Beggs, S., Ritchie, J., et al. (2012). Genetically determined P2X7 receptor pore formation regulates variability in chronic pain sensitivity. *Nat. Med.* 18, 595–599. doi:10.1038/nm.2710

Stock, T. C., Bloom, B. J., Wei, N., Ishaq, S., Park, W., Wang, X., et al. (2012). Efficacy and safety of CE-224, 535, an antagonist of P2X7 receptor, in treatment of patients with rheumatoid arthritis inadequately controlled by methotrexate. *J. Rheumatol.* 39, 720–727. doi:10.3899/jrheum.110874

Tao, J. H., Cheng, M., Tang, J. P., Dai, X. J., Zhang, Y., Li, X. P., et al. (2017). Single nucleotide polymorphisms associated with P2X7R function regulate the onset of gouty arthritis. *PLoS One* 12, e0181685. doi:10.1371/journal.pone.0181685

Zhu, J., Li, A., Jia, E., Zhou, Y., Xu, J., Chen, S., et al. (2017). Monosodium urate crystal deposition associated with the progress of radiographic grade at the sacroiliac joint in axial SpA: a dual-energy CT study. *Arthritis Res. Ther.* 19, 83. doi:10.1186/s13075-017-1286-0

frontiers | Frontiers in Pharmacology

TYPE Review
PUBLISHED 17 August 2022
DOI 10.3389/fphar.2022.964771

OPEN ACCESS

EDITED BY
Yan Huang,
Anhui Medical University, China

REVIEWED BY
Lifei Hou,
Harvard Medical School, United States
Chao Li,
University of Texas Southwestern Medical Center, United States
Yuanli Chen,
Hefei University of Technology, China

*CORRESPONDENCE
Zhixia Zhou,
zhou_zhixia@qdu.edu.cn
Shoushi Wang,
wangshoushi1226@126.com

SPECIALTY SECTION
This article was submitted to Inflammation Pharmacology, a section of the journal Frontiers in Pharmacology

RECEIVED 09 June 2022
ACCEPTED 11 July 2022
PUBLISHED 17 August 2022

CITATION
Yi S, Tao X, Wang Y, Cao Q, Zhou Z and Wang S (2022), Effects of propofol on macrophage activation and function in diseases.
Front. Pharmacol. 13:964771.
doi: 10.3389/fphar.2022.964771

Effects of propofol on macrophage activation and function in diseases

Shuyuan Yi[1,2,3], Xinyi Tao[3], Yin Wang[2], Qianqian Cao[3], Zhixia Zhou[2]* and Shoushi Wang[3]*

[1]School of Anesthesiology, Weifang Medical University, Weifang, China, [2]Institute for Translational Medicine, The Affiliated Hospital of Qingdao University, College of Medicine, Qingdao University, Qingdao, China, [3]Qingdao Central Hospital, Central Hospital Affiliated to Qingdao University, Qingdao, China

Macrophages work with monocytes and dendritic cells to form a monocyte immune system, which constitutes a powerful cornerstone of the immune system with their powerful antigen presentation and phagocytosis. Macrophages play an essential role in infection, inflammation, tumors and other pathological conditions, but these cells also have non-immune functions, such as regulating lipid metabolism and maintaining homeostasis. Propofol is a commonly used intravenous anesthetic in the clinic. Propofol has sedative, hypnotic, anti-inflammatory and anti-oxidation effects, and it participates in the body's immunity. The regulation of propofol on immune cells, especially macrophages, has a profound effect on the occurrence and development of human diseases. We summarized the effects of propofol on macrophage migration, recruitment, differentiation, polarization, and pyroptosis, and the regulation of these propofol-regulated macrophage functions in inflammation, infection, tumor, and organ reperfusion injury. The influence of propofol on pathology and prognosis via macrophage regulation is also discussed. A better understanding of the effects of propofol on macrophage activation and function in human diseases will provide a new strategy for the application of clinical narcotic drugs and the treatment of diseases.

KEYWORDS

macrophage, propofol, inflammation, tissue repair, tumor

1 Introduction

Propofol (2,6-diisopropylphenol) is a gamma-aminobutyric acid (GABA) receptor agonist and an intravenous anesthetic that is commonly used in the clinic. It is often used in the induction and maintenance of anesthesia. Propofol induction is rapid and stable with almost no excitation and a low incidence of postoperative nausea and vomiting (PONV) (Gao et al., 2020). Based on these advantages, propofol is suitable for sedation and anesthesia in most types of surgery. Propofol also regulates the inflammatory response (Ma et al., 2013; Li et al., 2015) and exerts antioxidant effects (Tanaka et al., 2010). Increasing evidence has shown that the use of propofol also affects the development of tumors and has long-term implications for

patient outcomes (Zhang et al., 2014; Cata et al., 2020). Increasing attention has been given to its possible mechanism. Propofol reduces the phagocytic activity of neutrophils in innate immunity and inhibits the release of pro-inflammatory cytokines, such as interleukin-6 (IL-6) and tumor necrosis factor-α (TNF-α), from peripheral blood mononuclear cells (Visvabharathy and Freitag, 2017). The regulation of propofol on the function of immune cells, including lymphocytes, neutrophils, natural killer (NK) cells and macrophages, and the potential mechanisms have been the focus of research in recent years.

Macrophages originate from progenitor cells in the bone marrow and enter the bloodstream, where monocytes migrate to tissues and differentiate into macrophages during inflammation or cancer (Gordon and Martinez, 2010). Macrophages are highly plastic immune cells that are involved in regulating the inflammatory response, secreting cytokines, removing cell fragments, killing pathogens, and maintaining tissue development and homeostasis (Varol et al., 2015). Macrophages play an important role in the development of inflammatory diseases, including diabetes (Meshkani and Vakili, 2016), infection (Kotani et al., 2001), atherosclerosis (Moore et al., 2013), reperfusion injury (Sousa et al., 2021), and cancer (Vitale et al., 2019; Wu et al., 2020). Depending on the local environment, macrophages differentiate into a variety of phenotypes and secrete a variety of inflammatory cytokines, which act as pro-inflammatory or anti-inflammatory agents. Increasing evidence shows that the inflammatory or anti-inflammatory response involved in macrophages is also regulated by perioperative anesthetics, which in turn affects the development and treatment of the disease. Dexmedetomidine and propofol inhibit the expression of lipopolysaccharide (LPS)-stimulated high mobility group box 1 (HMGB1) in macrophages (Chang et al., 2013; Jia et al., 2017). The volatile anesthetic sevoflurane modulates macrophage recruitment, polarization, differentiation, apoptosis and pyroptosis by regulating the caspase-1, reactive oxygen species (ROS), forkhead box O1 (FoxO1), p21, and glycogen synthase kinase-3 (GSK-3β)/nuclear factor-E2-related factor 2 (Nrf2) pathways, which are involved in local immunity and tumor growth (Jin et al., 2013; Fu et al., 2020; Sztwiertnia et al., 2020; Cai et al., 2021a). Opioids, such as morphine, also inhibit the phagocytosis of macrophages and are associated with the reduction of macrophage colony-stimulating factor-induced proliferation and differentiation (Sacerdote et al., 2003). Remifentanil increases osteoclasts by enhancing migration and cell fusion of bone marrow-derived macrophages (BMM_S) (Jeon et al., 2018). Therefore, the activation, polarization and function of macrophages are regulated by a variety of anesthetics during the perioperative period, especially propofol. Notably, increasing attention has been given to the prominent anti-inflammatory effect of propofol and its regulation of macrophage function, which reduce inflammation and reperfusion injury and improve tumor prognosis.

Therefore, a better understanding of the regulation of macrophage activation and function mediated by anesthetics and its consequent effects on the immune system and disease development will provide new strategies for clinical perioperative anesthetics and disease treatment. In this review, we summarize the effects of propofol on macrophage activation, including migration, recruitment, differentiation, polarization, and pyroptosis. Moreover, based on recent preclinical and clinical studies, the function of these propofol-related macrophages in local inflammation, infection, tumor, and tissue repair was highlighted. This review will enrich the theoretical basis of the research of anesthetics in human disease development and treatment.

2 Macrophage activation and function

Macrophages are one of the most important parts of the mononuclear phagocyte system (van Furth et al., 1972). There are two distinct origins of macrophages in tissues. Most macrophages in healthy tissues are established before birth. The other origin is associated with pathology, homeostasis, and tissue inflammation, where macrophages develop from tissue-infiltrating monocytes in adulthood (Varol et al., 2015). The $CD115^+$ mouse monocyte subsets are divided into $Ly6C^{hi}$ monocytes and $Ly6C^{low}$ monocytes (Ingersoll et al., 2010). The primary function of $Ly6C^{low}$ cells appears to involve surveying vascular endothelial integrity and involvement in early inflammation and tissue repair responses. In contrast, $Ly6C^{hi}$ monocytes in mice and $CD14^+$ monocytes in humans serve as precursors to tissue macrophages derived from monocytes and are recruited to pathological changes, such as tumors and inflammation, to exert pro-inflammatory and antibacterial activities (Auffray et al., 2007; Carlin et al., 2013). Under the stimulation of the microenvironment and cytokines, $Ly6C^{hi}$ cells enter damaged tissues and differentiate into macrophages to reduce inflammation and promote tissue repair by stimulating angiogenesis, suppressing neutrophil aggregation and removing cellular debris (Varol et al., 2015). Depending on the difference in anatomical locations and functional phenotypes, tissue-resident macrophages are divided into microglia, osteoclasts, alveolar macrophages, and Kupffer cells (Davies et al., 2013).

The activation and polarization of macrophages is always influenced by the surrounding microenvironments in inflammatory or tumor environments. Macrophages generally polarized into two subtypes, the classically activated type (M1) and the alternating activated type (M2). M1 macrophages are generally induced by Th1-type cytokines, such as interferon-γ (IFN-γ) and TNF-α, or recognized by bacterial LPS. These macrophages produce and secrete higher levels of proinflammatory cytokines, such as TNF-α, IL-1β, IL-6 and cyclooxygenase 2 (COX-2). Therefore, M1 macrophages have

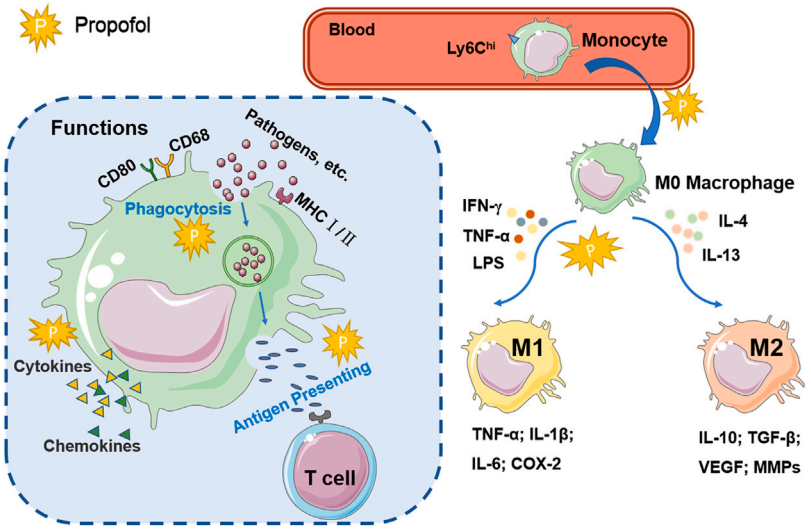

FIGURE 1
The activation and function of macrophages. Ly6C^{hi} monocytes in the blood enter the damaged tissue and differentiate into macrophages. Macrophages recruited by inflammation or tumors are stimulated by Th1 or Th2 cytokines to differentiate into two activated types: the classical activated type (M1) and the alternating activated type (M2). Activated macrophages express high levels of CD80, CD68, and MHC I/II. Macrophages phagocytize pathogens and cell fragments, recognize specific antigens, and transmit signals to T cells for antigen presentation. Macrophages participate in immune regulation by regulating the secretion of cytokines and chemokines. The explosion-shaped graphic represents propofol, suggesting that it may be involved in the signaling pathways and cellular processes of macrophages.

strong antigenic presentation, antimicrobial and antitumor activities, which also mediate ROS-induced tissue injury and promote tissue regeneration or wound healing. The Th2 cytokines IL-4 and IL-13 induce the activation of M2 macrophages and further induce the production of different surface receptors and effector molecules, such as IL-10 and TGF-β. M2 macrophages have a strong phagocytic capacity and remove debris and apoptotic cells, promote tissue repair and wound healing, and promote angiogenesis and fibrosis (Shapouri-Moghaddam et al., 2018; Wu et al., 2020). The exposure of M2 macrophages to M1 signals or the exposure of M1 macrophages to M2 signals induced the repolarization or rearrangement of differentiated macrophages. Therefore, the function of macrophages is usually depend on their polarization state.

As shown in Figure 1, the functional characteristics of macrophages are related to changes in the tissue microenvironment and cytokines. Macrophages play a role in immune surveillance via several receptors, including scavenger receptors, cytokine receptors, adhesion molecules, nuclear hormones and pattern recognition receptors, such as Toll-like receptors (TLRs) and Nod-like receptors (Varol et al., 2015). Activated macrophages highly express antigen-presenting molecules on the surface, such as CD80, CD68 and MHC class I and II molecules. As important antigen-presenting cells (APCs), macrophages play the role of antigen presentation by recognizing and phagocytizing pathogens and stimulating T cells (Wynn et al., 2013). During inflammation or infection, macrophage apoptosis is another strategy used by the host to limit infection and defend against pathogens, and it is an important process in the development of diseases associated with reduced pathogen activity. Macrophage apoptosis is associated with a reduction in lesion size in arteriosclerosis (Shapouri-Moghaddam et al., 2018). If the pathogen inhibits macrophage apoptosis and promotes necrosis, antigen presentation by macrophages may be impaired, and immune escape may occur (Moraco and Kornfeld, 2014). Macrophages are involved in the induction of adhesion molecules, pro-angiogenic factors, matrix metalloproteinase (MMP), nuclear factor-kappa B (NF-κB) and signal transducers and activators of transcription-1 (STAT1) via the regulation of interleukins (Wu et al., 2020). In conclusion, as a non-specific immune cell, macrophages exert phagocytic properties to directly engulf and break down cancer cells, antigens, senescent damaged cells and bacteria. Macrophages can take up and process antigens and deliver information to T lymphocytes. In addition, the ability to secrete bio-active mediators makes macrophages important cells involved in the inflammatory response.

3 Macrophages and anesthetic

A variety of anesthetics participate in macrophage activation, polarization, and functional regulation. Although the effects of

some anesthetics are controversial, it is well known that they influence the development and prognosis of disease by regulating macrophages.

In vivo animal models constructed with toxins and tumors showed that anesthetics and techniques had different effects on the progression of inflammation and tumor prognosis by regulating macrophage activation and function. Clinical histological studies showed that the distribution of multiple immune cells, especially macrophages, had the potential to predict prognosis and treatment in inflammatory sites and tumor tissues. Tissue damage and the use of opioids may activate neuroglia, and the early activation of microglia and macrophages after surgery or exposure to remifentanil may be related to the immune response to injury (Romero et al., 2013). Peroxisome proliferator-activated receptor gamma (PPARγ) negatively regulated macrophage activation. Dexmedetomidine also promotes the M2 activity of macrophages via the PPARγ/STAT3 pathway and inhibits the pro-inflammatory innate immune activation in the liver (Zhou et al., 2020). Dexmedetomidine also modulates the activation of Kupffer cells by activating alpha 2-adrenergic receptors (α2B-ARs), which transforms them into anti-inflammatory phenotypes and promotes liver regeneration (Yue et al., 2022).

Receptors, signaling pathways and transcription factors also influence macrophage polarization. Sevoflurane pretreatment promotes the formation of an anti-inflammatory phenotype in microglia/macrophages by up-regulating the phosphorylation of GSK-3β and Nrf2 nuclear transposition, and it has a neuroprotective effect on middle cerebral artery occlusion (MCAO) (Cai et al., 2021a). However, sevoflurane inhibits FoxO1, regulates p21 and increases the expression of TNF-α, monocyte chemotactic protein-1 (MCP-1) and IL-6, which may increase the polarization of M1 macrophages, induce a central nervous system (CNS) inflammatory response, and lead to cognitive impairment (Fu et al., 2020). This pathway suggests that inhaled anesthetics have different effects on prognosis via regulation of the process of M1-type polarization of macrophages due to different pathological conditions. Recent studies showed that electroacupuncture also prevented weight gain by regulating the inflammatory response in obese adipose tissue and promoting the polarization of M2 macrophages (Wang et al., 2021).

The volatile anesthetics isoflurane and sevoflurane inhibit macrophage phagocytosis. Sevoflurane binds directly to the Ras-like small GTPase RAP1 and inhibits its activity. Isoflurane may interact with molecules in the RAP1 cascades by inhibiting macrophage-1 antigen (Zha et al., 2019). Notably, another study demonstrated that sevoflurane upregulated inducible nitric oxide synthase (iNOS), inhibited the NF-κB pathway, enhanced the LPS-stimulated phagocytosis of macrophages on bacteria, and improved the bactericidal and anti-inflammatory mechanisms of endotoxemia (Gerber et al., 2019). This difference may be due to the different physical and chemical properties of macrophages under different stimuli and the multiple pathways of volatile anesthetic regulation of macrophages. Opioid analgesics also promoted macrophage apoptosis and reduced the expression of toll-like receptor 4 (TLR4) on macrophages (Franchi et al., 2012; Kim, 2018; Lin et al., 2021). Another intravenous anesthetic, ketamine, also had a significant effect on macrophage function. Nowak W et al. showed that ketamine promoted macrophage differentiation into M2 subtypes by modulating the N-methyl-D-aspartate receptor (NMDAR) and mammalian target of rapamycin (mTOR). Its prominent anti-inflammatory properties are important for the prognosis of patients with major depression and other inflammatory diseases (Nowak et al., 2019). Ketamine mediates the function of macrophages by decreasing the mitochondrial membrane potential and downregulating the activation of LPS-induced macrophages by regulating signaling pathways and transcription factors (Liu et al., 2012). However, the regulation of macrophages by anesthetics is not always beneficial to the body in disease progression. The use of sevoflurane is associated with reduced Tumor-associated macrophages (TAMs) and tumor growth in some cancer models (Sztwiertnia et al., 2020).

4 Propofol regulation of macrophage activation and function

Propofol, often referred to as “milk of anesthesia”, is an effective intravenous anesthetic. From the 1970s, James Baird Glen at British Chemical Industries promoted the use of propofol as a new and safe intravenous anesthetic, which was approved in the United Kingdom in 1987 and in the United States in 1989 (Walsh, 2018). Propofol can be used for induction and maintenance of general anesthesia and to enhance sedation in mechanically ventilated patients. The common pathophysiological functions of propofol mainly include inhibition of blood pressure and respiration, followed by immune system and nervous system abnormalities, and some gastrointestinal reactions, etc., which are related to the dose of propofol (Sahinovic et al., 2018). However, compared with other anesthetics, propofol induces anesthesia rapidly and steadily, and the probability of the above pathological effects is also lower (Eleveld et al., 2018). Therefore, propofol is one of the most widely used anesthetics in clinical practice.

The mechanism of action of propofol is related to the interaction of specific structures on the postsynaptic membrane. Extensive experiments have shown that inhibitory central GABAergic neurotransmission is the key to mediating the pharmacological effects of propofol (Trapani et al., 2000; Saraghi et al., 2013). GABA is an important inhibitory neurotransmitter in the central nervous system, and its effects are produced by selective interaction of GABA receptors (GABAA and GABAB) that are widely distributed in immune cells such as neutrophils, monocytes and macrophages (Bhat et al., 2010). Therefore, in addition to anesthesia, propofol also has non-anesthetic effects such as analgesia, organ protection, immunity, and anti-

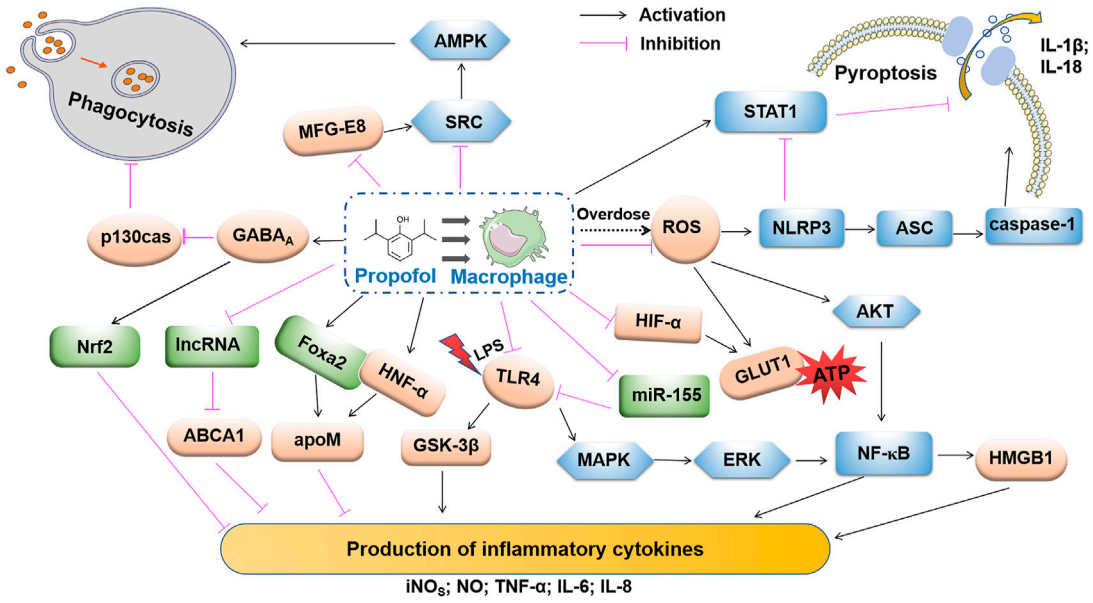

FIGURE 2
Propofol regulation in macrophage phagocytosis, pyroptosis and production of inflammatory cytokines. High-dose propofol activates pro-caspase-1 via NLRP3 and AIM2 inflammasomes via the inflammasome adaptor ASC. Propofol-induced mitochondrial ROS may trigger the activation of NLRP3. The clinical dose of propofol inhibits pyroptosis by activating STRT1. Propofol inhibits pressure effects on macrophage phagocytosis by activating the GABAA receptor and inhibiting p130cas. Propofol reduces microglial production of MFG-E8 and inhibits cellular phagocytosis using the MFG-E8-dependent SRC-AMPK pathway. Propofol inhibits the ROS-mediated AKT and NF-κB pathways. Propofol also inhibits MAPK/ERK, the upstream regulator of NF-κB. Dissociated NK-κB is transferred to the cytoplasm and further induces the release of HMGB1, which inhibits the production of pro-inflammatory factors. Propofol inhibits the release of inflammatory factors via apoM in an HNF-α- and Fox2-dependent manner. Through the expression of lncRNA LOC286367, the expression of ABCA1 inhibits the release of pro-inflammatory factors, and the inhibitory effect of propofol on LPS-activated TLR4 may be related to its down-regulation of miR-155 expression. Propofol also inhibits the expression of HIF-1α and GLUT1, which results in a decrease in ATP cytosolic accumulation and lactic acid accumulation. By regulating these signaling pathways and related molecules, propofol may play an anti-inflammatory role by inhibiting the secretion of inflammatory factors.

oxidation. Increasing attention has been given to propofol because of its outstanding anti-inflammatory and anti-oxidation characteristics. Immune cells targeted by propofol include lymphocytes, neutrophils, NK cells, and macrophages (Ji et al., 2011; Ulbrich et al., 2016; Lim et al., 2018).

Macrophages widely express GABA receptors and have a mechanism for GABA catabolism (Bhat et al., 2010). Sanders et al. detected mRNAs encoding GABAA receptor α1, α2, α3, β2 and γ2 subunits in mouse macrophages (Sanders et al., 2013). Several studies have demonstrated the role of GABA receptors in the development of macrophage-associated diseases. Januzi's team found that the expression levels of α2-type GABAA receptors were down-regulated and up-regulated respectively, during the activation of the M1 and M2 alveolar macrophage in mice (Januzi et al., 2018). For myocardial macrophages, GABAA receptors exacerbate myocardial hypertrophy and fibrosis by activating the AKT/mTOR signaling pathway and increasing the MHCII^{low}/MHCII^{high} ratio in Ly6C^{low} macrophage subsets (Bu et al., 2021). GABA transporter (GAT) 2 deficiency promotes the intracellular accumulation of hypoxanthine, which not only blocks the formation of the NLRP3-ASC-caspase-1 complex, but also enhances the expression of oxidative phosphorylation related genes, affecting the production of IL-1β (Xia et al., 2021). In summary, GABA signaling is involved in the regulation of immune responses mainly by affecting macrophage activation and function, which indicated that macrophages, are key cells involved in propofol regulation of the inflammatory response and tumor immunity. Indeed, propofol affects the biological behavior of macrophages by affecting signaling pathways, gene expression, and related mediators (Figure 2). Propofol has long-term effects on inflammatory disease and tumor prognosis by regulating macrophage recruitment, differentiation, polarization, pyroptosis and functions.

4.1 Regulation of macrophage migration and recruitment

Tissue-resident macrophages release a variety of pro-inflammatory mediators to facilitate circulation and macrophage recruitment in monocytes. Monocytes and

macrophages migrate to the site of inflammatory injury to eliminate inflammatory signals and promote wound healing and tissue repair (Shapouri-Moghaddam et al., 2018). Intraoperative hyperoxia leads to the aggregation of macrophages, as represented by an increased expression of IL-8. IL-8 and TNF-α are effective chemokines involved in the regulation of propofol on macrophages (Jia et al., 2017).

The integrity of mitochondrial function is the key to maintaining the chemotaxis, migration and phagocytosis of macrophages. Clinically relevant concentrations of propofol (3 and 30 μm) may inhibit macrophage function by inhibiting mitochondrial membrane potential and adenosine triphosphate (ATP) synthesis rather than exert direct cytotoxicity (Chen et al., 2003). Wu et al. also found that propofol reduced macrophage ATP biosynthesis and migration by inhibiting mitochondrial membrane potential (Wu et al., 2005). Mitochondrial dysfunction may be a key cause of propofol-induced immunosuppression of macrophages. Therefore, the inhibitory effect of propofol on macrophage migration and recruitment may be a new target in the treatment of macrophage-associated inflammatory diseases and tumors.

4.2 Regulation of macrophage differentiation and polarization

Macrophages migrate to the site of local injury and infection, which results in local and systemic acute and chronic inflammation. Phagocytosis, antibacterial activity, and cytotoxicity are enhanced, which contribute to initiating repair and resolving inflammation and tumor cells. Although propofol does not affect the recruitment of blood monocytes into the kidney in *Staphylococcus aureus* infection, it may prevent monocytes from differentiating into macrophages and expanding the inflammatory abscesses in the kidney (Visvabharathy and Freitag, 2017).

Propofol affects epigenetic pathways, such as long noncoding RNAs (lncRNAs), microRNAs (miRNAs), and histone acetylation, and it modulates genetic signaling pathways, including hypoxia, ROS, NF-κB, mitogen-activated protein kinase (MAPK), and Nrf2. Notably, propofol also affects tumor immune function and the degree of immunosuppression (Jawan et al., 2008; Ferrando et al., 2013; Ma et al., 2018; Gao et al., 2021). MiRNAs regulate genes at the transcriptional level and induce gene silencing, which play an important role in many aspects of macrophage biology, including influencing macrophage biology and pathological conditions. Propofol regulates the number and biological activity of macrophages by regulating miRNAs at the transcriptional level. MiR-142-3p exerts antitumor effects by regulating the differentiation of macrophages. However, propofol exerts antitumor activity by regulating the expression of miR-142-3p in macrophage-derived microvesicles (Zhang et al., 2014).

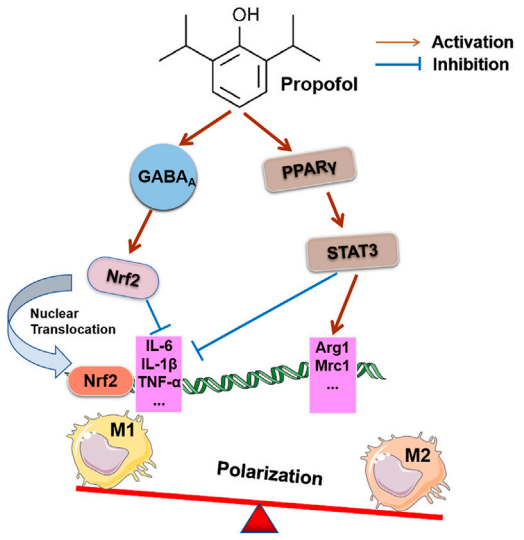

FIGURE 3
Effects of propofol on macrophage polarization. Invasive surgery may cause M1 macrophage polarization and related complications. Propofol inhibits the expression of IL-6 and IL-1β by activating the GABAA receptor to induce Nrf2 accumulation in the cytoplasm and its translocation into the nucleus, which prevents the inflammatory response during the polarization of human macrophages. Propofol treatment stimulated PPARγ activation in the rI/R model and enhanced PPARγ-mediated STAT3, decreased iNO$_S$ mRNA of the M1 target gene, increased Mrc1 and Arg1 mRNA expression of the M2 target gene, and promoted M2 polarization in macrophages.

Current studies show that propofol exposure to human monocytic leukemia THP-1 cells induces Nrf2 cytoplasmic accumulation and nuclear translocation by activating GABAA receptors, which inhibits the inflammatory response during the polarization of M1 macrophages and down-regulates the expression of IL-6 and IL-1β. However, it did not affect the function of M2 macrophages or change the gene expression of M2 markers [e.g., IL-10, transforming growth factor-(TGF-) β, and CD206]. The reason may be that propofol does not alter the anti-inflammatory or tissue repair functions of M2 macrophages (Kochiyama et al., 2019). However, a recent study suggested that propofol improved renal ischemia-reperfusion injury by inducing the expression of the M2 polarization marker via the PPARγ/STAT3 pathway (Liu et al., 2021b). The pathways and effect of propofol on the polarization of macrophages are shown in Figure 3. This result suggests that the degree of macrophage differentiation or the underlying state of the disease influences the effect of propofol on the classification and polarization of macrophages. Under pathological conditions, propofol may modulate the polarization of macrophages in different directions, which is influenced by local inflammatory signaling pathways, cytokines secreted by immune cells and the microenvironment. However, there are few studies on the role

of propofol in the polarization of macrophages, and its effect on the polarization of macrophages and its mechanism must be further studied.

4.3 Regulation of macrophage pyroptosis

Propofol inhibited macrophage phagocytosis, chemotaxis, and oxidative burst in the model of propofol infusion syndrome (PRIS) (Wheeler et al., 2011; Hsing et al., 2012; Sun et al., 2019), but the mechanism of this immune disorder is not clear. Exposure of macrophages to propofol may inhibit phagocytosis and apoptosis. Pyroptosis is a specific form of apoptosis that is involved in immune regulation and is caused by inflammatory bodies. Mitochondrial dysfunction induced specific activation of NLRP3-ASC inflammatory corpuscles, and propofol significantly induced mitochondrial dysfunction. High-dose propofol induced mitochondrial apoptosis and caspase-1-dependent pyroptosis in macrophages. Propofol-induced pyroptosis triggers macrophage death and mediates the release of IL-1β and IL-18 (Sun et al., 2019). However, Liu et al. found that a clinical dose of propofol inhibited the activation of IL-1β and IL-18 in rat alveolar macrophages or lung tissue and inhibited the activation of inflammatory bodies and pyroptosis by up-regulating sirtuin-1 (STRT1) in the lung, which attenuated acute lung injury caused by renal reperfusion injury (Liu et al., 2020). These results suggest that the regulatory effect of propofol on the focal death of macrophages may depend on the administration dose and pathological state of the body. Therefore, elucidating the mechanism of propofol-induced macrophage pyroptosis will further deepen our understanding of propofol-induced immune dysfunction.

4.4 Propofol regulation of macrophage function

Although macrophages effectively control infection, remove necrotic tissue and promote tissue repair and wound healing, they also cause tissue damage and pathological changes during infection and inflammatory disease. Several studies demonstrated that propofol participated in the regulation of macrophage function, regulated the energy metabolism of macrophages during inflammation and infection, altered the activated state of macrophages, and induced phagocytosis. As important immune cells, macrophages are not independent of their functional properties and effects on health or disease but are multidirectional and interconnected with each other. The effect of propofol on the function of macrophages has a significant impact on disease progression. We discuss the effects of propofol on human disease by regulating macrophages for inflammation, infection, and tumor and tissue repair. The potential anti-inflammatory effect of propofol on the disease of different organs or cells by mediating macrophages is summarized in Figure 4.

4.4.1 Inflammation

Mononuclear phagocytes are the host's first line of defense against infection and inflammation and play a vital role in wound repair. The mechanism of propofol on inflammation is not clear. However, propofol also inhibits macrophage function and reduces pro-inflammatory cytokine release under certain conditions (Chen et al., 2005). Propofol alleviates pulmonary inflammation in a respiratory distress model (Haitsma et al., 2009) and reduces endotoxin inflammation by inhibiting the production of ROS and downstream protein kinase B (AKT)/inhibitor of κB kinase (IKK β)/NF-κB signaling (Hsing et al., 2011). It also inhibits the activation of Kupffer cells and regulates the expression of NF-κB and P65 protein to alleviate LPS-induced inflammation and liver cell damage (Sung et al., 2005; Li et al., 2015; Li et al., 2016). Propofol inhibited acute local inflammation in the carrageenan-induced air pouch infection model by reducing the secretion of proinflammatory cytokines (TNF-α and IL-6) and neutrophil chemokines in intra-pouch secretion (Inada and Kamibayashi, 2021). However, propofol does not affect LPS-induced NO and TNF-α in mixed glial cells (Shibakawa et al., 2005), which suggests that the effect of propofol on inflammation may be related to the differentiation and expression pattern of macrophages.

LPS is an ingredient in the outer membrane of Gram-negative bacteria, and the activation of nuclear transcription factor NF-κB and activator protein-1 (AP-1) by TLR-4 on the surface of macrophages induced the release of a large number of inflammatory and cytokines, including IL-6, IL-8, and TNF-α (Jia et al., 2017). The inhibitory effect of propofol at clinically relevant concentrations on LPS-activated TNF-α may be related to the inhibition of NF-κB and TLR-4 expression (Wu et al., 2009). In conclusion, the anti-inflammatory and anti-oxidative effects of propofol are primarily mediated by its regulation of the biosynthesis of cytokines (e.g., TNF-α, TNF-β, IL-1, IL-6, and IL-10).

Propofol also inhibited nicotinamide adenine dinucleotide phosphate (NADPH) oxidase-mediated proinflammatory cytokine production. Long-chain non-coding RNALOC286367 is involved in propofol-induced inhibition of IL-6, TNF-α and IL-1β expression in THP-1 cells (Ma et al., 2018). *In vitro* experiments and many clinical studies observed the positive effect of propofol on the reduction of inflammation. Previous clinical trials demonstrated that the inhaled anesthetic and intravenous anesthetic propofol had a positive effect on proinflammatory cytokine gene expression. A clinical study compared gene expression changes in alveolar macrophages during general anesthesia with propofol and isoflurane. The gene expression of IL-8 and IFN-γ increased after 4 h of propofol anesthesia. IL-8 is an effective chemokine, and high expression of the IL-8 gene and intraoperative hyperoxia

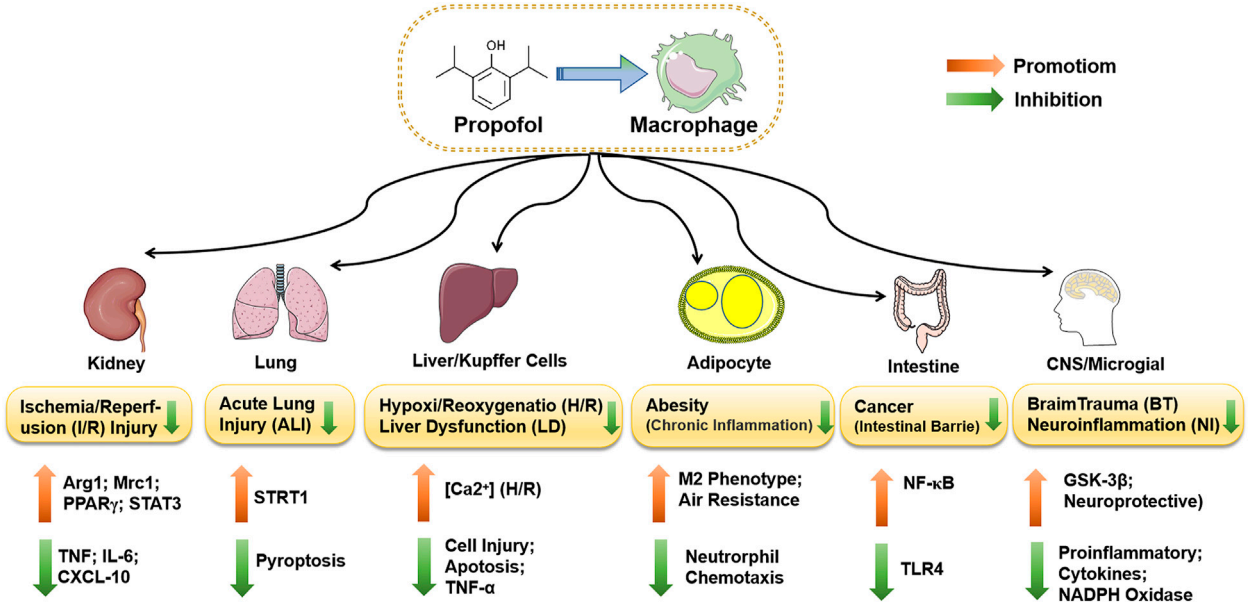

FIGURE 4
The functions of propofol-regulated macrophages in different diseases. Propofol suppresses the expression of STRT1 by inhibiting IL-1β and IL-18 in rat alveolar macrophages or lung tissue, which inhibits cell pyroptosis and attenuates ALI induced by rl/R. Propofol inhibits the activation of caspase-3 and the apoptosis of hepatocytes and alleviates LPS-induced liver dysfunction. During H/R, the inhibitory effect may be induced by the increase in [Ca2$^+$]i in Kupffer cells. Propofol also inhibits the TLR/NF-⊠B pathway via microRNA, reduces the release of inflammatory factors, and protects the intestinal mucosal barrier of colorectal cancer. Propofol partially protects microglia by downregulating TLR4 and inducing inactivation of GSK-3β, which inhibits the release of inflammatory factors and reduces LPS-induced neuroinflammation (NI). Neuroprotection after brain trauma (BT) may result from propofol reducing the expression of two key components of NADPH oxidase, P22phox and gp91phox.

exposure stimulate macrophage aggregation and enhance alveolar macrophage antibacterial and immune responses (Kotani et al., 2000). The anti-inflammatory effect of propofol in THP-1 cells may be mediated by apolipoprotein M (apoM) in a manner dependent on hepatocyte nuclear factor- (HNF-)1α (Ma et al., 2013). Prostaglandins are abundant in areas of trauma and inflammation. Prostaglandins are produced by COX and specific prostaglandin synthetase. Prostaglandin synthesis in macrophages primarily involves prostaglandin E2 (PGE_2) and thromboxane (TX) A_2 (Smith et al., 2000; Inada et al., 2010). PGE_1 reduces alveolar macrophage aggregation during anesthesia, possibly because it inhibits the expression of CD11A, CD18, CD54 and other adhesion molecules (Kotani et al., 2001). Propofol inhibits the production of PGE_2 in human peripheral blood mononuclear cells (Kambara et al., 2009) and peritoneal macrophages (Inada et al., 2010) by inhibiting COX-2 activity and promotes the production of IFN-γ by other immune cells, such as NK cells, to regulate inflammation and immune function.

4.4.2 Infection

Perioperative infections, such as surgical site infections and pneumonia, significantly increase mortality and economic burden. Although some *in vitro* studies showed that propofol decreased the secretion of proinflammatory cytokines and had an active anti-inflammatory effect, it may have a negative effect on the regulation of immune cells in a model of microbial infection. Lavanya. V et al. demonstrated that short-term exposure to propofol also significantly increased host susceptibility to microbial infection (Visvabharathy et al., 2015). Propofol is commonly used to sedate and anesthetize intensive care unit (ICU) patients, and *Staphylococcus aureus* infection is a common complication of nosocomial infection in long-term hospitalization or ICU patients (Pofahl et al., 2011). *Staphylococcus aureus* infection causes skin infection, severe sepsis and other clinical-pathological changes, and macrophages play an important role in the control of these infections. Previous studies showed that propofol inhibited a variety of functions of macrophages, including chemotaxis, phagocytosis, and ROS production. When *Staphylococcus* aureus-infected RAW264.7 cells were exposed to propofol, IL-1β secretion and ROS levels were significantly decreased, which increased bacterial survival, but propofol did not affect the expression of IL-1β mRNA (Chen et al., 2018). This inhibitory effect on the phagocytosis of RAW264.7 cells was also mediated by lipofundin in propofol (Chen et al., 2020). However, previous studies showed that propofol reduced the LPS-induced levels of IL-1β, IL-6, TNF-α mRNA, and

corresponding proteins at the pre-translation level (Chen et al., 2005). Propofol did not reduce the *in vitro* phagocytosis of *E. coli* by macrophages (Zha et al., 2019). This difference may be due to the different regulatory mechanisms of stimulating and proinflammatory cytokines. *In vivo* studies found that propofol anesthesia significantly increased the bacterial burden and renal pathology in mice infected with *Staphylococcus aureus*. This effect may be due to a reduction in the number of mature phagocytes in the kidney and increased dissemination of bacteria in the kidney tissue (Visvabharathy and Freitag, 2017). The effect of propofol on the phagocytic bacterial microbiome of macrophages strongly correlated with the type of infecting pathogen.

Mitochondria are important energy-producing organelles that participate in the activation of macrophages. Therefore, the integrity of mitochondrial function is the key to maintaining the chemotaxis, migration and phagocytosis of macrophages. Clinically relevant concentrations of propofol (3 and 30 μm) may inhibit macrophage function by decreasing mitochondrial membrane and ATP synthesis rather than direct cytotoxicity (Chen et al., 2003). Cellular ATP levels significantly correlated with macrophage function in mice with polymicrobial sepsis (Ayala and Chaudry, 1996; Chen et al., 2003). Propofol also significantly reduced the production of ATP in THP-1 cells by inhibiting LPS-induced Hypoxia inducible factor (HIF)-1 activation and the expression of the pyruvate dehydrogenase (PDH) kinase 1 (PDK-1) glycolytic process (Tanaka et al., 2010). Energy depletion of macrophages also reduces their ability to kill bacteria, which increases the risk of infection.

Studies showed that inflammation or edema increased tissue pressure, and the increase in extracellular pressure activated macrophage phagocytosis. Propofol inhibits the phagocytosis of pressure-stimulated macrophages via the GABAA receptor and p130cas phosphorylation dysregulation (Shiratsuchi et al., 2009). Propofol increases macrophage phagocytosis by inhibiting p130cas phosphorylation and reverses stress-stimulated macrophage phagocytosis mediated by GABAA receptors. Clinical studies are limited, but the incidence of postoperative pneumonia and surgical incision infection is lower with general intravenous anesthesia than volatile anesthetics in abdominal and rectal surgery (Von Dossow et al., 2007; Koo et al., 2016). It is a future target to develop new intravenous anesthetics that do not inhibit immune targets.

4.4.3 Tumor development

Surgery remains one of the most effective methods to treat solid tumors. Perioperative stress and the use of anesthetics may affect the entire process of tumor development. The surgical stress response is characterized by immunosuppression, systemic inflammatory response, and excessive production of reactive oxygen species. Propofol has anti-inflammatory and antioxidative effects, and it participates in inflammatory responses by regulating immune-related cells and the subsequent production of cytokines. It is generally accepted that propofol accelerates apoptosis, promotes autophagy of cancer cells, affects the serum microenvironment, inhibits the proliferation and migration of tumor cells, and improves the malignant potential of tumors (Jaura et al., 2014; Xu et al., 2020). Lymphocytes provide direct cytotoxicity to tumor cells, and monocytes and macrophages combine directly to kill tumors and enhance endogenous immunity via antigen presentation, which makes these cells a new approach to tumor immunotherapy in the future (Anderson et al., 2021). Propofol reduced the production of vascular endothelial growth factor (VEGF) and calmodulin-dependent kinase II (CaMK II) by inhibiting NMDAR, which blocks extracellular signal-regulated kinase (ERK)/protein kinase B (AKT) signaling and ultimately reduces the malignant potential of pancreatic cancer (Chen et al., 2017). Compared to inhalation anesthesia, propofol reduced the viability of serum-cultured cells, inhibited the invasion of cancer cells, and increased cancer cell death (Kirkegaard et al., 2017). However, other studies demonstrated that the use of propofol promoted cancer cell proliferation and invasion, which increased the risk of tumor recurrence and metastasis (Zhang et al., 2012; Liu et al., 2021a). In summary, a large number of laboratory and clinical studies concluded that propofol inhibited the development of cancer in the body, but only a few results suggest that propofol promotes the progression of certain cancers. This difference may depend largely on the type and biological behavior of the tumor cells. The effect of propofol on tumor cells depends greatly on the effect of propofol on various immune cells in the tumor microenvironment (TME), especially macrophages.

Mutations caused by DNA damage are important markers of cancer. *In vitro* experiments showed that propofol at 25 μg/ml caused DNA damage in RAW264.7 cells and inhibited the mRNA expression of repair-related genes, such as DNA-dependent serine/threonine protein kinase (DNA-Pk), breast cancer gene 1 (BRCA1), O^{6-}methylguanine-DNA methyltransferase (MGMT), and P50 (Wu et al., 2013). Another study showed that an overdose of propofol induced GSK-3-mediated apoptosis of lysosomes/mitochondria in macrophages (Hsing et al., 2012). The growth of malignant tumors is related to an increase in M2 cells in the TME (Najafi et al., 2019). M2 cells play a key role in tumor immune escape (Tan et al., 2018). Cytokines released by tumor cells regulate the expression of genes related to M2 angiogenesis and participate in angiogenesis. The metastasis of cancer cells may be due to the interaction with M2 cells in the TME. M2 cells release granular proteins, which act as TNF receptor inhibitors by inhibiting TNF-α binding to its receptors. TNF-α is generally released by M1 cells. As a result, the TME has a high degree of control over inflammation and tumor development. The inhibitory effect of propofol on COX-2 may also affect tumor progression because PGE_2 may promote tumor

progression by inducing bone marrow-derived suppressor cells in the TME (Sinha et al., 2007). Hypoxia significantly enhanced the pre-tumoral function of major histocompatibility complex-(MHC-)II^{low} M2-like TAMs by altering gene expression profiling rather than directly affecting TAM differentiation, which resulted in intra-tumoral heterogeneity of TAMs (Laoui et al., 2014). Under the influence of hypoxia, TAMs easily form an angiogenesis phenotype, which is involved in metabolism, angiogenesis and metastasis. HIF-1α is a key transcription factor regulating hypoxia-inducible gene expression. Hypoxia-directed TAMs promote angiogenesis by directly upregulating angiogenic molecules, such as VEGF-A, and angiogenic regulators, such as MMP7 (Henze and Mazzone, 2016). According to previous reports, propofol may inhibit the translation of HIF-1 protein via mRNA in THP-1 cells and its antioxidant activity, inhibit the accumulation of HIF-1α protein in LPS-induced macrophages (Tanaka et al., 2010). The role of macrophages and their polarization in propofol-induced tumor development has not been well studied, but the mechanism remains to be studied.

Propofol effectively inhibits the growth of hepatocellular carcinoma *in vivo* and stimulates the migration of miR-142-3p from macrophages to hepatocellular carcinoma (HCC) cells *in vitro* by down-regulating Ras-related C3 botulinum toxin substrate 1 (RAC1) and inhibiting the migration and proliferation of HCC cells (Zhang et al., 2014). Propofol also inhibits the activation of the TLR/NF-κB pathway by inhibiting the expression of miR-155, which reduces the release of inflammatory cytokines, protects the intestinal mucosal barrier and effectively inhibits bacterial translocation (Gao et al., 2021).

4.4.4 Tissue repair

Notably, many clinical and preclinical studies showed that propofol reduced ischemic damage to vital organs, such as the heart (Nederlof et al., 2017), brain (Sousa et al., 2021), kidney (Liu et al., 2021b), and lung (Sousa et al., 2021). Propofol reduced CD45^{+} and increased vascular cell adhesion molecule (VCAM)-1 in the ischemic stroke model, but it did not protect the brain or lung in experimental acute ischemic stroke. Propofol showed no reduction in IL-6 and IL-1β levels in alveolar macrophages and endothelial cells in this model (Sousa et al., 2021). During organ reperfusion, activation of the endothelium promotes the adhesion and infiltration of immune cells, such as lymphocytes, macrophages, dendritic cells, and neutrophils. The protective effect of propofol on reperfusion organs and tissue repair may be mediated by inhibiting the release of inflammatory mediators, such as TNF-α, IL-6 and IL-1β. Activated macrophages, neutrophils and lymphocytes release pro-inflammatory mediators that trigger inflammation and lead to dysfunction and tissue damage (Kezić et al., 2017). Peroxisome proliferator-activated receptor (PPAR)-γ is a member of the nuclear receptor PPAR subfamily and is widely expressed in many tissues (Singh et al., 2019). PPARγ also plays an important role in organ ischemia–reperfusion injury.

Propofol induced the infiltration of macrophages from the pro-inflammatory M1 phenotype to the anti-inflammatory M2 phenotype in a rat model of renal ischemia-reperfusion injury (rl/R). The M1 to M2 phenotypes of macrophages were reduced after reperfusion (Liu et al., 2021b), which accelerated the healing of ischemic tissue and promoted the formation of new blood vessels. Propofol may also reduce rl/R-induced acute lung injury (ALI) via the up-regulation of sirtuin (STRT)-1 in the lung, and rl/R stimulation may activate focal proteins caspase-1, nucleotide oligomerization domain (NOD)-like receptor pyrin domain-containing 3 (NLRP3), apoptosis-associated speck-like protein containing a CARD (ASC), IL-1β and IL-18 in the lung, but the expression of STRT1 mRNA and protein were decreased (Liu et al., 2020). STRT1 is an alveolar macrophage inhibitor, and NLRP3 recognizes elevated levels of inflammatory proteins in inflammatory bodies. It is an important stimulus for rl/R to induce ALI (Liu et al., 2018). The protective effect of propofol on organ ischemia-reperfusion and tissue repair may be based on its inhibition of macrophage-involved inflammatory responses and regulation of mitochondrial function.

Propofol attenuates the activation of Kupffer cells during hypoxia-reoxygenation and decreases the expression of TNF-α mRNA by inhibiting [Ca^{2+}]i, which attenuates the injury (Sung et al., 2005). The production of TNF-α in Kupffer cells also decreased the activity of caspase-3 and the apoptosis of hepatocytes to alleviate LPS-induced tissue injury and liver dysfunction (Li et al., 2016). Microglia are the resident macrophages of the CNS, and propofol may affect microglia phagocytosis of cell debris. Milk fat globule epidermal growth factor 8 (MFG-E8) is an important regulator of microglial phagocytosis. Cai et al. found that propofol inhibited microglial phagocytosis via the AMP-activated protein kinase (AMPK) and Src signaling pathways regulated by MFG-E8 (Cai et al., 2021b). The activation and proliferation of microglia are typical inflammatory responses to traumatic brain injury (TBI). Several studies suggested that propofol had neuroprotective effects on TBI, which may be due to its inhibitory effect on microglial NADPH oxidase and reduced inflammatory response because of the increased intracranial pressure (Yu et al., 2011; Luo et al., 2013). These findings support a role for propofol in improving brain damage and promoting cognitive recovery after injury by reducing microglial activation and associated neurotoxicity.

4.4.5 Other diseases

Obesity is a metabolic disorder associated with chronic inflammation throughout the body, and adipose tissue is rich in immune cells, including macrophages. An increase in adipose tissue induces chemokine and proinflammatory cytokine (TNF-α, IL-6, Il-12) secretion by monocytes and increases the production and activation of ROS. The resident macrophages in adipose tissue are more likely to differentiate into the pro-inflammatory M1 phenotype (Yu et al., 2011). Propofol may have different

TABLE 1 Regulation of propofol on macrophage activation and function.

Macrophage cell types	Propofol dose and time period	Model/Stimuli	Function in macrophages	Related genes	Reference
Murine RAW264.7	50 μM, 16/24 h, *in vitro*	None	↓chemotactic ↓migration ↑immunosuppression	↓mitochondrial membrane potential; ATP	Wu et al. (2005)
	30 μM, 1/6/4 h, *in vitro*	None	↓migration ↓oxidant production ↓phagocytosis	↓mitochondrial membrane potential; ATP; INF-γ; ROS	Chen et al. (2003)
	25/50 μmol, 16 h, *in vitro*	LPS	↓inflammation	↓HMGB1; IL-6; IL-8; TNF-α	Jia et al. (2017)
	25/50 mmol/ml, 2 h, *in vitro*	LPS	↓inflammation	↓HMGB1; NF-κB	Wang et al. (2015)
	50 μM, 24 h, *in vitro*	LPS	↓inflammation ↓oxidative	↓NO/iNOS; TNF-α; IL-1β; IL-6	Chen et al. (2005)
	<50 μM, 6/12/18/24 h, *in vitro*	LPS	↓inflammation ↓oxidative	↓NF-κB; TLR4; TNF-α	Wu et al. (2009)
	6 μg/ml, 5 h, *in vitro*	*s. aureus*	↓phagocytosis	↓IL -1β; ROS	Chen et al. (2020)
	1/5 μg, 24 h, *in vitro*; 20/50 mg/kg, q.h. 3 w, *in vivo*	HCC Model	↑antitumor ↓HCC cell invasion	↑miR-142-3p ↓RAC1	Zhang et al. (2014)
	25–200 μg/ml, 24/48/72 h, *in vitro*	None	↑DNA damage	↓DNA-PK; MGMT; BRCA1; p53; MDC1	Wu et al. (2013)
	10 mg/kg, 4 h, *in vivo*	CRC mice	↑intestinal barrier	↓miR-155 NLRP3; TLR4; NF-κB; MPO; TNF; IL-6; IL-1β ↑IL-10	Gao et al. (2021)
	10 μg/ml, 0.5 h, *in vitro*	LPS	↓inflammation ↓oxidative	↓ROS; AKT/IKKβ/NF-κB; TLR4; NO/iNO_S; TNF-α; IL-6; IL-10	Hsing et al. (2011)
	25 μg/ml, 24 h, *in vitro*; 10 mg/kg/h, 6 h, *in vivo*	overdose propofol	↑apoptosis	↑GSK-3β ↓Akt; Mcl	Hsing et al. (2012)
Peritoneal macrophages (PMs)	100 μM, 30 h, *in vitro*; 10 mg/kg + 5 mg/kg/h, 23 h, *in vivo*	rl/R	↑M2 polarization ↓M1 polarization ↓renal I/R injury	↑PPAR-γ; STAT3; IL-10; Arg1mRNA; mrc1mRNA ↓iNO_S; TNF-α; IL-6; CXCL-10	Liu et al. (2021b)
	50 μM, 18 h, *in vitro*; 18.75 mg/kg, *in vivo*	*listeria* monocytogenes (LM) or LPS	↓recruitment ↓activity ↑tissue damage ↑host susceptibility	↑IL-1β; IL-6; TNF-α; CCL2; CXCL1; IL-10	Visvabharathy et al. (2015)
	7.5/15/30 μM, 24 h	LPS	↑immune modulation ↓immunosuppression ↑anti-tumor immunity	↓COX activity; PGE2; IL-12 ↑TNF-α	Inada et al. (2010)
	5 mg/kg, 0.5 h, *in vivo*	LPS	↓inflammation ↓oxidant	↓Akt; NF-κB ↓NO/iNO_S	Hsing et al. (2011)
Human THP-1-cell	1–5 μM, 18 h, *in vitro*	None	↓M1 polarization	↑GABAA; nuclear translocation of Nrf2 ↓IL-6; IL-1β	Kochiyama et al. (2019)
	2.5–20 μg/ml, 30 min, *in vitro*	20 mmHg pressure	↓phagocytosis	↑GABAA; P130cas	Shiratsuchi et al. (2009)
	50 μM, 24 h, *in vitro*	LPS	↓inflammation	↓RNALOC286267; IL-6; TNF-α; IF-γ ↑ABCA1	Ma et al. (2018)
	50 μM, 24 h, *in vitro*	LPS	↓inflammation	↑APOM; HIF-1α ↓TNF-α; IL-1β; IL-6; iNO_S	Ma et al. (2013)
	50/100 μM, 4 h, *in vitro*	LPS	↓glucose metabolism	↓HIF-1α; ATP; LDHA; PDK-1; GLUT1 ↓VEGF; ENO-1	Tanaka et al. (2010)

(Continued on following page)

TABLE 1 (*Continued*) Regulation of propofol on macrophage activation and function.

Macrophage cell types	Propofol dose and time period	Model/Stimuli	Function in macrophages	Related genes	Reference
Rat alveolar macrophages	50/100 μM, 24 h, *in vitro*	rl/R	↓pyroptosis ↓acute lung injury	↓NLRPS; IL-1β; IL-18 ↑STRT1	Liu et al. (2020)
Mice bone marrow-derived macrophages (BMDMs)	50 μM, 18 h, *in vitro*; 18.75 mg/kg, *in vivo*	*listeria* monocytogenes (LM) or LPS	↓recruitment ↓activity ↑tissue damage ↑host susceptibility	↑IL-1β; IL-6; TNF-α; CCL2; CXCL1; IL-10	Visvabharathy et al. (2015)
	25/50 μM, 24 h, *in vitro*	LPS	↓inflammation ↓oxidative	↓ROS; NADPH; GLUT1	Zeng et al. (2021)
	300/600 μM, 30 min/3/6 h, *in vitro*	None	↑pyroptosis	↑NLRP 3-ASC; caspase-1; ROS ↑IL-1β; IL-18	Sun et al. (2019)
Human alveolar macrophages	1.5–2 mg/kg, *in vivo*	100% O_2 、30% O_2	↑phagocytosis ↑microbicidal	↑IL-1β; IL-8; IFN-γ; TNF-α	Kotani et al. (2000)
Human peripheral blood mononuclear cells (PBMCs)	0–60 μM, 18 h, *in vitro*	LPS	↓immunosuppression	↓COX-2 activity ↓PGE2; iNO/NOS; TNF-α; IL-10; TXB2	Kambara et al. (2009)
Rat Kupffer cell	0.5/5 μg/mg, 5 h, *in vitro*	hypoxia-reoxygenation	↑Kupffer cell activation ↓cell injury	↓[Ca^{2+}]i; TNF-α	Sung et al. (2005)
BV-2 microglia cells	30 μM, 4 h, *in vitro*	LPS	↓neuroinflammation	↓TLR4; GSK-3β; IL-1β; TNF-α; IL-10	Gui et al. (2012)
	12.5/25/50/100 μM, 4 h, *in vitro*	None	↓phagocytosis	↓MFG-E8; AMPK; Src	Cai et al. (2021b)
	25 μg/ml, 24 h, *in vitro*; 10 mg/kg/h, 6 h, *in vivo*	overdose propofol	↑apoptosis	↑GSK-3β ↓Akt; Mcl	Hsing et al. (2012)
	12.5–200 μM, 24 h, *in vitro*	TBI, LPS	↑neuroprotective ↓microglia activation	↓iNO_S; NO; TNF-α; IL-1β; ROS; NADPH oxidase; Iba-1	Luo et al. (2013)
Human microglia	2.5–2 mg/ml, 2/24 h, *in vitro*	15/30 mmHg pressure	↓phagocytosis ↓proliferation	↓TNF-α; IL-1β; NO	Yu et al. (2011)

immune effects in obese patients than normal-weight patients. A clinical trial that compared general anesthesia with sevoflurane and propofol in the regulation of immune function in patients undergoing laparoscopic weight loss surgery found that propofol differentiated macrophages from adipose tissue to the M2 phenotype (de Sousa et al., 2019). An animal model demonstrated that propofol and lipid excipients had different immunomodulatory effects in obesity, and the active components in propofol increased the expression of IL-10 and M2 phenotypes in macrophages from adipose tissue. Propofol and its active components increased IL-6 expression in obese animals (Heil et al., 2021). With the increase in the obese population, understanding the immune regulation of propofol on macrophages in obese patients will be helpful for proposing an anesthesia management program.

Increased expression of glucose transporter 1 (GLUT1) on the surface of macrophages in adipose tissue suggests that GLUT1 is associated with inflammation *in vivo*. Propofol also regulated the metabolism of macrophages, which regulates the metabolism of activated macrophages by inhibiting the overexpression of ROS and decreasing the expression of GLUT1 (Heil et al., 2021). Arteriosclerosis is a type of inflammatory vascular disease, and the regulation of propofol has a positive effect on arteriosclerosis formation. The expression of connexin 43 (Cx43) in arterial endothelial cells or monocytes induces monocytes to migrate and adhere to the arterial intima then transform into macrophage foam cells, which is a pathological marker for arteriosclerosis. Propofol up-regulates the expression of Cx43 in mononuclear cells and inhibits activation of the PI3K/AKT/NF-κB signaling pathway, which affects cell adhesion and arteriosclerosis formation (Ji et al., 2019).

5 Conclusion and outlook

Propofol is widely used in clinical anesthesia. In addition to its sedative and hypnotic effects as an intravenous anesthetic, its characteristics in inflammation, infection, tumor, and tissue

injury have attracted much attention in recent years. Macrophages are important immune cells that are involved in inflammation, infection, arteriosclerosis, organ damage and many other diseases. The effect of macrophage activation and polarization on the development of tumors and inflammatory diseases has become a research hotspot. Although some studies demonstrated the effects of propofol on various biological behaviors of macrophages, the mechanisms of propofol regulation of macrophage function are not fully understood. This review focused on the effects and mechanisms of perioperative anesthetics, especially propofol, on the activity and function of macrophages and explored the role of propofol-regulated macrophages in disease progression.

As shown in Table 1 and Figure 2, propofol regulates the role of macrophages in inflammation, infection, tumor, and organ reperfusion injury in cellular and molecular levels. Propofol affects the differentiation and polarization of macrophages in the microenvironment, which leads to different disease outcomes. Propofol inhibits the production of proinflammatory cytokines, which may help to alleviate inflammatory disease and reduce tissue damage. Moreover, it also affects the metabolic activity of macrophages and changes the functional characteristics of macrophages under the original stimulation to make the disease develop to the advantage or disadvantage of the body. The mechanism regulating macrophage function of propofol involves many molecules such as receptors, signaling pathways, epigenetics, and transcription factors. For example, GABAA receptor and TLR4 on the surface of macrophages are the directly or indirectly targets of propofol. Activation of the GABAA receptor pathway, on the one hand, induces the accumulation and nuclear translocation of Nrf2 in the cytoplasm, thereby inhibiting the M1 polarization of macrophages, and ultimately inhibits the secretion of pro-inflammatory cytokines; on the other hand, it inhibits p130cas phosphorylation and further Inhibits phagocytosis of macrophages in response to stress. On the contrary, the expression level of TLR4 is inhibited by propofol, which in turn affects the activation of its downstream NF-κB inflammatory signaling pathway to regulate the immune response. The other involved inflammation-related signaling include MAPK, Foxa2, HNF-α, and AKT. Furthermore, the scorch death pathway NLRP3/ASC/Caspase1 pathway is critical for propofol-induced macrophage pyroptosis. At the epigenetic and transcription factor levels, the expression of some noncoding RNA is regulated by propofol, such as lncRNA LOC286367 and miR-155. However, the mechanism of propofol regulation of transcription and translation and the induction of apoptosis of macrophage-related cytokines at the gene level are not clear and needs further study. Of course, with the deepening of research, the mechanism by which propofol regulates the activation and function of macrophages will become more and more clear, along with the discovery of more regulatory molecules or pathways. In particular, the role of GABA receptors in propofol-regulated macrophages and downstream signaling pathways need to be further investigated. After all, GABA receptor activation has been implicated not only in macrophage phagocytosis, polarization and secretion of inflammatory cytokines, but also in macrophage recruitment, antimicrobial responses and autophagy activation, which is mediated by Ca^{2+}, AKT/mTOR, or autophagy-related genes (ATGs) (Kim et al., 2018; Jiang et al., 2019; Bu et al., 2021).

However, propofol-mediated inflammatory diseases and tumors are mostly based on cellular or animal models, but few clinical studies have been conducted in patients. In addition, there are also few studies on the role of propofol in macrophage-associated tumor immunity. One new direction of tumor-targeted immunity is the seeking of new targets using macrophages to phagocytize tumor cells. Understanding the mechanism of macrophage differentiation, proliferation, polarization, apoptosis and phagocytosis is helpful to guide the use of perioperative anesthetics, improve the prognosis and improve the quality of life of patients. Surgical stress-induced immunosuppression is a well-recognized view. Whether the use of propofol inhibits the migration and proliferation of tumor cells by affecting the M1/M2 polarization of macrophages and inhibiting the drug resistance of chemotherapeutic agents to improve the long-term prognosis of tumors requires clarification in the future. To provide a theoretical basis for the development of tumor immunotherapy and related targeted drugs, it is necessary to deepen our understanding of propofol tumor-associated macrophages. The establishment of clinical trials or clinical retrospective investigations will help clarify the accuracy of the study. When propofol is used for general anesthesia and ICU sedation, the effect of propofol on immune cells and oxidative reactions should be considered.

Therefore, more research is needed to elucidate the potential effects of propofol on tumor and inflammation-related disease outcomes by modulating macrophage differentiation and polarization. More clinical studies are needed to confirm the association between perioperative propofol-regulated macrophages and patient morbidity and develop anesthetics with less suppression of immune cell function.

Author contributions

ZZ and SW designed the review and contributed to manuscript preparation. SY and ZZ wrote the manuscript. XT, YW, and QC provided technical and administrative support. SY and ZZ prepared the figures. ZZ and SW revised the manuscript. All authors read and approved the final manuscript.

Funding

This study was supported by the Natural Science Foundation of Shandong Province of China (ZR2020MH250), and the

Medical Health Science and Technology Development Plan of Shandong Province (202004111322).

Conflict of interest

The authors declare that the research was conducted in the absence of any commercial or financial relationships that could be construed as a potential conflict of interest.

Publisher's note

All claims expressed in this article are solely those of the authors and do not necessarily represent those of their affiliated organizations, or those of the publisher, the editors and the reviewers. Any product that may be evaluated in this article, or claim that may be made by its manufacturer, is not guaranteed or endorsed by the publisher.

References

Anderson, N. R., Minutolo, N. G., Gill, S., and Klichinsky, M. (2021). Macrophage-based approaches for cancer immunotherapy. *Cancer Res.* 81 (5), 1201–1208. doi:10.1158/0008-5472.CAN-20-2990

Auffray, C., Fogg, D., Garfa, M., Elain, G., Join-Lambert, O., Kayal, S., et al. (2007). Monitoring of blood vessels and tissues by a population of monocytes with patrolling behavior. *Science* 317 (5838), 666–670. doi:10.1126/science.1142883

Ayala, A., and Chaudry, I. H. (1996). Immune dysfunction in murine polymicrobial sepsis: Mediators, macrophages, lymphocytes and apoptosis. *Shock* 6 (1), S27–S38. doi:10.1097/00024382-199606001-00007

Bhat, R., Axtell, R., Mitra, A., Miranda, M., Lock, C., Tsien, R. W., et al. (2010). Inhibitory role for GABA in autoimmune inflammation. *Proc. Natl. Acad. Sci. U. S. A.* 107 (6), 2580–2585. doi:10.1073/pnas.0915139107

Bu, J., Huang, S., Wang, J., Xia, T., Liu, H., You, Y., et al. (2021). The GABAA receptor influences pressure overload-induced heart failure by modulating macrophages in mice. *Front. Immunol.* 12, 670153. doi:10.3389/fimmu.2021.670153

Cai, M., Sun, S., Wang, J., Dong, B., Yang, Q., Tian, L., et al. (2021a). Sevoflurane preconditioning protects experimental ischemic stroke by enhancing anti-inflammatory microglia/macrophages phenotype polarization through GSK-3β/Nrf2 pathway. *CNS Neurosci. Ther.* 27 (11), 1348–1365. doi:10.1111/cns.13715

Cai, X., Li, Y., Zheng, X., Hu, R., Li, Y., Xiao, L., et al. (2021b). Propofol suppresses microglial phagocytosis through the downregulation of MFG-E8. *J. Neuroinflammation* 18 (1). doi:10.1186/s12974-020-02061-3

Carlin, L. M., Stamatiades, E. G., Auffray, C., Hanna, R. N., Glover, L., Vizcay-Barrena, G., et al. (2013). Nr4a1-dependent Ly6C(low) monocytes monitor endothelial cells and orchestrate their disposal. *Cell* 153 (2), 362–375. doi:10.1016/j.cell.2013.03.010

Cata, J. P., Sood, A. K., and Eltzschig, H. K. (2020). Anesthetic drugs and cancer progression. *Anesthesiology* 133 (4), 698–699. doi:10.1097/ALN.0000000000003510

Chang, Y., Huang, X., Liu, Z., Han, G., Huang, L., Xiong, Y. C., et al. (2013). Dexmedetomidine inhibits the secretion of high mobility group box 1 from lipopolysaccharide-activated macrophages *in vitro*. *J. Surg. Res.* 181 (2), 308–314. doi:10.1016/j.jss.2012.07.017

Chen, M. S., Lin, W. C., Yeh, H. T., Hu, C. L., and Sheu, S. M. (2018). Propofol specifically suppresses IL-1β secretion but increases bacterial survival in Staphylococcus aureus-infected RAW264.7 cells. *Mol. Cell. Biochem.* 449 (1-2), 117–125. doi:10.1007/s11010-018-3348-2

Chen, M. S., Lu, P. K., Lin, W. C., Shin, H. C., Sie, S. R., and Sheu, S. M. (2020). Lipofundin mediates the major inhibition of intravenous propofol in IL-1β secretion and phagocytosis of Staphylococcus aureus-infected macrophages. *Lipids* 55 (1), 45–52. doi:10.1002/lipd.12207

Chen, R. M., Chen, T. G., Chen, T. L., Lin, L. L., Chang, C. C., Chang, H. C., et al. (2005). Anti-inflammatory and antioxidative effects of propofol on lipopolysaccharide-activated macrophages. *Ann. N. Y. Acad. Sci.* 1042, 262–271. doi:10.1196/annals.1338.030

Chen, R. M., Wu, C. H., Chang, H. C., Wu, G. J., Lin, Y. L., Sheu, J. R., et al. (2003). Propofol suppresses macrophage functions and modulates mitochondrial membrane potential and cellular adenosine triphosphate synthesis. *Anesthesiology* 98 (5), 1178–1185. doi:10.1097/00000542-200305000-00021

Chen, X., Wu, Q., You, L., Chen, S., Zhu, M., and Miao, C. (2017). Propofol attenuates pancreatic cancer malignant potential via inhibition of NMDA receptor. *Eur. J. Pharmacol.* 795, 150–159. doi:10.1016/j.ejphar.2016.12.017

Davies, L. C., Jenkins, S. J., Allen, J. E., and Taylor, P. R. (2013). Tissue-resident macrophages. *Nat. Immunol.* 14 (10), 986–995. doi:10.1038/ni.2705

de Sousa, G. C., Cruz, F. F., Heil, L. B., Sobrinho, C. J. S., Saddy, F., Knibel, F. P., et al. (2019). Intraoperative immunomodulatory effects of sevoflurane versus total intravenous anesthesia with propofol in bariatric surgery (the OBESITA trial): Study protocol for a randomized controlled pilot trial. *Trials* 20 (1), 300. doi:10.1186/s13063-019-3399-z

Eleveld, D. J., Colin, P., Absalom, A. R., and Struys, M. (2018). Pharmacokinetic-pharmacodynamic model for propofol for broad application in anaesthesia and sedation. *Br. J. Anaesth.* 120 (5), 942–959. doi:10.1016/j.bja.2018.01.018

Ferrando, C., Aguilar, G., Piqueras, L., Soro, M., Moreno, J., and Belda, F. J. (2013). Sevoflurane, but not propofol, reduces the lung inflammatory response and improves oxygenation in an acute respiratory distress syndrome model: A randomised laboratory study. *Eur. J. Anaesthesiol.* 30 (8), 455–463. doi:10.1097/EJA.0b013e32835f0aa5

Franchi, S., Moretti, S., Castelli, M., Lattuada, D., Scavullo, C., Panerai, A. E., et al. (2012). Mu opioid receptor activation modulates Toll like receptor 4 in murine macrophages. *Brain Behav. Immun.* 26 (3), 480–488. doi:10.1016/j.bbi.2011.12.010

Fu, J. B., Wang, Z. H., and Ren, Y. Y. (2020). Forkhead box O1-p21 mediates macrophage polarization in postoperative cognitive dysfunction induced by sevoflurane. *Curr. Neurovasc. Res.* 17 (1), 79–85. doi:10.2174/1567202617666200128142728

Gao, X., Mi, Y., Guo, N., Luan, J., Xu, H., Hu, Z., et al. (2020). The mechanism of propofol in cancer development: An updated review. *Asia. Pac. J. Clin. Oncol.* 16 (2), e3–e11. doi:10.1111/ajco.13301

Gao, Y., Han, T., Han, C., Sun, H., Yang, X., Zhang, D., et al. (2021). Propofol regulates the TLR4/NF-κB pathway through miRNA-155 to protect colorectal cancer intestinal barrier. *Inflammation* 44 (5), 2078–2090. doi:10.1007/s10753-021-01485-0

Gerber, T. J., Fehr, V. C. O., Oliveira, S. D. S., Hu, G., Dull, R., Bonini, M. G., et al. (2019). Sevoflurane promotes bactericidal properties of macrophages through enhanced inducible nitric oxide synthase expression in male mice. *Anesthesiology* 131 (6), 1301–1315. doi:10.1097/aln.0000000000002992

Gordon, S., and Martinez, F. O. (2010). Alternative activation of macrophages: Mechanism and functions. *Immunity* 32 (5), 593–604. doi:10.1016/j.immuni.2010.05.007

Gui, B., Su, M., Chen, J., Jin, L., Wan, R., and Qian, Y. (2012). Neuroprotective effects of pretreatment with propofol in LPS-induced BV-2 microglia cells: Role of TLR4 and GSK-3beta. *Inflammation* 35 (5), 1632–1640. doi:10.1007/s10753-012-9478-x

Haitsma, J. J., Lachmann, B., and Papadakos, P. J. (2009). Additives in intravenous anesthesia modulate pulmonary inflammation in a model of LPS-induced respiratory distress. *Acta Anaesthesiol. Scand.* 53 (2), 176–182. doi:10.1111/j.1399-6576.2008.01844.x

Heil, L. B. B., Cruz, F. F., Antunes, M. A., Braga, C. L., Agra, L. C., Bose Leao, R. M., et al. (2021). Effects of propofol and its formulation components on macrophages and neutrophils in obese and lean animals. *Pharmacol. Res. Perspect.* 9 (5), e00873. doi:10.1002/prp2.873

Henze, A. T., and Mazzone, M. (2016). The impact of hypoxia on tumor-associated macrophages. *J. Clin. Invest.* 126 (10), 3672–3679. doi:10.1172/jci84427

Hsing, C. H., Chen, Y. H., Chen, C. L., Huang, W. C., Lin, M. C., Tseng, P. C., et al. (2012). Anesthetic propofol causes glycogen synthase kinase-3β-regulated

lysosomal/mitochondrial apoptosis in macrophages. *Anesthesiology* 116 (4), 868–881. doi:10.1097/ALN.0b013e31824af68a

Hsing, C. H., Lin, M. C., Choi, P. C., Huang, W. C., Kai, J. I., Tsai, C. C., et al. (2011). Anesthetic propofol reduces endotoxic inflammation by inhibiting reactive oxygen species-regulated Akt/IKKβ/NF-κB signaling. *PLoS One* 6 (3), e17598. doi:10.1371/journal.pone.0017598

Inada, T., and Kamibayashi, T. (2021). Protective effect of the intravenous anesthetic propofol against a local inflammation in the mouse carrageenan-induced air pouch model. *Immunopharmacol. Immunotoxicol.* 43 (1), 100–104. doi:10.1080/08923973.2020.1869256

Inada, T., Kubo, K., and Shingu, K. (2010). Promotion of interferon-gamma production by natural killer cells via suppression of murine peritoneal macrophage prostaglandin E_2 production using intravenous anesthetic propofol. *Int. Immunopharmacol.* 10 (10), 1200–1208. doi:10.1016/j.intimp.2010.06.027

Ingersoll, M. A., Spanbroek, R., Lottaz, C., Gautier, E. L., Frankenberger, M., Hoffmann, R., et al. (2010). Comparison of gene expression profiles between human and mouse monocyte subsets. *Blood* 115 (3), e10–19. doi:10.1182/blood-2009-07-235028

Januzi, L., Poirier, J. W., Maksoud, M. J. E., Xiang, Y. Y., Veldhuizen, R. A. W., Gill, S. E., et al. (2018). Autocrine GABA signaling distinctively regulates phenotypic activation of mouse pulmonary macrophages. *Cell. Immunol.* 332, 7–23. doi:10.1016/j.cellimm.2018.07.001

Jaura, A. I., Flood, G., Gallagher, H. C., and Buggy, D. J. (2014). Differential effects of serum from patients administered distinct anaesthetic techniques on apoptosis in breast cancer cells *in vitro*: A pilot study. *Br. J. Anaesth.* 113 (1), i63–67. doi:10.1093/bja/aet581

Jawan, B., Kao, Y. H., Goto, S., Pan, M. C., Lin, Y. C., Hsu, L. W., et al. (2008). Propofol pretreatment attenuates LPS-induced granulocyte-macrophage colony-stimulating factor production in cultured hepatocytes by suppressing MAPK/ERK activity and NF-kappaB translocation. *Toxicol. Appl. Pharmacol.* 229 (3), 362–373. doi:10.1016/j.taap.2008.01.044

Jeon, H. O., Choi, I. S., Yoon, J. Y., Kim, E. J., Yoon, J. U., Cho, A. R., et al. (2018). Effect of remifentanil on pre-osteoclast cell differentiation *in vitro*. *J. Dent. Anesth. Pain Med.* 18 (1), 9–17. doi:10.17245/jdapm.2018.18.1.9

Ji, F. H., Wang, Y. L., and Yang, J. P. (2011). Effects of propofol anesthesia and sevoflurane anesthesia on the differentiation of human T-helper cells during surgery. *Chin. Med. J.* 124 (4), 525–529.

Ji, H., Qiu, R., Gao, X., Zhang, R., Li, X., Hei, Z., et al. (2019). Propofol attenuates monocyte-endothelial adhesion via modulating connexin43 expression in monocytes. *Life Sci.* 232, 116624. doi:10.1016/j.lfs.2019.116624

Jia, J., Sun, Y., Hu, Z., Li, Y., and Ruan, X. (2017). Propofol inhibits the release of interleukin-6, 8 and tumor necrosis factor-alpha correlating with high-mobility group box 1 expression in lipopolysaccharides-stimulated RAW 264.7 cells. *BMC Anesthesiol.* 17 (1), 148. doi:10.1186/s12871-017-0441-0

Jiang, S. H., Zhu, L. L., Zhang, M., Li, R. K., Yang, Q., Yan, J. Y., et al. (2019). GABRP regulates chemokine signalling, macrophage recruitment and tumour progression in pancreatic cancer through tuning KCNN4-mediated Ca(2+) signalling in a GABA-independent manner. *Gut* 68 (11), 1994–2006. doi:10.1136/gutjnl-2018-317479

Jin, Y., Li, H., Xie, G., Chen, S., Wu, S., and Fang, X. (2013). Sevoflurane combined with ATP activates caspase-1 and triggers caspase-1-dependent pyroptosis in murine J774 macrophages. *Inflammation* 36 (2), 330–336. doi:10.1007/s10753-012-9550-6

Kambara, T., Inada, T., Kubo, K., and Shingu, K. (2009). Propofol suppresses prostaglandin E2Production in human peripheral monocytes. *Immunopharmacol. Immunotoxicol.* 31 (1), 117–126. doi:10.1080/08923970802452046

Kezić, A., Stajic, N., and Thaiss, F. (2017). Innate immune response in kidney ischemia/reperfusion injury: Potential target for therapy. *J. Immunol. Res.* 2017, 6305439. doi:10.1155/2017/6305439

Kim, R. (2018). Effects of surgery and anesthetic choice on immunosuppression and cancer recurrence. *J. Transl. Med.* 16 (1), 8. doi:10.1186/s12967-018-1389-7

Kim, J. K., Kim, Y. S., Lee, H. M., Jin, H. S., Neupane, C., Kim, S., et al. (2018). GABAergic signaling linked to autophagy enhances host protection against intracellular bacterial infections. *Nat. Commun.* 9 (1), 4184. doi:10.1038/s41467-018-06487-5

Kirkegaard, T., Gögenur, M., and Gögenur, I. (2017). Assessment of perioperative stress in colorectal cancer by use of *in vitro* cell models: A systematic review. *PeerJ* 5, e4033. doi:10.7717/peerj.4033

Kochiyama, T., Li, X., Nakayama, H., Kage, M., Yamane, Y., Takamori, K., et al. (2019). Effect of propofol on the production of inflammatory cytokines by human polarized macrophages. *Mediat. Inflamm.* 2019, 1919538. doi:10.1155/2019/1919538

Koo, B. W., Sim, J. B., Shin, H. J., Kim, D. W., Kang, S. B., Do, S. H., et al. (2016). Surgical site infection after colorectal surgery according to the main anesthetic agent: A retrospective comparison between volatile anesthetics and propofol. *Korean J. Anesthesiol.* 69 (4), 332–340. doi:10.4097/kjae.2016.69.4.332

Kotani, N., Hashimoto, H., Kushikata, T., Yoshida, H., Muraoka, M., Takahashi, S., et al. (2001). Intraoperative prostaglandin E1 improves antimicrobial and inflammatory responses in alveolar immune cells. *Crit. Care Med.* 29 (10), 1943–1949. doi:10.1097/00003246-200110000-00016

Kotani, N., Hashimoto, H., Sessler, D. I., Muraoka, M., Hashiba, E., Kubota, T., et al. (2000). Supplemental intraoperative oxygen augments antimicrobial and proinflammatory responses of alveolar macrophages. *Anesthesiology* 93 (1), 15–25. doi:10.1097/00000542-200007000-00008

Laoui, D., Van Overmeire, E., Di Conza, G., Aldeni, C., Keirsse, J., Morias, Y., et al. (2014). Tumor hypoxia does not drive differentiation of tumor-associated macrophages but rather fine-tunes the M2-like macrophage population. *Cancer Res.* 74 (1), 24–30. doi:10.1158/0008-5472.Can-13-1196

Li, J., Kandatsu, N., Feng, G. G., Jiang, J. Z., Huang, L., Kinoshita, H., et al. (2016). Propofol reduces liver dysfunction caused by tumor necrosis factor-alpha production in Kupffer cells. *J. Anesth.* 30 (3), 420–426. doi:10.1007/s00540-016-2145-x

Li, S., Wang, C. X., Liu, N. Z., and Liu, P. (2015). Anti-inflammatory effects of propofol on lipopolysaccharides-treated rat hepatic Kupffer cells. *Cell biochem. Biophys.* 71 (2), 845–850. doi:10.1007/s12013-014-0272-2

Lim, J. A., Oh, C. S., Yoon, T. G., Lee, J. Y., Lee, S. H., Yoo, Y. B., et al. (2018). The effect of propofol and sevoflurane on cancer cell, natural killer cell, and cytotoxic T lymphocyte function in patients undergoing breast cancer surgery: An *in vitro* analysis. *BMC Cancer* 18 (1), 159. doi:10.1186/s12885-018-4064-8

Lin, M., Deng, K., Li, Y., and Wan, J. (2021). Morphine enhances LPS-induced macrophage apoptosis through a PPARγ-dependent mechanism. *Exp. Ther. Med.* 22 (1), 714. doi:10.3892/etm.2021.10146

Liu, F. L., Chen, T. L., and Chen, R. M. (2012). Mechanisms of ketamine-induced immunosuppression. *Acta Anaesthesiol. Taiwan* 50 (4), 172–177. doi:10.1016/j.aat.2012.12.001

Liu, Q., Sheng, Z., Cheng, C., Zheng, H., Lanuti, M., Liu, R., et al. (2021a). Anesthetic propofol promotes tumor metastasis in lungs via GABA(A) R-dependent TRIM21 modulation of Src expression. *Adv. Sci.* 8 (18), e2102079. doi:10.1002/advs.202102079

Liu, Z., Meng, Y., Miao, Y., Yu, L., Wei, Q., Li, Y., et al. (2021b). Propofol ameliorates renal ischemia/reperfusion injury by enhancing macrophage M2 polarization through PPARγ/STAT3 signaling. *Aging (Albany NY)* 13 (11), 15511–15522. doi:10.18632/aging.203107

Liu, Z., Meng, Y., Miao, Y., Yu, L., and Yu, Q. (2020). Propofol reduces renal ischemia/reperfusion-induced acute lung injury by stimulating sirtuin 1 and inhibiting pyroptosis. *Aging (Albany NY)* 13 (1), 865–876. doi:10.18632/aging.202191

Liu, Z., Qu, M., Yu, L., Song, P., and Chang, Y. (2018). Artesunate inhibits renal ischemia-reperfusion-mediated remote lung inflammation through attenuating ROS-induced activation of NLRP3 inflammasome. *Inflammation* 41 (4), 1546–1556. doi:10.1007/s10753-018-0801-z

Luo, T., Wu, J., Kabadi, S. V., Sabirzhanov, B., Guanciale, K., Hanscom, M., et al. (2013). Propofol limits microglial activation after experimental brain trauma through inhibition of nicotinamide adenine dinucleotide phosphate oxidase. *Anesthesiology* 119 (6), 1370–1388. doi:10.1097/aln.0000000000000020

Ma, X., Hu, Y. W., Zhao, Z. L., Zheng, L., Qiu, Y. R., Huang, J. L., et al. (2013). Anti-inflammatory effects of propofol are mediated by apolipoprotein M in a hepatocyte nuclear factor-1α-dependent manner. *Arch. Biochem. Biophys.* 533 (1-2), 1–10. doi:10.1016/j.abb.2013.03.002

Ma, X., Wang, T., Zhao, Z.-L., Jiang, Y., and Ye, S. (2018). Propofol suppresses proinflammatory cytokine production by increasing ABCA1 expression via mediation by the long noncoding RNA LOC286367. *Mediat. Inflamm.* 2018, 8907143–8907149. doi:10.1155/2018/8907143

Meshkani, R., and Vakili, S. (2016). Tissue resident macrophages: Key players in the pathogenesis of type 2 diabetes and its complications. *Clin. Chim. Acta.* 462, 77–89. doi:10.1016/j.cca.2016.08.015

Moore, K. J., Sheedy, F. J., and Fisher, E. A. (2013). Macrophages in atherosclerosis: A dynamic balance. *Nat. Rev. Immunol.* 13 (10), 709–721. doi:10.1038/nri3520

Moraco, A. H., and Kornfeld, H. (2014). Cell death and autophagy in tuberculosis. *Semin. Immunol.* 26 (6), 497–511. doi:10.1016/j.smim.2014.10.001

Najafi, M., Hashemi Goradel, N., Farhood, B., Salehi, E., Nashtaei, M. S., Khanlarkhani, N., et al. (2019). Macrophage polarity in cancer: A review. *J. Cell. Biochem.* 120 (3), 2756–2765. doi:10.1002/jcb.27646

Nederlof, R., Weber, N. C., Juffermans, N. P., de Mol, B. A., Hollmann, M. W., Preckel, B., et al. (2017). A randomized trial of remote ischemic preconditioning and control treatment for cardioprotection in sevoflurane-anesthetized CABG patients. *BMC Anesthesiol.* 17 (1), 51. doi:10.1186/s12871-017-0330-6

Nowak, W., Grendas, L. N., Sanmarco, L. M., Estecho, I. G., Arena Á, R., Eberhardt, N., et al. (2019). Pro-inflammatory monocyte profile in patients with major depressive disorder and suicide behaviour and how ketamine induces anti-inflammatory M2 macrophages by NMDAR and mTOR. *EBioMedicine* 50, 290–305. doi:10.1016/j.ebiom.2019.10.063

Pofahl, W. E., Ramsey, K. M., Nobles, D. L., Cochran, M. K., and Goettler, C. (2011). Importance of methicillin-resistant *Staphylococcus aureus* eradication in carriers to prevent postoperative methicillin-resistant *Staphylococcus aureus* surgical site infection. *Am. Surg.* 77 (1), 27–31. doi:10.1177/000313481107700116

Romero, A., Romero-Alejo, E., Vasconcelos, N., and Puig, M. M. (2013). Glial cell activation in the spinal cord and dorsal root ganglia induced by surgery in mice. *Eur. J. Pharmacol.* 702 (1-3), 126–134. doi:10.1016/j.ejphar.2013.01.047

Sacerdote, P., Limiroli, E., and Gaspani, L. (2003). Experimental evidence for immunomodulatory effects of opioids. *Adv. Exp. Med. Biol.* 521, 106–116.

Sahinovic, M. M., Struys, M., and Absalom, A. R. (2018). Clinical pharmacokinetics and pharmacodynamics of propofol. *Clin. Pharmacokinet.* 57 (12), 1539–1558. doi:10.1007/s40262-018-0672-3

Sanders, R. D., Godlee, A., Fujimori, T., Goulding, J., Xin, G., Salek-Ardakani, S., et al. (2013). Benzodiazepine augmented γ-amino-butyric acid signaling increases mortality from pneumonia in mice. *Crit. Care Med.* 41 (7), 1627–1636. doi:10.1097/CCM.0b013e31827c0c8d

Saraghi, M., Badner, V. M., Golden, L. R., and Hersh, E. V. (2013). Propofol: An overview of its risks and benefits. *Compend. Contin. Educ. Dent.* 34 (4), 252–258.

Shapouri-Moghaddam, A., Mohammadian, S., Vazini, H., Taghadosi, M., Esmaeili, S. A., Mardani, F., et al. (2018). Macrophage plasticity, polarization, and function in health and disease. *J. Cell. Physiol.* 233 (9), 6425–6440. doi:10.1002/jcp.26429

Shibakawa, Y. S., Sasaki, Y., Goshima, Y., Echigo, N., Kamiya, Y., Kurahashi, K., et al. (2005). Effects of ketamine and propofol on inflammatory responses of primary glial cell cultures stimulated with lipopolysaccharide. *Br. J. Anaesth.* 95 (6), 803–810. doi:10.1093/bja/aei256

Shiratsuchi, H., Kouatli, Y., Yu, G. X., Marsh, H. M., and Basson, M. D. (2009). Propofol inhibits pressure-stimulated macrophage phagocytosis via the GABAA receptor and dysregulation of p130cas phosphorylation. *Am. J. Physiol. Cell Physiol.* 296 (6), C1400–C1410. doi:10.1152/ajpcell.00345.2008

Singh, A. P., Singh, N., Pathak, D., and Bedi, P. M. S. (2019). Estradiol attenuates ischemia reperfusion-induced acute kidney injury through PPAR-γ stimulated eNOS activation in rats. *Mol. Cell. Biochem.* 453 (1-2), 1–9. doi:10.1007/s11010-018-3427-4

Sinha, P., Clements, V. K., Fulton, A. M., and Ostrand-Rosenberg, S. (2007). Prostaglandin E2 promotes tumor progression by inducing myeloid-derived suppressor cells. *Cancer Res.* 67 (9), 4507–4513. doi:10.1158/0008-5472.Can-06-4174

Smith, W. L., DeWitt, D. L., and Garavito, R. M. (2000). Cyclooxygenases: Structural, cellular, and molecular biology. *Annu. Rev. Biochem.* 69, 145–182. doi:10.1146/annurev.biochem.69.1.145

Sousa, G. C., Fernandes, M. V., Cruz, F. F., Antunes, M. A., da Silva, C. M., Takyia, C., et al. (2021). Comparative effects of dexmedetomidine and propofol on brain and lung damage in experimental acute ischemic stroke. *Sci. Rep.* 11 (1), 23133. doi:10.1038/s41598-021-02608-1

Sun, L., Ma, W., Gao, W., Xing, Y., Chen, L., Xia, Z., et al. (2019). Propofol directly induces caspase-1-dependent macrophage pyroptosis through the NLRP3-ASC inflammasome. *Cell Death Dis.* 10 (8), 542. doi:10.1038/s41419-019-1761-4

Sung, E. G., Jee, D., Song, I. H., Kim, H. S., Bae, J. H., and Park, S. H. (2005). Propofol attenuates Kupffer cell activation during hypoxia-reoxygenation. *Can. J. Anaesth.* 52 (9), 921–926. doi:10.1007/bf03022052

Sztwiertnia, I., Schenz, J., Bomans, K., Schaack, D., Ohnesorge, J., Tamulyte, S., et al. (2020). Sevoflurane depletes macrophages from the melanoma microenvironment. *PLoS One* 15 (5), e0233789. doi:10.1371/journal.pone.0233789

Tan, B., Shi, X., Zhang, J., Qin, J., Zhang, N., Ren, H., et al. (2018). Inhibition of rspo-lgr4 facilitates checkpoint blockade therapy by switching macrophage polarization. *Cancer Res.* 78 (17), 4929–4942. doi:10.1158/0008-5472.Can-18-0152

Tanaka, T., Takabuchi, S., Nishi, K., Oda, S., Wakamatsu, T., Daijo, H., et al. (2010). The intravenous anesthetic propofol inhibits lipopolysaccharide-induced hypoxia-inducible factor 1 activation and suppresses the glucose metabolism in macrophages. *J. Anesth.* 24 (1), 54–60. doi:10.1007/s00540-009-0829-1

Trapani, G., Altomare, C., Liso, G., Sanna, E., and Biggio, G. (2000). Propofol in anesthesia. Mechanism of action, structure-activity relationships, and drug delivery. *Curr. Med. Chem.* 7 (2), 249–271. doi:10.2174/0929867003375335

Ulbrich, F., Eisert, L., Buerkle, H., Goebel, U., and Schallner, N. (2016). Propofol, but not ketamine or midazolam, exerts neuroprotection after ischaemic injury by inhibition of toll-like receptor 4 and nuclear factor kappa-light-chain-enhancer of activated B-cell signalling: A combined *in vitro* and animal study. *Eur. J. Anaesthesiol.* 33 (9), 670–680. doi:10.1097/eja.0000000000000449

van Furth, R., Cohn, Z. A., Hirsch, J. G., Humphrey, J. H., Spector, W. G., and Langevoort, H. L. (1972). The mononuclear phagocyte system: A new classification of macrophages, monocytes, and their precursor cells. *Bull. World Health Organ.* 46 (6), 845–852.

Varol, C., Mildner, A., and Jung, S. (2015). Macrophages: Development and tissue specialization. *Annu. Rev. Immunol.* 33, 643–675. doi:10.1146/annurev-immunol-032414-112220

Visvabharathy, L., and Freitag, N. E. (2017). Propofol sedation exacerbates kidney pathology and dissemination of bacteria during *Staphylococcus aureus* bloodstream infections. *Infect. Immun.* 85 (7), e00097. doi:10.1128/IAI.00097-17

Visvabharathy, L., Xayarath, B., Weinberg, G., Shilling, R. A., and Freitag, N. E. (2015). Propofol increases host susceptibility to microbial infection by reducing subpopulations of mature immune effector cells at sites of infection. *Plos One* 10 (9), e0138043. doi:10.1371/journal.pone.0138043

Vitale, I., Manic, G., Coussens, L. M., Kroemer, G., and Galluzzi, L. (2019). Macrophages and metabolism in the tumor microenvironment. *Cell Metab.* 30 (1), 36–50. doi:10.1016/j.cmet.2019.06.001

Von Dossow, V., Baur, S., Sander, M., Tønnesen, H., Marks, C., Paschen, C., et al. (2007). Propofol increased the interleukin-6 to interleukin-10 ratio more than isoflurane after surgery in long-term alcoholic patients. *J. Int. Med. Res.* 35 (3), 395–405. doi:10.1177/147323000703500315

Walsh, C. T. (2018). Propofol: Milk of amnesia. *Cell* 175 (1), 10–13. doi:10.1016/j.cell.2018.08.031

Wang, H. F., Chen, L., Xie, Y., Wang, X. F., Yang, K., Ning, Y., et al. (2021). Electroacupuncture facilitates M2 macrophage polarization and its potential role in the regulation of inflammatory response. *Biomed. Pharmacother.* 140, 111655. doi:10.1016/j.biopha.2021.111655

Wang, T., Wei, X. Y., Liu, B., Wang, L. J., and Jiang, L. H. (2015). Effects of propofol on lipopolysaccharide-induced expression and release of HMGB1 in macrophages. *Braz. J. Med. Biol. Res.* 48 (4), 286–291. doi:10.1590/1414-431X20144222

Wheeler, D. W., Thompson, A. J., Corletto, F., Reckless, J., Loke, J. C., Lapaque, N., et al. (2011). Anaesthetic impairment of immune function is mediated via GABA(A) receptors. *PLoS One* 6 (2), e17152. doi:10.1371/journal.pone.0017152

Wu, G. J., Chen, T. L., Chang, C. C., and Chen, R. M. (2009). Propofol suppresses tumor necrosis factor-alpha biosynthesis in lipopolysaccharide-stimulated macrophages possibly through downregulation of nuclear factor-kappa B-mediated toll-like receptor 4 gene expression. *Chem. Biol. Interact.* 180 (3), 465–471. doi:10.1016/j.cbi.2009.05.003

Wu, G. J., Tai, Y. T., Chen, T. L., Lin, L. L., Ueng, Y. F., and Chen, R. M. (2005). Propofol specifically inhibits mitochondrial membrane potential but not complex I NADH dehydrogenase activity, thus reducing cellular ATP biosynthesis and migration of macrophages. *Ann. N. Y. Acad. Sci.* 1042, 168–176. doi:10.1196/annals.1338.019

Wu, K. C., Yang, S. T., Hsu, S. C., Chiang, J. H., Hsia, T. C., Yang, J. S., et al. (2013). Propofol induces DNA damage in mouse leukemic monocyte macrophage RAW264.7 cells. *Oncol. Rep.* 30 (5), 2304–2310. doi:10.3892/or.2013.2722

Wu, K., Lin, K., Li, X., Yuan, X., Xu, P., Ni, P., et al. (2020). Redefining tumor-associated macrophage subpopulations and functions in the tumor microenvironment. *Front. Immunol.* 11, 1731. doi:10.3389/fimmu.2020.01731

Wynn, T. A., Chawla, A., and Pollard, J. W. (2013). Macrophage biology in development, homeostasis and disease. *Nature* 496 (7446), 445–455. doi:10.1038/nature12034

Xia, Y., He, F., Wu, X., Tan, B., Chen, S., Liao, Y., et al. (2021). GABA transporter sustains IL-1β production in macrophages. *Sci. Adv.* 7 (15), eabe9274. doi:10.1126/sciadv.abe9274

Xu, Y., Pan, S., Jiang, W., Xue, F., and Zhu, X. (2020). Effects of propofol on the development of cancer in humans. *Cell Prolif.* 53 (8), e12867. doi:10.1111/cpr.12867

Yu, G., Dymond, M., Yuan, L., Chaturvedi, L. S., Shiratsuchi, H., Durairaj, S., et al. (2011). Propofol's effects on phagocytosis, proliferation, nitrate production, and cytokine secretion in pressure-stimulated microglial cells. *Surgery* 150 (5), 887–896. doi:10.1016/j.surg.2011.04.002

Yue, L. H., Wang, L. N., Zhu, X. C., and Peng, Y. H. (2022). The promotion of liver regeneration in mice after a partial hepatectomy as a result of the modulation of macrophage activation by dexmedetomidine. *Transpl. Immunol.* 72, 101577. doi:10.1016/j.trim.2022.101577

Zeng, W., Xing, Z., Tan, M., Wu, Y., and Zhang, C. (2021). Propofol regulates activated macrophages metabolism through inhibition of ROS-mediated GLUT1 expression. *Inflamm. Res.* 70 (4), 473–481. doi:10.1007/s00011-021-01449-y

Zha, H., Matsunami, E., Blazon-Brown, N., Koutsogiannaki, S., Hou, L., Bu, W., et al. (2019). Volatile anesthetics affect macrophage phagocytosis. *PLoS One* 14 (5), e0216163. doi:10.1371/journal.pone.0216163

Zhang, J., Shan, W. F., Jin, T. T., Wu, G. Q., Xiong, X. X., Jin, H. Y., et al. (2014). Propofol exerts anti-hepatocellular carcinoma by microvesicle-mediated transfer of miR-142-3p from macrophage to cancer cells. *J. Transl. Med.* 12, 279. doi:10.1186/s12967-014-0279-x

Zhang, L., Wang, N., Zhou, S., Ye, W., Jing, G., and Zhang, M. (2012). Propofol induces proliferation and invasion of gallbladder cancer cells through activation of Nrf2. *J. Exp. Clin. Cancer Res.* 31 (1), 66. doi:10.1186/1756-9966-31-66

Zhou, H., Sun, J., Zhong, W., Pan, X., Liu, C., Cheng, F., et al. (2020). Dexmedetomidine preconditioning alleviated murine liver ischemia and reperfusion injury by promoting macrophage M2 activation via PPARγ/STAT3 signaling. *Int. Immunopharmacol.* 82, 106363. doi:10.1016/j.intimp.2020.106363

Glossary

ATG autophagy-related gene
ALI acute lung injury
APCs antigen presenting cells
apoM apolipoprotein M
AMPK AMP-activated protein kinase
ASC apoptosis-associated speck-like protein containing a CARD
ATP adenosine triphosphate
BMMS bone marrow-derived macrophages
BRCA1 breast cancer gene 1(BRCA1)
CaMK II calmodulin-dependent kinase II
CNS central nervous system
COX cyclooxygenase
CX43 connexin 43
DNA-Pk DNA-dependent serine/threonine protein kinase
ERK extracellular signal-regulated kinase
FoxO1 forkhead box O1
GABA gamma-aminobutyric acid
GATs GABA transporters
GLUT1 glucose transporter 1
GSK-3β glycogen synthase kinase-3
HCC hepatocellular carcinoma
HIF-1 Hypoxia inducible factor-1
HMGB1 High mobility group box 1
HNF hepatocyte nuclear factor
ICU intensive care unit
IFN-γ interferon-γ
IL interleukin
iNOs nitric oxide synthase
lncRNAs long noncoding RNAs
LPS lipopolysaccharide
MAPK mitogen-activated protein kinase
MCAO middle cerebral artery occlusion
Mcl-1 myeloid cell leukemia 1
MCP-1 chemotactic protein-1
MFG-E8 milk fat globule epidermal growth factor 8
MGMT O6-methylguanine-DNA methyltransferase
MHC histocompatibility complex
miRNAs microRNAs
MMP matrix metalloproteinase
mTOR mammalian target of rapamycin
NF-κB nuclear factor-kappa B
NK natural killer
NLRP3 nucleotide oligomerization domain (NOD)-like receptor pyrin domain-containing 3
NMDAR N-methyl-D-aspartate receptor
Nrf2 nuclear factor-E2-related factor 2
PDK-1 pyruvate dehydrogenase (PDH) kinase 1
PGE2 prostaglandin E2
PI3K phosphatidylinositol 3 kinase
PONV post-operative nausea and vomiting
PPARγ peroxisome proliferator-activated receptor gamma
PRIS propofol infusion syndrome
RAC1 ras-related C3 botulinum toxin substrate 1
rl/R renal ischemia-reperfusion injury
ROS reactive oxygen species
STAT signal transducers and activators of transcriptions
STRT1 sirtuin-1
TAMs Tumor-associated macrophage
TBI traumatic brain injury
TLRs Toll-like receptors
TME tumor microenvironment
TNF-α tumor necrosis factors -α
TXA2 thromboxane A2
VCAM-1 vascular cell adhesion molecule-1
VEGF vascular endothelial growth factor
α2B-ARs alpha 2-adrenergic receptors

frontiers | Frontiers in Pharmacology

TYPE Review
PUBLISHED 09 September 2022
DOI 10.3389/fphar.2022.974794

OPEN ACCESS

EDITED BY
Li Wu,
Nanjing University of Chinese Medicine, China

REVIEWED BY
Ting Shen,
Huaiyin Normal University, China
Yunyao Jiang,
Tsinghua University, China

*CORRESPONDENCE
Ziping Jiang,
waterjzp@jlu.edu.cn
Bin Liu,
l_bin@jlu.edu.cn

†These authors have contributed equally to this work

SPECIALTY SECTION
This article was submitted to Inflammation Pharmacology, a section of the journal Frontiers in Pharmacology

RECEIVED 21 June 2022
ACCEPTED 17 August 2022
PUBLISHED 09 September 2022

CITATION
Xia Y, Wang D, Li J, Chen M, Wang D, Jiang Z and Liu B (2022), Compounds purified from edible fungi fight against chronic inflammation through oxidative stress regulation.
Front. Pharmacol. 13:974794.
doi: 10.3389/fphar.2022.974794

Compounds purified from edible fungi fight against chronic inflammation through oxidative stress regulation

Yidan Xia[1†], Dongxu Wang[2†], Jiaqi Li[1], Minqi Chen[1], Duo Wang[1], Ziping Jiang[1*] and Bin Liu[1*]

[1]Department of Hand and Foot Surgery, The First Hospital of Jilin University, Changchun, China, [2]Laboratory Animal Center, College of Animal Science, Jilin University, Changchun, China

Chronic inflammation is associated with various chronic diseases, including cardiovascular disease, neurodegenerative disease, and cancer, which severely affect the health and quality of life of people. Oxidative stress induced by unbalanced production and elimination of reactive oxygen species (ROS) is one of the essential risk factors for chronic inflammation. Recent studies, including the studies of mushrooms, which have received considerable attention, report that the antioxidant effects of natural compounds have more advantages than synthetic antioxidants. Mushrooms have been consumed by humans as precious nourishment for 3,000 years, and so far, more than 350 types have been identified in China. Mushrooms are rich in polysaccharides, peptides, polyphenols, alkaloids, and terpenoids and are associated with several healthy biological functions, especially antioxidant properties. As such, the extracts purified from mushrooms could activate the expression of antioxidant enzymes through the Keap1/Nrf2/ARE pathway to neutralize excessive ROS and inhibit ROS-induced chronic inflammation through the NF-κB pathway. Recently, the antioxidant properties of mushrooms have been successfully applied to treating cardiovascular disease (CAD), neurodegenerative diseases, diabetes mellitus, and cancer. The present review summarizes the antioxidant properties and the mechanism of compounds purified from mushrooms, emphasizing the oxidative stress regulation of mushrooms to fight against chronic inflammation.

KEYWORDS

chronic diseases, natural compounds, edible fungi, antioxidants, molecular mechanisms

Introduction

Mushrooms have been extensively cultivated in China using artificial techniques due to their high yield, desirable taste, and widespread consumption and application as a medicinal resource (Huang and Nie, 2015). Recently, various compounds have been isolated from mushrooms, such as polysaccharides, alkaloids, peptides, terpenoids, and polyphenols (Homer and Sperry, 2017; Zhou et al., 2020; Kuang et al., 2021; Leong et al., 2021; Zhang

et al., 2021). Mushroom extracts can resist free radicals, reduce the activities of pro-inflammatory factors, and relieve chronic inflammation, which are valuable natural antioxidants with the advantages of safety, nontoxic, and easy to obtain (Hu et al., 2021). Some studies have also demonstrated the therapeutic potential of mushroom extract for cardiovascular disease (CAD), neurodegenerative diseases, and cancer (Klupp et al., 2015; Jin et al., 2016; Chun et al., 2021). This review discusses the mechanisms underlying the effect of oxidative stress on chronic inflammation and summarizes the antioxidant properties of compounds purified from mushrooms. The anti-inflammatory effects of these compounds on CAD, neurodegenerative diseases, diabetes mellitus, and cancer provide potential treatment measures for chronic inflammation caused by oxidative stress.

Chronic inflammation and oxidative stress

Predisposing factors of oxidative stress

The predisposing factors, including diet, exercise, chemicals, radiation, and drugs, can increase reactive oxygen species (ROS) production and disrupt the antioxidant system, inducing oxidative stress (Klaunig et al., 2011; Quindry et al., 2016; Tan et al., 2018; Tan and Norhaizan, 2019). Similarly, eating habits, including refined carbohydrates, high-fat, and high-animal protein diets, can increase oxidative stress through the nuclear factor-kappa B (NF-κB) signaling pathways (Tan et al., 2018). High sugar intake can produce advanced glycation end products to promote oxidation and activate the protein phosphatase 2 A and NF-κB pathways, inducing oxidative stress in mitochondria (Man et al., 2020). Regular and moderate exercise has also been proven to inhibit ROS production, while high intensity and long-term exercise might induce oxidative stress in the skeletal muscle cells, causing muscle contractile dysfunction (Powers and Jackson, 2008; Thirupathi et al., 2020). A previous study has reported that the exposure of cells to metals and metal oxide nanoparticles induces oxidative stress, thereby damaging the deoxyribonucleic acids (DNAs), proteins, and lipids (Tee et al., 2016). For instance, aluminum accumulation could impair the oxidative function of mitochondria, especially in the brain, which is explicitly sensitive to oxidative stress and is one of the causes of neurodegenerative diseases (Kumar and Gill, 2014). Similarly, continuous exposure to ionizing radiation induces excessive production of hydroxyl radicals through water oxidation or secondary partially ROS formation (Klaunig et al., 2011). Drugs, including gentamicin and bleomycin, could produce free radicals during degeneration and metabolism (Pizzino et al., 2017). Additionally, the potential predisposing factors, including unhealthy living habits, exposure to harmful substances, and certain drugs, could induce oxidative stress and damage the cellular components through different mechanisms.

Mechanism of oxidative stress

In mitochondria, most oxygen is utilized for aerobic respiration and energy release, with ROS being produced as a byproduct (Cadenas and Davies, 2000). Mitochondria convert glucose to adenosine triphosphate (ATP) through the tricarboxylic acid cycle and oxidative phosphorylation by using nicotinamide adenine dinucleotide (NADH) and reduced flavin adenosine dinucleotide (FADH2) produced in the cytoplasmic matrix (Ryoo and Kwak, 2018). In the oxidative phosphorylation process, NADH and FADH2 efficiently reduce oxygen and release energy through the electron transport chain (ETC) (Bhatti et al., 2017). However, a small quantity of oxygen is still reduced prematurely by electrons, producing superoxide anion (O_2^-), a relatively stable intermediate, which can generate hydrogen peroxide (H_2O_2) by disproportionation reaction, or hydroxyl radicals (OH) by the Haber-Weiss and Fenton reaction (Figure 1) (Sinha et al., 2013).

Under physiological conditions, ROS can be removed by the antioxidant enzymes, including superoxide dismutase (SOD), catalase (CAT), glutathione peroxidase (GSH-PX), and peroxiredoxin/thioredoxin (Prx/Trx) (Griendling et al., 2021). SOD consists of manganese superoxide dismutase (MnSOD) located in the mitochondrial matrix and cuprum/zinc superoxide dismutase (Cu/ZnSOD) in the membrane gap, which can dismutate the O_2—produced by ETC into H_2O_2 (Peoples et al., 2019). The GSH-PX and Prx/Trx systems of the cytoplasmic matrix could reduce H_2O_2, while nicotinamide adenine dinucleotide phosphate (NADPH) maintains the reducing power of these two antioxidant systems (Nolfi-Donegan et al., 2020). Meanwhile, NADH/NADPH oxidase serves as an intracellular ROS source, especially in the vascular tissues and cardiomyocytes (Elahi et al., 2009). The persistence of ROS damages the somatic cells, including the cardiac muscle cells and nerve cells, while the antioxidant properties of the compounds in mushrooms neutralize the ROS (Chun et al., 2021).

Mechanism of oxidative stress in chronic inflammation

The persistence of inflammatory factors causing tissue damage, such as trauma, chemical erosion, microbial infection, and autoimmune reaction, significantly contributes to chronic inflammation (Medzhitov, 2008; Leuti et al., 2020). When inflammation occurs, oxygen uptake by the white blood cells and mast cells in the inflammatory area increases, leading to "respiratory burst," which enhances ROS production and release (Reuter et al., 2010). It is reported that low density lipoprotein (LDL) can be oxidized by ROS and phagocytosed by macrophages, thereby improving the release of pro-inflammatory factors and inducing inflammatory responses mediated by the NF-κB signal pathway (Zuo et al., 2019). The expression of phagocytic NADPH oxidase relying on NF-κB

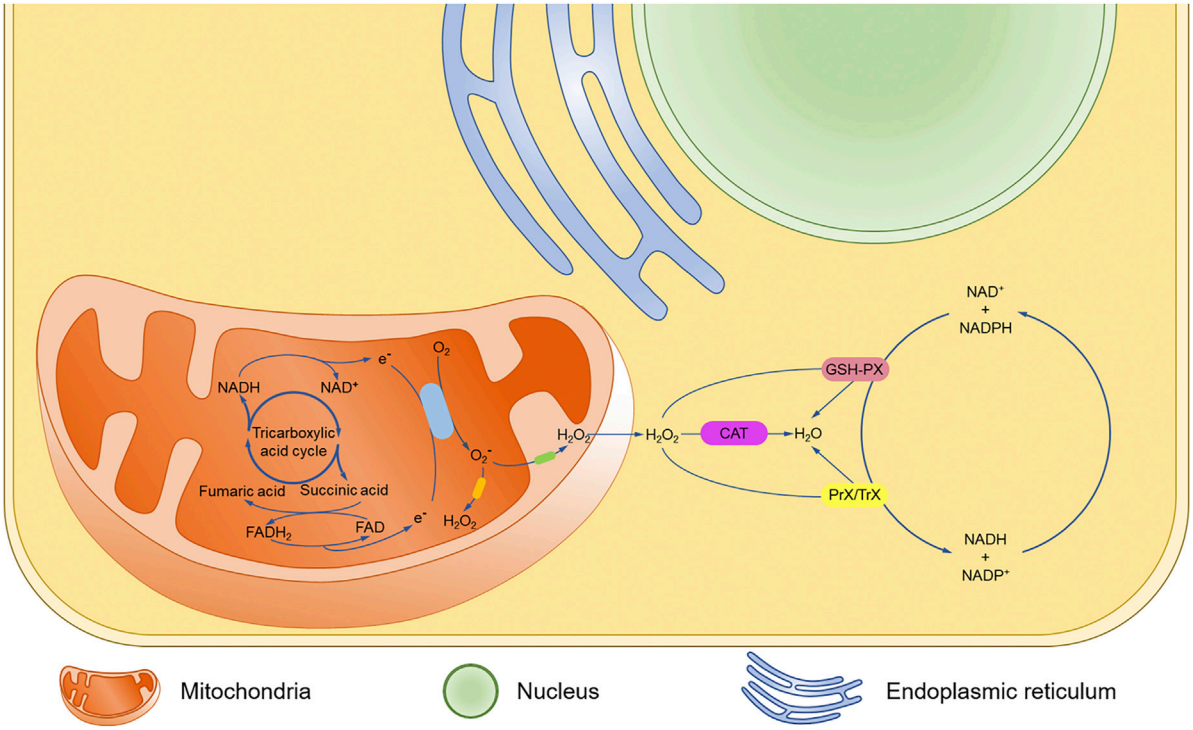

FIGURE 1
Mechanism of oxidative stress.

could produce ROS and increase the bactericidal activity of macrophages through the Toll-like receptors, including Toll-like receptor 1 (TLR1), TLR2, and TLR4 (West et al., 2011). However, excessive intracellular ROS stimulate the expression of NF-κB by activating the p38 signaling pathway and regulating the liberation of pro-inflammatory factors, including tumor necrosis factor-α (TNF-α), inducible nitric oxide synthase (iNOS), and cyclooxygenase-2 (COX-2) (Xi et al., 2020). Additionally, ROS could stimulate the expression of TLR4 and trigger an inflammatory response in the lungs by activating the NF-κB pathway (Mishra et al., 2018). Oxidative stress can induce chronic inflammation, while the inflammatory response can improve ROS release, primarily mediated through the NF-κB signal pathway (Figure 2).

Antioxidant effects and mechanisms of compounds purified from edible fungi

Extraction of compounds from edible fungi

Mushrooms are rich in polysaccharides, peptides, polyphenols, and other compounds beneficial to human health. Hence, mushrooms have been widely recognized as functional food resources and are being used for developing drugs and nutrients (Alves et al., 2012). In recent years, mushroom-derived polysaccharides have gained considerable attention due to their antioxidant, antibacterial, anti-tumor, and immunomodulatory effects (Wang et al., 2017). Most of the polysaccharides from mushrooms are water-soluble and can be extracted frequently by water extraction using heating, ultrasound, and microwave techniques (Leong et al., 2021). According to modern technology, water extraction has some disadvantages, such as long extraction time, low efficiency, and risk of biopolymer degradation. As such, the subcritical pressurized hot water extraction technology and deep eutectic solvent extraction technology have emerged as potential approaches to achieving efficient water extraction (Rodrigues Barbosa et al., 2020). Extracting mushroom-derived bioactive peptides is mostly dependent on the proteolytic action of exogenous enzymes and microbial fermentation technology (Zhou et al., 2020). Traditionally, microwave-assisted and ultrasound-assisted methods were used to extract the phenolic compounds (Petrovic et al., 2014). Different extraction methods may influence the antioxidant effects of different compounds in mushrooms, thus helping to select the appropriate extraction method to inhibit chronic inflammation by eliminating ROS.

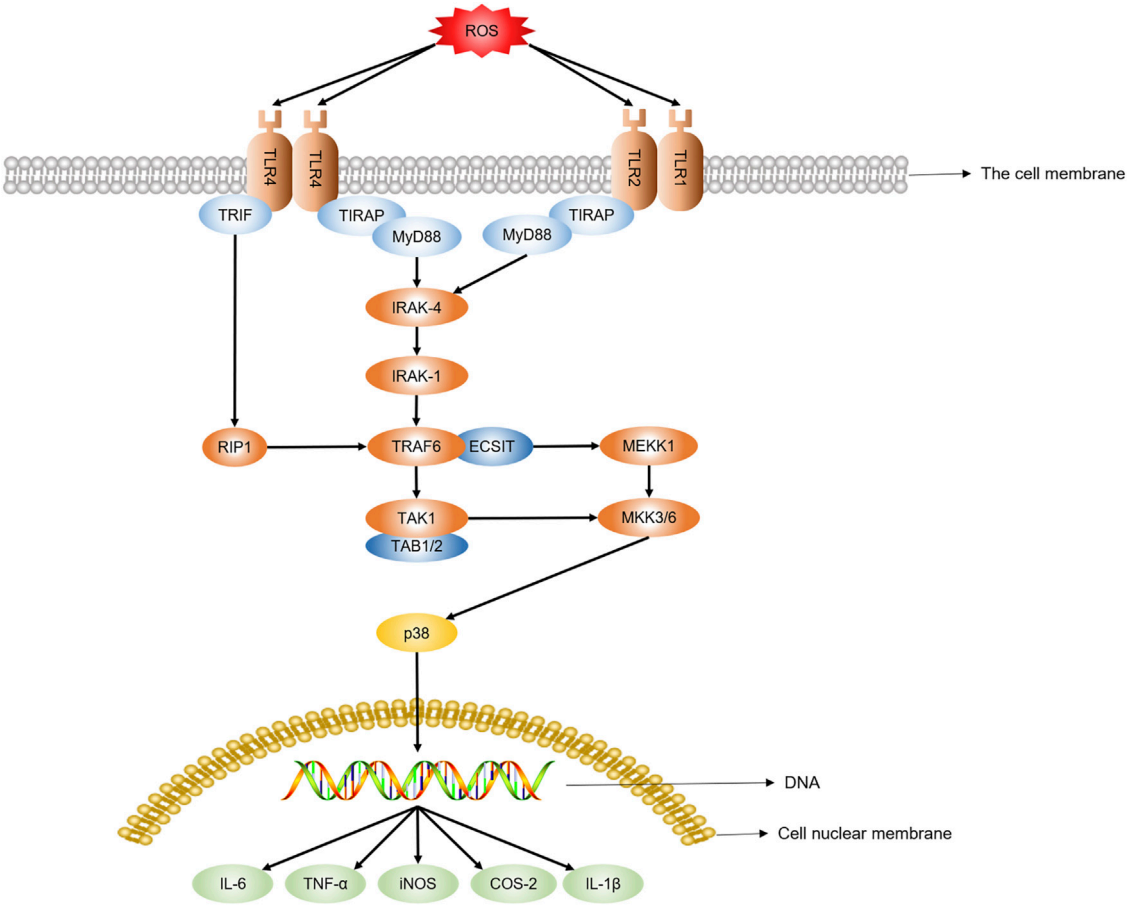

FIGURE 2
ROS promote pro-inflammatory factors release through the NF-KB pathway.

Polysaccharide

Polysaccharide, the most widely studied compound in mushrooms, is primarily composed of more than 10 monosaccharides linked with glycosidic bonds of polymeric sugar polymer carbohydrates (Supplementary Figure.S1) (Leong et al., 2021). The hydrogen ion on the sugar chain of polysaccharides can directly bind to OH and break down into harmless products (Lu et al., 2020). Polysaccharides can inhibit oxidative stress by improving the activities of antioxidant enzymes, including SOD, CAT, and GSH-PX, or chelate with metal ions, essential for ROS production (Huang et al., 2017). The antioxidant effect of polysaccharides is mainly mediated through the activation of the Keap1/Nrf2/ARE pathway to achieve the expression of downstream antioxidant enzymes (Figure 3A) (Chen et al., 2021). Nuclear factor erythroid-2 (Nrf2) is the major regulatory element of the antioxidant system *in vivo*, which can detach from the binding site of Kelch-like ECH-associated protein 1 (Keap1) in the cytoplasm after being stimulated and transferred to the nucleus to bind with the anti-oxidant response element (ARE) (Liao et al., 2019). Polysaccharides have been reported to regulate oxidative stress by upregulating the expression of phosphatidylinositol 3-kinase (P13K) and phosphorylation of protein kinase B (AKT) (Yun et al., 2020).

Poria cocos polysaccharide could eliminate O_2—and OH, while carboxymethylated pachymaran could promote the expression of SOD to achieve an antioxidant effect (Li et al., 2019). Lepista nuda polysaccharides extracted through water extraction and alcohol precipitation method could chelate iron ions and scavenge O_2—and 1,1-diphenyl-2-picrylhydrazyl free (DPPH) radicals and in a concentration-dependent manner (Shu et al., 2019). A water-soluble polysaccharide isolated from the alkaline extract of Entoloma lividoalbum could eliminate OH through the hydrogen atom donation ability of its hydroxyl group (Maity et al., 2014). In a previous study, the ultrasonic-assisted extraction of Flammulina velutipes polysaccharide showed stronger scavenging ability of DPPH, OH, and

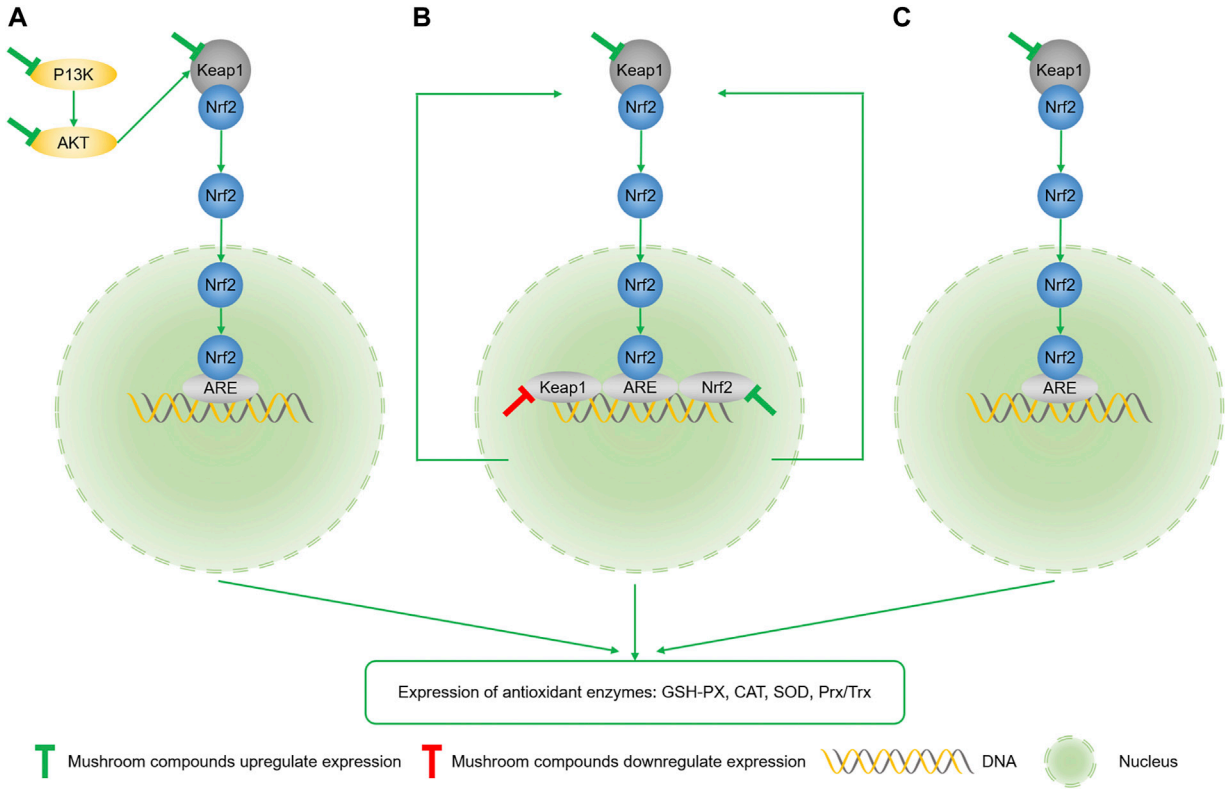

FIGURE 3
(A) Mushroom polysaccharides activate the Keap1/Nrf2/ARE pathway by upregulating the expression of P13K and AKT. **(B)** Mushroom peptides activate the Nrf2 pathway by downregulating the Keap1 gene and upregulating the Nrf2 gene expression. **(C)** Polyphenols directly promote the dissociation of Keap1 and Nrf2.

O_2—than hot water extraction, with better inflammation inhibitory ability (Chen et al., 2019). For instance, the polysaccharide purified for the first time from the floral mushrooms cultivated in Huangshan could scavenge 79.46% DPPH free radical and 74.18% OH at 5 mg/ml (Wang et al., 2015). A new polysaccharide AAP-3-1 isolated from the fruit body of Auricularia auricula could inhibit ROS production, reduce malondialdehyde content, and increase the activities of SOD, GSH-PX, and CAT (Qian et al., 2020).

Peptides

Peptides are composed of three or more amino acid molecules linked by peptide bonds, which can be easily absorbed by the intestine and pose excellent physiological characteristics than proteins (Erdmann et al., 2008). The aromatic amino acids and hydrophobic amino acid residues in the peptides could significantly increase the antioxidant activity, thereby inducing hydrogen atoms (Fontoura et al., 2019; Yang et al., 2020). Peptides can activate the Nrf2 pathway by downregulating the Keap1 gene and upregulating the Nrf2 gene expression to achieve antioxidant effects (Figure 3B) (Liu et al., 2021). Mushrooms are the primary sources of natural active peptides with significant potency, high tissue affinity, low toxicity, and high stability (Zhou et al., 2020). An analysis of the GSH levels in various mushroom species showed that the GSH content of Maitake was higher than most fruits and vegetables, indicating that mushrooms could be an indispensable source of GSH in the daily diet (Kalaras et al., 2017). In a previous study, Matsutake derived peptide WFNNAGP significantly inhibited glucan sulfate-induced oxidative stress in mice by scavenging OH and promoting the SOD activity, thereby preventing colon inflammation (Li et al., 2021a). Low molecular weight peptides decomposed from the protein hydrolysates of *Agaricus bisporus* by enzymatic processes are abundant in negatively charged amino acids, which can be applied to neutralize free radicals to resist oxidative stress (Kimatu et al., 2017).

Polyphenol

Polyphenols consisting of at least one aromatic ring with hydroxyl functional groups, including flavonoids, phenolic acids, stilbenes, and lignans, are the natural antioxidants in plant foods

(Kozarski et al., 2015). Polyphenols can provide electrons or hydrogen atoms to neutralize free radicals or chelate with metal ions to reduce the rate of Fenton reaction (Figure 3C) (Cheng et al., 2017). *Agaricus brasiliensis* mushroom containing phenolic compounds, such as gallic acid, serum acid, and pyrogallol, could inhibit ROS production by tert-butyl hydrogen peroxide stimulated macrophages (Navegantes-Lima et al., 2020). A novel polyphenol isolated from Phellinus linteus hispolon and its derivatives has been reported to have a strong free radical scavenging ability (Sarfraz et al., 2020). In a previous study, the release of phenolic compounds in agaricus bisporus, cantharellus cibarius, and lentinula edodes was determined by the simulating human gastrointestinal digestion method. The results indicated that lentinus edodes released the most phenolic acids, confirming that the phenolic compounds in lentinus edodes might easily improve the antioxidant capacity of the human body through consumption (Kala et al., 2021). Meanwhile, the flavonoids purified from Flammulina velutipes significantly increased the glutathione level, and the SOD activity of PC12 cells efficiently inhibited intracellular ROS accumulation (Hu et al., 2016). The phenolic compounds in the water extract of lentinus edobes and methanol extract of volvariella volvacea showed a higher hydrogen-providing ability to scavenge the DPPH radicals (Stajic et al., 2013).

Proteins, terpenoids, arene, and lipids

Polysaccharides, polypeptides, and polyphenols are the major antioxidant compounds in mushrooms, while other compounds, including proteins, terpenes, arene, and lipids, tend to have antioxidant properties (Kuang et al., 2021). A novel protein from edible fungi could effectively remove OH and DPPH *in vitro*, while promoting the apoptosis of breast cancer cells through anti-tumor activity (Zhang et al., 2014). Terpenoids isolated and identified from Sanghuangporus sanghuang could scavenge DPPH and 2,2′-Azinobis-(3-ethylbenzthiazoline-6-sulphonate) (ABTS) free radicals; however, their antioxidant activity is significantly inferior to the polysaccharides and phenolic compounds (Zhang et al., 2021). P-terphenyl compounds isolated from mushroom Boletopsis leucomelas through chromatography possess effective DPPH scavenging capacity, which can be enhanced with heating (Sakemi et al., 2021). 2,5-diarylcyclopentenone derivatives from Paxillus involutus possess clearing abilities of DPPH,·OH, and O_2—(Lv et al., 2021). Mushrooms are rich in fatty acids, much higher than in beef and pork, which might contribute to their antioxidant ability to fight against mitochondrial dysfunction (Fontes et al., 2019; Sande et al., 2019).

The antioxidant properties of compounds purified from mushrooms are affected by species, the extracted parts, and purification methods. Accumulating researchers have studied the polysaccharides, peptides, and phenolic compounds comprehensively, while studies focusing on protein, terpenoids, arene, and fatty acids are limited. The antioxidant effects of different compounds in mushrooms are presented in Table 1.

Applications of mushroom-derived compounds on chronic inflammatory diseases

Cardiovascular disease

Endothelial cells act as the barrier between the blood and blood vessel wall, mediating the synthesis and release of a series of active substances (Miller, 2020). Oxidative stress associated with increased ROS production and reduced nitric oxide (NO) availability in the blood vessels and myocardium could induce endothelial dysfunction, including impaired vasodilation, proinflammatory, and thrombogenic, a risk factor for cardiovascular disease (Zhao et al., 2021). Endothelial-derived NO is the primary vasodilator and can react with increased ROS to form toxic peroxynitrite (ONOO−) (Meng et al., 2021). Meanwhile, ROS can induce the uncoupling of endothelial NO synthase (eNOS), a vital enzyme for NO production (Wu et al., 2014). The mushroom-derived compounds exert antioxidant effects through the Nrf2 pathway to effectively treat chronic cardiovascular diseases caused by endothelial disorders (Cheng et al., 2017; Shen et al., 2019) (Figure 4A).

Ergothioneine is highly abundant in mushrooms and has the ability to scour ROS and chelate the metal cations. This phenomenon of ergothioneine could effectively regulate endovascular inflammation caused by endothelial dysfunction and reduce the release of pro-inflammatory factors, including interleukin-6 (IL-6), IL-1β, and TNF-α (Lam-Sidun et al., 2021). The water-soluble polysaccharide FC isolated from wild mushroom agaricus bitorquis could inhibit the NADPH oxidase activity, which might be used to treat myocardial infarction, hypertension, and atherosclerosis caused by excessive ROS (Jiao et al., 2019). In a previous study, the vasodilatation of phellinus linteus extracts was found in the rat mesenteric artery, which might induce the antioxidant and anti-inflammatory effects of polysaccharides, peptides, and terpenoids in the mycelium (Cai et al., 2019; Kwon et al., 2020; Zuo et al., 2021).

Neurodegenerative disease

Neurodegenerative diseases are characterized by the degeneration and loss of neurons in the brain and spinal cord, including Parkinson's disease (PD), Alzheimer's disease (AD), and Huntington's disease (Djajadikerta et al., 2020). Lipids in the

TABLE 1 Antioxidant effects of compounds purified from mushrooms.

Mushrooms	Compounds	Name	Antioxidant effects	References
Lepista nuda	Polysaccharide	LNP	Scavenge DPPH and $O_2^{\cdot-}$	Shu et al. (2019)
Entoloma lividoalbum	Polysaccharide	ELPS	Eliminate ·OH	Maity et al. (2015)
Flammulina velutipes	Polysaccharide	FVPs	Scavenge DPPH, ·OH, and $O_2^{\cdot-}$	Chen et al. (2019)
Floral mushroom	Polysaccharide	FMPS	Scavenge DPPH and ·OH	Wang et al. (2015)
Auricularia auricula	Polysaccharide	AAP-3-1	Increase the activities of SOD, GSH-PX, and CAT	Qian et al. (2020)
Oyster mushroom	Polysaccharide	Extract	Improve the antioxidant status during ageing	Jayakumar et al. (2007)
Pleurotus ostreatus	Polysaccharide	Extract	Protect against oxidative damage induced by H_2O_2	Barbosa et al. (2020)
Pleurotus djamor	Polysaccharide	Extract	Scavenge DPPH and ·OH	Maity et al. (2021)
Pleurotus eryngii	Polysaccharide	PERP	Scavenge reactive radicals and improve the antioxidant status	Zhang et al. (2021a)
Hohenbuehelia serotina	Polysaccharide	NTHSP-A1	Scavenging abilities of ABTS radical and ·OH radical	Li et al. (2017b)
Maitake	Peptide	Glutathione	Antioxidant property	Kalaras et al. (2017)
Matsutake	Peptide	WFNNAGP	Scavenge ·OH and promote the SOD activity	Li et al. (2021)
Agaricus bisporus	Peptide	MPI	Neutralize free radicals to resist oxidative stress	Kimatu et al. (2017)
Schizophyllum commune	Peptide	Extract	Free radical scavenging activity	Wongaem et al. (2021)
Ophiocordyceps sinensis	Peptide	COP	Scavenge DPPH radical and chelate heavy metal ions	Mishra et al. (2019)
Hericium erinaceus	Peptide	Extract	ABTS, DPPH and NO radical scavenging activities	Sangtitanu et al. (2020)
Agaricus blazei	Peptide	ABp	Change the contents of T-AOC, MDA, CAT, and ROS	Feng et al. (2021)
Pleurotus eryngii	Peptide	PEMP	Scavenge DPPH, ·OH, and $O_2^{\cdot-}$ radicals	Sun et al. (2017)
Sanghuangporus sanghuang	Polyphenol	Extract	Good cellular antioxidant activities	Zhang et al. (2021b)
Flammulina velutipes	Polyphenol	FFVP	Inhibit the secretion of NO and ROS	Ma et al. (2021)
Phlebopus portentosus	Polyphenol	Extract	DPPH scavenging activity and ferric reducing antioxidant power	Kumla et al. (2021)
Phellinus linteus	Polyphenol	Hispolon	Strong free radical scavenging ability	Sarfraz et al. (2020)
Flammulina velutipes	Polyphenol	FVF	Increase glutathione level and SOD activity and inhibit the accumulation of intracellular ROS	Hu et al. (2016)
Boletus edulis and *Cantharellus cibarius*	Polyphenol	Extract	The aqueous extract showed the strongest antioxidant activity	Fogarasi et al. (2021)
Sanghuangporus baumii	Polyphenol	Extract	Scavenge ·OH, DPPH, and ABTS	Zheng et al. (2021)
Boletopsis leucomelas	P-terphenyl compound	Extract	Effective DPPH scavenging capacity	Sakemi et al. (2021)
T. terrestris and T. vialis	P-terphenyl compound	Extract	Prevent VEGF-induced production of ROS and malondialdehyde	Sonowal et al. (2018)
Hericium erinaceum	Sterol	Extract	Cellular antioxidant activity	Li et al. (2017a)
Pholiota nameko	Protein	PNAP	Scavenge ·OH and DPPH	Zhang et al. (2014)
Sanghuangporus sanghuang	Terpenoid	Extract	Scavenge DPPH and ABTS free radicals	Zhang et al. (2021b)
Paxillus involutus	2,5-diarylcyclopentenone	Extract	Clearing abilities of DPPH, ·OH, and $O_2^{\cdot-}$	Lv et al. (2021)
Agaricomycetes	Extract	Extract	Significantly increase the activities of SOD, CAT and GSH-Px	Zhang et al. (2019)
Agaricus bisporus	Extract	Extract	Enhance the activities of antioxidant enzymes	Liu et al. (2013a)
Lactarius salmonicolor	Extract	Extract	Show the most potent radical scavenging activity	Athanasakis et al. (2013)
Ramaria flava	Extract	Extract	High DPPH and ·OH radical-scavenging activities	Liu et al. (2013b)
Chaga	Extract	Extract	Scavenging activity against the ABTS radical cation and DPPH radical.	Lee et al. (2007)
Porodaedalea chrysoloma	Extract	Extract	Possess considerable antioxidant effect	Sarkozy et al. (2020)
Orange coral mushroom	Extract	Extract	Good free radical scavenges and reduce capacities	Aprotosoaie et al. (2017)
Cynomorium coccineum	Extract	Extract	ORAC-PYR assay gives the highest antioxidant value in both cases	Zucca et al. (2013)
Entoloma lividoalbum	Extract	Extract	Possess hydroxyl and superoxide radical-scavenging activities	Maity et al. (2014)
Flammulina velutipes	Extract	Extract	High DPPH radical scavenging activity	Bao et al. (2008)
Pleurotus ostreatus	Extract	Extract	High DPPH and hydrogen peroxide scavenging potential	Udeh et al. (2021)
Agaricus brasiliensis	Extract	Extract	Protect against sepsis by alleviating oxidative and inflammatory response	Navegantes-Lima et al. (2020)

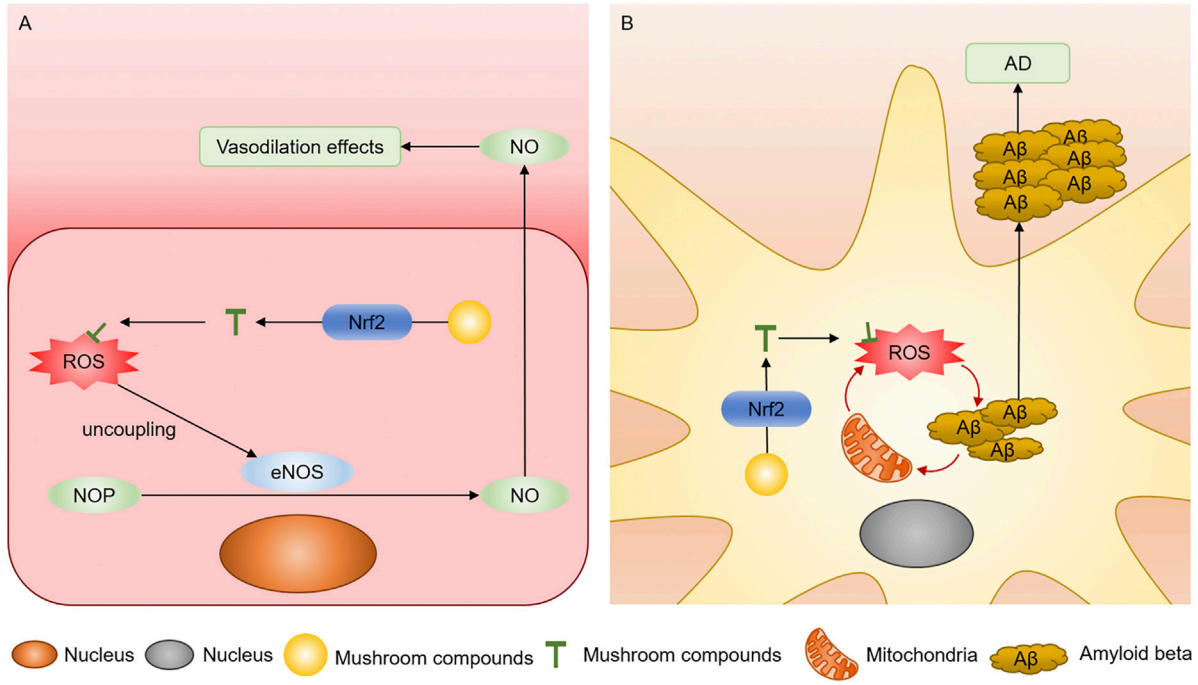

FIGURE 4
(A) Compounds in mushrooms inhibit eNOS uncoupling through the Nrf2 pathway. **(B)** Compounds in mushrooms neutralize ROS through the Nrf2 pathway and inhibit Aβ accumulation.

brain play a vital role in the function of neurons, which are vulnerable to being attacked by ROS and produce lipid peroxidation to form malondialdehyde (MDA), inducing reduced membrane fluidity and neuron degeneration (Singh et al., 2019). Meanwhile, the damaged neurons activate microglia and astrocytes to release the pro-inflammatory cytokines and ROS, further exacerbating neurodegeneration (Fischer and Maier, 2015). ROS produced by oxidative stress could damage and mutate the mitochondrial DNA, increasing oxidative decomposition of dopamine as the pathogenesis of neurodegenerative diseases and the accumulation of abnormal protein, such as amyloid beta (Aβ) in AD (Figure 4B) (Lin and Beal, 2006). Antioxidants in mushrooms could directly neutralize ROS or activate the Nrf2/ARE signaling pathway to induce the competence of antioxidant enzymes (Elfawy and Das, 2019).

Ethanol extracts from hericium erinaceus could alleviate the mitochondrial damage caused by H_2O_2 and activate antioxidant enzymes to treat hippocampal neurons' injury in mice (Kushairi et al., 2019). The polysaccharide peptides and vitamins in coriolus versicolor could significantly reduce the proportion of GSH and oxidized glutathione (GSSG) in the plasma to relieve the systemic oxidative stress state and nerve injury of patients (Scuto et al., 2019). Meroterpenoids from Albatrellus yasudae have been found to inhibit Aβ aggregation, which might be a therapeutic and health care product for AD (Masuda et al., 2021). Polyphenols, polysaccharides, and triterpenes in Amauroderma rugosum could reduce oxidative stress and 6-hydroxydopamine-induced mitochondria dysfunction in the PC12 cells (Li et al., 2021b).

Diabetes mellitus

The occurrence of diabetes mellitus is related to the dysfunction of islet β cells and insulin resistance, in which oxidative stress plays a vital role in regulating multiple signaling pathways (Zhang et al., 2020). Excessive ROS can activate the NF-κB, JNK/SAPK, and p38 MAPK pathways by activating TLR and inducing the dysfunction of islet β cells (Yaribeygi et al., 2020). A persistent hyperglycemic environment induces ROS production through the binding of advanced glycation end products (AGE) to peroxisome proliferators activated receptors (PPAR) (Deng et al., 2021). Additionally, excessive production of AGE increases the expression of inflammatory mediators through the NF-κB pathway (Karam et al., 2017). The inflammatory factor TNF-α activates the intracellular signaling factor IKKβ that affects insulin production through the NF-κB signaling pathway (Wellen and Hotamisligil, 2005; Rohm et al., 2022).

Polysaccharides isolated from Inonotus obliquus are the potential to treat type 2 diabetes by directly removing ROS or mediating lipid peroxidation (Lu et al., 2021). Terpenoids from Antrodia camphorata could significantly inhibit the binding of AGE to PPAR and reduce blood glucose levels, thus inhibiting ROS production and promoting insulin secretion (Kuang et al., 2021). Alkali-soluble polysaccharides from Amillariella mellea could improve pancreatic B-cell dysfunction caused by oxidative stress, thereby improving insulin sensitivity and reducing insulin resistance (Yang et al., 2019). As food supplements, *P. Ostreatus* and *L. Subnudus* have been shown to increase the activity of antioxidant enzymes and non-enzymatic antioxidants, inducing memory loss in diabetic rats (Agunloye and Oboh, 2021).

Cancer

ROS can induce chronic inflammation, and the continuous inflammatory environment and oxidative stress might damage the adjacent epithelial cells and stromal cells, inducing cancer (Reuter et al., 2010). Additionally, ROS induces the proliferation of cancer cells and promotes tumor growth by activating the MAPK pathway (Moloney and Cotter, 2018). Tumor cell metastasis depends on the epithelial-mesenchymal transformation process, in which ROS activates the proteins, including β -catenin, e-cadherin, and matrix metalloproteinases (MMP), through the Wnt/β -catenin signaling pathway (Sosa et al., 2013).

Termitomyces Clypeatus significantly inhibited the tumor volume and number of ascites carcinoma mice by inhibiting lipid peroxidation and increasing the levels of GSH, SOD, and CAT (Mondal et al., 2016). The extracts from Lactarius deliciosus and Coprinus comatus inhibited the activity of MMP produced by oxidative stress and induced apoptosis in gliomas associated with G1 or G2/M phase cell cycle stagnation (Nowakowski et al., 2021). Natural antioxidants isolated from Thelephora Ganbajun by ultrasonic-assisted technology exhibited anti-proliferation effects on the liver and lung cancer cells (Xu et al., 2016). Antrodia salmonea induces protective autophagy and apoptosis in colon cancer cells through cascades of extracellular signal kinase (ERK) signaling, which has been reported to mediate ROS due to the double-sided effects of antioxidants on cancer cells (Dastmalchi et al., 2020; Yang et al., 2021).

The compounds purified from mushrooms might possess promising applications in preventing and treating cardiovascular diseases, neurodegenerative diseases, and cancer by regulating oxidative stress and chronic inflammation.

Discussion

Excessive ROS increases the release of pro-inflammatory factors, thereby promoting ROS production, which is the primary reason for oxidative stress-induced chronic inflammation. Chronic inflammation can lead to organic diseases in different tissues and organs over time. Chronic inflammation in the blood vessels can affect the vascular endothelial relaxation function and form atherosclerosis, the root cause of coronary atherosclerotic heart disease (Golia et al., 2014). It is reported that chronic inflammatory response persists in the neurodegeneration of AD and is considered an important factor in accelerating the progression (Gasiorowski et al., 2018). In chronic inflammation, ROS can damage DNA and cause biological macromolecule dysfunction, such as proteins and lipids, inducing antioxidant dysfunction and a vicious cycle of oxidative stress, a risk factor for cancer (Murata, 2018). In recent years, antioxidants have attracted much attention due to their oxidative stress combating ability to inhibit chronic inflammation. Natural compounds are more easily recognized and absorbed by the body than synthetic antioxidants, with no toxic side effects (Liu, 2022). Chinese herbs, including Astragalus membranaceus, berberine, and curcumin have also been proven to have antioxidant properties (Kocaadam and Sanlier, 2017; Liu et al., 2017; Song et al., 2020). The separation and purification process of Chinese herbs extract is complicated, implying that purity can affect its application. Meanwhile, improper usage might lead to toxicoses (Hu et al., 2005; Liu et al., 2018). In contrast, mushrooms are widely distributed, easy to process, and can provide various nutrients with simple treatments (Ahmad et al., 2021). Additionally, mushrooms are well absorbed by the human body with no harm as the natural antioxidant (Fontes et al., 2019).

Mushrooms possess many biological and pharmacological characteristics, which are already applied in nutrition, health care, and medical treatment (Venturella et al., 2021). Therefore, studies pay more attention to mushroom-derived polysaccharides than other compounds, as the purification method is mature and the biological activity is stable and diverse (Muszynska et al., 2018). Mushroom polysaccharides mainly contain β-glucan chains, which have been proven to have antioxidant effects (Maity et al., 2021). The hydrogen ions of mushroom polysaccharides could inhibit oxidative stress by neutralizing ROS and enhance antioxidant effects through chemical modification, including carboxymethylation and sulphuration (Huang and Nie, 2015; Lu et al., 2020). The extraction method significantly affected the antioxidant activity of the compound. Water extraction of Lepista nuda polysaccharides showed better scavenging ability of free radicals than ethanol extraction (Shu et al., 2019). The same compound had different scavenging abilities for different free radicals. For instance, Sanghuang could scavenge 68% ·OH and 57% O_2—at 1 mg/ml, indicating that the scavenging ability of most compounds in the mushrooms is concentration-dependent (Zuo et al., 2021). Mushrooms are a promising source of natural antioxidants, ergothioneine, and glutathione, with the highest content in the mushroom cap of yellow oyster (Kalaras et al., 2017). However, more research on different species of natural compounds purified from mushrooms should be conducted to broaden their application.

In conclusion, the compounds in mushrooms could inhibit oxidative stress and chronic inflammation by neutralizing excessive ROS or activating antioxidant enzymes through the Nrf2 signaling pathway and have been applied to cardiovascular disease, neurodegenerative disease, and cancer.

Author contributions

YX and DW wrote the manuscript. JL, MC, DW, ZJ, and BL collected the references and prepared figures. All authors reviewed the manuscript.

Funding

This research was financially supported by the National Natural Science Foundation of China (Grant Nos. 52022095, 82071391, 51973216, 51873207, and 51833010), the Provincial Health Special Project of Jilin Province (Grant Nos. JLSCZD 2019-002 and JLSWSRCZX 2020-095), the Science and Technology Development Program of Jilin Province (Grant No. 20200404182YY), the Youth Innovation Promotion Association of Chinese Academy of Sciences (Grant No. 2019230), and Natural science Foundation of the Jilin province (Grant No. 20210101310JC). Project of science and Technology Department of Jilin Province (Grant No. 20220505033ZP).

Conflict of interest

The authors declare that the research was conducted in the absence of any commercial or financial relationships that could be construed as a potential conflict of interest.

Publisher's note

Supplementary material

The Supplementary Material for this article can be found online at: https://www.frontiersin.org/articles/10.3389/fphar.2022.974794/full#supplementary-material

SUPPLEMENTARY FIGURE S1
Structure of compounds purified from mushrooms, with hydrogen atoms in red as active sites against oxidative stress. N is the number of cycles. **(A)** Structure of mushroom polysaccharide. **(B)** Structure of mushroom peptides. **(C)** Structure of mushroom polyphenols, with flavonoids as an example.

References

Agunloye, O. M., and Oboh, G. (2021). Effect of diet supplemented with P. ostreatus and L. subnudus on memory index and key enzymes linked with Alzheimer's disease in streptozotocin-induced diabetes rats. *J. Food Biochem.* 45 (3), e13355. doi:10.1111/jfbc.13355

Ahmad, R., Riaz, M., Khan, A., Aljamea, A., Algheryafi, M., Sewaket, D., et al. (2021). Ganoderma lucidum (Reishi) an edible mushroom; a comprehensive and critical review of its nutritional, cosmeceutical, mycochemical, pharmacological, clinical, and toxicological properties. *Phytother. Res.* 35 (11), 6030–6062. doi:10.1002/ptr.7215

Alves, M. J., Ferreira, I. C., Dias, J., Teixeira, V., Martins, A., and Pintado, M. (2012). A review on antimicrobial activity of mushroom (Basidiomycetes) extracts and isolated compounds. *Planta Med.* 78 (16), 1707–1718. doi:10.1055/s-0032-1315370

Aprotosoaie, A. C., Zavastin, D. E., Mihai, C. T., Voichita, G., Gherghel, D., Silion, M., et al. (2017). Antioxidant and antigenotoxic potential of Ramaria largentii Marr & D. E. Stuntz, a wild edible mushroom collected from Northeast Romania. *Food Chem. Toxicol.* 108, 429–437. doi:10.1016/j.fct.2017.02.006

Athanasakis, G., Aligiannis, N., Gonou-Zagou, Z., Skaltsounis, A. L., and Fokialakis, N. (2013). Antioxidant properties of the wild edible mushroom Lactarius salmonicolor. *J. Med. Food* 16 (8), 760–764. doi:10.1089/jmf.2012.0297

Bao, H. N., Ushio, H., and Ohshima, T. (2008). Antioxidative activity and antidiscoloration efficacy of ergothioneine in mushroom (Flammulina velutipes) extract added to beef and fish meats. *J. Agric. Food Chem.* 56 (21), 10032–10040. doi:10.1021/jf8017063

Barbosa, J. R., Mm, S. F., Oliveira, L. C., Lh, S. M., Almada-Vilhena, A. O., Oliveira, R. M., et al. (2020). Obtaining extracts rich in antioxidant polysaccharides from the edible mushroom Pleurotus ostreatus using binary system with hot water and supercritical CO2. *Food Chem.* 330, 127173. doi:10.1016/j.foodchem.2020.127173

Bhatti, J. S., Bhatti, G. K., and Reddy, P. H. (2017). Mitochondrial dysfunction and oxidative stress in metabolic disorders - a step towards mitochondria based therapeutic strategies. *Biochim. Biophys. Acta. Mol. Basis Dis.* 1863 (5), 1066–1077. doi:10.1016/j.bbadis.2016.11.010

Cadenas, E., and Davies, K. J. (2000). Mitochondrial free radical generation, oxidative stress, and aging. *Free Radic. Biol. Med.* 29 (3-4), 222–230. doi:10.1016/s0891-5849(00)00317-8

Cai, C., Ma, J., Han, C., Jin, Y., Zhao, G., and He, X. (2019). Extraction and antioxidant activity of total triterpenoids in the mycelium of a medicinal fungus, Sanghuangporus sanghuang. *Sci. Rep.* 9 (1), 7418. doi:10.1038/s41598-019-43886-0

Chen, F., Huang, S., and Huang, G. (2021). Preparation, activity, and antioxidant mechanism of rice bran polysaccharide. *Food Funct.* 12 (2), 834–839. doi:10.1039/d0fo02498h

Chen, X., Fang, D., Zhao, R., Gao, J., Kimatu, B. M., Hu, Q., et al. (2019). Effects of ultrasound-assisted extraction on antioxidant activity and bidirectional immunomodulatory activity of Flammulina velutipes polysaccharide. *Int. J. Biol. Macromol.* 140, 505–514. doi:10.1016/j.ijbiomac.2019.08.163

Cheng, Y. C., Sheen, J. M., Hu, W. L., and Hung, Y. C. (2017). Polyphenols and oxidative stress in atherosclerosis-related ischemic heart disease and stroke. *Oxid. Med. Cell. Longev.* 2017, 8526438. doi:10.1155/2017/8526438

Chun, S., Gopal, J., and Muthu, M. (2021). Antioxidant activity of mushroom extracts/polysaccharides-their antiviral properties and plausible AntiCOVID-19 properties. *Antioxidants (Basel)* 10 (12), 1899. doi:10.3390/antiox10121899

Dastmalchi, N., Baradaran, B., Latifi-Navid, S., Safaralizadeh, R., Khojasteh, S. M. B., Amini, M., et al. (2020). Antioxidants with two faces toward cancer. *Life Sci.* 258, 118186. doi:10.1016/j.lfs.2020.118186

Deng, L., Du, C., Song, P., Chen, T., Rui, S., Armstrong, D. G., et al. (2021). The role of oxidative stress and antioxidants in diabetic wound healing. *Oxid. Med. Cell. Longev.* 2021, 8852759. doi:10.1155/2021/8852759

Djajadikerta, A., Keshri, S., Pavel, M., Prestil, R., Ryan, L., and Rubinsztein, D. C. (2020). Autophagy induction as a therapeutic strategy for neurodegenerative diseases. *J. Mol. Biol.* 432 (8), 2799–2821. doi:10.1016/j.jmb.2019.12.035

Elahi, M. M., Kong, Y. X., and Matata, B. M. (2009). Oxidative stress as a mediator of cardiovascular disease. *Oxid. Med. Cell. Longev.* 2 (5), 259–269. doi:10.4161/oxim.2.5.9441

Elfawy, H. A., and Das, B. (2019). Crosstalk between mitochondrial dysfunction, oxidative stress, and age related neurodegenerative disease: Etiologies and therapeutic strategies. *Life Sci.* 218, 165–184. doi:10.1016/j.lfs.2018.12.029

Erdmann, K., Cheung, B. W., and Schroder, H. (2008). The possible roles of food-derived bioactive peptides in reducing the risk of cardiovascular disease. *J. Nutr. Biochem.* 19 (10), 643–654. doi:10.1016/j.jnutbio.2007.11.010

Feng, Q., Li, Y., Lu, X., Yu, Y., Yuan, G., Sun, J., et al. (2021). Agaricus blazei polypeptide exerts a protective effect on D-galactose-induced aging mice via the Keap1/Nrf2/ARE and P53/Trim32 signaling pathways. *J. Food Biochem.* 45 (1), e13555. doi:10.1111/jfbc.13555

Fischer, R., and Maier, O. (2015). Interrelation of oxidative stress and inflammation in neurodegenerative disease: Role of TNF. *Oxid. Med. Cell. Longev.* 2015, 610813. doi:10.1155/2015/610813

Fontes, A., Alemany-Pages, M., Oliveira, P. J., Ramalho-Santos, J., Zischka, H., and Azul, A. M. (2019). Antioxidant versus pro-apoptotic effects of mushroom-enriched diets on mitochondria in liver disease. *Int. J. Mol. Sci.* 20 (16), E3987. doi:10.3390/ijms20163987

Fogarasi, M., Socaciu, M. I., Salagean, C. D., Ranga, F., Farcas, A. C., Socaci, S. A., et al. (2021). Comparison of different extraction solvents for characterization of antioxidant potential and polyphenolic composition in boletus edulis and cantharellus cibarius mushrooms from Romania. *Molecules* 26 (24), 7508. doi:10.3390/molecules26247508

Fontoura, R., Daroit, D. J., Correa, A. P. F., Moresco, K. S., Santi, L., Beys-da-Silva, W. O., et al. (2019). Characterization of a novel antioxidant peptide from feather keratin hydrolysates. *N. Biotechnol.* 49, 71–76. doi:10.1016/j.nbt.2018.09.003

Gasiorowski, K., Brokos, B., Echeverria, V., Barreto, G. E., and Leszek, J. (2018). RAGE-TLR crosstalk sustains chronic inflammation in neurodegeneration. *Mol. Neurobiol.* 55 (2), 1463–1476. doi:10.1007/s12035-017-0419-4

Golia, E., Limongelli, G., Natale, F., Fimiani, F., Maddaloni, V., Pariggiano, I., et al. (2014). Inflammation and cardiovascular disease: From pathogenesis to therapeutic target. *Curr. Atheroscler. Rep.* 16 (9), 435. doi:10.1007/s11883-014-0435-z

Griendling, K. K., Camargo, L. L., Rios, F. J., Alves-Lopes, R., Montezano, A. C., and Touyz, R. M. (2021). Oxidative stress and hypertension. *Circ. Res.* 128 (7), 993–1020. doi:10.1161/CIRCRESAHA.121.318063

Homer, J. A., and Sperry, J. (2017). Mushroom-Derived indole alkaloids. *J. Nat. Prod.* 80 (7), 2178–2187. doi:10.1021/acs.jnatprod.7b00390

Hu, Q., Yu, J., Yang, W., Kimatu, B. M., Fang, Y., Ma, N., et al. (2016). Identification of flavonoids from Flammulina velutipes and its neuroprotective effect on pheochromocytoma-12 cells. *Food Chem.* 204, 274–282. doi:10.1016/j.foodchem.2016.02.138

Hu, W., Li, Z., Wang, W., Song, M., Dong, R., Zhou, Y., et al. (2021). Structural characterization of polysaccharide purified from amanita caesarea and its pharmacological basis for application in alzheimer's disease: Endoplasmic reticulum stress. *Food Funct.* 12 (21), 11009–11023. doi:10.1039/d1fo01963e

Hu, Z., Yang, X., Ho, P. C., Chan, S. Y., Heng, P. W., Chan, E., et al. (2005). Herb-drug interactions: A literature review. *Drugs* 65 (9), 1239–1282. doi:10.2165/00003495-200565090-00005

Huang, G., Mei, X., and Hu, J. (2017). The antioxidant activities of natural polysaccharides. *Curr. Drug Targets* 18 (11), 1296–1300. doi:10.2174/1389450118666170123145357

Huang, X., and Nie, S. (2015). The structure of mushroom polysaccharides and their beneficial role in health. *Food Funct.* 6 (10), 3205–3217. doi:10.1039/c5fo00678c

Jayakumar, T., Thomas, P. A., and Geraldine, P. (2007). Protective effect of an extract of the oyster mushroom, Pleurotus ostreatus, on antioxidants of major organs of aged rats. *Exp. Gerontol.* 42 (3), 183–191. doi:10.1016/j.exger.2006.10.006

Jiao, Y., Kuang, H., Wu, J., and Chen, Q. (2019). Polysaccharides from the edible mushroom Agaricus bitorquis (quel.) sacc. Chaidam show anti-hypoxia activities in pulmonary artery smooth muscle cells. *Int. J. Mol. Sci.* 20 (3), E637. doi:10.3390/ijms20030637

Jin, X., Ruiz Beguerie, J., Sze, D. M., and Chan, G. C. (2016). Ganoderma lucidum (Reishi mushroom) for cancer treatment. *Cochrane Database Syst. Rev.* 4, CD007731. doi:10.1002/14651858.CD007731.pub3

Kala, K., Krakowska, A., Szewczyk, A., Ostachowicz, B., Szczurek, K., Fijalkowska, A., et al. (2021). Determining the amount of potentially bioavailable phenolic compounds and bioelements in edible mushroom mycelia of Agaricus bisporus, Cantharellus cibarius, and Lentinula edodes. *Food Chem.* 352, 129456. doi:10.1016/j.foodchem.2021.129456

Kalaras, M. D., Richie, J. P., Calcagnotto, A., and Beelman, R. B. (2017). Mushrooms: A rich source of the antioxidants ergothioneine and glutathione. *Food Chem.* 233, 429–433. doi:10.1016/j.foodchem.2017.04.109

Karam, B. S., Chavez-Moreno, A., Koh, W., Akar, J. G., and Akar, F. G. (2017). Oxidative stress and inflammation as central mediators of atrial fibrillation in obesity and diabetes. *Cardiovasc. Diabetol.* 16 (1), 120. doi:10.1186/s12933-017-0604-9

Kimatu, B. M., Zhao, L., Biao, Y., Ma, G., Yang, W., Pei, F., et al. (2017). Antioxidant potential of edible mushroom (Agaricus bisporus) protein hydrolysates and their ultrafiltration fractions. *Food Chem.* 230, 58–67. doi:10.1016/j.foodchem.2017.03.030

Klaunig, J. E., Wang, Z., Pu, X., and Zhou, S. (2011). Oxidative stress and oxidative damage in chemical carcinogenesis. *Toxicol. Appl. Pharmacol.* 254 (2), 86–99. doi:10.1016/j.taap.2009.11.028

Klupp, N. L., Chang, D., Hawke, F., Kiat, H., Cao, H., Grant, S. J., et al. (2015). Ganoderma lucidum mushroom for the treatment of cardiovascular risk factors. *Cochrane Database Syst. Rev.* 2021 (2), CD007259. doi:10.1002/14651858.CD007259.pub2

Kocaadam, B., and Sanlier, N. (2017). Curcumin, an active component of turmeric (Curcuma longa), and its effects on health. *Crit. Rev. Food Sci. Nutr.* 57 (13), 2889–2895. doi:10.1080/10408398.2015.1077195

Kozarski, M., Klaus, A., Jakovljevic, D., Todorovic, N., Vunduk, J., Petrovic, P., et al. (2015). Antioxidants of edible mushrooms. *Molecules* 20 (10), 19489–19525. doi:10.3390/molecules201019489

Kuang, Y., Li, B., Wang, Z., Qiao, X., and Ye, M. (2021). Terpenoids from the medicinal mushroom Antrodia camphorata: Chemistry and medicinal potential. *Nat. Prod. Rep.* 38 (1), 83–102. doi:10.1039/d0np00023j

Kumar, V., and Gill, K. D. (2014). Oxidative stress and mitochondrial dysfunction in aluminium neurotoxicity and its amelioration: A review. *Neurotoxicology* 41, 154–166. doi:10.1016/j.neuro.2014.02.004

Kumla, J., Suwannarach, N., Tanruean, K., and Lumyong, S. (2021). Comparative evaluation of chemical composition, phenolic compounds, and antioxidant and antimicrobial activities of tropical black bolete mushroom using different preservation methods. *Foods* 10 (4), 781. doi:10.3390/foods10040781

Kushairi, N., Phan, C. W., Sabaratnam, V., David, P., and Naidu, M. (2019). Lion's mane mushroom, hericium erinaceus (bull.: Fr.) pers. Suppresses H2O2-induced oxidative damage and LPS-induced inflammation in HT22 hippocampal neurons and BV2 microglia. *Antioxidants (Basel)* 8 (8), E261. doi:10.3390/antiox8080261

Kwon, Y., Haam, C. E., Byeon, S., Choi, S. J., Shin, D. H., Choi, S. K., et al. (2020). Vasodilatory effect of phellinus linteus extract in rat mesenteric arteries. *Molecules* 25 (14), E3160. doi:10.3390/molecules25143160

Lam-Sidun, D., Peters, K. M., and Borradaile, N. M. (2021). Mushroom-derived medicine? Preclinical studies suggest potential benefits of ergothioneine for cardiometabolic health. *Int. J. Mol. Sci.* 22 (6), 3246. doi:10.3390/ijms22063246

Lee, I. K., Kim, Y. S., Jang, Y. W., Jung, J. Y., and Yun, B. S. (2007). New antioxidant polyphenols from the medicinal mushroom Inonotus obliquus. *Bioorg. Med. Chem. Lett.* 17 (24), 6678–6681. doi:10.1016/j.bmcl.2007.10.072

Leong, Y. K., Yang, F. C., and Chang, J. S. (2021). Extraction of polysaccharides from edible mushrooms: Emerging technologies and recent advances. *Carbohydr. Polym.* 251, 117006. doi:10.1016/j.carbpol.2020.117006

Leuti, A., Fazio, D., Fava, M., Piccoli, A., Oddi, S., and Maccarrone, M. (2020). Bioactive lipids, inflammation and chronic diseases. *Adv. Drug Deliv. Rev.* 159, 133–169. doi:10.1016/j.addr.2020.06.028

Li, J., Li, R., Wu, X., Hoo, R. L., Lee, S. M., Cheung, T. M., et al. (2021). Amauroderma rugosum protects PC12 cells against 6-OHDA-induced neurotoxicity through antioxidant and antiapoptotic effects. *Oxid. Med. Cell. Longev.* 2021, 6683270. doi:10.1155/2021/6683270

Li, M., Lv, R., Wang, C., Ge, Q., Du, H., and Lin, S. (2021). Tricholoma matsutake-derived peptide WFNNAGP protects against DSS-induced colitis by ameliorating oxidative stress and intestinal barrier dysfunction. *Food Funct.* 12 (23), 11883–11897. doi:10.1039/d1fo02806e

Li, W., Lee, S. H., Jang, H. D., Ma, J. Y., and Kim, Y. H. (2017a). Antioxidant and anti-osteoporotic activities of aromatic compounds and sterols from hericium erinaceum. *Molecules* 22 (1), 108. doi:10.3390/molecules22010108

Li, X., Wang, L., and Wang, Z. (2017b). Structural characterization and antioxidant activity of polysaccharide from Hohenbuehelia serotina. *Int. J. Biol. Macromol.* 98, 59–66. doi:10.1016/j.ijbiomac.2016.12.089

Li, X., He, Y., Zeng, P., Liu, Y., Zhang, M., Hao, C., et al. (2019). Molecular basis for Poria cocos mushroom polysaccharide used as an antitumour drug in China. *J. Cell. Mol. Med.* 23 (1), 4–20. doi:10.1111/jcmm.13564

Liao, Z., Zhang, J., Liu, B., Yan, T., Xu, F., Xiao, F., et al. (2019). Polysaccharide from okra (abelmoschus esculentus (L.) moench) improves antioxidant capacity via PI3K/AKT pathways and Nrf2 translocation in a type 2 diabetes model. *Molecules* 24 (10), E1906. doi:10.3390/molecules24101906

Lin, M. T., and Beal, M. F. (2006). Mitochondrial dysfunction and oxidative stress in neurodegenerative diseases. *Nature* 443 (7113), 787–795. doi:10.1038/nature05292

Liu, J., Jia, L., Kan, J., and Jin, C. H. (2013a). *In vitro* and *in vivo* antioxidant activity of ethanolic extract of white button mushroom (Agaricus bisporus). *Food Chem. Toxicol.* 51, 310–316. doi:10.1016/j.fct.2012.10.014

Liu, J., Wu, Q., Yang, T., Yang, F., Guo, T., Zhou, Y., et al. (2021). Bioactive peptide F2d isolated from rice residue exerts antioxidant effects via Nrf2 signaling pathway. *Oxid. Med. Cell. Longev.* 2021, 2637577. doi:10.1155/2021/2637577

Liu, K., Wang, J., Zhao, L., and Wang, Q. (2013b). Anticancer, antioxidant and antibiotic activities of mushroom Ramaria flava. *Food Chem. Toxicol.* 58, 375–380. doi:10.1016/j.fct.2013.05.001

Liu, P., Zhao, H., and Luo, Y. (2017). Anti-aging implications of Astragalus membranaceus (huangqi): A well-known Chinese tonic. *Aging Dis.* 8 (6), 868–886. doi:10.14336/AD.2017.0816

Liu, Y., Gao, J., Peng, M., Meng, H., Ma, H., Cai, P., et al. (2018). A review on central nervous system effects of gastrodin. *Front. Pharmacol.* 9, 24. doi:10.3389/fphar.2018.00024

Liu, Z. Q. (2022). Why natural antioxidants are readily recognized by biological systems? 3D architecture plays a role. *Food Chem.* 380, 132143. doi:10.1016/j.foodchem.2022.132143

Lu, J., He, R., Sun, P., Zhang, F., Linhardt, R. J., and Zhang, A. (2020). Molecular mechanisms of bioactive polysaccharides from Ganoderma lucidum (Lingzhi), a review. *Int. J. Biol. Macromol.* 150, 765–774. doi:10.1016/j.ijbiomac.2020.02.035

Lu, Y., Jia, Y., Xue, Z., Li, N., Liu, J., and Chen, H. (2021). Recent developments in Inonotus obliquus (chaga mushroom) polysaccharides: Isolation, structural characteristics, biological activities and application. *Polym. (Basel)* 13 (9), 1441. doi:10.3390/polym13091441

Lv, J. H., Yao, L., Zhang, J. X., Wang, L. A., Zhang, J., Wang, Y. P., et al. (2021). Novel 2, 5-diarylcyclopentenone derivatives from the wild edible mushroom Paxillus involutus and their antioxidant activities. *J. Agric. Food Chem.* 69 (17), 5040–5048. doi:10.1021/acs.jafc.1c01160

Maity, P., Samanta, S., Nandi, A. K., Sen, I. K., Paloi, S., Acharya, K., et al. (2014). Structure elucidation and antioxidant properties of a soluble beta-D-glucan from mushroom Entoloma lividoalbum. *Int. J. Biol. Macromol.* 63, 140–149. doi:10.1016/j.ijbiomac.2013.10.040

Maity, P., Sen, I. K., Chakraborty, I., Mondal, S., Bar, H., Bhanja, S. K., et al. (2021). Biologically active polysaccharide from edible mushrooms: A review. *Int. J. Biol. Macromol.* 172, 408–417. doi:10.1016/j.ijbiomac.2021.01.081

Maity, P., Sen, I. K., Maji, P. K., Paloi, S., Devi, K. S., Acharya, K., et al. (2015). Structural, immunological, and antioxidant studies of beta-glucan from edible mushroom Entoloma lividoalbum. *Carbohydr. Polym.* 123, 350–358. doi:10.1016/j.carbpol.2015.01.051

Man, A. W. C., Li, H., and Xia, N. (2020). Impact of lifestyles (diet and exercise) on vascular health: Oxidative stress and endothelial function. *Oxid. Med. Cell. Longev.* 2020, 1496462. doi:10.1155/2020/1496462

Masuda, Y., Fujihara, K., Hayashi, S., Sasaki, H., Kino, Y., Kamauchi, H., et al. (2021). Inhibition of BACE1 and amyloid-beta aggregation by meroterpenoids from the mushroom Albatrellus yasudae. *J. Nat. Prod.* 84 (6), 1748–1754. doi:10.1021/acs.jnatprod.0c01329

Medzhitov, R. (2008). Origin and physiological roles of inflammation. *Nature* 454 (7203), 428–435. doi:10.1038/nature07201

Meng, P., Yang, R., Jiang, F., Guo, J., Lu, X., Yang, T., et al. (2021). Molecular mechanism of astragaloside IV in improving endothelial dysfunction of cardiovascular diseases mediated by oxidative stress. *Oxid. Med. Cell. Longev.* 2021, 1481236. doi:10.1155/2021/1481236

Miller, M. R. (2020). Oxidative stress and the cardiovascular effects of air pollution. *Free Radic. Biol. Med.* 151, 69–87. doi:10.1016/j.freeradbiomed.2020.01.004

Mishra, V., Banga, J., and Silveyra, P. (2018). Oxidative stress and cellular pathways of asthma and inflammation: Therapeutic strategies and pharmacological targets. *Pharmacol. Ther.* 181, 169–182. doi:10.1016/j.pharmthera.2017.08.011

Mishra, J., Rajput, R., Singh, K., Bansal, A., and Misra, K. (2019). Antioxidant-Rich peptide fractions derived from high-altitude Chinese caterpillar medicinal mushroom ophiocordyceps sinensis (ascomycetes) inhibit bacterial pathogens. *Int. J. Med. Mushrooms* 21 (2), 155–168. doi:10.1615/IntJMedMushrooms.2019030013

Moloney, J. N., and Cotter, T. G. (2018). ROS signalling in the biology of cancer. *Semin. Cell. Dev. Biol.* 80, 50–64. doi:10.1016/j.semcdb.2017.05.023

Mondal, A., Banerjee, D., Majumder, R., Maity, T. K., and Khowala, S. (2016). Evaluation of *in vitro* antioxidant, anticancer and *in vivo* antitumour activity of Termitomyces clypeatus MTCC 5091. *Pharm. Biol.* 54 (11), 2536–2546. doi:10.3109/13880209.2016.1168854

Murata, M. (2018). Inflammation and cancer. *Environ. Health Prev. Med.* 23 (1), 50. doi:10.1186/s12199-018-0740-1

Muszynska, B., Grzywacz-Kisielewska, A., Kala, K., and Gdula-Argasinska, J. (2018). Anti-inflammatory properties of edible mushrooms: A review. *Food Chem.* 243, 373–381. doi:10.1016/j.foodchem.2017.09.149

Navegantes-Lima, K. C., Monteiro, V. V. S., de Franca Gaspar, S. L., de Brito Oliveira, A. L., de Oliveira, J. P., Reis, J. F., et al. (2020). Agaricus brasiliensis mushroom protects against Sepsis by alleviating oxidative and inflammatory response. *Front. Immunol.* 11, 1238. doi:10.3389/fimmu.2020.01238

Nolfi-Donegan, D., Braganza, A., and Shiva, S. (2020). Mitochondrial electron transport chain: Oxidative phosphorylation, oxidant production, and methods of measurement. *Redox Biol.* 37, 101674. doi:10.1016/j.redox.2020.101674

Nowakowski, P., Markiewicz-Zukowska, R., Gromkowska-Kepka, K., Naliwajko, S. K., Moskwa, J., Bielecka, J., et al. (2021). Mushrooms as potential therapeutic agents in the treatment of cancer: Evaluation of anti-glioma effects of Coprinus comatus, Cantharellus cibarius, Lycoperdon perlatum and Lactarius deliciosus extracts. *Biomed. Pharmacother.* 133, 111090. doi:10.1016/j.biopha.2020.111090

Peoples, J. N., Saraf, A., Ghazal, N., Pham, T. T., and Kwong, J. Q. (2019). Mitochondrial dysfunction and oxidative stress in heart disease. *Exp. Mol. Med.* 51 (12), 1–13. doi:10.1038/s12276-019-0355-7

Petrovic, J., Papandreou, M., Glamoclija, J., Ciric, A., Baskakis, C., Proestos, C., et al. (2014). Different extraction methodologies and their influence on the bioactivity of the wild edible mushroom Laetiporus sulphureus (Bull.) Murrill. *Food Funct.* 5 (11), 2948–2960. doi:10.1039/c4fo00727a

Pizzino, G., Irrera, N., Cucinotta, M., Pallio, G., Mannino, F., Arcoraci, V., et al. (2017). Oxidative stress: Harms and benefits for human health. *Oxid. Med. Cell. Longev.* 2017, 8416763. doi:10.1155/2017/8416763

Powers, S. K., and Jackson, M. J. (2008). Exercise-induced oxidative stress: Cellular mechanisms and impact on muscle force production. *Physiol. Rev.* 88 (4), 1243–1276. doi:10.1152/physrev.00031.2007

Qian, L., Liu, H., Li, T., Liu, Y., Zhang, Z., and Zhang, Y. (2020). Purification, characterization and *in vitro* antioxidant activity of a polysaccharide AAP-3-1 from Auricularia auricula. *Int. J. Biol. Macromol.* 162, 1453–1464. doi:10.1016/j.ijbiomac.2020.07.314

Quindry, J., Dumke, C., Slivka, D., and Ruby, B. (2016). Impact of extreme exercise at high altitude on oxidative stress in humans. *J. Physiol.* 594 (18), 5093–5104. doi:10.1113/JP270651

Reuter, S., Gupta, S. C., Chaturvedi, M. M., and Aggarwal, B. B. (2010). Oxidative stress, inflammation, and cancer: How are they linked? *Free Radic. Biol. Med.* 49 (11), 1603–1616. doi:10.1016/j.freeradbiomed.2010.09.006

Rodrigues Barbosa, J., Dos Santos Freitas, M. M., da Silva Martins, L. H., and de Carvalho, R. N. J. (2020). Polysaccharides of mushroom Pleurotus spp.: New extraction techniques, biological activities and development of new technologies. *Carbohydr. Polym.* 229, 115550. doi:10.1016/j.carbpol.2019.115550

Rohm, T. V., Meier, D. T., Olefsky, J. M., and Donath, M. Y. (2022). Inflammation in obesity, diabetes, and related disorders. *Immunity* 55 (1), 31–55. doi:10.1016/j.immuni.2021.12.013

Ryoo, I. G., and Kwak, M. K. (2018). Regulatory crosstalk between the oxidative stress-related transcription factor Nfe2l2/Nrf2 and mitochondria. *Toxicol. Appl. Pharmacol.* 359, 24–33. doi:10.1016/j.taap.2018.09.014

Sakemi, Y., Hagiwara, M., Oikawa, A., Sato, M., Sato, S., Sawa, N., et al. (2021). Antioxidant p-terphenyl compounds in the mushroom Boletopsis leucomelas (PERS.) FAYOD and how they change via cooking. *Food Chem.* 363, 130281. doi:10.1016/j.foodchem.2021.130281

Sande, D., Oliveira, G. P., Moura, M., Martins, B. A., Lima, M., and Takahashi, J. A. (2019). Edible mushrooms as a ubiquitous source of essential fatty acids. *Food Res. Int.* 125, 108524. doi:10.1016/j.foodres.2019.108524

Sangtitanu, T., Sangtanoo, P., Srimongkol, P., Saisavoey, T., Reamtong, O., and Karnchanatat, A. (2020). Peptides obtained from edible mushrooms: Hericium erinaceus offers the ability to scavenge free radicals and induce apoptosis in lung cancer cells in humans. *Food Funct.* 11 (6), 4927–4939. doi:10.1039/d0fo00227e

Sarkozy, A., Kusz, N., Zomborszki, Z. P., Csorba, A., Papp, V., Hohmann, J., et al. (2020). Isolation and characterization of chemical constituents from the poroid medicinal mushroom porodaedalea chrysoloma (agaricomycetes) and their

antioxidant activity. *Int. J. Med. Mushrooms* 22 (2), 125–131. doi:10.1615/IntJMedMushrooms.2020033698

Sarfraz, A., Rasul, A., Sarfraz, I., Shah, M. A., Hussain, G., Shafiq, N., et al. (2020). Hispolon: A natural polyphenol and emerging cancer killer by multiple cellular signaling pathways. *Environ. Res.* 190, 110017. doi:10.1016/j.envres.2020.110017

Scuto, M., Di Mauro, P., Ontario, M. L., Amato, C., Modafferi, S., Ciavardelli, D., et al. (2019). Nutritional mushroom treatment in meniere's disease with coriolus versicolor: A rationale for therapeutic intervention in neuroinflammation and antineurodegeneration. *Int. J. Mol. Sci.* 21 (1), E284. doi:10.3390/ijms21010284

Shen, Y., Liu, X., Shi, J., and Wu, X. (2019). Involvement of Nrf2 in myocardial ischemia and reperfusion injury. *Int. J. Biol. Macromol.* 125, 496–502. doi:10.1016/j.ijbiomac.2018.11.190

Shu, X., Zhang, Y., Jia, J., Ren, X., and Wang, Y. (2019). Extraction, purification and properties of water-soluble polysaccharides from mushroom Lepista nuda. *Int. J. Biol. Macromol.* 128, 858–869. doi:10.1016/j.ijbiomac.2019.01.214

Singh, A., Kukreti, R., Saso, L., and Kukreti, S. (2019). Oxidative stress: A key modulator in neurodegenerative diseases. *Molecules* 24 (8), E1583. doi:10.3390/molecules24081583

Sinha, K., Das, J., Pal, P. B., and Sil, P. C. (2013). Oxidative stress: The mitochondria-dependent and mitochondria-independent pathways of apoptosis. *Arch. Toxicol.* 87 (7), 1157–1180. doi:10.1007/s00204-013-1034-4

Song, D., Hao, J., and Fan, D. (2020). Biological properties and clinical applications of berberine. *Front. Med.* 14 (5), 564–582. doi:10.1007/s11684-019-0724-6

Sonowal, H., Shukla, K., Kota, S., Saxena, A., and Ramana, K. V. (2018). Vialinin A, an edible mushroom-derived p-terphenyl antioxidant, prevents VEGF-induced neovascularization *in vitro* and *in vivo*. *Oxid. Med. Cell. Longev.* 2018, 1052102. doi:10.1155/2018/1052102

Sosa, V., Moline, T., Somoza, R., Paciucci, R., Kondoh, H., and Me, L. L. (2013). Oxidative stress and cancer: An overview. *Ageing Res. Rev.* 12 (1), 376–390. doi:10.1016/j.arr.2012.10.004

Stajic, M., Vukojevic, J., Knezevic, A., Lausevic, S. D., and Milovanovic, I. (2013). Antioxidant protective effects of mushroom metabolites. *Curr. Top. Med. Chem.* 13 (21), 2660–2676. doi:10.2174/15680266113136660192

Sun, Y., Hu, X., and Li, W. (2017). Antioxidant, antitumor and immunostimulatory activities of the polypeptide from Pleurotus eryngii mycelium. *Int. J. Biol. Macromol.* 97, 323–330. doi:10.1016/j.ijbiomac.2017.01.043

Tan, B. L., and Norhaizan, M. E. (2019). Effect of high-fat diets on oxidative stress, cellular inflammatory response and cognitive function. *Nutrients* 11 (11), E2579. doi:10.3390/nu11112579

Tan, B. L., Norhaizan, M. E., and Liew, W. P. (2018). Nutrients and oxidative stress: Friend or foe? *Oxid. Med. Cell. Longev.* 2018, 9719584. doi:10.1155/2018/9719584

Tee, J. K., Ong, C. N., Bay, B. H., Ho, H. K., and Leong, D. T. (2016). Oxidative stress by inorganic nanoparticles. *Wiley Interdiscip. Rev. Nanomed. Nanobiotechnol.* 8 (3), 414–438. doi:10.1002/wnan.1374

Thirupathi, A., Pinho, R. A., and Chang, Y. Z. (2020). Physical exercise: An inducer of positive oxidative stress in skeletal muscle aging. *Life Sci.* 252, 117630. doi:10.1016/j.lfs.2020.117630

Udeh, A. S., Ezebialu, C. U., Eze, E. A., and Engwa, G. A. (2021). Antibacterial and antioxidant activity of different extracts of some wild medicinal mushrooms from Nigeria. *Int. J. Med. Mushrooms* 23 (10), 83–95. doi:10.1615/IntJMedMushrooms.2021040197

Venturella, G., Ferraro, V., Cirlincione, F., and Gargano, M. L. (2021). Medicinal mushrooms: Bioactive compounds, use, and clinical trials. *Int. J. Mol. Sci.* 22 (2), E634. doi:10.3390/ijms22020634

Wang, J. H., Xu, J. L., Zhang, J. C., Liu, Y., Sun, H. J., and Zha, X. (2015). Physicochemical properties and antioxidant activities of polysaccharide from floral mushroom cultivated in Huangshan Mountain. *Carbohydr. Polym.* 131, 240–247. doi:10.1016/j.carbpol.2015.05.052

Wang, Q., Wang, F., Xu, Z., and Ding, Z. (2017). Bioactive mushroom polysaccharides: A review on monosaccharide composition, biosynthesis and regulation. *Molecules* 22 (6), 955. doi:10.3390/molecules22060955

Wellen, K. E., and Hotamisligil, G. S. (2005). Inflammation, stress, and diabetes. *J. Clin. Invest.* 115 (5), 1111–1119. doi:10.1172/JCI25102

West, A. P., Brodsky, I. E., Rahner, C., Woo, D. K., Erdjument-Bromage, H., Tempst, P., et al. (2011). TLR signalling augments macrophage bactericidal activity through mitochondrial ROS. *Nature* 472 (7344), 476–480. doi:10.1038/nature09973

Wongaem, A., Reamtong, O., Srimongkol, P., Sangtanoo, P., Saisavoey, T., and Karnchanatat, A. (2021). Antioxidant properties of peptides obtained from the split gill mushroom (Schizophyllum commune). *J. Food Sci. Technol.* 58 (2), 680–691. doi:10.1007/s13197-020-04582-4

Wu, J., Xia, S., Kalionis, B., Wan, W., and Sun, T. (2014). The role of oxidative stress and inflammation in cardiovascular aging. *Biomed. Res. Int.* 2014, 615312. doi:10.1155/2014/615312

Xi, X. J., Zeng, J. J., Lu, Y., Chen, S. H., Jiang, Z. W., He, P. J., et al. (2020). Extracellular vesicles enhance oxidative stress through P38/NF-kB pathway in ketamine-induced ulcerative cystitis. *J. Cell. Mol. Med.* 24 (13), 7609–7624. doi:10.1111/jcmm.15397

Xu, D. P., Zheng, J., Zhou, Y., Li, Y., Li, S., and Li, H. B. (2016). Extraction of natural antioxidants from the Thelephora ganbajun mushroom by an ultrasound-assisted extraction technique and evaluation of antiproliferative activity of the extract against human cancer cells. *Int. J. Mol. Sci.* 17 (10), E1664. doi:10.3390/ijms17101664

Yang, H. L., Liu, H. W., Shrestha, S., Thiyagarajan, V., Huang, H. C., and Hseu, Y. C. (2021). Antrodia salmonea induces apoptosis and enhances cytoprotective autophagy in colon cancer cells. *Aging (Albany NY)* 13 (12), 15964–15989. doi:10.18632/aging.203019

Yang, Q., Cai, X., Yan, A., Tian, Y., Du, M., and Wang, S. (2020). A specific antioxidant peptide: Its properties in controlling oxidation and possible action mechanism. *Food Chem.* 327, 126984. doi:10.1016/j.foodchem.2020.126984

Yang, S., Yan, J., Yang, L., Meng, Y., Wang, N., He, C., et al. (2019). Alkali-soluble polysaccharides from mushroom fruiting bodies improve insulin resistance. *Int. J. Biol. Macromol.* 126, 466–474. doi:10.1016/j.ijbiomac.2018.12.251

Yaribeygi, H., Sathyapalan, T., Atkin, S. L., and Sahebkar, A. (2020). Molecular mechanisms linking oxidative stress and diabetes mellitus. *Oxid. Med. Cell. Longev.* 2020, 8609213. doi:10.1155/2020/8609213

Yun, L., Wu, T., Mao, Z., Li, W., Zhang, M., and Sun, X. (2020). A novel wheat germ polysaccharide: Structural characterization, potential antioxidant activities and mechanism. *Int. J. Biol. Macromol.* 165, 1978–1987. doi:10.1016/j.ijbiomac.2020.10.112

Zhang, J., Zhang, J., Zhao, L., Shui, X., Wang, L. A., and Wu, Y. (2019). Antioxidant and anti-aging activities of ethyl acetate extract of the coral tooth mushroom, hericium coralloides (agaricomycetes). *Int. J. Med. Mushrooms* 21 (6), 561–570. doi:10.1615/IntJMedMushrooms.2019030840

Zhang, C., Song, X., Cui, W., and Yang, Q. (2021a). Antioxidant and anti-ageing effects of enzymatic polysaccharide from Pleurotus eryngii residue. *Int. J. Biol. Macromol.* 173, 341–350. doi:10.1016/j.ijbiomac.2021.01.030

Zhang, J. J., Chen, B. S., Dai, H. Q., Ren, J. W., Zhou, L. W., Wu, S. H., et al. (2021b). Sesquiterpenes and polyphenols with glucose-uptake stimulatory and antioxidant activities from the medicinal mushroom Sanghuangporus sanghuang. *Chin. J. Nat. Med.* 19 (9), 693–699. doi:10.1016/S1875-5364(21)60101-2

Zhang, P., Li, T., Wu, X., Nice, E. C., Huang, C., and Zhang, Y. (2020). Oxidative stress and diabetes: Antioxidative strategies. *Front. Med.* 14 (5), 583–600. doi:10.1007/s11684-019-0729-1

Zhang, Y., Liu, Z., Ng, T. B., Chen, Z., Qiao, W., and Liu, F. (2014). Purification and characterization of a novel antitumor protein with antioxidant and deoxyribonuclease activity from edible mushroom Pholiota nameko. *Biochimie* 99, 28–37. doi:10.1016/j.biochi.2013.10.016

Zhao, S., Cheng, C. K., Zhang, C. L., and Huang, Y. (2021). Interplay between oxidative stress, cyclooxygenases, and prostanoids in cardiovascular diseases. *Antioxid. Redox Signal.* 34 (10), 784–799. doi:10.1089/ars.2020.8105

Zheng, N., Ming, Y., Chu, J., Yang, S., Wu, G., Li, W., et al. (2021). Optimization of extraction process and the antioxidant activity of phenolics from sanghuangporus baumii. *Molecules* 26 (13), 3850. doi:10.3390/molecules26133850

Zhou, J., Chen, M., Wu, S., Liao, X., Wang, J., Wu, Q., et al. (2020). A review on mushroom-derived bioactive peptides: Preparation and biological activities. *Food Res. Int.* 134, 109230. doi:10.1016/j.foodres.2020.109230

Zucca, P., Rosa, A., Tuberoso, C. I., Piras, A., Rinaldi, A. C., Sanjust, E., et al. (2013). Evaluation of antioxidant potential of "Maltese mushroom" (Cynomorium coccineum) by means of multiple chemical and biological assays. *Nutrients* 5 (1), 149–161. doi:10.3390/nu5010149

Zuo, K., Tang, K., Liang, Y., Xu, Y., Sheng, K., Kong, X., et al. (2021). Purification and antioxidant and anti-Inflammatory activity of extracellular polysaccharopeptide from sanghuang mushroom, Sanghuangporus lonicericola. *J. Sci. Food Agric.* 101 (3), 1009–1020. doi:10.1002/jsfa.10709

Zuo, L., Prather, E. R., Stetskiv, M., Garrison, D. E., Meade, J. R., Peace, T. I., et al. (2019). Inflammaging and oxidative stress in human diseases: From molecular mechanisms to novel treatments. *Int. J. Mol. Sci.* 20 (18), E4472. doi:10.3390/ijms20184472

frontiers | Frontiers in Pharmacology

TYPE Correction
PUBLISHED 05 January 2023
DOI 10.3389/fphar.2022.1081523

OPEN ACCESS

EDITED AND REVIEWED BY
Li Wu,
Nanjing University of Chinese Medicine, China

*CORRESPONDENCE
Ziping Jiang,
waterjzp@jlu.edu.cn
Bin Liu,
l_bin@jlu.edu.cn

†These authors have contributed equally to this work

SPECIALTY SECTION
This article was submitted to Inflammation Pharmacology, a section of the journal Frontiers in Pharmacology

RECEIVED 27 October 2022
ACCEPTED 28 November 2022
PUBLISHED 05 January 2023

CITATION
Xia Y, Wang D, Li J, Chen M, Wang D, Jiang Z and Liu B (2023), Corrigendum: Compounds purified from edible fungi fight against chronic inflammation through oxidative stress regulation. *Front. Pharmacol.* 13:1081523. doi: 10.3389/fphar.2022.1081523

Corrigendum: Compounds purified from edible fungi fight against chronic inflammation through oxidative stress regulation

Yidan Xia[1†], Dongxu Wang[2†], Jiaqi Li[1], Minqi Chen[1], Duo Wang[1], Ziping Jiang[1*] and Bin Liu[1*]

[1]Department of Hand and Foot Surgery, The First Hospital of Jilin University, Changchun, China, [2]Laboratory Animal Center, College of Animal Science, Jilin University, Changchun, China

KEYWORDS

chronic diseases, natural compounds, edible fungi, antioxidants, molecular mechanisms

A Corrigendum on
Compounds purified from edible fungi fight against chronic inflammation through oxidative stress regulation

by Xia Y, Wang D, Li J, Chen M, Wang D, Jiang Z and Liu B (2022). Front. Pharmacol. 13:974794. doi: 10.3389/fphar.2022.974794

In the published article, the reference for "Recently, various compounds have been isolated from mushrooms, such as polysaccharides, alkaloids, peptides, terpenoids, and polyphenols (Leong et al., 2021)" was incorrectly written as (Leong et al., 2021). It should be (Homer and Sperry, 2017; Zhou et al., 2020; Kuang et al., 2021; Leong et al., 2021; Zhang et al., 2021).

In the published article, there was an error in **Table 1** as published. The references of Table 1 were incorrect due to our carelessness in proof section. The corrected Table 1 and its caption (Table 1 Antioxidant effects of compounds purified from mushrooms) appear below.

The authors apologize for this error and state that this does not change the scientific conclusions of the article in any way. The original article has been updated.

TABLE 1 Antioxidant effects of compounds purified from mushrooms.

Mushrooms	Compounds	Name	Antioxidant effects	References
Lepista nuda	Polysaccharide	LNP	Scavenge DPPH and $O_2^{\cdot-}$	Shu et al. (2019)
Entoloma lividoalbum	Polysaccharide	ELPS	Eliminate ·OH	Maity et al. (2015)
Flammulina velutipes	Polysaccharide	FVPs	Scavenge DPPH, ·OH, and $O_2^{\cdot-}$	Chen et al. (2019)
Floral mushroom	Polysaccharide	FMPS	Scavenge DPPH and ·OH	Wang et al. (2015)
Auricularia auricula	Polysaccharide	AAP-3-1	Increase the activities of SOD, GSH-PX, and CAT	Qian et al. (2020)
Oyster mushroom	Polysaccharide	Extract	Improve the antioxidant status during ageing	Jayakumar et al. (2007)
Pleurotus ostreatus	Polysaccharide	Extract	Protect against oxidative damage induced by H_2O_2	Barbosa et al. (2020)
Pleurotus djamor	Polysaccharide	Extract	Scavenge DPPH and ·OH	Maity et al. (2021)
Pleurotus eryngii	Polysaccharide	PERP	Scavenge reactive radicals and improve the antioxidant status	Zhang et al. (2021a)
Hohenbuehelia serotina	Polysaccharide	NTHSP-A1	Scavenging abilities of ABTS radical and ·OH radical	Li et al. (2017b)
Maitake	Peptide	Glutathione	Antioxidant property	Kalaras et al. (2017)
Matsutake	Peptide	WFNNAGP	Scavenge ·OH and promote the SOD activity	Li et al. (2021)
Agaricus bisporus	Peptide	MPI	Neutralize free radicals to resist oxidative stress	Kimatu et al. (2017)
Schizophyllum commune	Peptide	Extract	Free radical scavenging activity	Wongaem et al. (2021)
Ophiocordyceps sinensis	Peptide	COP	Scavenge DPPH radical and chelate heavy metal ions	Mishra et al. (2019)
Hericium erinaceus	Peptide	Extract	ABTS, DPPH and NO radical scavenging activities	Sangtitanu et al. (2020)
Agaricus blazei	Peptide	ABp	Change the contents of T-AOC, MDA, CAT, and ROS	Feng et al. (2021)
Pleurotus eryngii	Peptide	PEMP	Scavenge DPPH, ·OH, and $O_2^{\cdot-}$ radicals	Sun et al. (2017)
Sanghuangporus sanghuang	Polyphenol	Extract	Good cellular antioxidant activities	Zhang et al. (2021b)
Flammulina velutipes	Polyphenol	FFVP	Inhibit the secretion of NO and ROS	Ma et al. (2021)
Phlebopus portentosus	Polyphenol	Extract	DPPH scavenging activity and ferric reducing antioxidant power	Kumla et al. (2021)
Phellinus linteus	Polyphenol	Hispolon	Strong free radical scavenging ability	Sarfraz et al. (2020)
Flammulina velutipes	Polyphenol	FVF	Increase glutathione level and SOD activity and inhibit the accumulation of intracellular ROS	Hu et al. (2016)
Boletus edulis and *Cantharellus cibarius*	Polyphenol	Extract	The aqueous extract showed the strongest antioxidant activity	Fogarasi et al. (2021)
Sanghuangporus baumii	Polyphenol	Extract	Scavenge ·OH, DPPH, and ABTS	Zheng et al. (2021)
Boletopsis leucomelas	P-terphenyl compound	Extract	Effective DPPH scavenging capacity	Sakemi et al. (2021)
T. terrestris and T. vialis	P-terphenyl compound	Extract	Prevent VEGF-induced production of ROS and malondialdehyde	Sonowal et al. (2018)
Hericium erinaceum	Sterol	Extract	Cellular antioxidant activity	Li et al. (2017a)
Pholiota nameko	Protein	PNAP	Scavenge ·OH and DPPH	Zhang et al. (2014)
Sanghuangporus sanghuang	Terpenoid	Extract	Scavenge DPPH and ABTS free radicals	Zhang et al. (2021b)
Paxillus involutus	2,5-diarylcyclopentenone	Extract	Clearing abilities of DPPH, ·OH, and $O_2^{\cdot-}$	Lv et al. (2021)
Agaricomycetes	Extract	Extract	Significantly increase the activities of SOD, CAT and GSH-Px	Zhang et al. (2019)
Agaricus bisporus	Extract	Extract	Enhance the activities of antioxidant enzymes	Liu et al. (2013a)
Lactarius salmonicolor	Extract	Extract	Show the most potent radical scavenging activity	Athanasakis et al. (2013)
Ramaria flava	Extract	Extract	High DPPH and ·OH radical-scavenging activities	Liu et al. (2013b)

(Continued on following page)

TABLE 1 (*Continued*) Antioxidant effects of compounds purified from mushrooms.

Mushrooms	Compounds	Name	Antioxidant effects	References
Chaga	Extract	Extract	Scavenging activity against the ABTS radical cation and DPPH radical.	Lee et al. (2007)
Porodaedalea chrysoloma	Extract	Extract	Possess considerable antioxidant effect	Sarkozy et al. (2020)
Orange coral mushroom	Extract	Extract	Good free radical scavenges and reduce capacities	Aprotosoaie et al. (2017)
Cynomorium coccineum	Extract	Extract	ORAC-PYR assay gives the highest antioxidant value in both cases	Zucca et al. (2013)
Entoloma lividoalbum	Extract	Extract	Possess hydroxyl and superoxide radical-scavenging activities	Maity et al. (2014)
Flammulina velutipes	Extract	Extract	High DPPH radical scavenging activity	Bao et al. (2008)
Pleurotus ostreatus	Extract	Extract	High DPPH and hydrogen peroxide scavenging potential	Udeh et al. (2021)
Agaricus brasiliensis	Extract	Extract	Protect against sepsis by alleviating oxidative and inflammatory response	Navegantes-Lima et al. (2020)

Publisher's note

References

Aprotosoaie, A. C., Zavastin, D. E., Mihai, C. T., Voichita, G., Gherghel, D., Silion, M., et al. (2017). Antioxidant and antigenotoxic potential of Ramaria largentii Marr & D. E. Stuntz, a wild edible mushroom collected from Northeast Romania. *Food Chem. Toxicol.* 108, 429–437. doi:10.1016/j.fct.2017.02.006

Athanasakis, G., Aligiannis, N., Gonou-Zagou, Z., Skaltsounis, A. L., and Fokialakis, N. (2013). Antioxidant properties of the wild edible mushroom Lactarius salmonicolor. *J. Med. Food* 16 (8), 760–764. doi:10.1089/jmf.2012.0297

Bao, H. N., Ushio, H., and Ohshima, T. (2008). Antioxidative activity and antidiscoloration efficacy of ergothioneine in mushroom (Flammulina velutipes) extract added to beef and fish meats. *J. Agric. Food Chem.* 56 (21), 10032–10040. doi:10.1021/jf8017063

Barbosa, J. R., Mm, S. F., Oliveira, L. C., Lh, S. M., Almada-Vilhena, A. O., Oliveira, R. M., et al. (2020). Obtaining extracts rich in antioxidant polysaccharides from the edible mushroom Pleurotus ostreatus using binary system with hot water and supercritical CO2. *Food Chem.* 330, 127173. doi:10.1016/j.foodchem.2020.127173

Chen, X., Fang, D., Zhao, R., Gao, J., Kimatu, B. M., Hu, Q., et al. (2019). Effects of ultrasound-assisted extraction on antioxidant activity and bidirectional immunomodulatory activity of Flammulina velutipes polysaccharide. *Int. J. Biol. Macromol.* 140, 505–514. doi:10.1016/j.ijbiomac.2019.08.163

Feng, Q., Li, Y., Lu, X., Yu, Y., Yuan, G., Sun, J., et al. (2021). Agaricus blazei polypeptide exerts a protective effect on D-galactose-induced aging mice via the Keap1/Nrf2/ARE and P53/Trim32 signaling pathways. *J. Food Biochem.* 45 (1), e13555. doi:10.1111/jfbc.13555

Fogarasi, M., Socaciu, M. I., Salagean, C. D., Ranga, F., Farcas, A. C., Socaci, S. A., et al. (2021). Comparison of different extraction solvents for characterization of antioxidant potential and polyphenolic composition in boletus edulis and cantharellus cibarius mushrooms from Romania. *Molecules* 26 (24), 7508. doi:10.3390/molecules26247508

Homer, J. A., and Sperry, J. (2017). Mushroom-Derived indole alkaloids. *J. Nat. Prod.* 80 (7), 2178–2187. doi:10.1021/acs.jnatprod.7b00390

Hu, Q., Yu, J., Yang, W., Kimatu, B. M., Fang, Y., Ma, N., et al. (2016). Identification of flavonoids from Flammulina velutipes and its neuroprotective effect on pheochromocytoma-12 cells. *Food Chem.* 204, 274–282. doi:10.1016/j.foodchem.2016.02.138

Jayakumar, T., Thomas, P. A., and Geraldine, P. (2007). Protective effect of an extract of the oyster mushroom, Pleurotus ostreatus, on antioxidants of major organs of aged rats. *Exp. Gerontol.* 42 (3), 183–191. doi:10.1016/j.exger.2006.10.006

Kalaras, M. D., Richie, J. P., Calcagnotto, A., and Beelman, R. B. (2017). Mushrooms: A rich source of the antioxidants ergothioneine and glutathione. *Food Chem.* 233, 429–433. doi:10.1016/j.foodchem.2017.04.109

Kimatu, B. M., Zhao, L., Biao, Y., Ma, G., Yang, W., Pei, F., et al. (2017). Antioxidant potential of edible mushroom (Agaricus bisporus) protein hydrolysates and their ultrafiltration fractions. *Food Chem.* 230, 58–67. doi:10.1016/j.foodchem.2017.03.030

Kuang, Y., Li, B., Wang, Z., Qiao, X., and Ye, M. (2021). Terpenoids from the medicinal mushroom antrodia camphorata: Chemistry and medicinal potential. *Nat. Prod. Rep.* 38 (1), 83–102. doi:10.1039/d0np00023j

Kumla, J., Suwannarach, N., Tanruean, K., and Lumyong, S. (2021). Comparative evaluation of chemical composition, phenolic compounds, and antioxidant and antimicrobial activities of tropical black bolete mushroom using different preservation methods. *Foods* 10 (4), 781. doi:10.3390/foods10040781

Lee, I. K., Kim, Y. S., Jang, Y. W., Jung, J. Y., and Yun, B. S. (2007). New antioxidant polyphenols from the medicinal mushroom Inonotus obliquus. *Bioorg. Med. Chem. Lett.* 17 (24), 6678–6681. doi:10.1016/j.bmcl.2007.10.072

Leong, Y. K., Yang, F. C., and Chang, J. S. (2021). Extraction of polysaccharides from edible mushrooms: Emerging technologies and recent advances. *Carbohydr. Polym.* 251, 117006. doi:10.1016/j.carbpol.2020.117006

Li, M., Lv, R., Wang, C., Ge, Q., Du, H., and Lin, S. (2021). Tricholoma matsutake-derived peptide WFNNAGP protects against DSS-induced colitis by ameliorating oxidative stress and intestinal barrier dysfunction. *Food Funct.* 12 (23), 11883–11897. doi:10.1039/d1fo02806e

Li, W., Lee, S. H., Jang, H. D., Ma, J. Y., and Kim, Y. H. (2017a). Antioxidant and anti-osteoporotic activities of aromatic compounds and sterols from hericium erinaceum. *Molecules* 22 (1), 108. doi:10.3390/molecules22010108

Li, X., Wang, L., and Wang, Z. (2017b). Structural characterization and antioxidant activity of polysaccharide from Hohenbuehelia serotina. *Int. J. Biol. Macromol.* 98, 59–66. doi:10.1016/j.ijbiomac.2016.12.089

Liu, J., Jia, L., Kan, J., and Jin, C. H. (2013a). *In vitro* and *in vivo* antioxidant activity of ethanolic extract of white button mushroom (Agaricus bisporus). *Food Chem. Toxicol.* 51, 310–316. doi:10.1016/j.fct.2012.10.014

Liu, K., Wang, J., Zhao, L., and Wang, Q. (2013b). Anticancer, antioxidant and antibiotic activities of mushroom Ramaria flava. *Food Chem. Toxicol.* 58, 375–380. doi:10.1016/j.fct.2013.05.001

Lv, J. H., Yao, L., Zhang, J. X., Wang, L. A., Zhang, J., Wang, Y. P., et al. (2021). Novel 2, 5-diarylcyclopentenone derivatives from the wild edible mushroom paxillus involutus and their antioxidant activities. *J. Agric. Food Chem.* 69 (17), 5040–5048. doi:10.1021/acs.jafc.1c01160

Ma, S., Zhang, H., and Xu, J. (2021). Characterization, antioxidant and anti-inflammation capacities of fermented flammulina velutipes polyphenols. *Molecules* 26 (20), 6205. doi:10.3390/molecules26206205

Maity, G. N., Maity, P., Khatua, S., Acharya, K., Dalai, S., and Mondal, S. (2021). Structural features and antioxidant activity of a new galactoglucan from edible mushroom Pleurotus djamor. *Int. J. Biol. Macromol.* 168, 743–749. doi:10.1016/j.ijbiomac.2020.11.131

Maity, P., Samanta, S., Nandi, A. K., Sen, I. K., Paloi, S., Acharya, K., et al. (2014). Structure elucidation and antioxidant properties of a soluble beta-D-glucan from mushroom Entoloma lividoalbum. *Int. J. Biol. Macromol.* 63, 140–149. doi:10.1016/j.ijbiomac.2013.10.040

Maity, P., Sen, I. K., Maji, P. K., Paloi, S., Devi, K. S., Acharya, K., et al. (2015). Structural, immunological, and antioxidant studies of beta-glucan from edible mushroom Entoloma lividoalbum. *Carbohydr. Polym.* 123, 350–358. doi:10.1016/j.carbpol.2015.01.051

Mishra, J., Rajput, R., Singh, K., Bansal, A., and Misra, K. (2019). Antioxidant-Rich peptide fractions derived from high-altitude Chinese caterpillar medicinal mushroom ophiocordyceps sinensis (ascomycetes) inhibit bacterial pathogens. *Int. J. Med. Mushrooms* 21 (2), 155–168. doi:10.1615/IntJMedMushrooms.2019030013

Navegantes-Lima, K. C., Monteiro, V. V. S., de Franca Gaspar, S. L., de Brito Oliveira, A. L., de Oliveira, J. P., Reis, J. F., et al. (2020). Agaricus brasiliensis mushroom protects against sepsis by alleviating oxidative and inflammatory response. *Front. Immunol.* 11, 1238. doi:10.3389/fimmu.2020.01238

Qian, L., Liu, H., Li, T., Liu, Y., Zhang, Z., and Zhang, Y. (2020). Purification, characterization and *in vitro* antioxidant activity of a polysaccharide AAP-3-1 from Auricularia auricula. *Int. J. Biol. Macromol.* 162, 1453–1464. doi:10.1016/j.ijbiomac.2020.07.314

Sakemi, Y., Hagiwara, M., Oikawa, A., Sato, M., Sato, S., Sawa, N., et al. (2021). Antioxidant p-terphenyl compounds in the mushroom Boletopsis leucomelas (PERS.) FAYOD and how they change via cooking. *Food Chem.* 363, 130281. doi:10.1016/j.foodchem.2021.130281

Sangtitanu, T., Sangtanoo, P., Srimongkol, P., Saisavoey, T., Reamtong, O., and Karnchanatat, A. (2020). Peptides obtained from edible mushrooms: Hericium erinaceus offers the ability to scavenge free radicals and induce apoptosis in lung cancer cells in humans. *Food Funct.* 11 (6), 4927–4939. doi:10.1039/d0fo00227e

Sarfraz, A., Rasul, A., Sarfraz, I., Shah, M. A., Hussain, G., Shafiq, N., et al. (2020). Hispolon: A natural polyphenol and emerging cancer killer by multiple cellular signaling pathways. *Environ. Res.* 190, 110017. doi:10.1016/j.envres.2020.110017

Sarkozy, A., Kusz, N., Zomborszki, Z. P., Csorba, A., Papp, V., Hohmann, J., et al. (2020). Isolation and characterization of chemical constituents from the poroid medicinal mushroom porodaedalea chrysoloma (agaricomycetes) and their antioxidant activity. *Int. J. Med. Mushrooms* 22 (2), 125–131. doi:10.1615/IntJMedMushrooms.2020033698

Shu, X., Zhang, Y., Jia, J., Ren, X., and Wang, Y. (2019). Extraction, purification and properties of water-soluble polysaccharides from mushroom Lepista nuda. *Int. J. Biol. Macromol.* 128, 858–869. doi:10.1016/j.ijbiomac.2019.01.214

Sonowal, H., Shukla, K., Kota, S., Saxena, A., and Ramana, K. V. (2018). Vialinin A, an edible mushroom-derived p-terphenyl antioxidant, prevents VEGF-induced neovascularization *in vitro* and *in vivo*. *Oxid. Med. Cell. Longev.* 2018, 1052102. doi:10.1155/2018/1052102

Sun, Y., Hu, X., and Li, W. (2017). Antioxidant, antitumor and immunostimulatory activities of the polypeptide from Pleurotus eryngii mycelium. *Int. J. Biol. Macromol.* 97, 323–330. doi:10.1016/j.ijbiomac.2017.01.043

Udeh, A. S., Ezebialu, C. U., Eze, E. A., and Engwa, G. A. (2021). Antibacterial and antioxidant activity of different extracts of some wild medicinal mushrooms from Nigeria. *Int. J. Med. Mushrooms* 23 (10), 83–95. doi:10.1615/IntJMedMushrooms.2021040197

Wang, J. H., Xu, J. L., Zhang, J. C., Liu, Y., Sun, H. J., and Zha, X. (2015). Physicochemical properties and antioxidant activities of polysaccharide from floral mushroom cultivated in Huangshan Mountain. *Carbohydr. Polym.* 131, 240–247. doi:10.1016/j.carbpol.2015.05.052

Wongaem, A., Reamtong, O., Srimongkol, P., Sangtanoo, P., Saisavoey, T., and Karnchanatat, A. (2021). Antioxidant properties of peptides obtained from the split gill mushroom (Schizophyllum commune). *J. Food Sci. Technol.* 58 (2), 680–691. doi:10.1007/s13197-020-04582-4

Zhang, C., Song, X., Cui, W., and Yang, Q. (2021a). Antioxidant and anti-ageing effects of enzymatic polysaccharide from Pleurotus eryngii residue. *Int. J. Biol. Macromol.* 173, 341–350. doi:10.1016/j.ijbiomac.2021.01.030

Zhang, J. J., Chen, B. S., Dai, H. Q., Ren, J. W., Zhou, L. W., Wu, S. H., et al. (2021b). Sesquiterpenes and polyphenols with glucose-uptake stimulatory and antioxidant activities from the medicinal mushroom Sanghuangporus sanghuang. *Chin. J. Nat. Med.* 19 (9), 693–699. doi:10.1016/S1875-5364(21)60101-2

Zhang, J. J., Chen, B. S., Dai, H. Q., Ren, J. W., Zhou, L. W., Wu, S. H., et al. (2021). Sesquiterpenes and polyphenols with glucose-uptake stimulatory and antioxidant activities from the medicinal mushroom Sanghuangporus sanghuang. *Chin. J. Nat. Med.* 19 (9), 693–699. doi:10.1016/S1875-5364(21)60101-2

Zhang, J., Zhang, J., Zhao, L., Shui, X., Wang, L. A., and Wu, Y. (2019). Antioxidant and anti-aging activities of ethyl acetate extract of the coral tooth mushroom, hericium coralloides (agaricomycetes). *Int. J. Med. Mushrooms* 21 (6), 561–570. doi:10.1615/IntJMedMushrooms.2019030840

Zhang, Y., Liu, Z., Ng, T. B., Chen, Z., Qiao, W., and Liu, F. (2014). Purification and characterization of a novel antitumor protein with antioxidant and deoxyribonuclease activity from edible mushroom Pholiota nameko. *Biochimie* 99, 28–37. doi:10.1016/j.biochi.2013.10.016

Zheng, N., Ming, Y., Chu, J., Yang, S., Wu, G., Li, W., et al. (2021). Optimization of extraction process and the antioxidant activity of phenolics from sanghuangporus baumii. *Molecules* 26 (13), 3850. doi:10.3390/molecules26133850

Zhou, J., Chen, M., Wu, S., Liao, X., Wang, J., Wu, Q., et al. (2020). A review on mushroom-derived bioactive peptides: Preparation and biological activities. *Food Res. Int.* 134, 109230. doi:10.1016/j.foodres.2020.109230

Zucca, P., Rosa, A., Tuberoso, C. I., Piras, A., Rinaldi, A. C., Sanjust, E., et al. (2013). Evaluation of antioxidant potential of "Maltese mushroom" (Cynomorium coccineum) by means of multiple chemical and biological assays. *Nutrients* 5 (1), 149–161. doi:10.3390/nu5010149

frontiers | Frontiers in Pharmacology

TYPE Original Research
PUBLISHED 03 October 2022
DOI 10.3389/fphar.2022.995523

OPEN ACCESS

EDITED BY
Li Wu,
Nanjing University of Chinese Medicine, China

REVIEWED BY
Giovanni Tarantino,
University of Naples Federico II, Italy
Marta Chagas Monteiro,
Federal University of Pará, Brazil
JingHong Wan,
INSERM U1149 Centre de Recherche sur l'Inflammation, France

*CORRESPONDENCE
Mingrong Cao,
tcaomr@jnu.edu.cn
Jian Hong,
hongjian7@jnu.edu.cn

†These authors have contributed equally to this work and share first authorship

SPECIALTY SECTION
This article was submitted to Inflammation Pharmacology, a section of the journal Frontiers in Pharmacology

RECEIVED 16 July 2022
ACCEPTED 14 September 2022
PUBLISHED 03 October 2022

CITATION
Xiao Y, Gao C, Wu J, Li J, Wang L, You Y, Peng T, Zhang K, Cao M and Hong J (2022), Periplaneta americana extract alleviates steatohepatitis in a mouse model by modulating HMGB1-mediated inflammatory response.
Front. Pharmacol. 13:995523.
doi: 10.3389/fphar.2022.995523

Periplaneta americana extract alleviates steatohepatitis in a mouse model by modulating HMGB1-mediated inflammatory response

Yang Xiao[1†], Chongqing Gao[2†], Junru Wu[2†], Jing Li[2], Lijuan Wang[2], Yang You[2], Tianqi Peng[1], Keke Zhang[2], Mingrong Cao[1*] and Jian Hong[1,2*]

[1]Department of Hepatological Surgery, The First Affiliated Hospital, Jinan University, Guangzhou, China, [2]Department of Pathophysiology, School of Medicine, Jinan University, Guangzhou, China

Alcoholic abuse and obesity are the most common lifestyle implications of chronic liver injury, and always act synergistically to increase the risk of mortality. *Periplaneta americana* has a long history of being applied in medicine, including wound healing, antitumor, antibacterial, antiviral, antifibrotic, and cardiomyocyte-protecting. Ganlong capsule (GLC), a natural prescription drug extracted from *Periplaneta americana*, has been widely used in HBV-related symptoms. However, the anti-steatohepatitis efficacy and mechanisms of GLC have not yet been characterized. Here, we found the protective effect of GLC on the development of hepatic steatosis, oxidative stress, and inflammation *in vivo* under alcohol exposure combined with a high-fat and high-cholesterol diet (HFHC). Consistently, GLC exhibited a hepatoprotective property by preventing hepatocytes from oxidative stress injury and lipid accumulation *in vitro*. In addition, it exerted an anti-inflammation characteristic by reducing macrophage recruitment and decreasing the expression of pro-inflammatory genes *in vivo* and *in vitro*. Mechanically, GLC serum, isolated from GLC-treated mice, reduced extracellular high-mobility group box 1 (HMGB1) of dying hepatocytes; and suppressed subsequent M1 polarization of macrophages in the co-culture system. Furthermore, GLC serum inhibited inflammatory response *via* suppressing the HMGB1 release and blocking the downstream TLR4/NF-kB pathway. Collectively, GLC alleviates steatohepatitis induced by alcohol consumption and obesity through inhibition of the HMGB1-mediated inflammatory cascade. GLC might be a therapeutic candidate for the treatment of steatohepatitis developed by alcohol abuse and metabolic disorders.

KEYWORDS

steatohepatitis, alcohol consumption, obesity, periplaneta americana extractions (PAEs), high-mobility group box1 (HMGB1)

Introduction

Chronic liver disease (CLD) is one of the leading causes of death worldwide; around 844 million people suffer from CLD resulting in approximately two million deaths per year (Byass, 2014). At present, obesity and alcohol consumption are the two main causes of CLD (Ntandja Wandji., et al., 2020), promoting the development of alcoholic liver disease (ALD) and non-alcoholic fatty liver disease (NAFLD), respectively. While one of the two factors is always predominant, there is considerable evidence indicating that hazardous alcohol use and obesity-associated metabolic disorders act synergistically to aggravate the progression of fatty liver disease (Aberg., et al., 2020).

The spectrum of liver injury in ALD and NAFLD is quite similar, ranging from steatosis, and steatohepatitis to fibrosis, cirrhosis, and hepatocellular carcinoma (HCC) (MacSween and Burt, 1986; Matteoni., et al., 1999). However, although obesity is an essential contributor to NAFLD, less than 5% of NAFLD patients will ever develop a complicated liver disease (Tsukamoto., et al., 2009). Similarly, even though a strong dose-response relationship between alcohol intake and liver cirrhosis mortality in the ALD population, only 6.26%–10.7% of heavy drinkers develop cirrhosis during their lifetime (Roerecke., et al., 2019). The fact has led to a hypothesis that excessive intake of alcohol or calories is the first hit to induce hepatic steatosis, the early stage of ALD or NAFLD. The second hit is required in the progress of steatohepatitis and cirrhosis (Tsukamoto, Machida, Dynnyk and Mkrtchyan, 2009). Indeed, numerous studies have pointed out that alcohol and obesity synergistically increase the development of hepatic fibrosis and cirrhosis. The result of a French study showed that being overweight (defined as a BM1 $\geq$ 25 kg/m^2 in women and $\geq$27 in men) for at least 10 years was independently associated with the risk of steatosis, alcoholic hepatitis and cirrhosis (Raynard., et al., 2002).

Although a severe liver injury caused by alcohol abuse combined with obesity, the treatment for such a complicated liver disease remains unsatisfactory. Alcohol abstinence, nutrition intervention and controlling body weight are crucial for patients with ALD and NAFLD. However, only a minority of patients with NAFLD achieve weight loss and some regular drinkers still consume alcohol despite medical advice. Thus, pharmacological interventions may be needed. Corticosteroids are the only validated treatment for ALD in the subgroup of patients with severe alcoholic hepatitis (Louvet., et al., 2018). Although various pharmacological approaches aiming to alleviate NAFLD-NASH are currently being examined at different phases of clinical trials (Negi., et al., 2022); no drug is approved by Food and drug administration (FDA) for the treatment of NAFLD.

Periplaneta Americana, the American cockroach, has a long history of application for the treatment of various injuries (Wang., et al., 2011; Zhu., et al., 2018). Over the past few years, considerable studies have identified extracts of *Periplaneta* Americana (PAEs) have tissue repair (Yang., et al., 2015), antitumor (Zhao., et al., 2017), antibacterial (Ma et al., 2018), antifungal (Yun et al., 2017), antifibrotic, antiosteoporotic, cardiomyocyte-protecting, and immunity-enhancing efficacy (Zou et al., 2020). However, PAEs have not been explored in clinical applications as a result of the difficulty in purifying the active constituents and the unclear molecular mechanisms. There are only a few representative clinical PAEs prescriptions such as "Kangfuxin solution", "Xinmailong injection", and "Ganlong capsule (GLC)" that have been approved to use in clinical treatment until recent years. Particularly, GLC has been widely used in the treatment of chronic hepatitis B in China. The main ingredients of GLC are sticky sugar amino acid, which was identified as the property of immunological regulation and hepatoprotective (Lv, 2017). Sun analyzed the component of water-soluble polysaccharides from cockroaches. The immunological test in normal mice showed the polysaccharide of cockroaches could significantly increase the phagocytic percentage and index of macrophages (Sun et al., 2022). It has been reported that GLC showed a protective effect on chronic liver injury induced by alcohol (Zhang., et al., 2013). However, it remains unclear whether GLC could inhibit steatohepatitis progress driven by both alcohol and obesity.

Here, in this study, we explored the possible protective mechanisms of GLC on liver injury and the progression of steatohepatitis in a mouse model with alcoholics plus a high-fat high-cholesterol diet (EHFD).

Material and methods

Chemicals and reagents

Ganlong capsule was purchased from Kunming SINOWAY Natural Pharmaceuticals Co., Ltd (21062101). Palmitic acid was purchased from Sorabio Science and Technology Co., Ltd (Beijing, China).

Animals and treatments

Male C57BL/6J mice (5–8 weeks old, SPF grade), weighing 20 ± 2 g, were purchased from Zhejiang Vital River Laboratory Animal Technology Co., Ltd (Zhejiang, China) and Guangzhou Ruige Biological Technology Co., Ltd (Guangzhou, China) respectively. The animal welfare practices and animal experimental protocols were strictly consistent with the Guide for the Care and Use of Laboratory Animals, all experimental procedure was officially approved by The Animal Ethics Committee of Jinan University. Animals were maintained in a controlled environment with a temperature of 20°C–26°C and

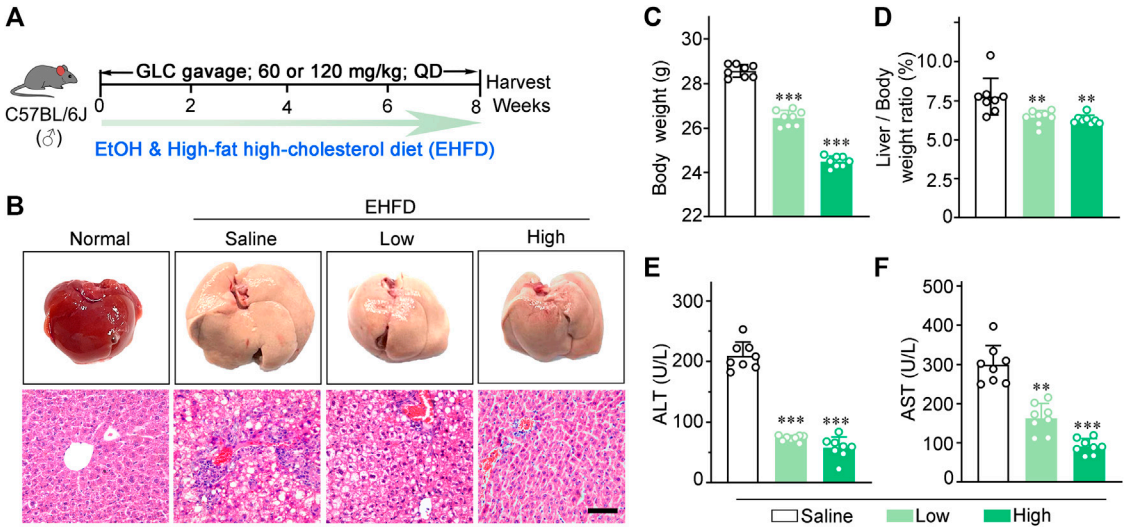

FIGURE 1
GLC alleviates steatohepatitis induced by EHFD diet. **(A)** Schematic of the liver injury mouse model induced by EHFD diet. **(B)** Representative images of the mouse liver and H&E staining with EHFD treatment. Scale bars, 50 μm. **(C)** The final body weight and **(D)** liver index of EHFD mice (n = 8 for each group). **(E)** Serum ALT and **(F)** AST levels of EHFD mice with or without GLC treatment $^{**}P < 0.01$ vs. the EHFD mice with the treatment of saline; $^{***}P < 0.001$ vs. the EHFD mice with the treatment of saline.

relative humidity of 40–70% under a 12-h light/dark cycle, with standard food and water *ad libitum*.

Mice were randomly assigned to the following groups: 1) the control group, which received a standard chow diet (5% fat w/w); 2) the EHFD group, which received a high-fat high-cholesterol diet (containing 17% fat and supplemented with 1.25% cholesterol and 0.5% cholate) which was obtained from Trophic Animal Feed High-tech Co. Ltd (China), with *ad libitum* access to alcohol in drinking water with increasing concentrations of alcohol (1% v/v of alcohol for the first 2 days, 2% from day 3 to day 7, 4% for the second week, and 5% for another 6 weeks); 3) the EHFD + Low group, based on EHFD group, mice were gavaged with 60 mg/kg BW GLC solution per day for 8 weeks; 4) the EHFD + High, based on EHFD group, mice were gavaged with 120 mg/kg BW GLC solution per day for 8 weeks. The control, EHFD mice were given saline at equivalent volumes as the treatment group. The schematic of the animal experiment was shown in Figure 1A. The mice were euthanized at the age of 14 weeks after fasting for 16 h, and the serum and liver tissue were harvested for subsequent measurement.

Collection of GLC serum

To determine the preventive effect of GLC on liver injury, some normal mice were given GLC treatment with a standard dose according to the clinical use for the patient. GLC-treated group mice were gavaged with GLC (90 mg/kg, twice per day) for 7 days. The control mice were given the same volume of normal 0.9% saline. After 2 h of the last gavage, the mice serum was collected and heat-inactivated at 56°C for 30min, then stored at -20°C for the subsequent experiment (Qin et al., 2021; Zhang, 2021).

Cell culture and treatments

NCTC1469 and J774A.1 cell line was obtained from the Procell Life Science & Technology Co., Ltd (Wuhan, China) and Newgainbio Co., Ltd (Wuxi, China), and cultured in DMEM supplemented with 10% fetal bovine serum and 1% penicillin streptomycin at 37°C in a 5% CO_2 humidified atmosphere. We collected portal vein serum from normal male C57BL/6J mice (Ctrl serum) and only GLC gavage-treated male C57BL/6J mice (GLC serum) at a dose of 90 mg/kg BW for 2 h. NCTC1469 cells were treated with GLC serum or other agents when they were 50–60% confluence. GLC serum was added 6h before the treatment of ethanol or palmitic acid.

Co-culture of hepatocytes and macrophages

NCTC1469 cell lines were seeded in 12-well plates, and different concentrations of GLC serum or Ctrl serum

dissolved in serum-free media were pretreated for 6 h when they were 50%–60% confluence. Ethanol (400 mM) was added to the culture medium 6 h later. The supernatant was collected as a condition medium for the macrophages. J774A.1 cell lines were seeded in a 12-well plate at a density of 5×10^5/well for 24 h, then treated with condition medium at 1:2 dilution in serum-free media for 24 h. Cells were collected for subsequent experiments.

Biochemical analysis

The serum biochemical markers, including alanine aminotransferase (ALT) (Servicebo, #GM1102) aspartate aminotransferase (AST) (Servicebo, #GM1103) triglyceride (TG) (Servicebio, #GM1114) and total cholesterol (TC) (Servicebio, #GM1113) hepatic TG (Sangon Biotech, #D799796) levels were measured with a biochemical autoanalyzer (Rayto, Shenzhen, China). The activity of High-mobility group box1 (HMGB1) in cell supernatant was determined by kits (Elabscience Biotechnology Co., Ltd, Wuhan, China) (Mei mian, #MM-44107M1), and the tissue IL-1β (Proteintech, #KE10003), CCL2 (Proteintech, #KE10006) levels were examined according to the manufactures' instructions.

Reactive oxygen species (ROS) analysis

Optimal cutting temperature (OCT)-embedded tissues were fixed in 4% paraformaldehyde. Tissue sections were incubated with either dihydroethidium (DHE, 5 μM, APExBio, #C3807) or 2′,7′-dichlorodihydrofluorescein diacetate (DCFDA, 5 μM, Beyotime, #S0033S) for 30 min at 37°C in a humidified chamber protected from light. Images were acquired by fluorescence microscopy (Germany, Leica).

Quantitative real-time polymerase chain reaction (qRT-PCR) analysis

Total RNA was isolated by using Trizol reagent (Accurate Biology, Changsha, China) according to the manufacturer's specifications. cDNA was reverse-transcribed using the RT-PCR system. Real-time PCR was performed by mixing cDNA with primers and SYBR Green qPCR Master Mix (APExBIO, Houston, United States). The sequences of the primers were as follows: *Actb* (forward: 5′-GTGACGTTGACATCCGTAAAGA-3'; reverse: 5′-GCCGGACTCATCGTACTCC)-3′, *Cd36* (forward: 5′-GACTGGGACCATTGGTGATGA-3'; reverse: 5′-AAGGCCATCTCTACCATGCC-3′), *Fabp1* (forward: 5′-TGG TCCGCAATGAGTTCACCCT-3'; reverse: 5′-CCAGCTTGA CGACTGCCTTGACTT-3′), *Fasn* (forward: 5′-CTGCGGAAA CTTCAGGAAATG-3'; reverse: 5′-GGTTCGGAATGCTAT CCAGG-3′), *Scd1*(forward: 5′-TCTTCCTTATCATTGCCA ACACCA-3'; reverse: 5′-GCGTTGAGCACCAGAGTGTAT CG-3′), *Pparγ* (forward: 5′-ATTCTGGCCCACCAACTTCGG-3'; reverse: 5′-TGGAAGCCTGATGCTTTATCCCCA-3′), *Pparα* (forward: 5′-TATTCGGCTGAAGCTGGTGTAC-3'; reverse: 5′-CTGGCATTTGTTCCGGTTCT-3′), *Cpt1α* (forward: 5′-AGG ACCCTGAGGCATCTATT-3'; reverse: 5′-ATGACCTCCTGG CATTCTCC-3′), *Gss* (forward: 5′-TGTGCCCTTTTACCC TCTTCCT-3'; reverse: 5′-TCTTTGGAGTGTGGGAATGGA-3′), *Gsr* (forward: 5′-AGCCGCCTGAACACCATCTA-3'; reverse: 5′-GATGTGTGGAGCGGTAAACTTTT-3′), *Gpx3* (forward: 5′-GCTTGGTCATTCTGGGCTTC-3'; reverse: 5′-CCCACCTGGTCGAACATACT-3′), *Sod1* (forward: 5′-TTG GCCGTACAATGGTGGT-3'; reverse: 5′-CGCAATCCCAAT CACTCCAC-3′), *Sod2* (forward: 5′- GGTGGCGTTGAGATT GTTCA-3'; reverse: 5′- CCCAGACCTGCCTTACGACTAT-3′), *Cat* (forward: 5′-TCACCCACGATATCACCAGA-3'; reverse: 5′-AGC TGA GCC TGA CTC TCC AG-3′), *Cyp2e1* (forward: 5′-ACAGAGACCACCAGCACAAC-3'; reverse: 5′-ATTCAT CCTGTCTCGGACTGC-3′), *Il-1β* (forward: 5′-CACTACAGG CTCCGAGATGAACAAC-3'; reverse: 5′-TGTCGTTGCTTG GTTCTCCTTGTAC-3′), *Il6* (forward: 5′-TACCACTTCACA AGTCGGAGGC-3'; reverse: 5′-CTGCAAGTGCATCATCGT TGTTC-3′), *Tnfα* (forward: 5′-CTGAACTTCGGGGTGATC GG-3'; reverse: 5′-GGCTTGTCACTCGAATTTTGAGA-3′), *Ccl2* (forward: 5′-CCACAACCACCTCAAGCACT-3'; reverse: 5′-TAAGGCATCACAGTCCGAGTC-3′).

Histopathology assessment

Liver tissues were sectioned and mounted on glass slides then stained with H&E and immunohistochemistry of F4/80 (Abcam, #111101), iNOS (Abcam, #15323), Ly6G (Abcam, #238132), CD86 (CST, #19589). Each sample was observed at a ×400 magnification of microscopic field. The liver cryostat section (Germany, Leica) (5 μm) was stained with Oil red O staining. Images were photographed under a microscope (Germany, Leica). Image Pro Plus 6.0 was used to measure the staining Area.

Nile red staining

Nile red staining was used to specifically stain the intracellular fat. The cells were fixed and stained with Nile red (100 ng/ml) (APExBio, #B8209) in PBS for 30 min. After being washed thrice with PBS, the cells were examined under a fluorescent microscope (Germany, Leica). Image Pro Plus 6.0 was used to measure the positive staining cells.

Western blot analysis

Liver tissues were lysed in RIPA lysis buffer (Beyotime) with 1 mM PMSF. An equal amount of protein was separated by SDS-PAGE and transferred to the PVDF membrane. The membranes were washed, blocked and incubated with specific primary anti-rabbit antibodies against CYP2E1 (Proteintech, #19937-1-AP), GAPDH (Cell signaling Technology, #2118S), pNF-kB p65 (Wanleibio, #WL02169), NF-kB p65 (Wanleibio, #WL01273b), TLR4 (PTMBIO, #PTM-5192).

Dataset analysis

The cDNA microarray data (GEO database: GSE28619) were used for relevant analysis.

Statistic analysis

The data were presented as the means ± standard deviation (SD). The statistical significance of the difference was analyzed by Student's t test. $p < 0.05$ was regulated as statistically significant. In this study, the statistical analyses were performed using GraphPad Prism eight software.

Results

GLC alleviates steatohepatitis induced by EHFD diet

The picture (Figure 1A) is the schematic of the liver injury mouse model induced by EHFD. H&E staining showed that GLC treatment ameliorated inflammatory necrosis and hepatic steatosis with a dose-dependent tendency (Figure 1B). In addition, GLC exerts a hepatic protective character by decreasing the final body weight (Figure 1C) and liver index (Figure 1D) as well as the serum level of ALT (Figure 1E) and AST (Figure 1F). We also developed a mouse model with alcohol alone to identify the effect of GLC on the chronic liver injury of ALD mice. (Supplementary Figure S1A). The results indicated that the mouse liver injury characterized by hepatocytes vacuolar and ballooning degeneration was alleviated by GLC treatment. (Supplementary Figure S1B). Moreover, the final body weight of ALD mice was decreased while the other was increased with the treatment of GLC (Supplementary Figure S1C). The liver index of ALD was decreased by the administration of GLC (Supplementary Figure S1D). And the serum level of ALT (Supplementary Figure S1E) and AST (Supplementary Figure S1F) was downregulated by GLC administration. Moreover, the lipid accumulation of ALD mice with GLC treatment declined (Supplementary Figures S1G, H). It also showed a declining trend in hepatic and serum TG levels, as well as TC levels in the treatment group (Supplementary Figures S1I, J, K).

GLC alleviates lipid accumulation by regulating lipogenesis *in vivo* and *in vitro*

To further investigate the impact of GLC on hepatic steatosis, we analyzed the lipid accumulation of the model mice and therapy groups. The Oil red O staining demonstrated that GLC treatment improved a remarkable accumulation of lipid droplets induced by the EHFD diet. (Figures 2A, B). Consistently, hepatic and serum TG, as well as TC levels, were significantly decreased in GLC-treated mice (Figures 2C–E). Moreover, GLC treatment strikingly decreased the mRNA levels of fatty acid uptake-related and synthesis-related genes (*Cd36, Fabp1, Fasn, Scd1, and Pparγ*) (Figure 2F). Additionally, the mRNA levels of β-oxidation genes (*Cpt1α*) were notably increased in GLC-treated mice compared to EHFD mice (Figure 2F). Considering the complexity of the component in traditional Chinese medicine, GLC-containing serum (GLC serum) and control serum (Ctrl serum) from normal mice was prepared for further study. The main steps were illustrated in the flow chart (Figure 2G). The GLC serum and Ctrl serum were collected for the subsequent experiment *in vitro*. Palmitic acid (PA) induced NCTC1469 cells were applied to study if the different concentrations of GLC serum could improve hepatocytes steatosis. Nile red staining demonstrated GLC serum exerted a dose-dependent decreasing trend of lipid droplets in hepatocytes induced by PA (Figures 2H, I, Supplementary Figure S2A). Consist with the results *in vivo*, GLC serum also declined the mRNA expression levels of genes related to lipogenesis while promoting mRNA expression of genes associated with fatty acid β-oxidation in the PA-induced NCTC1469 cells with different concentrations of GLC serum (Figure 2J, Supplementary Figure S2B). Compared with the vehicle group, Ctrl serum (PA + 10N) also downregulated the expression of genes related to lipid accumulation. The results may be attributed to the protective characteristics of the serum. Wang identified that inactive serum is better for cell growth, and different concentrations of serum had various efficacy for cell culturing (Wang et al., 2018). In our study, GLC serum performed a better effect on decreasing lipid accumulation than Ctrl serum.

GLC attenuates hepatotoxicity *via* inhibiting oxidative stress injury of hepatocytes

Histological analysis revealed that GLC effectively reduces reactive oxygen species (ROS) levels in the mouse model of

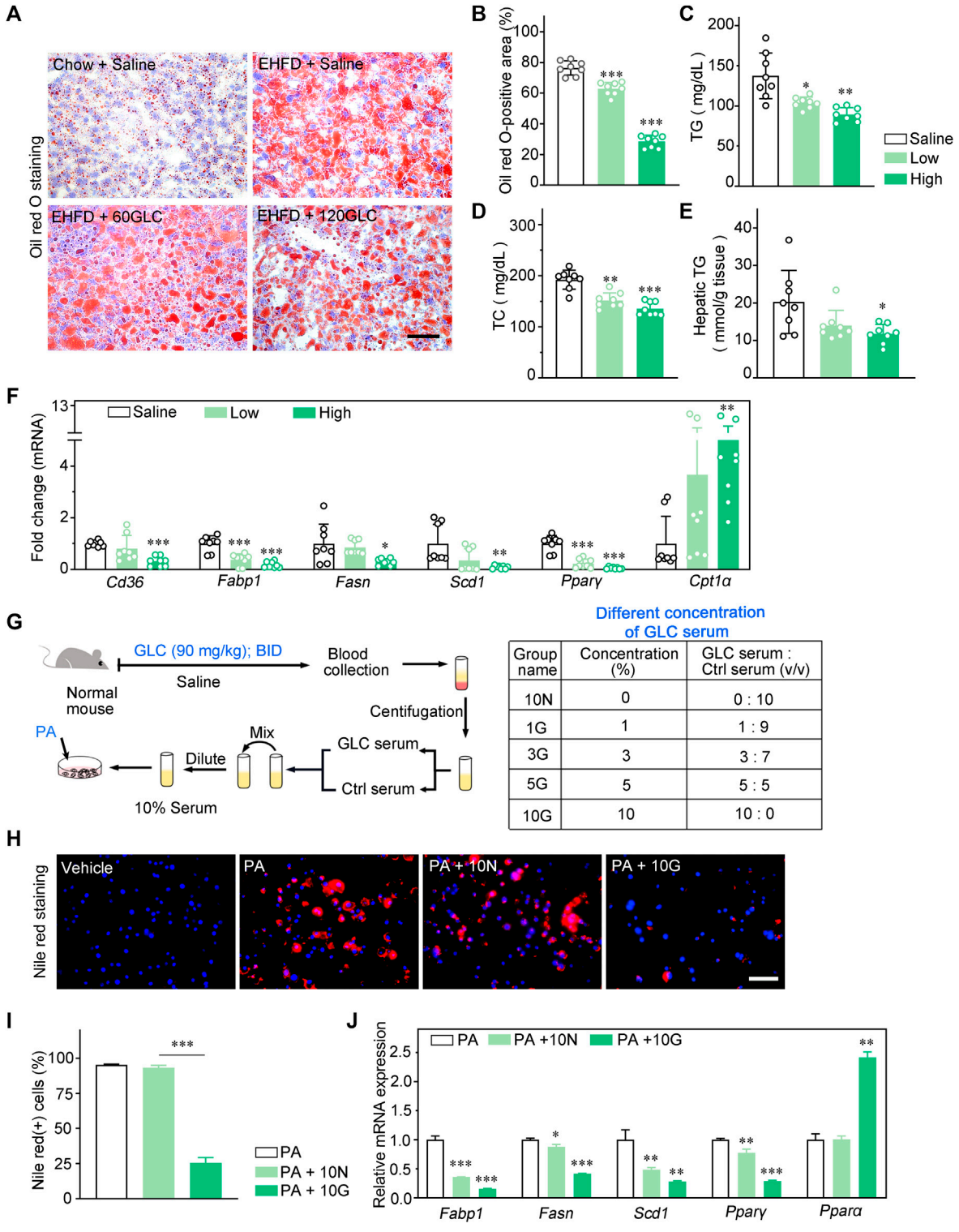

FIGURE 2
GLC alleviates lipid accummulatlon by regulating lipogenesis *in vivo* and *in vitro*. **(A)** Representative images of Oil red O Staining of the frozen liver sections. Scale bars, 50 μm. **(B)** The statistics of Oil red O-positive areas. **(C)** Serum TG and **(D)** TC levels in EHFD mice. **(E)** Hepatic TG levels in EHFD mice. **(F)** Quanttative PCR analysis of the hepatic mRNA levels of genes related to fatty acid metabolism in mice from the indicated groups. Gene expression was nomalized to actin beta (Actb) mRNA levels (n = 8 for each groups). **(G)** The flow chart of drug-containing serum preparation, the GLC-containing serum group are shown in table. **(H)** Representative images of nile red staining of hepatocytes Induced by EtOH and palmitic acid (PA) with the treatment of GLC-containing serum. Scale bars, 50 μm. **(I)** The statistics of nile red(+) cells. **(J)** Quantitative PCR analysis of the mRNA levels of genes related to fatty acid metabolsm in hepatocytes induced by PA with different concentrations of GLC-containing serum. $^{*}P < 0.05$; $^{**}P < 0.01$; $^{***}P < 0.001$.

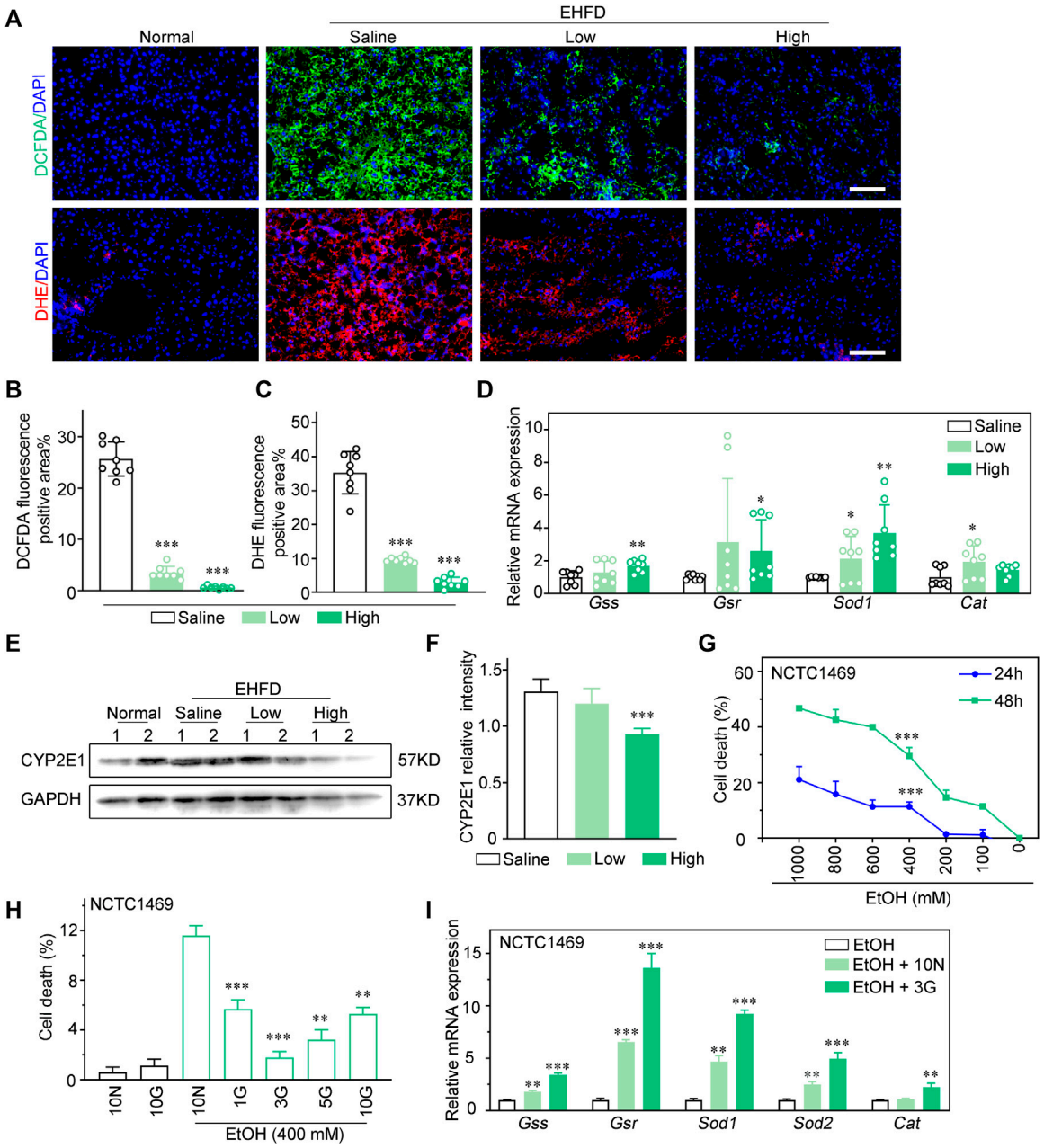

FIGURE 3
GLC attenuates hepatotoxicity via inhibiting oxidative stress injury of hepatocytes. **(A)** Fluorescence analysis of ROS using DCFDA and DHE dyes in mouse liver sections. Scale bars, 100 μm. **(B)** Statistics of DCFDA and **(C)** DHE positive areas. **(D)** Quantitative PCR analysis of hepatic mRNA levels of genes related to oxidative stress injury. **(E)** Expression of CYP2E1 and GAPDH were examined by western blotting. GAPDH as a loading control (n = 2 for each group). **(F)** Relative intensity of CYP2E1. **(G)** NCTC1469 cells were treated with different concentrations of EtOH (0–1000 mM) for 24 h or 48 h. **(H)** NCTC1469 cells were pretreated with different concentrations of GLC serum for 1 h followed by administrationwith EtOH (400 mM). The cell death was analyzed by CCK-8. $^{**}P < 0.01$ vs. NCTC1469 cells induced by ethanol with treatment of 10% Ctrl serum; $^{***}P < 0.001$ vs. NCTC1469 cells induced by ethanol with treatment of 10% Ctrl serum. **(I)** Quantitative PCR analysis of NCTC1469 cells mRNA levels of genes related to oxidative stress injury. The data were obtained from three dependent experiments per group. $^{**}P < 0.01$ vs. NCTC1469 cells treated with EtOH; $^{***}P < 0.001$ vs. NCTC1469 cells treated with EtOH.

EHFD (Figures 3A–C). Effects of GLC on mRNA levels of hepatic antioxidant genes (*Gss, Gsr, Gpx3, Sod1,* and *Cat*) were also investigated. The quantitative PCR analysis indicated that the expression of antioxidant genes mentioned above was potently less than those in the GLC treatment group (Figure 3D). CYP2E1 was reported as a major contributor to ROS

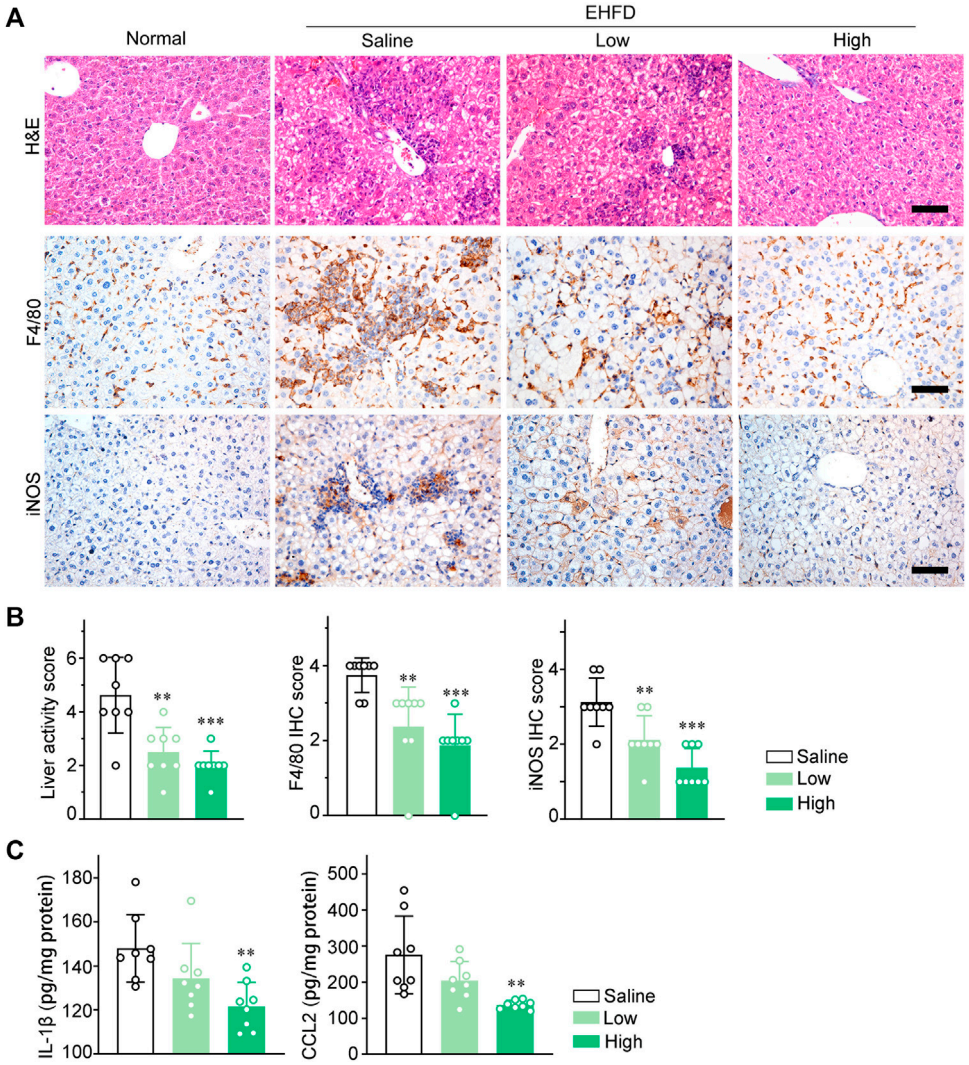

FIGURE 4
GLC suppresses macrophage infiltration and pro-inflammatory cytokines expression *in vivo*. **(A)** H&E staining and IHC staining of F4/80, iNOS of mouse liver sections. Scale bars, 50 μm. **(B)** Liver activity score, IHC score of F4/80 and iNOS of mouse liver sections. **(C)** IL-1β and CCL2 levels in liver tissue of EHFD mice with or without treatment of GLC (n = 8 for each group).

generation and played a pivotal role in ethanol-induced fatty liver and oxidative stress (Lu and Cedeerbaum, 2008; Lu et al., 2010; Yang et al., 2012). The results identified that the increase of CYP2E1 in the EHFD group was significantly reduced with GLC administration (Figures 3E, F). To further confirm the hepatoprotective property of GLC, we also used GLC serum to pretreat NCTC1469 cells before EtOH exposure. We found that EtOH dose-dependently increased NCTC1469 cell death (Figure 3G), while GLC serum could effectively inhibit EtOH-induced cell death in 3%GLC serum ($P < 0.0001$) (Figure 3H). According to the results, we then performed 3%GLC serum for further study. Quantitative PCR analysis also depicted that ethanol-induced reduction of gene expression related to the antioxidant enzyme was strongly inhibited by GLC serum. These data suggest that GLC serum increased the activity of antioxidant defenses. Furthermore, GLC also exerted a similar effect on injured hepatocytes induced by both EtOH and PA (Supplementary Figure S3).

GLC suppresses macrophages infiltration and pro-inflammatory cytokines expression *in vivo*

To investigate inflammatory response in EHFD model mice, H&E staining of liver sections was performed to

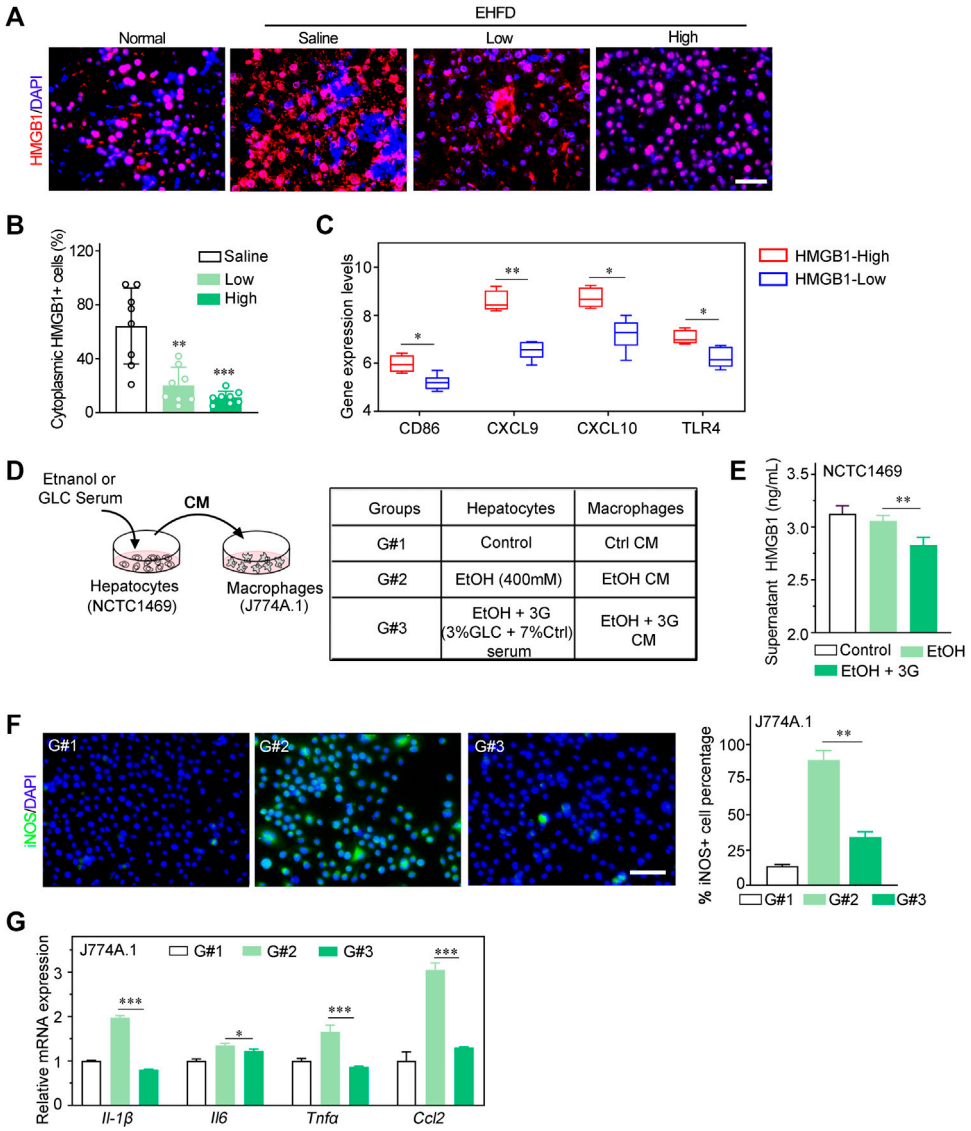

FIGURE 5
GLC blocks M1 polarization by decreasing HMGB1 released by hepatocytes. **(A)** Immunofluorescence staining of HMGB I in mouse liver tissues. Scale bars, 50 μm. **(B)** Statistics of cytoplasmic HMGB1 positive cells of IF staining sections **(C)** Dataset (GEO database- GSE28619) of patients with alcoholic hepatitis were analyzed. Expression levels of M1 related markers (CD86, CXCL9, CXCL1 0 and TLR4) in HMGB1-High group and HMGB1-Low group. **(D)** Schematic flow chart of co-culture system. NCTC1469 cells induced by EtOH with or without treatment of GLC serum. Supemetant was collected for ELISA and culturing macrophages. The treatment of NCTC1469 cells was displayed in table **(E)** Supernatant HMGB1 levels of NCTC1469 cells induced by EtOH. $^{**}P < 0.01$ vs. the NCTC1469 cells with EtOH treatment. **(F)** Representative iNOS immunofluorescence staining and statistics of macrophages treated with condition medium (CM) of NCTC1469 cells. Scale bars, 50 μm. **(G)** Quantitative PCR analysis of J774A.1 cell cocultured with NCTCI469 cells. The data were obtained from three dependent experiments per group. $^{*}P < 0.05$ vs. G#1, $^{***}P < 0.001$ vs. G#1.

compare inflammatory lesions between the model group and the therapy group. As shown in the images (Figure 4A), GLC treatment markedly attenuated inflammatory cell infiltration and hepatocyte necrosis. Ly6G immunohistochemistry (IHC) staining analysis indicated that GLC decreased neutrophil infiltration of EHFD mice (Supplementary Figure S4A). Furthermore, IHC staining of F4/80, iNOS, and CD86 identified that GLC decreased M1 macrophage infiltration (Figure 4A, Supplementary Figure S4A). The results of liver activity score and IHC score of F4/80, iNOS, and CD86 are also consistent with the outcome mentioned above (Figure 4B, Supplementary Figure S4B).

Correspondently, we subsequently found that expression of IL-1β and CCL2 were significantly reduced with the treatment of GLC in EHFD model mice (Figure 4C).

GLC blocks macrophage M1 polarization *via* decreasing HMGB1 released by hepatocytes

HMGB1 is recognized as a prototypical DAMP, which was identified to be released by necrotic and apoptotic cells (Scaffidi et al., 2002; Bell et al., 2006). Particularly, HMGB1 is also well known to play a key role in NAFLD, ALD and drug-induced liver injury (DILI) (Khambu et al., 2019). Therefore, we speculated that HMGB1 may act as a mediator of inflammatory response in an early stage of steatohepatitis induced by alcohol consumption and obesity. Consistently, in our study, the translocation of HMGB1 from the nucleus to the cytoplasm and extracellular hepatocytes was significantly lower in the treatment group compared to the EHFD model group (Figures 5A, B). In addition, the ELISA analysis of the supernatant of NCTC1469 cells induced by EtOH indicated that the expression level of HMGB1 was declined with GLC serum treatment (Figure 5E). Apart from that, by using Gene Expression Omnibus (GEO) database (GSE28619), we found that the high expression of HMGB1 was positively related to the M1-related markers (CD86, CXCL9, CXCL10, TLR4) of macrophages (Figure 5C) in patients with alcoholic steatohepatitis (AH), which indicated a closed relationship between HMGB1 expression and M1 polarization of macrophages in the development of steatohepatitis. To further study whether it is HMGB1 released by damaged hepatocytes promotes the M1 polarization of macrophages, a co-culture system was performed to identify the effect of GLC on the interaction between injured hepatocytes and macrophages (Figure 5D). Surprisingly, immunofluorescence (IF) analysis showed a significant reduction of iNOS-positive macrophages when co-cultured with GLC serum-treated hepatocytes induced by ethanol (Figure 5F). Correspondently, the mRNA expression of genes related to M1 markers (*Il-1β, Il6, Tnfα, Ccl2*) was dramatically downregulated in macrophages co-cultured with GLC serum-treated hepatocytes (Figure 5G). Interestingly, we found that GLC not only protected the hepatocytes from oxidative stress and steatosis but also inhibited the M1 polarization of macrophages triggered by LPS. IF staining demonstrated a decrease of iNOS-positive macrophages induced by LPS with the treatment of GLC serum (Supplementary Figure S5A, B). Similar results were detected in PA-treated macrophages. GLC serum reduced iNOS-positive macrophages with PA treatment (Supplementary Figure S5D, E). Particularly, western blot analysis suggested GLC serum alleviates the increase of HMGB1, TLR4, pNF-KB (Supplementary Figure S5F, G). Saturated fatty acids could polarize macrophages to an M1-predominant phenotype (Luo et al., 2017), the results of our study identified that PA promoted M1 polarization of macrophages, and GLC serum could suppress the activation of macrophages and block the HMGB1-modulated TLR4/NF-κB pathway. The detection illustrated that GLC exerted a multi-target efficacy in the progression of steatohepatitis. We need a further study to explore the bioactive chemicals of GLC serum and its underlying mechanism of inhibiting the inflammatory response.

GLC ameliorates the progression of steatohepatitis *via* the HMGB1-mediated TLR4/NF-κB pathway

TLR4 is one of the most prevalent and well-studied HMGB1 extracellular receptors (Khambu et al, 2019). The activation of TLR4 initiates a signaling cascade, and stimulates the downstream molecule like NF-kB, inducing the production of pro-inflammatory cytokines (Sung et al., 2013). In our study, western blot analysis demonstrated that GLC reduced the expression of TLR4 and phosphorylated NF-κB in the GLC treatment group compared with the EHFD model group (Figures 6A,B). In the progression of steatohepatitis, alcoholics and HFHC diet cause liver damage by the byproducts of ethanol and lipid metabolism, including ROS. GLC could protect hepatocytes from oxidative stress and steatosis, and reduce extracellular HMGB1 levels, which blocks activation of macrophages *via* TLR4/NF-κB, and the expression of inflammatory cytokines was decreased to alleviate progression of steatohepatitis (Figure 6C).

Discussion

Excess alcohol consumption and obesity promote the development of steatohepatitis, cirrhosis, and hepatocellular carcinoma (Hart et al., 2010; Naveau et al., 1997; Ruhl and Everhart, 2005; Diehl, 2004). However, the mechanisms underlying the interaction of fat and alcohol in the progression of steatohepatitis are still unclear, and there is lacking effective treatment for such a complex liver disease. *Periplaneta Americana* is a common source of animal medicine with a long history of use in traditional Chinese medicine. Over the past two decades, PAEs have been tested for the promotion of gastric and duodenal ulcer healing (Lu et al., 2019), treatment of hepatic fibrosis (Zeng et al., 2019), inhibition of tumor growth (Zhao et al, 2017), and stimulation of skin wound healing. Many researchers are actively engaged in the analysis and identification of ingredients of PAEs and have made

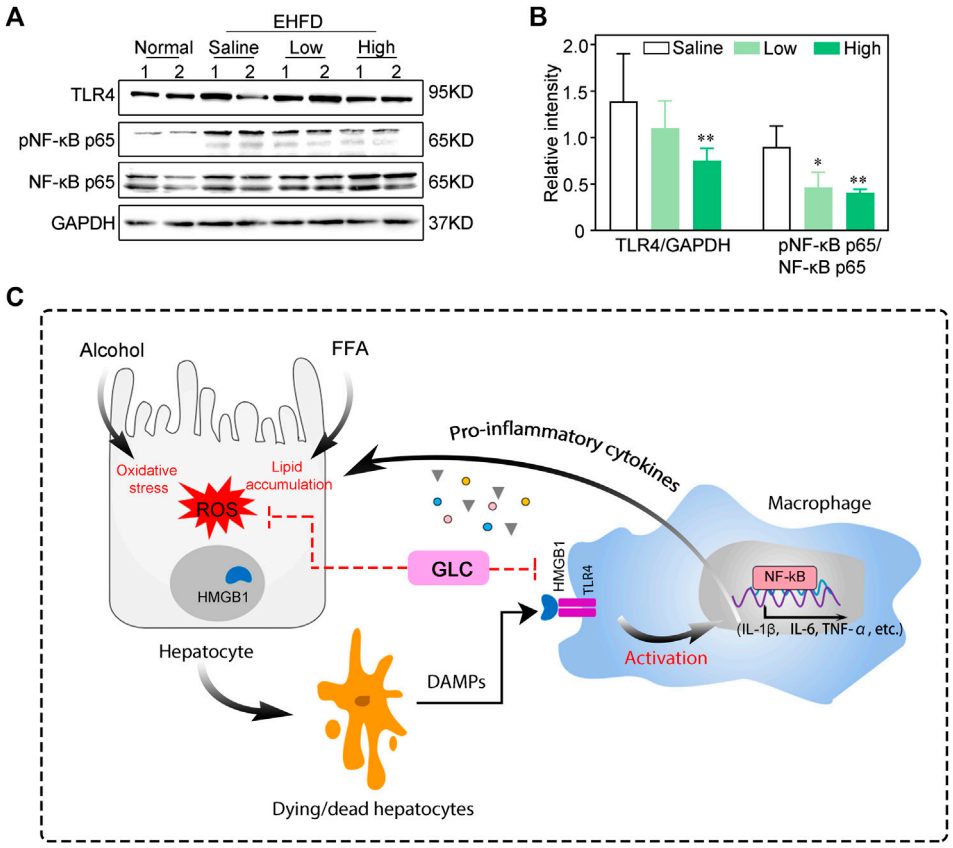

FIGURE 6
GLC ameliorates progression of steatohepatitis *via* HMGB1-mediated TLR4/NF-KB pathway **(A)** Western blot analysis of indicated proteins expression. **(B)** The relative intensity of indicated proteins expression. The data were obtained from three dependent experiments per group. **(C)** Process of GLC inhibiting HMGB1-mediated macrophage activation by TLR4/NF-KB in the progression of steatohepatitis. Alcoholics and free fatty acids cause oxidative stress injury and lipid accumulation of hepatocytes. The dying/dead hepatocytes release DAMPs - HMGB1 to the extracellular. HMGB1 combined with TLR4 of macrophages to activate the inflammatory response through the NF-KB pathway, which aggravated the hepatocyte injury. GLC exerts hepatoprotective properties by reducing lipid accumulation and oxidative stress. It decreases the HMGB1 in extracellular and blocks TLR4/NF-KB mediated inflammatory cytokines expression of macrophages.

some progress. It has been reported that PAEs contain polysaccharides, peptides, nucleosides, polyols, steroids, terpenes, alkaloids, flavonoids, and isocoumarins. Therefore, PAEs may have multiple targets and biochemical properties. GLC is a kind of crude PAEs, the main biologically active ingredients are sticky sugar amino acid, which was identified as the efficacy of hepatoprotective and immunological regulation (Lv, 2017). Thus, we developed a mouse model of liver injury induced by alcoholics combined with HFHC diet to explore the effect of GLC on steatohepatitis.

GLC is a kind of crude PAEs, PAEs contain polysaccharides, peptides, nucleosides, polyols, steroids, terpenes, alkaloids, flavonoids, and isocoumarins. It has been reported that PAEs could decrease the hepatic TG levels and upregulate the expression of antioxidative enzymes including SOD and GSH in the mouse model of acute liver injury (Zeng et al, 2019). Consistently, our results showed that GLC exerts a protective effect on oxidative stress injury of hepatocytes by increasing the expression of antioxidant genes (*Gss, Gsr, Sod, and Cat*) and reducing lipid accumulation *via* modulating genes related to lipid metabolism (*Cd36, Fabp1, Fasn, Scd1, Pparγ, Pparα, and Cpt1α*). The results suggested that GLC could regulate the oxidative balance and lipid metabolism. In addition, the decrease of HMGB1 of the supernatant of EtOH-induced hepatocytes with the treatment of GLC serum also identified the positive function of GLC in alleviating liver injury. Furthermore, our results also demonstrated that GLC could ameliorate liver inflammation by reducing inflammatory cytokines expression of macrophages *in vivo*.

Mechanically, Our study confirmed that GLC blocked the translocation of HMGB1 in the liver tissue of EHFD model mice, and downregulated the expression of TLR4 and NF-κB.

HMGB1 is the prototypical DAMP that could act as telltales of danger by eliciting an early immune response. HMGB1 plays a critical role in initiating and maintaining a chronic inflammatory state in the liver tissue, promoting the progression of steatosis to NASH(Khambu et al, 2019). Similarly, in the rodent model of ALD, alcohol intake elevated the expression of HMGB1, nucleocytoplasmic shutting, and secretion from the hepatocyte. The ROS generated during ethanol metabolism appears to regulate HMGB1 release. Therefore, the treatment of antioxidants in ALD prevented HMGB1 release (Ge et al., 2014). Despite several detrimental factors that can stimulate inflammatory response through diverse pathways mediated by HMGB1, the most important one of the pathways is characterized by the activation of NF-kB. Our results are consistent with the previous study that the inhibition of HMGB1 blocks the TLR4/NF-κB mediated inflammatory response (Tao et al., 2022). Our study indicated that GLC may play an important role in the inhibition of this positive feedback from multiple targets, which is a complicated process that needs further study.

In conclusion, this study suggests that GLC protects the liver against oxidative stress, lipid accumulation, and inflammatory response induced by the EHFD diet. Indeed, GLC suppresses the process of liver injury from hepatic steatosis to steatohepatitis by blocking inflammatory response through the HMGB1-directed pathway. However, we have not figured out the underlying mechanisms of GLC inhibiting the steatosis and oxidative stress of hepatocytes exposed to ethanol and free fatty acid. The precise composition of GLC serum also needs to be identified in the following research. Although the model in this study was established based on the pathogenesis of ALD with obesity, it could not completely mirror the truly human disease.

Data availability statement

The datasets presented in this study can be found in online repositories. The names of the repository/repositories and accession number(s) can be found in the article/ Supplementary Material.

Ethics statement

The animal study was reviewed and approved by Animal Ethics Committee of Jinan University.

Author contributions

YX conceived and designed the study; CG contributed to operating the research; JW collected animal samples; JL, LW, YY, TP, and KZ performed the study and collected the data; YX wrote the manuscript; JH and MC revised the manuscript. All authors approved the submission.

Funding

This work was funded by National Natural Science Foundation of China (Grant No. 81871987) and Fundamental Research Funds for the Central Universities (Grant No. 21620106).

Acknowledgments

The author thank the Medical Experimental center, School of Medicine, Jinan University, for providing the facilities and assistance that supported this research.

Conflict of interest

The authors declare that the research was conducted in the absence of any commercial or financial relationships that could be construed as a potential conflict of interest.

Publisher's note

Supplementary material

The Supplementary Material for this article can be found online at: https://www.frontiersin.org/articles/10.3389/fphar.2022.995523/full#supplementary-material

References

Bell, C. W., Jiang, W., Reich, C. F., 3rd, and Pisetsky, D. S. (2006). The extracellular release of HMGB1 during apoptotic cell death. *Am. J. Physiol. Cell Physiol.* 291, C1318–C1325. doi:10.1152/ajpcell.00616.2005

Byass, P. (2014). The global burden of liver disease: A challenge for methods and for public health. *BMC Med.* 12, 159. doi:10.1186/s12916-014-0159-5

Diehl, A. M. (2004). Obesity and alcoholic liver disease. *Alcohol* 34, 81–87. doi:10.1016/j.alcohol.2004.07.010

Ge, X., Antoine, D. J., Lu, Y., Arriazu, E., Leung, T. M., Klepper, A. L., et al. (2014). High mobility group box-1 (HMGB1) participates in the pathogenesis of alcoholic liver disease (ALD). *J. Biol. Chem.* 289, 22672–22691. doi:10.1074/jbc.M114.552141

Hart, C. L., Morrison, D. S., Batty, G. D., Mitchell, R. J., and Davey Smith, G. (2010). Effect of body mass index and alcohol consumption on liver disease: Analysis of data from two prospective cohort studies. *BMJ* 340, c1240. doi:10.1136/bmj.c1240

Khambu, B., Yan, S., Huda, N., and Yin, X. M. (2019). Role of high-mobility group box-1 in liver pathogenesis. *Int. J. Mol. Sci.* 20, E5314. doi:10.3390/ijms20215314

Louvet, A., Thursz, M. R., Kim, D. J., Labreuche, J., Atkinson, S. R., Sidhu, S. S., et al. (2018). Corticosteroids reduce risk of death within 28 Days for patients with severe alcoholic hepatitis, compared with Pentoxifylline or Placebo-a meta-analysis of individual data from controlled trials. *Gastroenterology* 155, 458–468. doi:10.1053/j.gastro.2018.05.011

Lu, S., Wu, D., Sun, G., Geng, F., Shen, Y., Tan, J., et al. (2019). Gastroprotective effects of kangfuxin against water-immersion and restraint stress-induced gastric ulcer in rats: Roles of antioxidation anti-inflammation and pro-survival. *Pharm. Biol.* 57, 770–777. doi:10.1080/13880209.2019.1682620

Lu, Y., and Cederbaum, A. I. (2008). CYP2E1 and oxidative liver injury by alcohol. *Free Radic. Biol. Med.* 44, 723–738. doi:10.1016/j.freeradbiomed.2007.11.004

Lu, Y., Wu, D., Wang, X., Ward, S. C., and Cederbaum, A. I. (2010). Chronic alcohol-induced liver injury and oxidant stress are decreased in cytochrome P4502E1 knockout mice and restored in humanized cytochrome P4502E1 knock-in mice. *Free Radic. Biol. Med.* 49, 1406–1416. doi:10.1016/j.freeradbiomed.2010.07.026

Luo, W., Xu, Q., Wang, Q., Wu, H., and Hua, J. (2017). Effect of modulation of PPAR-gamma activity on Kupffer cells M1/M2 polarization in the development of non-alcoholic fatty liver disease. *Sci. Rep.* 7, 44612. doi:10.1038/srep44612

Lv, N. L. G.-z. W. J.-c. S. L.-g. S. J.-y. (2017). Chemical components and biological activities in Periplaneta America. *Prog. Mod. Biomed.* 16, 3184–3190. doi:10.13241/j.cnki.pmb.2017.16.046

Ma, X., Hu, Y., Li, X., Zheng, X., Wang, Y., Zhang, J., et al. (2018). *Periplaneta americana* ameliorates dextran sulfate sodium-induced ulcerative colitis in rats by keap1/nrf-2 activation, intestinal barrier function, and gut microbiota regulation. *Front. Pharmacol.* 9, 944. doi:10.3389/fphar.2018.00944

MacSween, R. N., and Burt, A. D. (1986). Histologic spectrum of alcoholic liver disease. *Semin. Liver Dis.* 6, 221–232. doi:10.1055/s-2008-1040605

Matteoni, C. A., Younossi, Z. M., Gramlich, T., Boparai, N., Liu, Y. C., and McCullough, A. J. (1999). Nonalcoholic fatty liver disease: A spectrum of clinical and pathological severity. *Gastroenterology* 116, 1413–1419. doi:10.1016/s0016-5085(99)70506-8

Naveau, S., Giraud, V., Borotto, E., Aubert, A., Capron, F., and Chaput, J. C. (1997). Excess weight risk factor for alcoholic liver disease. *Hepatology* 25, 108–111. doi:10.1002/hep.510250120

Negi, C. K., Babica, P., Bajard, L., Bienertova-Vasku, J., and Tarantino, G. (2022). Insights into the molecular targets and emerging pharmacotherapeutic interventions for nonalcoholic fatty liver disease. *Metabolism.* 126, 154925. doi:10.1016/j.metabol.2021.154925

Ntandja Wandji, L. C., Gnemmi, V., Mathurin, P., and Louvet, A. (2020). Combined alcoholic and non-alcoholic steatohepatitis. *JHEP Rep.* 2, 100101. doi:10.1016/j.jhepr.2020.100101

Qin, M. Y., Huang, S. Q., Zou, X. Q., Zhong, X. B., Yang, Y. F., Zhang, Y. T., et al. (2021). Drug-containing serum of rhubarb-astragalus capsule inhibits the epithelial-mesenchymal transformation of HK-2 by downregulating TGF-β1/p38MAPK/Smad2/3 pathway. *J. Ethnopharmacol.* 280, 114414. doi:10.1016/j.jep.2021.114414

Raynard, B., Balian, A., Fallik, D., Capron, F., Bedossa, P., Chaput, J. C., et al. (2002). Risk factors of fibrosis in alcohol-induced liver disease. *Hepatology* 35, 635–638. doi:10.1053/jhep.2002.31782

Roerecke, M., Vafaei, A., Hasan, O. S. M., Chrystoja, B. R., Cruz, M., Lee, R., et al. (2019). Alcohol consumption and risk of liver cirrhosis: A systematic review and meta-analysis. *Am. J. Gastroenterol.* 114, 1574–1586. doi:10.14309/ajg.0000000000000340

Ruhl, C. E., and Everhart, J. E. (2005). Joint effects of body weight and alcohol on elevated serum alanine aminotransferase in the United States population. *Clin. Gastroenterol. Hepatol.* 3, 1260–1268. doi:10.1016/s1542-3565(0500743-3)

Scaffidi, P., Misteli, T., and Bianchi, M. E. (2002). Release of chromatin protein HMGB1 by necrotic cells triggers inflammation. *Nature* 418, 191–195. doi:10.1038/nature00858

Sun, L. F., Feng, Y., Zhao, H., and Chen, Z. Y. (2022). Study on extraction, analysis of water-soluble polysaccharide from Cockroaches and its immunologic activities. *For. Res.* 02, 256–261.

Sung, B., Pandey, M. K., Ahn, K. S., Kunnumakkara, A. B., Chaturvedi, M. M., and Aggarwal, B. B. (2013). Pandey MK, Sung B, Ahn KS, Kunnumakkara AB, Chaturvedi MM, Aggarwal BB. Gambogic acid, a novel ligand for transferrin receptor, potentiates TNF-induced apoptosis through modulation of the nuclear factor-κB signaling pathway. *Blood* 121, 3778. doi:10.1182/blood-2013-03-494385

Tao, Z., Helms, M. N., Leach, B. C. B., and Wu, X. (2022). Molecular insights into the multifaceted functions and therapeutic targeting of high mobility group box 1 in metabolic diseases. *J. Cell. Mol. Med.* 26, 3809–3815. doi:10.1111/jcmm.17448

Tsukamoto, H., Machida, K., Dynnyk, A., and Mkrtchyan, H. (2009). Second hit" models of alcoholic liver disease. *Semin. Liver Dis.* 29, 178–187. doi:10.1055/s-0029-1214373

Wang, G. B., Chen, J., He, J. H., and Bo, H. B. (2018). Effect of autologous serum on bone marrow stromal cell culture *in vitro*. *J. Guangdong Pharm.* 05, 618–622. doi:10.16809/j.cnki.2096-3653.2018062801

Wang, X. Y., He, Z. C., Song, L. Y., Spencer, S., Yang, L. X., Peng, F., et al. (2011). Chemotherapeutic effects of bioassay-guided extracts of the American cockroach, *Periplaneta americana*. *Integr. Cancer Ther.* 10, Np12–Np23. doi:10.1177/1534735411413467

Yang, L., Wu, D., Wang, X., and Cederbaum, A. I. (2012). Cytochrome P4502E1, oxidative stress, JNK, and autophagy in acute alcohol-induced fatty liver. *Free Radic. Biol. Med.* 53, 1170–1180. doi:10.1016/j.freeradbiomed.2012.06.029

Yang, Y. X., Luo, Q., Hou, B., Yan, Y. M., Wang, Y. H., Tang, J. J., et al. (2015). Periplanosides A-C: New insect-derived dihydroisocoumarin glucosides from *Periplaneta americana* stimulating collagen production in human dermal fibroblasts. *J. Asian Nat. Prod. Res.* 17, 988–995. doi:10.1080/10286020.2015.1047771

Yun, J., Hwang, J. S., and Lee, D. G. (2017). The antifungal activity of the peptide, periplanetasin-2, derived from American cockroach *Periplaneta americana*. *Biochem. J.* 474, 3027–3043. doi:10.1042/BCJ20170461

Zeng, C., Liao, Q., Hu, Y., Shen, Y., Geng, F., and Chen, L. (2019). The role of *Periplaneta americana* (blattodea: Blattidae) in modern versus traditional Chinese medicine. *J. Med. Entomol.* 56, 1522–1526. doi:10.1093/jme/tjz081

Zhang, B. (2021). Effect of qushi tongluo formula drug-containing serum on the expression of miR-155 and miR-146a in RAW264.7 cells and its clinical study China. *Acad. J. Electron. Publ. House*.

Zhang, X. Q., Wu, H. B., Peng, L., Gong, X. M., Li, J., Pu, X. F., et al. (2013). Preventive effect of ganlong capsule on chronic alcoholic hepatic injury in rats. *Zhongguo Zhong Yao Za Zhi* 38, 2197–2201.

Zhao, Y., Yang, A., Tu, P., and Hu, Z. (2017). Anti-tumor effects of the American cockroach, *Periplaneta americana*. *Chin. Med.* 12, 26. doi:10.1186/s13020-017-0149-6

Zhu, J. J., Yao, S., Guo, X., Yue, B. S., Ma, X. Y., and Li, J. (2018). Bioactivity-guided screening of wound-healing active constituents from American cockroach *Periplaneta americana*. *Molecules* 23, 101. doi:10.110.3390/molecules23010101

Zou, Y., Zhang, M., Zeng, D., Ruan, Y., Shen, L., Mu, Z., et al. (2020). *Periplaneta americana* extracts accelerate liver regeneration via a complex network of pathways. *Front. Pharmacol.* 11, 1174. doi:10.3389/fphar.2020.01174

frontiers | Frontiers in Pharmacology

TYPE Mini Review
PUBLISHED 19 October 2022
DOI 10.3389/fphar.2022.1042651

OPEN ACCESS

EDITED BY
Yan Huang,
Anhui Medical University, China

REVIEWED BY
Zhaoguo Liu,
Nantong University, China
Feixiang Liu,
First Affiliated Hospital of Henan University of Traditional Chinese Medicine, China

*CORRESPONDENCE
Zili Zhang,
zilizhang@njucm.edu.cn
Kuirong Jiang,
jiangkuirong@njmu.edu.cn

†These authors have contributed equally to this work

SPECIALTY SECTION
This article was submitted to Inflammation Pharmacology, a section of the journal Frontiers in Pharmacology

RECEIVED 12 September 2022
ACCEPTED 10 October 2022
PUBLISHED 19 October 2022

CITATION
Wu Y, Zhang C, Guo M, Hu W, Qiu Y, Li M, Xu D, Wu P, Sun J, Shi R, Zhang Z and Jiang K (2022), Targeting pancreatic stellate cells in chronic pancreatitis: Focus on therapeutic drugs and natural compounds.
Front. Pharmacol. 13:1042651.
doi: 10.3389/fphar.2022.1042651

Targeting pancreatic stellate cells in chronic pancreatitis: Focus on therapeutic drugs and natural compounds

Yang Wu[1†], Chun Zhang[2†], Mei Guo[3†], Weikang Hu[1†], Yangling Qiu[3], Mengran Li[3], Dong Xu[1], Pengfei Wu[1], Jing Sun[4], Run Shi[5], Zili Zhang[3*] and Kuirong Jiang[1*]

[1]Pancreas Center, The First Affiliated Hospital of Nanjing Medical University, Nanjing, China, [2]Gastroenterology Department, Jiangsu Province Hospital of Chinese Medicine, Affiliated Hospital of Nanjing University of Chinese Medicine, Nanjing, China, [3]Jiangsu Key Laboratory for Pharmacology and Safety Evaluation of Chinese Materia Medica, School of Pharmacy, Nanjing University of Chinese Medicine, Nanjing, China, [4]Department of Endocrinology, Jiangsu Province Hospital of Chinese Medicine, Affiliated Hospital of Nanjing University of Chinese Medicine, Nanjing, China, [5]Department of Oncology, The First Affiliated Hospital of Nanjing Medical University, Nanjing, China

Chronic pancreatitis (CP) is a precancerous illness linked to pancreatic ductal adenocarcinoma (PDAC), although the evolutionary mechanism is uncertain. CP is distinguished by severe fibrosis caused by the activation of pancreatic stellate cells (PSCs). The current clinical therapeutic protocol for CP lacks specific therapeutic medicines for the prevention and suppression of inflammation and fibrosis aggravating in CP. More research on specifically targeting PSCs would help facilitate the development of novel therapies for pancreatic fibrosis. Notably, using natural compounds from medicinal plants as new antifibrotic agents has become a focus of recent research and is widely employed as an alternative and complementary approach. Our goal was to shed light on the role of PSCs in the development of CP and provide a focused update on the new potential therapeutic strategies against PSCs in CP models. Future studies can refer to these possible strategies for drug design, bioavailability, pharmacokinetics, and other issues to obtain better clinical outcomes for treating CP.

KEYWORDS

CP, PSCs, natural compounds, pancreatic fibrosis, anti-fibrotic drug

Introduction

CP is characterized by inflammation, fibrosis, and loss of acinar and islet cells, which may present as abdominal pain, steatorrhea, pancreatic exocrine and endocrine insufficiency, and imaging-detectable pancreatic damage (Beyer et al., 2020). CP has a poorly known pathogenesis. Nonetheless, there appears to be a consistent sequence of an initial shock with damage, followed by recovery *via* fibrosis and regeneration. Recurrent oxidative stress or inflammation are fundamental causes of persistent pancreatic injury,

causing irreversible changes in pancreatic structure and function and eventually leading to the onset of CP (Ren et al., 2020).

Pathogenesis of chronic pancreatitis differs based on underlying etiology, genetic background, and environmental exposures. Alcohol, the most prevalent cause of CP, may induce damage *via* toxic alcohol metabolites, overexpression of numerous genes related to cell death, direct stimulation of PSCs (resulting in fibrosis), and other mechanisms (Setiawan et al., 2017). Abnormal stromal/desmoplastic response is the hallmark histological feature of CP, which is attributed mainly to the activation of PSCs. Targeting PSCs may be a viable treatment strategy for CP (Kandikattu et al., 2020).

Currently, there are still few clinically available therapeutic agents for CP. Recently, some preclinical research into PSCs has been conducted, which will aid in creating innovative therapeutics for CP. In addition, natural chemicals derived from medicinal plants have great potential as antifibrotic drugs for the treatment of CP and deserve more in-depth studies *in vivo* and *in vitro* (Calfio et al., 2020).

This paper focuses on research targeting PSCs in CP models and reviews in detail the antifibrotic capabilities of several potential drugs for treating CP.

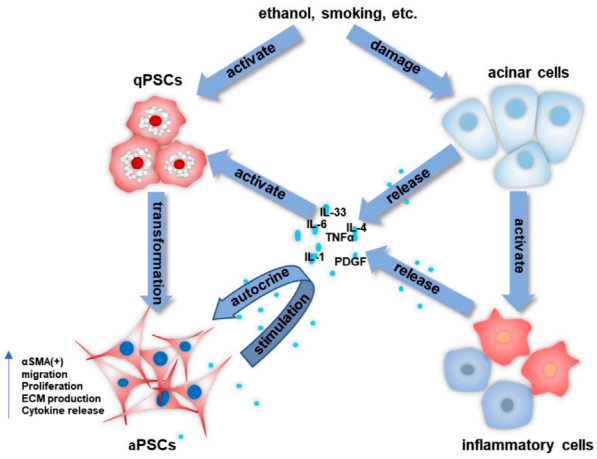

FIGURE 1
The activation process of PSCs in CP. The crosstalk among acinar cells, inflammatory cells, and stellate cells allows for the continued activation of PSCs and the progression of pancreatic fibrosis.

Pancreatic stellate cells

Nearly a century after Karl von Kupffer's discovery of hepatic stellate cells (HSCs) in 1876, Wateri's group first detected similar cells (later termed PSCs) in the pancreas (Watari et al., 1982). It was not until 1998 that two milestone studies detailed the isolation and culture procedures of PSCs *in vitro*, allowing researchers to examine them in health and disease (Apte et al., 1998; Bachem et al., 1998). Since then, a slew of new research has been conducted in this area, and PSCs have become widely recognized as the primary source of the stromal/desmoplastic response that is characteristic of pancreatic cancer and CP (Apte and Wilson, 2004; Apte and Wilson, 2012; Pang et al., 2017).

PSCs have two phenotypes: quiescent (qPSCs) and activated (aPSCs). Under normal physiological conditions, qPSCs can be found in the peri-acinar or interlobular areas and comprise around 4% of the pancreatic cells (Apte et al., 1998; Bachem et al., 1998). qPSCs play a role in vitamin A storage, immunity, and the preservation of the normal structure in the pancreas (Allam et al., 2017). qPSCs have many typical features, such as abundant perinuclear lipid droplets, molecular markers (cytoglobin and adipophilin), and a low capacity to proliferate, migrate and synthesize ECM (Apte et al., 2013; Nielsen et al., 2017). Several factors can contribute to the activation process of qPSCs, such as smoking, alcohol intake, oxidative stress, hypoxia, etc. (Fu et al., 2018). In diseases like PDAC or CP, qPSCs get continuously activated and transform into aPSCs (Apte et al., 1999; Bynigeri et al., 2017). aPSCs show a myofibroblast-like phenotype: positive staining of α-smooth muscle actin (αSMA), loss of lipid droplets, increased production of cytokines and ECM (collagens, hyaluronic acid, fibronectin, etc.), and elevated ability to migrate, proliferate (Apte et al., 1999; Bynigeri et al., 2017). We have previously given a detailed overview of PDAC-associated PSCs, and the following will focus on their role in CP and targeted strategies (Wu et al., 2020).

Pancreatic stellate cells in the development of chronic pancreatitis

PSCs are special pancreatic resident cells that provide critical functions in both normal and abnormal pancreata. PSCs activation is a crucial step in the fibrogenic process of the pancreas (Bynigeri et al., 2017; Beyer et al., 2020). Multiple stimuli (ethanol, hyperglycemia, oxidative stress, cytokines, chemokines, etc.) can activate PSCs, causing them to release an abundance of ECM and hence promote the severe interlobular and intralobular desmoplastic reaction. Increased pancreatic fibrosis can lead to impaired exocrine and endocrine function of the pancreas. In early CP, damaged acinar cells stimulate major inflammatory cells (macrophages, granulocytes, and lymphocytes) that subsequently release large amounts of cytokines, such as interleukin (IL)-1/-4/-6/-8, tumor necrosis factor-alpha (TNF-α), transforming growth factor-beta 1 (TGF-β1), platelet-derived growth factor (PDGF), etc. (Jin et al., 2020; Kandikattu et al., 2020; Zheng et al., 2021). These molecules then stimulate PSCs, while PSCs can also secrete cytokines and continue to activate themselves through an autocrine pathway.

TABLE 1 Potential antifibrotic drugs in the treatment of CP.

Drugs	Diseases	Main results
Dasatinib	CP	Dasatinib inhibited the growth and activation of PSCs by inhibiting various TKs and MAPK cascades (Zeng et al., 2019).
Olaparib	CP	Olaparib showed antifibrotic effects in cerulein-induced CP (El-Hamoly et al., 2021).
Imatinib	CP	Imatinib reduced ECM deposition and PSCs' activation while inhibiting the TGF-β1/Smad pathway (Bansod et al., 2021).
EGCG	CP	EGCG prevented fibrosis by decreasing PSCs' activation through the antioxidative effect (Asaumi et al., 2006).
Emodin	CP	Emodin showed an antifibrotic effect on pancreatic fibrosis (Lin et al., 2015).
Curcumin	CP	Curcumin decreased the activation markers of PSCs (Lin et al., 2015).
Saikosaponin d (SSd)	CP	SSd decreased fibrosis by inhibiting the autophagy of PSCs *via* PI3K/Akt/mTOR signaling (Cui et al., 2019).
NLPR3 siRNA	CP	NLPR3 siRNA reduced the activation markers of PSCs (αSMA, collagen I, Fibronectin) (Li et al., 2021b).
YAP siRNA	CP	Activated YAP enhanced PSCs proliferation, and YAP siRNA decreased the activation of PSCs and fibrosis in CP (Spanehl et al., 2022).
Metformin	PDAC	Metformin reduced the cytokines released from cancer cells and inhibited the activation of PSCs in paracrine under co-culture (Duan et al., 2017).
Rhein	PDAC	Rhein inhibited fibrosis by decreasing the immunoreactivity of fibrotic activators and reducing fibronectin (Tsang and Bian, 2015).
Resveratrol	PDAC	Resveratrol suppressed ROS/miR-21-mediated activation and glycolysis in PSCs, inhibiting tumor invasion and migration (Yan et al., 2018).
DHA	Liver fibrosis	DHA alleviated liver fibrosis by triggering HSCs ferroptosis in an autophagy-dependent way (Shen et al., 2022).
EA	Liver fibrosis	EA exerted its antifibrotic effects by inducing FPN-dependent ferroptosis of HSCs by disrupting the formation of SNARE complexes (Li et al., 2022).
Angelica sinensis polysaccharide (ASP)	Liver fibrosis	ASP effectively alleviates chronic liver fibrosis by inhibiting HSCs activation through the IL-22/STAT3 pathway (Wang et al., 2020a).
Dendrobium officinale Polysaccharide (DOP)	Liver fibrosis	DOP maintained intestinal homeostasis by enhancing tight junctions between intestinal cells and reducing apoptosis, thereby inhibiting activation of the LPS-TLR4-NF-κB signaling pathway to protect against liver fibrosis (Wang et al., 2020b).
Celastrol	Liver fibrosis	Celastrol exerted anti-fibrotic effects by promoting ROS production and inducing ferroptosis in activated HSCs (Luo et al., 2022).

The continuous stimulation of PSCs disrupts the synthesis-degradation balance of the ECM, ultimately leading to ECM deposition and fibrosis in the pancreas (Jin et al., 2020; Kandikattu et al., 2020; Zheng et al., 2021). Figure 1 is a schematic representation of the activation of PSCs in CP.

Several investigations on the mechanisms have been undertaken. Wu et al. indicated that TGF-β1 induced the activation of the nuclear factor kappa B (NF-κB) pathway in PSCs through modulating phospho-transforming growth factor beta-activated kinase 1 (p-TAK1), and this pathway might be a target for treating CP (Wu et al., 2021). Li et al. (2021a) showed that nicotine facilitated pancreatic fibrosis by inducing the activation of PSCs through Janus kinase 2/signal transducer and activator of transcription 3 (JAK2/STAT3) signaling pathway in rats, revealing the mechanism of smoking on CP. Lee et al. (2015) demonstrated that the cumulative effects of ethanol and cigarette components could activate PSCs in alcoholic smokers, accelerating the evolution of pancreatic fibrosis. Another study showed that the JAK/STAT pathway was essential for the proliferation and activation of PSCs and that inhibition of this pathway reduced caerulein-induced CP *in vivo* (Komar et al., 2017). Recently, Yang et al. indicated that very low-density lipoprotein receptor (VLDLR)-enhanced lipoprotein metabolism in PSCs increased fibrosis and that IL-33 played an essential role in this process in CP (Yang et al., 2022).

All these findings indicate that PSCs' activation plays a crucial role in the development of CP, making PSCs a promising therapeutic target for CP.

Drugs for the treatment of chronic pancreatitis by targeting pancreatic stellate cells

Even though the area of PSCs is still in its infancy, scientists have made significant efforts and proposed different strategies to target PSCs for treating CP. Recent research has indicated that siRNAs and small molecule kinase inhibitors can treat CP by targeting PSCs (Pezzilli et al., 2011; Tan et al., 2019; Mohanavelu et al., 2021). In addition, studies have shown that natural compounds from plants are widely used as complementary and alternative medications to treat diseases and extend life spans (Lin et al., 2015). Such drugs have promising clinical applications in the prevention and treatment of CP. The

following is a discussion of the current status of several potential drugs and their possible mechanisms in treating CP.

Since morphological, functional, and gene expression investigations revealed considerable similarities between PSCs and HSCs, research on HSCs will be very informative (Erkan et al., 2012; Paulo et al., 2013). In addition, considering that PSCs derived from PDAC and CP have much in common in causing pancreatic fibrosis, some drugs of potential research value will also be listed here. Table 1 provides a summary of the existing antifibrotic strategies.

siRNA

siRNAs represent a form of posttranscriptional gene silencing and have emerged as a fundamental and extensive regulator of gene expression. The most recent technology of high-throughput sequencing allows the analysis of siRNA abundance and expression profile in specific organs, tissues, and cells more and more precisely, allowing for the investigation of the roles of miRNAs and siRNAs (Fowler et al., 2018). mRNA transcripts of altered genes in genetic disorders and tumors are typical siRNA targets (Nambudiri and Widlund, 2013). Several studies have shown that the involvement of siRNAs in the expression of certain genes, which in turn influence the onset and progression of chronic pancreatitis, has potential therapeutic value (Charo et al., 2013). For instance, recent studies showed that the NACHT, LRR, and PYD domains-containing protein 3 (NLRP3) inflammatory bodies were directly involved in PSCs' activation *in vivo* and *in vitro*. NLPR3 siRNA decreased the activation markers of PSCs (αSMA, collagen I, fibronectin) expression (Li et al., 2021b). Another study indicated that activated yes-associated protein (YAP) enhanced PSCs proliferation and knockdown of YAP by siRNA decreased the activation of PSCs and fibrosis in the CP animal model (Spanehl et al., 2022). However, these studies are still in the laboratory stage and must be further validated in clinical trials.

Artemisinin and its derivatives

Artemisinin was identified as an isolated phytochemical derived from the Artemisia annua in 1972 (White et al., 2015). Several chemical derivatives have been developed to increase artemisinin's water and oil solubility without compromising its therapeutic effect. Artemisinin was first used by the ancient Chinese to treat "fever," commonly thought of as malaria (Miller and Su, 2011). This substance and its derivatives are still vital in treating malaria today.

Recent studies have also identified these chemicals' role in treating different diseases, including inflammation, infection, cancer, and fibrosis (Efferth, 2006; Lai et al., 2013; Kim et al., 2015; Shi et al., 2015). Our preliminary research found that dihydroartemisinin (DHA) reduced liver fibrosis *via* inducing ferroptosis in HSCs (Shen et al., 2022). However, artemisinin and its derivatives have not been reported in pancreatic fibrosis in CP, which is a potential hot spot for future research.

Vitamin A/D derivatives

In CP, vitamin A derivatives were reported to induce significant apoptosis, inhibit proliferation, and suppress ECM production of PSCs *in vitro*, indicating the potential of Vitamin A derivatives in reducing pancreatic fibrosis in CP (Xiao et al., 2015). However, the application of Vitamin A and its derivatives has been little studied in CP research. Therefore its use in targeting PSCs in PDAC is of a reference value. Previous research has demonstrated that Vitamin A analogs can inhibit the activation of PSCs in PDAC (Chronopoulos et al., 2016). ATRA (a Vitamin A analog) was found to reprise the quiescent state of PSCs in KPC mice (Froeling et al., 2011). All these studies show that Vitamin A analogs have potential research and clinical translational value in treating CP-related fibrosis.

A high prevalence of Vitamin D (VD) deficiency in CP patients is associated with the risk and prognosis of CP (Klapdor et al., 2012; Joker-Jensen et al., 2020). VD serves several biological roles in the body and has been extensively studied in inflammatory illnesses. VD and its derivatives have been found to inhibit PSCs' activation and decrease ECM deposition, therefore relieving pancreatic fibrosis. Several investigations have shown that VD analogs may reprise the quiescence of PSCs and reduce fibrosis in CP and PDAC (Sherman et al., 2014; Wallbaum et al., 2018). These findings imply that VD might be an effective antifibrotic treatment for CP. More high-quality research and clinical trials are necessary to validate the anti-fibrosis function of VD in CP.

Small molecule kinase inhibitors

Kinases have been the subject of contemporary pharmacological study due to their crucial function in cellular signal transmission (Wu et al., 2015). Previous research has shown that fibromodulin (FMOD) is increased in CP and is an essential downstream mediator of oxidative stress. The extracellular signal-regulated kinases (ERK) and c-Jun N-terminal kinases (JNK) inhibitors can decrease FMOD, thereby decreasing PSCs' activation (An et al., 2020). Dasatinib, an inhibitor of several tyrosine kinases (TKs), was shown to have possible anti-fibrosis effects on CP and decrease pancreatic fibrosis and macrophage infiltration (Zeng et al., 2019). Olaparib, a peroxisome proliferator-activated receptor gamma (PARP) inhibitor, was reported to have antifibrotic effects in cerulein-induced CP (El-Hamoly et al., 2021).

Imatinib, an inhibitor of discoidin domain receptor 1 (DDR1) and DDR2, can reduce ECM deposition and PSCs' activation while inhibiting the TGF-β1/Smad pathway (Bansod et al., 2021). Small molecule kinase inhibitors are one of the current research hotspots and have promising applications in the treatment of CP.

Resveratrol

Resveratrol is a polyphenolic stilbene in significant concentrations in grape, raspberry, blueberry, and peanut species (Rauf et al., 2018). Resveratrol has been shown to induce apoptosis of CP cells and alleviate fibrosis by promoting caspase-3 activation (Zhou et al., 2011). Previous studies have shown that resveratrol can suppress intracellular reactive oxygen species (ROS) and boost PSCs' activation and glycolytic metabolism by suppressing miR-21 expression (Yan et al., 2018). Resveratrol inhibited ROS-induced activation of PSCs by decreasing miR-21 expression and raising the phosphatase and tensin homolog deleted on Chromosome 10 (PTEN) (Yan et al., 2018). Another study reported that resveratrol could inhibit the activation markers of PSCs (αSMA, collagen I, and fibronectin) by downregulating NF-κB signaling (Lin et al., 2015).

Rhein

Rhein, the active component of rhubarb, is used extensively in treatment because of its anti-inflammatory, anti-angiogenic and anticancer characteristics (Xian et al., 2020; Li et al., 2021c). Rhein was reported to attenuate PSCs' activation and suppress sonic hedgehog (SHH)/glioma-associated oncogene homolog 1 (GLI1) signaling in pancreatic fibrosis (Tsang et al., 2013). Rhein was able to suppress αSMA, Fibronectin, and matrix metalloproteinases (MMPs) in cultured PSCs *via* modulating the SHH pathway (Tsang et al., 2013; Tsang and Bian, 2015). Studies have shown that down-regulation of NF-κB and STAT3 signaling pathways may be the potential mechanism of Rhein's anti-fibrosis and anti-tumor effects (Lin et al., 2015).

Epigallocatechin gallate

Epigallocatechin gallate (EGCG), the main phenolic compound in green tea, was reported to have antioxidant, anti-inflammatory, and anticancer functions (Lee et al., 2014; Hosseini and Ghorbani, 2015). Polyphenols in green tea can prevent fibrosis by decreasing the activation of PSCs (Asaumi et al., 2006). Masamune et al. indicated that EGCG could reduce the ability of PSCs to proliferate and migrate (Masamune et al., 2005). *In vitro* experiments showed that EGCG pretreatment could inhibit the ethanol-induced activation of PSCs (Asaumi et al., 2007). Ethanol was known to increase the protein expression of αSMA, activate TGF-β1, and induce p38 mitogen-activated protein kinase (MAPK) phosphorylation. After EGCG treatment, p38 MAPK phosphorylation was eliminated, and the activation process of PSCs was inhibited (Asaumi et al., 2006).

Metformin

Metformin has gained widespread use in treating type II diabetes. (Bailey, 2017). Studies have shown that metformin exerts anticancer effects by regulating inflammatory responses (Vancura et al., 2018). Previous studies have indicated that metformin significantly reduces the expression of αSMA and collagen and inhibits PSCs proliferation by upregulating phosphorylation-AMP-activated protein kinase (p-AMPK) expression (Duan et al., 2017).

Emodin

Emodin, a natural anthraquinone derivative in some herbs, was reported to have anti-inflammation, anti-angiogenesis, anti-dyslipidemia, and anticancer functions (Gaman et al., 2018; Semwal et al., 2021). According to the literature, after 4 mmol/l emodin treatment, emodin downregulated the expression of several fibrosis markers (αSMA, fibronectin, and collagen I), thereby reducing the cell viability of primary PSCs (Lin et al., 2015). Table 1 lists the drugs that may be explored in CP treatment.

Discussion

Multiple investigations have established that PSCs play a critical role in CP. All the above treatments have been reported to prevent the activation of PSCs in CP and the resulting fibrosis. These studies have also revealed the molecular mechanisms of the various drugs.

We address several drugs with antifibrotic effects that may serve as innovative antifibrotic treatments for PSCs in CP. Notably, phytochemicals should be encouraged for further in-depth research due to their cheap, non-toxic nature and sound therapeutic effects on PSCs in CP. Based on preclinical studies, given their potential as new antifibrotic drugs, it is important to consider drug delivery and low bioavailability. Recently, applications of nanoparticle systems have emerged in clinical practice related to drug delivery (Poilil Surendran et al., 2017; Sharma et al., 2017). We are confident that there will be relevant studies to test and validate these hypotheses and find new solutions for treating CP in the future.

Apart from these, some other promising options, such as ferroptosis inducers, have not been studied in CP. In recent years, ferroptosis has become a new hotspot to describe the regulatory form of cell death. Ferroptosis is closely related to tumors, degenerative diseases, ischemia-reperfusion injury, and cardiovascular diseases (Wei et al., 2020). Previous research showed that tripartite motif-containing protein 26 (TRIM26), a ferroptosis inducer, promoted ferroptosis in HSCs to inhibit liver fibrosis, which indicated that ferroptosis inducers might be potential anti-fibrosis agents (Zhu et al., 2021). Ellagic acid (EA), a natural product, exerted its antifibrotic effects by inducing ferroportin (FPN)-dependent ferroptosis of HSCs by disrupting the formation of SNARE complexes in liver fibrosis (Li et al., 2022). Luo et al. indicated that celastrol demonstrated anti-fibrotic effects on activated HSCs *via* boosting ROS generation and triggering ferroptosis (Luo et al., 2022). Our published paper has also revealed that DHA alleviates liver fibrosis by inducing ferroptosis in HSCs. We uncovered the possible mechanism of DHA against hepatic fibrosis and demonstrated that ferroptosis might be a novel method to remove activated HSCs (Zhang et al., 2021). Although these medications have not been investigated for CP fibrosis, their scientific value and clinical application possibilities in CP are promising.

However, drug research in CP still faces many challenges. When testing new treatments, it is vital to choose models that replicate the realities of CP in humans as closely as possible. There is still a long way to go in the development of new CP models. Besides, it is essential to note that the treatment modalities in these experimental models were performed at the same time as or before the induction of CP, which does not fully reflect the actual clinical situation. Therefore, the next major step is to construct phase I and subsequent trials for human CP so that the laboratory outcomes may be transferred to the bedside.

Author contributions

Investigate and write the original paper: YW, CZ, and WH; review and edit: YQ, DX, and ML; Supervision: MG and PW; Manuscript revision: JS and RS; Project administration: ZZ and KJ. All authors have read and agreed to the published version of the manuscript. All authors contributed to the article and approved the submitted version.

Funding

The work was supported by the National Natural Science Foundation of China (Nos. 82000572, 81871980, 82203850), the Natural Science Foundation of Jiangsu Province (No. BK20200840), General Projects of the Natural Science Research of Jiangsu Higher Education Institutions (No. 20KJB310003), the Natural Science Foundation of Nanjing University of Chinese Medicine (No. NZY82000572).

Conflict of interest

The authors declare that the research was conducted in the absence of any commercial or financial relationships that could be construed as a potential conflict of interest.

Publisher's note

All claims expressed in this article are solely those of the authors and do not necessarily represent those of their affiliated organizations, or those of the publisher, the editors and the reviewers. Any product that may be evaluated in this article, or claim that may be made by its manufacturer, is not guaranteed or endorsed by the publisher.

References

Allam, A., GothwalM.Saha, D., Maurer, J., and Brunner, T. B. (2017). Pancreatic stellate cells in pancreatic cancer: In focus. *Pancreatology* 17 (4), 514–522. doi:10.1016/j.pan.2017.05.390

An, W., Zhu, J. W., Jiang, F., Jiang, H., Zhao, J. L., Liu, M. Y., et al. (2020). Fibromodulin is upregulated by oxidative stress through the MAPK/AP-1 pathway to promote pancreatic stellate cell activation. *Pancreatology* 20 (2), 278–287. doi:10.1016/j.pan.2019.09.011

Apte, M. V., Haber, P. S., Applegate, T. L., Norton, I. D., McCaughan, G. W., Korsten, M. A., et al. (1998). Periacinar stellate shaped cells in rat pancreas: Identification, isolation, and culture. *Gut* 43 (1), 128–133. doi:10.1136/gut.43.1.128

Apte, M. V., Haber, P. S., Darby, S. J., Rodgers, S. C., McCaughan, G. W., Korsten, M. A., et al. (1999). Pancreatic stellate cells are activated by proinflammatory cytokines: Implications for pancreatic fibrogenesis. *Gut* 44 (4), 534–541. doi:10.1136/gut.44.4.534

Apte, M. V., and Wilson, J. S. (2012). Dangerous liaisons: Pancreatic stellate cells and pancreatic cancer cells. *J. Gastroenterol. Hepatol.* 27, 69–74. doi:10.1111/j.1440-1746.2011.07000.x

Apte, M. V., Wilson, J. S., Lugea, A., and Pandol, S. J. (2013). A starring role for stellate cells in the pancreatic cancer microenvironment. *Gastroenterology* 144 (6), 1210–1219. doi:10.1053/j.gastro.2012.11.037

Apte, M. V., and Wilson, J. S. (2004). Mechanisms of pancreatic fibrosis. *Dig. Dis.* 22 (3), 273–279. doi:10.1159/000082799

Asaumi, H., Watanabe, S., Taguchi, M., Tashiro, M., and Otsuki, M. (2007). Externally applied pressure activates pancreatic stellate cells through the generation of intracellular reactive oxygen species. *Am. J. Physiol. Gastrointest. Liver Physiol.* 293 (5), G972–G978. doi:10.1152/ajpgi.00018.2007

Asaumi, H., Watanabe, S., TaguchiM.TashiroM.Nagashio, Y., NomiYama, Y., et al. (2006). Green tea polyphenol (-)-epigallocatechin-3-gallate inhibits ethanol-induced activation of pancreatic stellate cells. *Eur. J. Clin. Invest.* 36 (2), 113–122. doi:10.1111/j.1365-2362.2006.01599.x

Bachem, M. G., SchnEidEr, E., Gross, H., WeidenbacH, H., Schmid, R. M., Menke, A., et al. (1998). Identification, culture, and characterization of pancreatic stellate cells in rats and humans. *Gastroenterology* 115 (2), 421–432. doi:10.1016/s0016-5085(98)70209-4

Bailey, C. J. (2017). Metformin: Historical overview. *Diabetologia* 60 (9), 1566–1576. doi:10.1007/s00125-017-4318-z

Bansod, S., Saifi, M. A., and Godugu, C. (2021). Inhibition of discoidin domain receptors by imatinib prevented pancreatic fibrosis demonstrated in experimental chronic pancreatitis model. *Sci. Rep.* 11 (1), 12894. doi:10.1038/s41598-021-92461-z

Beyer, G., Habtezion, A., Werner, J., Lerch, M. M., and Mayerle, J. (2020). Chronic pancreatitis. *Lancet* 396 (10249), 499–512. doi:10.1016/S0140-6736(20)31318-0

Bynigeri, R. R., Jakkampudi, A., Jangala, R., Subramanyam, C., Sasikala, M., Rao, G. V., et al. (2017). Pancreatic stellate cell: Pandora's box for pancreatic disease biology. *World J. Gastroenterol.* 23 (3), 382–405. doi:10.3748/wjg.v23.i3.382

Calfio, C., Gonzalez, A., Singh, S. K., Rojo, L. E., and Maccioni, R. B. (2020). The emerging role of nutraceuticals and phytochemicals in the prevention and treatment of alzheimer's disease. *J. Alzheimers Dis.* 77 (1), 33–51. doi:10.3233/JAD-200443

Charo, C., Holla, V., Arumugam, T., Hwang, R., Yang, P., Dubois, R. N., et al. (2013). Prostaglandin E2 regulates pancreatic stellate cell activity via the EP4 receptor. *Pancreas* 42 (3), 467–474. doi:10.1097/MPA.0b013e318264d0f8

Chronopoulos, A., Robinson, B., Sarper, M., Cortes, E., Auernheimer, V., Lachowski, D., et al. (2016). ATRA mechanically reprograms pancreatic stellate cells to suppress matrix remodelling and inhibit cancer cell invasion. *Nat. Commun.* 7, 12630. doi:10.1038/ncomms12630

Cui, L. H., Li, C. X., Zhuo, Y. Z., Yang, L., Cui, N. Q., and Zhang, S. K. (2019). Saikosaponin d ameliorates pancreatic fibrosis by inhibiting autophagy of pancreatic stellate cells via PI3K/Akt/mTOR pathway. *Chem. Biol. Interact.* 300, 18–26. doi:10.1016/j.cbi.2019.01.005

Duan, W., Chen, K., Jiang, Z., Chen, X., Sun, L., Li, J., et al. (2017). Desmoplasia suppression by metformin-mediated AMPK activation inhibits pancreatic cancer progression. *Cancer Lett.* 385, 225–233. doi:10.1016/j.canlet.2016.10.019

Efferth, T. (2006). Molecular pharmacology and pharmacogenomics of artemisinin and its derivatives in cancer cells. *Curr. Drug Targets* 7 (4), 407–421. doi:10.2174/138945006776359412

El-Hamoly, T., Hajnady, Z., Nagy-Penzes, M., Bakondi, E., Regdon, Z., Demeny, M. A., et al. (2021). Poly(ADP-Ribose) polymerase 1 promotes inflammation and fibrosis in a mouse model of chronic pancreatitis. *Int. J. Mol. Sci.* 22 (7), 3593. doi:10.3390/ijms22073593

Erkan, M., Adler, G., Apte, M. V., Bachem, M. G., Buchholz, M., Detlefsen, S., et al. (2012). StellaTUM: Current consensus and discussion on pancreatic stellate cell research. *Gut* 61 (2), 172–178. doi:10.1136/gutjnl-2011-301220

Fowler, E. K., Mohorianu, I., Smith, D. T., Dalmay, T., and Chapman, T. (2018). Small RNA populations revealed by blocking rRNA fragments in *Drosophila melanogaster* reproductive tissues. *PLoS One* 13 (2), e0191966. doi:10.1371/journal.pone.0191966

Froeling, F. E., Feig, C., Chelala, C., Dobson, R., Mein, C. E., Tuveson, D. A., et al. (2011). Retinoic acid-induced pancreatic stellate cell quiescence reduces paracrine Wnt-beta-catenin signaling to slow tumor progression. *Gastroenterology* 141 (4), 1486–1497. doi:10.1053/j.gastro.2011.06.047

Fu, Y., Liu, S., Zeng, S., and Shen, H. (2018). The critical roles of activated stellate cells-mediated paracrine signaling, metabolism and onco-immunology in pancreatic ductal adenocarcinoma. *Mol. Cancer* 17 (1), 62. doi:10.1186/s12943-018-0815-z

Gaman, L., Dragos, D., Vlad, A., Robu, G. C., Radoi, M. R., Stroica, L., et al. (2018). Phytoceuticals in acute pancreatitis: Targeting the balance between apoptosis and necrosis. *Evid. Based Complement. Altern. Med.* 2018, 5264592. doi:10.1155/2018/5264592

Hosseini, A., and Ghorbani, A. (2015). Cancer therapy with phytochemicals: Evidence from clinical studies. *Avicenna J. Phytomed.* 5 (2), 84–97.

Jin, G., Hong, W., Guo, Y., Bai, Y., and Chen, B. (2020). Molecular mechanism of pancreatic stellate cells activation in chronic pancreatitis and pancreatic cancer. *J. Cancer* 11 (6), 1505–1515. doi:10.7150/jca.38616

Joker-Jensen, H., Mathiasen, A. S., Kohler, M., Rasmussen, H. H., Drewes, A. M., and Olesen, S. S. (2020). Micronutrient deficits in patients with chronic pancreatitis: Prevalence, risk factors and pitfalls. *Eur. J. Gastroenterol. Hepatol.* 32 (10), 1328–1334. doi:10.1097/MEG.0000000000001866

Kandikattu, H. K., Venkateshaiah, S. U., and Mishra, A. (2020). Chronic pancreatitis and the development of pancreatic cancer. *Endocr. Metab. Immune Disord. Drug Targets* 20 (8), 1182–1210. doi:10.2174/1871530320666200423095700

Kim, W. S., Choi, W. J., Lee, S., Lee, D. C., Sohn, U. D., Kim, W. J., et al. (2015). Anti-inflammatory, antioxidant and antimicrobial effects of artemisinin extracts from Artemisia annua L. *Korean J. Physiol. Pharmacol.* 19 (1), 21–27. doi:10.4196/kjpp.2015.19.1.21

Klapdor, S., Richter, E., and Klapdor, R. (2012). Vitamin D status and per-oral vitamin D supplementation in patients suffering from chronic pancreatitis and pancreatic cancer disease. *Anticancer Res.* 32 (5), 1991–1998.

Komar, H. M., Serpa, G., Kerscher, C., Schwoegl, E., Mace, T. A., Jin, M., et al. (2017). Inhibition of Jak/STAT signaling reduces the activation of pancreatic stellate cells *in vitro* and limits caerulein-induced chronic pancreatitis *in vivo*. *Sci. Rep.* 7 (1), 1787. doi:10.1038/s41598-017-01973-0

Lai, H. C., Singh, N. P., and Sasaki, T. (2013). Development of artemisinin compounds for cancer treatment. *Invest. New Drugs* 31 (1), 230–246. doi:10.1007/s10637-012-9873-z

Lee, A. T., Xu, Z., Pothula, S. P., Patel, M. B., Pirola, R. C., Wilson, J. S., et al. (2015). Alcohol and cigarette smoke components activate human pancreatic stellate cells: Implications for the progression of chronic pancreatitis. *Alcohol. Clin. Exp. Res.* 39 (11), 2123–2133. doi:10.1111/acer.12882

Lee, L. S., Kim, S. H., Kim, Y. B., and Kim, Y. C. (2014). Quantitative analysis of major constituents in green tea with different plucking periods and their antioxidant activity. *Molecules* 19 (7), 9173–9186. doi:10.3390/molecules19079173

Li, C. X., Cui, L. H., Zhang, L. Q., Yang, L., Zhuo, Y. Z., Cui, N. Q., et al. (2021). Role of NLR family pyrin domain-containing 3 inflammasome in the activation of pancreatic stellate cells. *Exp. Cell Res.* 404 (2), 112634. doi:10.1016/j.yexcr.2021.112634

Li, G. M., Chen, J. R., Zhang, H. Q., Cao, X. Y., Sun, C., Peng, F., et al. (2021). Update on pharmacological activities, security, and pharmacokinetics of rhein. *Evid. Based. Complement. Altern. Med.* 2021, 4582412. doi:10.1155/2021/4582412

Li, L., Wang, K., Jia, R., Xie, J., Ma, L., Hao, Z., et al. (2022). Ferroportin-dependent ferroptosis induced by ellagic acid retards liver fibrosis by impairing the SNARE complexes formation. *Redox Biol.* 56, 102435. doi:10.1016/j.redox.2022.102435

Li, Z., Lu, D., Jin, T., Liu, X., and Hao, J. (2021). Nicotine facilitates pancreatic fibrosis by promoting activation of pancreatic stellate cells via α7nAChR-mediated JAK2/STAT3 signaling pathway in rats. *Toxicol. Lett.* 349, 84–91. doi:10.1016/j.toxlet.2021.06.012

Lin, Z., Zheng, L. C., Zhang, H. J., Tsang, S. W., and Bian, Z. X. (2015). Anti-fibrotic effects of phenolic compounds on pancreatic stellate cells. *BMC Complement. Altern. Med.* 15, 259. doi:10.1186/s12906-015-0789-y

Luo, P., Liu, D., Zhang, Q., Yang, F., Wong, Y. K., Xia, F., et al. (2022). Celastrol induces ferroptosis in activated HSCs to ameliorate hepatic fibrosis via targeting peroxiredoxins and HO-1. *Acta Pharm. Sin. B* 12 (5), 2300–2314. doi:10.1016/j.apsb.2021.12.007

Masamune, A., Kikuta, K., Satoh, M., Suzuki, N., and Shimosegawa, T. (2005). Green tea polyphenol epigallocatechin-3-gallate blocks PDGF-induced proliferation and migration of rat pancreatic stellate cells. *World J. Gastroenterol.* 11 (22), 3368–3374. doi:10.3748/wjg.v11.i22.3368

Miller, L. H., and Su, X. (2011). Artemisinin: Discovery from the Chinese herbal garden. *Cell* 146 (6), 855–858. doi:10.1016/j.cell.2011.08.024

Mohanavelu, P., Mutnick, M., Mehra, N., White, B., Kudrimoti, S., Hernandez Kluesner, K., et al. (2021). Meta-analysis of gastrointestinal adverse events from tyrosine kinase inhibitors for chronic myeloid leukemia. *Cancers (Basel)* 13 (7), 1643. doi:10.3390/cancers13071643

Nambudiri, V. E., and Widlund, H. R. (2013). Small interfering RNA. *J. Invest. Dermatol.* 133 (12), 1–4. doi:10.1038/jid.2013.411

Nielsen, M. F. B., Mortensen, M. B., and Detlefsen, S. (2017). Identification of markers for quiescent pancreatic stellate cells in the normal human pancreas. *Histochem. Cell Biol.* 148 (4), 359–380. doi:10.1007/s00418-017-1581-5

Pang, T. C. Y., Wilson, J. S., and Apte, M. V. (2017). Pancreatic stellate cells: what's new? *Curr. Opin. Gastroenterol.* 33 (5), 366–373. doi:10.1097/MOG.0000000000000378

Paulo, J. A., Kadiyala, V., Banks, P. A., Conwell, D. L., and Steen, H. (2013). Mass spectrometry-based quantitative proteomic profiling of human pancreatic and hepatic stellate cell lines. *Genomics Proteomics Bioinforma.* 11 (2), 105–113. doi:10.1016/j.gpb.2013.01.009

Pezzilli, R., Fabbri, D., Imbrogno, A., and Corinaldesi, R. (2011). Tyrosine kinase inhibitors, pancreatic hyperenzymemia and acute pancreatitis: A review. *Recent Pat. Inflamm. Allergy Drug Discov.* 5 (2), 165–168. doi:10.2174/187221311795399255

Poilil Surendran, S., George Thomas, R., Moon, M. J., and Jeong, Y. Y. (2017). Nanoparticles for the treatment of liver fibrosis. *Int. J. Nanomedicine* 12, 6997–7006. doi:10.2147/IJN.S145951

Rauf, A., Imran, M., Butt, M. S., Nadeem, M., Peters, D. G., and Mubarak, M. S. (2018). Resveratrol as an anti-cancer agent: A review. *Crit. Rev. Food Sci. Nutr.* 58 (9), 1428–1447. doi:10.1080/10408398.2016.1263597

Ren, Y., Zhang, J., Wang, M., Bi, J., Wang, T., Qiu, M., et al. (2020). Identification of irisin as a therapeutic agent that inhibits oxidative stress and fibrosis in a murine

model of chronic pancreatitis. *Biomed. Pharmacother.* 126, 110101. doi:10.1016/j.biopha.2020.110101

Semwal, R. B., Semwal, D. K., Combrinck, S., and Viljoen, A. (2021). Emodin - a natural anthraquinone derivative with diverse pharmacological activities. *Phytochemistry* 190, 112854. doi:10.1016/j.phytochem.2021.112854

Setiawan, V. W., Monroe, K., Lugea, A., Yadav, D., and Pandol, S. (2017). Uniting epidemiology and experimental disease models for alcohol-related pancreatic disease. *Alcohol Res.* 38 (2), 173–182.

Sharma, N., Bhandari, S., Deshmukh, R., Yadav, A. K., and Mishra, N. (2017). Development and characterization of embelin-loaded nanolipid carriers for brain targeting. *Artif. Cells Nanomed. Biotechnol.* 45 (3), 409–413. doi:10.3109/21691401.2016.1160407

Shen, M., Guo, M., Li, Y., Wang, Y., Qiu, Y., Shao, J., et al. (2022). m(6 A methylation is required for dihydroartemisinin to alleviate liver fibrosis by inducing ferroptosis in hepatic stellate cells. *Free Radic. Biol. Med.* 182, 246–259. doi:10.1016/j.freeradbiomed.2022.02.028

Sherman, M. H., Yu, R. T., Engle, D. D., Ding, N., Atkins, A. R., Tiriac, H., et al. (2014). Vitamin D receptor-mediated stromal reprogramming suppresses pancreatitis and enhances pancreatic cancer therapy. *Cell* 159 (1), 80–93. doi:10.1016/j.cell.2014.08.007

Shi, C., Li, H., Yang, Y., and Hou, L. (2015). Anti-inflammatory and immunoregulatory functions of artemisinin and its derivatives. *Mediat. Inflamm.* 2015, 435713. doi:10.1155/2015/435713

Spanehl, L., Revskij, D., Bannert, K., Ehlers, L., and Jaster, R. (2022). YAP activates pancreatic stellate cells and enhances pancreatic fibrosis. *Hepatobiliary Pancreat. Dis. Int.* doi:10.1016/j.hbpd.2022.06.004

Tan, P., Wang, A., Chen, H., Du, Y., Qian, B., Shi, H., et al. (2019). SPOP inhibits mice pancreatic stellate cell activation by promoting FADD degradation in cerulein-induced chronic pancreatitis. *Exp. Cell Res.* 384 (1), 111606. doi:10.1016/j.yexcr.2019.111606

Tsang, S. W., and Bian, Z. X. (2015). Anti-fibrotic and anti-tumorigenic effects of rhein, a natural anthraquinone derivative, in mammalian stellate and carcinoma cells. *Phytother. Res.* 29 (3), 407–414. doi:10.1002/ptr.5266

Tsang, S. W., Zhang, H., Lin, C., Xiao, H., Wong, M., Shang, H., et al. (2013). Rhein, a natural anthraquinone derivative, attenuates the activation of pancreatic stellate cells and ameliorates pancreatic fibrosis in mice with experimental chronic pancreatitis. *PLoS One* 8 (12), e82201. doi:10.1371/journal.pone.0082201

Vancura, A., Bu, P., Bhagwat, M., Zeng, J., and Vancurova, I. (2018). Metformin as an anticancer agent. *Trends Pharmacol. Sci.* 39 (10), 867–878. doi:10.1016/j.tips.2018.07.006

Wallbaum, P., Rohde, S., Ehlers, L., Lange, F., Hohn, A., Bergner, C., et al. (2018). Antifibrogenic effects of vitamin D derivatives on mouse pancreatic stellate cells. *World J. Gastroenterol.* 24 (2), 170–178. doi:10.3748/wjg.v24.i2.170

Wang, K., Wang, J., Song, M., Wang, H., Xia, N., and Zhang, Y. (2020). Angelica sinensis polysaccharide attenuates CCl4-induced liver fibrosis via the IL-22/STAT3 pathway. *Int. J. Biol. Macromol.* 162, 273–283. doi:10.1016/j.ijbiomac.2020.06.166

Wang, K., Yang, X., Wu, Z., Wang, H., Li, Q., Mei, H., et al. (2020). Dendrobium officinale polysaccharide protected CCl4-induced liver fibrosis through intestinal homeostasis and the LPS-TLR4-NF-κb signaling pathway. *Front. Pharmacol.* 11, 240. doi:10.3389/fphar.2020.00240

Watari, N., Hotta, Y., and Mabuchi, Y. (1982). Morphological studies on a vitamin A-storing cell and its complex with macrophage observed in mouse pancreatic tissues following excess vitamin A administration. *Okajimas Folia Anat. Jpn.* 58 (4-6), 837–858. doi:10.2535/ofaj1936.58.4-6_837

Wei, X., Yi, X., Zhu, X. H., and Jiang, D. S. (2020). Posttranslational modifications in ferroptosis. *Oxid. Med. Cell. Longev.* 2020, 8832043. doi:10.1155/2020/8832043

White, N. J., Hien, T. T., and Nosten, F. H. (2015). A brief history of qinghaosu. *Trends Parasitol.* 31 (12), 607–610. doi:10.1016/j.pt.2015.10.010

Wu, N., Xu, X. F., Xin, J. Q., Fan, J. W., Wei, Y. Y., Peng, Q. X., et al. (2021). The effects of nuclear factor-kappa B in pancreatic stellate cells on inflammation and fibrosis of chronic pancreatitis. *J. Cell. Mol. Med.* 25 (4), 2213–2227. doi:10.1111/jcmm.16213

Wu, P., Nielsen, T. E., and Clausen, M. H. (2015). FDA-approved small-molecule kinase inhibitors. *Trends Pharmacol. Sci.* 36 (7), 422–439. doi:10.1016/j.tips.2015.04.005

Wu, Y., Zhang, C., Jiang, K., Werner, J., Bazhin, A. V., and D'Haese, J. G. (2020). The role of stellate cells in pancreatic ductal adenocarcinoma: Targeting perspectives. *Front. Oncol.* 10, 621937. doi:10.3389/fonc.2020.621937

Xian, Z., Tian, J., Wang, L., Zhang, Y., Han, J., Deng, N., et al. (2020). Effects of rhein on bile acid homeostasis in rats. *Biomed. Res. Int.* 2020, 8827955. doi:10.1155/2020/8827955

Xiao, W., Jiang, W., Shen, J., Yin, G., Fan, Y., Wu, D., et al. (2015). Retinoic acid ameliorates pancreatic fibrosis and inhibits the activation of pancreatic stellate cells in mice with experimental chronic pancreatitis via suppressing the wnt/β-catenin signaling pathway. *PLoS One* 10 (11), e0141462. doi:10.1371/journal.pone.0141462

Yan, B., Cheng, L., Jiang, Z., Chen, K., Zhou, C., Sun, L., et al. (2018). Resveratrol inhibits ROS-promoted activation and glycolysis of pancreatic stellate cells via suppression of miR-21. *Oxid. Med. Cell Longev.* 2018, 1346958. doi:10.1155/2018/1346958

Yang, X., Chen, J., Wang, J., Ma, S., Feng, W., Wu, Z., et al. (2022). Very-low-density lipoprotein receptor-enhanced lipid metabolism in pancreatic stellate cells promotes pancreatic fibrosis. *Immunity* 55 (7), 1185–1199 e8. doi:10.1016/j.immuni.2022.06.001

Zeng, X. P., Wang, L. J., Guo, H. L., He, L., Bi, Y. W., Xu, Z. L., et al. (2019). Corrigendum to "Dasatinib ameliorates chronic pancreatitis induced by caerulein via anti-fibrotic and anti-inflammatory mechanism" [Pharmacol Res. 147 (2019) 104357]. *Pharmacol. Res.* 147, 104788. doi:10.1016/j.phrs.2020.104788

Zhang, Z., Wang, X., Wang, Z., Cao, Y., Wei, Z., Zhang, Z., et al. (2021). Dihydroartemisinin alleviates hepatic fibrosis through inducing ferroptosis in hepatic stellate cells. *Biofactors* 47 (5), 801–818. doi:10.1002/biof.1764

Zheng, M., Li, H., Sun, L., Brigstock, D. R., and Gao, R. (2021). Interleukin-6 participates in human pancreatic stellate cell activation and collagen I production via TGF-β1/Smad pathway. *Cytokine* 143, 155536. doi:10.1016/j.cyto.2021.155536

Zhou, J. H., Cheng, H. Y., Yu, Z. Q., He, D. W., Pan, Z., and Yang, D. T. (2011). Resveratrol induces apoptosis in pancreatic cancer cells. *Chin. Med. J.* 124 (11), 1695–1699.

Zhu, Y., Zhang, C., Huang, M., Lin, J., Fan, X., and Ni, T. (2021). TRIM26 induces ferroptosis to inhibit hepatic stellate cell activation and mitigate liver fibrosis through mediating SLC7A11 ubiquitination. *Front. Cell Dev. Biol.* 9, 644901. doi:10.3389/fcell.2021.644901

frontiers | Frontiers in Pharmacology

TYPE Original Research
PUBLISHED 20 October 2022
DOI 10.3389/fphar.2022.1002565

OPEN ACCESS

EDITED BY
Yan Huang,
Anhui Medical University, China

REVIEWED BY
Shaofeng Pu,
Shanghai Jiao Tong University, China
Dingsheng Zha,
First Affiliated Hospital of Jinan University, China

*CORRESPONDENCE
Lingsuo Kong,
konglingsuo3201@ustc.edu.cn

†These authors have contributed equally to this work and share first authorship

SPECIALTY SECTION
This article was submitted to Inflammation Pharmacology, a section of the journal Frontiers in Pharmacology

RECEIVED 25 July 2022
ACCEPTED 22 September 2022
PUBLISHED 20 October 2022

CITATION
Ge F, Li Z, Hu J, Pu Y, Zhao F and Kong L (2022), METTL3/m^{6}A/IFIT2 regulates proliferation, invasion and immunity in esophageal squamous cell carcinoma. *Front. Pharmacol.* 13:1002565. doi: 10.3389/fphar.2022.1002565

METTL3/m^{6}A/IFIT2 regulates proliferation, invasion and immunity in esophageal squamous cell carcinoma

Fangfang Ge[1,2†], Zhenyu Li[1,2†], Jiaru Hu[3], Youguang Pu[4], Fangfang Zhao[4] and Lingsuo Kong[1*]

[1]Department of Anesthesiology, the First Affiliated Hospital of USTC, Division of Life Sciences and Medicine, University of Science and Technology of China, Hefei, China, [2]Department of Provincial Clinical College, Wannan Medical College, Wuhu, China, [3]Division of Life Sciences and Medicine, Department of the First Affiliated Hospital of USTC, University of Science and Technology of China, Hefei, China, [4]Division of Life Sciences and Medicine, Department of Cancer Epigenetics Program, The First Affiliated Hospital of USTC, University of Science and Technology of China, Hefei, China

Epigenetic regulation plays a critical role in the development, progression, and treatment of tumors. The most common chemical modification of mRNA, called m^{6}A, is essential for controlling mRNA stability, splicing, and translation. Methyltransferase-like 3 (METTL3) is an important m6A methyltransferase. The mechanism of action of METTL3 in esophageal squamous cell carcinoma (ESCC) remains unclear. In this investigation, we sought to clarify the function and clinical importance of METTL3 in ESCC and investigate its underlying mechanisms. We discovered that METTL3 has a significant proliferative effect in ESCC cells by using lentiviral construction of stable cell lines overexpressing METTL3 (METTL3-OE) and knocking down METTL3 (sh-METTL3). To create a xenograft tumor model, we inoculated KYSE510 cells subcutaneously into BALB/c nude mice and discovered that sh-METTL3 inhibited the tumorigenicity of esophageal cancer KYSE510 cells in the nude mouse tumor model. MeRIP-seq and RNA-seq analysis revealed IFIT2 to be a METTL3 target gene. The findings revealed that METTL3 regulates IFIT2 and thus influences malignant biological behaviors such as proliferation, migration, and invasion of ESCC, as well as the immune microenvironment of tumors.

KEYWORDS

squamous cell carcinoma, N6-methyladenosine modification, METTL3, IFIT2, immune infiltration

Introduction

Esophageal cancer is the seventh most common malignant disease worldwide and the sixth leading cause of cancer-related mortality. Global cancer statistics for 2020 suggest 544,000 deaths and 604,000 new cases (Sung et al., 2021). One of the most aggressive tumors, squamous cell carcinoma, makes up 90% of metastatic

esophageal cancers (Liu et al., 2017). Despite notable improvements in the treatment of lung, breast, and other cancers over the past ten years, the number of people with esophageal cancer has remained stable (Lagergren et al., 2017). Surgery, radiation therapy, and chemotherapy are all effective treatments for esophageal cancer, but their long-term prognosis is still poor (Wang et al., 2018). In an effort to improve the prognosis and overall survival rate of the disease, we are actively exploring the pathogenesis of esophageal cancer.

Genetic abnormalities are what initiates and fuels the development of cancer, and tumorigenesis is greatly influenced by epigenetic pathways (Dawson and Kouzarides, 2012). Epigenetic modifications can alter gene expression without changing the base sequence (Toh et al., 2017). RNA modification widely affects the structure, function and stability of RNA and has been a research hotspot in recent years (Barbieri and Kouzarides, 2020). mRNA is a crucial step in the process of interpreting genetic information since it is the main molecular connection between DNA and protein (Delaveau et al., 2016). One-third of all mammalian mRNAs have an average of 3-5 m^{6}A modifications, which is the most common type of posttranscriptional modification in mRNA (Jiang et al., 2021). This modification has the potential to influence RNA stability, splicing, transport, and localization, and various diseases are influenced by its activity (Zhao et al., 2017). They are intently related to the regulation of current therapeutic approaches and may additionally supply new options for the fine cure of illness (Ma and Ji, 2020).

m^{6}A modification is a dynamic and reversible process achieved by "writer" methylesterase, "eraser" demethylase and "reader" methyl recognition protein (Ping et al., 2014; Wang et al., 2016). METTL3, the major catalytic component of the methyltransferase complex, recognizes a conserved sequence of RNA 5′-RRACU-3' (R = A or G) (Dominissini et al., 2012). METTL3 is mainly involved in posttranscriptional regulation. Abnormal expression alters the fate of m^{6}A transcripts (He and He, 2021). Loss of METTL3 results in a dramatic drop in m^{6}A levels and effects on other molecules (Koh et al., 2019a). Researchers have found that METTL3 is highly expressed in lung adenocarcinomas, while METTL3-silenced cells proliferate and migrate much less than those that are not silenced (Lin et al., 2016). In contrast, METTL3 regulates tumor growth by cooperating with YTHDF2 to modify tumor-associated neutrophils (TANs) infiltration and performs a key tumor suppressor role in papillary thyroid carcinoma (He et al., 2021). It appears that METTL3 plays a dual role, which may be related to the tumor's primary site of development, the cellular microenvironment, upstream and downstream regulatory elements, and resistance mechanisms.

The host immune system has an important influence on all aspects of tumor cell proliferation, epithelial mesenchymal transition, invasion, and metastasis (Liu et al., 2021). m^{6}A modification also affects the tumor immune microenvironment (Ma et al., 2021). Inhibition of METTL3 enhances the response to immunotherapy in colorectal cancer and melanoma. Through T-cell activation, depletion, and infiltration mediated by PD-L1, METTL3 improves antitumor immunity in breast cancer both *in vitro* and *in vivo* (Wan et al., 2022). METTL3-mediated m^{6}A modification has been shown to significantly improve the capacity of tumor-infiltrating myeloid cells to suppress the immune system and facilitate tumor immune evasion (Xiong et al., 2022). However, it is still unclear how METTL3 contributes to esophageal cancer and what its exact mechanism is. We also investigated whether METTL3's role in esophageal cancer is immune-related.

In this study, we demonstrate that METTL3 regulates esophageal cancer proliferation, invasion, and immunity *via* the downstream target IFIT2.

Materials and methods

Esophageal cancer specimens and cell lines

Eleven samples from esophageal cancer patients who underwent surgery were obtained from the West Hospital of the First Affiliated Hospital of Chinese University of Science and Technology. The Biomedical Ethics Committee of the University of Science and Technology of China conducted every experiment for this study. The clinicopathological details of every participant who gave their written consent are listed in Supplementary Table S1. HEEC and KYSE150, KYSE510, KYSE30, KYSE140, KYSE410, and KYSE450 cell lines were obtained from the China Cell Resource Center (Shanghai, China). The cells were cultured in RPMI 1640 (Gibco) supplemented with 10% fetal bovine serum (PAN) and 1% penicillin–streptomycin.

RNA extraction and quantitative RT–PCR analysis

Total RNA was extracted from tissues and cells using TRIzol reagent (Vazyme). A total of 1000 ng of total RNA was reverse transcribed to obtain cDNA using the HiScript®II 1st Strand cDNA Synthesis Kit (Vazyme). The relative mRNA expression was calculated using the $2^{-\Delta\Delta Ct}$ method. TaqMan probe quantitative PCR was used to locate the target gene's expression, and ACTB was used as an internal control. All qPCR primer sequences are presented in Supplementary Table S2.

Western blot

Lysis buffer was used to lyse esophageal tissue and cells. After boiling the proteins for 10 min in a metal bath, the proteins were denatured. SDS–PAGE (Beyotime Biotechnology) was used to separate the samples, which were then transferred to PVDF membranes (Millipore). Then, the cells were blocked with 5% nonfat milk for an hour. The primary antibody (1:2000) was placed on the membrane overnight in a 4° refrigerator, and then the secondary antibody (1:5000) was applied to the membrane for 1 h at room temperature. The signal band was exposed to ECL luminescence solution (Thermo). Proteintech provided all the antibodies used in this article. Detailed information on full-length gels is provided in Supplementary Figures S7–S15.

Plasmid and lentiviral transfection

The cells were seeded into 24-well plates, the cell density was increased to 30%, lentiviral infection (MOI = 3) was carried out, and puromycin was used to screen stable cell lines for overexpression and knockdown. Construction, sequencing, packaging, concentration, and purification were performed on the lentiviral plasmid containing the target gene. Virus titer determination was entrusted to Shanghai Hanheng Company. METTL3-OE (NM_019852.5) and IFIT2-OE (NM_001547.5). The IFIT2 gene was silenced using small interfering RNAs (siRNAs), all of which were produced by GenePharma. By using Lipofectamine 2000, plasmids containing the transgene and a packaging plasmid were cotransfected into KYSE510 and KYSE30 cells (Invitrogen, USA). The sh-RNA and siRNA sequences are listed in Supplementary Table S2.

CCK-8 assay

The proliferation assay was carried out in a 96-well plate with 3000 cells per well. After 0, 24, 48 and 72 h, 10 μL of CCK-8 solution (Bimake) was added to every well and then incubated for 2 h. The absorbance (OD) of each well at 450 nm was detected by an enzyme labeling instrument, and the cell viability was calculated.

Colony formation assay

In six-well plates, 300 or 400 cells were seeded per well and then cultured for two weeks in medium containing 10% FBS. After that, 4% paraformaldehyde was added for fixation for 15 min, followed by 0.1% crystal violet staining for 15 min. The staining solution was discarded, and the cells were air-dried and counted.

Wound healing assays

Once the density reached 100% in twelve-well plates, the cells were scraped vertically from top to bottom with a 10 μL sterile pipette tip. Serum-free medium was added after washing 3 times with precooled PBS. Pictures were taken at 0 h and 24 h. Analysis of area measurements for wound healing experiments using ImageJ software.

Transwell assay

Transwell chambers were covered with Matrigel (BD) for invasion assays, while those without Matrigel were used for migration assays. Differently treated cells (5×10^4 for the migration assay and 1×10^5 for the invasion assay) were loaded into 8 μm diameter 24-well transwells (Corning) and cultured without serum. In the lower compartment, 600 μL of medium containing 20% serum was added. Nonmigrating cells were scraped off after 24 h, and noninvasive cells were removed after 48 h. Migrating and invasive cells were fixed with 4% paraformaldehyde for 30 min. After staining with 1% crystal violet solution for 30 min, the cells in the upper chamber were wiped clean with a cotton swab, counted, and photographed.

Flow cytometry

After being collected and resuspended in binding buffer, the cells underwent an incubation period of 5 min at room temperature with fluorescently labeled APC and PI (Annexin V-APC/PI apoptosis kit).

Quantification of RNA m^{6}A modification

To each well, 200 ng–300 ng of RNA extracted from cells, capture antibody, detection antibody, enhancer solution, chromogenic reagent solution, and stop solution was added and incubated in the dark for 5–15 min. The optical density value (OD) (450) of the standard was detected by a microplate reader at 450 nm and used to calculate the relative m^{6}A content (m^{6}A%) of the RNA to be tested. EpiQuik M^{6}A RNA methylation quantitative kit (P9005; Epigentek).

RNA-sequencing, RNA-seq

The RNA library construction kit was used to build the library after the RNA had been quantified, and all operations were carried out in accordance with the instructions. Second-generation sequencing was carried out by Ribo after the

library was checked, double end sequenced, and used in a sequencer.

Model of xenotransplantation

ESCC tumor xenograft model establishment in 4-week-old male nude mice. Mice were subcutaneously injected with 1×10^7 cells resuspended in 100 μL PBS containing Matrigel (1:1). Every four days, the tumor volume was measured with calipers. The volume is calculated as 1/2×length×width squared. One month after injection, the mice were euthanized. The weight and images of subcutaneous tumors were taken. The mouse tumors were embedded and fixed before being stained with HE on dewaxed sections. IHC staining of Ki67 revealed the proliferation index. TUNEL was used to detect apoptotic cells. All animal research procedures were carried out under a program approved by the Animal Laboratory Center of University of Science and Technology of China.

Immunohistochemistry

Dewaxed and hydrated paraffin sections were incubated with the primary antibodies Ki67 (1:200), METTL3 (1:500) and IFIT2 (1:500) overnight at 4°C before being incubated with the secondary antibody for two hours at room temperature. The antigen was then repaired and titrated with a blocking endogenous peroxidase blocker.

For 7 pairs of cancer and paracancerous tissue samples, the H-Score method was used to analyze them by ImageJ's IHC Profiler software (Varghese et al., 2014). The result obtained was scored as 0 (negative), 1+ (low positive), 2+ (positive) and 3+ (high positive). For IHC staining of METTL3, an IHC score ≥2 was defined as high METTL3 expression, and an IHC score <2 was defined as low METTL3 expression. Ki67 was detected in animal specimens, and the positive area of Ki67 was counted by ImageJ.

Bioinformatics analysis

The Gene Expression Profiling Interactive Analysis (GEPIA) database was used to analyze the total expression level of METTL3 in ESCC and normal esophageal epithelial samples. The TCGA dataset was used to download the TRNA-sequencing expression profiles for ESCC along with the associated clinical data. Based on the prognostic data of esophageal cancer patients and METTL3 and IFIT2 expression data, a prognostic model was constructed using the LASSO Cox regression model (R package "glmnet"). The risk score was calculated by normalizing the TCGA expression data (R package "scale" function) with the following formula: Risk Score = (X: regression coefficient; Y: gene expression level), and the ROC prognostic assessment curve was constructed based on the risk score.

ROC curve analysis by muti_cox. R package and pROC package. The pathways that were enriched by GSEA. TIMER is a convenient method for analyzing immune infiltrates in TCGA tumors. Multigene correlation was visualized using the R programming language's pheatmap package.

Statistical analysis

The experimental results were analyzed using GraphPad Prism 9.0 statistical software. The data are at least the average of three experimental data points, and the *t* test was used to compare groups and analyze differences between them ($^*p < 0.05$, $^{**}p < 0.01$, $^{***}p < 0.001$, $^{****}p < 0.0001$).

Results

METTL3 is upregulated in esophageal squamous cell carcinoma

We gathered 11 pairs of clinical samples from esophageal cancer and paracancerous tissue. Following the extraction of RNA and protein from 4 pairs, it was discovered that the levels of METTL3 mRNA and protein expression in tumor tissues were higher than those in adjacent tissues (Figures 1A,B). This is in line with the TCGA database's findings that esophageal cancer tumor tissues exhibit high levels of METTL3 expression (Figure 1C). Seven esophageal cancer cell lines expressed METLL3 at levels higher than those of human esophageal epithelial cells (HEECs) (Figure 1D). After that, immunohistochemistry was used to examine seven pairs of clinical specimens that had been fixed, dehydrated, and paraffin-embedded, and the results revealed that METTL3 expression was higher than that of adjacent tumors (Figure 1E). Collectively, these results clearly demonstrated that METTL3 is highly expressed in esophageal cancer patients.

High METTL3 expression is associated with ESCC proliferation, apoptosis, migration and invasion

We constructed stable cells using lentiviral METTL3 expression constructs. As shown, the results indicated that not only the METTL3 expression of this protein but also the expression at the mRNA level was increased (Figure 2A). The results from CCK-8 and colony experiments revealed that overexpressing METTL3 significantly increased the ability of KYSE510 and KYSE30 cells to proliferate. Likewise, flow cytometry measurements were employed to evaluate the apoptotic capacity

of cells. These results confirmed that METTL3 overexpression notably decreased the percentage of apoptotic cells (Figure 2B–D). Wound-healing assays showed that METTL3-overexpressing cells had a markedly increased wound closure area at 24 h (Figure 2E). To similarly reflect the effect of METTL3 on cell invasion, transwell invasion and migration assays were performed. The results implied that METTL3 overexpression promoted cell migration and invasion (Figure 2F). In the detection of associated apoptosis proteins, BCL2 and cyclin D1 protein levels were upregulated in the METTL3-OE group. At the same time, overexpressing METTL3 inhibited the expression of Caspase3. Moreover, we noted that the expression of EMT-related proteins varied, with MMP19 and Vimentin showing increased expression, while E-cadherin showed diminished expression (Figure 2G).

Low METTL3 expression is associated with proliferation, apoptosis, migration and invasion in ESCC cells

We performed the assay utilizing shRNA lenticular METTL3 knockdown. The results confirmed that the

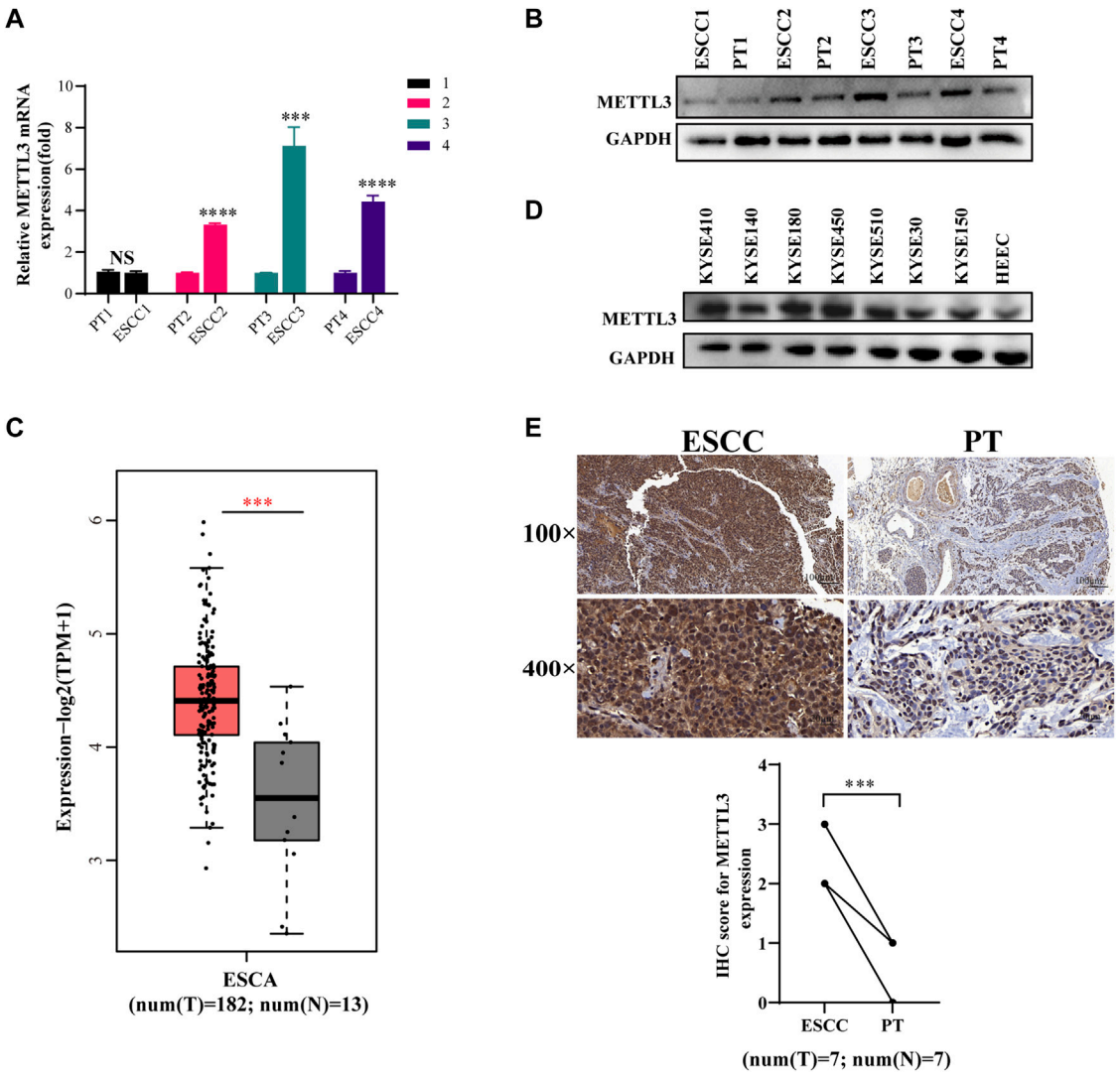

FIGURE 1
METTL3 is upregulated in esophageal squamous cell carcinoma **(A,B)**. qPCR and WB were used to measure METTL3 expression in 4 pairs of ESCC tissues and corresponding adjacent tissues. **(C)**. METTL3 expression levels in the TCGA database. **(D)**. METTL3 was expressed in seven ESCC cell lines and HEEC cells. **(E)**. Representative image of immunohistochemical staining by METTL3 in 100-fold (scaled bar = 100 μm) and 400-fold (scaled bar = 20 μm) magnified ESCC tissues and paired normal tissues in human samples (above). Immunohistochemical expression of METTL3 in ESCC tumor tissue and paired paracancerous tissues (PT) was quantitatively analyzed using ImageJ Profiler software (n = 7). n.s, no statistical significance, ***p < 0.001, ****p < 0.0001.

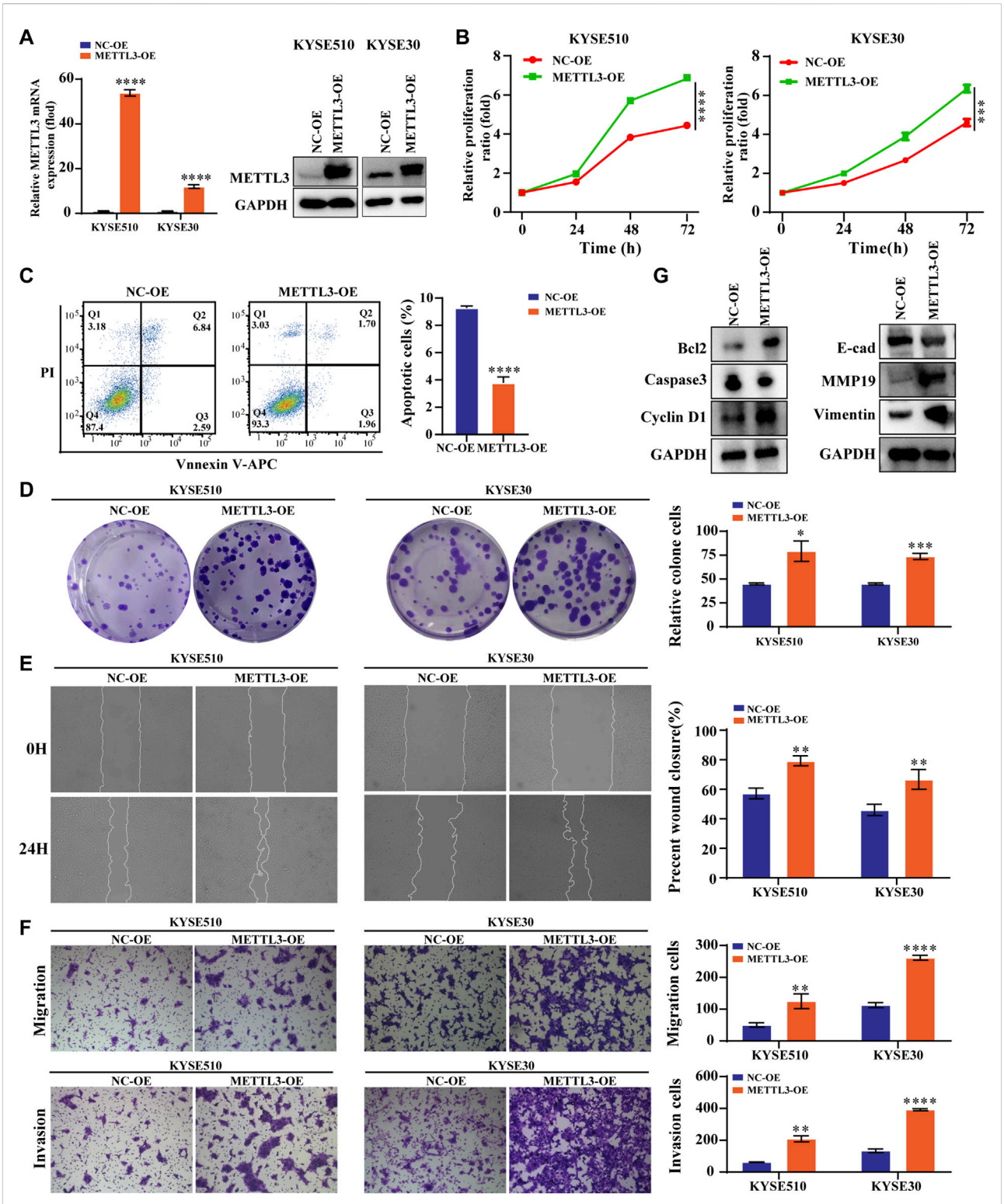

FIGURE 2
High METTL3 expression is associated with proliferation, apoptosis, migration and invasion in ESCC cells **(A)**. METTL3 mRNA and protein levels were drastically elevated following lentiviral transfection of KYSE510 and KYSE30 cells. **(B)**. The CCK-8 assay assessed the proliferation ability of METTL3-overexpressing KYSE510 and KYSE30 cells. **(C)**. Flow cytometric analysis was conducted to assess apoptosis in KYSE510 METTL3-overexpressing cells. **(D)**. The clonality of KYSE510 and KYSE30 cells was measured by the plate clone. **(E)**. The wound scratch test and **(F)**. Transwell migration and invasion assays were conducted to examine the migratory and invasion capacities of KYSE510 and KYSE30 cells overexpressing METTL3. **(G)**. Expression of E-cadherin, MMP19 and Vimentin proteins was detected *via* western transfer in METTL3-overexpressing cells. The protein levels of Bcl2, Caspase 3 and Cyclin D1 were detected by western blotting in METTL3-overexpressing cells. *$p < 0.05$, **$p < 0.01$, ***$p < 0.001$, ****$p < 0.0001$.

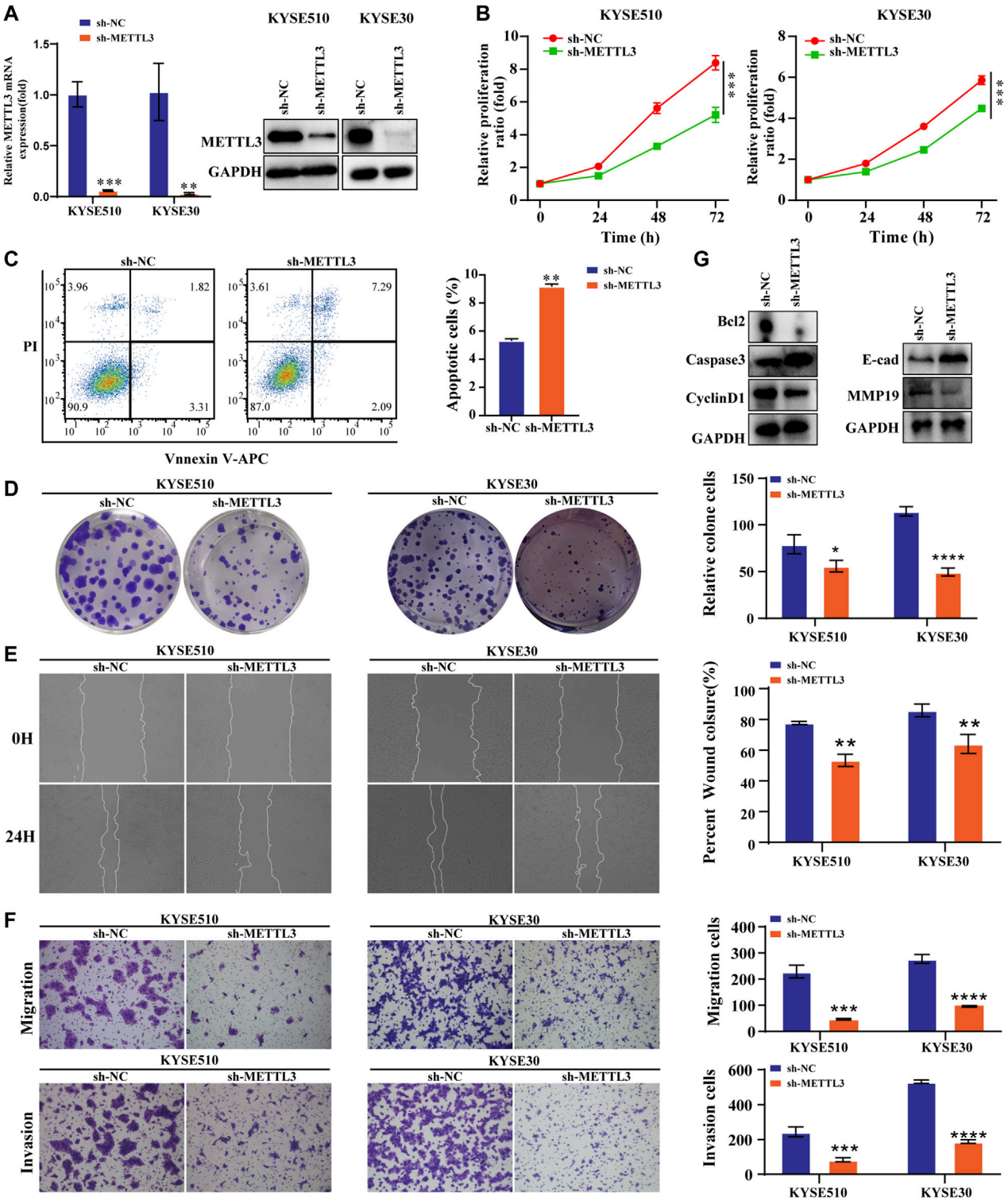

FIGURE 3
Low METTL3 expression is associated with proliferation, apoptosis, migration and invasion in ESCC cells **(A)**. The mRNA and protein levels of METTL3 were drastically decreased following lentiviral transfection of KYSE510 and KYSE30 cells. **(B)**. The CCK-8 assay assessed the proliferation ability of METTL3-knockdown cells. **(C)**. Flow cytometric analysis was conducted to assess apoptosis in KYSE510 METTL3-knockdown cells. **(D)**. The clonality of KYSE510 and KYSE30 cells was measured by the plate clone. **(E)**. The wound scratch test and **(F)**. Transwell migration and invasion assays were conducted to examine the migratory and invasion capacities of METTL3 knockdown cells. **(G)**. Expression of E-cadherin and MMP19 proteins was detected *via* western transfer in METTL3-knockdown cells. The protein levels of Bcl2, Caspase 3 and Cyclin D1 were detected by western blotting in METTL3-knockdown cells. *$p < 0.05$, **$p < 0.01$, ***$p < 0.001$, ****$p < 0.0001$.

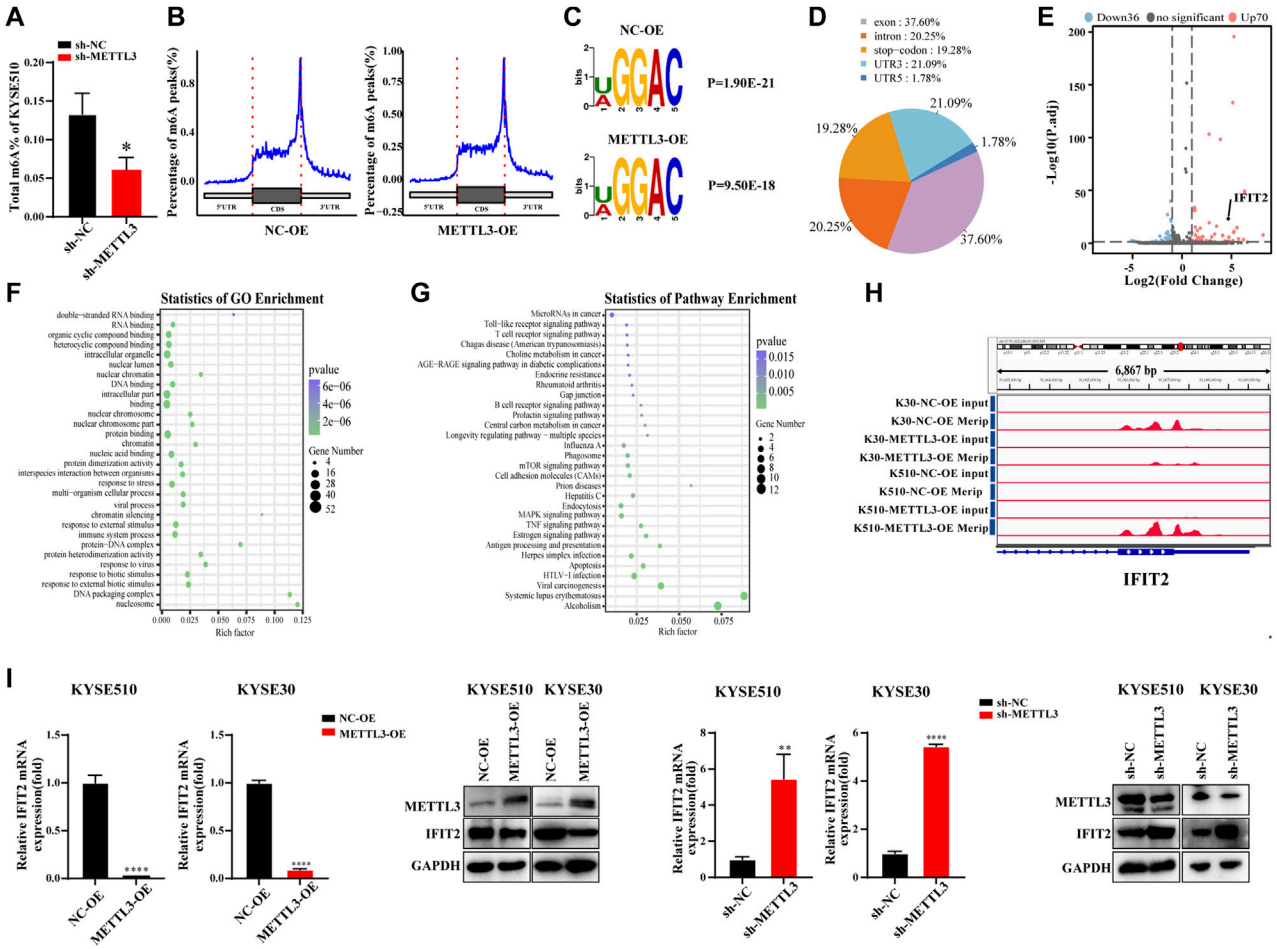

FIGURE 4
MeRIP-seq analysis of the effect of overexpression on the methylation of target genes **(A)**. The m^{6}A RNA methylation assay revealed the m^{6}A content in KYSE510 cells with METTL3 **(B)**. Peak distribution in CDS, 5′UTR and 3′UTR regions (The abscissa is the CDS, 5′UTR, and 3′UTR regions, and the ordinate is the distribution ratio of the peaks corresponding to the positions of each region). **(C)**. The predominant consensus motif GGAC was detected in m6A-seq. **(D)**. Statistical results of the regional distribution of the difference peak. **(E)**. The volcano plot shows the distribution of differential genes. **(F)**. The results of GO biological process enrichment. **(G)**. The results of KEGG pathways analysis. **(H)**. m^{6}A peaks were enriched from m^{6}A RIP-seq data. **(I)**. Effects of METTL3 overexpression or knockdown on IFIT2 mRNA and protein expression in KYSE510 and KYSE30 cells. *p < 0.05, **p < 0.01, ****p < 0.0001.

expression of this protein at the mRNA level as well as at METTL3 was reduced (Figure 3A). The viability and proliferation of cells were markedly reduced by METTL3 knockdown, as tested through CCK8 and colony formation assays. In contrast, sh-METTL3 significantly promoted apoptosis (Figures 3B–D). We further explored the invasive and migratory abilities of the cells. The scratch healing ability of the sh-METTL3 group was slowed (Figure 3E). The low expression of METTL3 in the invasion assay reduced the number of invading cells, which was consistent with the results of the migration assay (Figure 3F). The apoptosis and expression of EMT-related proteins after METTL3 knockdown were opposite to those after METTL3 overexpression (Figure 3G).

MeRIP-seq analysis of the effect of overexpression on the methylation of target genes

We detected the m^{6}A contents of the total mRNA in METTL3-silenced KYSE510 cells. As expected, METTL3 silencing dramatically decreased the m^{6}A content in KYSE510 cells (Figure 4A). Taking the sample as the unit to annotate the peaks of the sample and counting and annotating the annotation results, the results show that the m^{6}A peaks are abundant in coding sequences (CDS), especially near stop codons in the 3′UTR of mRNA (Figure 4B). The RMBase database determined that the consensus motif for the genes with m^{6}A modification is U/AGGAC (p = 2.3e-022), which is the common

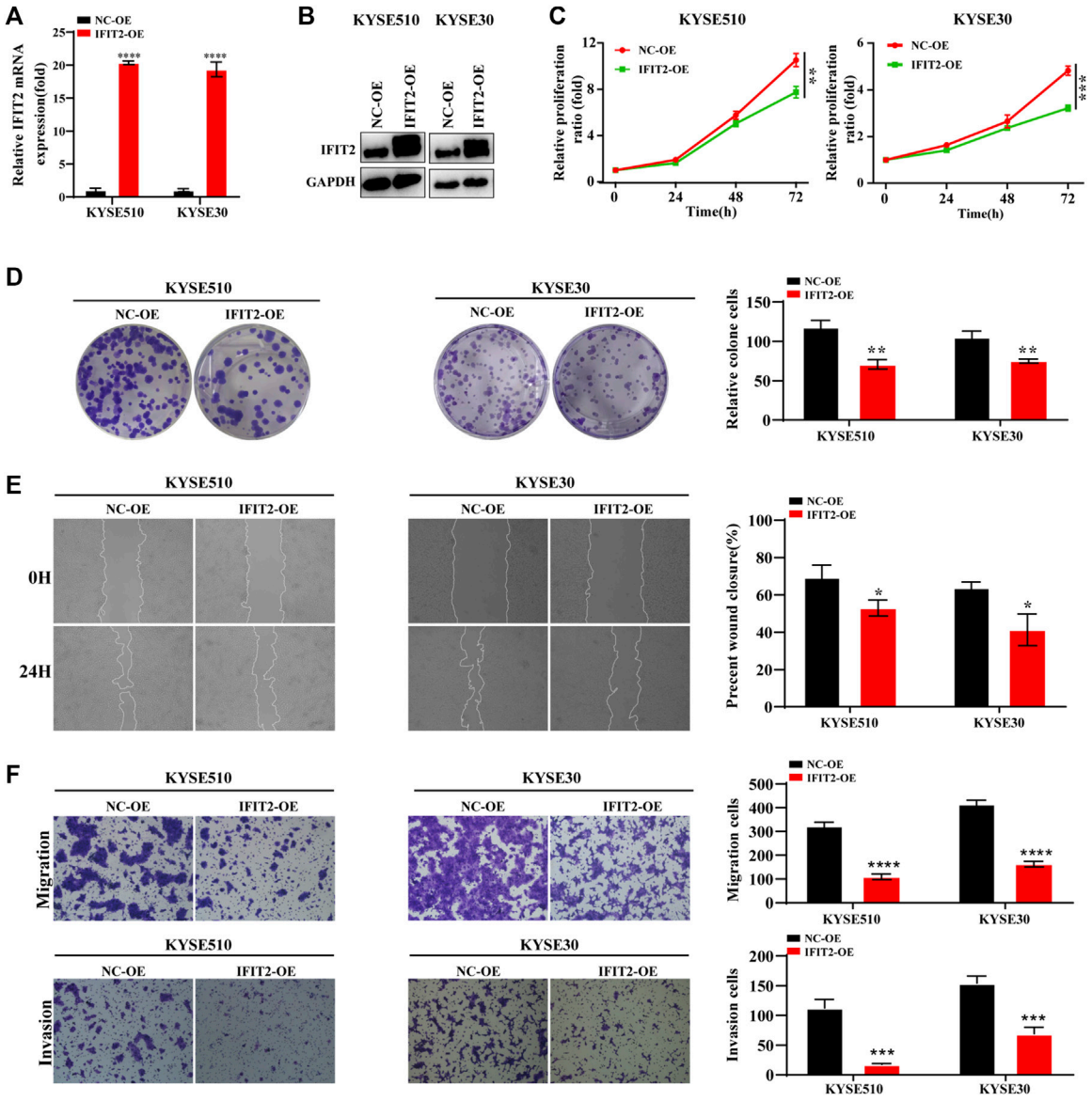

FIGURE 5
IFIT2 overexpression inhibited ESCC cell proliferation and invasion **(A, B)**. To evaluate the effectiveness of the IFIT2 overexpression lentivirus, qRT–PCR was used to detect mRNA levels, and western blot analyses were used to detect protein levels. **(C)**. A CCK-8 assay was used to evaluate the proliferation ability of KYSE510 and KYSE30 cells after IFIT2 overexpression. **(D)**. Cell proliferation capabilities were identified through colony formation tests in transfected KYSE510 and KYSE30 cells. **(E)**. The wound healing assay reduced the KYSE510 and KYSE30 cell ability to migrate. **(F)**. Transwell assays were used to analyze transfected cell migration and invasion. *$p < 0.05$, **$p < 0.01$, ***$p < 0.001$, ****$p < 0.0001$.

feature among the genes with m^{6}A methylation (Figure 4C). The main distribution area of the difference peak was in the exon (37.6%), intron (20.25%), 3′UTR (21.09%) and stop codon (19.28%). Only a small portion (1.78%) was distributed in the 5′UTR (Figure 4D). The significantly differentially expressed genes between samples can be further selected by the fold difference and significance level. Notably, 70 transcripts were upregulated, and 36 transcripts were downregulated in the RNA-seq and MeRIP-seq data (Figure 4E and Supplementary Figure S1). We took the intersection of the downregulated peak after overexpression of METTL3 and the upregulated peak after interference with METTL3 and then enriched the GO and KEGG functions of the intersected genes. GO analyses showed that immune system processes were significantly enriched. KECG has been shown to be associated with immune signaling pathways, including the Toll-like, T-cell and B-cell

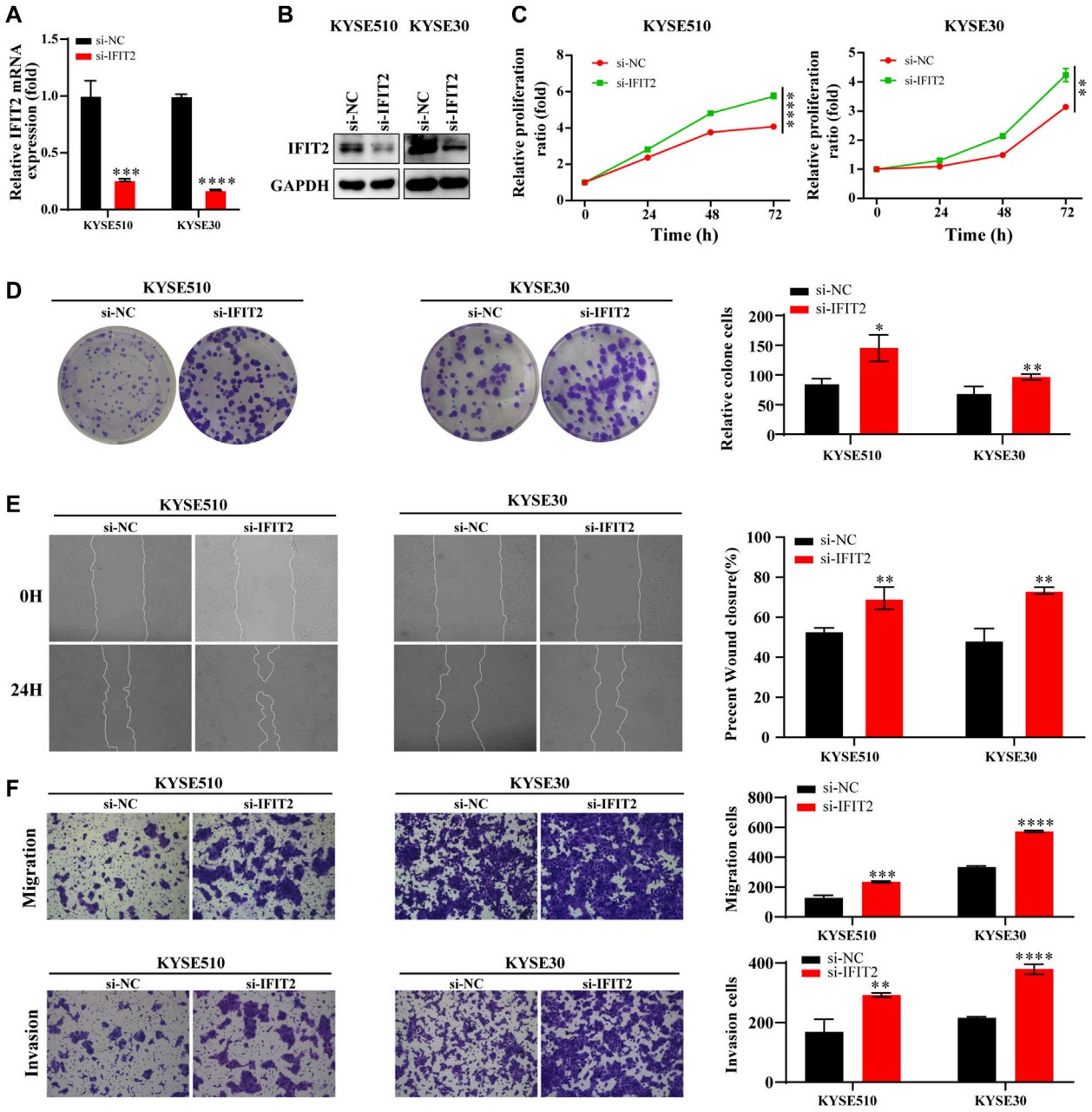

FIGURE 6
Effect of IFIT2 siRNA on ESCC cell proliferation, migration, and invasion **(A, B)**. To evaluate the effectiveness of si-IFIT2, qRT–PCR was used to detect mRNA levels, and western blot analyses were used to detect protein levels. **(C)**. A CCK-8 assay was used to evaluate the proliferation ability of KYSE510 and KYSE30 cells after si-IFIT2. **(D)**. Cell proliferation capabilities were identified through colony formation tests in transfected KYSE510 and KYSE30 cells. **(E)**. The healing experience reduced the KYSE510 and KYSE30 cell ability to migrate. **(F)**. Transwell assays were used to analyze transfected cell migration and invasion. *$p < 0.05$, **$p < 0.01$, ***$p < 0.001$, ****$p < 0.0001$.

receptor signaling pathways. Moreover, genes were also significantly enriched in apoptosis (Figures 4F,G and Supplementary Figures S2, S3). Among these genes, we chose and verified the gene that was most strongly associated using qRT–PCR and WB. We thus detected the m^{6}A abundance on IFIT2 mRNA transcripts in KYSE30 and KYSE150 cells by m^{6}A-seq, and the results showed that m^{6}A methylation was enriched in the exon and 3′UTR regions of IFIT2 with a clustered distribution (Figure 4H). We then characterized the expression relationship of IFIT2 with METTL3 in esophageal

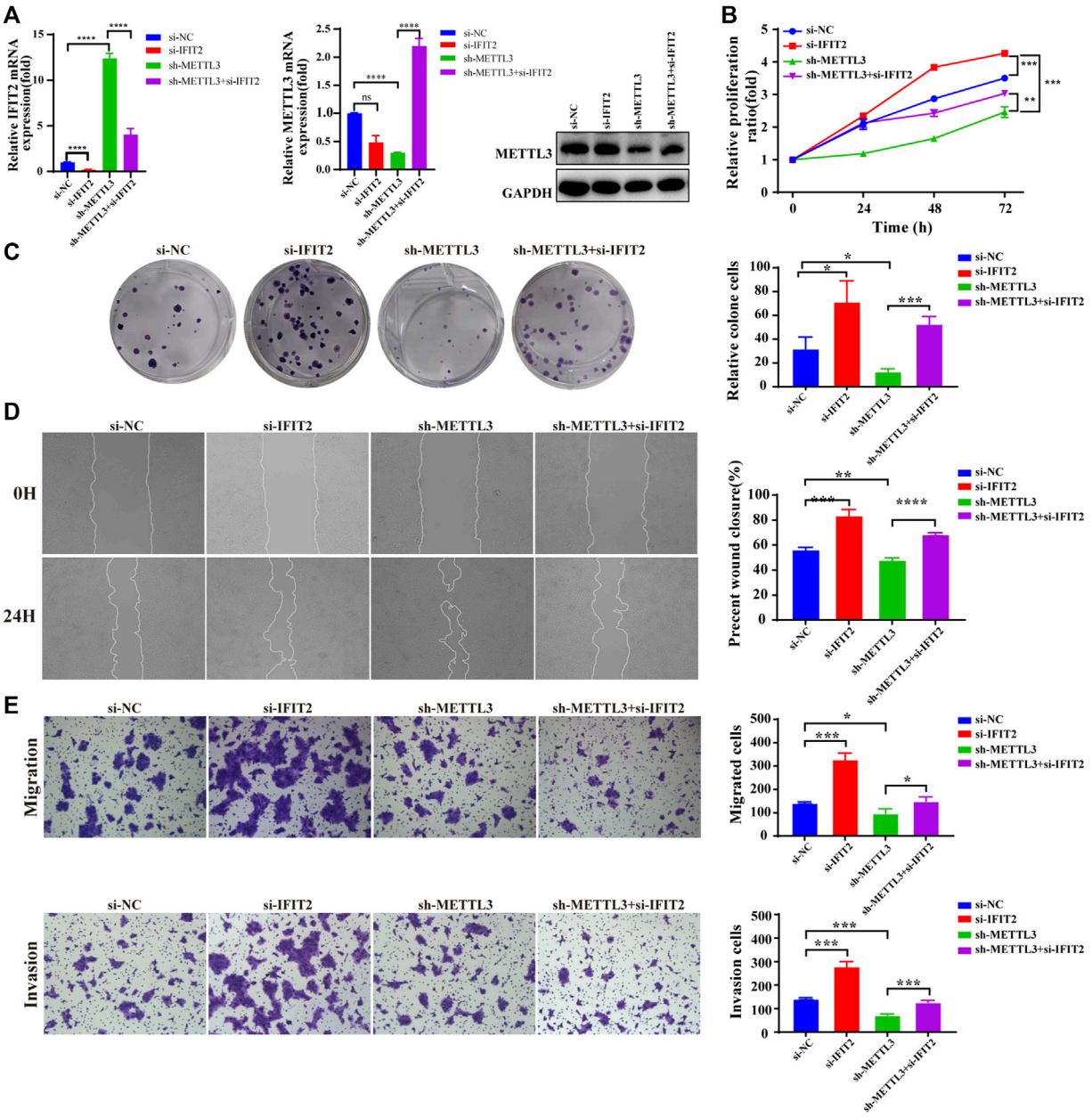

FIGURE 7
METTL3 reverses the biological effects of IFIT2 with respect to ESCC proliferation, invasion and metastasis **(A)**. Effects of siRNA-IFIT2 on METTL3 mRNA and protein expression following METTL3 knockdown. **(B,C)**. In the CCK-8 and colony formation assays, the inhibition of KYSE150 cell proliferation caused by poorly regulated METTL3 was restored by increased regulation of IFIT2 expression. **(D)**. The wound healing of cells demonstrated that upregulating IFIT2 restored the inhibition of METTL3-induced cell migration. **(E)**. The transwell migration and invasion tests were successful in rescuing the inhibition of migration and invasion capacity induced by sh-METTL3. n.s, no statistical significance, $*p < 0.05$, $**p < 0.01$, $***p < 0.001$, $****p < 0.0001$.

cancer cells. Notably, IFIT2 mRNA and protein expression were both significantly downregulated by METTL3 overexpression in KYSE510 cells (Figure 4I), whereas IFIT2 mRNA and protein expression were upregulated by METTL3 knockdown in KYSE510 cells (Figure 4I).

IFIT2 overexpression inhibited ESCC cell proliferation and invasion

The IFIT2 transfection efficiency was confirmed to be increased at both the mRNA and protein levels (Figure 5A,

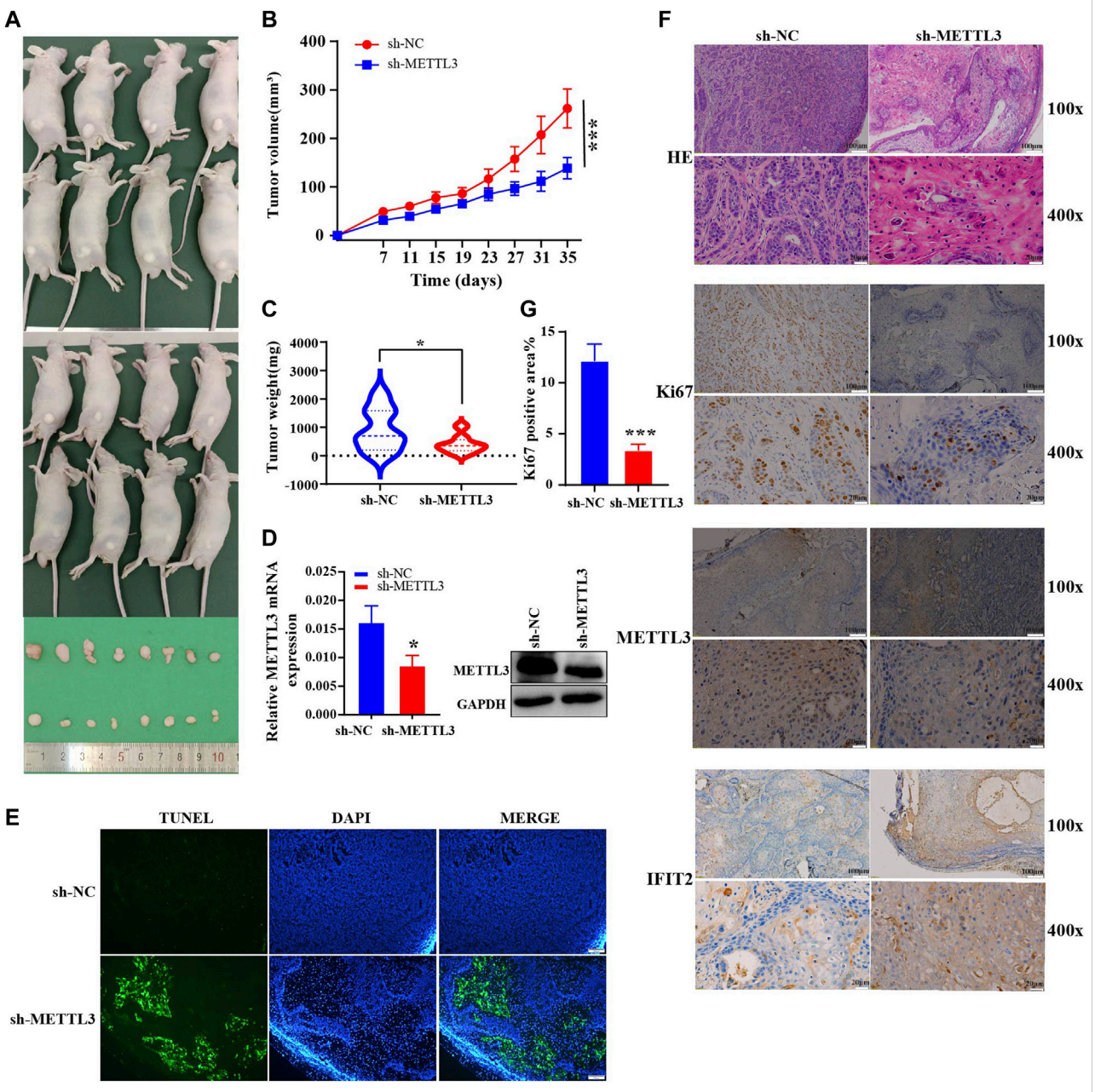

FIGURE 8
In vivo experimental validations in mice **(A)**. An analysis of the shape of transplanted tumors, changes in body weight of nude mice **(B)** and growth curves of tumor volume for each group **(C)** (n = 8). **(D)**. Expression of mouse tumor protein and mRNA. **(E)**. TUNEL staining of the paraffin sections of the xenograft tumors. Evaluation of tumor cell apoptosis by TUNEL staining (scale bar = 100 μm). **(F)**. Ki67 expression and HE coloration in mouse tumor tissue. Immunohistochemical recovery of the expression of METTL3 and IFIT2 (Scale bars are indicated in the figure). **(G)**. The ratio of KI67-positive area in the sh-NC and sh-METTL3 groups was analyzed using ImageJ software. *$p < 0.05$, ***$p < 0.001$.

B). Next, we verified the function of downstream target genes of IFIT2. The results of CCK-8 and cloning experiments showed that IFIT2 overexpression attenuated the proliferation of esophageal cancer cells (Figures 5C,D). IFIT2 overexpression prevented cell migration, according to scratch experiments (Figure 5E). It was determined whether IFIT2 in cells affected cell invasion and migration using a transwell assay. These cells displayed less cell migration and invasion (Figure 5F).

Effect of IFIT2 siRNA on ESCC cell proliferation, migration, and invasion

The transfection efficiency of si-IFIT2 was confirmed at both the protein and mRNA levels (Figures 6A,B). siRNA-IFIT2-transfected KYSE510 and KYSE30 cells significantly enhanced cell proliferation, as shown by CCK8 and colony formation assays (Figures 6C,D). In comparison to control and untransfected siRNA, the scratch wound healing and migration assays showed that siRNA transfection significantly accelerated cell migration and facilitated wound healing and increased the number of cell invasions (Figures 6E,F).

METTL3 reverses the biological effects of IFIT2 on ESCC proliferation, invasion, and metastasis

To further investigate the relationship between METTL3 and IFIT2 in the tumorigenesis of esophageal cancer, we knocked down IFIT2 in KYSE150 cells, accompanied by METTL3 knockdown. In siRNA-IFIT2-transfected cells, IFIT2 mRNA levels were decreased 6.5-fold, whereas IFIT2 expression was increased 12-fold in METTL3-silenced KYSE150 cells. IFIT2 expression in METLL3-silenced KYSE150 cells transfected with the si-IFIT2 vector (sh-METTL3+si-IFIT2) increased approximately 3-fold. Meanwhile, we confirmed that si-IFIT2 partially rescued METTL3 mRNA and protein upregulation in sh-METTL3 cells (Figure 7A). In fact, the reduction in KYSE510 cell proliferation following METTL3 knockdown was rescued by ectopic expression of IFIT2, as shown by CCK-8 and colony formation assays (Figures 7B,C). The expression of IFIT2 during wound healing partially rescued sh-METTL3 cells in the wound healing area (Figure 7D). *In vitro* cell migration and invasion assays, si-IFIT2 effectively restored the mechanical properties of METTL3 knockdown cells (Figure 7E).

In vivo experimental validations in mice

We investigated the effect of METTL3 on tumorigenicity *in vivo* using a xenograft model of sh-METTL3 KYSE510 cells. Mice were inoculated subcutaneously with KYSE510 sh-NC and sh-METTL3 cells, and tumor size were measured every 4 days. Thirty-five days after tumor cell injection, subcutaneous tumor tissue was dissected, and tumor weight and volume were measured (Figure 8A). The tumor growth rate in the experimental group was substantially inhibited, and the tumor volume was significantly reduced (Figures 8B,C). By extracting RNA and proteins from mouse tumors, METTL3 was effectively silenced in the sh-METTL3 group (Figure 8D). After TUNEL staining, the range of TUNEL-positive cells improved in sh-METTL3 tumor tissue sections, consistent with the tumor size results (Figure 8E). Under the light microscope with HE staining in the transplanted tumor tissue, the nuclear volume of the tumor cells increased, as did the nuclear-cytoplasmic ratio. Meanwhile, immunohistochemistry also showed that METTL3 was successfully knocked out. METTL3 and IFIT2 were negatively correlated with immunohistochemistry (Figure 8F). In addition, the proliferation marker Ki67 was noticeably lower in sh-METTL3 cells than in sh-NC cells, according to IHC staining of the resected tumor tissue. ImageJ software statistics showed that the positive area of Ki67 in the sh-NC group was higher than that in the sh-METTL3 group (Figure 8G).

METTL3 and IFIT2 are associated with prognostic immune infiltration

When we used TCGA pancancer data to analyze the expression levels of the model's key genes, METTL3 and IFIT2 were observed to have extensively different expression levels in regular and tumor tissues (Figure 9A). We developed a prognostic model using the genes METLL3 and IFIT2. According to the median risk score, ESCC cancer patients were divided into two groups: low-risk and high-risk (Figure 9B). Kaplan–Meier (K-M) analysis was utilized to explore the prognostic value of scores (Supplementary Figure S4). ROC curve analysis showed that the risk model constructed by the expression and prognosis of IFIT2 and METTL3 in esophageal cancer patients was closely related to the prognosis survival of more than 3 years (AUC = 0.77) (Figure 9C). In TCGA esophageal cancer samples, IFIT2 gene expression and pathway enrichment were correlated by GSEA enrichment analysis. The findings demonstrate that IFIT2 expression is linked to the suppression of the oxidative phosphorylation pathway in tissues from esophageal cancer (Figure 9D). The tumor immune microenvironment is associated with the prognostic survival of patients. Therefore, we investigated the correlation of METTL3 and IFIT2 expression with immune cells in esophageal cancer. The findings of the TIMER database showed that the expression of METTL3 was appreciably correlated with the diploma of infiltration of B cells (p = 3.41e-03) and macrophages (p = 3.96e-04). IFIT2 was significantly inversely correlated with tumor purity (p = 9.77e-05), B cells (p = 9.68e-03), $CD4^+$ T cells (p = 7.10e-04), macrophages (p = 2.20e-03) and neutrophils (p = 6.34e-03) (Figure 9E). We performed multigene correlation analysis using the R package pheatmap, and METTL3 and IFIT2 showed a negative correlation. METLL3 was significantly correlated with $CD8^+$ T cells and uncharacterized cells ($p < 0.01$). IFIT2 was correlated with $CD8^+$ T cells and uncharacterized cells ($p < 0.05$) (Figure 9F).

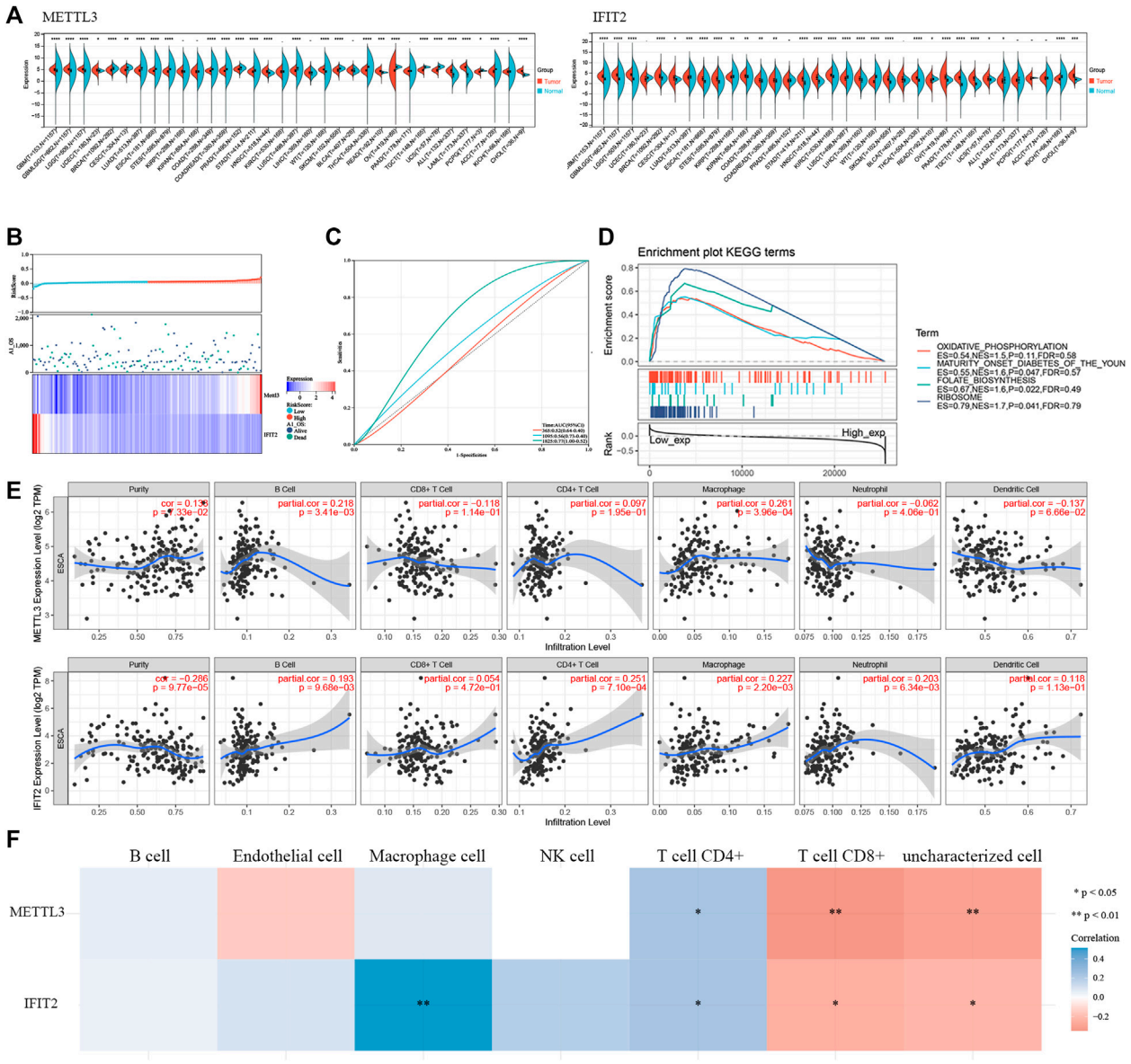

FIGURE 9
METTL3 and IFIT2 are associated with prognostic immune infiltration **(A)**. Pancancer analysis of METTL3 and IFIT2 expression across cancers from TCGA. **(B)**. The expression profiles that correspond to the distributions of prognostic signature-based risk scores. Low-risk patients are represented by green dots, while high-risk patients are represented by red dots. **(C)**. The ROC curve for evaluating the prediction efficiency of the prognostic signature. **(D)**. Correlation of IFIT2 gene expression and pathway enrichment in TCGA esophageal cancer samples by GSEA enrichment analysis. **(E)**. Correlation of IFIT2 and METTL3 expression levels with immune infiltration of B cells, CD4 T cells, CD8 T cells, neutrophils, macrophages, and dendritic cells in ESCC. **(F)**. A heatmap of the correlation between METTL3, IFIT2 and immune score.

Discussion

Studies have shown that proteins related to m^{6}A modification are dysregulated and carcinogenic in esophageal cancer. Wang W found that METTL3 expression was significantly elevated in esophageal squamous cell carcinoma and was associated with poor patient prognosis (Han et al., 2021; Wang et al., 2021). FTO demethylase overexpression enhances esophageal cancer cell proliferation and tumor development (Cui et al., 2021). In a prior study, our team discovered that ESCC had significantly higher FTO levels, which in conjunction with ERBB2 controlled ESCC tumorigenesis and metastasis (Zhao et al., 2022). Li J showed that in the pathophysiology of ESCC, ALKBH5 acts as a tumor suppressor (Li et al., 2021). Due to advances in biological technologies such as high-throughput sequencing and the discovery of abnormal expression of METTL3, ALKBH5, and

FTO, the role of m^{6}A methylation in ESCC has gradually been revealed (Zhang et al., 2021). The insidious onset of ESCC is primarily responsible for the patients' poor prognosis, and by the time of diagnosis, the majority had advanced to the middle and late stages of lymphatic metastasis. As a result, to find reliable prognostic biomarkers and therapeutic targets, it is imperative to research the molecular pathogenesis of esophageal cancer.

METTL3 is the most important methylase of m^{6}A. In recent years, it has become clear that METTL3 is aberrantly expressed in gastric (Yue et al., 2019), breast (Pan et al., 2021), prostate (Chen et al., 2021) and non-small cell lung cancers (Xue et al., 2021), which raises the possibility that METTL3 could be a useful diagnostic marker and therapeutic target (Zeng et al., 2020). Our study shows that METTL3, a protein highly expressed in esophageal cancer tissues, can promote the proliferation, invasion and metastasis of esophageal cancer both *in vitro* and *in vivo*. These results are consistent with previously reported results. Although the trend of m^{6}A modification levels is constant, it may have different effects by controlling different target genes, and the impact on tumor prognosis may be different (Li et al., 2019). In this study, we mainly found that METTL3 affects the occurrence and development of ESCC by regulating the downstream target IFIT2. Interestingly, METTL3 was recently reported to regulate IFIT2 expression in a m^{6}A-YTHDF2-dependent manner in cholangiocarcinoma (Xu et al., 2022). However, the difference is that their findings were in bile duct cancer. Because of the clear differences between the pathogenesis of ESCC and ICC, the distribution of m^{6}A modifications in various tissue types varies widely. Whether it has the same effect is still controversial.

IFIT is a family of tetrapeptide repeat genes induced by interferon. It is commonly studied for its antiviral properties, known as an interferon-stimulated gene, and is located on the human chromosome (Pidugu et al., 2019). IFIT2 can be induced by viral infection, interferon or other pathogen-associated molecular pattern recognition and is involved in inhibiting viral replication and governing apoptosis and antitumor activity (Liu et al., 2011). IFIT2 may be crucial in controlling the inflammatory tumor environment during metastasis in OSCC, which results in cachexia (Lai et al., 2022). Koh et al. found that low IFIT2 expression in triple-negative breast cancer patients increases the risk of recurrence (Koh et al., 2019b). In particular, overexpression of IFIT2 promotes tumor cell death (Mbofung et al., 2017). IFIT2 balances pro- and antiapoptotic Bcl-2 family proteins to alter mitochondrial membrane permeability and cause apoptosis (Tait and Green, 2010; Stawowczyk et al., 2011). In colorectal cancer, IFIT2 expression is induced by IRF1, and Wnt/β-catenin signaling, which has antiapoptotic properties, inhibits it (Ohsugi et al., 2019).

In our study, a significant amount of METTL3 was detected in tissues from esophageal cancer patients compared to adjacent tissues. The METTL3 downstream target gene IFIT2 was identified in esophageal cancer cells using MeRIP-seq. *In vitro* rescue assays showed that IFIT2 could rescue the biological function of METTL3 elimination. *In vivo* research on mouse tumors using immunohistochemistry revealed a negative correlation between METTL3 and IFIT2. Furthermore, from the tail vein, we injected 1×10^6 sh-METTL3 cells. The sh-NC group had liver metastases after two months (Supplementary Figure S5). Mouse lung metastases did not appear as obvious nodules (Supplementary Figure S6); this is likely because KYSE510 is a moderately aggressive cell type. When the calibration curve and ROC curve were examined, we also created a prognostic risk model using METTL3 and IFIT2 that performed well at predicting prognosis. Additionally, the immune response during the development of esophageal cancer may be mediated by METTL3 and IFIT2, which would explain why patients with esophageal cancer have a poor prognosis. These findings offer a solid foundation for future immunotherapy.

Conclusion

In conclusion, IFIT2 and METTL3 may serve as targets for immunotherapy in addition to being potential pathogenic factors in esophageal cancer development. METTL3 and IFIT2, which may serve as prognostic or diagnostic indicators for esophageal cancer, also offer fresh evidence in favor of immunotherapy and customized treatment for ESCC patients. To assess the therapeutic potential of METTL3-regulated IFIT2 more fully in ESCC, a more thorough study with a larger sample size and multicenter clinical study should be conducted.

Data availability statement

The data presented in the study are deposited in the SRA database, accession number PRJNA889200.

Ethics statement

The animal study was reviewed and approved by all animal research procedures are carried out under a program approved by the Animal Laboratory Center of the University of Science and Technology of China. Written informed consent was obtained from the individual(s) for the publication of any potentially identifiable images or data included in this article.

Author contributions

YP and FZ contributed to the conception and manuscript writing. FG, FZ, ZL, and JH were involved in the experimental work. LK acquired funding and assisted with the manuscript development. All authors read and approved the final manuscript.

Funding

This work was supported by the Fundamental Research Funds for the Central Universities granted to FZ (WK9110000008), LK (WK9110000090) and CBZ (WK9110000132), respectively. The Youth Fund of Anhui Cancer Hospital granted grants to FZ and LK, respectively. The Youth Technical Backbone Fund of West Branch of the First Affiliated Hospital of USTC granted to LK.

Conflict of interest

The authors declare that the research was conducted in the absence of any commercial or financial relationships that could be construed as a potential conflict of interest.

Publisher's note

Supplementary material

The Supplementary Material for this article can be found online at: https://www.frontiersin.org/articles/10.3389/fphar.2022.1002565/full#supplementary-material

References

Barbieri, I., and Kouzarides, T. (2020). Role of RNA modifications in cancer. *Nat. Rev. Cancer* 20 (6), 303–322. doi:10.1038/s41568-020-0253-2

Chen, Y., Pan, C., Wang, X., Xu, D., Ma, Y., Hu, J., et al. (2021). Silencing of METTL3 effectively hinders invasion and metastasis of prostate cancer cells. *Theranostics* 11 (16), 7640–7657. doi:10.7150/thno.61178

Cui, Y., Zhang, C., Ma, S., Li, Z., Wang, W., Li, Y., et al. (2021). RNA m^{6}A demethylase FTO-mediated epigenetic up-regulation of LINC00022 promotes tumorigenesis in esophageal squamous cell carcinoma. *J. Exp. Clin. Cancer Res.* 40 (1), 294. doi:10.1186/s13046-021-02096-1

Dawson, M. A., and Kouzarides, T. (2012). Cancer epigenetics: From mechanism to therapy. *Cell* 150 (1), 12–27. doi:10.1016/j.cell.2012.06.013

Delaveau, T., Davoine, D., Jolly, A., Vallot, A., Rouviere, J. O., Gerber, A., et al. (2016). Tma108, a putative M1 aminopeptidase, is a specific nascent chain-associated protein in *Saccharomyces cerevisiae*. *Nucleic Acids Res.* 44 (18), 8826–8841. doi:10.1093/nar/gkw732

Dominissini, D., Moshitch-Moshkovitz, S., Schwartz, S., Salmon-Divon, M., Ungar, L., Osenberg, S., et al. (2012). Topology of the human and mouse m^{6}A RNA methylomes revealed by m6A-seq. *Nature* 485 (7397), 201–206. doi:10.1038/nature11112

Han, H., Yang, C., Zhang, S., Cheng, M., Guo, S., Zhu, Y., et al. (2021). METTL3-mediated m(6)A mRNA modification promotes esophageal cancer initiation and progression via Notch signaling pathway. *Mol. Ther. Nucleic Acids* 26, 333–346. doi:10.1016/j.omtn.2021.07.007

He, J., Zhou, M., Yin, J., Wan, J., Chu, J., Jia, J., et al. (2021). METTL3 restrains papillary thyroid cancer progression via m(6)A/c-Rel/IL-8-mediated neutrophil infiltration. *Mol. Ther.* 29 (5), 1821–1837. doi:10.1016/j.ymthe.2021.01.019

He, P. C., and He, C. (2021). m(6) A RNA methylation: from mechanisms to therapeutic potential. *EMBO J.* 40 (3), e105977. doi:10.15252/embj.2020105977

Jiang, X., Liu, B., Nie, Z., Duan, L., Xiong, Q., Jin, Z., et al. (2021). The role of m^{6}A modification in the biological functions and diseases. *Signal Transduct. Target. Ther.* 6 (1), 74. doi:10.1038/s41392-020-00450-x

Koh, C. W. Q., Goh, Y. T., and Goh, W. S. S. (2019a). Atlas of quantitative single-base-resolution N(6)-methyl-adenine methylomes. *Nat. Commun.* 10 (1), 5636. doi:10.1038/s41467-019-13561-z

Koh, S. Y., Moon, J. Y., Unno, T., and Cho, S. K. (2019b). Baicalein suppresses stem cell-like characteristics in radio- and chemoresistant MDA-MB-231 human breast cancer cells through up-regulation of IFIT2. *Nutrients* 11 (3), E624. doi:10.3390/nu11030624

Lagergren, J., Smyth, E., Cunningham, D., and Lagergren, P. (2017). Oesophageal cancer. *Lancet* 390 (10110), 2383–2396. doi:10.1016/s0140-6736(17)31462-9

Lai, K. C., Hong, Z. X., Hsieh, J. G., Lee, H. J., Yang, M. H., Hsieh, C. H., et al. (2022). IFIT2-depleted metastatic oral squamous cell carcinoma cells induce muscle atrophy and cancer cachexia in mice. *J. Cachexia Sarcopenia Muscle* 13 (2), 1314–1328. doi:10.1002/jcsm.12943

Li, J., Liu, H., Dong, S., Zhang, Y., Li, X., and Wang, J. (2021). ALKBH5 is lowly expressed in esophageal squamous cell carcinoma and inhibits the malignant proliferation and invasion of tumor cells. *Comput. Math. Methods Med.* 2021, 1001446. doi:10.1155/2021/1001446

Li, Y., Xiao, J., Bai, J., Tian, Y., Qu, Y., Chen, X., et al. (2019). Molecular characterization and clinical relevance of m(6)A regulators across 33 cancer types. *Mol. Cancer* 18 (1), 137. doi:10.1186/s12943-019-1066-3

Lin, S., Choe, J., Du, P., Triboulet, R., and Gregory, R. I. (2016). The m(6)A methyltransferase METTL3 promotes translation in human cancer cells. *Mol. Cell* 62 (3), 335–345. doi:10.1016/j.molcel.2016.03.021

Liu, C., Yang, Z., Li, R., Wu, Y., Chi, M., Gao, S., et al. (2021). Potential roles of N6-methyladenosine (m^{6}A) in immune cells. *J. Transl. Med.* 19 (1), 251. doi:10.1186/s12967-021-02918-y

Liu, X. Y., Chen, W., Wei, B., Shan, Y. F., and Wang, C. (2011). IFN-induced TPR protein IFIT3 potentiates antiviral signaling by bridging MAVS and TBK1. *J. Immunol.* 187 (5), 2559–2568. doi:10.4049/jimmunol.1100963

Liu, X., Zhang, M., Ying, S., Zhang, C., Lin, R., Zheng, J., et al. (2017). Genetic alterations in esophageal tissues from squamous dysplasia to carcinoma. *Gastroenterology* 153 (1), 166–177. doi:10.1053/j.gastro.2017.03.033

Ma, Z., Gao, X., Shuai, Y., Xing, X., and Ji, J. (2021). The m^{6}A epitranscriptome opens a new charter in immune system logic. *Epigenetics* 16 (8), 819–837. doi:10.1080/15592294.2020.1827722

Ma, Z., and Ji, J. (2020). N6-methyladenosine (m^{6}A) RNA modification in cancer stem cells. *Stem Cells* 38, 1511–1519. doi:10.1002/stem.3279

Mbofung, R. M., McKenzie, J. A., Malu, S., Zhang, M., Peng, W., Liu, C., et al. (2017). HSP90 inhibition enhances cancer immunotherapy by upregulating interferon response genes. *Nat. Commun.* 8 (1), 451. doi:10.1038/s41467-017-00449-z

Ohsugi, T., Yamaguchi, K., Zhu, C., Ikenoue, T., Takane, K., Shinozaki, M., et al. (2019). Anti-apoptotic effect by the suppression of IRF1 as a downstream of Wnt/β-catenin signaling in colorectal cancer cells. *Oncogene* 38 (32), 6051–6064. doi:10.1038/s41388-019-0856-9

Pan, X., Hong, X., Li, S., Meng, P., and Xiao, F. (2021). METTL3 promotes adriamycin resistance in MCF-7 breast cancer cells by accelerating pri-microRNA-221-3p maturation in a m^{6}A-dependent manner. *Exp. Mol. Med.* 53 (1), 91–102. doi:10.1038/s12276-020-00510-w

Pidugu, V. K., Pidugu, H. B., Wu, M.-M., Liu, C.-J., and Lee, T.-C. (2019). Emerging functions of human IFIT proteins in cancer. *Front. Mol. Biosci.* 6, 148. doi:10.3389/fmolb.2019.00148

Ping, X. L., Sun, B. F., Wang, L., Xiao, W., Yang, X., Wang, W. J., et al. (2014). Mammalian WTAP is a regulatory subunit of the RNA N6-methyladenosine methyltransferase. *Cell Res.* 24 (2), 177–189. doi:10.1038/cr.2014.3

Stawowczyk, M., Van Scoy, S., Kumar, K. P., and Reich, N. C. (2011). The interferon stimulated gene 54 promotes apoptosis. *J. Biol. Chem.* 286 (9), 7257–7266. doi:10.1074/jbc.M110.207068

Sung, H., Ferlay, J., Siegel, R. L., Laversanne, M., Soerjomataram, I., Jemal, A., et al. (2021). Global cancer statistics 2020: GLOBOCAN estimates of incidence and

mortality worldwide for 36 cancers in 185 countries. *Ca. Cancer J. Clin.* 71 (3), 209–249. doi:10.3322/caac.21660

Tait, S. W., and Green, D. R. (2010). Mitochondria and cell death: Outer membrane permeabilization and beyond. *Nat. Rev. Mol. Cell Biol.* 11 (9), 621–632. doi:10.1038/nrm2952

Toh, T. B., Lim, J. J., and Chow, E. K. (2017). Epigenetics in cancer stem cells. *Mol. Cancer* 16 (1), 29. doi:10.1186/s12943-017-0596-9

Varghese, F., Bukhari, A. B., Malhotra, R., and De, A. (2014). IHC Profiler: an open source plugin for the quantitative evaluation and automated scoring of immunohistochemistry images of human tissue samples. *PLoS One* 9 (5), e96801–639. doi:10.1371/journal.pone.0096801

Wan, W., Ao, X., Chen, Q., Yu, Y., Ao, L., Xing, W., et al. (2022). METTL3/IGF2BP3 axis inhibits tumor immune surveillance by upregulating N(6)-methyladenosine modification of PD-L1 mRNA in breast cancer. *Mol. Cancer* 21 (1), 60. doi:10.1186/s12943-021-01447-y

Wang, M., Smith, J. S., and Wei, W. Q. (2018). Tissue protein biomarker candidates to predict progression of esophageal squamous cell carcinoma and precancerous lesions. *Ann. N. Y. Acad. Sci.* 1434 (1), 59–69. doi:10.1111/nyas.13863

Wang, W., Shao, F., Yang, X., Wang, J., Zhu, R., Yang, Y., et al. (2021). METTL3 promotes tumour development by decreasing APC expression mediated by APC mRNA N6-methyladenosine-dependent YTHDF binding. *Nat. Commun.* 12 (1), 3803. doi:10.1038/s41467-021-23501-5

Wang, X., Feng, J., Xue, Y., Guan, Z., Zhang, D., Liu, Z., et al. (2016). Structural basis of N(6)-adenosine methylation by the METTL3-METTL14 complex. *Nature* 534 (7608), 575–578. doi:10.1038/nature18298

Xiong, J., He, J., Zhu, J., Pan, J., Liao, W., Ye, H., et al. (2022). Lactylation-driven METTL3-mediated RNA m(6)A modification promotes immunosuppression of tumor-infiltrating myeloid cells. *Mol. Cell* 82 (9), 1660–1677.e10. doi:10.1016/j.molcel.2022.02.033

Xu, Q. C., Tien, Y. C., Shi, Y. H., Chen, S., Zhu, Y. Q., Huang, X. T., et al. (2022). METTL3 promotes intrahepatic cholangiocarcinoma progression by regulating IFIT2 expression in an m(6)A-YTHDF2-dependent manner. *Oncogene* 41 (11), 1622–1633. doi:10.1038/s41388-022-02185-1

Xue, L., Li, J., Lin, Y., Liu, D., Yang, Q., Jian, J., et al. (2021). m(6) A transferase METTL3-induced lncRNA ABHD11-AS1 promotes the Warburg effect of non-small-cell lung cancer. *J. Cell. Physiol.* 236 (4), 2649–2658. doi:10.1002/jcp.30023

Yue, B., Song, C., Yang, L., Cui, R., Cheng, X., Zhang, Z., et al. (2019). METTL3-mediated N6-methyladenosine modification is critical for epithelial-mesenchymal transition and metastasis of gastric cancer. *Mol. Cancer* 18 (1), 142. doi:10.1186/s12943-019-1065-4

Zeng, C., Huang, W., Li, Y., and Weng, H. (2020). Roles of METTL3 in cancer: Mechanisms and therapeutic targeting. *J. Hematol. Oncol.* 13 (1), 117. doi:10.1186/s13045-020-00951-w

Zhang, X., Lu, N., Wang, L., Wang, Y., Li, M., Zhou, Y., et al. (2021). Recent advances of m^6A methylation modification in esophageal squamous cell carcinoma. *Cancer Cell Int.* 21 (1), 421. doi:10.1186/s12935-021-02132-2

Zhao, B. S., Roundtree, I. A., and He, C. (2017). Post-transcriptional gene regulation by mRNA modifications. *Nat. Rev. Mol. Cell Biol.* 18 (1), 31–42. doi:10.1038/nrm.2016.132

Zhao, F., Ge, F., Xie, M., Li, Z., Zang, C., Kong, L., et al. (2022). FTO mediated ERBB2 demethylation promotes tumor progression in esophageal squamous cell carcinoma cells. *Clin. Exp. Metastasis* 39, 623–639. doi:10.1007/s10585-022-10169-4

frontiers | Frontiers in Pharmacology

TYPE Original Research
PUBLISHED 21 October 2022
DOI 10.3389/fphar.2022.1011406

OPEN ACCESS

EDITED BY
Songyan Liao,
The University of Hong Kong, Hong Kong SAR, China

REVIEWED BY
Xuan Yuan,
The Affiliated Hospital of Qingdao University, China
Fei Luan,
Chengdu University of Traditional Chinese Medicine, China
Meizhu Zheng,
Changchun Normal University, China

*CORRESPONDENCE
Qin Li,
2020000301@hmc.edu.cn

†These authors have contributed equally to this work

SPECIALTY SECTION
This article was submitted to Inflammation Pharmacology, a section of the journal Frontiers in Pharmacology

RECEIVED 04 August 2022
ACCEPTED 11 October 2022
PUBLISHED 21 October 2022

CITATION
Zhou X, Shi Q, Li J, Quan S, Zhang X, Gu L, Li H, Ju Y, Hu M and Li Q (2022), Medicinal fungus Phellinus igniarius alleviates gout in vitro by modulating TLR4/NF-kB/NLRP3 signaling.
Front. Pharmacol. 13:1011406.
doi: 10.3389/fphar.2022.1011406

Medicinal fungus *Phellinus igniarius* alleviates gout *in vitro* by modulating TLR4/NF-kB/NLRP3 signaling

Xuebin Zhou†, Qiyuan Shi†, Jinhua Li, Shengli Quan, Xinyue Zhang, Lili Gu, Hongxing Li, Yue Ju, Min Hu and Qin Li*

School of Pharmacy, Hangzhou Medical College, Hangzhou, ZheJiang, China

Background: *Phellinus igniarius* (*P. igniarius*) is a valuable medicinal and edible fungus with various biological activities such as anti-inflammation, antioxidation, and immune regulation. In this study, we explored the effects of *P. igniarius* on a gout model *in vitro*.

Methods: The DPPH, ABTS, and FRAP methods were combined to determine and compare the antioxidant activities of wild *P. igniarius* total polyphenols (WPP) and cultivated *P. igniarius* total polyphenols (CPP) *in vitro*. Spectrophotometry was used to compare the inhibitory effect of WPP and CPP on xanthine oxidase (XO) activity to evaluate anti-hyperuricemia activity *in vitro*. HUVECs were stimulated with monosodium urate (MSU) crystals for 24 h to establish an acute gouty inflammation model *in vitro*. The protective effects were compared by measuring cell viability; the contents of ICAM-1, IL-1β, IL-6 and VCAM-1; the protein expressions of TLR4 and NLRP3; reactive oxygen species production; and the nuclear translocation of NF-κB p65. UHPLC-QE-MS technology was used to explore the potential metabolic mechanism of *P. igniarius* against gout.

Results: WPP and CPP had strong antioxidant capacity, and the antioxidant capacity of CPP was similar to that of WPP. In a comparative experiment of xanthine oxidase activity inhibition by WPP and CPP, the IC_{50} values were 88.19 μg/ml and 108.0 μg/ml, respectively. At a dose of 40 μg/ml, WPP and CPP significantly improved the decrease in cell viability induced by monosodium urate (150 μg/ml) and inhibited the increase in inflammatory factors such as ICAM-1, IL-1β, IL-6, and VCAM-1. The increase in TLR4 and NLRP3 protein expression induced by MSU crystals in HUVECs was also significantly inhibited by total polyphenols from wild and cultivated *P. igniarius*. In addition, both significantly improved MSU-induced ROS overproduction and NF-κB p65 nuclear translocation. WPP and CPP may primarily be involved in phenylalanine metabolism and lysophosphatidylcholine metabolism in their role in the treatment of gout.

Conclusion: CPP and WPP both showed good antioxidant activity and xanthine oxidase inhibitory activity and had good therapeutic effects on the gout model *in vitro*. Furthermore, this study indicated that cultivated *P. igniarius* had a protective effect similar to that of wild *P. igniarius*, which would be expected to

improve the shortage of wild *P. igniarius* and promote the development of the cultivated *P. igniarius* industry and product development.

KEYWORDS

medicinal fungus Phellinus igniarius, anti-gout, metabolic mechanism, TLR4, NF-κB, NLRP3 inflammasome

Introduction

Gout is a clinically common metabolic disease, which is a major problem impacting human health (Stack et al., 2019; Ashiq et al., 2021). Gout is a disorder of purine metabolism in the body, leading to high concentrations of uric acid in the blood and deposition of sodium urate crystals in the joints, which induces an inflammatory response that manifests as the pathogenesis of gouty arthritis as the main disease, affecting the quality of life of patients (Ghaemi-Oskouie and Shi, 2011; Singh and Gaffo, 2020; Yin et al., 2020).

An increase in serum urate concentrations (hyperuricemia, ≥7.0 mg/dl) manifests as inflammation induced by the deposition of MSU crystals in cartilage, synovial bursa, tendons, or soft tissues (Garcia et al., 2016). MSU crystals are known to activate TLR4, a key factor in the initiation of neuroinflammation, and TLR4 expression further activates and phosphorylates NF-κB (Zeng, 2019). NF-κB, a downstream target protein of TLR4 (Yin et al., 2021), is activated to promote the release of a range of inflammatory factors (Guo et al., 2020), such as TNF-α, IL-6 (Fan, 2017), IL-1β and others (Borstad et al., 2004). Normally, IκBα and NF-κB exist in the cytoplasm as an inactive dimer. After phosphorylation of IκBα by IκB kinase, phosphorylated NF-κB translocates from the cytoplasm to the nucleus, thus inducing transcriptional activation of NLRP3 inflammatory vesicles and increased expression of inflammatory factors. NLRP3 inflammasomes produce reactive oxygen species (ROS) during activation, but the sources of these ROS and the mechanism by which NLRP3 participates in their production have not been clarified.

Given the intensity of the inflammatory reactions that characterize an acute attack, oral colchicines and nonsteroidal anti-inflammatory drugs (NSAIDs) are appropriate first-line drugs for this phase. However, oral colchicines and NSAIDs have adverse effects such as severe gastrointestinal reactions and toxicity (Borstad et al., 2004; Sabina et al., 2011). Therefore, the need to identify new anti-inflammatory treatments for gouty arthritis has stimulated many recent studies to focus on natural products (Ahmad et al., 2008) such as herbs (An et al., 2010), as people urgently need anti-gout drugs.

P. igniarius, a well-known mushroom belonging to the family Polyporaceae, is distributed in many East Asian countries such as China, Korea, and Japan (Mao, 2000; Dong et al., 2019) and is commonly referred to as "*Sanghuang*" in China (Dong et al., 2019). Its main components include polysaccharides, flavonoids, polyphenols, steroids, and organic acids, and it therefore has good anti-inflammatory, antioxidant and antitumor activities (Ding et al., 2016; Wang et al., 2018; Gu et al., 2019; Luan et al., 2022). Many studies have shown that it has good anti-uric acid activity, but the specific mechanism has not been clarified (Liu et al., 2019; Xing et al., 2021).

In conclusion, we hypothesize that *P. igniarius* may down-regulate MSU crystal-induced gout-related inflammatory factor expression in HUVECs through mediating the TLR4/NF-κB/NLRP3 signaling pathway. In this study, MSU was used to induce HUVECs to produce an acute gouty inflammation model *in vitro* to study the anti-inflammatory effects of wild and cultivated *P. igniarius* and further explore the specific mechanism of its inhibitory effect through enzyme kinetics and metabolomics studies. In addition, the medicinal value of wild *P. igniarius* is high, but the supply is insufficient and therefore the price is high, which has limited the development and utilization of *P. igniarius* as a medicinal fungal resource. Fortunately, artificial cultivation is effective. However, there are few comparative studies on wild and cultivated *P. igniarius*. Another purpose of this study was to compare and evaluate the efficacy of wild *P. igniarius* and cultivated *P. igniarius* in the treatment of hyperuricemia and gouty arthritis and to promote its industrial development and product development.

Materials and methods

Plant material

The Zhejiang Qiandao Lake Sangdu Edible Fungus Professional Cooperative sold us wild *P. igniarius* samples (Hangzhou, China). The *Phellinus igniarius* that was artificially cultivated was a strain known as "Zhehuang No. 1," which was also supplied by Zhejiang Qiandao Lake Sangdu Edible Fungus Professional Cooperative. The Horticulture Institute of Zhejiang Academy of Agricultural Sciences and the Institute of Edible Fungi of Shanghai Academy of Agricultural Sciences both recognized it as *Phellinus igniarius*. All samples were kept in a dim setting with constant humidity and temperature.

Preparation of polyphenols from P. igniarius

Response surface approach was used to identify the ideal conditions for the extraction and purification of polyphenols from *P. igniarius* by referring to the polyphenol concentrations and adhering to scientific standards and environmental protection protocols. In particular, the *P. igniarius* dried fruit body was crushed and put through a 40-mesh filter. The powder was extracted with 16-fold 70% ethanol for 2 h at 80°C in the dark after being steeped in 70% ethanol for 30 min. Under the same circumstances, the residue was removed once more. An ethanol extract of both wild and cultivated *P. igniarius* was produced by combining these two filtrates and removing the solvent under negative pressure at 60°C without light. After that, the crude extract solution was adsorbed by an HP20 macroporous resin, contaminants were cleaned up with 10% ethanol using five times the volume of the solution, and then the solution was eluted with 40% ethanol using five times the volume of the solution. The eluates were gathered, pooled, and then turned into a powder by freeze-drying. WPP and CPP were created in succession, stored at -20°C, and kept in the dark. The amount of total polyphenols was calculated using the Folin-Ciocalteu technique.

Comparison of total antioxidant capacity between WPP and CPP *in vitro*

Determination of total antioxidant capacity by the DPPH method

Aliquots of 2.5, 5, 10, 20, 40 and 80 μg/ml Vc, WPP or CPP 133.3 μl were added to a 200 μl DPPH working solution (Jiancheng, Nanjing, China). As a control, 2.5, 5, 10, 20, 40 and 80 μg/ml Vc, WPP or CPP 133.3 μl were added to 200 μL 80% ethanol. The blank tube contained 200 μl of 80% ethanol and 300 μl of the DPPH working solution. The absorbance (A) was measured at 517 nm after mixing and incubation at room temperature for 30 min. The DPPH free radical clearance rate (%) = $[1- (A_{sample}- A_{control})/A_{blank}] \times 100\%$. The IC_{50} value was calculated using a logistic regression curve.

Determination of total antioxidant capacity by the FRAP method

Aliquots of 2.5, 5, 10, 20, 40 and 80 μg/ml Vc, WPP or CPP 5 μl were added to 180 μl of FRAP working solution (Jiancheng, Nanjing, China) with four wells each. Distilled water was added to three wells as a blank control. A standard curve was drawn with $FeSO_4$ as the standard. Absorbance (A) was determined at 593 nm after incubation at 37°C for 5 min. The absorbance measured for each sample was compared with the standard curve, and the concentration equivalent to the $FeSO_4$ standard solution was used to represent the antioxidant capacity. The FRAP was used to compare the total antioxidant capacity of the sample and the positive control: 1 unit FRAP = 0.5 mM $FeSO_4$. The smaller the FRAP, the higher the total antioxidant capacity.

Determination of total antioxidant capacity by the ABTS method

Aliquots of 2.5, 5, 10, 20, 40 and 80 μg/ml Vc, WPP or CPP 10 μl, and 20 μl enzyme application solution were added to 170 μl of ABTS working solution (Jiancheng, Nanjing, China) with four wells each. Distilled water was added to three wells as a blank control. A standard curve was drawn with Trolox as the standard. The absorbance (A) at 405 nm was determined after incubation at ambient temperature for 6 min. The absorbance measured for each sample was compared with the standard curve, and the concentration equivalent to the Trolox standard solution was used to represent the antioxidant capacity. The total antioxidant capacity of the tested samples and the positive control were compared by ABTS, with 1 unit ABTS = 0.5 mM Trolox. The smaller the ABTS, the higher the total antioxidant capacity.

Comparison of inhibition of XO activity *in vitro* between WPP and CPP

Four groups were established: a blank control group, a positive control group, the WPP group and the CPP group. The WPP group and the CPP group were treated with a drug solution at different concentrations, with four wells per concentration. PBS was added to the blank group, and an allopurinol solution was added to the positive control group at different concentrations, with four wells for each concentration. The XO solution (Yuanye, Shanghai, China) was added to the wells of each group, and incubated at 37°C with an enzyme label. The XA solution (Yuanye, Shanghai, China) was then added to each well, and the absorbance (A) was measured immediately at 295 nm and read every 1 min. The change value was recorded for 6 min, and the XO inhibition rate (IR) and half-maximum inhibitory concentration (IC_{50}) were calculated.

$$IR\,(\%) = \left[\left(dA/dt\right)_{blank} - \left(dA/dt\right)_{sample}\right] \Big/ \left(dA/dt\right)_{blank} \times 100\% \quad (1)$$

The reaction time was chosen based on variations in absorbance, and in this formula, dA represents the absorbance difference from the time the reaction started

and when it finished. The IR was calculated from the average values of the four wells. The IC_{50} value was calculated using a logistic regression curve.

Cell culture and treatment

HUVECs (Bogoo Biological Technology, Shanghai, China) were grown in DMEM (Gibco, United States) culture medium containing 10% FBS (Siji Green, Zhejiang, China), 100 units/ml penicillin, and streptomycin at 37°C in a humidified atmosphere with 5% CO_2. The cells in the logarithmic phase were subcultured and tested.

MTT assay

MTT was used to detect cellular activity. The HUVEC monolayers were digested with pancreatin (Solarbio, Beijing, China), and then the HUVECs were plated in a 96-well plate and allowed to attach overnight. Next, the HUVECs were treated with different concentrations of MSU (Yuanye, Shanghai, China), WPP and CPP. The supernatant was discarded after incubation for 24 h, and 20 μl of MTT solution was added. The supernatant was discarded after incubation for 4 h, and 150 μl of DMSO was added with oscillation for 10 min. The OD was measured at 490 nm:

$$\text{Cell Viability}\,(\%) = \left(\text{OD}_{\text{drug}} - \text{OD}_{\text{control}}\right) \Big/ \left(\text{OD}_{\text{blank}} - \text{OD}_{\text{control}}\right) \times 100\% \quad (2)$$

Determination of ICAM-1, VCAM-1, IL-1β and IL-6 in cell culture medium by ELISA

HUVECs were plated in a 6-well plate and allowed to attach overnight before they were treated with different concentrations of WPP or CPP and MSU for 24 h. The culture medium of each group was then extracted. The levels of ICAM-1, VCAM-1, IL-1β and IL-6 in the cell culture medium were determined with an ELISA kit (Mlbio, Shanghai, China).

Western blot analysis

The cells were lysed in ice-cold RIPA buffer, and cell lysates were clarified by centrifugation, diluted in 2× SDS loading buffer, resolved by SDS–PAGE and transferred onto PVDF, which was subsequently blocked with 5% skimmed milk. The membranes were then incubated overnight at 4°C with primary antibodies followed by incubation with horseradish peroxidase-conjugated antibodies. The immunoreactive protein bands were visualized with an enhanced chemiluminescence (ECL) kit (New Cell & Molecular Biotech, Suzhou, China).

DCFH-DA fluorescent probe assay

The cell culture medium was withdrawn, the DCFH-DA was diluted with PBS (Biosharp, Anhui, China), and the cells were then given two PBS washes. The cells were then added to the diluted DCFH-DA solution, and they were incubated at 37°C. To completely eliminate any DCFH-DA that did not reach the cells, PBS was applied three times to the cells. Following the addition of PBS, the fluorescence was observed, captured on camera, and its average optical density was measured and quantitatively analyzed using ImageJ software. The excitation and emission wavelengths were 485 nm and 528 nm, respectively.

Immunofluorescence assay

The cell culture medium was discarded, PBS (Biosharp, Anhui, China) was used to wash the cells three times, a 4% paraformaldehyde solution (Solarbio, Beijing, China) was added to fix the cells, the fixative was removed, and an immunostaining blocking solution was added at room temperature. The primary antibody was incubated overnight at 4°C, and goat anti-rabbit IgG H&L (Alexa Fluor® 488) was diluted at 37 °C. A blocking solution (including DAPI) was added. The cells were observed under a fluorescence microscope.

UHPLC-QE-MS for cell metabolomics analysis

Cell sample preparation

The cells in each group were removed from the culture medium, quickly washed with precooled PBS solution, digested with trypsin, and then added to the culture medium. The medium was gently shaken to stop digestion of the infiltrated cells. With rapid counting, 1×10^7 cells per bottle were taken as samples (i.e., 1 unit), quickly placed in a precooled 5 unit quencher containing 60% methanol (Macklin, Shanghai, China) and 8.5 g/L ammonium bicarbonate, adjusted to pH 7.4 with 12 M hydrochloric acid, and placed in a slightly oscillating centrifuge tube for 10 s. The mixture was allowed to cool at -20°C, centrifuged at 4°C and 1,000 × g for 1 min, and then the supernatant was removed, and the cells were placed in liquid nitrogen for 30 s and preserved at -80°C.

Metabolite extraction

For lyophilization, the materials were moved to a 2 ml EP tube. 200 L of water were then added to the samples. The samples were vortexed for 30 s before being frozen with liquid nitrogen and thawed three times. The samples were sonicated in an ice-water bath for 10 min. The protein concentration was assessed using 50 μl of homogenate. The leftover amount was then mixed with 600 L of acetonitrile:methanol (1:1) and put to a 2 ml EP tube. The samples were vortexed for 30 s, then incubated at -40°C for 1 h, and then centrifuged for 15 min at 4°C at 12000 (RCF = 13800 g, R = 8.6 cm) rpm. The supernatant was transferred to an EP tube in an amount of 660 L, and it was dried in a vacuum concentrator. After drying, a proportionate amount of acetonitrile, methanol, and water (2:2:1) with an internally labeled standard mixture was added. The samples were vortexed for 30 s before being sonicated for 10 min in an ice-water bath. The materials were then centrifuged for 15 min at 4°C at 12000 (RCF = 13800 g, R = 8.6 cm) rpm. A new glass vial was used to transfer the resultant supernatant for analysis. An equivalent quantity of the supernatant was mixed to create the quality control (QC) sample.

LC–MS/MS analysis

A UHPLC system (Vanquish, Thermo Fisher Scientific) with a UPLC BEH Amide column (2.1 mm 100 mm, 1.7 m) connected to a Q Exactive HFX mass spectrometer was used to perform the LC-MS/MS analysis (Orbitrap MS, Thermo). 25 mmol/L each of ammonium acetate and ammonia hydroxide in water (pH = 9.75) (A) and acetonitrile made up the mobile phase (B). The injection volume was 2 L, and the autosampler's temperature was 4°C. Because it can acquire MS/MS spectra in information-dependent acquisition (IDA) mode under the control of the acquisition software, the QE HFX mass spectrometer was chosen (Xcalibur, Thermo). The acquisition program constantly assesses the complete scan MS spectrum in this mode. The following parameters were adjusted for the ESI source: spray voltage of 3.6 kV (positive) or -3.2 kV, sheath gas flow rate of 30 arb, aux gas flow rate of 25 arb, capillary temperature of 350°C, full MS resolution of 60000, MS/MS resolution of 7,500, collision energy of 10/30/60 in NCE mode (negative).

Data annotation, multivariate statistical analysis and metabolic pathway analysis

The raw data was programmatically converted to the mzXML format and then ordered to perform metabolic annotations. This information included peak detection, extraction, alignment, and integration. For logarithmic conversion and centralized formatting, the final datasets were entered into the SIMCA V15.0.2 software program (Sartorius Stedim Data Analytics AB, Umea, Sweden). Principal component analysis (PCA) and orthogonal projections to latent structures-discriminate analysis (OPLS-DA) were carried out in succession to depict group separation and identify significantly altered metabolites. The OPLS-DA was used to calculate the VIP value, or variable importance in the projection.

For the purposes of the following study, metabolites between the two groups that had P 0.05 (Student's t test) and VIP >1 were regarded as differential metabolites. Utilizing volcano plots, the up- and downregulation of various metabolites was demonstrated. To identify the key metabolic pathways with the highest correlation, the differential metabolites were subjected to pathway enrichment analysis using the KEGG database and MetaboAnalyst (http://www.metaboanalyst.ca/), which further revealed the related metabolic mechanism of wild and cultivated *Phellinus igniarius* in the treatment of hyperuricacidemia.

LC-MS/MS data

The original data of HPLC chromatogram has been uploaded to the public database "MetaboLights", and the original data can be downloaded according to the database number MTBLS5795.

Statistical analysis

GraphPad Prism V8.0.2 software was used for statistical analysis and data visualization. Multiple comparisons between groups were performed using a one-way ANOVA or two-way ANOVA. The data are expressed as the mean ± standard deviation (SD), and a $p < 0.05$ was considered statistically significant.

Results

The total antioxidant capacity of CPP is similar to that of WPP

With vitamin C (Vc) as the positive control, the total antioxidant capacities of WPP and CPP were detected using the DPPH, FRAP and ABTS methods. As shown in Figure 1, 1A, the IC_{50} values of Vc, WPP and CPP for DPPH radical scavenging were 9.994 μg/ml, 12.28 μg/ml and 21.00 μg/ml, respectively. The FRAP values (Figure 1B) of Vc, WPP and

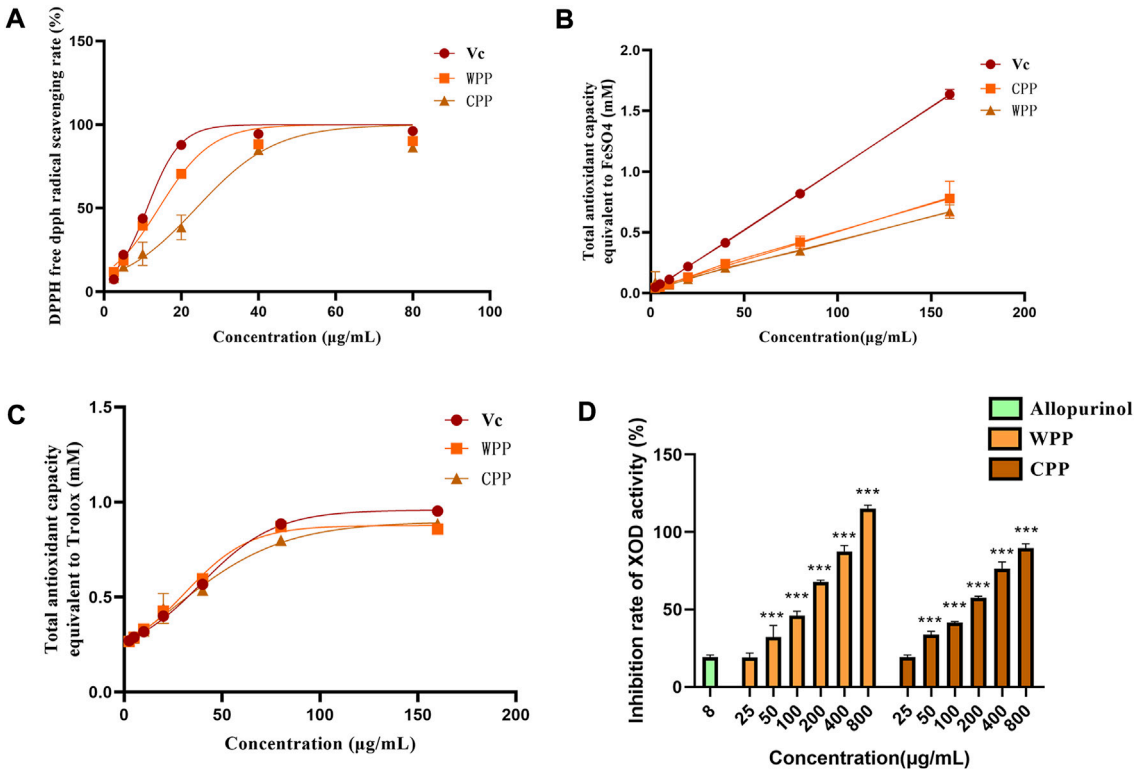

FIGURE 1
Comparison of DPPH free radical scavenging rates between WPP and CPP **(A)**, comparison of FRAP values between WPP and CPP **(B)**, and comparison of ABTS values between WPP and CPP **(C)**. Comparison of inhibitory effects of WPP and CPP on XO, ***$p < 0.001$ vs. allopurinol (8 μg/ml), $n = 4$ **(D)**.

CPP were 47.83 μg/ml, 98.75 μg/ml and 116.97 μg/ml, respectively. The ABTS values (Figure 1C) of Vc, WPP and CPP were 39.69 μg/ml, 40.44 μg/ml and 44.40 μg/ml, respectively. In conclusion, WPP and CPP have a strong total antioxidant capacity, and the total antioxidant capacity of CPP is similar to that of WPP.

The inhibitory effect of CPP on XO activity was similar to that of WPP

As shown in Figure 1D, with allopurinol (8 μg/ml) as the control, WPP and CPP significantly inhibited XO activity and showed dose-dependent tolerance within a certain concentration range. The XO inhibition of both in the dose range of 50–800 μg/ml was statistically significant ($p < 0.001$). The IC_{50} values of WPP and CPP for the inhibition of XO activity were 88.19 μg/ml and 108.0 μg/ml, respectively. The ability of CPP to inhibit XO activity was similar to that of WPP.

WPP and CPP attenuated the decrease in cell viability and cell cytotoxicity caused by MSU in HUVECs

To evaluate the toxicity of MSU, WPP and CPP, HUVECs were treated with different concentrations of MSU (0–500 μg/ml), WPP or CPP (0–800 μg/ml for both) for 24 h, and cell viability was evaluated by the MTT assay. As shown in Figure 2, 2A, MSU concentrations above 150 μg/ml had an extremely significant inhibitory effect on cell viability. WPP and CPP had no significant cytotoxic effect on cells below 200 μg/ml (Figure 2B) and 100 μg/ml (Figure 2C), respectively. We chose these concentrations for the following experiments. To evaluate the protective effects of WPP and CPP on MSU-induced cell death, HUVECs were treated with MSU and WPP or CPP for 24 h. At a concentration of 40 μg/ml, both WPP and CPP reduced the loss of cell viability induced by MSU (Figures 2D,E). In summary, WPP and CPP at a dose of 40 μg/ml were selected for subsequent studies on efficacy and mechanism.

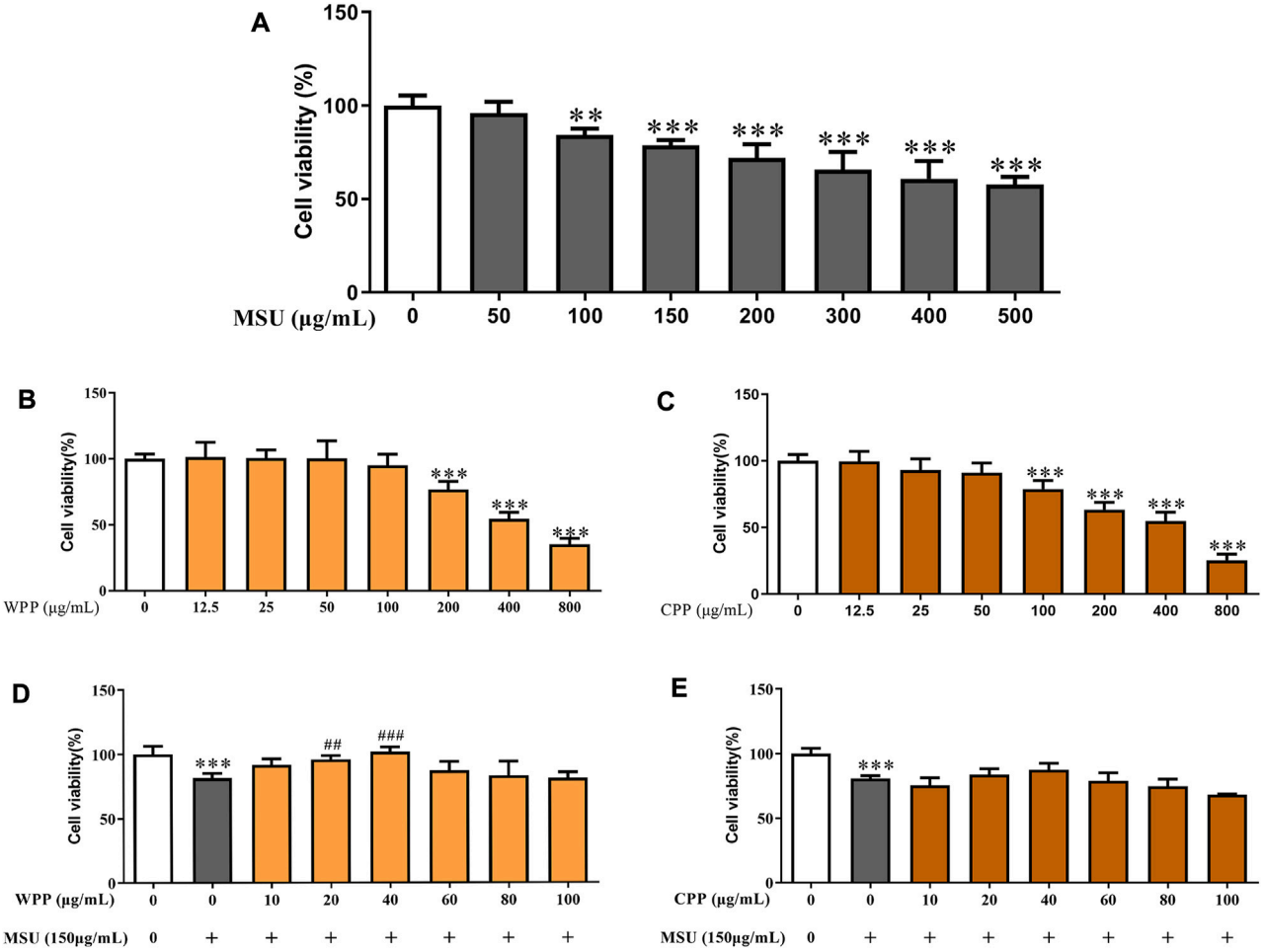

FIGURE 2
The effects of MSU on cell viability, *$p < 0.05$, **$p < 0.01$, ***$p < 0.001$ vs. the control group, $n = 6$ **(A)**. Cell viability of HUVECs treated with different concentrations of WPP as determined by the MTT assay, ***$p < 0.001$ vs. the control group, $n = 6$ **(B)**. Cell viability of HUVECs treated with different concentrations of CPP as determined by the MTT assay, ***$p < 0.001$ vs. control group; $n = 6$ **(C)**. Protective effect of WPP on MSU-induced HUVEC injury, ***$p < 0.001$ vs. control group; $^{\#\#}p < 0.01$, $^{\#\#\#}p < 0.001$ vs. positive group, n = 6 **(D)**. Protective effect of CPP on MSU-induced HUVEC injury, ***$p < 0.001$ vs. the control group, $n = 6$ **(E)**.

WPP and CPP can reduce the production of inflammatory factors in an acute gouty inflammation model *in vitro*

As shown in Figure 3, compared with the control group, the ICAM-1 ($p < 0.05$), VCAM-1 ($p < 0.05$), IL-1β ($p < 0.01$) and IL-6 ($p < 0.01$) contents in the model group were significantly increased, suggesting that MSU induces inflammatory injury in HUVECs. Compared with the model group, the ICAM-1 ($p < 0.05$), VCAM-1 ($p < 0.01$), IL-1β ($p < 0.001$) and IL-6 ($p < 0.001$) contents were significantly decreased after treatment with 40 μg/ml WPP and MSU. The ICAM-1 ($p < 0.05$), VCAM-1 ($p < 0.01$), IL-1β ($p < 0.01$) and IL-6 ($p < 0.01$) contents were also significantly decreased after treatment with 40 μg/ml CPP and MSU. The results indicated that both WPP and CPP could alleviate MSU-induced inflammatory injury by downregulating the expression of ICAM-1, VCAM-1, IL-1β and IL-6.

WPP and CPP can reduce the expression of TLR4 and NLRP3

As shown in Figure 4, compared with the control group, the protein expressions of TLR4 ($p < 0.05$) and NLRP3 ($p < 0.01$) in the model group were significantly increased, indicating that the NLRP3 inflammatory corpuscle pathway recognized and mediated by TLR4 was activated. After the 40 μg ml WPP treatment, the protein expressions of TLR4 ($p < 0.05$) and NLRP3 ($p < 0.01$) were significantly decreased. At 40 μg/ml,

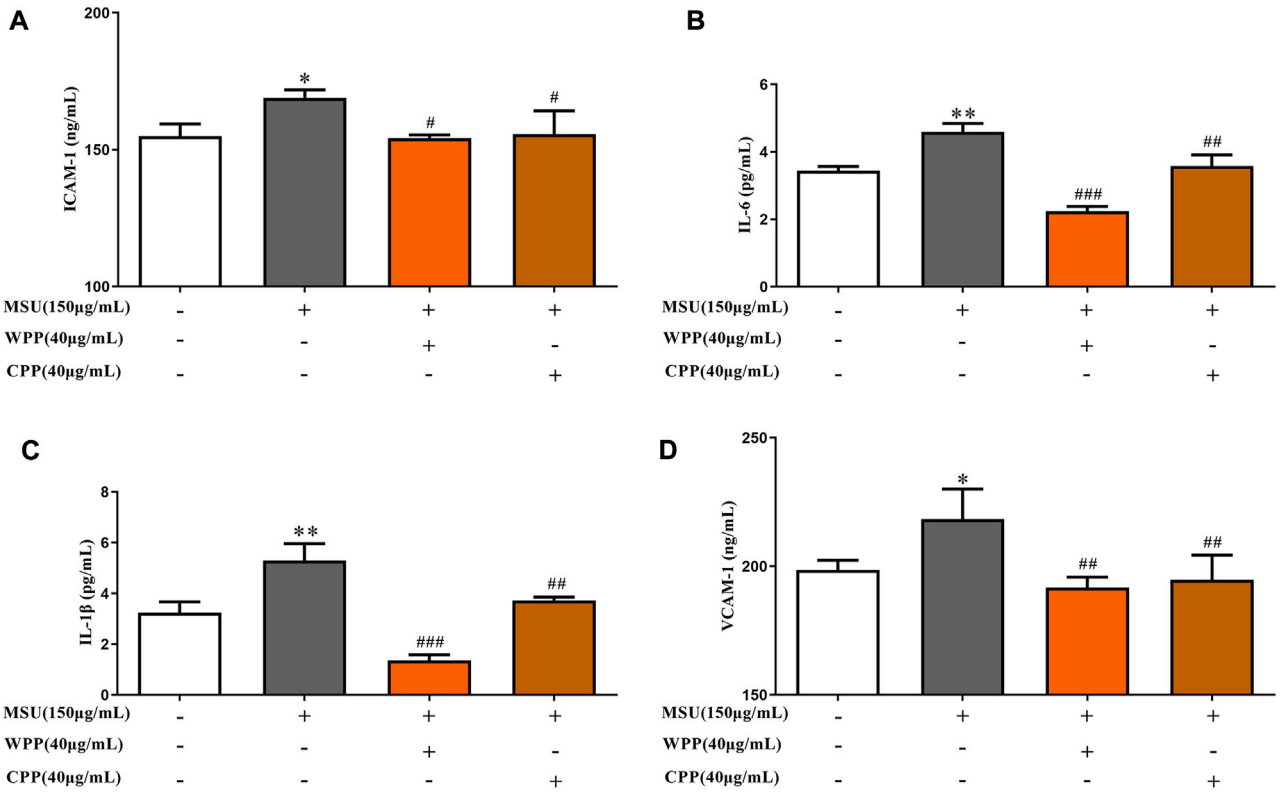

FIGURE 3
Effects of WPP and CPP on ICAM-1 **(A)**, IL-6 **(B)**, IL-1β **(C)** and VCAM-1 **(D)** in the *in vitro* gout model, $^{*}p < 0.05$, $^{**}p < 0.01$ vs. control group; $^{\#}p < 0.05$, $^{\#\#}p < 0.01$, $^{\#\#\#}p < 0.001$ vs. model group; $n = 3$.

CPP also significantly downregulated the protein expression of TLR4 ($p < 0.05$) and NLRP3 ($p < 0.001$).

WPP and CPP can inhibit ROS

As shown in Figures 5A,B, compared with the control group, the ROS content in the model group was significantly increased after MSU stimulation ($p < 0.001$), indicating that the intracellular oxidative stress response was activated. Compared with the model group, 40 μg/ml WPP or CPP cotreated with MSU for 24 h significantly inhibited ROS production ($p < 0.001$), indicating that oxidative stress injury was alleviated and inhibited. Therefore, WPP and CPP can alleviate MSU-induced oxidative stress injury by inhibiting ROS generation.

WPP and CPP inhibited NF-κB activation

In the control group, NF-κB p65 was mainly expressed in the cytoplasm, and there was no obvious nuclear entry, as fluorescent nuclear division was clearly observed. After MSU stimulation, the nuclear translocation of NF-κB p65 in the model group was significantly increased, there was no obvious nuclear-cytoplasmic division indicated by fluorescence, and the nuclear green fluorescence intensity was significantly enhanced, indicating that the NF-κB pathway was activated and had triggered downstream inflammatory reactions. Compared with the model group, the nuclear translocation of NF-κB p65 was significantly improved after treatment with 40 μg/ml WPP or CPP and MSU for 24 h, and fluorescent nuclear division was enhanced. The above results showed (Figure 5C) that WPP and CPP could inhibit activation of the NF-κB pathway by inhibiting NF-κB p65 translocation into the nucleus, thereby alleviating the inflammatory response induced by MSU.

UHPLC-QE-MS for cell metabolomics analysis

PCA was used to evaluate the treatment of gout with WPP (40 g/ml) and CPP (40 g/ml) to the control group and the

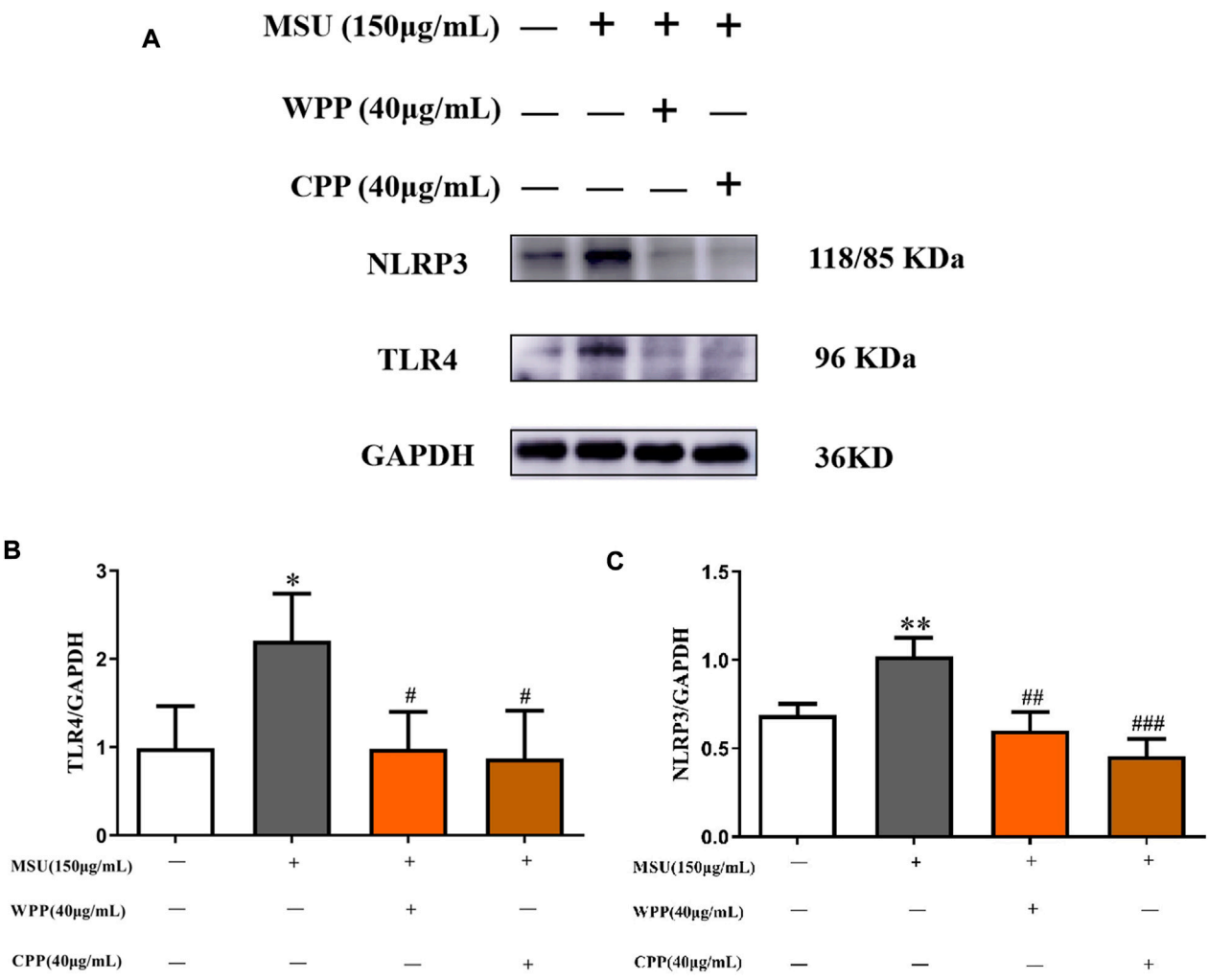

FIGURE 4
Western blotting was used to detect the effect of WPP and CPP on the protein expression of TLR4 and NLRP3 **(A)**, and ImageJ was used to measure the gray value of the protein bands **(B,C)**, $^{*}p < 0.05$, $^{**}p < 0.01$ vs. the control group; $^{\#}p < 0.05$, $^{\#\#}p < 0.01$, $^{\#\#\#}p < 0.001$ vs. the model group; $n = 3$.

model group to determine changes in the metabolic spectrum. According to the PCA score (Figure 6), there were some differences between the metabolite spectra of the four groups in ESI+ and ESI. Additionally, the OPLS-DA diagram (Figures 7A–C) demonstrated that there may be a substantial difference between the control group, model group, WPP treatment group, and CPP treatment group. Since the database contains more data about chemicals in ESI + than in ESI-, differential metabolites between the groups were screened using a $p < 0.05$ (Student's t test) and a VIP >1 in ESI+. Specifically, there were 90 upregulated metabolites and 16 downregulated metabolites between the control group and the model group (Figure 7D), 25 downregulated metabolites between the model group and the WPP treatment group (Figure 7E), and upregulated metabolites between the model group and the CPP treatment group (Figure 7F).

Finally, according to the topological analysis, the method of determining the path affects the value (ln p) generated in the flow analysis. Therefore, the topological analysis method determines a higher level of metabolic path and is displayed in the bubble diagram. The results (Figure 8) showed that the biosynthesis of glycerophosphate, thiamine, pantothenic acid and coenzyme a may lead to the production and development of uric acid. These altered metabolites were discovered to play a major role in the effects of the treatment on gout, specifically in the phenylalanine metabolism of WPP and the lysophosphatidylcholine metabolism of CPP.

10.3389/fphar.2022.1011406

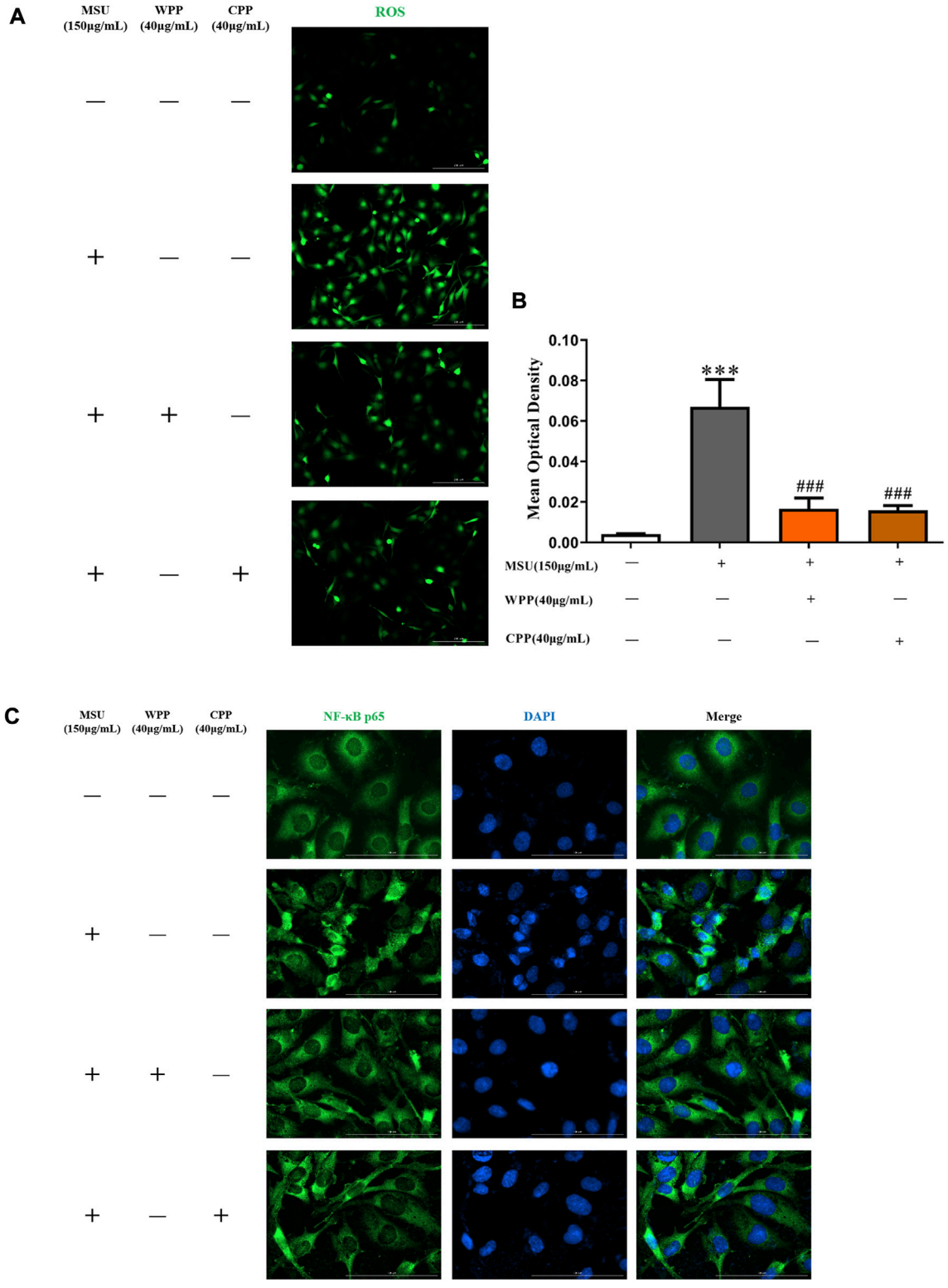

FIGURE 5
The generation of ROS was compared by IF **(A)**, scale bar = 200 μm, and the fluorescence intensity was quantitatively analyzed **(B)**, $^{***}p < 0.001$ vs. the control group; $^{###}p < 0.001$ vs. the model group; $n = 3$. Effect of WPP and CPP on NF-κB p65 nuclear translocation by IF **(C)**.

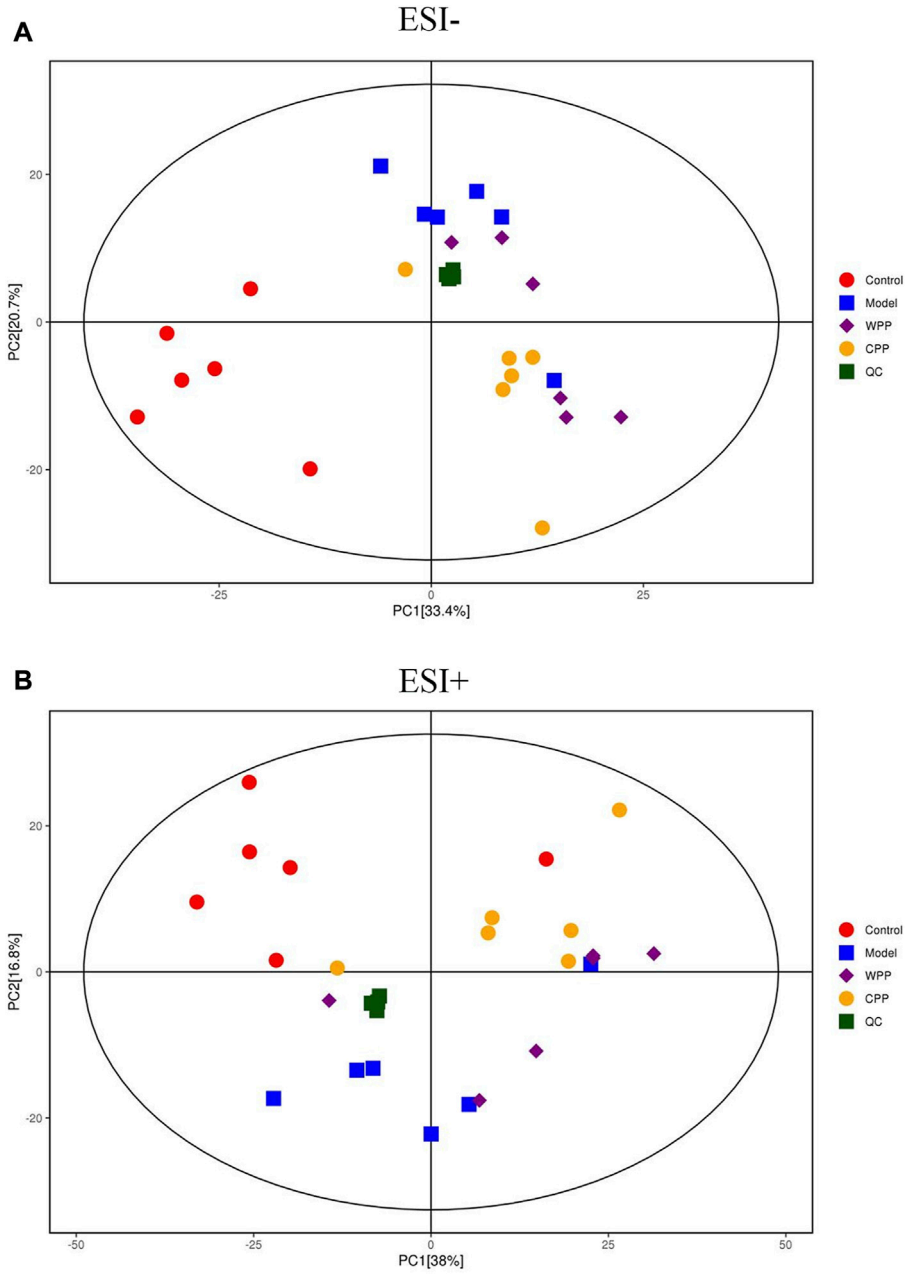

FIGURE 6
Principal component analysis (PCA) score plot of the control group, model group, WPP-treated group (40 μg/ml) and CPP-treated group (40 μg/ml) in the negative ion mode (NEG) **(A)** and positive ion mode (POS) **(B)** (*n* = 6).

Discussion

P. igniarius is a traditional Chinese herbal medicine that has a long history of application in China. In modern times, it has gradually become the focus of attention in China and abroad because of its outstanding regulation of immunity and its antitumor and antioxidant activities. A series of studies have shown that *P. igniarius* has antiviral (H Dogan et al., 2018), anti-inflammatory (Nakayama et al., 2014), antioxidant (Kottgen et al., 2013), antineoplastic (Li et al., 2015), and immunoregulatory (Li et al., 2015) pharmacological effects, whereas documentation of the anti-uric acid activity of *P. igniarius* is still rare. This study focused on oxidative stress, NF-κB signal transduction and NLRP3 inflammation to study

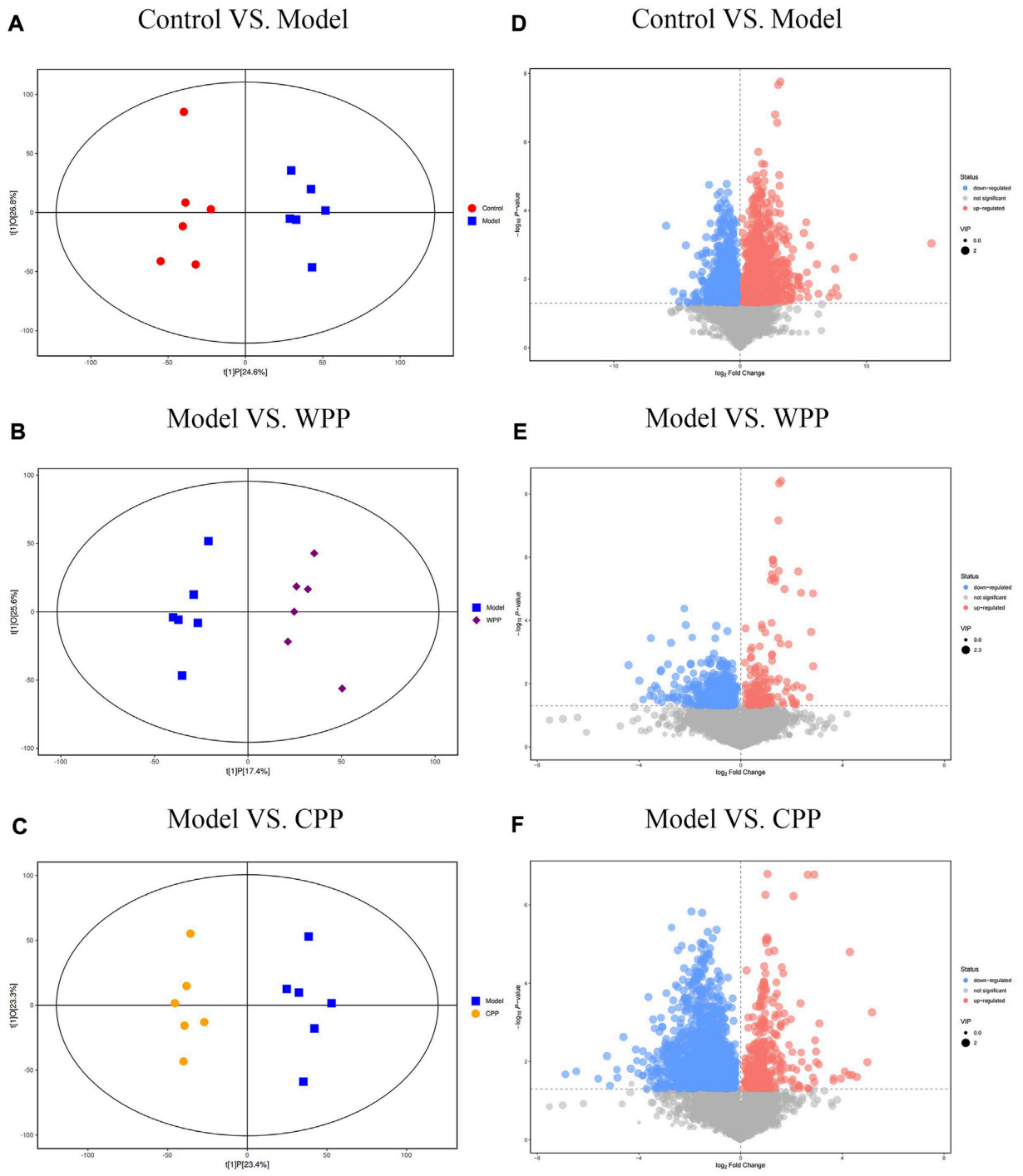

FIGURE 7
Orthogonal projections for the latent structures-discriminate analysis (OPLS-DA) score plot and volcano plot between the control group, model group, WPP-treated group (40 μg/ml), and CPP-treated group (40 μg/ml) in the positive ion mode (POS) (n = 6). OPLS-DA score plots between the control group and model group **(A)**, model group and WPP-treated group (40 μg/ml) **(B)**, and model group and CPP-treated group (40 μg/ml) **(C)**. The volcano plots between the control group and model group **(D)**, model group and WPP-treated group (40 μg/ml) **(E)**, and model group and CPP-treated group (40 μg/ml) **(F)** are also shown above. The *X*-axis and *Y*-axis represent the log2-fold change and $-\log_{10} p$ value, respectively.

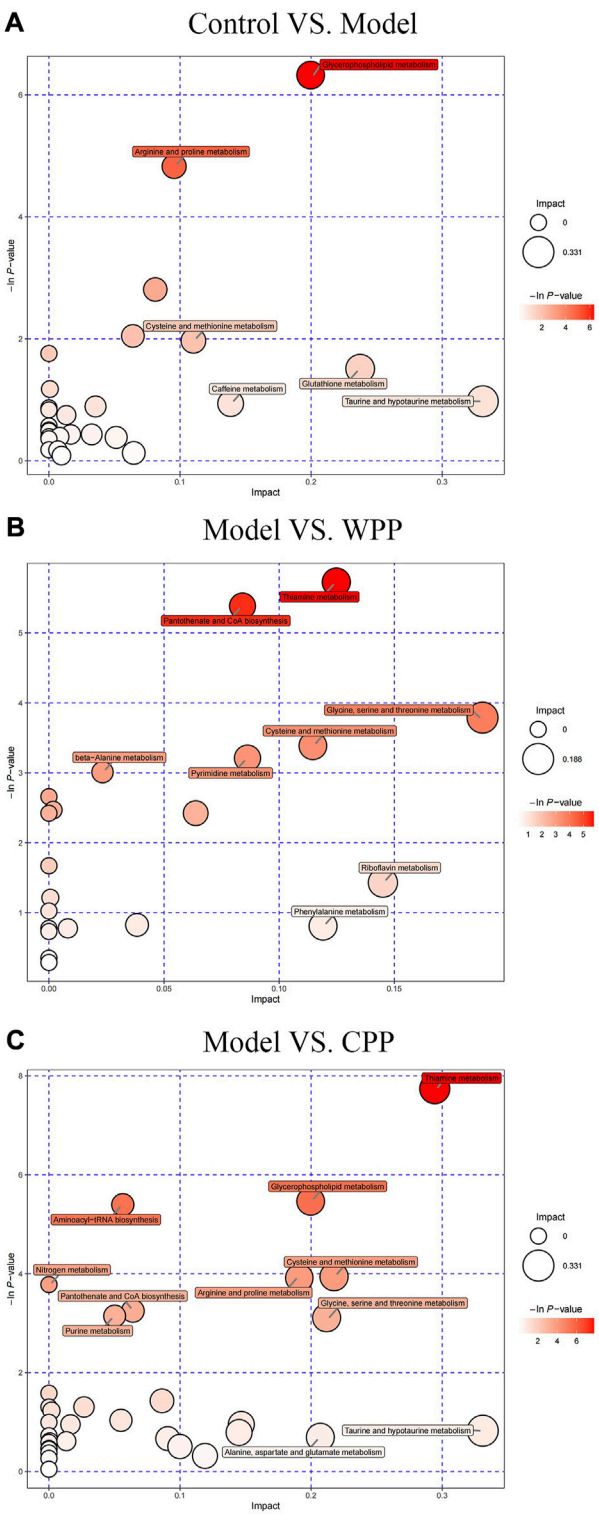

FIGURE 8
Metabolic pathway bubble plots of the control group and model group **(A)**, the model group and WPP-treated group (40 μg/ml) **(B)**, and the model group and CPP-treated group (40 μg/ml) **(C)**. The *X*-axis and *Y*-axis represent the impact and −ln *p* values, respectively.

the molecular mechanism of *P. igniarius* on gout-related inflammation caused by MSU crystals in HUVECs. We have proven that *P. igniarius* is an effective oxidative scavenger that plays a key role in regulating the NF-κB pathway and NLRP3 inflammatory bodies through ROS generation during MSU crystal-induced inflammation.

However, the shortage of wild *P. igniarius* resources and the high market prices have indirectly limited the in-depth study of the medicinal value of *P. igniarius* and restricted the development and application of *P. igniarius*. Therefore, artificial cultivation is an important way to efficiently obtain fruiting bodies of *P. igniarius*, and research on the cultivation of *P. igniarius* will effectively alleviate this situation. Our research team has analyzed and studied the main active components of wild and cultivated *P. igniarius*, and the results showed that wild and cultivated samples were similar in composition (Li et al., 2021). Therefore, we used wild and cultivated *P. igniarius* to prepare WPP and CPP, respectively, to study their efficacy and mechanism *in vitro*.

ROS are crucial bioactive mediators that act as second messengers in signal transduction during the pathogenesis of MSU crystal-induced inflammation (Cheng et al., 2015; Choe et al., 2015). Inhibition of ROS production is an important indicator that can be used to evaluate the anti-inflammatory effect of drugs and can demonstrate the antioxidant capacity of drugs (Ren et al., 2020). The antioxidant capacity of known drugs can be determined by the DPPH, FRAP and ABTS methods. In 293 cells derived from the human embryonic kidney, ascorbic acid (Vc), which has antioxidant characteristics and functions as a powerful ROS scavenger, inhibits the production of ROS (Ozgen et al., 2006); Vc was used as a positive control. This study showed that the total polyphenol extracts (WPP and CPP) from *P. igniarius* had good antioxidant capacity, which could theoretically effectively inhibit the production of ROS and have certain anti-inflammatory effects. This study also demonstrated that the total polyphenol content in the prepared WPP and CPP was high.

XO is an enzyme that produces uric acid in the body. Evolutionarily, primates lack uric acid oxidase, and thus they are prone to hyperuricemia and gout (Zulueta et al., 2009; Neogi, 2010). Therefore, XO is the target of therapeutic drugs for hyperuricemia and gout (Nishino, 1994; Hille, 1996). Allopurinol is a commonly used drug in clinical practice for the treatment of gout (Elion, 1966). In this study, WPP and CPP showed similar XO inhibitory effects in a concentration-dependent manner. This suggests that *P. igniarius* may be a potential XO inhibitor.

The main pathological trait of gout is endothelial activation brought on by IL-1 and IL-6 while inducing ICAM-1 expression, which increases the influx of neutrophils into the joint fluid and the subsequent influx of monocytes. Following activation, monocytes and neutrophils actively phagocytose MSU crystals, which sets off inflammatory reactions (Cronstein and Terkeltaub, 2006; Shi et al., 2013; Han et al., 2021). In this study, the ELISA experiment showed that WPP and CPP can inhibit the

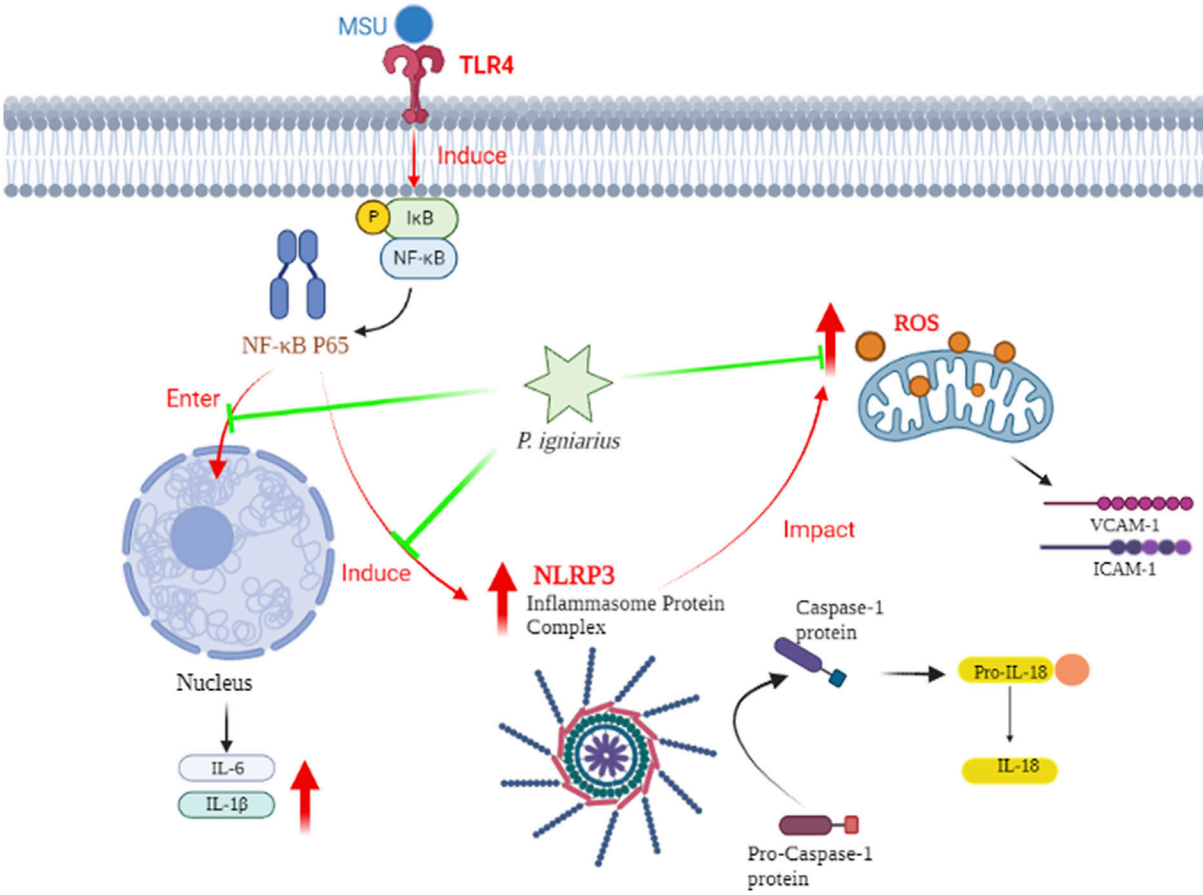

FIGURE 9
The hypothetical mechanism of *P. igniarius* in HUVECs.

expression of IL-1β, IL-6, ICAM-1 and VCAM-1 to inhibit the phagocytosis of MSUs. The expression of the inflammasome (TLR4 and NLRP3) is associated with acute gout inflammation (Kim et al., 2016; Zhang et al., 2022), which was determined by western blot, and WPP and CPP inhibited the expression of TLT4 and NLRP3. Thus, *P. igniarius* further inhibited the occurrence of acute gout inflammation. This study proves that *P. igniarius* is an effective drug for gout. Moreover, WPP and CPP have similar effects at the same concentration. This suggests that high-priced WPP can be replaced with low-priced CPP.

The NF-κB signaling pathway is an important signaling pathway regulating inflammation *in vivo*. Its activation is determined by the nuclear entry of NF-κB p65. Immunofluorescence results showed that WPP and CPP could inhibit NF-κB p65 entry into the nucleus and alleviate the inflammatory response induced by MSU, which is consistent with our previous conclusion.

In conclusion, we can speculate on the mechanism of *P. igniarius*. MSU crystals induce inflammasome maturation and inflammatory factor secretion (IL-1, IL-6, ICAM-1, and VCAM-1) in HUVECs through activating the NF-κB pathway and producing ROS. *P. igniarius* reduced the production of ROS and NF-κB activation, which in turn prevented the activation of inflammasomes (Figure 9).

Metabolomics has made significant advances in helping to understand the pathogenesis of many metabolic diseases, which has proven the validity of metabolite profiling (Shan et al., 2021). Various methods have been conducted to explore effective treatments for hyperuricemia such as magnetic resonance spectroscopy and liquid and gas chromatography-tandem mass spectrometry (Wang et al., 2020). Therefore, metabolomics based on UHPLC-QE-MS, which is suitable for the simultaneous and systemic analysis of multiple metabolite fingerprinting, was employed to generate metabolite profiles of cells to characterize the metabolic changes related to hyperuricemia and uncover the underlying metabolic mechanism of the therapeutic effects of WPP and CPP on gout. In our study, it was found that the *in vitro* model of MSU-induced gouty arthritis in HUVECs was mainly related to lysophosphatidylcholine metabolism and phenylalanine

metabolism. Studies have shown that lysophosphatidylcholine (lysoPC) is the end product of glycerophospholipid metabolism. Abnormal levels of lysoPC can lead to lipid peroxidation damage and inflammation (van der Veen et al., 2017). From the biomarkers found in metabolomics, the expression level of lysoPC in the model group was upregulated, whereas lysoPC in the WPP and CPP groups was downregulated. Therefore, WPP and CPP may treat gouty arthritis by affecting the metabolism of lysoPC. However, phenylpyruvate, a dimethyl compound, is a product of phenylalanine metabolism, and several studies have reported that hyperuricemia and gout are related to phenylalanine metabolism (Liu et al., 2012; Jiang et al., 2017). Phenylpyruvate can further generate phenylacetaldehyde, which generates phenylacetaldehyde-CoA, which is related to pantothenate and CoA biosynthesis through acetyl-CoA (Wu et al., 2018). According to our research results, the expression of L-phenylalanine in the model group was upregulated, whereas those in the WPP and CPP groups were downregulated.

Conclusion

In conclusion, we showed that both wild and cultivated *P. igniarius* have anti-gout arthritis properties; their similar active ingredients and pharmacological properties are anticipated to encourage the development and use of cultivated *P. igniarius* to fill the void left by wild *P. igniarius*. In the future, we'll concentrate on the targets and pathways involved in *P. igniarius*'s treatment of gout (Dalbeth et al., 2016).

Data availability statement

The raw data supporting the conclusions of this article will be made available by the authors, without undue reservation.

Author contributions

XZ, QS, QL implement the concept, design and definition of knowledge content, document retrieval, data collection, data analysis and manuscript preparation. JL and SQ provide help for data collection, data analysis and statistical analysis. XZ, LG and HL conducted document retrieval, data collection and manuscript editing. YJ and MH conducted manuscript review. All authors have read and approved the manuscript.

Funding

This study was financially supported by the Project of Zhejiang Administration of Traditional Chinese Medicine (2020ZB038), the Zhejiang Provincial Department of Science and Technology of Institution Special Funds (12002Y-04), the Zhejiang Provincial Natural Science Foundation (LY21H280010), the Zhejiang Medical and Health Science Research Foundation (2021KY136), and the Zhejiang Province Health High-level Talent Training Project (WJW2022007).

Acknowledgments

We are thankful to all the authors of the study. We would like to thank Shanghai Biotree Biotechnology for the UHPLC-QE-MS/MS and data analyses.

Conflict of interest

The authors declare that the research was conducted in the absence of any commercial or financial relationships that could be construed as a potential conflict of interest.

Publisher's note

References

Ahmad, N. S., Farman, M., Najmi, M. H., Mian, K. B., and Hasan, A. (2008). Pharmacological basis for use of Pistacia integerrima leaves in hyperuricemia and gout. *Journal of Ethnopharmacology* 117 (3), 478–482. doi:10.1016/j.jep.2008.02.031

An, J., Yang, H., Park, K., Lee, J., and Kim, B. W. (2010). Reparatory and preventive effects of oriental herb extract mixture (OHEM) on hyperuricemia and gout. *Food Science and Biotechnology* 19 (2), 517–524. doi:10.1007/s10068-010-0072-4

Ashiq, K., Bajwa, M. A., Tanveer, S., Qayyum, M., Ashiq, S., Khokhar, R., Abid, F., et al. (2021). A comprehensive review on gout: The epidemiological trends, pathophysiology, clinical presentation, diagnosis and treatment. *Journal of the Pakistan Medical Association*, 71 (4), 1234–1238. doi:10.47391/JPMA.313

Borstad, G. C., Bryant, L. R., Abel, M. P., Scroggie, D. A., Harris, M. D., and Alloway, J. A. (2004). Colchicine for prophylaxis of acute flares when initiating allopurinol for chronic gouty arthritis. *Journal of Rheumatology* 31 (12), 2429–2432.

Choe, J. Y., Ki-Yeun, P., and Seong-Kyu, K. (2015). Oxidative stress by monosodium urate crystals promotes renal cell apoptosis through mitochondrial caspase-dependent pathway in human embryonic kidney 293 cells: Mechanism for

urate-induced nephropathy. *Apoptosis* 20 (1), 38–49. doi:10.1007/s10495-014-1057-1

Cronstein, B. N., and Terkeltaub, R. (2006). The inflammatory process of gout and its treatment, *Arthritis Research Therapy* 8, (1), 1-7. doi:10.1186/ar1908

Dalbeth, N., Merriman, T. R., and Stamp, L. K. (2016). Gout. *Lancet* 388 (10055), 2039–2052. doi:10.1016/S0140-6736(16)00346-9

Ding, Y., Liu, F., Shi, C., and Zhang, Y. (2016). Chemical constituents from Phellinus igniarius and their anti-tumor activity *in vitro*. *China Journal of Chinese Materia Medica* 41 (16), 3042–3048. doi:10.4268/cjcmm20161617

Dong, Y., Qiu, P., Zhu, R., Zhao, L., Zhang, P., Wang, Y., et al. (2019). A combined phytochemistry and network Pharmacology approach to reveal the potential antitumor effective substances and mechanism of Phellinus igniarius, *Frontiers in Pharmacology* 10, 10266. doi:10.3389/fphar.2019.00266

Elion, G. B. (1966). Enzymatic and metabolic studies with allopurinol. *Annals of the Rheumatic Diseases* 25 (6), 608–614. doi:10.1136/ard.25.Suppl_6.608

Fan, L. (2017). Curcumin attenuates neuronal damage in Alzheimer s disease model by inhibiting TLR4/NF kB signaling pathway, *Anatomy research* 39 (2), 102–105. doi:10.1136/ard.25.suppl_6.608

Garcia, P. J., Beltran, L., Mejia Chew, -C., ToRRes, R., Tebar Marquez, D., and Pose Reino, A. (2016). Ultrasound in the diagnosis of asymptomatic hyperuricaemia and gout. *Revista Clínica Española* 216 (8), 445–450. doi:10.1016/j.rce.2016.05.007

Ghaemi-Oskouie, F., and Shi, Y. (2011). The role of uric acid as an endogenous danger signal in immunity and inflammation, *Current Rheumatology Reports* 13, (2), 160–166. doi:10.1007/s11926-011-0162-1

Gu, L., Cai, W., and Jin, Q. (2019). Effect of sanghuang decoction on oxidative damage induced by D-galactose in mice. *Chinese Journal of Modern Applied Pharmacy* 36 (17), 2144–2148. doi:10.13748/j.cnki.issn1007-7693.2019.17.006

Guo, Q., He, Q., Hu, F., Cai, Y., and Li, Y. (2020). Chrysophanol regulates microglial inflammatory response through TLR4/NF-kB signaling pathway. *Medical information* 33 (19), 51–54. doi:10.3969/j.issn.1006-1959.2020.19.016

Dogan, H. H., Karagoz, S., and Duman, R. (2018). *In vitro* evaluation of the antiviral activity of some mushrooms from Turkey, *International Journal of Medicinal Mushrooms* 20 (3), 201–212. doi:10.1615/IntJMedMushrooms.2018025468

Han, J., Shi, G., Li, W., Wang, S., Bai, J., Sun, X., et al. (2021). Zisheng shenqi decoction ameliorates monosodium urate-mediated gouty arthritis in rats via promotion of autophagy through the AMPK/mTOR signaling pathway. *Evidence-Based Complementary and Alternative Medicine* 2021, 1–12. doi:10.1155/2021/6918026

Hille, R. (1996). The mononuclear molybdenum enzymes. *Chemical Reviews* 96 (7), 2757–2816. doi:10.1021/cr950061t

Jhang, J. J., Cheng, Y. T., Ho, C. Y., and Yen, G. C., (2015). Monosodium urate crystals trigger Nrf2- and heme oxygenase-1-dependent inflammation in THP-1 cells. *Cellular & Molecular Immunology* 12 (4), 424–434. doi:10.1038/cmi.2014.65

Jiang, T., Qian, J., Ding, J., Wang, G., Ding, X., Liu, S., et al. (2017). Metabolomic profiles delineate the effect of Sanmiao wan on hyperuricemia in rats. *Biomedical Chromatography* 31 (2), e3792. doi:10.1002/bmc.3792

Kim, S. K., Choe, J. Y., and Park, K. Y. (2016). Rebamipide suppresses monosodium urate crystal-induced interleukin-1β production through regulation of oxidative stress and caspase-1 in THP-1 cells. *Inflammation* 39 (1), 473–482. doi:10.1007/s10753-015-0271-5

Kottgen, A., Albrecht, E., Teumer, A., Vitart, V., Krumsiek, J., Hundertmark, C., et al. (2013). Genome-wide association analyses identify 18 new loci associated with serum urate concentrations. *Nature Genetics* 45 (2), 145–154. doi:10.1038/ng.2500

Li, C., Li, Z., Liu, S., Wang, C., Han, L., and Cui, L. (2015). Genome-wide association analysis identifies three new risk loci for gout arthritis in Han Chinese. *Nature Communications* 6, 67041. doi:10.1038/ncomms8041

Li, H., Zhang, X., Gu, L., Li, Q., Ju, Y., Zhou, X., et al. (2021). Anti-gout effects of the medicinal fungus Phellinus igniarius in hyperuricaemia and acute gouty arthritis rat models. *Frontiers in Pharmacology* 12, 12. doi:10.3389/fphar.2021.801910

Liu, S., Liao, X., and Yu, R. (2019). Research on the inhibition of uric acid synthesis by the extract of Phellinus Igniarius. *Ginseng Research* 31 (4), 17–20. doi:10.19403/j.cnki.1671-1521.2019.04.005

Liu, Y., Yu, P., Sun, X., and Di, D. (2012). Metabolite target analysis of human urine combined with pattern recognition techniques for the study of symptomatic gout. *Molecular Biosystems* 8 (11), 2956–2963. doi:10.1039/c2mb25227a

Luan, F., Peng, X., Zhao, G., Zeng, J., Zou, J., Rao, Z., et al. (2022). Structural diversity and bioactivity of polysaccharides from medicinal mushroom Phellinus spp.: A review. *Food Chemistry* 397, 397133731. doi:10.1016/j.foodchem.2022.133731

Mao, X. (2000). *The macrofungi in China*. Zhengzhou: Henan Science and Technology Publishing, 477.

Nakayama, A., Matsuo, H., Nakaoka, H., Nakamura, T., Nakashima, H., Takada, Y., et al. (2014). Common dysfunctional variants of ABCG2 have stronger impact on hyperuricemia progression than typical environmental risk factors. *Scientific Reports* 4, 45227. doi:10.1038/srep05227

Neogi, T. (2010). Interleukin-1 antagonism in acute gout: Is targeting a single cytokine the answer? *Arthritis and rheumatism* 62 (10), 2845–2849. doi:10.1002/art.27635

Nishino, T. (1994). The conversion of xanthine dehydrogenase to xanthine oxidase and the role of the enzyme in reperfusion Injury1. *Journal of Biochemistry* 116 (1), 1–6. doi:10.1093/oxfordjournals.jbchem.a124480

Ozgen, M., Reese, R-N., Tulio, A. Z., Scheerens, J. C., and Miller, A. R. (2006). Modified 2, 2-azino-bis-3-ethylbenzothiazoline-6-sulfonic acid (abts) method to measure antioxidant capacity of Selected small fruits and comparison to ferric reducing antioxidant power (FRAP) and 2, 2'-diphenyl-1-picrylhydrazyl (DPPH) methods. *Journal Agricultural and Food Chemistry* 54 (4), 1151–1157. doi:10.1021/jf051960d

Ren, J., Su, D., Li, L., Cai, H., Zhang, M., Zhai, J., et al. (2020). Anti-inflammatory effects of Aureusidin in LPS-stimulated RAW264.7 macrophages via suppressing NF-κB and activating ROS- and MAPKs-dependent Nrf2/HO-1 signaling pathways, *Toxicology and Applied Pharmacology* 387, 387114846. doi:10.1016/j.taap.2019.114846

Sabina, E. P., Shruthi, N., and Mahaboobkhan, R. (2011). A role of piperine on monosodium urate crystal-induced inflammation-an experimental model of gouty arthritis. *Inflammation* 34 (3), 184–192. doi:10.1007/s10753-010-9222-3

Shan, B., Ting, C., Huang, B., Liu, Y., and Chen, J. (2021). Untargeted metabolomics reveal the therapeutic effects of Ermiao wan categorized formulas on rats with hyperuricemia. *Journal of Ethnopharmacol* 281, 281114545. doi:10.1016/j.jep.2021.114545

Shi, L., Xu, L., Yang, Y., Song, H., Pan, H., Yin, L., et al. (2013). Suppressive effect of modified simiaowan on experimental gouty arthritis: An *in vivo* and *in vitro* study. *Journal of Ethnopharmacol* 150 (3), 1038–1044. doi:10.1016/j.jep.2013.10.023

Singh, J. A., and Gaffo, A. (2020). Gout epidemiology and comorbidities, *Seminars in Arthritis and Rheumatism* 50 (3), S11–S16. doi:10.1016/j.semarthrit.2020.04.008

Stack, A-G., Johnson, M-E., Blak, B., Klein, A., Carpenter, L., Morlock, R., et al. (2019). Gout and the risk of advanced chronic kidney disease in the UK health system: A national cohort study. *BMJ Open* 9 (8), e031550. doi:10.1136/bmjopen-2019-031550

van der Veen, J-N., Kennelly, J-P., Wan, S., Vance, J. E., Vance, D. E., and Jacobs, R. L. (2017). The critical role of phosphatidylcholine and phosphatidylethanolamine metabolism in health and disease, *Biochimica et Biophysica Acta* 1859 (9), 1558–1572. doi:10.1016/j.bbamem.2017.04.006

Wang, F., Sun, L., Zong, G., Gao, X., Zhang, H., Xiong, Q., et al. (2020). Associations of amino acid and acylcarnitine profiles with incident hyperuricemia in middle-aged and older Chinese individuals. *Arthritis Care and research* 72 (9), 1305–1314. doi:10.1002/acr.24013

Wang, F. F., Shi, C., Yang, Y., Fang, Y., Sheng, L., and Li, N., (2018). Medicinal mushroom Phellinus igniarius induced cell apoptosis in gastric cancer SGC-7901 through a mitochondria-dependent pathway. *Biomedicine and pharmacotherapy* 102, 10218–10225. doi:10.1016/j.biopha.2018.03.038

Wu, P., Jing, L., Zhang, X., Zeng, F., Liu, Y., Sun, W., et al. (2018). Study of the treatment effects of compound tufuling granules in hyperuricemic rats using serum metabolomics. *Evidence-Based Complementary and Alternative Medicine* 2018, 3458185. doi:10.1155/2018/3458185

Xing, L., Chu, F., Jiang, S., and Jin, X., (2021). Preliminary study on effect of Phellinus igniarius ethanol extract on serum uric acid metabolism and gut microbiome in rats. *China Journal of Chinese Materia Medica* 46 (1), 177–182. doi:10.19540/j.cnki.cjcmm.20200915.403

Yin, C., Liu, B., Li, Y., Li, X., Wang, J., Chen, R., et al. (2020). IL-33/ST2 induces neutrophil-dependent reactive oxygen species production and mediates gout pain. *Theranostics* 10 (26), 12189–12203. doi:10.7150/thno.48028

Yin, X., Wang, S., and Qin, T., (2021). Anti-inflammatory effect of Compound Yinhua Jiedu Granules on LPS induced acute pneumonia in juvenile rats and its effect on TLR4/NF-κB/NLRP3 signaling pathway. *Chinese Traditional and Herbal Drugs* 52 (01), 203–210.

Zeng, Q., (2019). *The expression and significance of TLR4 NF-κB and NLRP3 in gastric cancer tissues*. Luzhou, Sichuan Province: CNKI.

Zhang, B., Huang, R., Yang, D., Chen, G., Chen, Y., Han, J., et al. (2022). Combination of colchicine and ticagrelor inhibits carrageenan-induced thrombi in mice, *Oxidative Medicine and Cellular Longevity* 2022, 3087198. doi:10.1155/2022/3087198

Zulueta, A., Esteve, M. J., and Ana, F. (2009). ORAC and TEAC assays comparison to measure the antioxidant capacity of food products. *Food Chemistry* 114 (1), 310–316. doi:10.1016/j.foodchem.2008.09.033

Glossary

DPPH 2,2-diphenyl-1-(2,4,6-trinitrophenyl) hydrazyl stable free radical assay

ABTS 2,2-azino-bis-3-ethylbenzothiazoline-6-sulfonic acid assay

FRAP Ferric Reducing/Antioxidant Power assay

IR Inhibition rate

WPP Wild P. igniarius total polyphenols

CPP Cultivated P. igniarius total polyphenols

XO Xanthine Oxidase

MSU Monosodium urate

ICAM-1 Intercellular adhesion molecule-1

IL-1β Interleukin-1β

IL-6 Interleukin-6

TNF-α Tumour necrosis factor

VCAM-1 Vascular cell adhesion molecular-1

TLR4 Toll like receptor 4

NLRP3 NOD-like receptor thermal protein domain associated protein 3

ROS Reaction oxygen species

NF-κB p65 Nuclear factor-κB p65

NF-kB Nuclear factor-κB

IκBα Nuclear factor-κB inhibitor protein

NSAIDs Nonsteroidal anti-inflammatory drugs

Vc Ascorbic acid

lysoPC Lysophosphatidylcholine

IC_{50} Half-maximum inhibitory concentration

DMSO Dimethyl sulfoxide

OD Optical density

DCFH-DA dichloro-dihydro-fluorescein diacetate

LC-MS/MS Liquid chromatography-tandem mass spectrometric

IDA Information-dependent acquisition

PCA Principal component analysis

OPLS-DA Orthogonal projections to latent structures-discriminate analysis

SD Standard deviation

Vc Vitamin C

XO Xanthaxanthin oxidase

PVDF Polyvinylidene fluoride

ECL Enhanced chemiluminescence

QC Quality control

UHPLC-QE-MS Ultra-high-performance liquid chromatography/Q Exactive HF-X Hybrid Quadrupole-Orbitrap Mass

IDA Information-dependent acquisition

PCA Principal component analysis

OPLS-DA Orthogonal projections to latent structures-discriminate analysis

VIP Variable importance in the projection

ANOVA Analysis of variance

MTT Methyl thiazole tetrazolium

PCA Principal component analysis

ELISA Enzyme-linked immunosorbent assay

POS Positive ion mode

NEG Negative ion mode

frontiers | Frontiers in Pharmacology

TYPE Original Research
PUBLISHED 11 November 2022
DOI 10.3389/fphar.2022.1004619

OPEN ACCESS

EDITED BY
Yan Huang,
Anhui Medical University, China

REVIEWED BY
Na Liu,
Tongji University, China
Lihong Chen,
Dalian Medical University, China

*CORRESPONDENCE
Zhanjun Jia,
jiazj72@hotmail.com
Xianrui Dou,
betty9911@163.com

†These authors have contributed equally to this work and share first authorship

SPECIALTY SECTION
This article was submitted to Inflammation Pharmacology, a section of the journal Frontiers in Pharmacology

RECEIVED 27 July 2022
ACCEPTED 28 October 2022
PUBLISHED 11 November 2022

CITATION
Luo Q, Liu M, Tan Y, Chen J, Zhang W, Zhong S, Pan J, Zheng Q, Gong L, Su L, Jia Z and Dou X (2022), Blockade of prostaglandin E2 receptor 4 ameliorates peritoneal dialysis-associated peritoneal fibrosis.
Front. Pharmacol. 13:1004619.
doi: 10.3389/fphar.2022.1004619

Blockade of prostaglandin E2 receptor 4 ameliorates peritoneal dialysis-associated peritoneal fibrosis

Qimei Luo[1†], Mi Liu[1†], Yanhong Tan[1], Jinzhong Chen[1], Wei Zhang[1], Shaoxin Zhong[1], Jianyi Pan[1], Qingkun Zheng[1], Lewei Gong[1], Lijuan Su[1], Zhanjun Jia[2*] and Xianrui Dou[1*]

[1]Department of Nephrology, Shunde Hospital, Southern Medical University (The First People's Hospital of Shunde), Foshan, China, [2]Nanjing Key Laboratory of Pediatrics, Children's Hospital of Nanjing Medical University, Nanjing, China

Inflammatory responses in the peritoneum contribute to peritoneal dialysis (PD)-associated peritoneal fibrosis. Results of our previous study showed that increased microsomal prostaglandin E synthase-1-mediated production of prostaglandin E2 (PGE2) contributed to peritoneal fibrosis. However, the role of its downstream receptor in the progression of peritoneal fibrosis has not been established. Here, we examined the role of PGE2 receptor 4 (EP4) in the development of peritoneal fibrosis. EP4 was significantly upregulated in peritoneal tissues of PD patients with ultrafiltration failure, along with the presence of an enhanced inflammatory response. *In vitro* experiments showed that exposure to high glucose concentrations enhanced EP4 expression in rat peritoneal mesothelial cells (RPMCs). High-glucose–induced expression of inflammatory cytokines (monocyte chemoattractant protein-1, tumour necrosis factor α, and interleukin 1β) was significantly reduced in RPMCs treated with ONO-AE3-208, an EP4 receptor antagonist. ONO-AE3-208 also significantly decreased the expression of extracellular matrix proteins induced by high glucose concentrations. Furthermore, ONO-AE3-208 blunted activation of the NLR family pyrin domain containing 3 (NLRP3) inflammasome and phosphorylation of nuclear factor kappa B (NF-κB) (p-p65). To further investigate the functional role of EP4, ONO-AE3-208 was administrated for 4 weeks in a rat model of PD, the results of which showed that ONO-AE3-208 inhibited peritoneal fibrosis and improved peritoneal dysfunction. Additionally, inflammatory cytokines in the peritoneum of PD rats treated with ONO-AE3-208 were downregulated, in line with inhibition of the NLRP3 inflammasome and NF-κB phosphorylation. In conclusion, an EP4 antagonist reduced the development of peritoneal fibrosis, possibly by suppressing NLRP3 inflammasome- and p-p65–mediated inflammatory responses. Our findings suggest that an EP4 antagonist may be therapeutically beneficial for PD-associated peritoneal fibrosis.

KEYWORDS
prostaglandin E2 receptor 4, ONO-AE3-208, peritoneal dialysis, fibrosis, inflammation

Introduction

Peritoneal dialysis (PD) is a well-established treatment option for patients with end-stage renal disease (ESRD). After continuous exposure to high-glucose PD fluid, histologic changes occur in the peritoneum, presenting as loss of the mesothelial monolayer, increased deposition of extracellular matrix, and angiogenesis (Zhou et al., 2016). Long-term infusion of bioincompatible PD fluid can lead to peritoneal fibrosis, eventually resulting in discontinuation of PD therapy (Fusshoeller, 2008; Morelle et al., 2015). Currently, no effective therapies are available to prevent the development of peritoneal fibrosis in clinical practice. Thus, there is an urgent need to develop a specific and effective therapy to prevent the development and progression of peritoneal fibrosis.

Several studies have demonstrated that chronic sterile inflammation induced by PD solutions with a high glucose content is involved in the pathogenesis of peritoneal fibrosis (Lai et al., 2007; Rosengren et al., 2013). Peritoneal injury caused by PD fluid leads to activation of nuclear factor kappa B (NF-κB); promotes the release of proinflammatory cytokines, including interleukin-6 (IL-6), IL-1β, tumour necrosis factor-α (TNF-α), and monocyte chemoattractant protein-1 (MCP-1); and increases the synthesis of extracellular matrix protein (Liu et al., 2015; Chu et al., 2017). Additionally, our recent study showed that microsomal prostaglandin E synthase-1 (mPGES-1), a catalytic enzyme for the production of prostaglandin E2 (PGE2), was induced in peritoneal mesothelial cells treated with high levels of glucose. We also found that mPGES-1 increased the synthesis of extracellular matrix proteins by activating the NLR family pyrin domain containing 3 (NLRP3) inflammasome (Luo et al., 2021). These findings suggest that targeting mPGES-1 may attenuate the progression of peritoneal fibrosis; however, the use of mPGES-1 inhibitors in clinical practice is limited because they also inhibit physiologic functions of PGE2.

Results from previous research and our recent study showed that PGE2 secretion was significantly elevated in peritoneal mesothelial cells treated with high levels of glucose (Sitter et al., 1998; Liu et al., 2007; Luo et al., 2021). PGE2 exerts its pharmacologic activity *via* four receptor subtypes: EP1, EP2, EP3, and EP4. EP1 regulates intracellular Ca^{2+} concentration, EP3 inhibits the intracellular increase in cyclic adenosine 3′,5′-monophosphate (cAMP) concentration, EP2, and EP4 increase intracellular levels of cAMP, and EP4 is involved in the phosphatidylinositol 3-kinase signal pathway by regulating NF-κB (Tang et al., 2012; Sheppe et al., 2018). Recent studies have shown that PGE2 participates in inflammation by acting on the EP4 receptor. For example, PGE2 stimulated the EP4 receptor to promote a chronic inflammatory response in a rat model of rheumatoid arthritis (Chen et al., 2010). Furthermore, PGE2 facilitated T helper type 1 (TH1) cell differentiation and amplified TH17 cell expansion *in vitro*, and administration of an EP4 antagonist in an animal model of experimental autoimmune encephalomyelitis decreased the accumulation of TH1 and TH17 cells and suppressed disease progression (Yao et al., 2009). However, the role of EP4 in modulating the inflammatory process during PD-associated peritoneal fibrosis remains unclear.

In this study, we examined EP4 expression in the peritoneum of PD patients with ultrafiltration failure (UFF) and rat peritoneal mesothelial cells (RPMCs) stimulated with high concentrations of glucose. Additionally, we evaluated the effects of ONO-AE3-208, a highly selective and potent functional EP4 receptor antagonist, on pathologic changes associated with fibrosis *in vitro* and *in vivo*. We also determined the mechanisms by which EP4 receptor inhibition reduces the progression of peritoneal fibrosis.

Materials and methods

Reagents

ONO-AE3-208 was purchased from Cayman Chemistry (Michigan, United States). We obtained 4.25% PD fluid from Baxter Healthcare (Guangzhou, China). The sources for the primary and secondary antibodies used in this study were as follows: rabbit polyclonal anti-EP4 (no. 101775) was obtained from Cayman Chemistry; rabbit monoclonal anti-fibronectin (no. ab45688), rabbit monoclonal anti-collagen I (no. ab138492), rabbit monoclonal anti-NLRP3 (no. ab263899), rabbit monoclonal anti–caspase-1 (no. ab179515), rabbit monoclonal anti-vimentin (no. ab92547), goat anti-rabbit IgG H&L Alexa Fluor 488-conjugated secondary antibody (no. ab150077), and goat anti-mouse IgG H&L Alexa Fluor 647-conjugated secondary antibody (no. ab150115) were obtained from Abcam (Cambridge, MA, United States); and mouse monoclonal anti-E-cadherin (no. 14472), rabbit monoclonal anti-phospho-NF-κB (p-p65, no. 3033), rabbit monoclonal anti-NF-κB (p65, no. 8242), β-actin (no.3700), horseradish peroxidase (HRP)-conjugated anti-mouse IgG (no. 7076), and HRP-conjugated anti-rabbit IgG (no.7074) were obtained from Cell Signaling Technology (Danvers, MA, United States). IL-1β, IL-18, TNF-α, and MCP-1 enzyme-linked immunosorbent assay (ELISA) kits were purchased from Dakewe Biotech (Shenzhen, China). The PrimeScript™ RT Reagent Kit (no. RR470A) and the SYBR Green PCR Kit (no. RR820A) were purchased from TaKaRa (Japan). The DAB Kit (no. GK500710) was purchased from Gene Tech (China).

Human sample collection

Peritoneal tissues and nocturnal peritoneal dialysate samples were collected from ESRD patients, new-onset PD patients and PD patients with UFF at Shunde Hospital of Southern Medical University. New-onset PD patients were defined as patients who had started PD therapy within the previous 6 months. UFF was defined as failing to achieve at least 400 ml of net ultrafiltration in a 4-h dwell period with 4.25% PD fluid (Teitelbaum, 2015). Peritoneal tissues were collected at the time of laparoscopy for PD catheter implantation or withdrawal. The peritoneal dialysate was drained after at least 8 h of dwell exchange.

Patients were excluded if they refused to provide written informed consent; had a malignancy, diabetes mellitus, or heterotopia endometriosis; or received nonselective non-steroidal anti-inflammatory drugs or cyclooxygenase 2 (COX-2)-selective inhibitors (e.g., celecoxib, nimesulide, meloxicam, rofecoxib) in the past 2 weeks. All patients provided written informed consent. The use of human biopsy and dialysate samples were approved by the Ethical Review Board of Shunde Hospital of Southern Medical University.

Cell culture and treatment

RPMCs were cultured at 37°C with 5% carbon dioxide in Dulbecco's Modified Eagle Medium/Nutrient Mixture F-12 medium containing 10% fetal bovine serum (FBS, Gibco, United States), 1% penicillin, and 1% streptomycin. RPMCs were treated with the following glucose concentrations: 5.5 mmol/L, 83.3 mmol/L, 138 mmol/L, and 234.6 mmol/L. The 83.3 mmol/L, 138 mmol/L, and 234.6 mmol/L concentrations represent the glucose concentrations in 1.5%, 2.5%, and 4.25% PD fluid. Cell Counting Kit-8 (CCK-8, Solarbio, China) was used to assess the effects of different glucose concentrations on cell viability. To examine the expression of EP4 in RPMCs, cells were first deprived of serum for 24 h and then treated with D-glucose at high (138 mmol/L) concentration for 0, 24, 48, and 72 h. RPMCs were also treated with 138 mmol/L mannitol. RPMCs were treated with different concentrations of ONO-AE3-208 for 24 h, and then CCK-8 was used to determine cell viability. To examine the effects of ONO-AE3-208 on high-glucose–induced inflammation and fibrosis, RPMCs were deprived of serum for 24 h and then exposed to 138 mmol/L glucose in the presence of ONO-AE3-208 (100 and 200 nM). After exposure for 24 or 48 h, the cells were harvested for quantitative reverse-transcription polymerase chain reaction testing (RT-PCR) or western blotting. All *in vitro* experiments were repeated at least thrice.

Animal models and experimental design

Male Sprague–Dawley rats weighing 200–220 g were purchased from the Guangdong Medical Laboratory Animal Center (Guangdong, China). A rat model of peritoneal fibrosis was created by intraperitoneal injection of 4.25% PD fluid at a dose of 100 ml/kg daily for 4 weeks (Zhou et al., 2013). To investigate the effects of ONO-AE3-208 on peritoneal fibrosis, rats were intraperitoneally injected with ONO-AE3-208 at 0.2 mg/kg per day (Wang et al., 2014). Rats were randomly divided into three groups: 1) rats injected intraperitoneally with 100 ml/kg saline (control group; $n = 6$); 2) rats injected intraperitoneally with 100 ml/kg PD fluid (PD group; $n = 6$); and 3) rats injected intraperitoneally with 100 ml/kg PD fluid + ONO-AE3-208 (PD + ONO-AE3-208 group; $n = 6$).

After 28 days of PD, a peritoneal equilibrium test was performed on each rat before they were killed. Briefly, 100 ml/kg of 4.25% PD fluid was injected intraperitoneally, and dialysate and blood samples were collected at 0 and 4 h of dwell time. Parietal and visceral peritoneal tissues were collected for further analysis. The animal protocol was reviewed and approved by the Animal Experimental Ethics Committee at Southern Medical University.

Analysis of peritoneal permeability

Concentrations of glucose and creatinine in the dialysate and plasma were assessed using an automatic biochemical instrument (AU5800; Beckman Coulter, California, United States). Absorption of glucose from the dialysate (D/D0) and the dialysate-to-plasma ratio of creatinine (D/P_{Scr}) were used to determine peritoneal permeability.

Histology and immunohistochemistry

Changes in peritoneal tissues were assessed by haematoxylin and eosin staining or Masson's trichrome staining of paraformaldehyde-fixed, paraffin-embedded 4-μm–thick sections. Peritoneum thickness was expressed as the mean of five independent measurements for each section. A microwave-based antigen retrieval technique was used to examine the immunohistochemistry results, as previously described (Luo et al., 2021). Briefly, 4-μm–thick sections were de-paraffinised, rehydrated, and incubated in hydrogen peroxide to block endogenous peroxidase, then antigen retrieval was performed. The signal was visualised using a DAB kit, and slides were viewed with a Leica microscope equipped with a digital camera.

TABLE 1 Primer sequences for q-PCR.

Gene symbol	Primer sequences
β-actin	5′-TGTGACGTTGACATCCGTAAAG-3′
	5′-GGCAGTAATCTCCTTCTGCATC-3′
IL-1β	5′-CTATGGCAACTGTCCCTGAA-3′
	5′-GGCTTGGAAGCAATCCTTAATC-3′
TNF-α	5′-CGTGTTCATCCGTTCTCTACC-3′
	5′-CAGAGCCACAATTCCCTTTCTA-3′
MCP-1	5′-GATCTCTCTTCCTCCACCACTA-3′
	5′-TTAACTGCATCTGGCTGAGAC-3
Fibronectin	5′-ACCGAAATCACAGCCAGTAG-3
	5′-CCTCCTCACTCAGCTCATATTC-3
Collagen I	5′-CCTGTCTGCTTCCTGTAAACTC-3
	5′-GTTCAGTTTGGGTTGCTTGTC -3
Vimentin	5′- GTCCGTGTCCTCGTCCTCCTAC -3
	5′- AGGTGCGGGTGGATGTGGTC -3

Western blotting

Western blotting analysis of peritoneal tissues and cell samples was conducted as previously described (Luo et al., 2021). The densitometry analysis was performed using the ImageJ software.

RNA extraction and quantitative RT-PCR

Total RNA was extracted from the peritoneal tissues and cell samples using Trizol reagent. cDNA was synthesised using the PrimeScript™ RT Reagent Kit according to the manufacturer's protocol. Real-time PCR was performed using the SYBR Green PCR Kit according to the manufacturer's instructions. Primers used in this study are listed in Table 1. Levels of mRNAs were normalised to β-actin in each sample, and data were presented as the relative fold change.

Immunofluorescence staining

Two-colour immunofluorescence staining was performed on the paraformaldehyde-fixed, paraffin-embedded sections. Sections were de-paraffinised, rehydrated, and antigen repaired. Sections were incubated with blocking buffer (3% bovine serum albumin [BSA] in phosphate-buffered saline [PBS]). Peritoneal tissues were incubated overnight at 4°C with polyclonal rabbit anti-EP4 (1:100) and monoclonal mouse anti-E-cadherin (1:100), followed by incubation with goat anti-rabbit IgG (Alexa Fluor 488, 1:1,000) and goat anti-mouse IgG (Alexa Fluor 647, 1:1,000) for 1 h at room temperature. Nuclei were counterstained with 4′,6-diamidino-2-phenylindole (DAPI). Positive staining was measured using a fluorescent microscope (Leica, Germany).

Cells were cultured on glass coverslips and fixed with methanol for 10 min at room temperature. They were then washed with PBS and permeabilised in 0.1% Triton-X for 10 min at room temperature, followed by incubation in blocking buffer (5% BSA in PBS) for 1 h at room temperature. The cells were subsequently incubated with monoclonal rabbit anti–phospho-NF-κB (1:100) at 4°C overnight, and then incubated with Alexa Fluor 488-conjugated anti-rabbit IgG (1:1,000) antibody for 1 h at room temperature, followed by staining with DAPI. Positive staining was measured using a fluorescent microscope (Leica, Germany).

ELISA

ELISA detection of IL-1β, IL-18, TNF-α, and MCP-1 proteins in the dialysate was performed according to the manufacturer's instructions.

Statistical analysis

All data are presented as mean ± standard error of the mean (SEM). Significant differences between two groups were assessed using unpaired, two-tailed Student's t-test. Multiple groups were compared using one-way analysis of variance (ANOVA), followed by Dunnett's multiple comparisons test *versus* the high-glucose group (Figures 2B–D,F,H,J, 3B,D,F,H) or *versus* the high-glucose 0-h group, vehicle group, 5.5 mmol/L glucose group, or mannitol 0-h group (Figures 1I, 2A, Supplementary Figures 1A,C). For *in vivo* data, statistical differences were assessed using one-way ANOVA, followed by comparisons of the mean of each column with the mean of every other column. $p < 0.05$ was deemed indicative of statistical significance. Statistical and data analyses were conducted using GraphPad Prism 7.

Results

Expression of EP4 increased during peritoneal fibrosis in patients with UFF and high-glucose–induced RPMCs

We first evaluated the expression of EP4 in the peritoneal tissues of ESRD patients and PD patients with UFF. On Masson's trichrome staining, the peritoneal tissues of ESRD patients exhibited no substantial peritoneal fibrosis, whereas the peritoneal tissues of PD patients with UFF showed severe peritoneal fibrosis, with increased accumulation of extracellular matrix (Figure 1A). Double indirect immunofluorescent staining for EP4 and E-cadherin showed partial loss of E-cadherin and increased EP4 expression in the peritoneum of PD patients with UFF, and the EP4 staining co-localized with the E-cadherin staining (Figure 1B). As E-cadherin is a mesothelial cell

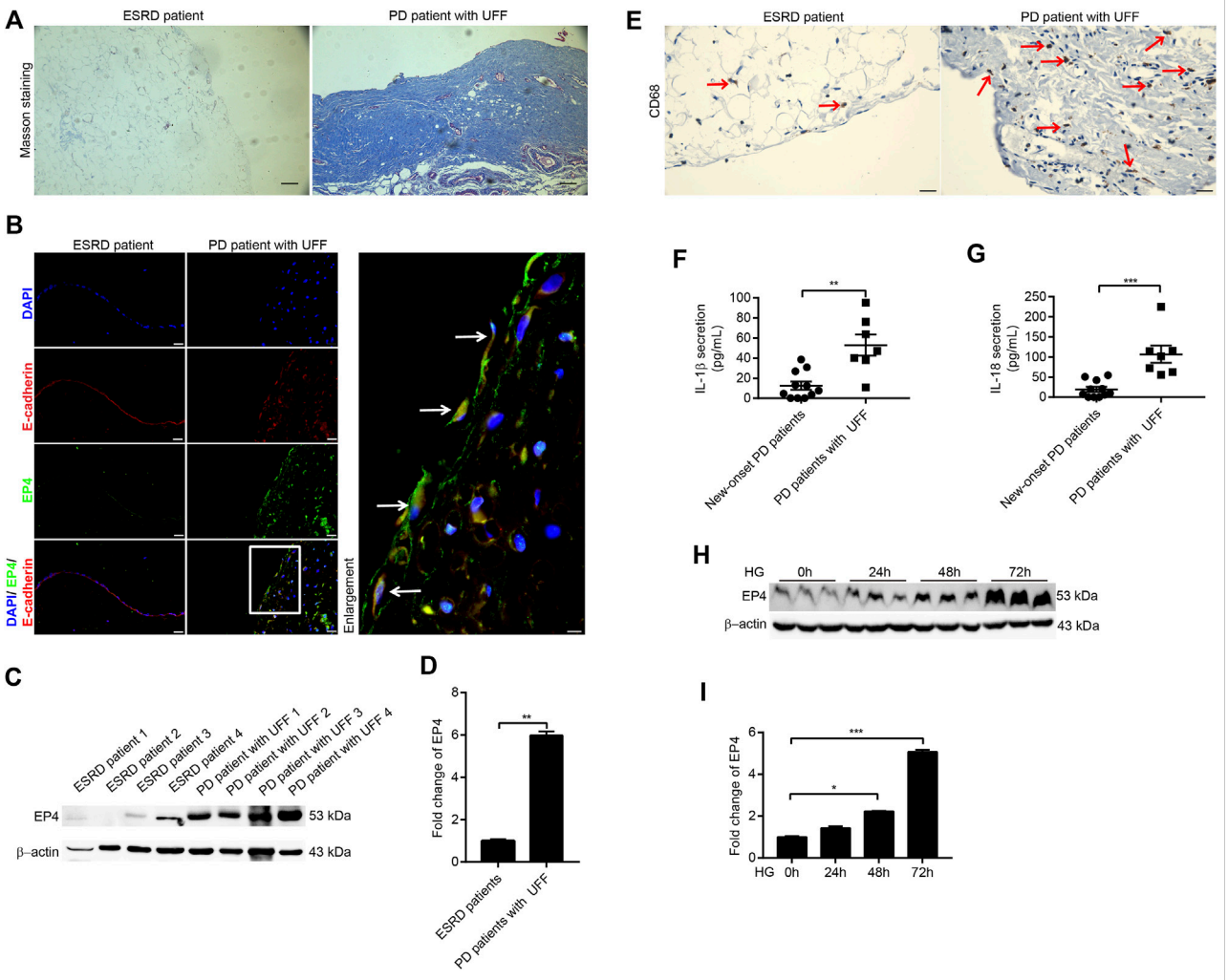

FIGURE 1
Expression of EP4 increased during peritoneal fibrosis in patients with UFF and high-glucose–induced RPMCs. **(A)** Masson staining from peritoneal tissues of ESRD patient and PD patient with UFF. Scale bar = 100 μm. **(B)** Immunofluorescence microscopy of peritoneal tissue sections stained for EP4 (green) and E-cadherin (red) with DAPI (blue). Arrows represent EP4- and E-cadherin–positive mesothelial cells. Scale bar = 25 μm. **(C)** Peritoneal tissue lysates from ESRD patients and PD patients with UFF were subjected to western blotting analysis with specific antibodies against EP4 and β-actin. **(D)** EP4 expression levels were quantified by densitometry, normalised with β-actin, and presented as fold changes. **(E)** Immunohistochemistry analysis of peritoneal tissue sections stained for CD68. Arrows represent CD68-positive cells. Scale bar = 25 μm. **(F,G)** Dialysates from new-onset PD patients (n = 11) and PD patients with UFF (n = 7) were subjected to ELISA analysis to detect secretion of IL-1β **(F)** and IL-18 **(G)**. **(H)** Cell lysates from RPMCs exposed to 138 mmol/L glucose at different times were subjected to western blotting analysis with specific antibodies against EP4 and β-actin. **(I)** EP4 expression levels were quantified by densitometry, normalised with β-actin, and presented as fold changes. Data are presented as mean ± SEM. *p < 0.05, **p < 0.01, ***p < 0.001.

marker, these results indicate that EP4 was expressed in the residual mesothelial cells in PD patients with UFF.

Next, 4 peritoneal tissues from ESRD patients and 4 peritoneal tissues from PD patients with UFF were used for western blotting to investigate EP4 protein expression. The western blotting results showed that EP4 expression was significantly increased in the peritoneal tissues of PD patients with UFF (Figures 1C,D). We also found that CD68-positive cells were increased in the peritoneum of PD patients with UFF, whereas these cells were rarely found in the peritoneum of ESRD patients (Figure 1E). Dialysate concentrations of IL-1β and IL-18 of new-onset PD patients and PD patients with UFF were also analyzed. As shown in Figures 1F,G, levels of both IL-1β and IL-18 were significantly increased in PD patients with UFF. These results suggest that an increased inflammatory response was observed in the peritoneum of PD patients with UFF.

We also investigated changes in EP4 expression in RPMCs after damage induced by high levels of glucose. CCK-8 testing showed that cell viability was not affected by a glucose concentration of 138 mmol/L (Supplementary Figure 1A). After exposing RPMCs to

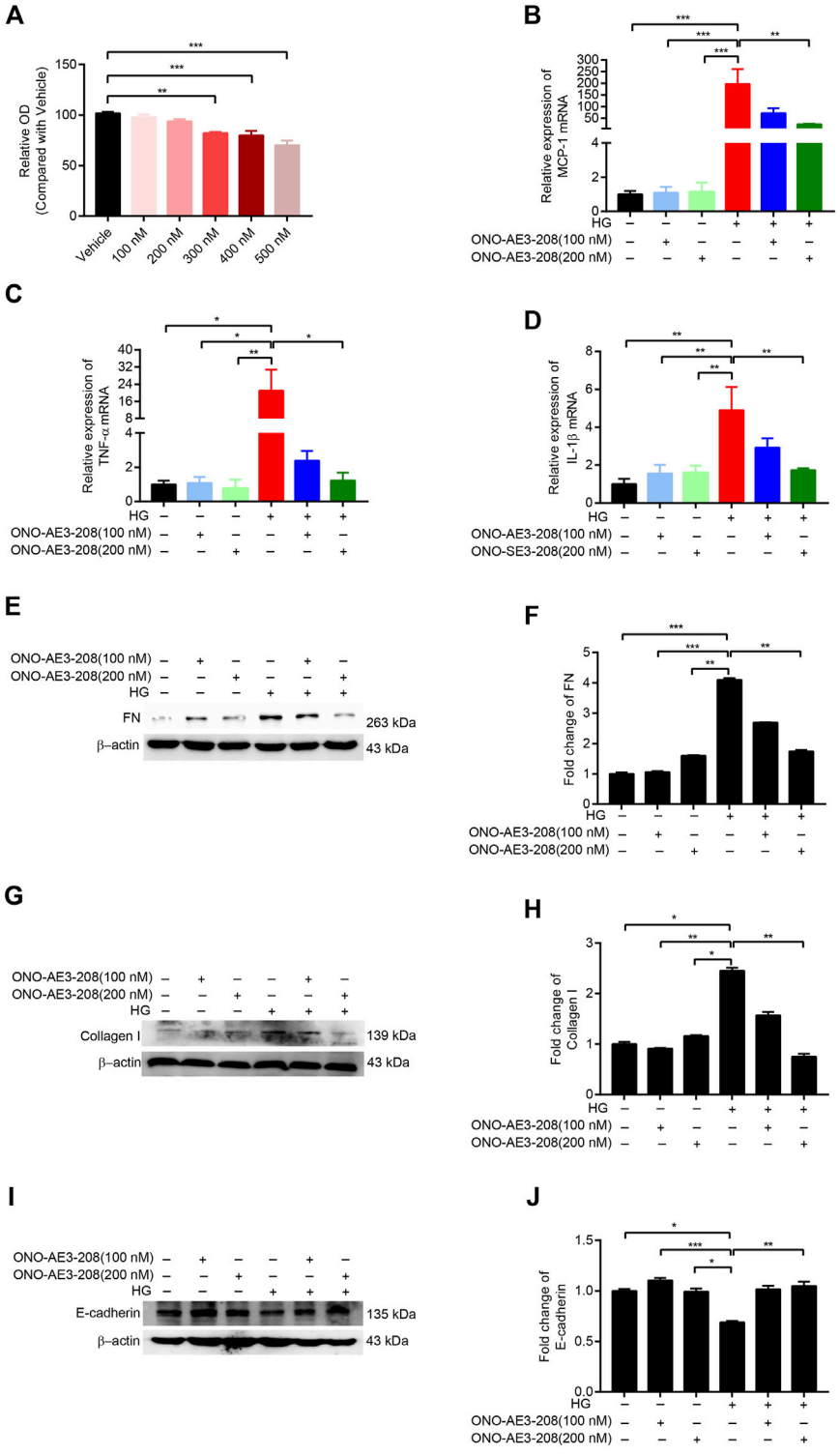

FIGURE 2
ONO-AE3-208 decreased inflammatory activity and synthesis of extracellular matrix in cultured RPMCs. **(A)** Cell viability from RPMCs treated with different doses of ONO-AE3-208 was examined by CCK-8. **(B–D)** Real-time quantitative PCR analysis of MCP-1, TNF-α, and IL-1β levels in RPMCs exposed to different doses of ONO-AE3-208 or 138 mmol/L glucose. **(E,G,I)** Cell lysates from RPMCs treated with different doses of ONO-AE3-208 or 138 mmol/L glucose were subjected to western blotting analysis with specific antibodies against fibronectin (FN), collagen I, E-cadherin, and β-actin. **(F,H,J)** Expression levels of FN, collagen I, and E-cadherin were quantified by densitometry, normalised with β-actin, and presented as fold changes. Data are presented as mean ± SEM. *$p < 0.05$, **$p < 0.01$, ***$p < 0.001$.

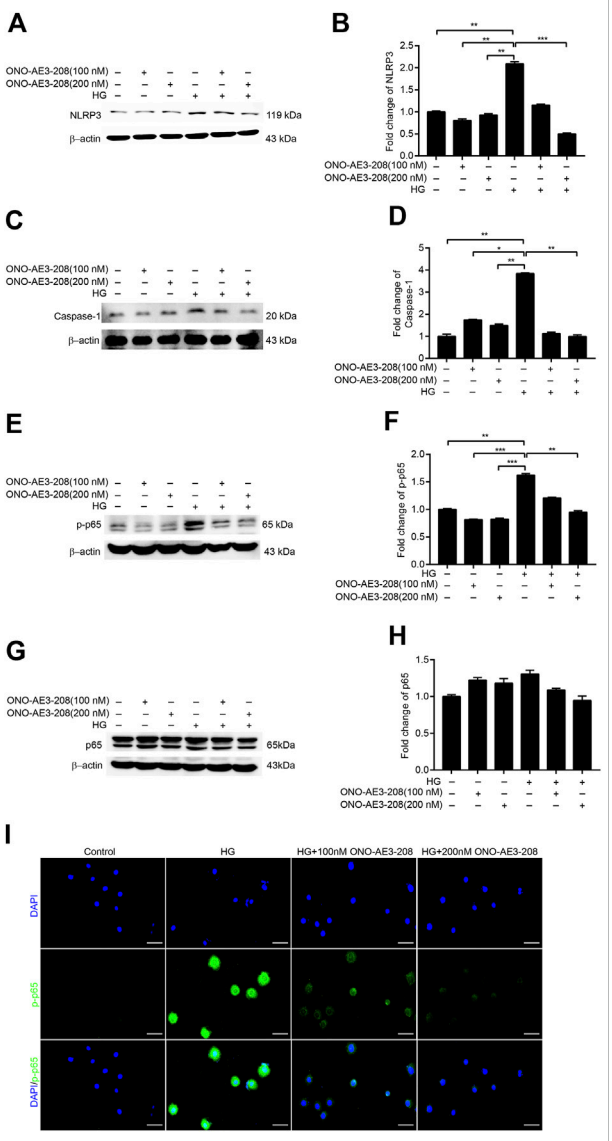

FIGURE 3
ONO-AE3-208 inhibited activation of the NRLP3 inflammasome and phosphorylation of NF-κB in cultured RPMCs. **(A,C)** Cell lysates from RPMCs treated with different doses of ONO-AE3-208 or 138 mmol/L glucose were subjected to western blotting analysis with specific antibodies against NLRP3, caspase-1, and β-actin. **(B,D)** Expression levels of NLRP3 and caspase-1 were quantified by densitometry, normalised with β-actin, and presented as fold changes. **(E,G)** Cell lysates from RPMCs treated with different doses of ONO-AE3-208 or 138 mmol/L glucose were subjected to western blotting analysis with specific antibodies against p-p65, p65, and β-actin. **(F,H)** Expression levels of p-p65 and p65 were quantified by densitometry, normalised with β-actin, and presented as fold changes. **(I)** Photomicrographs showing immunofluorescence staining of p-p65 and DAPI in RPMCs exposed to different doses of ONO-AE3-208 or 138 mmol/L glucose. Scale bar = 50 μm. Data are represented as mean ± SEM. $*p < 0.05$, $**p < 0.01$, $***p < 0.001$.

138 mmol/L glucose for 0, 24, 48, and 72 h, EP4 expression was significantly increased in these high-glucose–induced RPMCs (Figures 1H,I). By contrast, 138 mmol/L mannitol did not increase EP4 expression (Supplementary Figures 1B,C). Taken together, these results indicate that there is an increased inflammatory response in the peritoneum of PD patients with UFF and that EP4 is upregulated in the peritoneum of PD patients with UFF and RPMCs exposed to high glucose levels.

ONO-AE3-208 decreased inflammatory activity and synthesis of extracellular matrix in cultured RPMCs

Cultured RPMCs were treated with varying concentrations of ONO-AE3-208. CCK-8 results showed that 100 nM and 200 nM concentrations of ONO-AE3-208 had no significant effect on cell viability (Figure 2A). We then incubated RPMCs with 138 mmol/L glucose and 100 nM or 200 nM ONO-AE3-208. Quantitative RT-PCR assay showed that mRNA levels of MCP-1, TNF-α, and IL-1β were significantly increased in response to high glucose, and ONO-AE3-208 treatment inhibited this expression (Figures 2B–D). Exposure of RPMCs to 138 mmol/L glucose increased the expression of fibronectin (FN) and collagen I and decreased the expression of E-cadherin; treatment with ONO-AE3-208 inhibited this high-glucose–induced upregulation of FN and collagen I and downregulation of E-cadherin (Figures 2E–J). These results demonstrate the inhibitory effects of ONO-AE3-208 on inflammatory activity and extracellular matrix synthesis *in vitro*.

ONO-AE3-208 inhibited activation of NLRP3 inflammasome and phosphorylation of NF-κB in cultured RPMCs

Our previous study showed that mPGES-1 contributed to peritoneal fibrosis by activating the NLRP3 inflammasome (Luo et al., 2021); thus, in this study, we examined the effects of ONO-AE3-208 on NLRP3 inflammasome activation. NLRP3 and caspase-1 activation were induced in cultured RPMCs treated with 138 mmol/L glucose, a phenomenon that was markedly blocked by treatment with ONO-AE3-208 (Figures 3A–D).

As NF-κB–induced inflammatory signalling pathways play a pivotal role in peritoneal fibrosis (Shi et al., 2021), we also explored whether the anti-inflammatory effects of ONO-AE3-208 were mediated by changes in phosphorylated NF-κB. We found that phosphorylated NF-κB (p-p65) was substantially increased in cultured RPMCs stimulated with 138 mmol/L

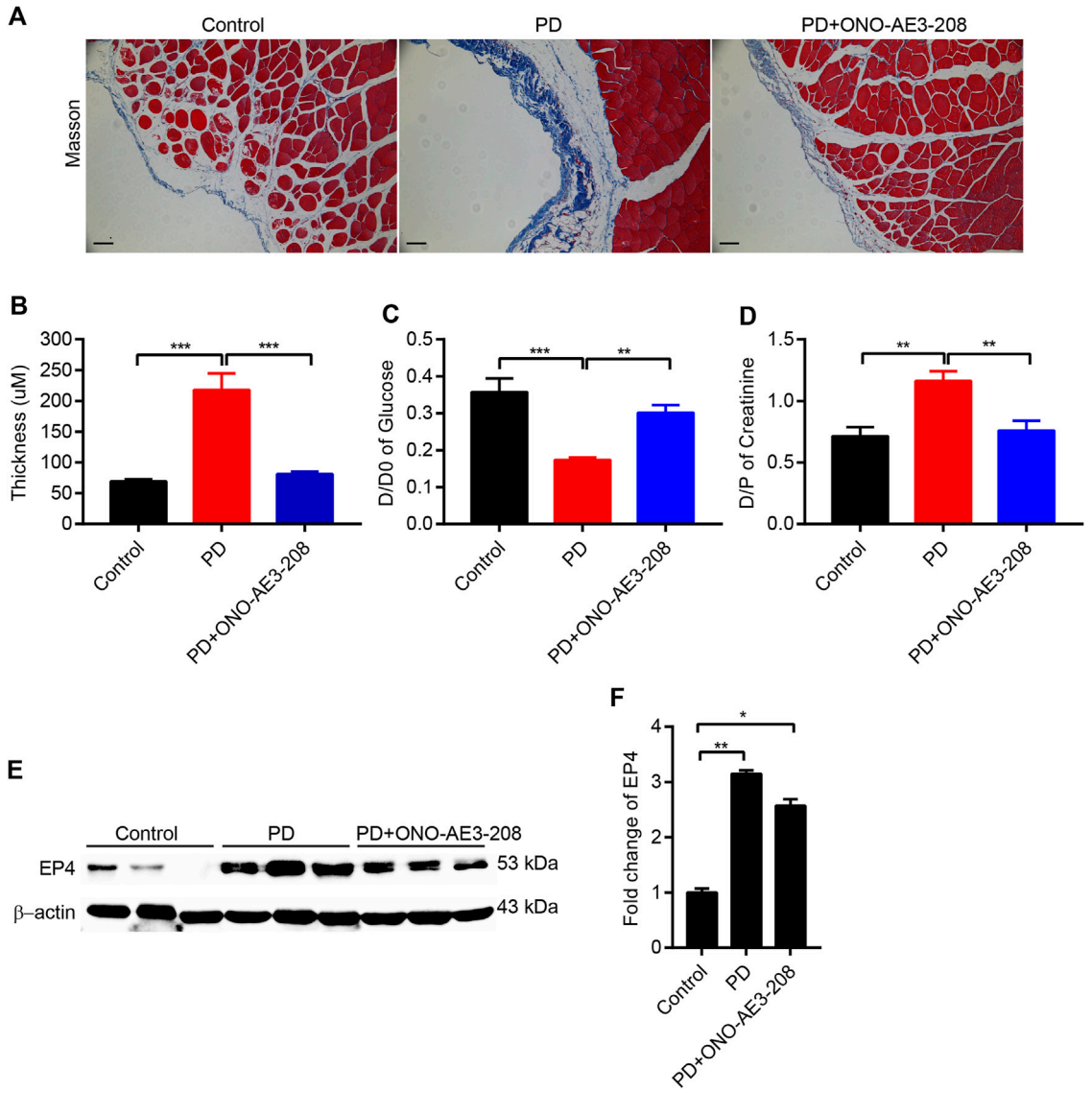

FIGURE 4
Administration of ONO-AE3-208 reduced peritoneal pathologic injury and improved peritoneal dysfunction in a rat model of peritoneal fibrosis. **(A)** Photomicrographs illustrating Masson staining of the parietal peritoneum in each animal group. **(B)** Thickness of the peritoneal membrane in each group. **(C,D)** Peritoneal function was assessed by the transfer of glucose (D/D0) and creatinine (D/P_{Scr}). **(E)** Peritoneal tissue lysates from each group were subjected to western blotting analysis with specific antibodies against EP4 and β-actin. **(F)** Expression levels of EP4 were quantified by densitometry, normalised with β-actin, and presented as fold changes. Data are presented as mean ± SEM. *$p < 0.05$, **$p < 0.01$, ***$p < 0.001$.

glucose, and that ONO-AE3-208 downregulated phosphorylated NF-κB (p-p65) but had no significant effect on total NF-κB (p-65) (Figures 3E–H). Additionally, immunofluorescence staining revealed increased nuclear translocation of phosphorylated NF-κB (p-p65) in cultured RPMCs treated with high glucose, whereas ONO-AE3-208 abrogated high-glucose–induced translocation of phosphorylated NF-κB (p-p65) (Figure 3I). These data suggest that ONO-AE3-208 regulates activation of the NLRP3 inflammasome and phosphorylation of NF-κB *in vitro*.

Administration of ONO-AE3-208 reduced peritoneal pathologic injury and improved peritoneal dysfunction in a rat model of peritoneal dialysis

To further elucidate the role of ONO-AE3-208 in the development of peritoneal fibrosis and functional injury in response to chronic PD fluid infusion, we established a rat model of peritoneal fibrosis and concurrently treated the animals with ONO-AE3-208. Masson's trichrome staining

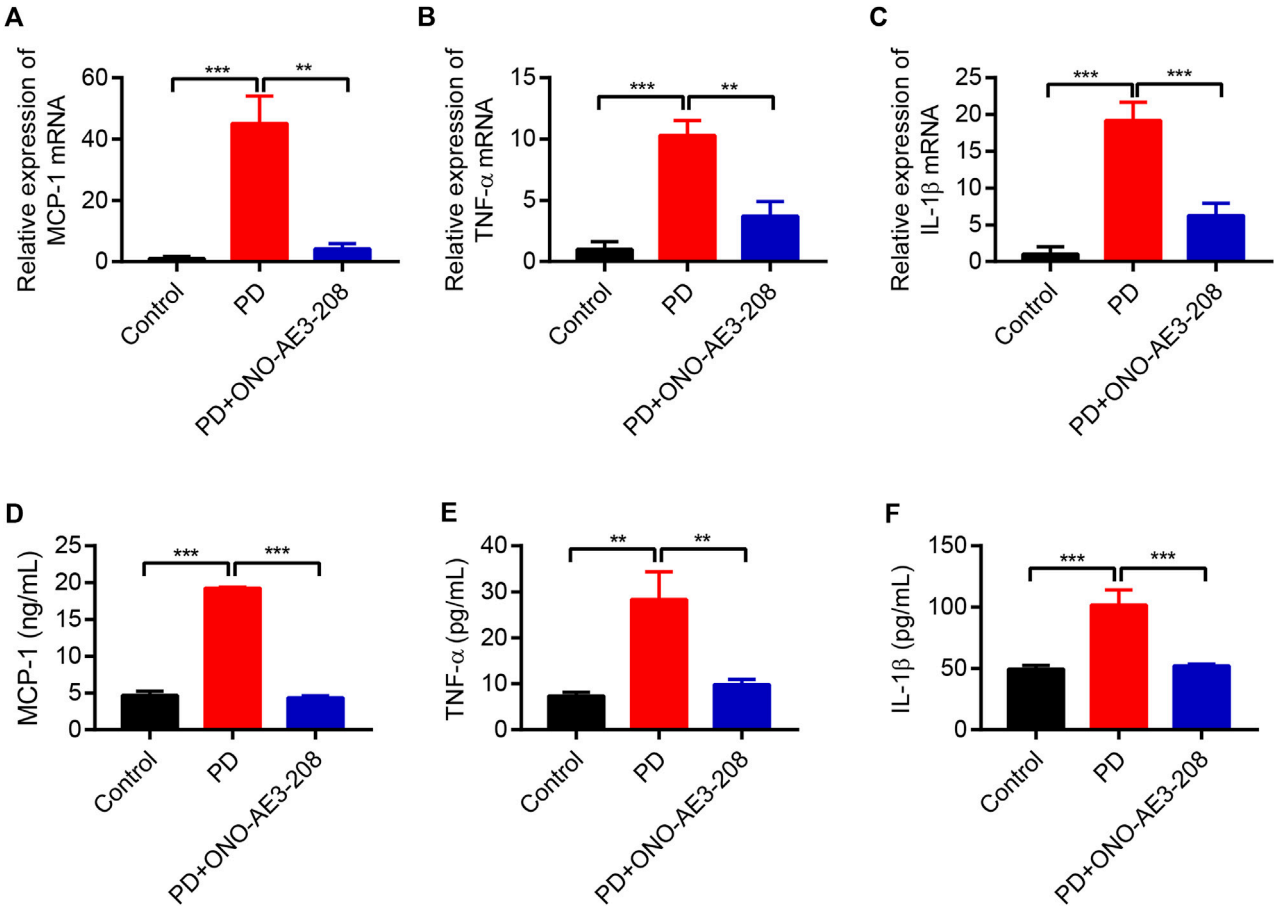

FIGURE 5
Administration of ONO-AE3-208 prevented inflammation in a rat model of peritoneal fibrosis. **(A–C)** Real-time quantitative PCR analysis of MCP-1, TNF-α, and IL-1β levels in the visceral peritoneum for each animal group. **(D–F)** ELISA results of the secretion of MCP-1, TNF-α, and IL-1β in the dialysate for each group. Data are presented as mean ± SEM. $^{**}p < 0.01$, $^{***}p < 0.001$.

showed that compared with the peritoneal tissues of control rats, those in the PD group exhibited loss of the mesothelial cell monolayer and increased thickness of the submesothelial compact zone (Figures 4A,B). These histologic changes were accompanied by increased peritoneal transport of glucose (D/D0) and increased peritoneal transport of creatinine (D/P_{Scr}) (Figures 4C,D), indicating increased peritoneal permeability in PD rats. In contrast, administering ONO-AE3-208 prevented peritoneal thickening and improved peritoneal transport function, as indicated by a decreased D/D0 and decreased D/P_{Scr} (Figures 4A–D). We also evaluated EP4 expression in the peritoneum *in vivo*. Upregulation of EP4 in the fibrotic peritoneal tissues was confirmed, and ONO-AE3-208 had little effect on EP4 expression (Figures 4E,F). These results indicate that ONO-AE3-208 can alleviate peritoneal pathologic injury and improve peritoneal dysfunction *in vivo*.

Administration of ONO-AE3-208 prevented inflammation in a rat model of peritoneal dialysis

Based on the results of our *in vitro* study, we further evaluated the effects of ONO-AE3-208 on inflammatory cytokine expression *in vivo*. Levels of MCP-1, TNF-α, and IL-1β mRNA in the visceral peritoneum increased in rats receiving 4.25% PD fluid, and these levels decreased after treatment with ONO-AE3-208 (Figures 5A–C). Secretion of these inflammatory cytokines in the PD fluid was further evaluated using ELISA. Injection of 4.25% PD fluid significantly increased MCP-1, TNF-α, and IL-1β concentrations in the effluent, and treatment with ONO-AE3-208 effectively reduced their secretion (Figures 5D–F). These results demonstrate that ONO-AE3-208 inhibits peritoneal inflammation during PD *in vivo*.

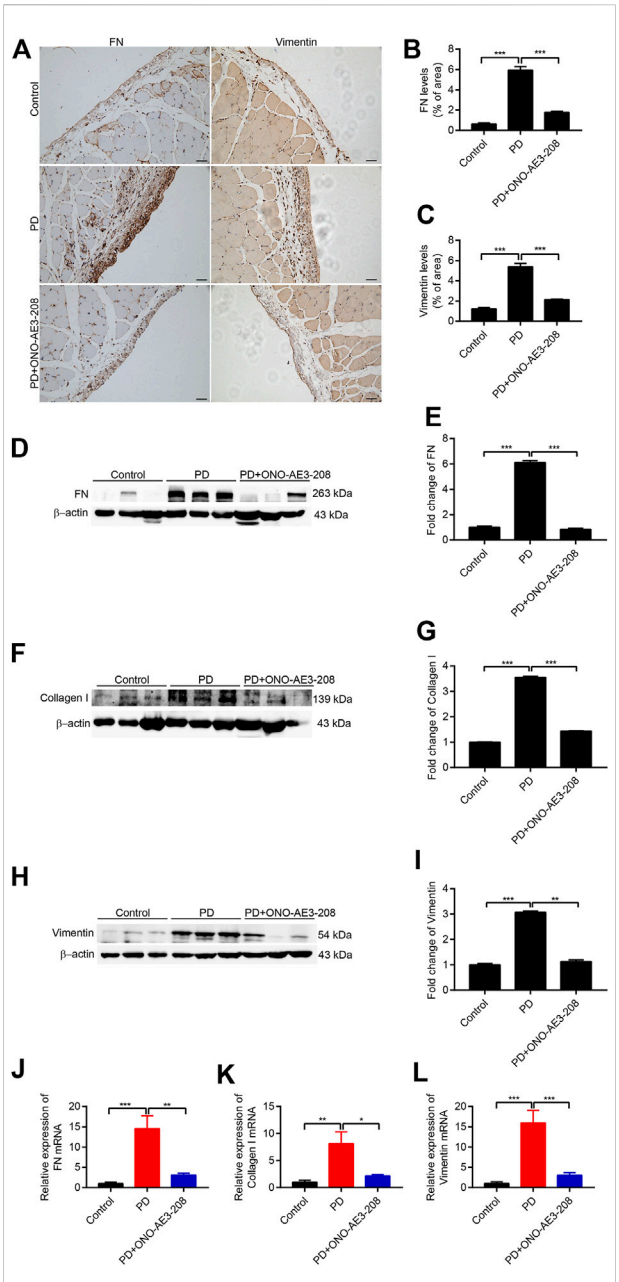

FIGURE 6
Administration of ONO-AE3-208 prevented peritoneal fibrosis in a rat model of peritoneal fibrosis. **(A)** Photomicrographs showing immunohistochemistry staining of FN and vimentin from peritoneal tissues in each group. Scale bar = 50 μm. **(B,C)** Areas positive for FN and vimentin. **(D,F,H)** Peritoneal tissue lysates from each animal group were subjected to western blotting analysis with specific antibodies against FN, collagen I, vimentin, and β-actin. **(E,G,I)** Expression levels of FN, collagen I, and vimentin were quantified by densitometry, normalised with β-actin, and presented as fold changes. **(J–L)** Real-time quantitative PCR analysis of FN, collagen I, and vimentin levels in the visceral peritoneum for each group. Data are presented as mean ± SEM. $*p < 0.05$, $**p < 0.01$, $***p < 0.001$.

Administration of ONO-AE3-208 prevented peritoneal fibrosis in a rat model of peritoneal dialysis

We next examined the preventive effects of ONO-AE3-208 on peritoneal fibrosis in response to long-term PD fluid infusion. Results of immunohistochemical staining demonstrated that ONO-AE3-208 inhibited the formation of FN and vimentin and significantly reduced FN- and vimentin-positive areas (Figures 6A–C). The protective effects of ONO-AE3-208 on peritoneal fibrosis were further demonstrated by its ability to inhibit FN, collagen I, and vimentin at both the mRNA and protein levels (Figures 6D–L). These data thereby suggest that ONO-AE3-208 prevents peritoneal fibrosis *in vivo*.

Administration of ONO-AE3-208 inhibited NLRP3 inflammasome activation and NF-κB phosphorylation in a rat model of peritoneal dialysis

Finally, we investigated the effects of ONO-AE3-208 on activation of the NLRP3 inflammasome and NF-κB in peritoneal tissues *in vivo*. Western blotting analysis revealed that NLRP3 and p-p65 expression were significantly induced in the peritoneum of PD rats and significantly inhibited in the peritoneal tissues of rats treated with ONO-AE3-208 (Figures 7A–D). These data indicate that ONO-AE3-208 inhibits activation of the NLRP3 inflammasome and phosphorylation of NF-κB *in vivo*.

Discussion

PGE2 is the major product of COX-2 and mPGES-1, and these two enzymes were previously reported to be increased in the peritoneum of a mouse model of PD and PD patients with UFF (Aroeira et al., 2009; Luo et al., 2021). PGE2 can bind to different EP receptors (EP1 to EP4), which are expressed in different cells and have opposing effects; therefore, blocking PGE2 using COX-2 or mPGES-1 inhibitors is clinically problematic. Targeting an EP receptor that specifically regulates the deleterious effects of COX-2/mPGES-1/PGE2 would be beneficial for preventing or treating peritoneal fibrosis. In this study, we found that PD-related peritoneal fibrosis was associated with increased expression of EP4 and that administration of an EP4 receptor antagonist (ONO-AE3-208) prevented progressive peritoneal fibrosis and functional injury of the peritoneal membrane. These results suggest that EP4 may be a potential therapeutic target for PD-associated peritoneal fibrosis.

Previous studies showed that EP4 was expressed in the brain, thymus, heart, lung, uterus, and kidney tissues of mice (Sugimoto

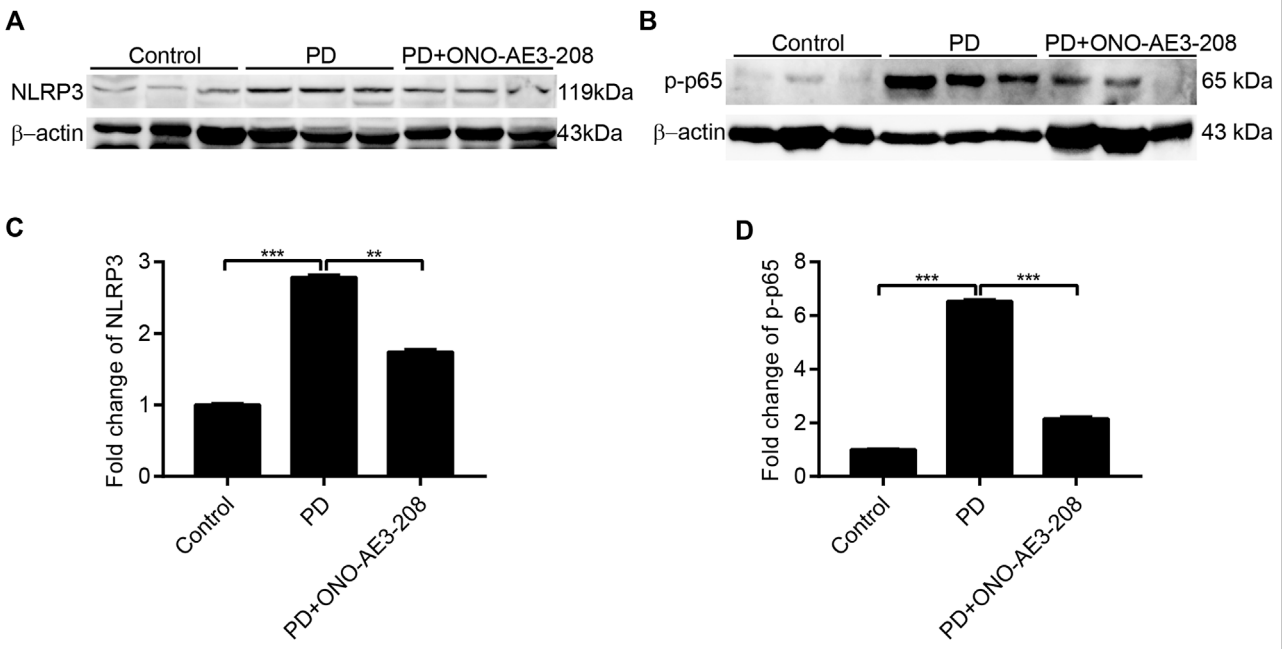

FIGURE 7
Administration of ONO-AE3-208 inhibited NLRP3 inflammasome activation and NF-κB phosphorylation in a rat model of peritoneal dialysis. **(A,B)** Peritoneal tissue lysates from each animal group were subjected to western blotting analysis with specific antibodies against NLRP3, p-p65, and β-actin. **(C,D)** Expression levels of NLRP3 and p-p65 were quantified by densitometry, normalised with β-actin, and presented as fold changes. Data are presented as mean ± SEM. $^{**}p < 0.01$, $^{***}p < 0.001$.

and Narumiya, 2007; Aringer et al., 2018). Our study demonstrated that EP4 is also distributed in human peritoneal tissues. Peritoneal fibrosis is a common complication in patients undergoing long-term PD, and our findings of enhanced EP4 expression in the peritoneum of PD patients with UFF and RPMCs stimulated with high levels of glucose suggest that EP4 may play an important role in the development of this complication. Chronic inflammation promotes the development of peritoneal fibrosis. Our results are consistent with previous reports of the EP4 receptor playing a key role in a variety of disease models associated with increased inflammation, including type 1 diabetes (Rahman et al., 2018), endometritis (Li et al., 2019), angiotensin II-induced abdominal aortic aneurysm (Hiromi et al., 2020), airway inflammation (van Geffen et al., 2021), and nephrotoxic serum nephritis (Aringer et al., 2018).

The current study adds new evidence in support of the important role of EP4 in promoting inflammation, as indicated by the findings that EP4 blockade suppressed the expression of inflammatory cytokines in RPMCs in response to high glucose levels and in the peritoneal tissues of a rat model of PD. However, the role of EP4 in inflammation varies. In a mouse model of inflammatory bowel disease, PGE2 signalling repressed intestinal epithelial cell necroptosis and induced resolution of colitis through the EP4 receptor (Patankar et al., 2021). In addition, blockade of the EP4 receptor in a mouse model of autosomal dominant polycystic kidney disease resulted in more severe cystic disease and increased macrophage infiltration in the kidney tissue (Lannoy et al., 2020). Thus, functions of the EP4 receptor appear to be cell type- and context-dependent, and the differing effects on inflammation may be attributed to different disease models.

Emerging evidence shows that targeting the EP4 receptor has clear effects in various animal models of fibrosis. A specific EP4 antagonist significantly inhibited the autophagy of M2 macrophage-mediated hepatic stellate cells and improved liver fibrosis (Cao et al., 2022). Chronic repeated administration of an EP4 receptor-selective antagonist significantly attenuated the development of glomerulosclerosis and tubulointerstitial fibrosis in 5/6 nephrectomised rats (Mizukami et al., 2019). Administration of a PGE2 receptor EP4-selective agonist increased TNF-α (an inflammatory cytokine) levels and exacerbated renal fibrosis in an animal model of type 1 diabetes (Mohamed et al., 2013). Our results showed that the EP4 antagonist ONO-AE3-208 had beneficial effects in an experimental model of PD-associated peritoneal fibrosis. This was further demonstrated by the findings that ONO-AE3-208 protected against PD-induced peritoneal fibrosis and functional impairment of the peritoneal membrane, thus

suggesting that ONO-AE3-208 may be a potential therapeutic agent for peritoneal fibrosis.

ONO-AE3-208 is a well-characterized EP4 receptor antagonist, which binds to the EP4 receptor, thereby blocking the interaction of PGE2 with the EP4 receptor and thus inhibiting downstream inflammatory responses (Kabashima et al., 2003; Jones et al., 2009; Esaki et al., 2010). Local inflammatory responses in the peritoneum contribute to deterioration of peritoneal transport function and peritoneal fibrosis (de Lima et al., 2013). The results of our *in vivo* experiments showed that ONO-AE3-208 reduced the high-glucose–induced inflammatory response in the peritoneum and peritoneal fibrosis, thereby reducing peritoneal pathologic injury and improving peritoneal function. Our *in vivo* experiments also revealed that ONO-AE3-208 had little effect on EP4 in the peritoneum. Although ONO-AE3-208 reduced the peritoneal inflammatory response, the peritoneum was still surrounded by PD fluid containing a high concentration of glucose; therefore, increased expression of EP4 was still observed in PD rats treated with ONO-AE3-208. The EP4 antagonist can be administered orally and is not associated with changes in blood pressure (Aringer et al., 2018); therefore, clinical application of the EP4 antagonist is more promising. To date, the novel EP4 receptor antagonist has been studied in phase II clinical trials in patients with rheumatoid arthritis (ClinicalTrials.gov Identifier: NCT03163966) and patients with advanced prostate, breast, or non-small cell lung cancers (ClinicalTrials.gov Identifier: NCT02538432). Although our current results for ONO-AE3-208 are promising, further research will be necessary to investigate the efficacy and safety of different doses of this antagonist for the prevention and treatment of PD-associated peritoneal fibrosis.

The results of our previous study showed that mPGES-1 promoted the synthesis of extracellular matrix protein *via* activation of the NLRP3 inflammasome in RPMCs exposed to high levels of glucose (Luo et al., 2021), indicating that the NLRP3 inflammasome participated in peritoneal fibrosis. EP4 is one of the main downstream receptors of mPGES-1. Previous studies have shown that the PGE2/EP4 pathway is closely related to the activation of the NLRP3 inflammasome. For example, the PGE2 synthetic pathway was shown to promote albumin-induced renal tubular injury *via* an NLRP3 inflammasome-mediated mechanism (Zhuang et al., 2017). *Tityus serrulatus* venom triggered lung resident cells to release PGE2, which induced activation of the NLRP3 inflammasome *via* EP4-cAMP-PKA-NF-κB-dependent mechanisms, leading to an increase in IL-1β (Zoccal et al., 2016). In the present study, we further demonstrated that an EP4 antagonist attenuated peritoneal fibrosis by inhibiting activation of the NLRP3 inflammasome. Moreover, EP4 signalling has been shown to regulate NF-κB signalling. EP4 stimulation increased IL-6 production *via* PKA-NF-κB pathways in vascular smooth muscle cells isolated from the mouse aorta and human abdominal aortic aneurysms (Hiromi et al., 2020). Peptidoglycan-mediated IL-6 production was mediated by the PGE2/EP4/NF-κB pathway in RAW 264.7 macrophages (Chen et al., 2006). We further demonstrated that EP4 signalling regulated NF-κB signalling in RPMCs exposed to high concentrations of glucose.

In summary, we confirmed that the EP4 receptor promotes peritoneal fibrosis and that pharmacologic blockade of EP4 protects against peritoneal injury. EP4 was highly enhanced in the fibrotic peritoneum of PD patients with UFF and in cultured RPMCs stimulated with high glucose concentrations. Treatment with ONO-AE3-208 significantly prevented peritoneal inflammation and peritoneal fibrosis by inhibiting activation of the NLRP3 inflammasome and reducing phosphorylation of NF-κB. Therefore, EP4 inhibition may be a new strategy for the prevention and treatment of PD-associated peritoneal fibrosis in the future.

Data availability statement

The original contributions presented in the study are included in the article/Supplementary Material, further inquiries can be directed to the corresponding authors.

Ethics statement

The studies involving human participants were reviewed and approved by the Ethical Review Board of Shunde Hospital of Southern Medical University. The patients/participants provided their written informed consent to participate in this study. The animal study was reviewed and approved by the Animal Experimental Ethics Committee at Southern Medical University. Written informed consent was obtained from the individual(s) for the publication of any potentially identifiable images or data included in this article.

Author contributions

Designed the study: QL, ML, ZJ, and XD. Undertook the experimental work: QL, ML, YT, JC, WZ, SZ, JP, QZ, LG, and LS. Analyzed the data: QL, ML, and YT. Contributed the figures and manuscript preparation: QL, ML, YT, JC, WZ, SZ, JP, QZ, LG, LS, ZJ, and XD. The manuscript was written through contributions of all authors. All authors have approved the final version of the manuscript.

Funding

This work was supported by grants from the National Natural Science Foundation for Yong Scholars of China (81800674), Natural Science Foundation of Guangdong Province (2018A030310428), China Postdoctoral Science Foundation funded project (2019M663006), and Scientific Research Start Plan of Shunde Hospital, Southern Medical University (SRSP2019007).

Conflict of interest

The authors declare that the research was conducted in the absence of any commercial or financial relationships that could be construed as a potential conflict of interest.

Publisher's note

Supplementary material

The Supplementary Material for this article can be found online at: https://www.frontiersin.org/articles/10.3389/fphar.2022.1004619/full#supplementary-material

References

Aringer, I., Artinger, K., Kirsch, A. H., Schabhüttl, C., Jandl, K., Bärnthaler, T., et al. (2018). Blockade of prostaglandin E(2) receptor 4 ameliorates nephrotoxic serum nephritis. *Am. J. Physiol. Ren. Physiol.* 315 (6), F1869–F1880. doi:10.1152/ajprenal.00113.2018

Aroeira, L. S., Lara-Pezzi, E., Loureiro, J., Aguilera, A., Ramírez-Huesca, M., González-Mateo, G., et al. (2009). Cyclooxygenase-2 mediates dialysate-induced alterations of the peritoneal membrane. *J. Am. Soc. Nephrol.* 20 (3), 582–592. doi:10.1681/asn.2008020211

Cao, Y., Mai, W., Li, R., Deng, S., Li, L., Zhou, Y., et al. (2022). Macrophages evoke autophagy of hepatic stellate cells to promote liver fibrosis in NAFLD mice via the PGE2/EP4 pathway. *Cell. Mol. Life Sci.* 79 (6), 303. doi:10.1007/s00018-022-04319-w

Chen, B. C., Liao, C. C., Hsu, M. J., Liao, Y. T., Lin, C. C., Sheu, J. R., et al. (2006). Peptidoglycan-induced IL-6 production in RAW 264.7 macrophages is mediated by cyclooxygenase-2, PGE2/PGE4 receptors, protein kinase A, I kappa B kinase, and NF-kappa B. *J. Immunol.* 177 (1), 681–693. doi:10.4049/jimmunol.177.1.681

Chen, Q., Muramoto, K., Masaaki, N., Ding, Y., Yang, H., Mackey, M., et al. (2010). A novel antagonist of the prostaglandin E(2) EP(4) receptor inhibits Th1 differentiation and Th17 expansion and is orally active in arthritis models. *Br. J. Pharmacol.* 160 (2), 292–310. doi:10.1111/j.1476-5381.2010.00647.x

Chu, Y., Wang, Y., Zheng, Z., Lin, Y., He, R., Liu, J., et al. (2017). Proinflammatory effect of high glucose concentrations on HMrSV5 cells via the autocrine effect of HMGB1. *Front. Physiol.* 8, 762. doi:10.3389/fphys.2017.00762

de Lima, S. M., Otoni, A., Sabino Ade, P., Dusse, L. M., Gomes, K. B., Pinto, S. W., et al. (2013). Inflammation, neoangiogenesis and fibrosis in peritoneal dialysis. *Clin. Chim. Acta.* 421, 46–50. doi:10.1016/j.cca.2013.02.027

Esaki, Y., Li, Y., Sakata, D., Yao, C., Segi-Nishida, E., Matsuoka, T., et al. (2010). Dual roles of PGE2-EP4 signaling in mouse experimental autoimmune encephalomyelitis. *Proc. Natl. Acad. Sci. U. S. A.* 107 (27), 12233–12238. doi:10.1073/pnas.0915112107

Fusshoeller, A. (2008). Histomorphological and functional changes of the peritoneal membrane during long-term peritoneal dialysis. *Pediatr. Nephrol.* 23 (1), 19–25. doi:10.1007/s00467-007-0541-z

Hiromi, T., Yokoyama, U., Kurotaki, D., Mamun, A., Ishiwata, R., Ichikawa, Y., et al. (2020). Excessive EP4 signaling in smooth muscle cells induces abdominal aortic aneurysm by amplifying inflammation. *Arterioscler. Thromb. Vasc. Biol.* 40 (6), 1559–1573. doi:10.1161/atvbaha.120.314297

Jones, R. L., Giembycz, M. A., and Woodward, D. F. (2009). Prostanoid receptor antagonists: Development strategies and therapeutic applications. *Br. J. Pharmacol.* 158 (1), 104–145. doi:10.1111/j.1476-5381.2009.00317.x

Kabashima, K., Sakata, D., Nagamachi, M., Miyachi, Y., Inaba, K., and Narumiya, S. (2003). Prostaglandin E2-EP4 signaling initiates skin immune responses by promoting migration and maturation of Langerhans cells. *Nat. Med.* 9 (6), 744–749. doi:10.1038/nm872

Lai, K. N., Tang, S. C., and Leung, J. C. (2007). Mediators of inflammation and fibrosis. *Perit. Dial. Int.* 27 (2), S65–S71. doi:10.1177/089686080702702s12

Lannoy, M., Valluru, M. K., Chang, L., Abdela-Ali, F., Peters, D. J. M., Streets, A. J., et al. (2020). The positive effect of selective prostaglandin E2 receptor EP2 and EP4 blockade on cystogenesis *in vitro* is counteracted by increased kidney inflammation *in vivo*. *Kidney Int.* 98 (2), 404–419. doi:10.1016/j.kint.2020.02.012

Li, T., Liu, B., Guan, H., Mao, W., Wang, L., Zhang, C., et al. (2019). PGE2 increases inflammatory damage in Escherichia coli-infected bovine endometrial tissue *in vitro* via the EP4-PKA signaling pathway. *Biol. Reprod.* 100 (1), 175–186. doi:10.1093/biolre/ioy162

Liu, H., Peng, Y., Liu, F., Li, J., Chen, X., Liu, Y., et al. (2007). A selective cyclooxygenase-2 inhibitor decreases transforming growth factor-beta1 synthesis and matrix production in human peritoneal mesothelial cells. *Cell. Biol. Int.* 31 (5), 508–515. doi:10.1016/j.cellbi.2006.11.018

Liu, Y., Dong, Z., Liu, H., Zhu, J., Liu, F., and Chen, G. (2015). Transition of mesothelial cell to fibroblast in peritoneal dialysis: EMT, stem cell or bystander? *Perit. Dial. Int.* 35 (1), 14–25. doi:10.3747/pdi.2014.00188

Luo, Q., Hu, Q., Zheng, Q., Gong, L., Su, L., Ren, B., et al. (2021). Enhanced mPGES-1 contributes to PD-related peritoneal fibrosis via activation of the NLRP3 inflammasome. *Front. Med.* 8, 675363. doi:10.3389/fmed.2021.675363

Mizukami, K., Yoshida, H., Nozawa, E., Wada, K., and Ugawa, T. (2019). Renoprotective effects of the novel prostaglandin EP4 receptor-selective antagonist ASP7657 in 5/6 nephrectomized chronic kidney disease rats. *Naunyn. Schmiedeb. Arch. Pharmacol.* 392 (4), 451–459. doi:10.1007/s00210-018-01600-3

Mohamed, R., Jayakumar, C., and Ramesh, G. (2013). Chronic administration of EP4-selective agonist exacerbates albuminuria and fibrosis of the kidney in streptozotocin-induced diabetic mice through IL-6. *Lab. Invest.* 93 (8), 933–945. doi:10.1038/labinvest.2013.85

Morelle, J., Sow, A., Hautem, N., Bouzin, C., Crott, R., Devuyst, O., et al. (2015). Interstitial fibrosis restricts osmotic water transport in encapsulating peritoneal sclerosis. *J. Am. Soc. Nephrol.* 26 (10), 2521–2533. doi:10.1681/asn.2014090939

Patankar, J. V., Müller, T. M., Kantham, S., Acera, M. G., Mascia, F., Scheibe, K., et al. (2021). E-type prostanoid receptor 4 drives resolution of intestinal inflammation by blocking epithelial necroptosis. *Nat. Cell. Biol.* 23 (7), 796–807. doi:10.1038/s41556-021-00708-8

Rahman, M. J., Rodrigues, K. B., Quiel, J. A., Liu, Y., Bhargava, V., Zhao, Y., et al. (2018). Restoration of the type I IFN-IL-1 balance through targeted blockade of PTGER4 inhibits autoimmunity in NOD mice. *JCI Insight* 3 (3), 97843. doi:10.1172/jci.insight.97843

Rosengren, B. I., Sagstad, S. J., Karlsen, T. V., and Wiig, H. (2013). Isolation of interstitial fluid and demonstration of local proinflammatory cytokine production and increased absorptive gradient in chronic peritoneal dialysis. *Am. J. Physiol. Ren. Physiol.* 304 (2), F198–F206. doi:10.1152/ajprenal.00293.2012

Sheppe, A. E. F., Kummari, E., Walker, A., Richards, A., Hui, W. W., Lee, J. H., et al. (2018). PGE2 augments inflammasome activation and M1 polarization in macrophages infected with Salmonella typhimurium and Yersinia enterocolitica. *Front. Microbiol.* 9, 2447. doi:10.3389/fmicb.2018.02447

Shi, Y., Hu, Y., Wang, Y., Ma, X., Tang, L., Tao, M., et al. (2021). Blockade of autophagy prevents the development and progression of peritoneal fibrosis. *Front. Pharmacol.* 12, 724141. doi:10.3389/fphar.2021.724141

Sitter, T., Haslinger, B., Mandl, S., Fricke, H., Held, E., and Sellmayer, A. (1998). High glucose increases prostaglandin E2 synthesis in human peritoneal mesothelial cells: Role of hyperosmolarity. *J. Am. Soc. Nephrol.* 9 (11), 2005–2012. doi:10.1681/asn.v9112005

Sugimoto, Y., and Narumiya, S. (2007). Prostaglandin E receptors. *J. Biol. Chem.* 282 (16), 11613–11617. doi:10.1074/jbc.R600038200

Tang, E. H., Libby, P., Vanhoutte, P. M., and Xu, A. (2012). Anti-inflammation therapy by activation of prostaglandin EP4 receptor in cardiovascular and other inflammatory diseases. *J. Cardiovasc. Pharmacol.* 59 (2), 116–123. doi:10.1097/FJC.0b013e3182244a12

Teitelbaum, I. (2015). Ultrafiltration failure in peritoneal dialysis: A pathophysiologic approach. *Blood Purif.* 39 (1-3), 70–73. doi:10.1159/000368972

van Geffen, C., Deißler, A., Beer-Hammer, S., Nürnberg, B., Handgretinger, R., Renz, H., et al. (2021). Myeloid-derived suppressor cells dampen airway inflammation through prostaglandin E2 receptor 4. *Front. Immunol.* 12, 695933. doi:10.3389/fimmu.2021.695933

Wang, F., Lu, X., Peng, K., Du, Y., Zhou, S. F., Zhang, A., et al. (2014). Prostaglandin E-prostanoid4 receptor mediates angiotensin II-induced (pro) renin receptor expression in the rat renal medulla. *Hypertension* 64 (2), 369–377. doi:10.1161/hypertensionaha.114.03654

Yao, C., Sakata, D., Esaki, Y., Li, Y., Matsuoka, T., Kuroiwa, K., et al. (2009). Prostaglandin E2-EP4 signaling promotes immune inflammation through Th1 cell differentiation and Th17 cell expansion. *Nat. Med.* 15 (6), 633–640. doi:10.1038/nm.1968

Zhou, Q., Bajo, M. A., Del Peso, G., Yu, X., and Selgas, R. (2016). Preventing peritoneal membrane fibrosis in peritoneal dialysis patients. *Kidney Int.* 90 (3), 515–524. doi:10.1016/j.kint.2016.03.040

Zhou, Q., Yang, M., Lan, H., and Yu, X. (2013). miR-30a negatively regulates TGF-β1-induced epithelial-mesenchymal transition and peritoneal fibrosis by targeting Snai1. *Am. J. Pathol.* 183 (3), 808–819. doi:10.1016/j.ajpath.2013.05.019

Zhuang, Y., Zhao, F., Liang, J., Deng, X., Zhang, Y., Ding, G., et al. (2017). Activation of COX-2/mPGES-1/PGE2 cascade via NLRP3 inflammasome contributes to albumin-induced proximal tubule cell injury. *Cell. Physiol. biochem.* 42 (2), 797–807. doi:10.1159/000478070

Zoccal, K. F., Sorgi, C. A., Hori, J. I., Paula-Silva, F. W., Arantes, E. C., Serezani, C. H., et al. (2016). Opposing roles of LTB4 and PGE2 in regulating the inflammasome-dependent scorpion venom-induced mortality. *Nat. Commun.* 7, 10760. doi:10.1038/ncomms10760

frontiers | Frontiers in Pharmacology

TYPE Original Research
PUBLISHED 15 November 2022
DOI 10.3389/fphar.2022.1041671

OPEN ACCESS

EDITED BY
Li Wu,
Nanjing University of Chinese Medicine, China

REVIEWED BY
Kelong Ai,
Xiangya School of Medicine, Central South University, China
Lei Zhu,
Chinese Academy of Medical Sciences and Peking Union Medical College, China

*CORRESPONDENCE
Wu-Yi Sun,
sunwuyi51@aliyun.com
Wei Wei,
wwei@ahmu.edu.cn

†These authors have contributed equally to this work

SPECIALTY SECTION
This article was submitted to Inflammation Pharmacology, a section of the journal Frontiers in Pharmacology

RECEIVED 11 September 2022
ACCEPTED 01 November 2022
PUBLISHED 15 November 2022

CITATION
Li N, Wu J-J, Qi M, Wang Z-Y, Zhang S-N, Li X-Q, Chen T-T, Wang M-F, Zhang L-L, Wei W and Sun W-Y (2022), CP-25 exerts a protective effect against ConA-induced hepatitis *via* regulating inflammation and immune response.
Front. Pharmacol. 13:1041671.
doi: 10.3389/fphar.2022.1041671

CP-25 exerts a protective effect against ConA-induced hepatitis *via* regulating inflammation and immune response

Nan Li[1†], Jing-Jing Wu[1,2†], Meng Qi[1], Zi-Ying Wang[1], Sheng-Nan Zhang[1], Xiu-Qin Li[1], Ting-Ting Chen[1], Mei-Fang Wang[1], Ling-Ling Zhang[1], Wei Wei[1*] and Wu-Yi Sun[1*]

[1]Institute of Clinical Pharmacology, Anhui Medical University, Key Laboratory of Anti-inflammatory and Immune Medicine, Ministry of Education, Anhui Collaborative Innovation Center of Anti-inflammatory and Immune Medicine, Hefei, China, [2]Department of Oncology, The Second Affiliated Hospital of Anhui Medical University, Hefei, China

Hepatitis is a complex multifactorial pathological disorder, which can eventually lead to liver failure and even potentially be life threatening. Paeoniflorin-6′-O-benzene sulfonate (CP-25) has proven to have critical anti-inflammatory effects in arthritis. However, the effects of CP-25 in the pathogenesis of hepatitis remains unclear. In this experiment, mice were intragastrically administered with CP-25 (25, 50 and 100 mg/kg), and then ConA (25 mg/kg) was intravenous injected to establish hepatitis model *in vivo*. CP-25 administration attenuated liver damage and decreased ALT and AST activities in mice with hepatitis. Besides, CP-25 modulated immune responses including down-regulated the proportions of activated $CD4^+$, activated $CD8^+$ T cells, and ratio of Th1/Th2 in ConA-injected mice. Furthermore, ConA-mediated production of reactive oxygen species (ROS), release of inflammatory cytokines including IFN-γ, TNF-α, activation of MAPK pathways and nuclear translocation of nuclear factor-kappaB (NF-κB) were significantly decreased in CP-25 administrated mice. In ConA-stimulated RAW264.7 cells, CP-25 suppressed inflammatory cytokines secretion and reduced ROS level, which were consistent with animal experiments. Otherwise, the data showed that CP-25 restrained phosphorylation of ERK, JNK and p38 MAPK pathways influenced by ROS, accompanied with inhibiting NF-κB nuclear translocation. In conclusion, our findings indicated that CP-25 protected against ConA-induced hepatitis may through modulating immune responses and attenuating ROS-mediated inflammation via the MAPK/NF-κB signaling pathway.

KEYWORDS

concanavalin A, CP-25, inflammation, hepatitis, inflammatory response

Introduction

Liver is the pivotal digestive organ and plays a crucial role in detoxification, metabolism, and immunity (Kubes and Jenne, 2018). Hepatitis caused by viral infections, drugs, food additives and alcohol can progress into cirrhosis, resulting in a significant health issue. It is reported that an inflammatory process would lead to hepatitis, which was characterized by excessive macrophages infiltration and propagation of inflammatory mediators (Jothimani et al., 2020). However, the precise mechanism of inflammatory regulation in hepatitis remains poorly understood.

Inflammation is considered to be an automatic defense response that benefits to maintain normal tissue function from potential harm caused by autoimmune damage or injury. But excessive accumulation of inflammatory cytokines could induce kidney, heart, lung and liver damage (Karki et al., 2021). Macrophages are the primary contributors to release amounts of inflammatory cytokines in response to liver inflammation and damage. The imbalance level of reactive oxygen species (ROS) in macrophages has evolved in liver tissue destruction, accompanying with oxidative stress and production of inflammatory cytokines (Zhang P et al., 2020). Concanavalin A (ConA)-induced hepatitis has been considered as a well-established experimental model due to its obvious pathological changes in inflammatory cytokines production and immune response (Rani et al., 2018). Multiple T cell subsets have been confirmed to be involved in the etiology of autoimmune disorders including hepatitis (Graham et al., 2021). We have previously shown that increased proportions of activated T cells and T helper (Th) cells contribute to liver injury in CCl_4-induced fibrotic mice, and inhibiting the disorders of immune responses from various aspects could alleviate liver fibrosis (Sun J. C et al., 2020). Therefore, developing inflammatory and immunomodulatory agents could provide new prophylaxis or therapeutic approaches for hepatitis.

Paeonia lactiflora pall root exhibits multiple pharmacological activities, which has been an integral part of effective prescriptions for treatment of inflammatory and immune diseases. Paeoniflorin is the main bioactivity ingredient of total glycosides of paeony that presents in the root of *Paeonia lactiflora* (Zhang and Wei, 2020). Our lab has composed an innovative ester derivative of paeoniflorin named paeoniflorin-6′-O-benzene sulfonate (CP-25, patent number in China: ZL201210030616.4). CP-25 has superior intestinal absorption and improved lipid solubility compared with the paeoniflorin. Our lab has reported that CP-25 could reduce pro-inflammatory cytokines production in adjuvant-induced arthritis (Chang et al., 2016). Consistent with another study, CP-25 treatment showed a disease-attenuating effect on modulating T lymphocyte subsets in primary Sjögren's syndrome mice (Gu et al., 2018). Our previous study presented that paeoniflorin displayed antifibrotic effects on liver fibrosis rats induced by porcine serum (Sun et al., 2012). Despite advanced evidence displayed the role of CP-25 in multiple diseases, it is still unclear whether it has an effect on ConA-induced hepatitis and the probable mechanisms.

In present experiments, ConA administration was used to establish hepatitis model. Our results displayed that CP-25 is not only as an immune response modulator in ConA-induced hepatitis, but restraining of inflammatory cytokines release may through down-regulating ROS influenced MAPK pathways activation and NF-κB nuclear translocation. Altogether, our findings indicated that CP-25 is a potential therapeutic agent in hepatitis.

Materials and methods

Animals and treatment

Male C57BL/6J mice (18 ± 22) g were purchased from the Animal Center of Anhui Medical University. The mice were kept in a temperature- and humidity-controlled room under standard 12-h light/dark cycles, maintained with administered food and water *ad libitum*. The Ethics Review Committee approved the animal experimental protocol at the Animal Experimentation of Anhui Medical University.

In this experiment, seven groups were divided at random from the mice: normal group, ConA-induced hepatitis model group, three dosages of CP-25-treated groups (25, 50, and 100 mg/kg), paeoniflorin-treated group (100 mg/kg), bicyclol-treated group (100 mg/kg). The effect of CP-25 and paeoniflorin at the same dose in the treatment of liver injury was compared. Meanwhile, bicyclol (Beijing Union Pharmaceutical Factory, Beijing, China) was served as a positive control. To establish the hepatitis mice model, mice received an intravenous injection of ConA (Solarbio, Beijing, China, C8110) at dose of 25 mg/kg. All drugs were diluted with 0.5% carboxymethyl cellulose sodium (CMC-Na) solution and intragastrically treated for 10 days before ConA injection. Other mice were intragastrically administered with an equivalent volume of CMC-Na solution. Then sacrificed the mice at indicated time point for liver, thymus, spleen and blood samples gathering.

Cell culture and treatment

RAW264.7 cells were purchased from ATCC (Manassas, VA, United States), routinely maintained in DMEM (Gibco, CA, United States) supplemented with 10% fetal bovine serum (Zhejiang Tianhang Biotechnology Co., Ltd, Zhejiang, China) in a humidified incubator at 37°C in 5% CO_2.

Several studies indicated that ConA administration obviously elevated inflammation in RAW264.7 cells (Zhang Z et al., 2020). Thus *in vitro*, RAW264.7 cells stimulated with ConA (10 μg/ml) was taken as model group, the cells treated by the same cell medium without ConA was taken as control group. The treatment groups were cultured with CP-25 (10^{-7}–10^{-5} mol/L), meanwhile, ConA-stimulated group was treated with equal-volume DMEM. Then following experiments were conducted to verify the potential effect of CP-25.

Ratio of liver, spleen and thymus weight to body weight

The liver, spleen and thymus were separated from the mice and immediately weighed. The liver, spleen and thymus indices were defined as: Liver, spleen or thymus index = liver, spleen or thymus weight/body weight × 100%.

Liver histopathology

Mice liver tissues were collected and fixed with 4% formalin, the paraffin-embedded tissues cut into 4 μm sections. The prepared liver slices were stained by hematoxylin and eosin staining (H&E). Samples were photographed under a DFC7000 T color microscope camera (Leica Microsystems, Wetzlar, Germany) to display the pathological damage.

Analysis of liver function

The serum was collected from blood samples by centrifugation at 3,000 r/min for 20 min and stored at -20 °C. The activities of serum alanine aminotransferase (ALT) and aspartate aminotransferase (AST) were detected by spectrophotometric assay kits (Nanjing Jiancheng Bioengineering Institute, Jiangsu, China, C009-two to one and C010-2–1), and showed as an international unit per litre (U/L).

T cell viability assay

Thymus were aseptically separated from mice. Then, thymocyte suspensions were prepared by mechanical dissociation of the tissues. Thymocytes was re-suspended in a DMEM medium, and incubated with ConA in 96-well plates. 10 μl cell counting kit-8 (CCK-8) (Biosharp, Hefei, China, BS350A) reagents were supplied to each well after the incubation period. The absorbance at 450 nm was measured using an Infinite M1000 PRO microplate reader (Tecan Group Ltd., Männedorf, Switzerland).

Preparation of spleen mononuclear cells and T cell subset analysis

The spleen tissue was removed and a single spleen suspension was harvested by mechanical separation of spleen through 70 μm filter and erythrocytes were lysed. Splenocytes were washed with PBS and re-suspended in DMEM medium. The antibody combinations CD3-PE (12-0038-42)/CD4-FITC (11-0041-81)/CD8-APC (17-0081-81) or CD4-FITC/CD8-APC/CD69-PE (12-0691-81) (eBioscience, San Diego, United States) were added into each tube, the expression of CD4 (CD8) was observed in $CD3^+$ or $CD69^+$ cell gate. Moreover, for intracellular IL-4 and IFN-γ staining, CD4-FITC antibody was used to stain surface marker, then samples were fixed, permeabilized to prevent nonspecific binding before staining with labelled IL-4-PE (12-7041-81)/IFN-γ-APC (17-7311-81) (eBioscience, San Diego, United States) antibodies. A single fluorescent dye sample was stained with CD3-PE, CD4-FITC, CD8-APC, CD69-PE, IL-4-PE and IFN-γ-APC respectively. Negative cells were stained without fluorescent dye. All the samples were tested using a CytoFLEX flow cytometry (Beckman, CA, United States), the data analysis was performed using a CytExpert software, and we have chosen the gate from comparing between negative and single fluorescent dye cells.

Determination of cytokines by ELISA

Weighed fresh liver tissues were homogenized with PBS and centrifuged (4°C, 5,000×*g* for 5 min). *In vitro*, the cell supernatants in ConA-stimulated RAW264.7 cells were acquired. The levels of IFN-γ (ml063132), TNF-α (ml002095), IL-4 (ml002149) and IL-1β (ml063132) in all supernatants were measured by enzyme-linked immunosorbent assay (ELISA) kits (Shanghai Enzyme-linked Biotechnology Co., Ltd, Shanghai, China) according to the manufacturer's instructions.

Immunostaining and confocal microscopy

Liver sections were blocking in 3% BSA undertaken for 2 h to prevent nonspecific staining. After rinsing with PBS, sections were incubated with following primary and secondary antibodies: F4/80 (BioLegend, San Diego, CA, 123,101), Alexa Fluor 488 (Thermo Fisher, MA, United States, A11001). Negative control sections were incubated with PBS instead of primary antibody. Before imaging, sections should be counterstained with DAPI (Beyotime, Shanghai, China) to label the nuclei. Then

tissue images were taken with a Leica TCS SP8 confocal microscope (Leica, Wetzlar, Germany).

Determination of ROS production

ROS production in liver tissues and cells was detected by the oxidation of dihydroethidium (DHE, S0063) and 2′,7′-dichlorodihydrofluorescein diacetate (DCFH-DA, S0033S) (Beyotime Biotechnology, Shanghai, China). For DHE staining, liver cryosections were cultivated with 5 μmol/L DHE at the indicated temperature for 30 min and then photographed using DFC7000 T color microscope camera. Average staining intensities were quantified by ImageJ software (National Institutes of Health, MD, United States). *In vitro*, ConA-stimulated RAW264.7 cells were cultured with DCFH-DA and then analyzed on a CytoFLEX flow cytometer at excitation and emission wavelengths of 488 nm.

Western blot analysis

Total proteins were harvested from liver tissues or RAW264.7 cells. Immunoblotting detection was conducted as previously described (Sun W. Y et al., 2020). The following antibodies were used: p-JNK (#9251S), JNK (#9252), p-ERK (#9101s), ERK (#9102), p-p38 (#9212s), and p38 (#9211s) (Cell Signaling Technology, Danvers, MA). Immunoblot band densitometry was quantified using ImageJ software. Three independent experiments were performed.

Nuclear factor-kappaB (NF-κB) nuclear translocation assay

NF-κB p65 translocation of liver tissues was detected by immunohistochemical staining. The streptavidin/peroxidase method (Zhongshan Goldenbridge, LTD, Beijing, China, PV-9000) was used to detect the immunoreactivity. Each section was placed in 3% H_2O_2 in methanol and covered with anti-NF-κB p65 (Cell Signaling Technology, Danvers, MA, #8242). Then, peroxidase was visualized by incubation with Diaminobenzidine (DAPI, ZLI-9017) and counterstaining was done with hematoxylin. Slides were viewed through a DFC7000 T color microscope camera. Semiquantitative analysis was performed using ImageJ software.

RAW264.7 cells were incubated with ConA and then rinsed, fixed, permeabilized and incubated primary anti-NF-κB p65, followed by Alexa Fluor 555 (Thermo Fisher, MA, United States, A31572). Then counterstained with DAPI nuclear stain. Data of 1,000 cells per sample were acquired by an Amnis ImageStream X Mark II imaging flow cytometer (Amnis Corporation, Seattle, WA). IDEAS software was used to show brightfield images and obtain the proportions of NF-κB nuclear localization.

Statistical analysis

All results were analyzed by SPSS software version 24.0 (SPSS Inc., Chicago, Illinois, United States), and data represented using GraphPad Prism Software 8.0 (San Diego, CA, United States). Values in figures are given as means ± SD if not otherwise indicated. Statistical significance was determined by one-way analysis of variance (ANOVA) for multiple comparisons. $p < 0.05$ was considered to be significant.

Results

CP-25 attenuated ConA-induced hepatitis

To investigate the effects of CP-25 on hepatitis, mice received an intragastric administration of CP-25 (25, 50 and 100 mg/kg) and intravenous tail injection of 25 mg/kg ConA (Figure 1A). Our results showed that the liver, spleen and thymus indices were increased post ConA injection. CP-25 (50, 100 mg/kg) gradually declined the above indices, and the liver and thymus indices in CP-25 100 mg/kg group were obviously reduced compared with the equal dose of paeoniflorin (Figures 1B–D). In addition, H&E staining observed visible histopathological changes of model mice, such as disorganized cell arrangement, necrosis with extensive inflammatory infiltration and hepatocyte nuclear lysis (Figure 1E), CP-25 treatment gradually alleviated the degree of liver injury. To further support histological analysis, the activities of AST and ALT were significantly elevated in liver injury mice (Figure 1F). CP-25 (50, 100 mg/kg) treated mice showed reduced AST and ALT activity. Additionally, CP-25 at 100 mg/kg obviously decreased AST activity as compared to the same dosage of paeoniflorin. These data preliminarily suggested a protective effect of CP-25 on ConA-induced hepatitis.

CP-25 ameliorated T cells activation in hepatitis

Inflammatory immune dysfunction supports the development of hepatitis (Zhao et al., 2020). Therefore, we used CCK-8 to test the T cell viability, which was markedly higher in ConA-injected mice than in normal mice (Figure 2A). But CP-25 (50, 100 mg/kg) treatment groups significantly reversed the changes of T cell viability in hepatitis.

T cell-mediated immune responses are thought to be involved in the process of ConA-induced hepatitis. To determine whether CP-25 altered T cell subsets in spleen, the proportion of $CD3^+CD4^+$, $CD3^+CD8^+$, activated $CD4^+$ ($CD4^+CD69^+$), activated $CD8^+$ ($CD8^+CD69^+$), $CD4^+IFN\text{-}\gamma^+$ (Th1 cells) and $CD4^+IL\text{-}4^+$ (Th2 cells) T cells were examined by flow cytometry (Figures 2B–H). The proportions of $CD4^+$, $CD8^+$, activated $CD8^+$, activated $CD4^+$ T cells and the ratio of

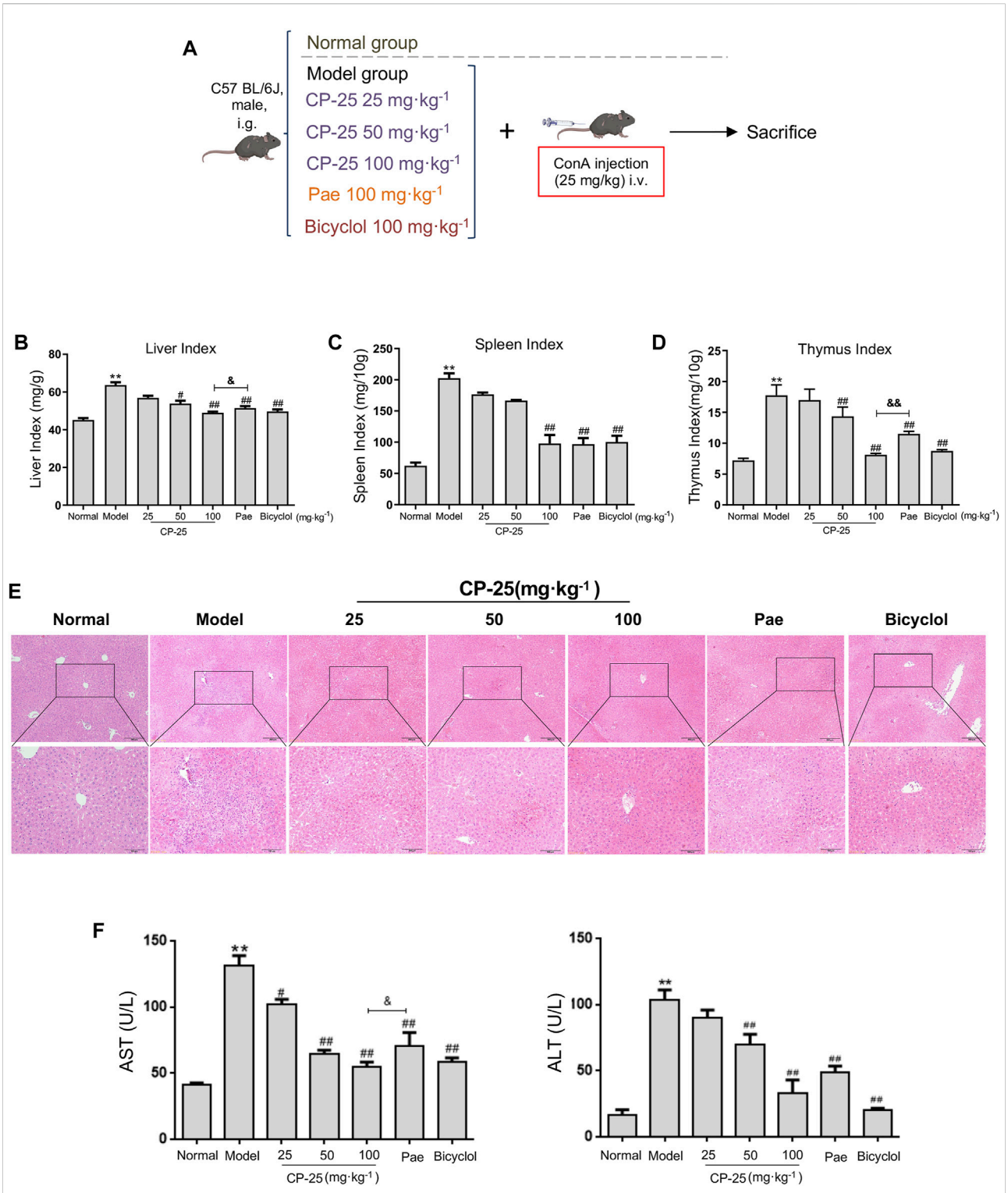

FIGURE 1
CP-25 attenuated ConA induced hepatitis. **(A)** ConA-induced hepatitis model and pretreatment of drugs. **(B)** Liver index. **(C)** Spleen index. **(D)** Thymus index. **(E)** The photomicrographs are of representative H&E-stained liver tissues after ConA injection of mice. **(F)** The serum AST and ALT activities. Data were representative as the means ± SD. $^{**}p < 0.01$ *versus* normal, $^{\#}p < 0.05$, $^{\#\#}p < 0.01$ *versus* model, $^{\&}p < 0.05$, $^{\&\&}p < 0.01$ *versus* paeoniflorin.

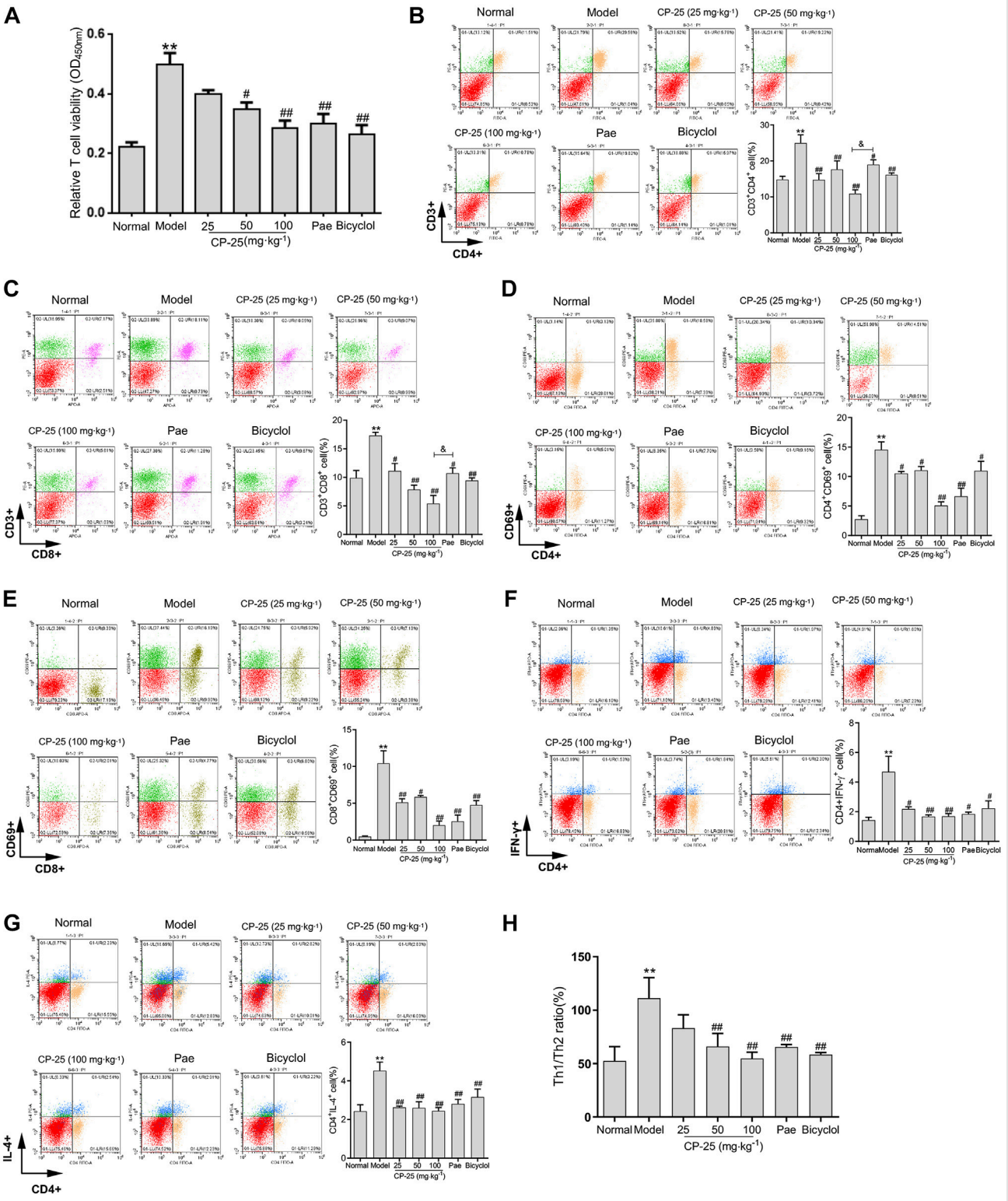

FIGURE 2
CP-25 ameliorated T cells activation in hepatitis. **(A)** The CCK-8 absorbance values of T cells from mice thymus. Flow cytometry analysis of single-cell suspensions of live immunocytes, which were isolated from freshly dissociated spleen of mice injected with ConA. The representative pictures and bar graphs showed the percentages of $CD3^+CD4^+$ T cell **(B)**, $CD3^+CD8^+$ T cell **(C)**, activated $CD4^+$ T cell **(D)**, activated $CD8^+$ T cell **(E)**, Th1 **(F)** and Th2 **(G)** cells. And the ratio of Th1/Th2 on each group **(H)**. Data of each marker were expressed as the mean ± SD at least three independent experiments. $^{**}p < 0.01$ *versus* normal, $^{\#}p < 0.05$, $^{\#\#}p < 0.01$ *versus* model, $^{\&}p < 0.05$ *versus* paeoniflorin.

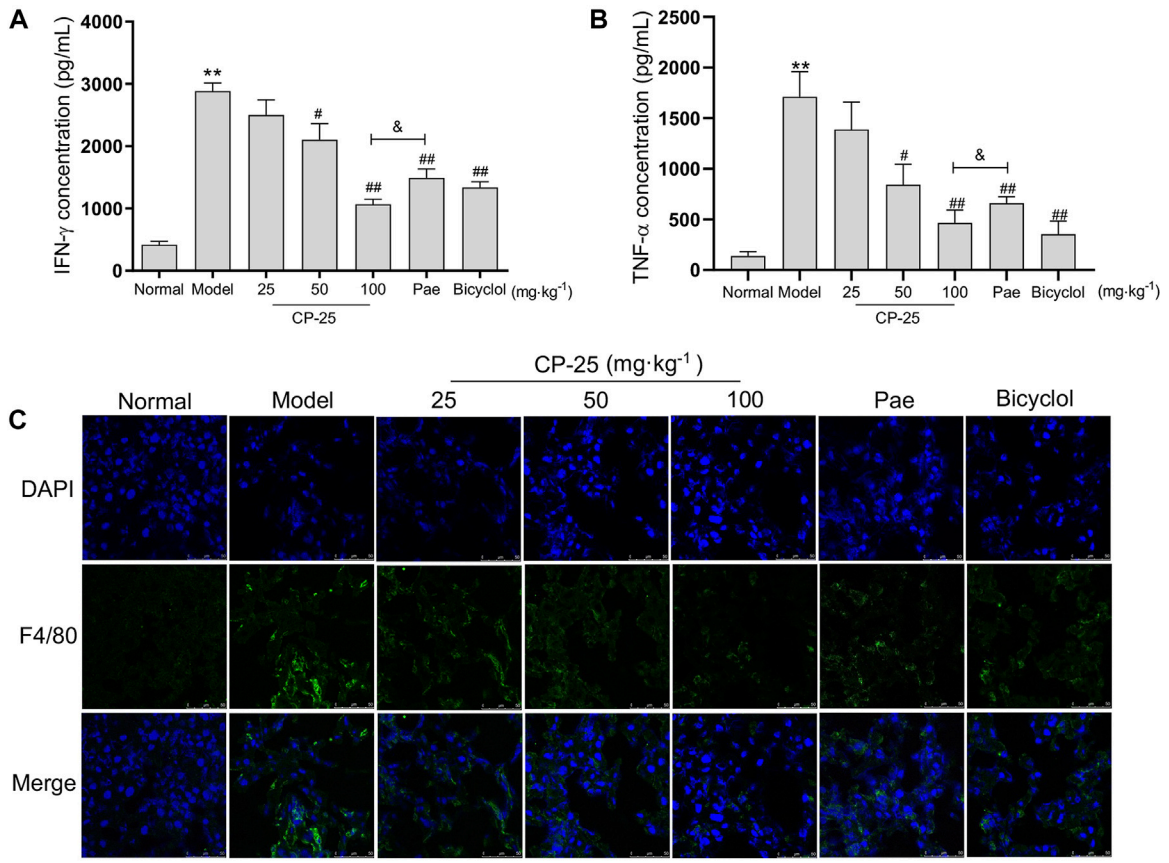

FIGURE 3
CP-25 down-regulated the inflammatory cytokines release in ConA-induced hepatitis. Comparison inflammatory factor expressions of IFN-γ **(A)** and TNF-α **(B)** in liver homogenate by ELISA. **(C)** Representative images showed the F4/80 positive staining cells (green) in liver sections by immunofluorescence (Scale bar = 50 μm). $^{**}p < 0.01$ *versus* normal, $^{\#}p < 0.05$, $^{\#\#}p < 0.01$ *versus* model, $^{\&}p < 0.05$ *versus* paeoniflorin.

Th1/Th2 were obviously elevated in hepatitis. In contrast, CP-25 treatment gradually down-regulated the proportions of $CD4^+$, $CD8^+$, activated $CD4^+$, activated $CD8^+$ T cells and the Th1/Th2 ratio. Moreover, the proportions of $CD4^+$ and $CD8^+$ T cells were significantly lower in CP-25 (100 mg/kg) administration than in the same dosage of paeoniflorin. These data suggested that CP-25 might attenuate T cell-mediated immune response through inhibiting the ratio of Th1/Th2 in hepatitis.

CP-25 down-regulated the inflammatory cytokines release in ConA-induced hepatitis

To further characterize CP-25 has a protective effect on inflammation in ConA-induced hepatitis, the production of IFN-γ and TNF-α were measured by ELISA (Figures 3A,B). ConA injection elevated the levels of IFN-γ and TNF-α, but CP-25 at dose of 50 and 100 mg/kg treatment suppressed the release of inflammatory cytokines. More importantly, mice given CP-25 (100 mg/kg) by oral gavage displayed lower levels of TNF-α and IFN-γ than mice treated with the equal dose of paeoniflorin. Due to macrophages are major sources of inflammatory cytokines during liver injury, hence we next analyzed the accumulation of macrophages (F4/80) in liver tissues by immunofluorescence staining (Figure 3C). Immunofluorescence staining showed an increase of F4/80 in ConA-injected mice compared to normal mice. However, CP-25 treatment suppressed ConA-induced F4/80 accumulation. Based on the above results, CP-25 might alleviate ConA-induced hepatitis via suppressing inflammatory cytokines release.

CP-25 inhibited the activation of MAPK pathway and nuclear translocation of NF-κB mediated by ROS *in vivo*

Since ROS acts as secondary messenger affecting macrophage activation leading to inflammatory cytokines secretion (Du et al., 2020), the results of ROS level in liver

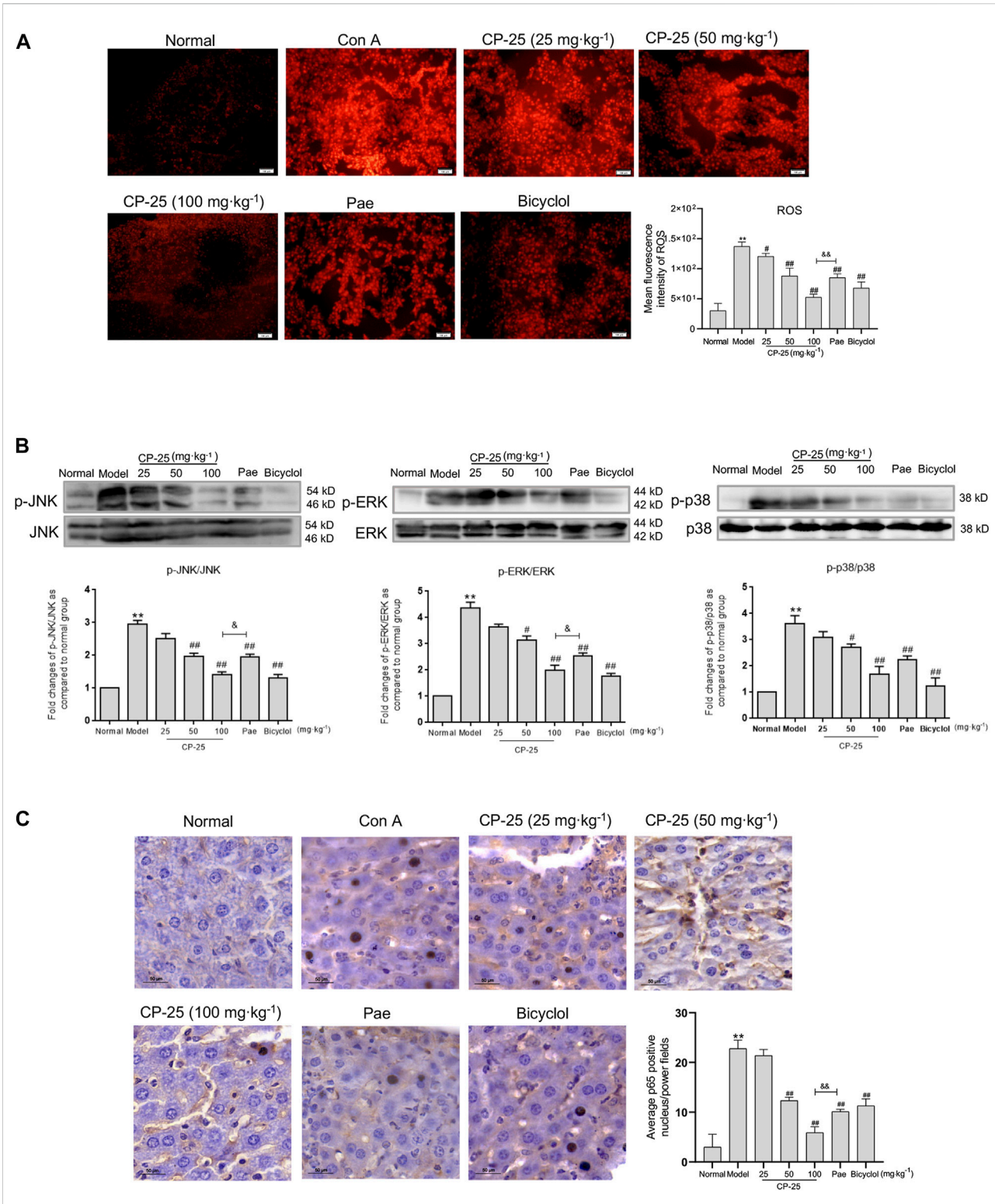

FIGURE 4
CP-25 inhibited the activation of MAPK pathway and nuclear translocation of NF-κB mediated by ROS *in vivo*. **(A)** Representative micrographs of ROS production in liver tissues were stained with DHE (Scale bar = 100 μm), and was quantitated by measuring the fluorescence intensity. **(B)** Representative immunoblotting bands of p-JNK, p-ERK and p-p38 in ConA-injected mice were showed, the semi-quantitative analysis was shown as the bar diagram. Densitometry values were expressed as-fold change relative to the normal group. **(C)** Representative images of NF-κB nuclear translocation in liver tissues were detected by immunohistochemistry staining (Scale bar = 50 μm). Results from three independent experiments are reported as the means ± SD. $^{**}p < 0.01$ *versus* normal, $^{\#}p < 0.05$, $^{\#\#}p < 0.01$ *versus* model, $^{\&}p < 0.05$, $^{\&\&}p < 0.01$ *versus* paeoniflorin.

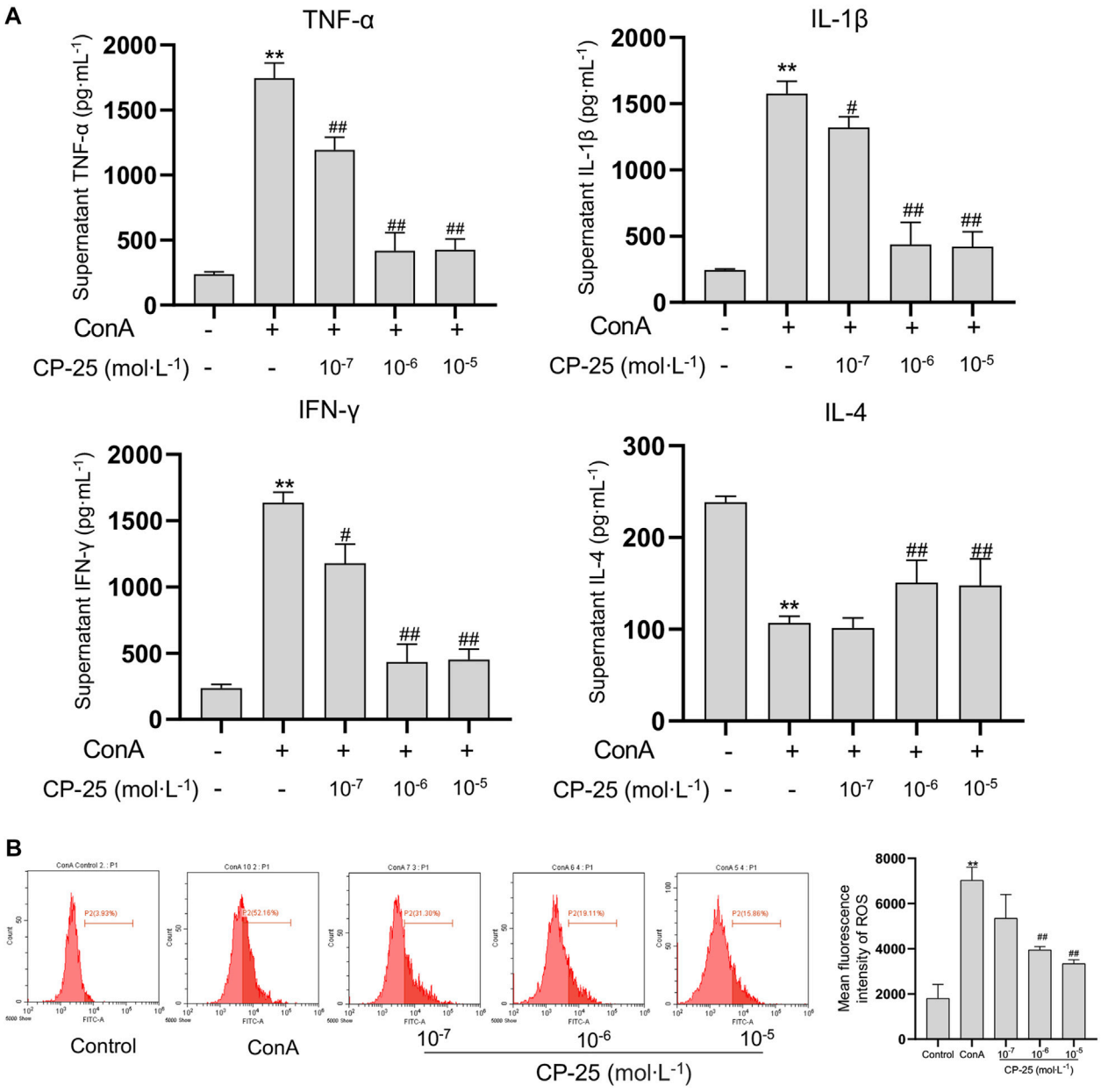

FIGURE 5
CP-25 inhibited inflammatory cytokines and ROS release in RAW264.7 cells. **(A)** Comparison inflammatory cytokine levels of TNF-α, IL-1β, IFN-γ and IL-4 in the supernatant of RAW264.7 cells by ELISA. **(B)** Decreased ROS levels were observed in CP-25 administrated RAW264.7 cells. $^{**}p < 0.01$ *versus* control, $^{\#}p < 0.05$, $^{\#\#}p < 0.01$ *versus* ConA. Data were showed as the mean ± SD of three independent experiments.

tissues were showed in Figure 4A. ROS level was significantly upregulated in livers of ConA-injected mice, but CP-25 treatment downregulated the increased level of ROS. Researches have demonstrated that ROS induced the phosphorylation of downstream MAPK pathway (Gong et al., 2019; Wu et al., 2021). Additionally, NF-κB has been proposed to be the sensor for oxidative stress that can be activated by ROS (Morgan and Liu, 2011). When exogenous inducers were applied into cells, NF-κB dissociated from the cytoplasmic complex and translocated to the nucleus, which contributed to inflammatory cytokines production (Giustarini et al., 2020). Therefore, we detected MAPK activation and NF-κB nuclear colocalization in liver tissues. ConA-stimulated group exhibited that upregulated phosphorylation of MAPK pathways and increased nuclear translocation of NF-κB, but CP-25 treatment suppressed MAPK pathway activation and

NF-κB nuclear translocation (Figures 4B,C). In addition, the highest dosage of CP-25 could obviously disrupt the levels of ROS, p-JNK, p-ERK and NF-κB nuclear translocation compared to the same dosage of paeoniflorin. These data indicated that CP-25 suppressed inflammation of hepatitis may be associated with down-regulating the MAPK activation and NF-κB nuclear translocation influenced by ROS.

CP-25 inhibited inflammatory cytokines and ROS release in RAW264.7 cells

Due to macrophages play an essential role in initiating inflammation, we utilized RAW264.7 cells *in vitro* to evaluate the anti-inflammatory effect of CP-25 (Wang et al., 2019). The levels of cytokines including IL-1β, TNF-α, IL-4 and IFN-γ were examined to verify whether CP-25 regulated inflammatory cytokines production *in vitro*. Results showed that ConA stimulation upregulated IL-1β, TNF-α and IFN-γ production, but reduced IL-4 release in RAW264.7 cells as compared to the untreated cells (Figure 5A). Furthermore, CP-25 treatment reversed the changes of inflammatory cytokines levels caused by ConA. Research showed that ROS as an effective molecule for determining the extent of inflammation (Ma et al., 2018). Hence the DCFH-DA fluorescent probe was used to detect ROS formation in ConA-stimulated RAW264.7 cells. The results showed that ConA stimulation significantly increased ROS production compared to the controls, while CP-25 (10^{-6}–10^{-5} mol/L) ameliorated ROS production (Figure 5B). These data showed that CP-25 may inhibit inflammatory cytokines secretion accompanied with down-regulating ROS production in RAW264.7 cells.

CP-25 suppressed ROS influenced MAPK pathway activation and NF-κB nuclear translocation in RAW264.7 cells

To further examine whether CP-25 has an effect on ConA-induced MAPK activation and NF-κB nuclear translocation *in vitro*. The activation of MAPK pathway was detected by Western blot and the nuclear localization of NF-κB was examined by imaging flow cytometry. Results showed that ConA stimulation significantly up-regulated phosphorylation of MAPK pathways and nuclear localization of NF-κB compared to the controls (Figures 6A,B). CP-25 supplementation reduced the phosphorylation of MAPK signaling pathways and the proportion of NF-κB nuclear localization, which suggested that CP-25 could suppress inflammation may be through inhibiting MAPK activation and NF-κB nuclear localization in macrophages.

Discussion

Hepatitis has been risen worldwide mainly due to exogenous substances (drug misuse, alcohol abuse, toxins), disease or external stimuli (viral infection, COVID-19), and others, which threatened human health recent decades (Liu et al., 2022). ConA-induced hepatitis was first established in 1992, which is now the most widely used tool to reveal liver injury in mice (Tiegs et al., 1992). Advanced evidence confirmed that various degrees of oxidative stress, inflammation, and necrosis could impair tissue function and integrity in ConA-treated mice (Khan et al., 2021). ConA altered cellular metabolic processes, which was contributed to disrupting oxidative phosphorylation and aggravating mitochondrial damage. Exhausted energy storage and accelerated production of ROS would cause damage to macrophages (Zanluqui et al., 2020). In this study, hepatitis model was established by intravenous injection of ConA and to explore the potential effect of CP-25. Pretreatment of CP-25 (100 mg/kg) exerted obviously hepatoprotective effects compared to the equal dose of paeoniflorin, includes reduced necrotic areas, decreased inflammatory cell infiltration.

CP-25, a novel ester from structural modification of paeoniflorin, has been shown to obviously anti-inflammatory activity in various diseases. Both in collagen and adjuvant-induced arthritis, CP-25 exhibited powerful anti-inflammatory and immunoregulatory effects and attenuated synovium inflammation (Chen et al., 2018; Wang et al., 2018). Furthermore, CP-25 alleviated kidney injuries in rats with arthritis through reducing the number of renal $CD68^+$ cells and downregulating the levels of TNF-α and IL-6 (Wang et al., 2020). As we all known $CD4^+$ cells are T helper cells which could differentiate into several subpopulations, and the activated $CD8^+$ T cell subsets generally perform cytotoxic T cell functions (Basu et al., 2021). Research determined that the upregulated ratio of $CD4^+/CD8^+$ occurred the pivotal contributing factor in autoimmune diseases, virus infections and cancers. It was obvious that bulk $CD4^+$ T cells differentiated into Th1 and Th2 subsets during autoimmune diseases progression (Zolfaghari et al., 2021). Th1 cells secreted Th1-type cytokines, such as IFN-γ, which positively fed back to promote further T cell differentiation and proliferation, and were associated to the cellular immunity response. Th2 cells could produce IL-4, which mainly participated in the humoral immunity in pathogenesis of autoimmune diseases. The dysregulation of Th1/Th2 would contribute to immunologic disease, such as osteoarthritis, hepatitis, type-1 diabetes and COVID-19 pandemic. Additionally, CP-25 reduced the infiltration of Th1/Th2 cells, and reduced inflammatory cytokines production in autoantigen-induced Sjögren's syndrome mice (Gu et al., 2018). Then, we paid more attention on the relationship between CP-25 and T cell activation in ConA-induced hepatitis. The results confirmed that CP-25 treated mice performed a lower proportion of

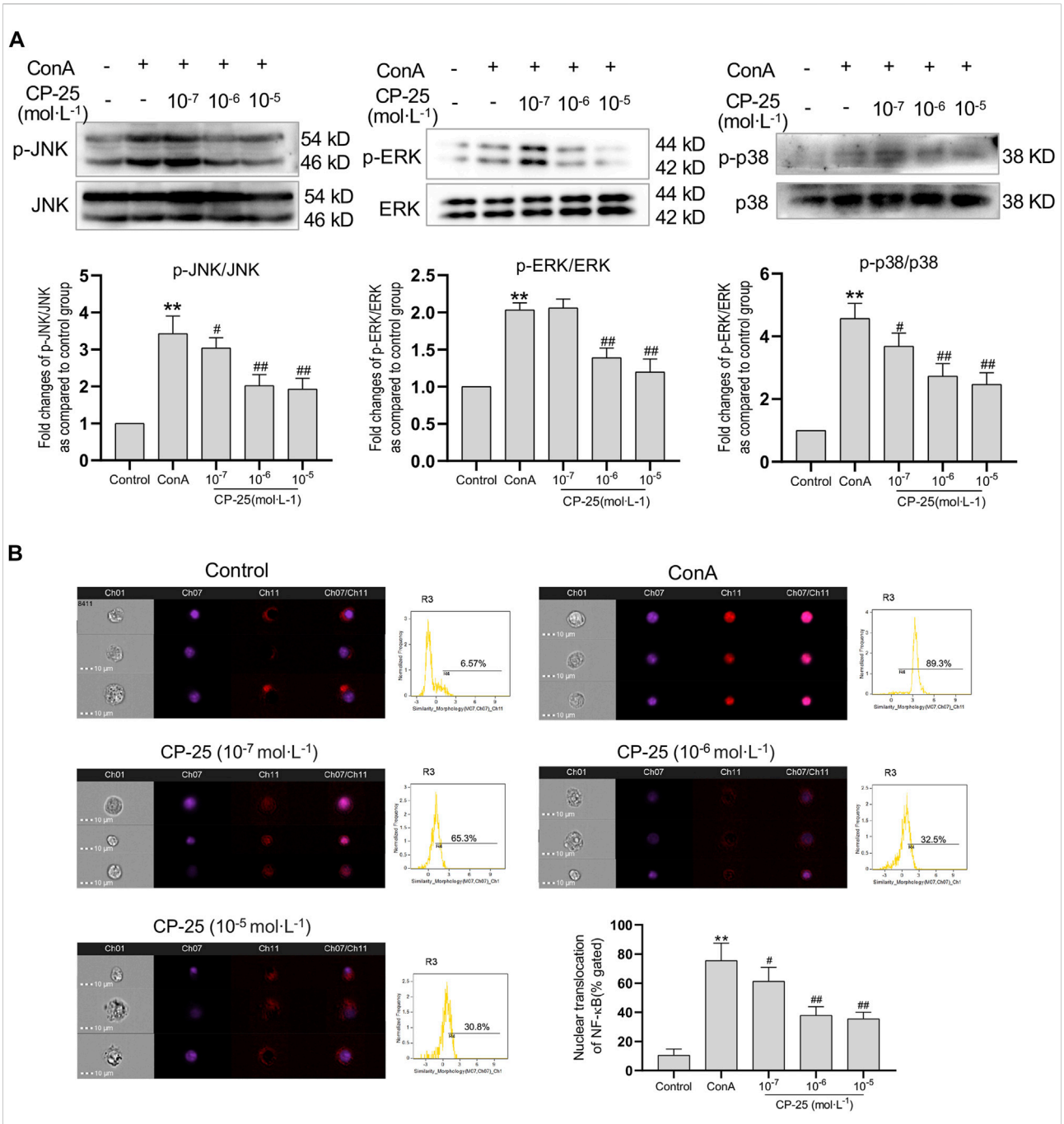

FIGURE 6
CP-25 suppressed ROS influenced MAPK pathway activation and NF-κB nuclear translocation in RAW264.7 cells. **(A)** Representative immunoblotting bands of p-JNK, p-ERK and p-p38 in ConA-stimulated RAW264.7 cells. Data were expressed as-fold change relative to the control group, which was assigned as a value of 1. **(B)** NF-κB nuclear colocalization in CP-25-administrated RAW264.7 cell was analyzed by image flow cytometry, and representative images were shown including brightfield, NF-κB (red), nucleus (purple), and merged images (Scale bars = 10 μm), and statistic results were shown. $^{**}p < 0.01$ *versus* control, $^{\#}p < 0.05$, $^{\#\#}p < 0.01$ *versus* ConA. Data were expressed as the mean ± SD from three independent experiments.

activated $CD4^+$, $CD8^+$ T lymphocytes and the ratio of Th1/Th2 than in ConA-injected mice. Furthermore, the highest dosage of CP-25 significantly reduced the proportion of $CD4^+$ and $CD8^+$ T cells compared with the same dosage of paeoniflorin group. These results indicated that CP-25 attenuated ConA-induced hepatitis may through modulating immune responses.

It is well-known that pro-inflammatory cytokines secretion could amplify inflammatory responses in immune cells (Feng et al., 2021). Our present findings occurred that CP-25 reduced inflammatory cytokines production and ROS levels in ConA-induced hepatitis. A sensible reduction in inflammation and ROS production was determined in CP-25 (100 mg/kg) treated mice compared with the equal dose of paeoniflorin. Paeoniflorin has been reported that inhibited TNF-α expression in BCG plus LPS induced liver injury (Liu et al., 2006). And other study revealed that CP-25 concentration was higher in liver tissue compared to paeoniflorin due to its elevated oral bioavailability (Zhao et al., 2019). Research supported that there was a positive correlation between ROS elevation and inflammation related pathways activation (Brennan and Gilmore, 2018; Yunrong Yang et al., 2022). And oxidative stress was happened accompanied by excessive ROS levels, which acting as signaling molecules contributing to abnormal cell growth, metastasis, disordered function, as well as enlarged proinflammatory cytokines production, allowing inflammation to progress (Li et al., 2020). Research showed that excessive ROS production may contribute to M1-like pro-inflammatory macrophages during the development of diabetes (Wada et al., 2017; Rendra et al., 2019). CP-25 regulated macrophage polarization from a M1 to a M2 phenotype to attenuate DSS-induced colitis and inhibited IL-1β and IL-18 production in mice (Li et al., 2021). As expected, our study determined that F4/80 positive staining was enhanced in hepatitis and decreased after CP-25 administration. Meanwhile, CP-25 treatment inhibited ROS production accompanied with down-regulation of inflammatory cytokines. Therefore, we speculated that CP-25 may protect hepatitis through prevention of ROS-mediated inflammatory cytokines released.

Then we identified the underlying mechanisms related to anti-inflammatory effects of CP-25 in hepatitis. The activation of MAPK was involved in macrophages accumulation, release of inflammatory factors and chemokine expression, which was involved in regulating tissue inflammation (Zhang et al., 2017). Studies presented that Zeaxanthin could induce a mass apoptosis of gastric cancer cells following by activation of ROS-mediated MAPK and NF-κB signaling pathways (Sheng et al., 2020). Another research demonstrated klotho downregulated inflammatory responses through inactivation of ROS/p38 MAPK pathways, leading to alleviate paraquat-induced lung injury (Zhang P et al., 2020). In present experiment, we demonstrated that CP-25 decreased the activation of MAPK signaling pathways. Besides there was compelling evidence to suggest that NF-κB could be activated by various stimuli including excessive ROS. H_2O_2 could rapidly activate NF-κB, which participated in ROS-induced cell death (Lingappan, 2018; Tian et al., 2021). It has been reported that sub-anesthetic ISO post-conditioning decreased the inflammation in OGD-insulted microglia partly *via* blocking ROS-NF-κB signaling pathways (Yao et al., 2020). Moreover, the NF-κB molecules were usually retained in cytoplasm in untreated cells. Upon stimulation, NF-κB p65 was able to migrate from the cytoplasm into the nucleus (Zinatizadeh et al., 2021). NF-κB p65 translocation promoted alveolar hypercoagulation and fibrinolysis in LPS-induced acute respiratory distress syndrome mice (Wu et al., 2020). NF-κB p65 has the tendency of translocation towards nucleus in LPS-induced BV2 cells to support the transcription of downstream pro-inflammatory factors such as IL-1β (Chen et al., 2022). Once activated by stimulators, NF-κB translocated into nucleus and involved in pro-inflammatory cytokines production (Luo et al., 2022). And in our results, CP-25 inhibited NF-κB nuclear translocation *in vivo* and *in vitro*. We supposed that the protective mechanisms of CP-25 against hepatitis had a direct relation to shut down ROS influenced MAPK activation and NF-κB nuclear translocation.

Conclusion

In summary, our present data suggested that the protective effects of CP-25 administration on ConA-induced hepatitis through inhibiting immune response and inflammatory cytokines production. The underlying mechanism of CP-25 may relate to regulate ROS influenced MAPK activation and NF-κB nuclear translocation. Our studies contribute to providing new insights into the pathogenesis of hepatitis, and future research will focus on CP-25 as a potential therapeutic candidate for the treatment of hepatitis.

Data availability statement

The original contributions presented in the study are included in the article/supplementary material, further inquiries can be directed to the corresponding authors.

Ethics statement

The animal study was reviewed and approved by the Ethics Review Committee for Animal Experimentation of Anhui Medical University.

Author contributions

NL wrote the manuscript and prepared the figures. JW, MQ, SZ, ZW and XL conducted the experiments and collected the data. TC and MW analyzed the data. LZ, WW and WS contributed to the conception and design of the study, and revised the manuscript. All authors have read and approved the final manuscript.

Funding

This work was supported by grants from the National Natural Science Foundation of China (No.81770605), Research Level Improvement Program of Anhui Medical University (No.2021xkjT016), Postgraduate Innovation Research and Practice Program of Anhui Medical University (No.YJS20210262), Anhui Provincial Natural Science Foundation (No.2008085QH413), Open Fund of Key Laboratory of Antiinflammatory and Immune Medicine, Ministry of Education, P.R. China (No.KFJJ-2020-10). The authors acknowledge the help of the staff members of the Institute of Clinical Pharmacology, Anhui Medical University.

Conflict of interest

The authors declare that the research was conducted in the absence of any commercial or financial relationships that could be construed as a potential conflict of interest.

Publisher's note

All claims expressed in this article are solely those of the authors and do not necessarily represent those of their affiliated organizations, or those of the publisher, the editors and the reviewers. Any product that may be evaluated in this article, or claim that may be made by its manufacturer, is not guaranteed or endorsed by the publisher.

References

Basu, A., Ramamoorthi, G., Albert, G., Gallen, C., Beyer, A., Snyder, C. G., et al. (2021). Differentiation and regulation of TH cells: A balancing act for cancer immunotherapy. *Front. Immunol.* 12, 669474. doi:10.3389/fimmu.2021.669474

Brennan, J. J., and Gilmore, T. D. (2018). Evolutionary origins of Toll-like receptor signaling. *Mol. Biol. Evol.* 35 (7), 1576–1587. doi:10.1093/molbev/msy050

Chang, Y., Jia, X., Wei, F., Wang, C., Sun, X., Xu, S., et al. (2016). CP-25, a novel compound, protects against autoimmune arthritis by modulating immune mediators of inflammation and bone damage. *Sci. Rep.* 6, 26239. doi:10.1038/srep26239

Chen, J., Wang, Y., Wu, H., Yan, S., Chang, Y., and Wei, W. (2018). A modified compound from paeoniflorin, CP-25, suppressed immune responses and synovium inflammation in collagen-induced arthritis mice. *Front. Pharmacol.* 9, 563. doi:10.3389/fphar.2018.00563

Chen, S., Liu, H., Wang, S., Jiang, H., Gao, L., Wang, L., et al. (2022). The neuroprotection of verbascoside in alzheimer's disease mediated through mitigation of neuroinflammation via blocking NF-κB-p65 signaling. *Nutrients* 14 (7), 1417. doi:10.3390/nu14071417

Du, J. J., Sun, J. C., Li, N., Li, X. Q., Sun, W. Y., and Wei, W. (2020). β-Arrestin2 deficiency attenuates oxidative stress in mouse hepatic fibrosis through modulation of NOX4. *Acta Pharmacol. Sin.* 42 (7), 1090–1100. doi:10.1038/s41401-020-00545-9

Feng, J. Y., Su, W. J., Chuang, F. Y., Pan, S. W., Yeh, Y. C., Lin, Y. Y., et al. (2021). TREM-1 enhances Mycobacterium tuberculosis-induced inflammatory responses in macrophages. *Microbes Infect.* 23 (1), 104765. doi:10.1016/j.micinf.2020.10.001

Giustarini, G., Huppelschoten, S., Barra, M., Oppelt, A., Wagenaar, L., Weaver, R. J. M., et al. (2020). The hepatotoxic fluoroquinolone trovafloxacin disturbs TNF- and LPS-induced p65 nuclear translocation *in vivo* and *in vitro*. *Toxicol. Appl. Pharmacol.* 391, 114915. doi:10.1016/j.taap.2020.114915

Gong, L., Lei, Y., Liu, Y., Tan, F., Li, S., Wang, X., et al. (2019). Vaccarin prevents ox-LDL-induced HUVEC EndMT, inflammation and apoptosis by suppressing ROS/p38 MAPK signaling. *Am. J. Transl. Res.* 11 (4), 2140–2154. https://www.ncbi.nlm.nih.gov/pmc/articles/PMC6511755/

Graham, J. J., Longhi, M. S., and Heneghan, M. A. (2021). T helper cell immunity in pregnancy and influence on autoimmune disease progression. *J. Autoimmun.* 121, 102651. doi:10.1016/j.jaut.2021.102651

Gu, F., Xu, S., Zhang, P., Chen, X., Wu, Y., Wang, C. M., et al. (2018). CP-25 alleviates experimental Sjogren's Syndrome features in NOD/Ltj mice and modulates T lymphocyte subsets. *Basic Clin Pharmacol Toxicol* 123 (4), 423–434.

Jothimani, D., Venugopal, R., Abedin, M. F., Kaliamoorthy, I., and Rela, M. (2020). COVID-19 and the liver. *J. Hepatol* 73 (5), 1231–1240. doi:10.1016/j.jhep.2020.06.006

Karki, R., Sharma, B. R., Tuladhar, S., Williams, E. P., Zalduondo, L., Samir, P., et al. (2021). Synergism of TNF-alpha and IFN-gamma triggers inflammatory cell death, tissue damage, and mortality in SARS-CoV-2 infection and cytokine shock syndromes. *Cell* 184 (1), 149–168.e17. doi:10.1016/j.cell.2020.11.025

Khan, H. A., Munir, T., Khan, J. A., Gul, A. H. S. T., Ahmad, M. Z., Aslam, M. A., et al. (2021). IL-33 ameliorates liver injury and inflammation in Poly I:C and Concanavalin-A induced acute hepatitis. *Microb. Pathog.* 150, 104716. doi:10.1016/j.micpath.2020.104716

Kubes, P., and Jenne, C. (2018). Immune responses in the liver. *Annu. Rev. Immunol.* 36, 247–277. doi:10.1146/annurev-immunol-051116-052415

Li, Y., Chen, X., Zhang, H., Xiao, J., Yang, C., Chen, W., et al. (2020). 4-Octyl itaconate alleviates lipopolysaccharide-induced acute lung injury in mice by inhibiting oxidative stress and inflammation. *Drug Des. Devel. Ther.* 14, 5547–5558. doi:10.2147/DDDT.S280922

Li, Y., Jiang, M. Y., Chen, J. Y., Xu, Z. W., Zhang, J. W., Li, T., et al. (2021). CP-25 exerts therapeutic effects in mice with dextran sodium sulfate-induced colitis by inhibiting GRK2 translocation to downregulate the TLR4-NF-κB-NLRP3 inflammasome signaling pathway in macrophages. *IUBMB Life* 73 (12), 1406–1422. doi:10.1002/iub.2564

Lingappan, K. (2018). NF-kappaB in oxidative stress. *Curr Opin Toxicol.* 7, 81–86. doi:10.1016/j.cotox.2017.11.002

Liu, D. F., Wei, W., and Song, L. H. (2006). Protective effect of paeoniflorin on immunological liver injury induced by bacillus calmette-guerin plus lipopolysaccharide: modulation of tumour necrosis factor-alpha and interleukin-6 MRNA. *Clin. Exp. Pharmacol. Physiol.* 33 (4), 332–339. doi:10.1111/j.1440-1681.2006.04371.x

Liu, M., Huang, Q., Zhu, Y., Chen, L., Li, Y., Gong, Z., et al. (2022). Harnessing reactive oxygen/nitrogen species and inflammation: Nanodrugs for liver injury. *Mat. Today. Bio* 13, 100215. doi:10.1016/j.mtbio.2022.100215

Luo, X., Bao, X., Weng, X., Bai, X., Feng, Y., Huang, J., et al. (2022). The protective effect of quercetin on macrophage pyroptosis via TLR2/Myd88/NF-κB and ROS/AMPK pathway. *Life Sci.* 291, 120064. doi:10.1016/j.lfs.2021.120064

Ma, Y. F., Tang, T., Sheng, L. L., Wang, Z. Q., Tao, H., Zhang, Q., et al. (2018). Aloin suppresses lipopolysaccharide-induced inflammation by inhibiting JAK1-STAT1/3 activation and ROS production in RAW264.7 cells. *Int. J. Mol. Med.* 42 (4), 1925–1934. doi:10.3892/ijmm.2018.3796

Morgan, M. J., and Liu, Z. G. (2011). Crosstalk of reactive oxygen species and NF-κB signaling. *Cell Res.* 21 (1), 103–115. doi:10.1038/cr.2010.178

Rani, R., Kumar, S., Sharma, A., Mohanty, S. K., Donnelly, B., Tiao, G. M., et al. (2018). Mechanisms of Concanavalin A-induced cytokine synthesis by hepatic stellate cells: Distinct roles of interferon regulatory factor-1 in liver injury. *J. Biol. Chem.* 293 (48), 18466–18476. doi:10.1074/jbc.RA118.005583

Rendra, E., Riabov, V., Mossel, D. M., Sevastyanova, T., Harmsen, M. C., and Kzhyshkowska, J. (2019). Reactive oxygen species (ROS) in macrophage activation and function in diabetes. *Immunobiology* 224 (2), 242–253. doi:10.1016/j.imbio.2018.11.010

Sheng, Y. N., Luo, Y. H., Liu, S. B., Xu, W. T., Zhang, Y., Zhang, T., et al. (2020). Zeaxanthin induces apoptosis via ROS-regulated MAPK and AKT signaling pathway in human gastric cancer cells. *Onco. Targets. Ther.* 13, 10995–11006. doi:10.2147/OTT.S272514

Sun, J. C., Du, J. J., Li, X. Q., Li, N., Wei, W., and Sun, W. Y. (2020). Depletion of beta-arrestin 2 protects against CCl_4-induced liver injury in mice. *Biochem. Biophys. Res. Commun.* 522 (2), 485–491. doi:10.1016/j.bbrc.2019.11.093

Sun, W. Y., Gu, Y. J., Li, X. R., Sun, J. C., Du, J. J., Chen, J. Y., et al. (2020). β-arrestin2 deficiency protects against hepatic fibrosis in mice and prevents synthesis of extracellular matrix. *Cell Death Dis.* 11 (5), 389. doi:10.1038/s41419-020-2596-8

Sun, W. Y., Wang, L., Liu, H., Li, X., and Wei, W. (2012). A standardized extract from Paeonia lactiflora and Astragalus membranaceus attenuates liver fibrosis induced by porcine serum in rats. *Int. J. Mol. Med.* 29 (3), 491–498. doi:10.3892/ijmm.2011.844

Tian, W., Heo, S., Kim, D. W., Kim, I. S., Ahn, D., Tae, H. J., et al. (2021). Ethanol extract of maclura tricuspidata fruit protects SH-SY5Y neuroblastoma cells against H_2O_2-induced oxidative damage via inhibiting MAPK and NF-kappaB signaling. *Int. J. Mol. Sci.* 22 (13), 6946. doi:10.3390/ijms22136946

Tiegs, G., Hentschel, J., and Wendel, A. (1992). A T cell-dependent experimental liver injury in mice inducible by concanavalin A. *J. Clin. Invest.* 90 (1), 196–203. doi:10.1172/JCI115836

Wada, T., Ishikawa, A., Watanabe, E., Nakamura, Y., Aruga, Y., Hasegawa, H., et al. (2017). Eplerenone prevented obesity-induced inflammasome activation and glucose intolerance. *J. Endocrinol.* 235 (3), 179–191. doi:10.1530/JOE-17-0351

Wang, C., Wei, X., Wu, Y., Tang, H., Wang, B., Wang, Y., et al. (2020). CP-25 improves nephropathy in collagen-induced arthritis rats by inhibiting the renal inflammatory response. *Int. Immunopharmacol.* 88, 106997. doi:10.1016/j.intimp.2020.106997

Wang, Y., Han, C. C., Cui, D., Luo, T. T., Li, Y., Zhang, Y., et al. (2018). Immunomodulatory effects of CP-25 on splenic T cells of rats with adjuvant arthritis. *Inflammation* 41 (3), 1049–1063. doi:10.1007/s10753-018-0757-z

Wang, Y. Q., Lan, Y. Y., Guo, Y. C., Yuan, Q. W., and Liu, P. (2019). Down-regulation of microRNA-138 improves immunologic function via negatively targeting p53 by regulating liver macrophage in mice with acute liver failure. *Biosci. Rep.* 39 (7), BSR20190763. doi:10.1042/BSR20190763

Wu, D., Liu, Z., Wang, Y., Zhang, Q., Li, J., Zhong, P., et al. (2021). Epigallocatechin-3-Gallate alleviates high-fat diet-induced nonalcoholic fatty liver disease via inhibition of apoptosis and promotion of autophagy through the ROS/MAPK signaling pathway. *Oxid. Med. Cell. Longev.* 2021, 5599997. doi:10.1155/2021/5599997

Wu, Y., Wang, Y., Liu, B., Cheng, Y., Qian, H., Yang, H., et al. (2020). SN50 attenuates alveolar hypercoagulation and fibrinolysis inhibition in acute respiratory distress syndrome mice through inhibiting NF-κB p65 translocation. *Respir. Res.* 21 (1), 130. doi:10.1186/s12931-020-01372-6

Yao, Z., Liu, N., Zhu, X., Wang, L., Zhao, Y., Liu, Q., et al. (2020). Subanesthetic isoflurane abates ROS-activated MAPK/NF-κB signaling to repress ischemia-induced microglia inflammation and brain injury. *Aging (Albany NY)* 12 (24), 26121–26139. doi:10.18632/aging.202349

Yunrong Yang, M. L., Zhao, T., Chen, Q., Yang, Y., Wang, S., Wang, S., et al. (2022). Epigallocatechin-3-gallate Mo nanoparticles (EGM NPs) efficiently treat liver injury by strongly reducing oxidative stress, inflammation and endoplasmic reticulum stress. *Front. Pharmacol.* 13, 1039558. doi:10.3389/fphar.2022.1039558

Zanluqui, N. G., Lovo-Martins, M. I., Malvezi, A. D., Panis, C., da Silva, R. V., Tatakihara, V. L. H., et al. (2020). Concanavalin-A stimulates IL-17 and nitric oxide production and induces macrophage polarization and resistance to Trypanosoma cruzi infection. *Life Sci.* 258, 118137. doi:10.1016/j.lfs.2020.118137

Zhang, L., and Wei, W. (2020). Anti-inflammatory and immunoregulatory effects of paeoniflorin and total glucosides of paeony. *Pharmacol. Ther.* 207, 107452. doi:10.1016/j.pharmthera.2019.107452

Zhang, P., Yin, Y., Wang, T., Li, W., Li, C., Zeng, X., et al. (2020). Maresin 1 mitigates concanavalin A-induced acute liver injury in mice by inhibiting ROS-mediated activation of NF-κB signaling. *Free Radic. Biol. Med.* 147, 23–36. doi:10.1016/j.freeradbiomed.2019.11.033

Zhang, T., Zhu, Q., Shao, Y., Wang, K., and Wu, Y. (2017). Paeoniflorin prevents TLR2/4-mediated inflammation in type 2 diabetic nephropathy. *Biosci. Trends* 11 (3), 308–318. doi:10.5582/bst.2017.01104

Zhang, Z., Nian, Q., Chen, G., Cui, S., Han, Y., and Zhang, J. (2020). Klotho alleviates lung injury caused by paraquat via suppressing ROS/P38 MAPK-regulated inflammatory responses and apoptosis. *Oxid. Med. Cell. Longev.* 2020, 1854206. doi:10.1155/2020/1854206

Zhao, J., Park, S., Kim, J. W., Qi, J., Zhou, Z., Lim, C. W., et al. (2020). Nicotine attenuates concanavalin A-induced liver injury in mice by regulating the α7-nicotinic acetylcholine receptor in Kupffer cells. *Int. Immunopharmacol.* 78, 106071. doi:10.1016/j.intimp.2019.106071

Zhao, M., Zhou, P., Yu, J., James, A., Xiao, F., Wang, C., et al. (2019). The tissue distribution and excretion study of paeoniflorin-6'-O-benzene sulfonate (CP-25) in rats. *Inflammopharmacology* 27 (5), 969–974. doi:10.1007/s10787-018-0463-3

Zinatizadeh, M. R., Schock, B., Chalbatani, G. M., Zarandi, P. K., Jalali, S. A., and Miri, S. R. (2021). The Nuclear Factor Kappa B (NF-kB) signaling in cancer development and immune diseases. *Genes Dis.* 8 (3), 287–297. doi:10.1016/j.gendis.2020.06.005

Zolfaghari, M. A., Arefnezhad, R., Parhizkar, F., Hejazi, M. S., Khiavi, F. M., Mahmoodpoor, A., et al. (2021). T lymphocytes and preeclampsia: The potential role of T-cell subsets and related microRNAs in the pathogenesis of preeclampsia. *Am. J. Reprod. Immunol.* 86 (5), e13475. doi:10.1111/aji.13475

frontiers | Frontiers in Pharmacology

TYPE Original Research
PUBLISHED 23 November 2022
DOI 10.3389/fphar.2022.1047463

OPEN ACCESS

EDITED BY
Yan Huang,
Anhui Medical University, China

REVIEWED BY
Xiangyan Liu,
Shandong Provincial Hospital, China
Yilan Sun,
Zhejiang Provincial People's Hospital, China

*CORRESPONDENCE
Feng Xu,
xufeng99@zju.edu.cn
Pin Wu,
pinwu@zju.edu.cn

†These authors have contributed equally to this work

SPECIALTY SECTION
This article was submitted to Inflammation Pharmacology, a section of the journal Frontiers in Pharmacology

RECEIVED 18 September 2022
ACCEPTED 03 November 2022
PUBLISHED 23 November 2022

CITATION
He T, Qiao Y, Yang Q, Chen J, Chen Y, Chen X, Hao Z, Lin M, Shao Z, Wu P and Xu F (2022), NMI: a potential biomarker for tumor prognosis and immunotherapy. *Front. Pharmacol.* 13:1047463. doi: 10.3389/fphar.2022.1047463

NMI: a potential biomarker for tumor prognosis and immunotherapy

Teng He[1†], Yinbiao Qiao[2†], Qi Yang[3†], Jie Chen[1], Yongyuan Chen[4,5], Xiaoke Chen[4,5], Zhixing Hao[4,5], Mingjie Lin[4,5], Zheyu Shao[4,5], Pin Wu[4,5]* and Feng Xu[1]*

[1]Department of Infectious Diseases, The Second Affiliated Hospital, Zhejiang University School of Medicine, Zhejiang University, Hangzhou, China, [2]Division of Hepatobiliary and Pancreatic Surgery, Department of Surgery, The First Affiliated Hospital, Zhejiang University School of Medicine, Zhejiang University, Hangzhou, China, [3]Department of Emergency, The Second Affiliated Hospital, Zhejiang University School of Medicine, Zhejiang University, Hangzhou, China, [4]Department of Thoracic Surgery, The Second Affiliated Hospital, Zhejiang University School of Medicine, Zhejiang University, Hangzhou, China, [5]Key Laboratory of Tumor Microenvironment and Immune Therapy of Zhejiang Province, The Second Affiliated Hospital, Zhejiang University School of Medicine, Zhejiang University, Hangzhou, China

N-Myc and STAT Interactor protein (NMI) is an interferon inducible protein participating in various cellular activities, and is widely involved in the process of tumorigenesis and progression. Studies have shown that the loss of NMI expression in breast cancer can promote its progression by inducing epithelial-mesenchymal transition (EMT). However, the expression level of NMI in other tumors and its impact on immune cell infiltration, patient prognosis, and drug treatment are still unclear. Here, we analyzed the role of NMI in pan-cancer through multiple omics data. We found that NMI was abnormally expressed in a variety of tumor tissues. The expression of NMI was closely related to the unique molecular and immunotyping, diagnosis and prognosis of various tumor tissues. In addition, we identified the main proteins that interact with NMI, and focused on the relationship between the clinical parameters of lower grade glioma (LGG) and NMI expression. Subsequently, we found that the expression of NMI was correlated with the infiltration of multiple immune cells and the expression of immune checkpoints. Finally, we also found that the expression of NMI was correlated with the sensitivity to multiple antitumor drugs. In conclusion, our comprehensive pan-cancer analysis of NMI revealed that it is a potential molecular marker for tumor diagnosis and treatment, plays an important role in tumor immunity, and is a promising molecular target for cancer treatment.

KEYWORDS

NMI, pan-cancer, prognostic biomarker, immune infiltration, bioinformatics

Introduction

In recent years, the incidence rate of cancer has increased year by year, which has placed a serious burden on society (Ali et al., 2022). At present, cancer treatment mainly includes chemotherapy, surgery, radiotherapy, targeted therapy and immunotherapy. Although the treatment of cancer is constantly improving, the overall prognosis and survival of cancer patients have not significantly improved (Sung et al., 2021). Therefore, finding suitable biomarkers for tumor diagnosis and prognosis has become an urgent problem.

The N-Myc and STAT interactor (NMI) is encoded by the NMI gene and consists of a coiled coil domain (CC) at the N-terminus and two tandem domains (NID1, NID2) at the C-terminus, which can interact with transcription factors containing zip, helix-loop-helix (HLH) or HLH zip motifs (Zhu et al., 1999; Weng et al., 2022). Existing studies have shown that NMI plays an important role in the differentiation of the breast lumen (Pruitt et al., 2018) and the maintenance of alveoli (Alsheikh et al., 2021). The loss of NMI in breast cancer cells reduces their autophagy reactivity and chemosensitivity (Metge et al., 2015), and the recovery of NMI expression can be achieved by inhibiting the Wnt/β-catenin signaling pathway to play an antitumor role (Fillmore et al., 2009). Interestingly, NMI can also negatively regulate the expression of hTERT in breast cancer through the Yin Yang 1 (YY1) protein, to control tumor growth (Feng et al., 2017). In addition, Nagel et al. (Nagel et al., 2011) found that NMI was involved in the apoptotic activity of acute lymphoblastic leukemia. In a lung adenocarcinoma model, Wang et al. (Wang et al., 2017) found that NMI could inhibit multiple signaling pathways including p300-mediated NF- κB acetylation to control tumor growth. However, a recent study by Meng et al. (Meng et al., 2015) showed that high expression of NMI was significantly correlated with poor prognosis in glioblastoma multiforme (GBM) patients and was an independent risk factor for the prognosis of GBM patients. Subsequently, they also found that the expression of NMI was correlated with PTEN deletion and EGFR amplification in GBM patients.

Therefore, NMI may play different roles in different types of tumors, which may be caused by the heterogeneity of tumors. In addition, the specific mechanism of NMI and its correlation with immunotherapy need to be further elucidated. Therefore, we aimed to comprehensively evaluate the role of NMI at the pan-cancer level, establish the relationship between NMI expression and tumor diagnosis and prognosis, and determine the correlation between NMI expression and immune cell infiltration and immune checkpoint expression. Thus, this study provides new targets for cancer diagnosis, immunotherapy and prognosis.

Materials and methods

Gene expression analysis

NMI expression data in different types of normal tissues were obtained from the genotype-tissue expression (GTEx, http://commonfund.nih.gov/GTEx/) database. The expression data of NMI in tumor and normal tissues, and the clinical information of patients were obtained from The Cancer Genome Atlas (TCGA, http://cancergenome.nih.gov) and GTEx databases. NMI expression data in tumor cell lines were obtained from the Human Protein Atlas (HPA, https://www.proteinatlas.org/) database. The above data were analyzed by R software (version 3.6.3) and visualized by the ggplot2 R package. A p value <0.05 was set as the critical value and was considered statistically significant by the Wilcoxon test.

Correlation analysis of NMI expression with tumor molecular and immune types

The correlation between the expression of NMI and the 6 immune types of tumors (C1 (wound healing); C2 (IFN-gamma dominant); C3 (inflammatory); C4 (lymphocyte depleted); C5 (immunologically quiet); C6 (TGF-β dominant) and their unique molecular types were obtained from the TISIDB (http://cis.hku.hk/TISIDB/) database.

Functional enrichment analysis

The STRING database was used to analyze the top 50 proteins that strongly interact with NMI, and the parameters were set as follows: meaning of network edges: evidence, active interaction sources: Textmining, Experiments, Databases, minimum required interaction score: medium confidence (0.400). Subsequently, we performed Kyoto Encyclopedia of Genes and Genomes (KEGG) and Gene Ontology (GO) analyses of the above proteins using the clusterprofiler package and visualized them using the ggplot2 package.

Analysis of the diagnostic and prognostic value of NMI

Receiver operating characteristic (ROC) curves were used to characterize the correlation between NMI expression and tumor diagnosis. Analysis was performed using the proc package and visualized using the ggplot2 package. An area under the curve (AUC) > 0.7 is regarded as having diagnostic accuracy, and an AUC >0.9 is regarded as having high diagnostic accuracy.

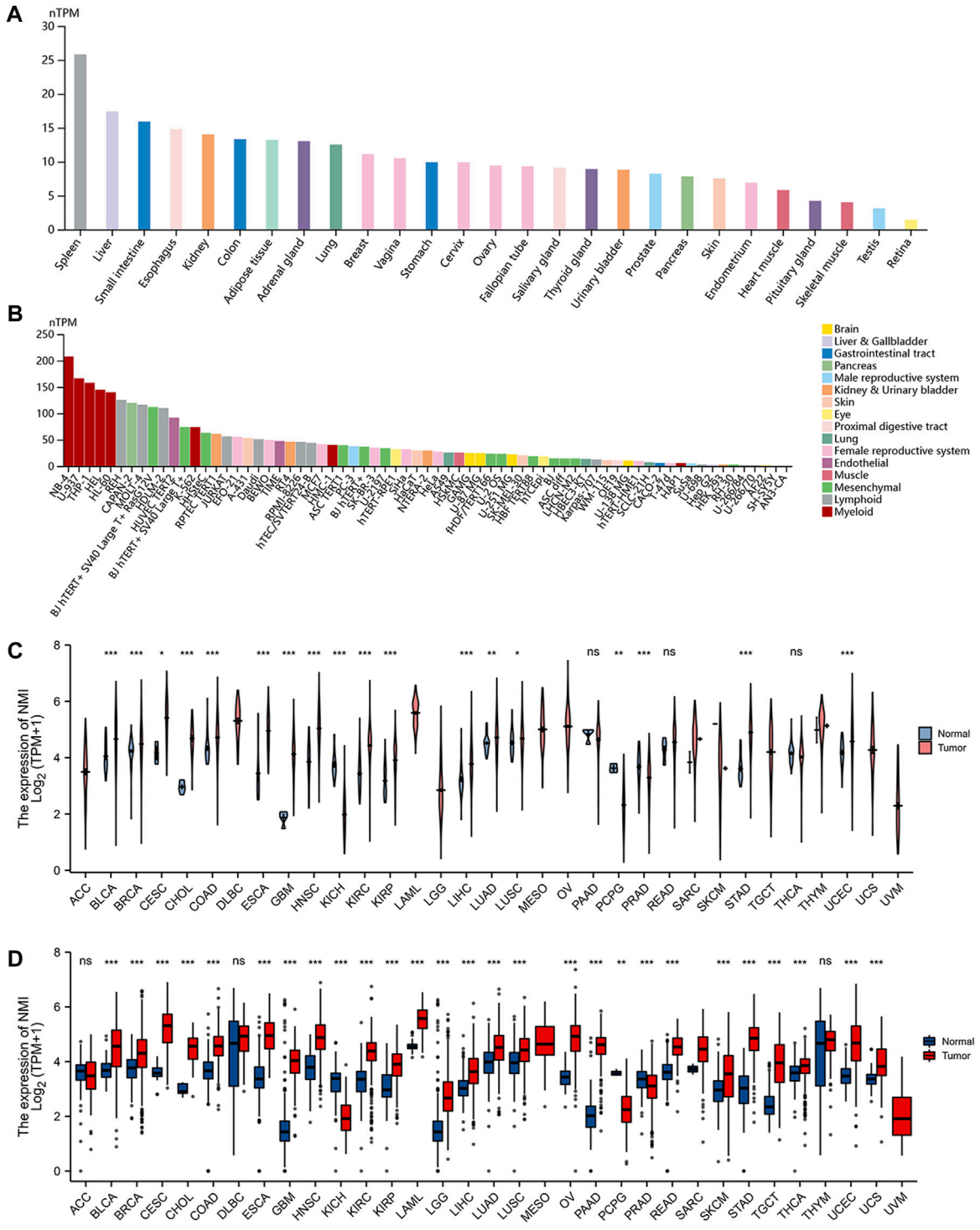

FIGURE 1
Expression level of NMI mRNA in pan-cancer. **(A)** NMI expression in normal tissues from GTEx database. **(B)** NMI expression in tumor cell lines from the HPA database. **(C)** Expression of NMI in tumor tissues and adjacent normal tissues from TCGA database. Pink represents tumor tissue and blue represents adjacent normal tissue. **(D)** Expression of NMI in tumor tissues and normal tissues in GTEx database. Red represents tumor tissue and blue represents adjacent normal tissue. *$p < 0.05$, **$p < 0.01$, ***$p < 0.001$. ns, not significant.

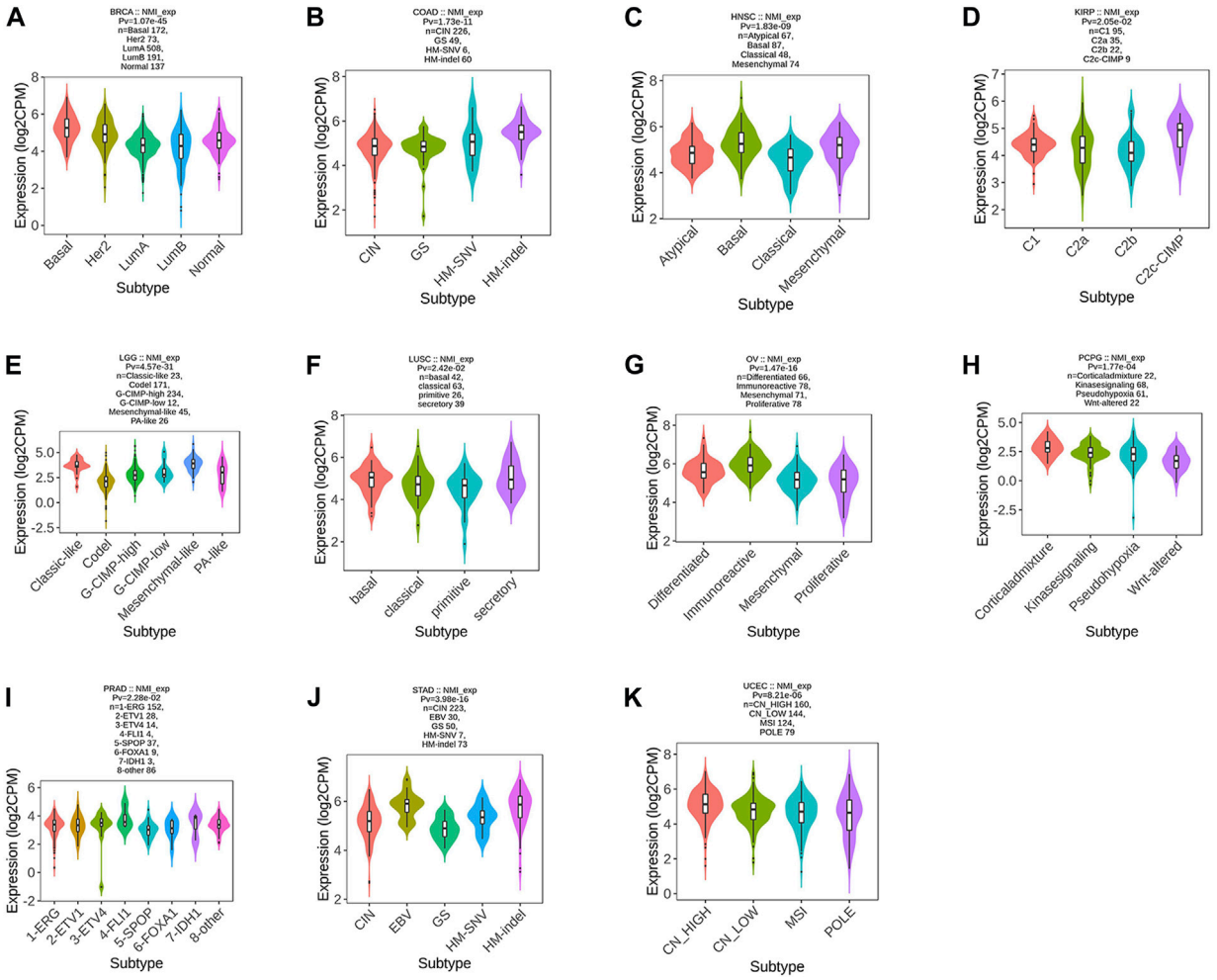

FIGURE 2
Correlation analysis between NMI expression and tumor molecular subtypes. **(A)** BRCA, **(B)** COAD, **(C)** HNSC, **(D)** KIRP, **(E)** LGG, **(F)** LUSC, **(G)** OV, **(H)** PCPG, **(I)** PRAD, **(J)** STAD, and **(K)** UCEC.

The value of NMI in the prognosis of tumor patients is characterized by its correlation with overall survival (OS), disease specific survival (DSS) and progression free interval (PFI). Correlation analysis of OS, DSS, PFI and clinical characteristics was performed in lower grade glioma (LGG) tumor types. Analysis was performed using the survival package and visualized using the survminer package. The median level of NMI expression was set as the cutoff value and statistical significance was tested by Cox regression analyses.

Correlation between NMI expression and immune cell infiltration

The correlation between NMI expression and the infiltration of 28 immune cell subtypes was analyzed at the pan-cancer level by searching the TISIDB database. Subsequently, the correlation between the abundance of T cells, B cells, DCs, macrophages, $CD8^+$ T cells, NK cells, cytotoxic cells and Treg cells and NMI expression in LGG was analyzed by the R package (GSVA). The Wilcoxon rank sum test was used for significance analysis.

Correlation analysis of NMI expression with immune stimulatory and inhibitory molecules

The correlation between NMI expression and 45 immunostimulatory molecules and 24 immunosuppressive molecules was analyzed by the TISIDB database.

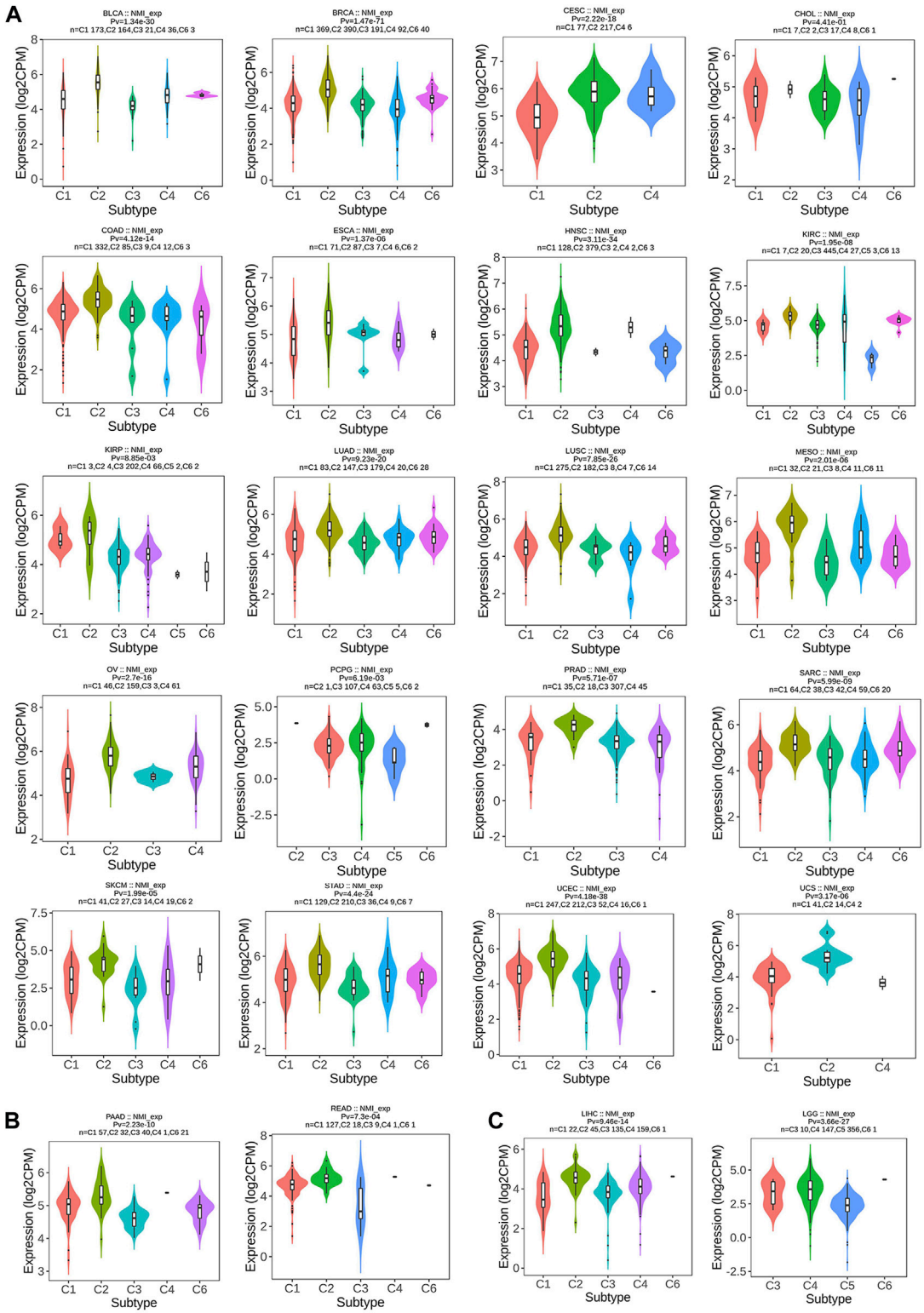

FIGURE 3
Correlation analysis between NMI expression and tumor immune subtypes. **(A)** BLCA, BRCA, CESC, CHOL, COAD, ESCA, HNSC, KIRC, KIRP, LUAD, LUSC, MESO, OV, PCPG, PRAD, SARC, SKCM, STAD, UCEC, and UCS. **(B)** PAAD and READ. **(C)** LIHC and LGG.

Drug sensitivity analysis

We analyzed the relationship between the expression of NMI and the nomenclature of various types of antitumor drugs through the RNAactDrug database (http://bio-bigdata.hrbmu.edu.cn/RNAactDrug), and showed the top 20 drugs with the strongest correlation. Pearson and Spearman correlation methods were used to analyze the correlation.

Results

Analysis of gene expression

Using the GTEx database, we analyzed the expression of NMI in normal tissues. We found that NMI was expressed in most tissues and organs, and it was the most highly expressed in the spleen and liver (Figure 1A). Subsequently, by analyzing the HPA database, we found that NMI was also expressed in a variety of tumor cell lines, especially in bone marrow-derived tumor cells (Figure 1B). Compared with adjacent normal tissues, NMI was significantly upregulated in 15 tumor types, including bladder urothelial carcinoma (BLCA), breast invasive carcinoma (BRCA), cervical squamous cell carcinoma and endocervical adenocarcinoma (CESC), cholangiocarcinoma (CHOL), colon adenocarcinoma (COAD), esophageal carcinoma (ESCA), GBM, head and neck squamous cell carcinoma (HNSC), kidney renal clear cell carcinoma (KIRC), kidney renal papillary cell carcinoma (KIRP), liver hepatocellular carcinoma (LIHC), lung adenocarcinoma (LUAD), lung squamous cell carcinoma (LUSC), stomach adenocarcinoma (STAD) and uterine corpus endometrial carcinoma (UCEC), while it was downregulated in kidney chromophobe (KICH), pheochromocytoma and paraganglioma (PCPG) and prostate adenocarcinoma (PRAD) (Figure 1C). Compared with the normal organization of GTEx database, NMI was significantly upregulated in 24 tumor types, including BLCA, BRCA, CESC, CHOL, COAD, ESCA, GBM, HNSC, KIRC, KIRP, acute myeloid leukemia (LAML), LGG, LIHC, LUAD, LUSC, ovarian serous cystadenocarcinoma (OV), pancreatic adenocarcinoma (PAAD), rectum adenocarcinoma (READ), skin cutaneous melanoma (SKCM), STAD, testicular germ cell tumors (TGCT), thyroid carcinoma (THCA), UCEC and uterine carcinosarcoma (UCS). However it was downregulated in KICH, PCPG and PRAD (Figure 1D).

Correlation analysis of NMI with tumor molecules and immune subtypes

In the past, the classification of tumors was mainly based on pathological classification. With the rapid development of genomics and immunotherapy, molecular typing and immunotyping are urgently needed to guide the treatment of patients. Therefore, we first analyzed the correlation between NMI expression and tumor molecular type at the pan-cancer level. We found that the expression of NMI was mainly related to 11 types of tumors, including BRCA (Figure 2A), COAD (Figure 2B), HNSC (Figure 2C), KIRP (Figure 2D), LGG (Figure 2E), LUSC (Figure 2F), OV (Figure 2G), PCPG (Figure 2H), PRAD (Figure 2I), STAD (Figure 2J) and UCEC (Figure 2K).

Next, we focused on analyzing the relationship between NMI expression and tumor immunotyping. We found that the expression of NMI was correlated with the immunotyping of 24 types of cancer. Among the 20 cancer types, high expression of NMI was mainly associated with C2 type, including BLCA, BRCA, CESC, CHOL, COAD, ESCA, HNSC, KIRC, KIRP, LUAD, LUSC, MESO, OV, PCPG, PRAD, SARC, SKCM, STAD, UCEC and UCS (Figure 3A). This suggests that the effect of NMI on tumorigenesis and progression may be mainly mediated by the expression of IFN-γ, which is also consistent with previous studies (Zhu et al., 1999). Interestingly, we observed that the highest expression of NMI was associated with C4 type (lymphocyte depleted) in PAAD and READ (Figure 3B), while the highest expression of NMI was associated with C6 type (TGF-β dominant) in LIHC and LGG (Figure 3C). This may be related to the small sample size of this subtype, but it also indicates that NMI may play different roles in different types of tumors.

Functional enrichment analysis

NMI proteins have attracted the attention of researchers because of their extensive interactions with transcription factors. Therefore, to further explore the protein interaction network of NMI, we analyzed the STRING database and obtained 50 proteins that closely interacted with NMI (Figure 4A). Subsequently, we performed KEGG and GO analysis of these proteins and visualized them (Figure 4B). GO enrichment analyses showed that NMI was mainly associated with “Kinase regulator activity”, “protein kinase regulator activity”, “transferase complex”, “transferring phosphorus-containing groups”, “protein kinase complex” and “serine/threonine protein kinase complex” (Figure 4C). KEGG enrichment analysis showed that NMI was mainly associated with “JAK-STAT signaling pathway”, “Human T-cell leukemia virus 1 infection”, “Measles” and “Hepatitis” (Figure 4D). Currently, many studies have established that NMI interacts with all signal transducers and activators of transcription (STATs) except STAT2 and enhances STAT-mediated transcription in response to the cytokines IL-2 and IFN-γ (Wang et al., 2017).

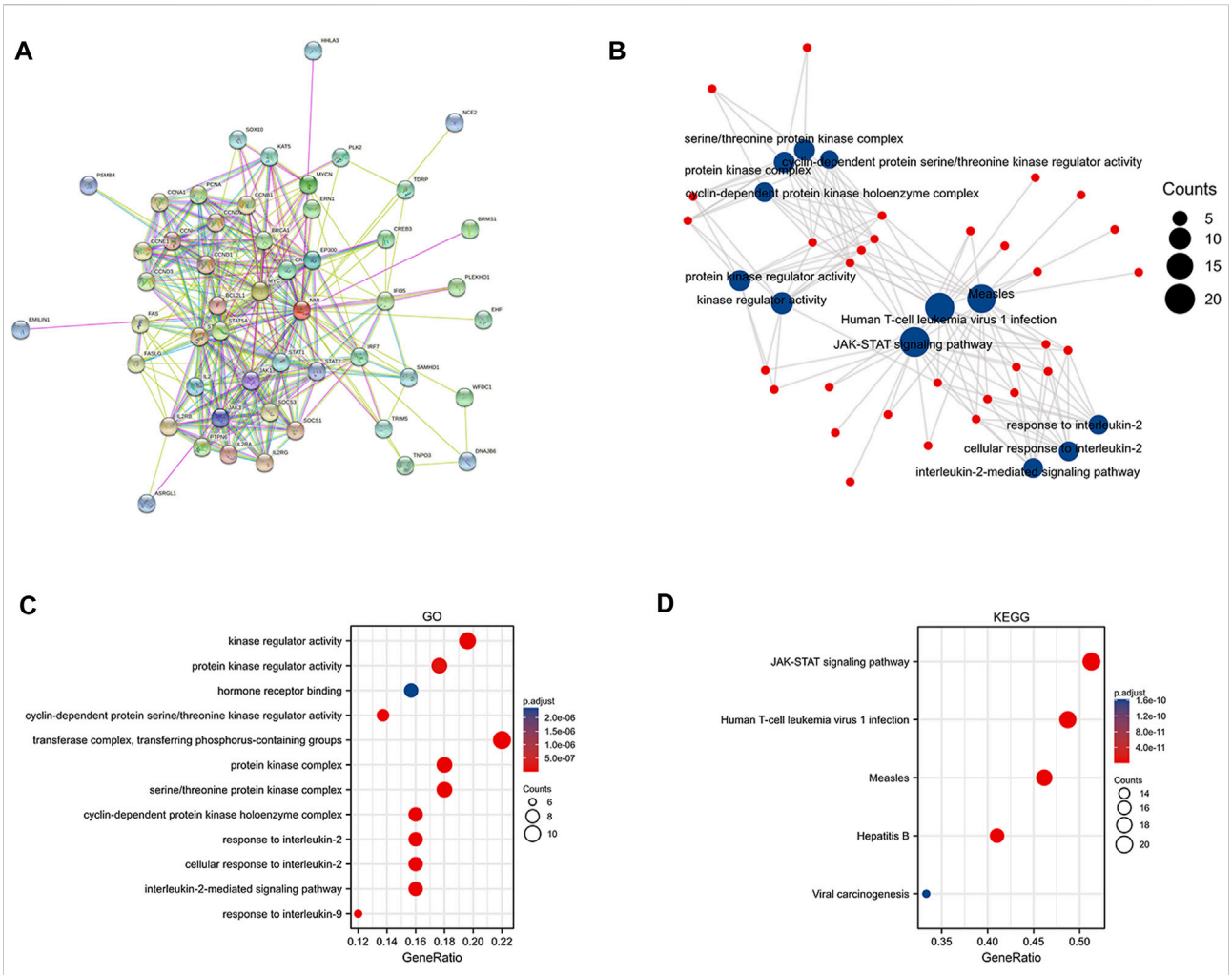

FIGURE 4
Functional enrichment analysis of NMI. **(A)** Protein network interaction diagram of NMI. **(B)** Scatter plot of GO and KEGG analyses of NMI interacting proteins **(C)** GO analysis of NMI-interacting proteins. **(D)** KEGG analysis of NMI-interacting proteins.

The value of NMI in tumor diagnosis

To further clarify whether NMI can be used as a biomarker for tumor diagnosis, ROC curves were used to explore the value of NMI in tumor diagnosis. We found that NMI accurately (AUC>0.7) predicted 8 types (Supplementary Figures S1A–H) and had higher accuracy (AUC>0.9) in 11 cancer types including CESC (AUC = 0.961) (Figure 5A), CHOL (AUC = 0.981) (Figure 5B), GBM (AUC = 0.979) (Figure 5C), KICH (AUC = 0.974) (Figure 5D), LAML (AUC = 0.965) (Figure 5E), LGG (AUC = 0.905) (Figure 5F), OV (AUC = 0.955) (Figure 5G), PAAD (AUC = 0.973) (Figure 5H), READ (AUC = 0.900) (Figure 5I), STAD (AUC = 0.935) (Figure 5J) and TGCT (AUC = 0.908) (Figure 5K).

The value of NMI in tumor prognosis

To determine whether NMI has predictive value for tumor prognosis, we analyzed the relationship between NMI expression and the OS, DSS and PFI of tumor patients. We found that NMI was highly correlated with three prognostic indicators in LGG, LUAD and SKCM. For LGG, high expression of NMI was associated with worse OS (hazard ratio (HR) = 3.30, $p < 0.001$), DSS (HR = 3.46, $p < 0.001$) and PFI (HR = 2.25, $p < 0.001$) (Figure 6A). For LUAD, high expression of NMI was associated with worse OS (HR = 1.50, $p = 0.006$), DSS (HR = 1.58, $p = 0.015$) and PFI (HR = 1.60, $p < 0.001$) (Figure 6B). However, in SKCM, high expression of NMI was associated with better OS (HR = 0.51, $p < 0.001$), DSS (HR = 0.46, $p < 0.001$) and PFI (HR = 0.71, $p = 0.003$) (Figure 6C). In

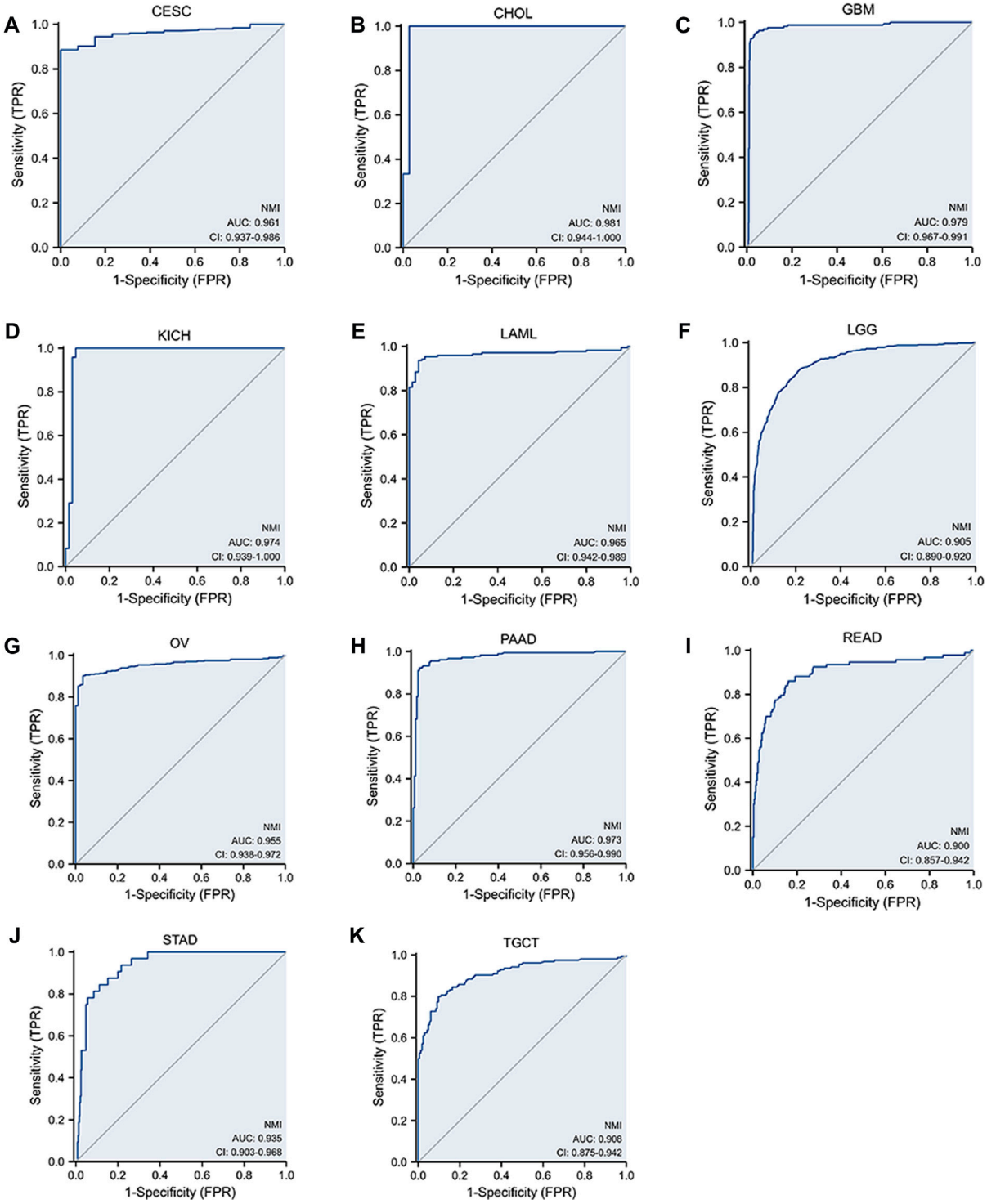

FIGURE 5
The sensitivity of NMI to tumor diagnosis is represented by the ROC curve. **(A)** CESC, **(B)** CHOL, **(C)** GBM, **(D)** KICH, **(E)** LAML, **(F)** LGG, **(G)** OV, **(H)** PAAD, **(I)** READ, **(J)** STAD, and **(K)** TGCT.

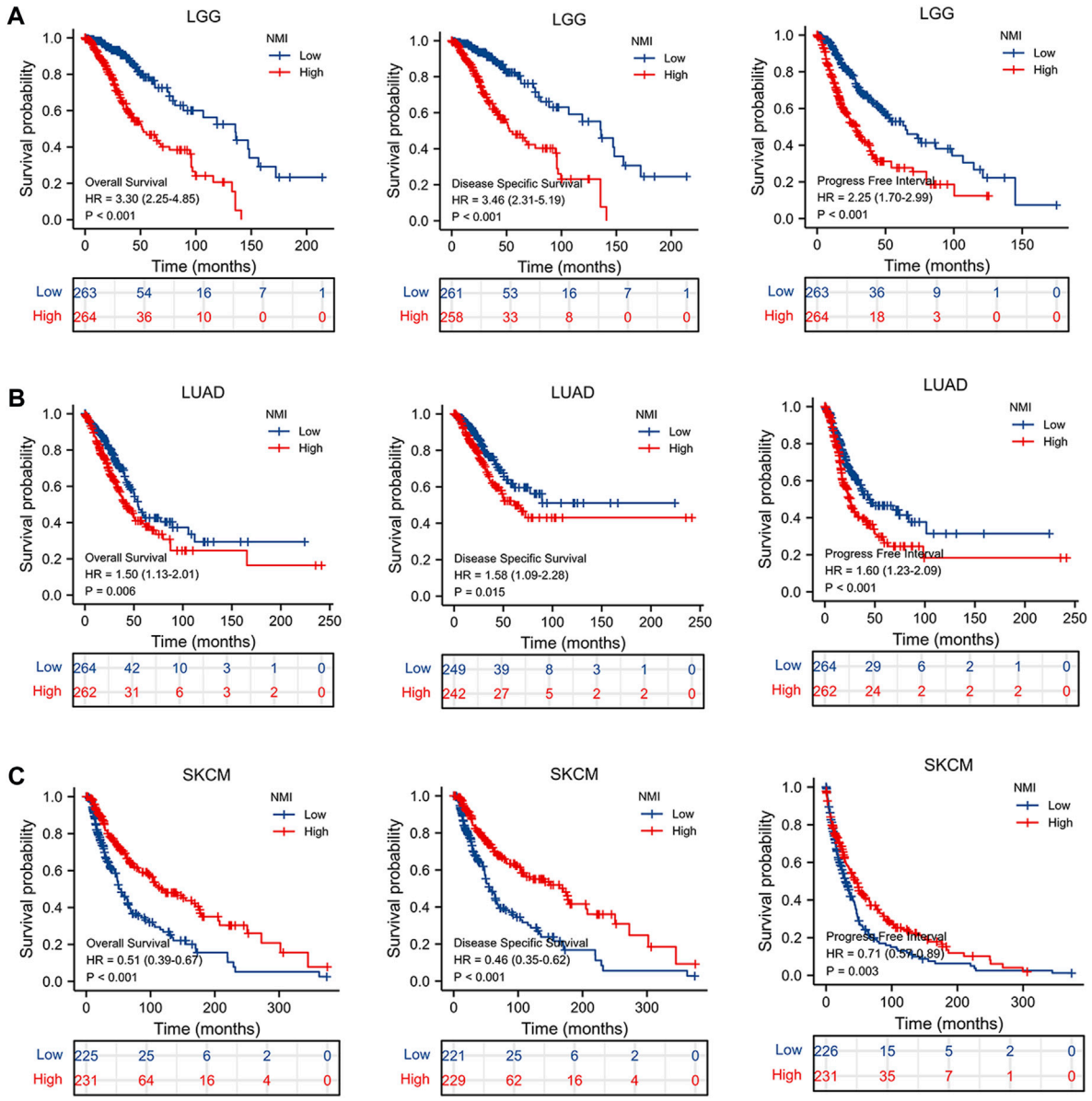

FIGURE 6
The relationship between NMI and OS, DSS and PFI in tumor patients. **(A)** LGG, **(B)** LUAD, and **(C)** SKCM.

addition, the high expression of NMI was associated with poor PFI in ACC (HR = 3.52, $p < 0.001$) (Supplementary Figure S2A) and GBM (HR = 1.44, $p = 0.041$) (Supplementary Figure S2B) and better PFI in COAD (HR = 0.68, $p = 0.029$) (Supplementary Figure S2C) and READ (HR = 0.50, $p = 0.04$) (Supplementary Figure S2D). The high expression of NMI was also associated with poor OS (HR = 1.57, $p = 0.032$) and DSS (HR = 1.64, $p = 0.038$) of PAAD (Supplementary Figure S2E), poor OS (HR = 1.47, $p = 0.029$) of LIHC (Supplementary Figure S2F) and poor OS (HR = 0.40, $p = 0.005$) of osteosarcoma (Supplementary Figure S2G).

Through the above analysis, we found that the expression of NMI was significantly correlated with the diagnosis and prognosis of LGG patients. Therefore, we further analyzed the correlation between NMI expression and the clinical characteristics of LGG patients. We found that the expression of NMI was closely related to tumor histological type, 1p/19q codeletion, WHO grade, primary therapy outcome and isocitrate dehydrogenase (IDH) status (Figure 7A) but not to age, race, sex or laterality (Supplementary Figure S3A). In addition, we further explored the impact of NMI expression in different clinical

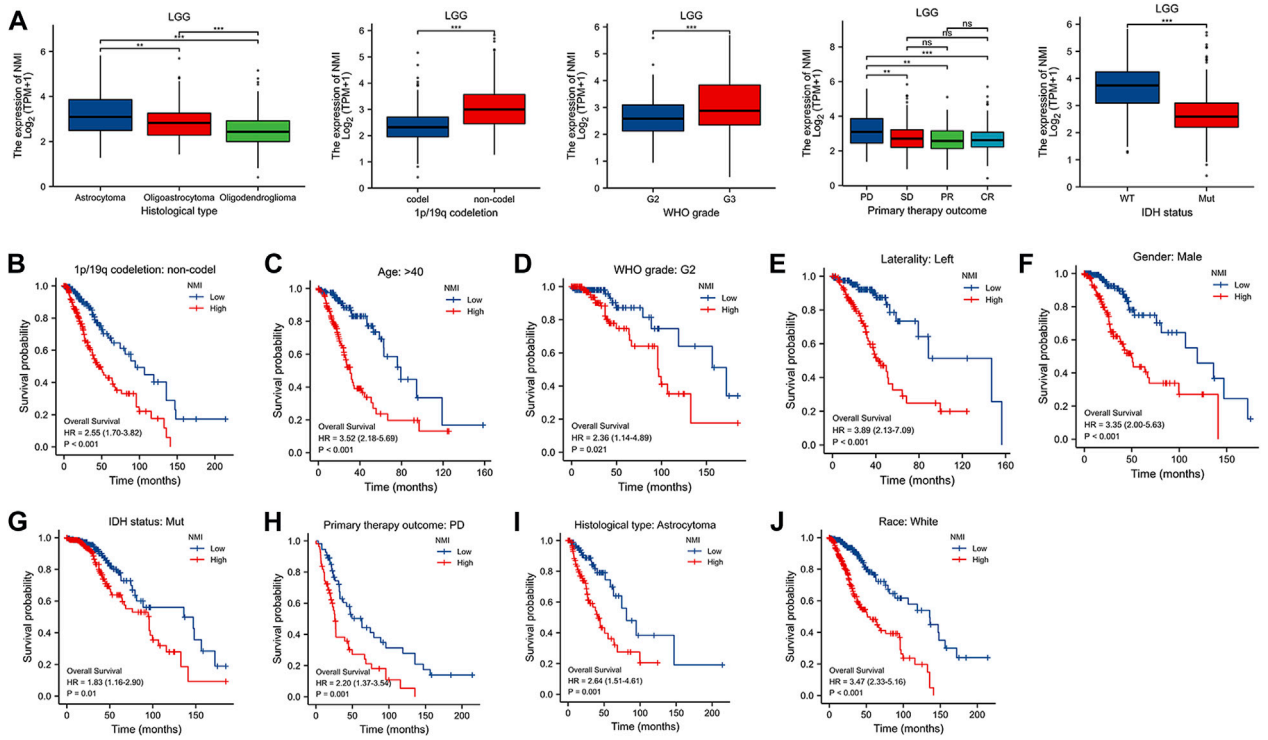

FIGURE 7
(A) Correlation between NMI and clinical features of LGG patients. $^{**}p < 0.01$, $^{***}p < 0.001$. ns, not significant. **(B–J)** The relationship between the expression of NMI and OS in different clinical subtypes of LGG. **(B)** 1p/19q codeletion: non-codel, **(C)** age>40, **(D)** WHO grade: G2, **(E)** laterality: left, **(F)** sex: male, **(G)** IDH status: mutation, **(H)** primary therapy outcome: PD, **(I)** histological: astrocytoma, **(J)** race: white.

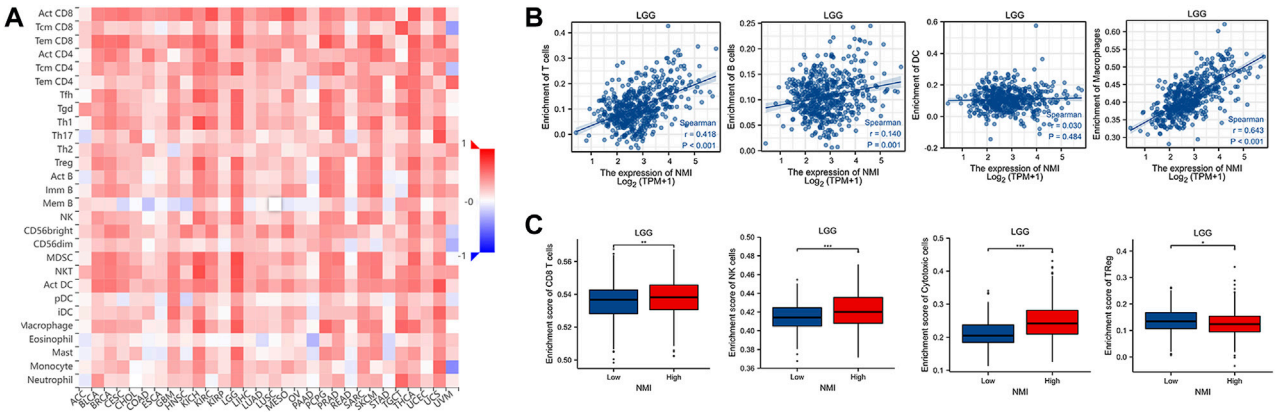

FIGURE 8
Correlation between NMI expression and immune cell infiltration. **(A)** The correlation heatmap between NMI expression at the pan cancer level and 28 immune cell subtypes was obtained from the TISIDB database. **(B)** Scatter plot of the correlation between NMI expression and T cells, B cells, DCs and macrophages in LGG. **(C)** In LGG, the correlation box diagram of NMI expression with $CD8^+$ T cells, NK cells, cytotoxic cells and Treg cells. $^{*}p < 0.05$, $^{**}p < 0.01$, $^{***}p < 0.001$.

subtypes on OS in LGG patients. The results showed that higher NMI expression was associated with worse OS in 1p/19q codeletion = non–codel (HR = 2.55, $p < 0.001$) (Figure 7B), age >40 years (HR = 3.52, $p < 0.001$) (Figure 7C), WHO grade = G2 (HR = 2.36, $p = 0.021$) (Figure 7D), laterality = left (HR = 3.89, $p < 0.001$)

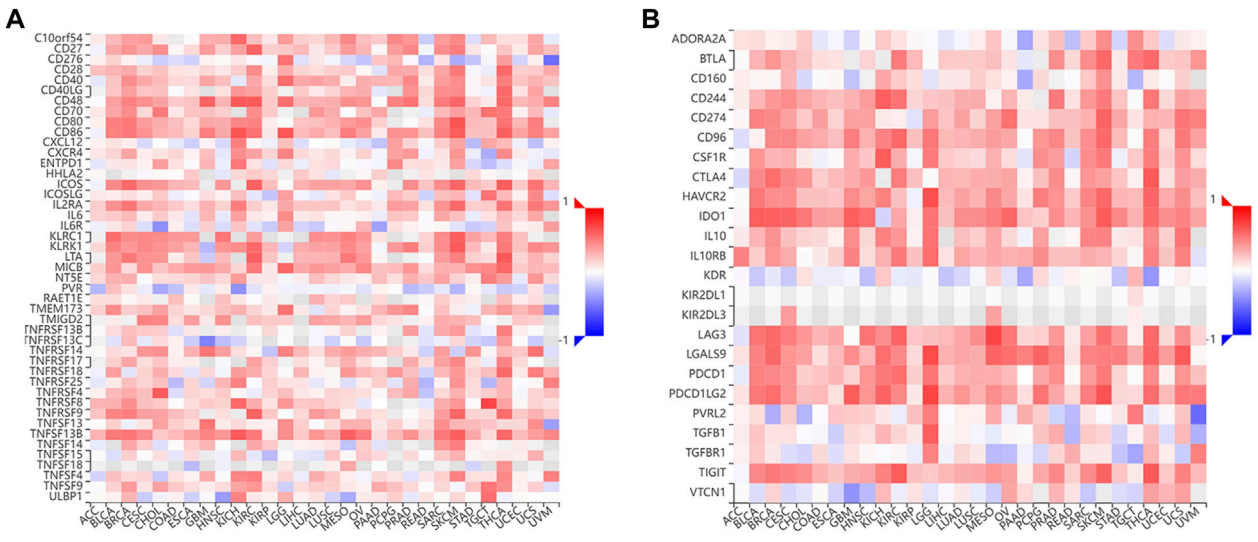

FIGURE 9
Correlation between NMI expression and immune checkpoint molecules. **(A)** The correlation heatmap between NMI expression and 45 immunostimulatory molecules was obtained from the TISIDB database. **(B)** The correlation Heatmap between NMI expression and 24 immunosuppressive molecules was obtained from the TISIDB database.

(Figure 7E), sex = male (HR = 3.35, $p < 0.001$) (Figure 7F), IDH status = mutation (HR = 1.83, $p = 0.01$) (Figure 7G), primary therapy outcome = progressive disease (PD) (HR = 2.2, $p = 0.001$) (Figure 7H), histological type = astrocytoma (HR = 2.64, $p = 0.001$) (Figure 7I), and race = white (HR = 3.47, $p < 0.001$) (Figure 7J).

Correlation between NMI expression and immune cell infiltration

Immunotherapy is the fastest developing type of cancer treatment. Finding suitable biomarkers before and after treatment has become an urgent issue. A previous analysis suggested that NMI is closely related to the diagnosis and prognosis of tumor patients. We found that the expression of NMI was highly correlated with the abundance of various tumor infiltrating immune cells, especially in LGG, KICH, and UCS tumor types (Figure 8A). Next, we focused on analyzing the relationship between NMI expression and immune cell infiltration in LGG. The results showed that the high expression of NMI was accompanied by high infiltration of T cells, B cells and macrophages, but not DCs (Figure 8B). Interestingly, the expression of NMI was also associated with major innate and adaptive toxic cells ($CD8^+$ T cells and NK cells) (Figure 8C). The high expression of NMI was accompanied by an overall increase in toxic cells, and the abundance of Treg cells decreased significantly.

Correlation between NMI expression and immune checkpoint molecules

Immune checkpoint blockade (ICB) therapy is a new model of immunotherapy, that has profoundly changed the prognosis of many types of tumors. Therefore, we further explored the relationship between the expression of NMI and the expression of immune checkpoint molecules. We found that the expression of NMI was related to the expression of 45 immunostimulatory molecules, especially the immunostimulatory molecules CD28, CD40, ICOS and the CD28 ligand CD80/86 (Figure 9A). In addition, we also found that the expression of NMI was related to 24 immunosuppressive molecules, especially PDCD-1, LAG-3, CTLA-4, TIGIT and IDO1 (Figure 9B). This suggests that the abnormal expression of NMI may be a biomarker for ICB treatment.

Drug sensitivity analysis

We explored the relationship between NMI mRNA expression and various types of antitumor drugs by searching the RNAactDrug database. We found that the top 20 drugs most closely related to NMI expression were Pcliainib, bosutinib, AICA Ribonucleotide, WHI-P97, idelalisib, BIX02189, TPCA-1, afatinib, SNX-2112, AT-7519, FR-180204, methotrexate, enzastaurin, OSU-03012, AZD7762, gemcitabine, AS605240, ZSTK474, CP466722 and VNLG/124 (Table 1).

TABLE 1 The correlation between NMI mRNA and anticancer drug sensitivity based on RNAactDrug data. ***$p < 0.001$.

Compound	RNAtype	RNAmoleade	Omits	Source	Peanon stat	Pearson.fdr	Spearmanstat	Spearman.dr
Pcliainib	mRNA	NMI	Expression	GDSC	−0.2490565	***	0.2946408	***
Bosutinib	mRNA	NMI	Expression	GDSC	−0.2363505	***	0.2504253	***
AICA Ribonueleotide	mRNA	NMI	Expression	GDSC	−0.1681221	***	0.2137404	***
WH1-P97	mRNA	NMI	Expression	GDSC	−0.1927539	***	0.2270336	***
Idelalisib	mRNA	NMI	Expression	GDSC	−0.2039266	***	0.2024053	***
B1X02189	mRNA	NMI	Expression	GDSC	−0.1779594	***	0.1952747	***
TPCA-I	mRNA	NMI	Expression	GDSC	−0.1651384	***	0.1916956	***
AICA Ribonueleotide	mRNA	NMI	Methylation	GDSC	0.14491277	***	0.20265865	***
Afatinib	mRNA	NMI	Expression	GDSC	0.1400821	***	0.1960697	***
SNX-2112	mRNA	NMI	Expression	GDSC	0.1475029	***	0.1897817	***
AT-7519	mRNA	NMI	Expression	GDSC	0.1375211	***	0.1839012	***
FR-180204	mRNA	NMI	Expression	GDSC	0.1633403	***	0.1868138	***
Methotrexate	mRNA	NMI	Expression	GDSC	0.1434948	***	0.1811458	***
Enzastaurin	mRNA	NMI	Expression	GDSC	0.1733262	***	0.1966106	***
OSU-03012	mRNA	NMI	Expression	GDSC	0.1685606	***	0.2017743	***
AZD7762	mRNA	NMI	Methylation	GDSC	0.14467147	***	0.19235985	***
Gcmciaabine	mRNA	NMI	Expression	GDSC	0.1880426	***	0.2103153	***
AS605240	mRNA	NMI	Expression	GDSC	0.1577792	***	0.1876233	***
ZSTK474	mRNA	NMI	Expression	GDSC	0.1659785	***	0.182499	***
CP466722	mRNA	NMI	Expression	GDSC	0.1495175	***	0.1771389	***

Discussion

Tumorigenesis is a gradual process, involving changes in many genes and signal transduction pathways (Todorovic-Rakovic, 2022). Pan-cancer analysis can reveal tumor heterogeneity and provide options for finding personalized biomarkers and drug screening (Chen et al., 2022). Here, we analyzed the expression of NMI at the pan-cancer level and the relationship between the expression level and tumor molecules and immune typing through bioinformatics. Subsequently, we further evaluated the PPI of NMI and its relationship with tumor diagnosis, prognosis, immunotherapy and antitumor drug sensitivity.

Our results showed that NMI was expressed in a variety of normal tissues, but was significantly elevated in 24 tumor types and correlated significantly with molecular type in 11 tumor types. These results suggest that changes in NMI expression are deeply involved in tumorigenesis and progression. This also indicates that NMI may play different roles due to the heterogeneity of tumors.

In recent years, researchers have realized that type II interferon (IFN-γ) plays an important role in the tumor immune surveillance of tumors (Dunn et al., 2005). IFN-γ in tumor tissues is mainly produced by TILs, which can play the role of regulatory and cellular effector factors (Angelicola et al., 2021). IFN-γ can upregulate the expression of MHC-I molecules on the surface of tumor cells, inhibit the proliferation of tumor cells and promote their apoptosis (Chin et al., 1997; Hobeika et al., 1999; Castro et al., 2018). However, the activation of IFN-γ receptor (IFNGR) on tumor cells can mediate the upregulation of PD-L1 through the JAK/STAT signaling pathway (Ribas et al., 2015; Garcia-Diaz et al., 2017). IFN-γ can also promote tumor growth by affecting the number of vascular endothelial growth inhibitors (VEGIs) (Lu et al., 2014) and the infiltration of immunosuppressive cells (Nishibori et al., 2004). In our study, we found that the high expression of NMI was associated with the formation of C2 (IFN gamma dominant) type tumors. In addition, we observed that the expression of NMI was related to the C6 type (TGF-β dominant) of LGG. Studies have shown that TGF- β can promote the metastasis of glioma by upregulating synthesis and matrix metalloproteinase-2 (MMP-2), and downregulating metalloproteinase-2 (TIMP-2) (Zhang et al., 2021). TGF- β can also induce epithelial-mesenchymal transition (EMT) and stemness by enhancing the signal transduction of NF-κb and Wnt (Kashani et al., 2022). This may explain how the expression of NMI is related to the C6 type of LGG. Enrichment analysis also showed that NMI mainly affected the "JAK/STAT signaling pathway" and "kinase regulation activity". This finding indicates that NMI may affect the JAK/STAT signaling pathway by regulating the expression of IFN-γ, thereby mediating the effect on tumorigenesis and progression. Moreover, NMI may play different roles in different types of tumors precisely because of the bidirectional regulatory effect of IFN-γ on tumors.

Adult glioma is a highly malignant tumor of the nervous system, that usually develops infiltratively (Figarella-Branger et al., 2011). According to the different types of origin, gliomas can be divided into three types: astrocytoma, oligoastrocytoma and oligodendroglioma (Davis, 2018). Common indicators for prognosis monitoring mainly include 1p/19q codeletion, IDH mutation, G-CIMP phenotype, TP53 mutation, and MGMT methylation (Baldock et al., 2014; Gusyatiner and Hegi, 2018; Guerrini et al., 2021). IDH mutation is currently recognized as an indicator of better prognosis. Our study found that the expression of NMI was negatively correlated with IDH mutation and 1p/19q codeletion, while high expression of NMI was associated with poor OS in LGG patients. Previous studies have shown that the high expression of NMI is related to the poor clinical prognosis of GBM patients, and the mechanism for this effect is that NMI regulates G1/S progression and cell proliferation through the interaction between STAT1 and NMI (Meng et al., 2015). Interestingly, we also found that the high expression of NMI was associated with the infiltration of toxic cells. This result may be related to that LGG with high NMI expression is more malignant, has higher heterogeneity, and can induce more immune cells to infiltrate, but the immune cells may be inhibited or exhausted.

Currently, immunotherapy is an important type of cancer treatment, that has profoundly changed the mode of cancer treatment (Zhu et al., 2021). However, there are still limitations in the effect of immunotherapy, which requires personalized selection of the treatment population (Zhang and Zhang, 2020). The foundation of immunotherapy is the number and status of infiltrating lymphocytes in tumor tissue, especially the existence of a depletion phenotype (Tan et al., 2020). In this study, we found that NMI is an important biomarker of immune cell infiltration and immune checkpoint expression. The expression of NMI was positively correlated with the number of infiltrating immune cells in most tumor tissues, especially the infiltration of tumor killer cells represented by $CD8^+$ T cells and NK cells. In addition, the expression of NMI is also related to the expression of a variety of immune checkpoint molecules that have been widely studied. This provides an opportunity for us to accurately select the appropriate treatment population for ICB. Of course, our study still has limitations. Our results are based on the mRNA level and need further verification at the protein level. In addition, multicenter, large sample clinical studies are needed to further confirm this conclusion.

Conclusion

Here, we revealed the expression changes of NMI in different tumor tissues, clarified its relationship with tumor molecules and immune typing, and confirmed that it can be used as a molecular marker for tumor diagnosis and prognosis. In addition, we also explored the relationship between NMI expression and immune cell infiltration and immune checkpoints, and identified it as a potential molecular marker for immunotherapy.

Data availability statement

The original contributions presented in the study are included in the article/Supplementary Material, further inquiries can be directed to the corresponding authors.

Author contributions

PW and TH designed this project. TH, YQ, and QY analyzed the data, interpreted the data, and wrote the manuscript. TH and QY designed the figures. ZH, YC, XC, ZS, and ML provided comments for the writing of the manuscript. FX and PW supervised the project, all authors reviewed and edited the manuscript.

Funding

This work was supported by funding from the National Natural Science Foundation of China (81572800 and 81970004).

Acknowledgments

We thank all the members of the PW and FX lab for discussions and comments on the manuscript.

Conflict of interest

The authors declare that the research was conducted in the absence of any commercial or financial relationships that could be construed as a potential conflict of interest.

Publisher's note

Supplementary material

The Supplementary Material for this article can be found online at: https://www.frontiersin.org/articles/10.3389/fphar.2022.1047463/full#supplementary-material

References

Ali, A., Manzoor, M. F., Ahmad, N., Aadil, R. M., Qin, H., Siddique, R., et al. (2022). The burden of cancer, government strategic policies, and challenges in Pakistan: A comprehensive review. *Front. Nutr.* 9, 940514. doi:10.3389/fnut.2022.940514

Alsheikh, H. A. M., Metge, B. J., Pruitt, H. C., Kammerud, S. C., Chen, D., Wei, S., et al. (2021). Disruption of STAT5A and NMI signaling axis leads to ISG20-driven metastatic mammary tumors. *Oncogenesis* 10 (6), 45. doi:10.1038/s41389-021-00333-y

Angelicola, S., Ruzzi, F., Landuzzi, L., Scalambra, L., Gelsomino, F., Ardizzoni, A., et al. (2021). IFN-Gamma and CD38 in hyperprogressive cancer development. *Cancers* 13 (2), 309. doi:10.3390/cancers13020309

Baldock, A. L., Yagle, K., Born, D. E., Ahn, S., Trister, A. D., Neal, M., et al. (2014). Invasion and proliferation kinetics in enhancing gliomas predict IDH1 mutation status. *Neuro. Oncol.* 16 (6), 779–786. doi:10.1093/neuonc/nou027

Castro, F., Cardoso, A. P., Gonçalves, R. M., Serre, K., and Oliveira, M. J. (2018). Interferon-gamma at the crossroads of tumor immune surveillance or evasion. *Front. Immunol.* 9, 847. doi:10.3389/fimmu.2018.00847

Chen, R., Wu, W., Chen, S. Y., Liu, Z. Z., Wen, Z. P., Yu, J., et al. (2022). A pan-cancer analysis reveals CLEC5A as a biomarker for cancer immunity and prognosis. *Front. Immunol.* 13, 831542. doi:10.3389/fimmu.2022.831542

Chin, Y. E., Kitagawa, M., Kuida, K., Flavell, R. A., and Fu, X. Y. (1997). Activation of the STAT signaling pathway can cause expression of caspase 1 and apoptosis. *Mol. Cell. Biol.* 17 (9), 5328–5337. doi:10.1128/mcb.17.9.5328

Davis, M. E. (2018). Epidemiology and overview of gliomas. *Semin. Oncol. Nurs.* 34 (5), 420–429. doi:10.1016/j.soncn.2018.10.001

Dunn, G. P., Ikeda, H., Bruce, A. T., Koebel, C., Uppaluri, R., Bui, J., et al. (2005). Interferon-γ and cancer immunoediting. *Immunol. Res.* 32 (1-3), 231–245. doi:10.1385/ir:32:1-3:231

Feng, X., Xu, X., Xiao, X., Zou, K., Yu, W., Wu, J., et al. (2017). NMI inhibits cancer stem cell traits by downregulating hTERT in breast cancer. *Cell Death Dis.* 8 (5), e2783. doi:10.1038/cddis.2017.200

Figarella-Branger, D., Maues de Paula, A., Colin, C., and Bouvier, C. (2011). Histomolecular classification of adult diffuse gliomas: The diagnostic value of immunohistochemical markers. *Rev. Neurol.* 167 (10), 683–690. doi:10.1016/j.neurol.2011.07.006

Fillmore, R. A., Mitra, A., Xi, Y., Ju, J., Scammell, J., Shevde, L. A., et al. (2009). Nmi (N-Myc interactor) inhibits Wnt/beta-catenin signaling and retards tumor growth. *Int. J. Cancer* 125 (3), 556–564. doi:10.1002/ijc.24276

Garcia-Diaz, A., Shin, D. S., Moreno, B. H., Saco, J., Escuin-Ordinas, H., Rodriguez, G. A., et al. (2017). Interferon receptor signaling pathways regulating PD-L1 and PD-L2 expression. *Cell Rep.* 19 (6), 1189–1201. doi:10.1016/j.celrep.2017.04.031

Guerrini, F., Mazzeo, L. A., Rossi, G., Verlotta, M., Del Maestro, M., Rampini, A. D., et al. (2021). Is it worth considering multicentric high-grade glioma a surgical disease? Analysis of our clinical experience and literature review. *Tomography* 7 (4), 523–532. doi:10.3390/tomography7040045

Gusyatiner, O., and Hegi, M. E. (2018). Glioma epigenetics: From subclassification to novel treatment options. *Semin. Cancer Biol.* 51, 50–58. doi:10.1016/j.semcancer.2017.11.010

Hobeika, A. C., Etienne, W., Fau - Torres, B. A., Torres Ba Fau - Johnson, H. M., Johnson Hm Fau - Subramaniam, P. S., and Subramaniam, P. S. (1999). IFN-gamma induction of p21(WAF1) is required for cell cycle inhibition and suppression of apoptosis. *J. Interferon Cytokine Res.* 19 (12), 1351–1361. doi:10.1089/107999099312812

Kashani, E., Schnidrig, D., Hashemi Gheinani, A., Ninck, M. S., Zens, P., Maragkou, T., et al. (2022). Integrated longitudinal analysis of adult grade 4 diffuse gliomas with long-term relapse interval revealed upregulation of TGF-beta signaling in recurrent tumors. *Neuro. Oncol.* 17, noac220. doi:10.1093/neuonc/noac220

Lu, Y., Gu, X., Chen, L., Yao, Z., Song, J., Niu, X., et al. (2014). Interferon-γ produced by tumor-infiltrating NK cells and CD4+ T cells downregulates TNFSF15 expression in vascular endothelial cells. *Angiogenesis* 17 (3), 529–540. doi:10.1007/s10456-013-9397-y

Meng, D., Chen, Y., Yun, D., Zhao, Y., Wang, J., Xu, T., et al. (2015). High expression of N-myc (and STAT) interactor predicts poor prognosis and promotes tumor growth in human glioblastoma. *Oncotarget* 6 (7), 4901–4919. doi:10.18632/oncotarget.3208

Metge, B. J., Mitra, A., Chen, D., Shevde, L. A., and Samant, R. S. (2015). N-Myc and STAT Interactor regulates autophagy and chemosensitivity in breast cancer cells. *Sci. Rep.* 5, 11995. doi:10.1038/srep11995

Nagel, S., Venturini, L., Meyer, C., Kaufmann, M., Scherr, M., Drexler, H. G., et al. (2011). Transcriptional deregulation of oncogenic myocyte enhancer factor 2C in T-cell acute lymphoblastic leukemia. *Leuk. Lymphoma* 52 (2), 290–297. doi:10.3109/10428194.2010.537003

Nishibori, T., Tanabe, Y., Su, L., and David, M. (2004). Impaired development of CD4+ CD25+ regulatory T cells in the absence of STAT1: Increased susceptibility to autoimmune disease. *J. Exp. Med.* 199 (1), 25–34. doi:10.1084/jem.20020509

Pruitt, H. C., Metge, B. J., Weeks, S. E., Chen, D., Wei, S., Kesterson, R. A., et al. (2018). Conditional knockout of N-Myc and STAT interactor disrupts normal mammary development and enhances metastatic ability of mammary tumors. *Oncogene* 37 (12), 1610–1623. doi:10.1038/s41388-017-0037-7

Ribas, A., Butler, M., Lutzky, J., Lawrence, D. P., Robert, C., Miller, W., et al. (2015). Phase I study combining anti-PD-L1 (MEDI4736) with BRAF (dabrafenib) and/or MEK (trametinib) inhibitors in advanced melanoma. *J. Clin. Oncol.* 33 (15), 3003. doi:10.1200/jco.2015.33.15_suppl.3003

Sung, H., Ferlay, J., Siegel, R. L., Laversanne, M., Soerjomataram, I., Jemal, A., et al. (2021). Global cancer statistics 2020: GLOBOCAN estimates of incidence and mortality worldwide for 36 cancers in 185 countries. *Ca. Cancer J. Clin.* 71 (3), 209–249. doi:10.3322/caac.21660

Tan, S., Li, D., and Zhu, X. (2020). Cancer immunotherapy: Pros, cons and beyond. *Biomed. Pharmacother.* 124, 109821. doi:10.1016/j.biopha.2020.109821

Todorovic-Rakovic, N. (2022). The role of cytokines in the evolution of cancer: IFN-Gamma paradigm. *Cytokine* 151, 155442. doi:10.1016/j.cyto.2021.155442

Wang, J., Zou, K., Feng, X., Chen, M., Li, C., Tang, R., et al. (2017). Downregulation of NMI promotes tumor growth and predicts poor prognosis in human lung adenocarcinomas. *Mol. Cancer* 16 (1), 158. doi:10.1186/s12943-017-0705-9

Weng, J., Li, S., Zhu, Z., Liu, Q., Zhang, R., Yang, Y., et al. (2022). Exploring immunotherapy in colorectal cancer. *J. Hematol. Oncol.* 15 (1), 95. doi:10.1186/s13045-022-01294-4

Zhang, H., Luo, Y. B., Wu, W., Zhang, L., Wang, Z., Dai, Z., et al. (2021). The molecular feature of macrophages in tumor immune microenvironment of glioma patients. *Comput. Struct. Biotechnol. J.* 19, 4603–4618. doi:10.1016/j.csbj.2021.08.019

Zhang, Y. Y., and Zhang, Z. M. (2020). The history and advances in cancer immunotherapy: Understanding the characteristics of tumor-infiltrating immune cells and their therapeutic implications. *Cell. Mol. Immunol.* 17 (8), 807–821. doi:10.1038/s41423-020-0488-6

Zhu, M., John, S., Fau - Berg, M., Berg, M., Fau - Leonard, W. J., and Leonard, W. J. (1999). Functional association of nmi with Stat5 and Stat1 in IL-2- and IFNgamma-mediated signaling. *Cell* 96 (1), 121–130. doi:10.1016/s0092-8674(00)80965-4

Zhu, S., Zhang, T., Zheng, L., Liu, H., Song, W., Liu, D., et al. (2021). Combination strategies to maximize the benefits of cancer immunotherapy. *J. Hematol. Oncol.* 14 (1), 156. doi:10.1186/s13045-021-01164-5

frontiers | Frontiers in Pharmacology

TYPE Review
PUBLISHED 09 December 2022
DOI 10.3389/fphar.2022.1093244

OPEN ACCESS

EDITED BY
Yan Huang,
Anhui Medical University, China

REVIEWED BY
Qingshan Chen,
Eastern Hepatobiliary Surgery Hospital, China
Rui Zhou,
Anhui Provincial Cancer Hospital, China

*CORRESPONDENCE
Yongzhong Wang,
wyzhmail@163.com

SPECIALTY SECTION
This article was submitted to Inflammation Pharmacology, a section of the journal Frontiers in Pharmacology

RECEIVED 08 November 2022
ACCEPTED 29 November 2022
PUBLISHED 09 December 2022

CITATION
Pan L, Gong C, Sun Y, Jiang Y, Duan X, Han Y and Wang Y (2022), Induction mechanism of ferroptosis: A novel therapeutic target in lung disease. *Front. Pharmacol.* 13:1093244. doi: 10.3389/fphar.2022.1093244

Induction mechanism of ferroptosis: A novel therapeutic target in lung disease

Lingyu Pan[1], Chunxia Gong[2], Yehong Sun[2], Yeke Jiang[2], Xianchun Duan[1], Yanquan Han[1] and Yongzhong Wang[1]*

[1]The First Affiliated Hospital of Anhui University of Chinese Medicine, Hefei, Anhui, China, [2]College of Pharmacy, Anhui University of Chinese Medicine, Hefei, Anhui, China

Ferroptosis is a newly discovered form of non-apoptotic regulatory cell death driven by iron-dependent lipid peroxidation. Ferroptosis significantly differs from other forms of cell death in terms of biochemistry, genetics, and morphology. Ferroptosis affects many metabolic processes in the body, resulting in disruption of homeostasis, and is related to many types of lung disease. Although current research on ferroptosis remains in the early stage, existing studies have confirmed that ferroptosis is regulated by a variety of genes, mainly involving changes in genes involved in iron homeostasis and lipid peroxidation metabolism. Furthermore, the mechanism of ferroptosis is complex. This review summarizes the confirmed mechanisms that can cause ferroptosis, including activation of glutathione peroxidase 4, synthesis of glutathione, accumulation of reactive oxygen species, and the influence of ferrous ions and p53 proteins. In recent years, the mechanism of ferroptosis in the occurrence and development of many diseases has been studied; the occurrence of ferroptosis will produce an inflammatory storm, and most of the inducing factors and pathological manifestations of lung diseases are also inflammatory reactions. Therefore, we believe that the association between ferroptosis and lung disease deserves further study. This article aims to help readers to better understand the mechanism of ferroptosis, provide new ideas and targets for the treatment of lung diseases, and point out the direction for the development of new targeted drugs for the clinical treatment of lung diseases.

KEYWORDS

ferroptosis, lung disease, glutathione peroxidase 4, glutathione, reactive oxygen species

1 Introduction

Cell death is an irreversible process that often occurs in normal tissues and is a necessary life process to maintain the function and morphology of tissues. Previous studies have suggested that there are two main pathways of cell death: apoptosis and necrosis. In recent years, a growing number of studies have indicates that there are other types of cell death besides apoptosis and necrosis, such as autophagy, necrotic apoptosis, scorch death, and ferroptosis. In 2003, Dolma et al. (2003) found that cells treated with

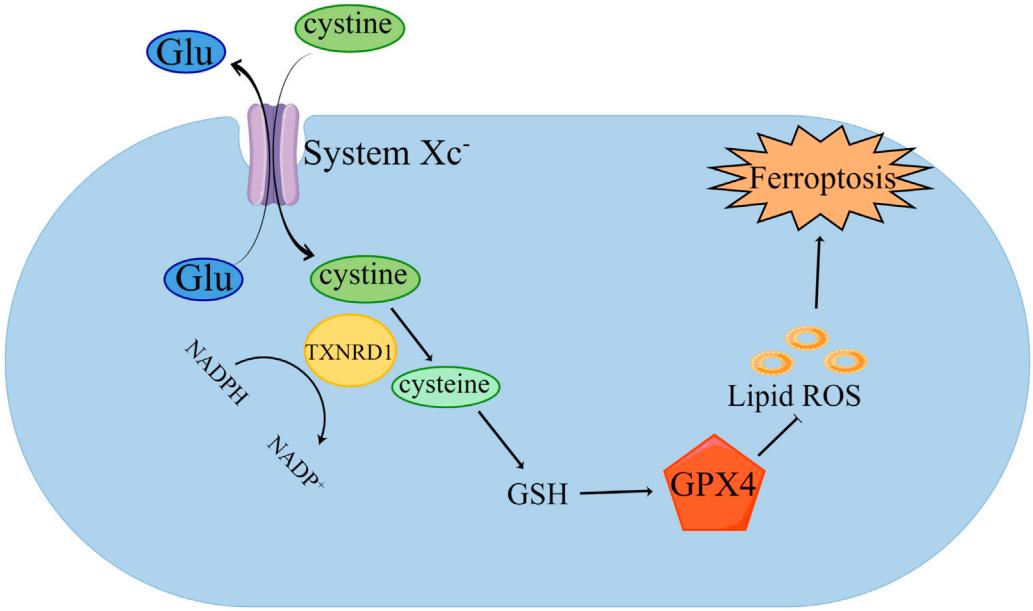

FIGURE 1
Inhibition of GPX4 induced ferroptosis. Cystine is transported into cells by System xc−and transformed into cysteine by TXNRD1, which further synthesizes GSH. GPX4 uses GSH to remove the phospholipid peroxide (PLOOH). The decrease of GSH leads to the weakening of GPX4's scavenging effect on lipid peroxides, thus inducing ferroptosis.

erastin, a small molecule compound that can be precisely targeted at human cancer cells, did not show the classic characteristics of apoptosis when screening selective lethal anti-tumor drugs in RAS mutated tumor cells. In 2012, Dixon et al. (2012) named this type of death as ferroptosis, an iron-dependent non-apoptotic form of cell death.

Regarding the common cell morphologies in ferroptosis that distinguish it from apoptosis, necrosis, and autophagy, during the process the size of the mitochondria decreases, the density of bilayer membranes increases, and the mitochondrial cristae decrease or disappear; however, the cell membrane remains intact, the size of nucleus is normal, and there is no evidence of nuclear concentration or chromatin marginalization (Peng et al., 2021). In terms of biochemistry, ferroptosis is mainly manifested by the exhaustion of glutathione (GSH), a decline in glutathione peroxidase 4 (GPX4) activity, and the inability of lipid peroxides to be metabolized through the GSH reduction reaction catalyzed by GPX4. Then, ferrous ions (Fe^{2+}) mediate lipid oxidation in a manner similar to the Fenton reaction to produce a large number of reactive oxygen species (ROS) (Park and Chung, 2019; Wang et al., 2020). Ferroptosis intersects with multiple cell death pathways were shown by many studies. Furthermore, the working mechanism of ferroptosis is being revealed and clarified underway.

Ferroptosis cells trigger the innate immune system by releasing inflammation related damage factors, and then stimulate the inflammatory response. Pulmonary diseases, such as asthma, acute lung injury, COPD, and pulmonary fibrosis, are closely related to inflammatory response. Therefore, based on the inducing the operating mechanism of ferroptosis, the exploration on the relevance between ferroptosis and lung diseases will conribute to a deeper perspective on pathogenesis of asthma, COPD and other lung diseases, and provide new ideas and directions in treatment methods and new drug research and development.

This review aims to improve our comprehension on the ferroptosis working mechanism so as to provide novel insights during the process of the clinical treatment of lung diseases, and identify the direction for the development of new targeted drugs for the clinical treatment of lung diseases.

2 The mechanism of the induction of ferroptosis

2.1 Suppression of GPX4

GPX4 plays an essential part in ferroptosis in ferroptosis (Figure 1) (Zhang et al., 2021b). Studies have shown that inhibiting the expression of GPX4 can induce iron- dependent cell death (Ding et al., 2021). GPX4 is required to participate in ferroptosis through the induction of erastin and RSL3 (Sui et al., 2018; Zhang et al., 2020b). GPX4 is a GSH-dependent enzyme, which can convert reduced GSH into oxidized GSH, reduce lipid

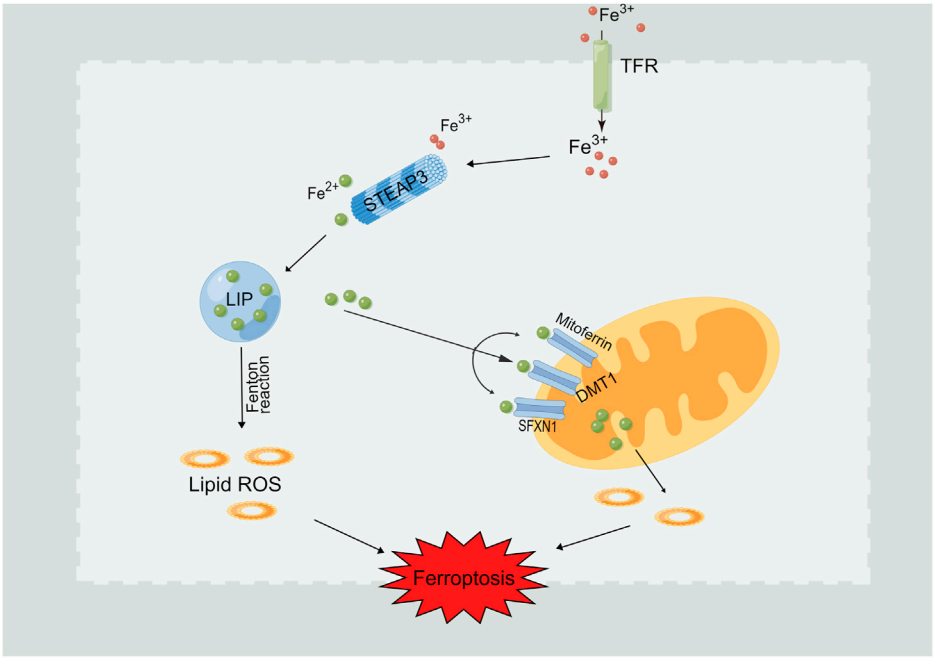

FIGURE 2
Intracellular Fe^{2+} overload induces ferroptosis. Fe^{3+} flows into the cell through the transferrin receptor (TFR). $Fe^{3+}$is reduced to Fe^{2+} through prostate six times transmembrane protein 3 (STEAP3) and stored in the labile iron pool (LIP). Fe^{2+} can also be further released from the endosome into LIP with the assistance of divalent metal transporter 1 (DMT1). Iron boosts the free radicals generation under the effect of Fenton reaction, which further promoting the occurence of lipid peroxidation and ferroptosis induction.

hydroperoxide into lipid alcohol, and convert free hydrogen peroxide into water to reduce iron-dependent lipid peroxidation (Liu et al., 2022a; Dang et al., 2022). GPX4 has selenocysteine (Sec) in its structure (Schwärzler et al., 2022). Sec can bind with RSL3, inhibiting the viability of GPX4 protease, resulting in the lipid peroxides accumulation in cells, which mediates ferroptosis (Shin et al., 2018; Wang et al., 2021). The activity of GPX4 is affected by Sec. As an essential donor in the mevalonate pathway (MVA), the Sec tRNA is modified by isopentenyltransferase. Therefore, inhibition of the MVA can lead to Sel RNA maturation disorder, affecting the normal function of GPX4, and inducing ferroptosis (Chen et al., 2021).

2.2 Inhibition of GSH synthesis

GSH is an important antioxidant in cells; it plays a protective role as it can reduce excessive lipid peroxide in cells (Lotocki et al., 2021; Sun et al., 2021). When the synthesis of GSH is blocked, the systems of intracellular oxidation and antioxidant are in a state of out-of-balance, and a large amount of polyunsaturated fatty acid peroxidation cannot be cleared in time; therefore, ferroptosis will occur. The synthesis of GSH depends on System Xc^-, which is anchored on the cell membrane and consists of seven members of the solute carrier family 11 (SLC7A11) and three members of the solute carrier family 2 (SLC3A2) (Dong et al., 2021). It can transfer cysteine into cells to synthesize GSH. Therefore, inhibiting the activity of System Xc^- leads to the inhibition of GSH synthesis and the depletion of GSH in cells, which in turn prevents the effective elimination of lipid peroxides in cells and mediates ferroptosis (Ma et al., 2021).

2.3 Intracellular Fe^{2+} overload

Normally, the iron ions inside and outside the cell are in a state of dynamic balance. The main iron ion used in cells is Fe^{2+}, which is stored in the cell marginal iron pool (LIP) (Krijt et al., 2018). The main routes of iron ions in the LIP are: 1) direct use in cells, 2) enter the mitochondria for biotransformation, 3) bound with ferritin (Fn) and stored in cells, and 4) they are transported out of cells (Xie et al., 2022). As shown in Figure 2, if the cell state is abnormal or the above process is inhibited, it will lead to an overload of Fe^{2+} in the cell. Affected by the Fenton reaction, iron will catalyze the generation of free radicals and promote to the peroxidation of lipid so as to lead to the lipid peroxides accumulation in cells, which eventually brings on the consequence of ferroptosis (He et al., 2020; Fu et al., 2021). In addition, iron reaction element binding protein 2 (IREB2) can significantly increase the expression of ferritin heavy chain and

light chain after inhibition, leading to a decreased intracellular free iron level and inhibiting the emergence of ferroptosis (Zhu et al., 2022).

2.4 ROS accumulation

The main cause of ferroptosis is the accumulation of lipid peroxides (Gao et al., 2019). Abnormal lipid metabolism leads to the formation of oxidized phospholipids and the accumulation of oxygen free radicals, thus inducing cell death (Zhang et al., 2022). As mentioned above, GPX4 and GSH are inhibited, and the result is the accumulation of ROS, which leads to ferroptosis. Polyunsaturated fatty acids (PUFA) are essential for ferroptosis (Zou et al., 2020), and PUFA is the main substrate for membrane lipid peroxidation. Acyl-CoA synthase long chain family member 4 (ACSL4) and lysophosphatidyltransferase 3 (LPCAT3) play roles in lipid synthesis and modification, respectively. The revelation of ACSL4 and LPCAT3 in ferroptosis resistant cells was significantly decreased (Liao et al., 2022). Furthermore, by downregulating the gene level of ACSL4 and LPCAT3 in cells, the production of lipid peroxides could be effectively prevented, and the ferroptosis resistance could be improved (Reed et al., 2022).

2.5 p53 and ferroptosis

p53 is a classical tumor suppressor gene that participates in a variety of cellular metabolic reactions through interactions with other proteins and selective transcriptional regulation of a variety of target genes (Zhao et al., 2021; Zheng et al., 2022). The accumulation of GPX4, GSH, and ROS mentioned above can be regulated by the signaling pathway mediated by p53, thus leading to ferroptosis. p53 can inhibit the activity of solute carrier family 7 member 11 (SLC7A11); cystathionine β synthase (CBS) has a regulatory effect (Hong et al., 2021). p53 can inhibit SLC7A11, reduce the synthesis of GSH through specific pathways, inhibit the viability of GPX4, lead to the accumulation of ROS, and induce ferroptosis (Guan et al., 2020). This discovery has important guiding significance in the treatment of cancer.

3 Ferroptosis and lung diseases

3.1 Chronic obstructive pulmonary disease (COPD)

COPD is a lung disease characterized by airflow restriction and persistent respiratory symptoms. An abnormal inflammatory reaction caused by exposure to chronic cigarette smoke (CS), harmful particles, or gases is one of the main causes of COPD (Vij et al., 2018). CS is composed of a complex mixture of chemical substances, including free radicals (Zhou et al., 2020). Previous studies have shown that there is iron accumulation in the lungs of long-term smokers, and CS promotes unstable iron accumulation through nuclear receptor coactivator 4-mediated ferritin autophagy, leading to an increase in free iron, and subsequently to phospholipid peroxidation and ferroptosis of pulmonary epithelial cells (Yoshida et al., 2019; Liu et al., 2022b). In a mouse model of CS-induced ferroptosis leading to COPD, GPX4 was shown to be a regulatory target that plays a therapeutic role. Yoshida et al. (2019) reported that accumulation of unstable iron and enhanced lipid peroxidation occurred in cells exposed to CS, and that the accumulation of iron was more severe after GPX4 was knocked out, indicating that ferroptosis may participate in the process of COPD. Furthermore, particle matter 2.5 (PM 2.5) has been shown to induce ferroptosis; the mechanism may be closely related to iron overload, lipid peroxidation, and redox imbalance (Ren et al., 2021).

3.2 Acute lung injury

Acute lung injury is characterized by acute systemic inflammation. Its clinical manifestations include pulmonary edema, hypoxemia, diffuse alveolar injury, and lung infiltration (Ren et al., 2021). Acute lung injury can further cause multiple organ dysfunction syndrome or acute respiratory distress syndrome. Acute lung injury is generally caused by extrapulmonary factors and pulmonary inflammation, and its pathogenesis is very complex. Zhou et al. (2019) reported an increase in iron accumulation in the lungs of mice with acute lung injury. The production of superoxide were promoted by the excess iron and leads to lipid peroxidation through the generation of free radicals from the Fenton reaction. The down-regulation of GSH and GPX4 also induces ferroptosis. Liu et al. (2020) showed evidence that ferroptosis plays an important role in lipopolysaccharide (LPS)-induced acute lung injury, and that treatment with the ferroptosis inhibitor ferrostatin-1 (Fer-1) resulted in a significantly improved effect in LPS-induced acute lung injury. Li et al. (2020) listed decreased expression of GPX4 and increased levels of ROS in the cells of mice with acute lung injury induced by radiation; after treatment with liproxstatin-1, an ferroptosis inhibitor, assumed the trend of escalation significantly while the expression of ROS reflected the trend the other way around.

3.3 Lung cancer

An increasing number of studies have reported the role of ferroptosis in the pathogenesis and treatment of cancer, including many malignant tumors such as breast cancer (Zhang et al., 2021a), liver cancer (Yang et al., 2020), stomach

cancer (Zhang et al., 2020a), rectal cancer (Xian et al., 2020), glioma (Zhuo et al., 2020), and pancreatic cancer (Ye et al., 2021). Typically, immune balance occurs when a tumor is present; the interaction between ferroptosis and lipid metabolism is very important in tumor immune regulation. Researches have proved that the content of prostaglandin-endoperoxide synthase 2 in tumor cells undergoing ferroptosis is abnormally increased, resulting in the production of the immunosuppressive factor prostaglandin E2, thereby inhibiting the tumor immune function of traditional type 1 dendritic cells, natural killer cells, and cytotoxic T cells (Zhao et al., 2022). In recent years, the relationship between lung cancer and ferroptosis has increasingly studied with a focus on NSCLC and lung adenocarcinoma (Tang et al., 2021; Yao et al., 2021).

There is a close relationship between ferroptosis and COPD and lung cancer. COPD caused by excessive smoking is one of the main causes of lung cancer (V et al., 2021). Many substances in CS can induce ferroptosis of airway epithelial cells, which in turn promotes the onset of COPD in lung cancer patients. Research has shown that the combined use of erastin and acetaminophen can promote cell apoptosis and ferroptosis and induce NSCLC cell death (Gai et al., 2020). Furthermore, it can decrease the GSH content and increase lipid peroxide levels to abnormal levels in NSCLC cells. In the radiation resistant subtype NSCLC cells, erastin not only can erastin induce ferroptosis, but also partially reduce cell resistance to radiation (Pan et al., 2019).

3.4 Pulmonary fibrosis

Ferroptosis is closely related to the pathogenesis of pulmonary fibrosis. The accumulation of iron ions, ROS, lipid peroxides, and inhibition of GPX4 activity features critically in the pathogenesis of pulmonary fibrosis (V et al., 2021). An imbalance of iron and lipid peroxide metabolism often accompanies pulmonary fibrosis (Hanania et al., 2019). Therefore, inhibiting the accumulation of lipid peroxide and iron in cells is an effective measure to prevent iron-dependent death of alveolar cells and the progression of pulmonary fibrosis. Radiation-induced lung fibrosis (RILF) is a serious and life-threatening complication of radiotherapy treatment for lung cancer; symptoms occur in the first few months after radiotherapy and can last for up to 2 years. The latest research shows that ferroptosis is a novel mechanism of radiation-induced cancer cell death. Inducers of ferroptosis cause biological molecule oxidation (such as lipid oxidation) by enhancing ROS generated by radiation, and drive ferroptosis through phospholipid peroxidation (Ye et al., 2020). Li et al. showed that the level of GPX4 was significantly down-regulated in a RILF mouse model, and that liproxstatin-1 could down-regulate transforming growth factor (TGF) by activating the nuclear factor-erthroid factor 2-related factor 2 (Nrf2) pathway-β1 to alleviate RILF (Li et al., 2019).

4 Discussion

Since Dixon and others put forward the concept of ferroptosis in 2012, it has received increasing research attention, with a particular focus on the mechanism. Ferroptosis is a novel form of cell death that disticts from common modes such as apoptosis and autophagy; the occurrence of ferroptosis is regulated by iron metabolism-related mechanisms. This controllable regulatory cell death mode provides new opportunities for the treatment of human diseases.

With increased research, the inducers, inhibitors, and related mechanisms of ferroptosis have been identified. From the perspective of biochemistry, the cause of ferroptosis can be contributed to GSH depletion, intracellular iron accumulation, lipid peroxidation and GPX4 inactivation. In recent years, more and more inducers and inhibitors of ferroptosis have been identified. For example, Nrf2 and heat shock proteins can regulate ferroptosis. Furthermore, the results of a large number of clinical trials and animal experiments indicates that ferroptosis can be closely attributes to a variety of human diseases and pathological processes. The treatment of pathway intervantion proves effectively delay on the process of certain diseases and relieves the symptoms (Chang et al., 2021). Although research on ferroptosis is far from complete at present, the research on ferroptosis and lung diseases has made some progress, Sorafenib, the representative of ferroptosis inducer, has been used as an anti-tumor drug in the treatment of liver and kidney cancer (Sun et al., 2017). RSL3 is one of the representative drugs of GPX4 inhibitors, which can directly target GPX4. RSL3 can trigger ferroptosis by directly inhibiting GPX4 activity and inhibit the growth of glioma cells (Wang et al., 2019). The use of ferroptosis inducers as new adjuvants to traditional treatment schemes in lung cancer has been shown to be effective. The research and development of new inducers of ferroptosis and the employment of a variety form of integrated treatments are promising in the field of lung cancer treatment research. Furthermore, inducing or inhibiting ferroptosis may become a new therapeutic method and drug development target in the treatment of other lung diseases. Relatively speaking, research on ferroptosis and acute lung injury, COPD, and pulmonary fibrosis remains very limited at present; however, there is clear evidence to show the relationship that exists between them. Considering that there is still a large gap to be filled regarding the proposed concept of ferroptosis, with future research, the relationship between ferroptosis and many lung-related diseases will become increasingly clear.

In conclusion, ferroptosis is a newly discovered form of cell death. With continuous in-depth research, new mechanisms and regulatory factors have been identified, and the connection with the processes of many diseases has been confirmed. It has important theoretical and practical value in guiding the development of new therapeutic schemes and targeted drugs for various diseases presenting with ferroptosis as the entry point.

Author contributions

CG wrote the review, YW and LP designed the idea of overall review. YS and YJ responsible for consulting relevant references. YH and XD draws the mechanism figures. All authors read and approved the final manuscript.

Funding

The work was funded by Anhui Provincial College Natural Science Research Key Project supports this review Fund Nos KJ2019A0440, KJ2020A0409.

Conflict of interest

The authors declare that the research was conducted in the absence of any commercial or financial relationships that could be construed as a potential conflict of interest.

Publisher's note

References

Chang, M., Hou, Z., Wang, M., Yang, C., Wang, R., Li, F., et al. (2021). Single-atom Pd nanozyme for ferroptosis-boosted mild-temperature photothermal therapy. *Angew. Chem. Int. Ed. Engl.* 60 (23), 12971–12979. doi:10.1002/anie.202101924

Chen, W., Fu, J., Chen, Y., Li, Y., Ning, L., Huang, D., et al. (2021). Circular RNA circKIF4A facilitates the malignant progression and suppresses ferroptosis by sponging miR-1231 and upregulating GPX4 in papillary thyroid cancer. *Aging (Albany NY)* 13 (12), 16500–16512. doi:10.18632/aging.203172

Dang, R., Wang, M., Li, X., Wang, H., Liu, L., Wu, Q., et al. (2022). Edaravone ameliorates depressive and anxiety-like behaviors via Sirt1/Nrf2/HO-1/Gpx4 pathway. *J. Neuroinflammation* 19 (1), 41. doi:10.1186/s12974-022-02400-6

Ding, Y., Chen, X., Liu, C., Ge, W., Wang, Q., Hao, X., et al. (2021). Identification of a small molecule as inducer of ferroptosis and apoptosis through ubiquitination of GPX4 in triple negative breast cancer cells. *J. Hematol. Oncol.* 14 (1), 19. doi:10.1186/s13045-020-01016-8

Dixon, S. J., Lemberg, K. M., Lamprecht, M. R., Skouta, R., Zaitsev, E. M., Gleason, C. E., et al. (2012). Ferroptosis: An iron-dependent form of nonapoptotic cell death. *Cell.* 149 (5), 1060–1072. doi:10.1016/j.cell.2012.03.042

Dolma, S., Lessnick, S. L., Hahn, W. C., and Stockwell, B. R. (2003). Identification of genotype-selective antitumor agents using synthetic lethal chemical screening in engineered human tumor cells. *Cancer Cell.* 3 (3), 285–296. doi:10.1016/s1535-6108(03)00050-3

Dong, H., Xia, Y., Jin, S., Xue, C., Wang, Y., Hu, R., et al. (2021). Nrf2 attenuates ferroptosis-mediated IIR-ALI by modulating TERT and SLC7A11. *Cell. Death Dis.* 12 (11), 1027. doi:10.1038/s41419-021-04307-1

Fu, J., Li, T., Yang, Y., Jiang, L., Wang, W., Fu, L., et al. (2021). Activatable nanomedicine for overcoming hypoxia-induced resistance to chemotherapy and inhibiting tumor growth by inducing collaborative apoptosis and ferroptosis in solid tumors. *Biomaterials* 268, 120537. doi:10.1016/j.biomaterials.2020.120537

Gai, C., Yu, M., Li, Z., Wang, Y., Ding, D., Zheng, J., et al. (2020). Acetaminophen sensitizing erastin-induced ferroptosis via modulation of Nrf2/heme oxygenase-1 signaling pathway in non-small-cell lung cancer. *J. Cell. Physiol.* 235 (4), 3329–3339. doi:10.1002/jcp.29221

Gao, M., Yi, J., Zhu, J., Minikes, A. M., Monian, P., Thompson, C. B., et al. (2019). Role of mitochondria in ferroptosis. *Mol. Cell.* 73 (2), 354–363. e353. doi:10.1016/j.molcel.2018.10.042

Guan, Z., Chen, J., Li, X., and Dong, N. (2020). Tanshinone IIA induces ferroptosis in gastric cancer cells through p53-mediated SLC7A11 down-regulation. *Biosci. Rep.* 40 (8), BSR20201807. doi:10.1042/bsr20201807

Hanania, A. N., Mainwaring, W., Ghebre, Y. T., Hanania, N. A., and Ludwig, M. (2019). Radiation-induced lung injury: Assessment and management. *Chest* 156 (1), 150–162. doi:10.1016/j.chest.2019.03.033

He, Y. J., Liu, X. Y., Xing, L., Wan, X., Chang, X., and Jiang, H. L. (2020). Fenton reaction-independent ferroptosis therapy via glutathione and iron redox couple sequentially triggered lipid peroxide generator. *Biomaterials* 241, 119911. doi:10.1016/j.biomaterials.2020.119911

Hong, T., Lei, G., Chen, X., Li, H., Zhang, X., Wu, N., et al. (2021). PARP inhibition promotes ferroptosis via repressing SLC7A11 and synergizes with ferroptosis inducers in BRCA-proficient ovarian cancer. *Redox Biol.* 42, 101928. doi:10.1016/j.redox.2021.101928

Krijt, M., Jirkovska, A., Kabickova, T., Melenovsky, V., Petrak, J., and Vyoral, D. (2018). Detection and quantitation of iron in ferritin, transferrin and labile iron pool (LIP) in cardiomyocytes using (55)Fe and storage phosphorimaging. *Biochim. Biophys. Acta. Gen. Subj.* 1862 (12), 2895–2901. doi:10.1016/j.bbagen.2018.09.005

Li, X., Duan, L., Yuan, S., Zhuang, X., Qiao, T., and He, J. (2019). Ferroptosis inhibitor alleviates Radiation-induced lung fibrosis (RILF) via down-regulation of TGF-β1. *J. Inflamm.* 16, 11. doi:10.1186/s12950-019-0216-0

Li, Y., Cao, Y., Xiao, J., Shang, J., Tan, Q., Ping, F., et al. (2020). Inhibitor of apoptosis-stimulating protein of p53 inhibits ferroptosis and alleviates intestinal ischemia/reperfusion-induced acute lung injury. *Cell. Death Differ.* 27 (9), 2635–2650. doi:10.1038/s41418-020-0528-x

Liao, P., Wang, W., Wang, W., Kryczek, I., Li, X., Bian, Y., et al. (2022). CD8(+) T cells and fatty acids orchestrate tumor ferroptosis and immunity via ACSL4. *Cancer Cell.* 40 (4), 365–378.e6. e366. doi:10.1016/j.ccell.2022.02.003

Liu, H., Forouhar, F., Seibt, T., Saneto, R., Wigby, K., Friedman, J., et al. (2022a). Characterization of a patient-derived variant of GPX4 for precision therapy. *Nat. Chem. Biol.* 18 (1), 91–100. doi:10.1038/s41589-021-00915-2

Liu, J., Zhang, Z., Yang, Y., Di, T., Wu, Y., and Bian, T. (2022b). NCOA4-Mediated ferroptosis in bronchial epithelial cells promotes macrophage M2 polarization in COPD emphysema. *Int. J. Chron. Obstruct. Pulmon. Dis.* 17, 667–681. doi:10.2147/copd.S354896

Liu, P., Feng, Y., Li, H., Chen, X., Wang, G., Xu, S., et al. (2020). Ferrostatin-1 alleviates lipopolysaccharide-induced acute lung injury via inhibiting ferroptosis. *Cell. Mol. Biol. Lett.* 25, 10. doi:10.1186/s11658-020-00205-0

Lotocki, V., Yazdani, H., Zhang, Q., Gran, E. R., Nyrko, A., Maysinger, D., et al. (2021). Miktoarm star polymers with environment-selective ROS/GSH responsive locations: From modular synthesis to tuned drug release through micellar partial corona shedding and/or core disassembly. *Macromol. Biosci.* 21 (2), e2000305. doi:10.1002/mabi.202000305

Ma, L., Zhang, X., Yu, K., Xu, X., Chen, T., Shi, Y., et al. (2021). Targeting SLC3A2 subunit of system X(C)(-) is essential for m(6)A reader YTHDC2 to be an endogenous ferroptosis inducer in lung adenocarcinoma. *Free Radic. Biol. Med.* 168, 25–43. doi:10.1016/j.freeradbiomed.2021.03.023

Pan, X., Lin, Z., Jiang, D., Yu, Y., Yang, D., Zhou, H., et al. (2019). Erastin decreases radioresistance of NSCLC cells partially by inducing GPX4-mediated ferroptosis. *Oncol. Lett.* 17 (3), 3001–3008. doi:10.3892/ol.2019.9888

Park, E., and Chung, S. W. (2019). ROS-mediated autophagy increases intracellular iron levels and ferroptosis by ferritin and transferrin receptor regulation. *Cell. Death Dis.* 10 (11), 822. doi:10.1038/s41419-019-2064-5

Peng, J., Hao, Y., Rao, B., and Zhang, Z. (2021). A ferroptosis-related lncRNA signature predicts prognosis in ovarian cancer patients. *Transl. Cancer Res.* 10 (11), 4802–4816. AME Publishing Company. doi:10.21037/tcr-21-1152

Reed, A., Ichu, T. A., Milosevich, N., Melillo, B., Schafroth, M. A., Otsuka, Y., et al. (2022). LPCAT3 inhibitors remodel the polyunsaturated phospholipid content of human cells and protect from ferroptosis. *ACS Chem. Biol.* 17 (6), 1607–1618. doi:10.1021/acschembio.2c00317

Ren, J. Y., Yin, B. W., Li, X., Zhu, S. Q., Deng, J. L., Sun, Y. T., et al. (2021). Sesamin attenuates PM(2.5)-induced cardiovascular injury by inhibiting ferroptosis in rats. *Food Funct.* 12 (24), 12671–12682. doi:10.1039/d1fo02913d

Schwärzler, J., Mayr, L., Radlinger, B., Grabherr, F., Philipp, M., Texler, B., et al. (2022). Adipocyte GPX4 protects against inflammation, hepatic insulin resistance and metabolic dysregulation. *Int. J. Obes.* 46 (5), 951–959. doi:10.1038/s41366-022-01064-9

Shin, D., Kim, E. H., Lee, J., and Roh, J. L. (2018). Nrf2 inhibition reverses resistance to GPX4 inhibitor-induced ferroptosis in head and neck cancer. *Free Radic. Biol. Med.* 129, 454–462. doi:10.1016/j.freeradbiomed.2018.10.426

Subramoniam, M., Binson, V. A., and Mathew, L. (2021). Detection of COPD and Lung Cancer with electronic nose using ensemble learning methods. *Clin. Chim. Acta* 523, 231–238. doi:10.1016/j.cca.2021.10.005

Sui, X., Zhang, R., Liu, S., Duan, T., Zhai, L., Zhang, M., et al. (2018). RSL3 drives ferroptosis through GPX4 inactivation and ROS production in colorectal cancer. *Front. Pharmacol.* 9, 1371. doi:10.3389/fphar.2018.01371

Sun, J., Wei, Q., Zhou, Y., Wang, J., Liu, Q., and Xu, H. (2017). A systematic analysis of FDA-approved anticancer drugs. *BMC Syst. Biol.* 11 (5), 87. doi:10.1186/s12918-017-0464-7

Sun, L., Dong, H., Zhang, W., Wang, N., Ni, N., Bai, X., et al. (2021). Lipid peroxidation, GSH depletion, and SLC7A11 inhibition are common causes of EMT and ferroptosis in A549 cells, but different in specific mechanisms. *DNA Cell. Biol.* 40 (2), 172–183. doi:10.1089/dna.2020.5730

Tang, X., Ding, H., Liang, M., Chen, X., Yan, Y., Wan, N., et al. (2021). Curcumin induces ferroptosis in non-small-cell lung cancer via activating autophagy. *Thorac. Cancer* 12 (8), 1219–1230. doi:10.1111/1759-7714.13904

V, A. B., Subramoniam, M., and Mathew, L. (2021). Detection of COPD and Lung Cancer with electronic nose using ensemble learning methods. *Clin Chim Acta* 523, 231–238. doi:10.1016/j.cca.2021.10.005

Vij, N., Chandramani-Shivalingappa, P., Van Westphal, C., Hole, R., and Bodas, M. (2018). Cigarette smoke-induced autophagy impairment accelerates lung aging, COPD-emphysema exacerbations and pathogenesis. *Am. J. Physiol. Cell. Physiol.* 314 (1), C73-C87–c87. doi:10.1152/ajpcell.00110.2016

Wang, L., Liu, Y., Du, T., Yang, H., Lei, L., Guo, M., et al. (2020). ATF3 promotes erastin-induced ferroptosis by suppressing system Xc. *Cell. Death Differ.* 27 (2), 662–675. doi:10.1038/s41418-019-0380-z

Wang, Q., Bin, C., Xue, Q., Gao, Q., Huang, A., Wang, K., et al. (2021). GSTZ1 sensitizes hepatocellular carcinoma cells to sorafenib-induced ferroptosis via inhibition of NRF2/GPX4 axis. *Cell. Death Dis.* 12 (5), 426. doi:10.1038/s41419-021-03718-4

Wang, X., Lu, S., He, C., Wang, C., Ge, P., Piao, M., et al. (2019). RSL3 induced autophagic death in glioma cells via causing glycolysis dysfunction. *Biochem. Biophys. Res. Commun.* 518 (3), 590–597. doi:10.1016/j.bbrc.2019.08.096

Xian, Z. Y., Hu, B., Wang, T., Cai, J. L., Zeng, J. Y., Zou, Q., et al. (2020). CircABCB10 silencing inhibits the cell ferroptosis and apoptosis by regulating the miR-326/CCL5 axis in rectal cancer. *Neoplasma* 67 (5), 1063–1073. doi:10.4149/neo_2020_191024N1084

Xie, S. S., Deng, Y., Guo, S. L., Li, J. Q., Zhou, Y. C., Liao, J., et al. (2022). Endothelial cell ferroptosis mediates monocrotaline-induced pulmonary hypertension in rats by modulating NLRP3 inflammasome activation. *Sci. Rep.* 12 (1), 3056. doi:10.1038/s41598-022-06848-7

Yang, Y., Lin, J., Guo, S., Xue, X., Wang, Y., Qiu, S., et al. (2020). RRM2 protects against ferroptosis and is a tumor biomarker for liver cancer. *Cancer Cell. Int.* 20 (1), 587. doi:10.1186/s12935-020-01689-8

Yao, J., Chen, X., Liu, X., Li, R., Zhou, X., and Qu, Y. (2021). Characterization of a ferroptosis and iron-metabolism related lncRNA signature in lung adenocarcinoma. *Cancer Cell. Int.* 21 (1), 340. doi:10.1186/s12935-021-02027-2

Ye, L. F., Chaudhary, K. R., Zandkarimi, F., Harken, A. D., Kinslow, C. J., Upadhyayula, P. S., et al. (2020). Radiation-induced lipid peroxidation triggers ferroptosis and synergizes with ferroptosis inducers. *ACS Chem. Biol.* 15 (2), 469–484. doi:10.1021/acschembio.9b00939

Ye, Z., Zhuo, Q., Hu, Q., Xu, X., Mengqi, L., Zhang, Z., et al. (2021). FBW7-NRA41-SCD1 axis synchronously regulates apoptosis and ferroptosis in pancreatic cancer cells. *Redox Biol.* 38, 101807. doi:10.1016/j.redox.2020.101807

Yoshida, M., Minagawa, S., Araya, J., Sakamoto, T., Hara, H., Tsubouchi, K., et al. (2019). Involvement of cigarette smoke-induced epithelial cell ferroptosis in COPD pathogenesis. *Nat. Commun.* 10 (1), 3145. doi:10.1038/s41467-019-10991-7

Zhang, H., Deng, T., Liu, R., Ning, T., Yang, H., Liu, D., et al. (2020a). CAF secreted miR-522 suppresses ferroptosis and promotes acquired chemo-resistance in gastric cancer. *Mol. Cancer* 19 (1), 43. doi:10.1186/s12943-020-01168-8

Zhang, H. L., Hu, B. X., Li, Z. L., Du, T., Shan, J. L., Ye, Z. P., et al. (2022). PKCβII phosphorylates ACSL4 to amplify lipid peroxidation to induce ferroptosis. *Nat. Cell. Biol.* 24 (1), 88–98. doi:10.1038/s41556-021-00818-3

Zhang, K., Ping, L., Du, T., Liang, G., Huang, Y., Li, Z., et al. (2021a). A ferroptosis-related lncRNAs signature predicts prognosis and immune microenvironment for breast cancer. *Front. Mol. Biosci.* 8, 678877. doi:10.3389/fmolb.2021.678877

Zhang, Y., Swanda, R. V., Nie, L., Liu, X., Wang, C., Lee, H., et al. (2021b). mTORC1 couples cyst(e)ine availability with GPX4 protein synthesis and ferroptosis regulation. *Nat. Commun.* 12 (1), 1589. doi:10.1038/s41467-021-21841-w

Zhang, Z., Guo, M., Li, Y., Shen, M., Kong, D., Shao, J., et al. (2020b). RNA-binding protein ZFP36/TTP protects against ferroptosis by regulating autophagy signaling pathway in hepatic stellate cells. *Autophagy* 16 (8), 1482–1505. doi:10.1080/15548627.2019.1687985

Zhao, C., Ghosh, B., Chakraborty, T., and Roy, S. (2021). Bavachinin mitigates DMH induced colon cancer in rats by altering p53/Bcl2/BAX signaling associated with apoptosis. *Biotech. Histochem.* 96 (3), 179–190. doi:10.1080/10520295.2020.1778087

Zhao, R., Lv, Y., Feng, T., Zhang, R., Ge, L., Pan, J., et al. (2022). ATF6α promotes prostate cancer progression by enhancing PLA2G4A-mediated arachidonic acid metabolism and protecting tumor cells against ferroptosis. *Prostate* 82 (5), 617–629. doi:10.1002/pros.24308

Zheng, Q., Lu, W., Yan, H., Duan, X., Chen, Y., Zhang, C., et al. (2022). Established pulmonary hypertension in rats was reversed by a combination of a HIF-2α antagonist and a p53 agonist. *Br. J. Pharmacol.* 179 (5), 1065–1081. doi:10.1111/bph.15696

Zhou, H., Li, F., Niu, J. Y., Zhong, W. Y., Tang, M. Y., Lin, D., et al. (2019). Ferroptosis was involved in the oleic acid-induced acute lung injury in mice. *Sheng Li Xue Bao* 71 (5), 689–697.

Zhou, J. S., Li, Z. Y., Xu, X. C., Zhao, Y., Wang, Y., Chen, H. P., et al. (2020). Cigarette smoke-initiated autoimmunity facilitates sensitisation to elastin-induced COPD-like pathologies in mice. *Eur. Respir. J.* 56 (3), 2000404. doi:10.1183/13993003.00404-2020

Zhu, T., Xiao, Z., Yuan, H., Tian, H., Chen, T., Chen, Q., et al. (2022). ACO1 and IREB2 downregulation confer poor prognosis and correlate with autophagy-related ferroptosis and immune infiltration in KIRC. *Front. Oncol.* 12, 929838. doi:10.3389/fonc.2022.929838

Zhuo, S., Chen, Z., Yang, Y., Zhang, J., Tang, J., and Yang, K. (2020). Clinical and biological significances of a ferroptosis-related gene signature in glioma. *Front. Oncol.* 10, 590861. doi:10.3389/fonc.2020.590861

Zou, Y., Henry, W. S., Ricq, E. L., Graham, E. T., Phadnis, V. V., Maretich, P., et al. (2020). Plasticity of ether lipids promotes ferroptosis susceptibility and evasion. *Nature* 585 (7826), 603–608. doi:10.1038/s41586-020-2732-8

frontiers | Frontiers in Pharmacology

TYPE Review
PUBLISHED 14 December 2022
DOI 10.3389/fphar.2022.1091779

OPEN ACCESS

EDITED BY
Yan Huang,
Anhui Medical University, China

REVIEWED BY
Guanglun Xie,
Henan Provincial Cancer Hospital, China
Hui' Dan Lin,
Ningbo First Hospital, China

*CORRESPONDENCE
Lingsuo Kong,
konglingsuo3201@ustc.edu.cn

†These authors have contributed equally to this work and share first authorship

SPECIALTY SECTION
This article was submitted to Inflammation Pharmacology, a section of the journal Frontiers in Pharmacology

RECEIVED 07 November 2022
ACCEPTED 05 December 2022
PUBLISHED 14 December 2022

CITATION
Zhou D, Duan Z, Li Z, Ge F, Wei R and Kong L (2022), The significance of glycolysis in tumor progression and its relationship with the tumor microenvironment.
Front. Pharmacol. 13:1091779.
doi: 10.3389/fphar.2022.1091779

The significance of glycolysis in tumor progression and its relationship with the tumor microenvironment

Daoying Zhou[1,2†], Zhen Duan[3†], Zhenyu Li[1,2†], Fangfang Ge[1,2], Ran Wei[1] and Lingsuo Kong[1*]

[1]Department of Anesthesiology, The First Affiliated Hospital of USTC, Division of Life Sciences and Medicine, University of Science and Technology of China, Hefei, China, [2]Department of Provincial Clinical College, Wannan Medical College, Wuhu, China, [3]Function Examination Center, Anhui Chest Hospital, Hefei, China

It is well known that tumor cells rely mainly on aerobic glycolysis for energy production even in the presence of oxygen, and glycolysis is a known modulator of tumorigenesis and tumor development. The tumor microenvironment (TME) is composed of tumor cells, various immune cells, cytokines, and extracellular matrix, among other factors, and is a complex niche supporting the survival and development of tumor cells and through which they interact and co-evolve with other tumor cells. In recent years, there has been a renewed interest in glycolysis and the TME. Many studies have found that glycolysis promotes tumor growth, metastasis, and chemoresistance, as well as inhibiting the apoptosis of tumor cells. In addition, lactic acid, a metabolite of glycolysis, can also accumulate in the TME, leading to reduced extracellular pH and immunosuppression, and affecting the TME. This review discusses the significance of glycolysis in tumor development, its association with the TME, and potential glycolysis-targeted therapies, to provide new ideas for the clinical treatment of tumors.

KEYWORDS

glycolysis, tumor microenvironment, immune cells, inflammatory factors, targeted therap

1 Introduction

Cancer is a massive global health challenge (Yang X et al., 2022), and is a major contributor to the universal disease burden. The global burden of disease is expected to continue to grow in the next 20 years. It is estimated that 23.6 million (95% UI, 22.2–24.9 million) new cases and 10 million (95% UI, 9.36–10.6 million) cancer-associated deaths occurred in 2019. According to the Global Burden of Disease cancer deaths, with a 26.3% (95% UI, 20.3%–32.3%) rise in novel cancer cases, and a 20.9% (95% UI, 14.2%–27.6%) elevation in cancer-related mortality since 2010, cancer ranked second to cardiovascular disease among global deaths in 2019 (Kocarnik et al., 2022). Owing to the persistence of the COVID-19 pandemic, and subsequent delays and disruptions in

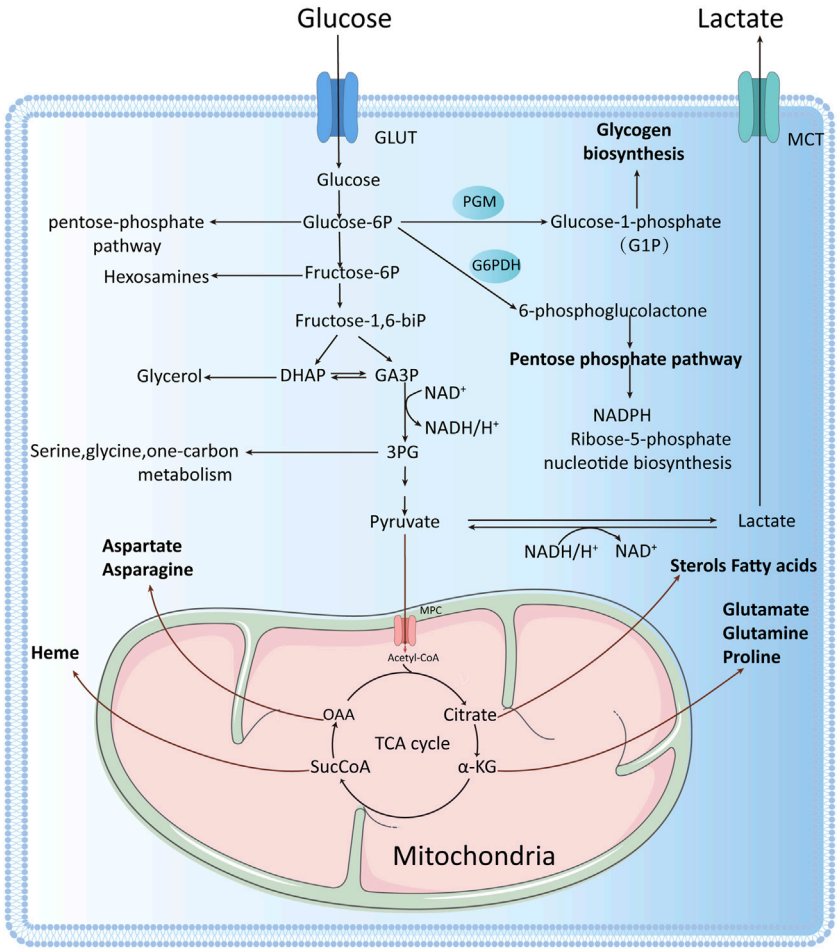

FIGURE 1
One glucose molecule is broken down intracellularly to two pyruvate molecules, which can enter the mitochondrion to participate in the tricarboxylic acid (TCA) cycle under aerobic conditions or to produce lactate under anaerobic conditions. Tumor cells rely mainly on aerobic glycolysis for energy production, even under oxygen-sufficient conditions, with one glucose molecule entering the glycolytic pathway to produce two net ATP molecules. Glycolysis involves the production of many intermediate metabolites apart from ATP. These intermediate metabolites can participate in other biosynthetic pathways, for example, glucose-6-phosphate can enter the pentose phosphate pathway, fructose 6-phosphate can enter the hexosamine biosynthesis pathway, dihydroxyacetone phosphate can be converted to glycerol 3-phosphate, and glycerol 3-phosphate can be converted to serine, cysteine, and glycine, among others.

cancer screening, diagnosis, and therapy worldwide (Kocarnik et al., 2022), the number of avoidable cancer deaths has increased dramatically (Maringe et al., 2020). Hence, it is critical to elucidate the occurrence and development of tumors and clinical therapeutic targets to reduce the morbidity and mortality of cancer patients. Glycolysis is a process of oxidative glucose catabolism, whereby glucose is broken down to lactate with a small amount of ATP production under anaerobic conditions (Fuller and Kim, 2021). Recent studies have demonstrated the essential roles of glycolysis in numerous tumors (Wang L et al., 2022; Xu et al., 2022; Yang J et al., 2022). These include the regulation of tumor growth, invasion, chemoresistance, and the tumor microenvironment (TME) (Bi et al., 2021). Studies have revealed that the TME strongly modulates tumorigenesis, tumor development, metastasis, and therapeutic response (Xiao and Yu, 2021). The TME is a complex tumor-associated environment, specifically supporting the survival and development of the tumor cells. It includes tumor cells, various immune cells, secretory factors, and extracellular matrix (ECM). Tumor cells and the TME constantly interact with one another and co-evolve (Xiao and Yu, 2021). In this review, we mainly discuss the significance of glycolysis in tumorigenesis and tumor development, the relationship between glycolysis and various types of cells and cytokines within the TME, and glycolysis-targeted anti-tumor therapy.

2 Tumor cell metabolism and glycolysis

Cellular energy is primarily derived from glucose conversion. Under conditions of sufficient oxygen, cells undergo aerobic oxidation, whereby glucose oxidizes to water and carbon dioxide. This is the main form of sugar oxidation, as well as the main process of cellular energy production. Under anaerobic conditions, however, glucose or glycogen breaks down to form lactate and energy. This process is known as anaerobic glycolysis (Figure 1).

Glycolysis has three main features: 1. It is the only way to produce ATP under anaerobic conditions or in cells with no mitochondria like erythrocytes and hyperthyroid cells. Under these circumstances, pyruvate is converted to lactate; 2. In presence of oxygen, glycolysis produces pyruvate, which enters into the tricarboxylic acid (TCA) cycle (also known as the citric acid or Krebs cycle) within the mitochondria to produce ATP; 3. Multiple glycolytic and TCA cycle metabolites can also become involved in anabolic networks to produce NADPH and intermediates required for glycogen, lipids, nucleotides and protein syntheses (Chandel, 2021). Thus, the primary goal of glycolysis is to produce intermediates that activate biosynthetic networks. Taken together, under oxygen availability, mitochondria provide a large amount of ATP to most cells. When oxygen is no longer available, glycolysis is activated to generate ATP for cell survival (Chandel, 2021).

Malignant tumor cells undergo excessive proliferation and detachment from neighboring cells to translocate to distant locations for metastasis. This requires ample energy and biosynthetic precursors that accelerate cell division, invasion, and migration. As an early tumor expands, it grows beyond the diffusion limit of local blood supply, which leads to hypoxia and upregulation of hypoxia-inducible transcription factor (HIF) expression (Infantino et al., 2021). Owing to the resulting reduced dependence on aerobic respiration, tumor cell metabolism generally switches to glycolysis by enhancing the production of glycolytic enzymes, glucose transporter proteins, and mitochondrial metabolic inhibitors (Hsu and Sabatini, 2008). By altering their energy metabolism, tumor cells gain a strong ability to survive in a hostile environment. This is known as “metabolic reprogramming”, and this mostly occurs due to enhanced glycolysis (Hsu and Sabatini, 2008).

Under oxygenated conditions, normally differentiated cells maximize ATP synthesis *via* mitochondria-mediated glucose oxidative phosphorylation. In contrast, tumor cells consume excess glucose and synthesize massive quantities of lactate, thereby relying on glycolysis for energy production even in a well-oxygenated environment (Zahra et al., 2020). This process is aerobic glycolysis or the Warburg effect (Wong et al., 2013). Although glycolysis is considerably less efficient in producing ATP per molecule of glucose, it produces ATP at a faster pace than oxidative phosphorylation. Thus, the unlimited tumor cell proliferation is amply supplied with rapidly producing energy (Zhang et al., 2020a; Domiński et al., 2020). Therefore, glycolysis is a critical element in tumor progression.

3 The significance and related mechanism of glycolysis in tumorigenesis and tumor development

Tumor cells exhibit a specific pattern of glucose metabolism, namely aerobic glycolysis, which is critical for tumorigenesis and tumor development, and it affects tumor growth, invasion, chemoresistance, and the TME (Bi et al., 2021). In pancreatic ductal adenocarcinoma, glycolysis was shown to promote tumor invasion and migration *via* large amounts of substrate production, and glycolytic enzymes and actin association, which ultimately support vigorous tumor cell growth (Yang et al., 2020). In addition, essential enzymes and glycolysis intermediates may modulate pancreatic ductal adenocarcinoma metastasis *via* participation in colonization-related networks, angiogenesis, epigenetic mechanisms, or activation of the epithelial-mesenchymal transition (Tsutsumi et al., 2004; Azoitei et al., 2016; McDonald et al., 2017; Liu et al., 2021). Non-coincidentally, Deng et al. (2019) also reported that aerobic glycolysis is essential for angiogenesis in colorectal cancer (CRC) cells, and angiogenesis is a critical modulator of tumor progression and metastasis. In CRC cells, glucose-derived aerobic glycolysis-generated lactic acid accumulates in the TME, wherein it stimulates the formation of vascular endothelial cells, which, in turn, promote tumor progression and metastasis. CRC cells also rely on aerobic glycolysis-derived ATP for rapid growth and chemoresistance (Wang et al., 2020). Emerging reports suggested that hypoxic tumors with enhanced glycolysis are more prone to metastasis than normoxic tumors. Therefore, augmented glycolysis is a major contributor to metastasis, and is a poor prognostic phenotype in cancers such as prostate cancer (Ghanavat et al., 2021).

Impaired energy metabolism and immune evasion are two major characteristics of cancer. Cancer cells employ the glycolytic network for energy production and reprogram the TME *via* the abundant energy supply (Chang et al., 2015; Ganapathy-Kanniappan, 2017; Vaupel et al., 2019). Multiple reports have suggested that tumor metabolism and tumor-based immune evasion are dependent on one another (Cascone et al., 2018). On the one hand, Jiang et al. (2019) revealed a strong direct association between tumor glycolysis and tumor immunity in various cancers, with glycolytic activity being more predictive of immune signaling in different cancers compared to tumor mutational burden and tumor aneuploidy. In addition, glycolysis also increased the programmed cell death ligand 1 (PD-L1) content in tumor cells, thereby enhancing the anti-PD-1/PD-L1 immunotherapeutic response. Tumors with enhanced

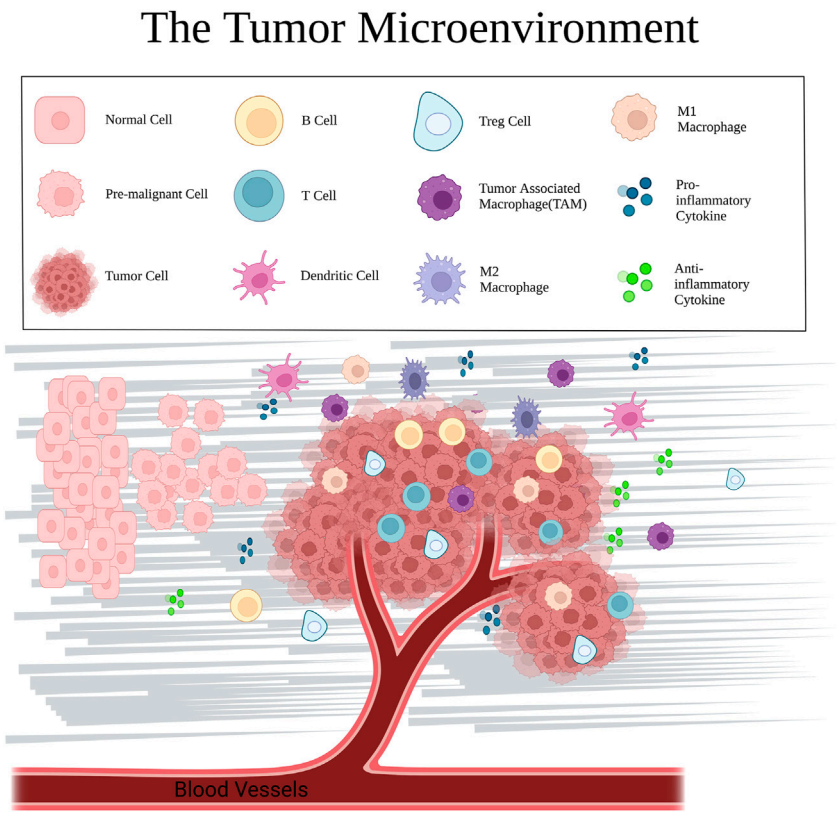

FIGURE 2
Major cellular components and mediators in the TME, including normal cells, cancer cells, immune cells (T cells, B cells, dendritic cells, TAMs, and macrophages), cytokines, and extracellular matrix.

glycolysis exhibit better immunotherapeutic response and good survival in an immunotherapeutic setting. Therefore, tumor glycolytic activity is a potential prognostic indicator for immunotherapeutic response in a variety of cancers (Jiang et al., 2019). On the other hand, Li et al. (2020) reported a strong association between enhanced glycolytic activity and pro-tumor immunity/inflammation in breast cancer. In the high-glycolysis group, there was a marked elevation in the tumor immunity/inflammation-associated gene expression and immune/inflammatory networks, particularly the IL-17 axis. Moreover, several immune/inflammatory cells such as Th2 cells and macrophages were enriched, whereas the invasion of killer immune cells such as NKT cells was diminished, and the immune checkpoint genes PD-L1, CTLA4, FOXP3, and IDO1 were elevated. This evidence suggests that tumor glycolysis can accelerate tumor immunity/inflammation *via* the IL-17 axis to enhance the immune/inflammatory functions of tumor cells (Li et al., 2020).

Furthermore, glycolytic activity is also closely related to apoptosis, a strong direct indicator of immune function. This indicates that apoptosis may serve as a bridge between glycolytic and immune activities in tumors (Jiang et al., 2019). It was revealed that increased aerobic glycolysis in nasopharyngeal carcinoma cells *via* the IRF2/CENP-N/AKT axis promoted malignant biological behavior while inhibiting apoptosis (Qi et al., 2021). In hepatocellular carcinoma (HCC), aerobic glycolysis was also found to inhibit Silibinin-triggered apoptosis in human HCC HepG2 and Hep3B cells (Yang et al., 2021). In addition to the glycolysis-mediated suppression of tumor cell apoptosis, its metabolite lactate accumulates in the TME, leading to acidification of the extracellular pH and immunosuppression, which, in turn, affect the TME (de la Cruz-López et al., 2019).

4 The TME

Cell proliferation and apoptosis in normal tissues remain in a state of equilibrium. Disruption of this balance can result in the development of various benign and malignant neoplastic diseases. The TME is a cellular niche comprising a dynamic heterogeneous collection of tumor or cancer stem cells, as well as being involved in the constant modulation of infiltrating and resident host cells, secretory factors, and ECM (Xiao and Yu,

2021). This niche not only includes the structure, function and metabolism of the tumor-host tissue, but also the internal environment (nucleus and cytoplasm) of the tumor cells themselves (Anderson and Simon, 2020; Cao et al., 2022). The cellular components of the TME include the tumor cells themselves, as well as adipocytes, fibroblasts, tumor vascular system, lymphocytes, dendritic cells, and tumor-related fibroblasts (Figure 2), each of which has a unique immune capacity that will determine the survivability and influence of tumor cells on neighboring cells (Arneth, 2019). The non-cellular components include chemokines and cytokines (for example, IL-1β, IL-33, IL-6, TNF-α, and IL-17). The cellular and non-cellular components together form a complex TME that synergistically supports tumor growth (Arneth, 2019). Parenchymal and mesenchymal cells are morphologically, phenotypically, and functionally distinct among patients, between primary and metastatic tumors, and even within individual tumors at multiple levels (Naxerova et al., 2014; Naxerova and Jain, 2015). Tumor cells cross-talk with neighboring cells using the circulatory and lymphatic systems to regulate tumor development. During tumor cell proliferation, tumor cells recruit surrounding non-tumor cells (Balamurugan, 2016) to foster a specific TME that facilitates local tumor development and metastasis to distant organs. These tumor cells associate with host cells to generate an aberrant organoid structure (Ge and Ding, 2020; Uneda et al., 2021). The available literature establishes TME as an essential niche for tumor development, heterogeneity among and within tumors, and systemic therapy resistance (Jin and Jin, 2020; Wang and Ilyas, 2021). It is well established that glycolysis modulates the TME, and, in recent years, numerous studies have reported links among glycolysis, immune cells, and inflammatory factors within the TME.

5 Relationships between glycolysis and immune cells in the TME

Glycolysis is inseparable from the immune cells present in the TME. Macrophages are specialized phagocytic cells belonging to the innate immune system, and they serve an essential function in the TME, along with their ability to fight inflammation. Macrophages are typically classified as M1 and M2 types, with M1-type macrophages promoting inflammatory responses, and M2-type macrophages promoting tumor development (Jablonski et al., 2015). The M2-type macrophages differentiate to form tumor-associated macrophages (TAM), which are critical regulatory cells for tumor immunity and immunotherapy (DeNardo and Ruffell, 2019). Glycolysis produces lactate, a pro-tumor metabolite, and lactate promotes M2-like gene expression in M1 macrophages, and enhances PD-L1 expression in M1 macrophages, which leads to an M1 phenotype that is both pro-inflammatory and potentially oncogenic (Morrissey et al., 2021). In HCC, cancer cell-based fibronectin 1 (FN-1) activates glycolysis within macrophages by triggering TLR4, which results in the significant upregulation of pyruvate kinase M2 (PKM2), which, in turn, enhances the syntheses of IL-1β, IL-12p70, TNF-α, HLA-DR, and PD-L1. In addition to being a glycolytic rate-limiting enzyme, PKM2 enters the nucleus to maintain HIF-1α stability, while inducing macrophage polarization, which diminishes the anti-tumor activity of macrophages (Lu et al., 2022). Similarly, lactate accumulation in breast cancer contributes to the M2-type macrophage polarization, which promotes tumor development both *in vivo* and *in vitro*. Additionally, this is correlated with worse outcomes in breast cancer patients (Jiang et al., 2022). It was revealed that, in pancreatic cancer (PC), the TAM paracrine factor CCL18 promotes malignant tumor progression and induces glycolysis by upregulating VCAM-1. In contrast, VCAM-1-triggered lactate formation in PC cells enhances aerobic glycolysis while activating macrophages to form a TAM-like phenotype, creating a positive feedback loop (Ye et al., 2018). The first rate-limiting enzyme in glycolysis is hexokinase. Hexokinase 3 (HK3) expression was shown to be strongly correlated with macrophage and dendritic cell infiltration. Moreover, it can promote the progression of renal clear cell carcinoma (Xu et al., 2021). Fructose-2,6-bisphosphatase 3 (PFKFB3) is a glycolytic activator, and PFKFB3 upregulation in peritumor-associated monocytes/macrophages in HCC promotes tumor progression *via* attenuation of the cytotoxic T lymphocyte response in tumor tissue using the PFKFB3/NF-κB/PD-L1 axis (Chen D.P et al., 2019).

Lymphocytes are another critical element for the TME. Moreover, the antitumor activity of lymphocytes is influenced by multiple factors. Cancer cell-mediated glycolysis is known to impair T cell activation and antitumor responses. For example, lactic acid accumulation impairs the activation and migration of T cells and promotes the immune escape of tumor cells (Beckermann et al., 2017). Among them, regulatory T cells (Tregs) strongly modulate homeostasis of the immune system, body immune tolerance, enhanced angiogenesis, tumor growth, and proliferation, as well as tumor transformation into metastatic disease (Paluskievicz et al., 2019). PD-1 expression of Treg cells is markedly increased in highly glycolytic tumors, relative to effector T cells (Kumagai et al., 2022). Tumor glycolytic activity is directly associated with PD-L1 levels and the immune response. Hence, tumor glycolytic activity can serve as a marker for tumor immunotherapeutic response prediction (Jiang et al., 2019).

NK cells exhibit antitumor cytotoxicity. Moreover, glycolysis-induced lactate production and the acid environment resulting from the excess lactate markedly reduce NK cell cytotoxicity, causing them to lose their antitumor function. In addition, the nuclear factor of activated T cells (NFAT) axis-related genes are suppressed, which leads to a decrease in NFAT-regulated IFN-γ production, an essential

factor for the hypoxia-induced accelerated glycolysis in cancer cells (Brand et al., 2016; Hasan et al., 2022). One study revealed that glycolysis-related genes are highly enriched in advanced cancer patients, particularly, when tumors undergo hypoxia. Moreover, pre-activated NK cell regulation *via* the ERK/STAT3 pathway enhances NK cell proliferation and cytotoxicity (Lim et al., 2021). Knockdown of CIS, an intracellular protein, in induced pluripotent stem cell-derived NK cells (iPSC-NK cells) improves metabolic adaptations, as evidenced by enhanced basal glycolytic and glycolytic capacities, which contributes to marked increases in NK cytotoxicity and antitumor activity (Zhu et al., 2020).

Dendritic cells (DCs) are antigen-presenting cells, and are responsible for the capture of pathogen- or tumor-associated antigens for T cell presentation to induce an immune response. However, the DC-based immune activity in the TME is usually suppressed. Moreover, lactate activates G protein-coupled receptors (GPR81) on murine DCs (which inhibit MHC II presentation on the DC surface), as well as the lactate-induced acidic TME (which inhibits antigen uptake by DCs and stabilizes antigen-MHC-I complexes) to promote tumor escape (Peng et al., 2021). Furthermore, HIF-1α and c-Myc convert more pyruvate to lactate by interacting with the lactate dehydrogenase (LDH-A) promoter in the hypoxic environment within tumor cells, and the resulting lactate accumulation within the TME further suppresses DC activation and antigen expression (Burgdorf et al., 2020).

6 Relationship between glycolysis and inflammatory factors in the TME

Inflammatory cells are also present in the TME, where they modulate tumor growth by the secretion of active molecules (such as IL-1β, IL-33, IL-6, TNF-α, and IL-17) into the TME. Moreover, chronic inflammation leads to the reprogramming of the tumor cell glucose metabolism to promote tumorigenesis (Vaughan et al., 2013). The IL-1 family encompasses essential inflammatory cytokines such as IL-1α, IL-1β, and IL-33, which modulate immune and inflammatory responses and regulate glycolysis by activating the glycolytic enzymes HK, glucokinase, PFK, and LDHA (Tan et al., 2018). IL-1β has been intensively studied, and IL-1β production by M2 macrophages promotes glycerol-3 -phosphate dehydrogenase (GPD2) phosphorylation, which, in turn, accelerates the glycolytic rate to promote glioma cell proliferation (Lu et al., 2020). IL-1β also promotes glycolysis in lung adenocarcinoma cells *via* the p38 axis, which further enhances lung adenocarcinoma cell migration and invasion (Tan et al., 2021). IL-33, on the other hand, accelerates Th2-associated cytokine synthesis and upregulates glucose transporter protein 1 (GLUT1) through the IL-33/ST2 pathway to enhance glucose uptake and glycolysis in tumor cells, while promoting growth and metastasis of non-small cell lung cancer (Wang et al., 2016).

Expression of the pro-inflammatory cytokine IL-6 is significantly elevated in numerous malignancies and is correlated with poor survival outcomes in several cancer types. IL-6 is a major modulator of the STAT3 signaling pathway, and it activates Glut5 by triggering the STAT3 axis to regulate fructose metabolism and tumorigenesis (Huang et al., 2022). Chen X et al. (2019) reported that IL-6 stimulates PC cell proliferation, survival, and glycolysis *via* the GP130/STAT3 axis. Zhang et al. (2021) also revealed that the immunoglobulin superfamily containing leucine-rich repeat (ISLR) gene deficiency markedly reduced JAK2 and STAT3 phosphorylation, thereby inhibiting the IL - 6/JAK/STAT3 axis, which, in turn, accelerates apoptosis, and suppresses non-small cell lung cancer cell proliferation, migration, invasion, and glycolysis. In addition, IL-6 was also shown to enhance glycolysis by upregulating the expression of the glycolytic enzyme PFKFB3 to promote colorectal carcinogenesis and progression (Han et al., 2016). Zhang et al. (2018) observed that the IL-6-induced enhancement of phosphoglycerate kinase 1 (PGK1) threonine (T) 243 phosphorylation was mediated by the 3-phosphatidylinositol-dependent protein kinase 1 (PDPK1) in tumor cells. This phosphorylation enhances PGK1-catalyzed glycolytic reactions by modulating their substrate affinities and has been correlated with human glioblastoma multiforme (GBM) malignancy and prognosis.

TNF-α and IL-17 are produced ubiquitously in acute and chronic inflammation, and both are associated with CRC. TNF-α and IL-17 synergistically enhance glycolysis and lactate production in CRC HT-29 cells *via* activation of the NF-κB axis in tumor cells, and they promote GLUT1 and hexokinase 2 (HK2), as well as expression of the common target genes HIF-1α and c-myc which, in turn, promote tumorigenesis (Straus, 2013). Emerging reports have suggested that the treatment of human colon cancer adenocarcinoma with the two pro-inflammatory cytokines, TNF-α and IL-17, also altered LDH activity, leading to an LDH shift to the A isoform, LDH-A, a major modulator of aerobic glycolysis. This effectively reduces pyruvate and enhances lactate levels in tumor tissue, thereby increasing cancer cell migration. Meanwhile, these two cytokines also induce the epithelial-mesenchymal transition characteristics of human colon cancer adenocarcinoma cells, including decreased e-calcineurin levels and increased metalloproteinase secretion (Baumann et al., 2009; Manerba et al., 2017). The stimulatory role of glycolysis in tumorigenesis and tumor progression has brought the glycolytic pathway into the public eye as a potential therapeutic target of anti-tumor therapy.

7 Glycolysis-targeted cancer therapy

Aerobic glycolysis is a critical metabolic property of tumor cells, and it provides rapid energy, essential precursors for a variety of other metabolic pathways, and raw materials for the synthesis of multiple biomolecules (Pavlova and Thompson, 2016). More significantly, enhanced glycolysis within tumor cells results in the synthesis of excess lactate which, along with the reduced glucose metabolic environment, sustains the

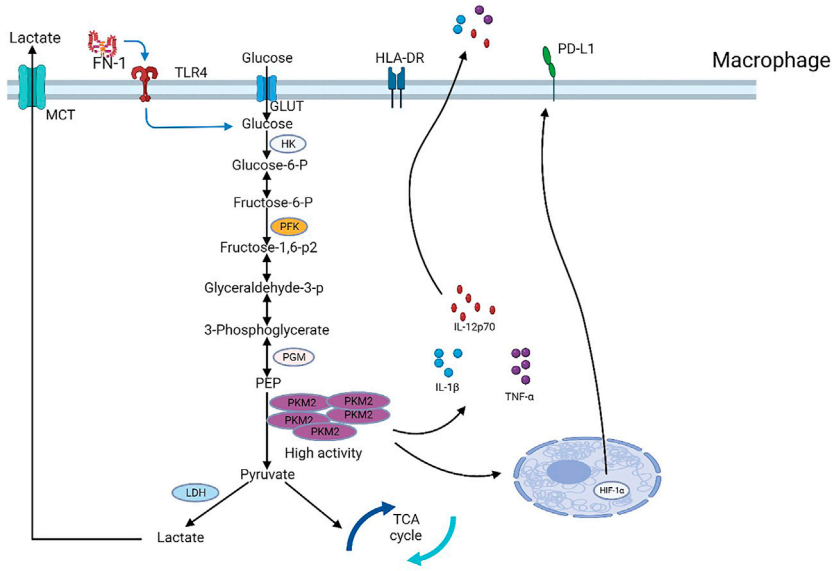

FIGURE 3
Major rate-limiting enzymes, metabolic enzymes, and transporters in the glycolytic pathway. PKM2, a key glycolytic enzyme regulated by fibronectin 1 (FN-1) secreted by hepatocellular carcinoma cells, controls PD-L1 expression in macrophages in a HIF-1α-dependent manner.

immunosuppressive TME (Ippolito et al., 2019). The aerobic glycolysis phenomenon is further accompanied by an upregulation of glycolysis-related rate-limiting enzymes, transporters, and other metabolic enzyme levels, namely, GLUT1, HK2, phosphofructokinase 1 (PFK1), PKM2, LDH-A, and monocarboxylate transporter protein 1 (MCT1) (Tanner et al., 2018) (Figure 3).

GLUT1 is a glucose transporter protein that plays a role in transporting glucose or fructose in cells. Xiao et al. (2018) showed that GLUT1 knockdown inhibits prostate cancer growth by suppressing tumor-cell glycolysis and proliferation while promoting cell cycle arrest. Similarly, other researchers reported that GLUT1 deficiency also inhibited CRC cell proliferation, migration, and glycolysis (Zhang et al., 2020b), while reversing the Warburg effect in gastric cancer cells, while enhancing cellular apoptosis (Dai et al., 2021). Dihydroartemisinin and rhodopsin are also reported to exert anticancer effects by inhibiting GLUT1 (Gao et al., 2020; Wang et al., 2021). Furthermore, HK is the first rate-limiting enzyme in the glycolytic reaction. It converts glucose to glucose-6-phosphate (G-6-P). HK2 is an isoform of HK, and in human glioblastoma cells, elevated glucose levels induce the mitochondrial separation of HK2, which then phosphorylates IκBα, and causes its destruction, thereby transcriptionally enhancing PD-L1, which promotes tumor cell immune evasion and brain tumor development (Guo et al., 2022). It is reported that HK2 deficiency significantly inhibits glycolysis and tumor cell growth in HCC (Wu et al., 2019), while HK2 activity suppression promotes cell death in glioblastoma (Uludağ et al., 2022). Current studies have demonstrated that 2-deoxy-D-glucose (2-DG) and 3-bromopyruvate (3-BrPA) can act as inhibitors of HK2 and inhibit the glycolytic process of tumor cells, thereby exerting an anti-tumor effect (Fan et al., 2019; Pajak et al., 2019).

PFK1 is the second rate-limiting enzyme in the glycolytic process. It was found that siRNA-based PFK1 deficiency enhanced apoptosis and inhibited rectal cancer cell migration and proliferation (Tian et al., 2020). Moreover, the stable downregulation of PFK1 expression suppresses human nasopharyngeal carcinoma CNE2 cell development, while inducing apoptosis, and reducing cell invasion and metastasis (Li S et al., 2021). So, PFK1 is a promising new target for nasopharyngeal and rectal cancer therapy, and it has great potential that can be extended to other malignancies. The activity of PFK1 is regulated by PFKFB3. PFKFB3 catalyzes fructose 6-phosphate to produce fructose 2,6-diphosphate, which is a metabotropic activator of PFK1 and can significantly increase the catalytic activity of PFK1. There are a number of PFKFB3 inhibitors developed so far, including KAN0438757, 3PO, and PFK15 (Hu et al., 2020; De Oliveira et al., 2021; Yan et al., 2021). Moreover, PKM2 is an enzyme that modulates the final rate-limiting glycolytic step, and it is a critical modulator of tumor metabolism. PKM2 is overexpressed in multiple cancers, and it promotes tumor cell proliferation and metastasis (Zhu et al., 2021). PKM2 methylation reversibly shifts the metabolic balance in breast cancer cells from oxidative phosphorylation to aerobic glycolysis, whereas inhibition of PKM2 methylation disrupts this intricate balance in cancer

cells and suppresses breast cancer cell proliferation, migration, and metastasis (Liu et al., 2017). Recent studies have reported that shikonin and its analogs, flavonoid derivatives, 2,3-dithiocarbamate substituted naphthoquinones, benserazide, and Compounds 3 k and 10i, can act as inhibitors of PKM2 and inhibit aerobic glycolysis of tumor cells to exert anti-tumor effects (Zahra et al., 2020; Zhu et al., 2021).

LDH-A is a cytoplasmic enzyme that is primarily involved in anaerobic and aerobic glycolytic processes, and elevated LDH-A levels are strongly correlated with worse prognosis among tumor patients (Valvona et al., 2016). It was reported that reduced LDH-A expression suppresses glycolysis, tumor growth, and lung metastasis in thyroid cancer *in vitro* and *in vivo* (Huo et al., 2021). LDH-A knockdown in triple-negative breast (TNBC) cell lines impairs the aerobic glycolytic process, thereby significantly inhibiting the proliferation, migration, and invasion of TNBC cells (Wang W et al., 2022). Currently, gossypol (AT-101) and its derivatives FX-11, galloflavin, and N-hydroxy indole-based compounds have been shown to selectively and preferentially inhibit LDHA and suppress tumor progression (Ippolito et al., 2019). Moreover, MCTs modulate glycolytic metabolism and tumor cell survival using a proton-linked transmembrane lactate transport, and it was revealed that the pharmacological inhibition of MCT1 effectively inhibits glioma angiogenesis, which leads to a reduction in glioma cell growth, proliferation, and migration (Miranda-Gonçalves et al., 2013). Similarly, the siRNA-mediated MCT1 knockdown suppresses kidney cancer cell proliferation and migration, thereby suppressing tumor progression (Li M et al., 2021). To date, α-cyano-4-hydroxycinnamate (CHC), phloretin, quercetin, AZD3965, and AR-C155858 have been found to have some anticancer potential as inhibitors of MCT1 (Puri and Juvale, 2020). Therefore, targeting GLUT1, HK2, PFK1, PKM2, LDH-A, or MCT1 in various tumors may be an effective approach for treating tumors, and all these possibilities have the potential to be effective therapeutic targets against tumors.

In addition, there are numerous other therapeutic targets for tumors. For example, mTOR is a major direct regulator of the Warburg effect, while HIF1α, a downstream mTOR target, is highly expressed and synergizes with c-Myc-hnRNP splicing modulators to enhance PKM2 expression, which, in turn, promotes tumor progression. Thus, the entire mTOR/HIF1α/Myc -hnRNPs/PKM2 axis components can serve as potential glycolytic therapeutic targets for tumors (Sun et al., 2011). Others also revealed that PD-L1 is highly expressed in Tregs and that PD-L1 inhibition in Tregs or Tregs may be an effective measure against cancer (Kim et al., 2019). CTLA-4 is constitutively expressed in tumor-infiltrating Tregs, while it is only expressed in low amounts of the surfaces of circulating Tregs and lymphoid organs. Therefore, it can also be selectively used in tumor tissues with anti-CTLA-4 antibodies (Paluskievicz et al., 2019). Drugs for these therapeutic targets are being researched and developed, and a growing number of researchers are dedicating themselves to them.

8 Conclusion

In summary, TME-based glycolysis is closely related to a variety of immune cells, namely, macrophages, T lymphocytes, NK cells, DCs, and inflammatory cytokines such as IL-1β, IL-33, IL-6, IL-17, and TNF-α. Together, these promote tumor development, invasion, metastasis, chemoresistance, and regulate tumor immune function. Recent studies have revealed that tumor glycolytic activity can also serve as a biomarker for tumor immunotherapeutic response prediction. Given that aerobic glycolysis is critical for tumor progression, the targeting of aerobic glycolysis has become a current research hotspot for the development of new anti-cancer treatments. Tumor cells mainly rely on aerobic glycolysis for the specific reprogramming of glucose metabolism, and many metabolic enzymes are involved in the glycolytic process. Targeting these metabolic enzymes to inhibit tumor progression requires the design of drugs that specifically target metabolic enzymes in the tumor, thus inhibiting tumor progression and minimizing the side effects on normal tissues. Targeted glycolytic therapy may enhance the clinical treatment of tumor patients through its combination with other therapeutic approaches, such as immune- and chemotherapies. It is critical to gain a deeper knowledge of the mechanism by which glucose metabolism is altered in tumors and how it regulates cancer cells. Hence, further investigation into the metabolic enzymes associated with glycolysis as therapeutic targets in tumors is warranted. This requires the design and development of highly specific and selective inhibitors for these enzymes and the development of treatment protocols that both improve efficacy and reduce toxicity when combined with other chemotherapeutic agents. This will help create a positive atmosphere for the fight against cancer and will bring new hope to patients with cancer.

Author contributions

DZ designed and wrote this manuscript, ZD and ZL revised the manuscript. FG and RW checked the manuscript. LK designed and checked the manuscript.

Funding

This study is supported by the Fundamental Research Funds for the Central Universities granted to LK (WK9110000090).

Acknowledgments

The authors would like to thank all the reviewers who participated in the review, as well as MJEditor (www.mjeditor.

com) for providing English editing services during the preparation of this manuscript.

Conflict of interest

The authors declare that the research was conducted in the absence of any commercial or financial relationships that could be construed as a potential conflict of interest.

Publisher's note

All claims expressed in this article are solely those of the authors and do not necessarily represent those of their affiliated organizations, or those of the publisher, the editors and the reviewers. Any product that may be evaluated in this article, or claim that may be made by its manufacturer, is not guaranteed or endorsed by the publisher.

References

Anderson, N. M., and Simon, M. C. (2020). The tumor microenvironment. *Curr. Biol.* 30 (16), R921. doi:10.1016/j.cub.2020.06.081

Arneth, B. (2019). Tumor microenvironment. *Med. Kaunas.* 56 (1), 15. doi:10.3390/medicina56010015

Azoitei, N., Becher, A., Steinestel, K., Rouhi, A., Diepold, K., Genze, F., et al. (2016). PKM2 promotes tumor angiogenesis by regulating HIF-1α through NF-κB activation. *Mol. Cancer* 15, 3. doi:10.1186/s12943-015-0490-2

Balamurugan, K. (2016). HIF-1 at the crossroads of hypoxia, inflammation, and cancer. *Int. J. Cancer* 138 (5), 1058–1066. doi:10.1002/ijc.29519

Baumann, F., Leukel, P., Doerfelt, A., Beier, C. P., Dettmer, K., Oefner, P. J., et al. (2009). Lactate promotes glioma migration by TGF-beta2-dependent regulation of matrix metalloproteinase-2. *Neuro. Oncol.* 11 (4), 368–380. doi:10.1215/15228517-2008-106

Beckermann, K. E., Dudzinski, S. O., and Rathmell, J. C. (2017). Dysfunctional T cell metabolism in the tumor microenvironment. *Cytokine Growth Factor Rev.* 35, 7–14. doi:10.1016/j.cytogfr.2017.04.003

Bi, J., Bi, F., Pan, X., and Yang, Q. (2021). Establishment of a novel glycolysis-related prognostic gene signature for ovarian cancer and its relationships with immune infiltration of the tumor microenvironment. *J. Transl. Med.* 19 (1), 382. doi:10.1186/s12967-021-03057-0

Brand, A., Singer, K., Koehl, G. E., Kolitzus, M., Schoenhammer, G., Thiel, A., et al. (2016). LDHA-associated lactic acid production blunts tumor immunosurveillance by T and NK cells. *Cell Metab.* 24 (5), 657–671. doi:10.1016/j.cmet.2016.08.011

Burgdorf, S., Porubsky, S., Marx, A., and Popovic, Z. V. (2020). Cancer acidity and hypertonicity contribute to dysfunction of tumor-associated dendritic cells: Potential impact on antigen cross-presentation machinery. *Cancers (Basel)* 12 (9), 2403. doi:10.3390/cancers12092403

Cao, H., Huang, T., Dai, M., Kong, X., Liu, H., Zheng, Z., et al. (2022). Tumor microenvironment and its implications for antitumor immunity in cholangiocarcinoma: Future perspectives for novel therapies. *Int. J. Biol. Sci.* 18 (14), 5369–5390. doi:10.7150/ijbs.73949

Cascone, T., McKenzie, J. A., Mbofung, R. M., Punt, S., Wang, Z., Xu, C., et al. (2018). Increased tumor glycolysis characterizes immune resistance to adoptive T cell therapy. *Cell Metab.* 27 (5), 977–987. doi:10.1016/j.cmet.2018.02.024

Chandel, N. S. (2021). Glycolysis. *Cold Spring Harb. Perspect. Biol.* 13 (5), a040535. doi:10.1101/cshperspect.a040535

Chang, C. H., Qiu, J., O'Sullivan, D., Buck, M. D., Noguchi, T., Curtis, J. D., et al. (2015). Metabolic competition in the tumor microenvironment is a driver of cancer progression. *Cell* 162 (6), 1229–1241. doi:10.1016/j.cell.2015.08.016

Chen, D. P., Ning, W. R., Jiang, Z. Z., Peng, Z. P., Zhu, L. Y., Zhuang, S. M., et al. (2019). Glycolytic activation of peritumoral monocytes fosters immune privilege via the PFKFB3-PD-L1 axis in human hepatocellular carcinoma. *J. Hepatol.* 71 (2), 333–343. doi:10.1016/j.jhep.2019.04.007

Chen, X., Tian, J., Su, G. H., and Lin, J. (2019). Blocking IL-6/GP130 signaling inhibits cell viability/proliferation, glycolysis, and colony forming activity in human pancreatic cancer cells. *Curr. Cancer Drug Targets* 19 (5), 417–427. doi:10.2174/1568009618666180430123939

Dai, Z., Zhang, X., Li, W., Tang, J., Pan, T., Ma, C., et al. (2021). Salidroside induces apoptosis in human gastric cancer cells via the downregulation of ENO1/PKM2/GLUT1 expression. *Biol. Pharm. Bull.* 44 (11), 1724–1731. doi:10.1248/bpb.b21-00443

de la Cruz-López, K. G., Castro-Muñoz, L. J., Reyes-Hernández, D. O., García-Carrancá, A., and Manzo-Merino, J. (2019). Lactate in the regulation of tumor microenvironment and therapeutic approaches. *Front. Oncol.* 9, 1143. doi:10.3389/fonc.2019.01143

De Oliveira, T., Goldhardt, T., Edelmann, M., Rogge, T., Rauch, K., Kyuchukov, N. D., et al. (2021). Effects of the novel PFKFB3 inhibitor KAN0438757 on colorectal cancer cells and its systemic toxicity evaluation *in vivo*. *Cancers (Basel)* 13 (5), 1011. doi:10.3390/cancers13051011

DeNardo, D. G., and Ruffell, B. (2019). Macrophages as regulators of tumour immunity and immunotherapy. *Nat. Rev. Immunol.* 19 (6), 369–382. doi:10.1038/s41577-019-0127-6

Deng, F., Zhou, R., Lin, C., Yang, S., Wang, H., Li, W., et al. (2019). Tumor-secreted dickkopf2 accelerates aerobic glycolysis and promotes angiogenesis in colorectal cancer. *Theranostics* 9 (4), 1001–1014. doi:10.7150/thno.30056

Domiński, A., Krawczyk, M., Konieczny, T., Kasprów, M., Foryś, A., Pastuch-Gawołek, G., et al. (2020). Biodegradable pH-responsive micelles loaded with 8-hydroxyquinoline glycoconjugates for Warburg effect based tumor targeting. *Eur. J. Pharm. Biopharm.* 154, 317–329. doi:10.1016/j.ejpb.2020.07.019

Fan, T., Sun, G., Sun, X., Zhao, L., Zhong, R., and Peng, Y. (2019). Tumor energy metabolism and potential of 3-bromopyruvate as an inhibitor of aerobic glycolysis: Implications in tumor treatment. *Cancers (Basel)* 11 (3), 317. doi:10.3390/cancers11030317

Fuller, G. G., and Kim, J. K. (2021). Compartmentalization and metabolic regulation of glycolysis. *J. Cell Sci.* 134 (20), jcs258469. doi:10.1242/jcs.258469

Ganapathy-Kanniappan, S. (2017). Taming tumor glycolysis and potential implications for immunotherapy. *Front. Oncol.* 7, 36. doi:10.3389/fonc.2017.00036

Gao, P., Shen, S., Li, X., Liu, D., Meng, Y., Liu, Y., et al. (2020). Dihydroartemisinin inhibits the proliferation of leukemia cells K562 by suppressing PKM2 and GLUT1 mediated aerobic glycolysis. *Drug Des. devel. Ther.* 14, 2091–2100. doi:10.2147/dddt.S248872

Ge, Z., and Ding, S. (2020). The crosstalk between tumor-associated macrophages (TAMs) and tumor cells and the corresponding targeted therapy. *Front. Oncol.* 10, 590941. doi:10.3389/fonc.2020.590941

Ghanavat, M., Shahrouzian, M., Deris Zayeri, Z., Banihashemi, S., Kazemi, S. M., and Saki, N. (2021). Digging deeper through glucose metabolism and its regulators in cancer and metastasis. *Life Sci.* 264, 118603. doi:10.1016/j.lfs.2020.118603

Guo, D., Tong, Y., Jiang, X., Meng, Y., Jiang, H., Du, L., et al. (2022). Aerobic glycolysis promotes tumor immune evasion by hexokinase2-mediated phosphorylation of IκBα. *Cell Metab.* 34 (9), 1312–1324. doi:10.1016/j.cmet.2022.08.002

Han, J., Meng, Q., Xi, Q., Zhang, Y., Zhuang, Q., Han, Y., et al. (2016). Interleukin-6 stimulates aerobic glycolysis by regulating PFKFB3 at early stage of colorectal cancer. *Int. J. Oncol.* 48 (1), 215–224. doi:10.3892/ijo.2015.3225

Hasan, M. N., Capuk, O., Patel, S. M., and Sun, D. (2022). The role of metabolic plasticity of tumor-associated macrophages in shaping the tumor microenvironment immunity. *Cancers (Basel)* 14 (14), 3331. doi:10.3390/cancers14143331

Hsu, P. P., and Sabatini, D. M. (2008). Cancer cell metabolism: warburg and beyond. *Cell* 134 (5), 703–707. doi:10.1016/j.cell.2008.08.021

Hu, X., Xu, Q., Wan, H., Hu, Y., Xing, S., Yang, H., et al. (2020). PI3K-Akt-mTOR/PFKFB3 pathway mediated lung fibroblast aerobic glycolysis and collagen synthesis in lipopolysaccharide-induced pulmonary fibrosis. *Lab. Invest.* 100 (6), 801–811. doi:10.1038/s41374-020-0404-9

Huang, X., Fang, J., Lai, W., Hu, Y., Li, L., Zhong, Y., et al. (2022). IL-6/STAT3 Axis activates Glut5 to regulate fructose metabolism and tumorigenesis. *Int. J. Biol. Sci.* 18 (9), 3668–3675. doi:10.7150/ijbs.68990

Huo, N., Cong, R., Sun, Z. J., Li, W. C., Zhu, X., Xue, C. Y., et al. (2021). STAT3/LINC00671 axis regulates papillary thyroid tumor growth and metastasis via LDHA-mediated glycolysis. *Cell Death Dis.* 12 (9), 799. doi:10.1038/s41419-021-04081-0

Infantino, V., Santarsiero, A., Convertini, P., Todisco, S., and Iacobazzi, V. (2021). Cancer cell metabolism in hypoxia: Role of HIF-1 as key regulator and therapeutic target. *Int. J. Mol. Sci.* 22 (11), 5703. doi:10.3390/ijms22115703

Ippolito, L., Morandi, A., Giannoni, E., and Chiarugi, P. (2019). Lactate: A metabolic driver in the tumour landscape. *Trends biochem. Sci.* 44 (2), 153–166. doi:10.1016/j.tibs.2018.10.011

Jablonski, K. A., Amici, S. A., Webb, L. M., Ruiz-Rosado Jde, D., Popovich, P. G., Partida-Sanchez, S., et al. (2015). Novel markers to delineate murine M1 and M2 macrophages. *PLoS One* 10 (12), e0145342. doi:10.1371/journal.pone.0145342

Jiang, H., Wei, H., Wang, H., Wang, Z., Li, J., Ou, Y., et al. (2022). Zeb1-induced metabolic reprogramming of glycolysis is essential for macrophage polarization in breast cancer. *Cell Death Dis.* 13 (3), 206. doi:10.1038/s41419-022-04632-z

Jiang, Z., Liu, Z., Li, M., Chen, C., and Wang, X. (2019). Increased glycolysis correlates with elevated immune activity in tumor immune microenvironment. *EBioMedicine* 42, 431–442. doi:10.1016/j.ebiom.2019.03.068

Jin, M. Z., and Jin, W. L. (2020). The updated landscape of tumor microenvironment and drug repurposing. *Signal Transduct. Target. Ther.* 5 (1), 166. doi:10.1038/s41392-020-00280-x

Kim, H. R., Park, H. J., Son, J., Lee, J. G., Chung, K. Y., Cho, N. H., et al. (2019). Tumor microenvironment dictates regulatory T cell phenotype: Upregulated immune checkpoints reinforce suppressive function. *J. Immunother. Cancer* 7 (1), 339. doi:10.1186/s40425-019-0785-8

Kocarnik, J. M., Compton, K., Dean, F. E., Fu, W., Gaw, B. L., Harvey, J. D., et al. (2022). Cancer incidence, mortality, years of life lost, years lived with disability, and disability-adjusted life years for 29 cancer groups from 2010 to 2019: A systematic analysis for the global burden of disease study 2019. *JAMA Oncol.* 8 (3), 420–444. doi:10.1001/jamaoncol.2021.6987

Kumagai, S., Koyama, S., Itahashi, K., Tanegashima, T., Lin, Y. T., Togashi, Y., et al. (2022). Lactic acid promotes PD-1 expression in regulatory T cells in highly glycolytic tumor microenvironments. *Cancer Cell* 40 (2), 201–218. doi:10.1016/j.ccell.2022.01.001

Li, M., Long, X., Wan, H., Yin, M., Yang, B., Zhang, F., et al. (2021). Monocarboxylate transporter 1 promotes proliferation and invasion of renal cancer cells by mediating acetate transport. *Cell Biol. Int.* 45 (6), 1278–1287. doi:10.1002/cbin.11571

Li, S., He, P., Wang, Z., Liang, M., Liao, W., Huang, Y., et al. (2021). RNAi-mediated knockdown of PFK1 decreases the invasive capability and metastasis of nasopharyngeal carcinoma cell line, CNE-2. *Cell Cycle* 20 (2), 154–165. doi:10.1080/15384101.2020.1866279

Li, W., Xu, M., Li, Y., Huang, Z., Zhou, J., Zhao, Q., et al. (2020). Comprehensive analysis of the association between tumor glycolysis and immune/inflammation function in breast cancer. *J. Transl. Med.* 18 (1), 92. doi:10.1186/s12967-020-02267-2

Lim, S. A., Moon, Y., Shin, M. H., Kim, T. J., Chae, S., Yee, C., et al. (2021). Hypoxia-Driven HIF-1α activation reprograms pre-activated NK cells towards highly potent effector phenotypes via ERK/STAT3 pathways. *Cancers (Basel)* 13 (8), 1904. doi:10.3390/cancers13081904

Liu, F., Ma, F., Wang, Y., Hao, L., Zeng, H., Jia, C., et al. (2017). PKM2 methylation by CARM1 activates aerobic glycolysis to promote tumorigenesis. *Nat. Cell Biol.* 19 (11), 1358–1370. doi:10.1038/ncb3630

Liu, M., Zhang, Y., Yang, J., Zhan, H., Zhou, Z., Jiang, Y., et al. (2021). Zinc-dependent regulation of ZEB1 and YAP1 coactivation promotes epithelial-mesenchymal transition plasticity and metastasis in pancreatic cancer. *Gastroenterology* 160 (5), 1771–1783. doi:10.1053/j.gastro.2020.12.077

Lu, J., Xu, Z., Duan, H., Ji, H., Zhen, Z., Li, B., et al. (2020). Tumor-associated macrophage interleukin-β promotes glycerol-3-phosphate dehydrogenase activation, glycolysis and tumorigenesis in glioma cells. *Cancer Sci.* 111 (6), 1979–1990. doi:10.1111/cas.14408

Lu, L. G., Zhou, Z. L., Wang, X. Y., Liu, B. Y., Lu, J. Y., Liu, S., et al. (2022). PD-L1 blockade liberates intrinsic antitumourigenic properties of glycolytic macrophages in hepatocellular carcinoma. *Gut* 71, 2551–2560. doi:10.1136/gutjnl-2021-326350

Manerba, M., Di Ianni, L., Govoni, M., Roberti, M., Recanatini, M., and Di Stefano, G. (2017). Lactate dehydrogenase inhibitors can reverse inflammation induced changes in colon cancer cells. *Eur. J. Pharm. Sci.* 96, 37–44. doi:10.1016/j.ejps.2016.09.014

Maringe, C., Spicer, J., Morris, M., Purushotham, A., Nolte, E., Sullivan, R., et al. (2020). The impact of the COVID-19 pandemic on cancer deaths due to delays in diagnosis in england, UK: a national, population-based, modelling study. *Lancet. Oncol.* 21 (8), 1023–1034. doi:10.1016/s1470-2045(20)30388-0

McDonald, O. G., Li, X., Saunders, T., Tryggvadottir, R., Mentch, S. J., Warmoes, M. O., et al. (2017). Epigenomic reprogramming during pancreatic cancer progression links anabolic glucose metabolism to distant metastasis. *Nat. Genet.* 49 (3), 367–376. doi:10.1038/ng.3753

Miranda-Gonçalves, V., Honavar, M., Pinheiro, C., Martinho, O., Pires, M. M., Pinheiro, C., et al. (2013). Monocarboxylate transporters (MCTs) in gliomas: expression and exploitation as therapeutic targets. *Neuro. Oncol.* 15 (2), 172–188. doi:10.1093/neuonc/nos298

Morrissey, S. M., Zhang, F., Ding, C., Montoya-Durango, D. E., Hu, X., Yang, C., et al. (2021). Tumor-derived exosomes drive immunosuppressive macrophages in a pre-metastatic niche through glycolytic dominant metabolic reprogramming. *Cell Metab.* 33 (10), 20402040–20402058. doi:10.1016/j.cmet.2021.09.002

Naxerova, K., Brachtel, E., Salk, J. J., Seese, A. M., Power, K., Abbasi, B., et al. (2014). Hypermutable DNA chronicles the evolution of human colon cancer. *Proc. Natl. Acad. Sci. U. S. A.* 111 (18), E1889–E1898. doi:10.1073/pnas.1400179111

Naxerova, K., and Jain, R. K. (2015). Using tumour phylogenetics to identify the roots of metastasis in humans. *Nat. Rev. Clin. Oncol.* 12 (5), 258–272. doi:10.1038/nrclinonc.2014.238

Pajak, B., Siwiak, E., Sołtyka, M., Priebe, A., Zieliński, R., Fokt, I., et al. (2019). 2-Deoxy-d-Glucose and its analogs: From diagnostic to therapeutic agents. *Int. J. Mol. Sci.* 21 (1), 234. doi:10.3390/ijms21010234

Paluskievicz, C. M., Cao, X., Abdi, R., Zheng, P., Liu, Y., and Bromberg, J. S. (2019). T regulatory cells and priming the suppressive tumor microenvironment. *Front. Immunol.* 10, 2453. doi:10.3389/fimmu.2019.02453

Pavlova, N. N., and Thompson, C. B. (2016). The emerging hallmarks of cancer metabolism. *Cell Metab.* 23 (1), 27–47. doi:10.1016/j.cmet.2015.12.006

Peng, X., He, Y., Huang, J., Tao, Y., and Liu, S. (2021). Metabolism of dendritic cells in tumor microenvironment: For immunotherapy. *Front. Immunol.* 12, 613492. doi:10.3389/fimmu.2021.613492

Puri, S., and Juvale, K. (2020). Monocarboxylate transporter 1 and 4 inhibitors as potential therapeutics for treating solid tumours: A review with structure-activity relationship insights. *Eur. J. Med. Chem.* 199, 112393. doi:10.1016/j.ejmech.2020.112393

Qi, C. L., Huang, M. L., Zou, Y., Yang, R., Jiang, Y., Sheng, J. F., et al. (2021). The IRF2/CENP-N/AKT signaling axis promotes proliferation, cell cycling and apoptosis resistance in nasopharyngeal carcinoma cells by increasing aerobic glycolysis. *J. Exp. Clin. Cancer Res.* 40 (1), 390. doi:10.1186/s13046-021-02191-3

Straus, D. S. (2013). TNFα and IL-17 cooperatively stimulate glucose metabolism and growth factor production in human colorectal cancer cells. *Mol. Cancer* 12, 78. doi:10.1186/1476-4598-12-78

Sun, Q., Chen, X., Ma, J., Peng, H., Wang, F., Zha, X., et al. (2011). Mammalian target of rapamycin up-regulation of pyruvate kinase isoenzyme type M2 is critical for aerobic glycolysis and tumor growth. *Proc. Natl. Acad. Sci. U. S. A.* 108 (10), 4129–4134. doi:10.1073/pnas.1014769108

Tan, Q., Duan, L., Huang, Q., Chen, W., Yang, Z., Chen, J., et al. (2021). Interleukin -1β promotes lung adenocarcinoma growth and invasion through promoting glycolysis via p38 pathway. *J. Inflamm. Res.* 14, 6491–6509. doi:10.2147/jir.S319433

Tan, Q., Huang, Q., Ma, Y. L., Mao, K., Yang, G., Luo, P., et al. (2018). Potential roles of IL-1 subfamily members in glycolysis in disease. *Cytokine Growth Factor Rev.* 44, 18–27. doi:10.1016/j.cytogfr.2018.11.001

Tanner, L. B., Goglia, A. G., Wei, M. H., Sehgal, T., Parsons, L. R., Park, J. O., et al. (2018). Four key steps control glycolytic flux in mammalian cells. *Cell Syst.* 7 (1), 49–62. doi:10.1016/j.cels.2018.06.003

Tian, R. F., Li, X. F., Xu, C., Wu, H., Liu, L., Wang, L. H., et al. (2020). SiRNA targeting PFK1 inhibits proliferation and migration and enhances radiosensitivity by suppressing glycolysis in colorectal cancer. *Am. J. Transl. Res.* 12 (9), 4923–4940.

Tsutsumi, S., Yanagawa, T., Shimura, T., Kuwano, H., and Raz, A. (2004). Autocrine motility factor signaling enhances pancreatic cancer metastasis. *Clin. Cancer Res.* 10 (22), 7775–7784. doi:10.1158/1078-0432.Ccr-04-1015

Uludağ, D., Bay, S., Sucu, B. O., Şavluğ İpek, Ö., Mohr, T., Güzel, M., et al. (2022). Potential of novel methyl jasmonate analogs as anticancer agents to metabolically target HK-2 activity in glioblastoma cells. *Front. Pharmacol.* 13, 828400. doi:10.3389/fphar.2022.828400

Uneda, A., Kurozumi, K., Fujimura, A., Fujii, K., Ishida, J., Shimazu, Y., et al. (2021). Differentiated glioblastoma cells accelerate tumor progression by shaping the tumor microenvironment via CCN1-mediated macrophage infiltration. *Acta Neuropathol. Commun.* 9 (1), 29. doi:10.1186/s40478-021-01124-7

Valvona, C. J., Fillmore, H. L., Nunn, P. B., and Pilkington, G. J. (2016). The regulation and function of lactate dehydrogenase A: Therapeutic potential in brain tumor. *Brain Pathol.* 26 (1), 3–17. doi:10.1111/bpa.12299

Vaughan, R. A., Garcia-Smith, R., Dorsey, J., Griffith, J. K., Bisoffi, M., and Trujillo, K. A. (2013). Tumor necrosis factor alpha induces Warburg-like metabolism and is reversed by anti-inflammatory curcumin in breast epithelial cells. *Int. J. Cancer* 133 (10), 2504–2510. doi:10.1002/ijc.28264

Vaupel, P., Schmidberger, H., and Mayer, A. (2019). The Warburg effect: essential part of metabolic reprogramming and central contributor to cancer progression. *Int. J. Radiat. Biol.* 95 (7), 912–919. doi:10.1080/09553002.2019.1589653

Wang, C., Chen, Z., Bu, X., Han, Y., Shan, S., Ren, T., et al. (2016). IL-33 signaling fuels outgrowth and metastasis of human lung cancer. *Biochem. Biophys. Res. Commun.* 479 (3), 461–468. doi:10.1016/j.bbrc.2016.09.081

Wang, J., and Ilyas, S. (2021). Targeting the tumor microenvironment in cholangiocarcinoma: implications for therapy. *Expert Opin. Investig. Drugs* 30 (4), 429–438. doi:10.1080/13543784.2021.1865308

Wang, K. J., Meng, X. Y., Chen, J. F., Wang, K. Y., Zhou, C., Yu, R., et al. (2021). Emodin induced necroptosis and inhibited glycolysis in the renal cancer cells by enhancing ROS. *Oxid. Med. Cell. Longev.* 2021, 8840590. doi:10.1155/2021/8840590

Wang, L., Liu, Y., Dai, Y., Tang, X., Yin, T., Wang, C., et al. (2022). Single-cell RNA-seq analysis reveals BHLHE40-driven pro-tumour neutrophils with hyperactivated glycolysis in pancreatic tumour microenvironment. *Gut* 2021, 326070. doi:10.1136/gutjnl-2021-326070

Wang, W., He, X., Wang, Y., Liu, H., Zhang, F., Wu, Z., et al. (2022). LINC01605 promotes aerobic glycolysis through lactate dehydrogenase A in triple-negative breast cancer. *Cancer Sci.* 113 (8), 2484–2495. doi:10.1111/cas.15370

Wang, X., Zhang, H., Yang, H., Bai, M., Ning, T., Deng, T., et al. (2020). Exosome-delivered circRNA promotes glycolysis to induce chemoresistance through the miR-122-PKM2 axis in colorectal cancer. *Mol. Oncol.* 14 (3), 539–555. doi:10.1002/1878-0261.12629

Wong, N., De Melo, J., and Tang, D. (2013). PKM2, a central point of regulation in cancer metabolism. *Int. J. Cell Biol.* 2013, 242513. doi:10.1155/2013/242513

Wu, H., Pan, L., Gao, C., Xu, H., Li, Y., Zhang, L., et al. (2019). Quercetin inhibits the proliferation of glycolysis-addicted HCC cells by reducing hexokinase 2 and akt-mTOR pathway. *Molecules* 24 (10), 1993. doi:10.3390/molecules24101993

Xiao, H., Wang, J., Yan, W., Cui, Y., Chen, Z., Gao, X., et al. (2018). GLUT1 regulates cell glycolysis and proliferation in prostate cancer. *Prostate* 78 (2), 86–94. doi:10.1002/pros.23448

Xiao, Y., and Yu, D. (2021). Tumor microenvironment as a therapeutic target in cancer. *Pharmacol. Ther.* 221, 107753. doi:10.1016/j.pharmthera.2020.107753

Xu, M., Zhou, C., Weng, J., Chen, Z., Zhou, Q., Gao, J., et al. (2022). Tumor associated macrophages-derived exosomes facilitate hepatocellular carcinoma malignance by transferring lncMMPA to tumor cells and activating glycolysis pathway. *J. Exp. Clin. Cancer Res.* 41 (1), 253. doi:10.1186/s13046-022-02458-3

Xu, W., Liu, W. R., Xu, Y., Tian, X., Anwaier, A., Su, J. Q., et al. (2021). Hexokinase 3 dysfunction promotes tumorigenesis and immune escape by upregulating monocyte/macrophage infiltration into the clear cell renal cell carcinoma microenvironment. *Int. J. Biol. Sci.* 17 (9), 2205–2222. doi:10.7150/ijbs.58295

Yan, S., Li, Q., Zhang, D., Wang, X., Xu, Y., Zhang, C., et al. (2021). Necroptosis pathway blockage attenuates PFKFB3 inhibitor-induced cell viability loss and genome instability in colorectal cancer cells. *Am. J. Cancer Res.* 11 (5), 2062–2080.

Yang, J., Liu, D. J., Zheng, J. H., He, R. Z., Xu, D. P., Yang, M. W., et al. (2022). IRAK2-NF-κB signaling promotes glycolysis-dependent tumor growth in pancreatic cancer. *Cell. Oncol.* 45 (3), 367–379. doi:10.1007/s13402-022-00670-z

Yang, J., Ren, B., Yang, G., Wang, H., Chen, G., You, L., et al. (2020). The enhancement of glycolysis regulates pancreatic cancer metastasis. *Cell. Mol. Life Sci.* 77 (2), 305–321. doi:10.1007/s00018-019-03278-z

Yang, J., Sun, Y., Xu, F., Liu, W., Hayashi, T., Mizuno, K., et al. (2021). Autophagy and glycolysis independently attenuate silibinin-induced apoptosis in human hepatocarcinoma HepG2 and Hep3B cells. *Hum. Exp. Toxicol.* 40 (12), 2048–2062. doi:10.1177/09603271211017609

Yang, X., Zhang, T., Zhang, X., Chu, C., and Sang, S. (2022). Global burden of lung cancer attributable to ambient fine particulate matter pollution in 204 countries and territories, 1990-2019. *Environ. Res.* 204, 112023. doi:10.1016/j.envres.2021.112023

Ye, H., Zhou, Q., Zheng, S., Li, G., Lin, Q., Wei, L., et al. (2018). Tumor-associated macrophages promote progression and the Warburg effect via CCL18/NF-kB/VCAM-1 pathway in pancreatic ductal adenocarcinoma. *Cell Death Dis.* 9 (5), 453. doi:10.1038/s41419-018-0486-0

Zahra, K., Dey, T., AshishMishra, S. P., and Pandey, U. (2020). Pyruvate kinase M2 and cancer: The role of PKM2 in promoting tumorigenesis. *Front. Oncol.* 10, 159. doi:10.3389/fonc.2020.00159

Zhang, J., Yang, J., Lin, C., Liu, W., Huo, Y., Yang, M., et al. (2020a). Endoplasmic Reticulum stress-dependent expression of ERO1L promotes aerobic glycolysis in Pancreatic Cancer. *Theranostics* 10 (18), 8400–8414. doi:10.7150/thno.45124

Zhang, J., Zhang, Y. H., Qin, X. J., Wang, Y. X., and Fu, J. (2020b). Circular RNA circDENND4C facilitates proliferation, migration and glycolysis of colorectal cancer cells through miR-760/GLUT1 axis. *Eur. Rev. Med. Pharmacol. Sci.* 24 (5), 2387–2400. doi:10.26355/eurrev_202003_20506

Zhang, P., Li, Z., and Yang, G. (2021). Silencing of ISLR inhibits tumour progression and glycolysis by inactivating the IL-6/JAK/STAT3 pathway in non-small cell lung cancer. *Int. J. Mol. Med.* 48 (6), 222. doi:10.3892/ijmm.2021.5055

Zhang, Y., Yu, G., Chu, H., Wang, X., Xiong, L., Cai, G., et al. (2018). Macrophage-associated PGK1 phosphorylation promotes aerobic glycolysis and tumorigenesis. *Mol. Cell* 71 (2), 201201–201215. doi:10.1016/j.molcel.2018.06.023

Zhu, H., Blum, R. H., Bernareggi, D., Ask, E. H., Wu, Z., Hoel, H. J., et al. (2020). Metabolic reprograming via deletion of CISH in human iPSC-derived NK cells promotes *in vivo* persistence and enhances anti-tumor activity. *Cell Stem Cell* 27 (2), 224–237. doi:10.1016/j.stem.2020.05.008

Zhu, S., Guo, Y., Zhang, X., Liu, H., Yin, M., Chen, X., et al. (2021). Pyruvate kinase M2 (PKM2) in cancer and cancer therapeutics. *Cancer Lett.* 503, 240–248. doi:10.1016/j.canlet.2020.11.018

frontiers | Frontiers in Pharmacology

TYPE Review
PUBLISHED 15 December 2022
DOI 10.3389/fphar.2022.1096984

OPEN ACCESS

EDITED BY
Yan Huang,
Anhui Medical University, China

REVIEWED BY
Teng He,
Zhejiang University, China
Xianrui Dou,
Southern Medical University, China

*CORRESPONDENCE
Zhong Zheng,
zhengz1993@163.com

†These authors have contributed equally to this work

SPECIALTY SECTION
This article was submitted to Inflammation Pharmacology, a section of the journal Frontiers in Pharmacology

RECEIVED 13 November 2022
ACCEPTED 05 December 2022
PUBLISHED 15 December 2022

CITATION
Zheng Z and Yu Y (2022), A review of recent advances in exosomes and allergic rhinitis.
Front. Pharmacol. 13:1096984.
doi: 10.3389/fphar.2022.1096984

A review of recent advances in exosomes and allergic rhinitis

Zhong Zheng[1*†] and Yangyang Yu[2†]

[1]Department of Child Otorhinolaryngology, Anhui Provincial Children's Hospital, Hefei, China, [2]Department of Function Examination Center, Anhui Chest Hospital, Hefei, China

Allergic rhinitis is a chronic inflammatory disease of nasal mucosa caused by the presence of IgE after exposure to allergens, characterized by nasal irritation, hypersecretion of the nasal passages and sneezing, which frequently occurs in children and adolescents. There has been an increase in allergic rhinitis over the past few years due to air pollution. Exosomes have been discovered to be nano-sized vesicles, which contain a wide range of substances, including proteins and nucleic acids, numerous studies indicates that exosomes play a vital role in cells communication. Recently there have been more and more studies exploring the role of exosomes in allergic rhinitis. Therefore, here we will present a comprehensive review of the research on exosomes and their role in allergic rhinitis for the purpose of providing new understanding of potential value of exosomes applied to the treatment of allergic rhinitis.

KEYWORDS

exosome, allergic rhinitis, mechanism, miRNA, lncRNA, treatment

Introduction

Allergic rhinitis is a common disease, which is becoming an increasingly serious global problem related to health, medicine, and economics. High-income countries show a prevalence of up to 50%, making it one of the most common chronic conditions, while the prevalence is comparatively low in low- and middle-income countries, despite the fact that it is steadily rising in these nations (Bousquet et al., 2020; Liu and Liu, 2022). In Europe, over the last 3 decades, there has been a gradual increase from 19% to 32% of Danish adults suffering from allergic rhinitis (Leth-Moller et al., 2020). Its high incidence imposes a substantial burden on our general welfare, as well as significant financial costs, both direct and indirect. In allergic rhinitis, inhaled particles cause an inflammatory response led by IgE, which may result in sneezing, nasal itching, rhinorrhea, or nasal obstruction, among other symptoms (Mims, 2014). A number of allergens can trigger allergic rhinitis, including pollen (from trees, grass, and weeds), mould and dust mites et al. During the year, allergens are classified into perennial and seasonal triggers according to their temporal pattern. In some cases, perennial symptoms occur in patients because of things in their homes all year round, it may include mold, dust mites, or animals (especially cats and dogs) (Schuler Iv and Montejo, 2019). Lifestyle factors and climate change contribute to high prevalence of allergic rhinitis, including antibiotic use, contact with farm animals, exposure to air pollution, and parental smoking et al. It is noteworthy that genetic and environmental factors also contribute to other

allergic diseases, such as atopic dermatitis and asthma, which are often comorbid with allergic rhinitis (2020; Zhang et al., 2021). In terms of treating allergic rhinitis, there are three main approaches. These approaches are avoidance, medications, and immunotherapy (Schuler Iv and Montejo, 2021). However, allergic rhinitis cannot be cured completely at present, and can only be prevented and controlled through standardized comprehensive treatment. There is a mental health impact associated with allergic rhinitis as well as physical health effects (Amritwar et al., 2017). Due to its high prevalence and the difficulty in treating allergic rhinitis, the exploration of active and effective diagnoses and treatments is essential.

Exosomes are lipid bilayer vesicles released *via* exocytosis, an exocytotic process, with a diameter of 40–100 nm. A wide variety of bioactive molecules can be found in exosomes, including proteins, lipids, DNA, and microRNA. There is evidence of its presence in various body fluids, including urine, blood, breast milk, saliva, cerebrospinal fluid and amniotic fluid (Konala et al., 2016; Pegtel and Gould, 2019; Kalluri and LeBleu, 2020). Recently researchers have found that exosomes may be involved in occurrence and progression of a variety of diseases, such as tumors (Zhang and Yu, 2019), neurodegenerative diseases (Jiang et al., 2019; Wang et al., 2020), infection (Choi et al., 2020; Ocansey et al., 2020), autoimmune diseases (Robak et al., 1998; Lee et al., 2016) and cardiovascular disorders (Zamani et al., 2019) et al., among them allergic rhinitis is a newly studied exosome related disease. Currently, research on exosomes and allergic rhinitis has gained increasing attention among scholars. As a result, here we will present a comprehensive review of the research on exosomes in order to understand how exosomes might be useful in treating allergic rhinitis.

Allergic rhinitis pathogenesis

It remains to be explored in greater depth about the mechanisms underlying allergic rhinitis pathology, despite extensive studies of the mechanisms that contribute to the disease. Allergic rhinitis is a result of specific IgE-mediated responses to allergens inhaled, which is leaded by T helper two cells (Th2). Eosinophils and basophils are influxed into the mucosa when allergic rhinitis causes mucosal inflammation (Bernstein et al., 2016). IgE is provided by B cells, T cells and basophils et al. in conjunction with each other, which is also involved in multiple cytokines. An understanding of allergic rhinitis pathogenesis may lead to better treatment. Therefore, this review summarizes recent studies that illustrate the role of important cells and proteins in allergic rhinitis pathogenesis, to provide support for relevant research. Numerous studies indicate that several cell types play a role in allergic rhinitis' occurrence and progression. These cells consist mainly of epithelial cells, dendritic cells (DCs), type 2 follicular helper T cells (Tfh2), basophils, mast cells, Th2 cells, B cells, group 2 innate lymphoid cells (ILC2s), eosinophils and neutrophils (Drazdauskaite et al., 2020; Zhang et al., 2022). Among these cells, the ILC2s play a crucial role in airway inflammation as a component of the Th2 innate immunity. In fact, within an ILC2-mediated immune microenvironment, mast cells, histiocytes and Th2 cells can produce IL-4, IL-5, IL-9, IL-13, IL-25, and IL-33 (Peng et al., 2020). In addition, many proteins contribute to the occurence and progression of allergic rhinitis. Toll-like receptor 4 (TLR4) binds to the corresponding ligands (HMGB1 and LPS et al.) to activate the relevant signaling pathway, resulting to the activation and translocation of NF-κB, which induces allergic rhinitis by mediating cytokine secretion (Sha et al., 2008; Lauriello et al., 2012; Cui et al., 2015; Radman et al., 2015; Haruna et al., 2019). YKL-40 (chitinase-3-like-1; CHI3L1) is primarily known as human cartilage glycoprotein 39 (HCgp-39), which is an important protein that plays a crucial role in chronic hypersensitivity inflammation. A high level of YKL-40 expression is found in nasal mucosa of patients with mild and moderate/severe allergic rhinitis (Pirayesh et al., 2020), which participates in mucosal remodeling in the nasal cavity, mediates the epithelial detachment of nasal mucosa, tissue edema and small vessel hyperplasia, and aggravating the symptoms of allergic rhinitis (Sanai et al., 1999; Kim et al., 2019). YKL-40 may promote nasal mucosa remodeling by activating fibroblasts and producing TIMP1 and MMP-9 (Park et al., 2013). Histone deacetylase (HDAC) is an important driver of inflammation in response to allergies, as well as tight junction dysfunction, which may be a pathogenesis of airway epithelial tissue and cell damage, and that inhibiting HDAC may restore epithelial barrier integrity (Steelant et al., 2019). There is also evidence that periostin may be important in allergic rhinitis. It has been suggested that it transmits signals to trigger allergic diseases while secreting mucus (Izuhara et al., 2016; Izuhara et al., 2019). Moreover, the CD86 may function as a second activation signal for T cells, make the initial T lymphocytes differentiate to Th2 cells, lead to the imbalance of Th1/Th2 cytokines in the body, and mediate the occurrence of allergic rhinitis (Gunawan et al., 2015; Li et al., 2016b; Sun et al., 2019).

Exosomes in allergic diseases

The exosome is a type of small extracellular vesicle secreted by cells that contains protein, lipid, and nucleic acid for physiological and pathological processes. According to cellular biogenesis and sizes, they can be divided into three groups to deliver their contents and enable the exchange of information between cells, including docking and fusing with the recipient cell plasma membrane, targeting the recipient's signals, and internalizing into the recipient (Konala et al., 2016; Kalluri and LeBleu, 2020; Zhang et al., 2020). Exosomes are found in

a variety of body fluids, which can be produced by almost all types of normal cells, including mesenchymal stem cells, T cells, B cells, and macrophages et al. (Cheng et al., 2017; He et al., 2020). Exosomes were originally regarded as molecular 'garbage bags' associated with cell waste disposal (Harischandra et al., 2019). Nevertheless, recently they have become crucial devices for intercellular communication, modulating and mediating various cellular functions. (Shekari et al., 2021). Studies have shown that RNA (including mRNAs, miRNAs, and other non-coding RNAs), DNA, and lipids can be incorporated into intraluminal vesicles from exosomes actively and selectively (van Niel et al., 2018). According to the ExoCarta database (http://www.exocarta.org/), 9769 proteins, 3408 mRNAs, 2838 miRNAs, and 116 lipids have been discovered in exosomes as of 2020 (Zhou et al., 2020). Almost all cells can communicate from cell to cell by secreting exosomes, which are closely related to their physiological effects (Mathieu et al., 2019). Research has shown that exosomes are important in treating inflammatory diseases (Harrell et al., 2019; Zhao and Luo, 2019; Choi et al., 2020; Ocansey et al., 2020), neurological diseases (Jiang et al., 2019; Wang et al., 2020; Harrell et al., 2021) and autoimmune diseases (Robak et al., 1998; Lee et al., 2016; Riazifar et al., 2019). Furthermore, exosomes have been identified as tumor markers and a diagnostic tool (Sharma and Johnson, 2020; Li et al., 2021). This review focuses primarily on recent research progress related to exosomes in allergies. As a result of exposure to allergens, the body's initial T cells differentiate into Th2 cells, which produce cytokines that promote allergic reactions. A study has shown that exosomes secreted by T cells reduce the production of inflammatory mediators when worms cause host allergic reactions. Additionally, exosomes secreted by worms contain miRNA, which can enter immune cells and promote their proliferation and differentiation (Siles-Lucas et al., 2015). Moreover, Li et al. found that exosomes secreted by bone marrow mast cells (BMMCs) promoted the proliferation of naive $CD4^+$ T cells, and significantly enhanced Th2 cell differentiation by ligation of OX40L and OX40 between BMMC-exosomes and $CD4^+$ T cells and this may represent a novel mechanism for communicating between cells (Li et al., 2016a). Interestingly, Gao et al. discovered that exosomes from septic mice have been shown to enhance differentiation of Th1 and Th2 cells and promote proliferation and migration of T cells for the first time (Gao et al., 2019). Generally, studies on exosomes in allergic reactions mainly focus on T cells and mast cells. Exosomes may play a significant role in activating or suppressing immune cells in this process. In addition, there is something worth mentioning that for allergy, Villalba et al. (2014) have demonstrated that exosomes derived from bronchoalveolar lavage of Ole e 1-tolerized mice were effective in protecting animals against allergic sensitization to Ole e 1 and the non-related allergen Bet v 1, as opposed to naive mice's exosomes, this suggested that exosomes could be a better allergy vaccine due to their properties.

Overview of research related to allergic rhinitis and exosomes

A growing body of researches has been conducted on exosomes and allergic rhinitis in recent years. It has been demonstrated that exosomes play a vital role in allergic rhinitis' occurrence and progression. In this section, we review the relevant studies regarding exosomes and allergic rhinitis to clarify the corresponding mechanisms and provide theoretical support for targeting exosomes therapy of allergic rhinitis.

In a study by Qiu et al., they found that exosomes can be discovered in the patients with chronic atypical allergic rhinitis, and these exosomes containing microbial products and airborne antigens, which can influence DCs maturation and major histocompatibility class I (MHCI) production, thereby promoting antigen specific $CD8^+$ T cell development, eventually this leads to allergic rhinitis (Qiu et al., 2011; Qiu et al., 2012). In another study by Wu et al. (2015) they found that in nasal mucus from allergic rhinitis patients, 21 vesicle miRNAs were up-regulated and 14 were down-regulated significantly compared to healthy controls. And the studied vesicles were confirmed to be exosomes by FACS analysis and binding specifically to antiCD63 coated latex beads. By bioinformatic analysis, this study demonstrated that vesicle miRNA may be a regulator for the development of allergic rhinitis. Interestingly, Jiang et al. (2022) indicated that there are 812 miRNAs were detected in the serum exosomes, including 16 upregulated and 14 downregulated ones. Their study also suggested that children suffering from allergic rhinitis were predicted to respond to SCIT by serum exosomal hsa-miR-4669. Actually, there are many studies on miRNA secreted by exosome and allergic rhinitis. For example, Luo et al. (2015) found that patients with allergic rhinitis had much lower miR146a levels than healthy subjects in nasal epithelial specimens. And there is evidence that human nasal epithelial cells produce miR-146a, which can be released to the microenvironment carried by exosomes. Their results indicated that miRNA-146a can inhibit $CD4^+$ effector T cell activity and Th2 polarization by enhancing monocyte interleukin-10 expression and the allergic reaction was suppressed in the mouse nasal mucosa ultimately. Furthermore, Zhou et al. (2021) discovered that there was a significant increase in Th2 cells in allergic rhinitis patients compared to healthy donors, while exosomes from HMSCs could reduce the expression of SERPINB2 and facilitate the differentiation of Th2 cells. They concluded that the miR-146a-5p and SERPINB2 genes can serve as potential targets for allergic rhinitis therapy . Additionally, it is acknowleged that exosomes can influence the DCs maturation. Teng et al. used RNA-seq and results showed that miR-142-5p was the differentially decreased gene in Tfh-derived exosomes. In depth, they indicated that miR-142-5p inhibited DCs maturation by inhibiting CDK5 and STAT3 expression. According to their findings, Tfh-derived exosomes play a

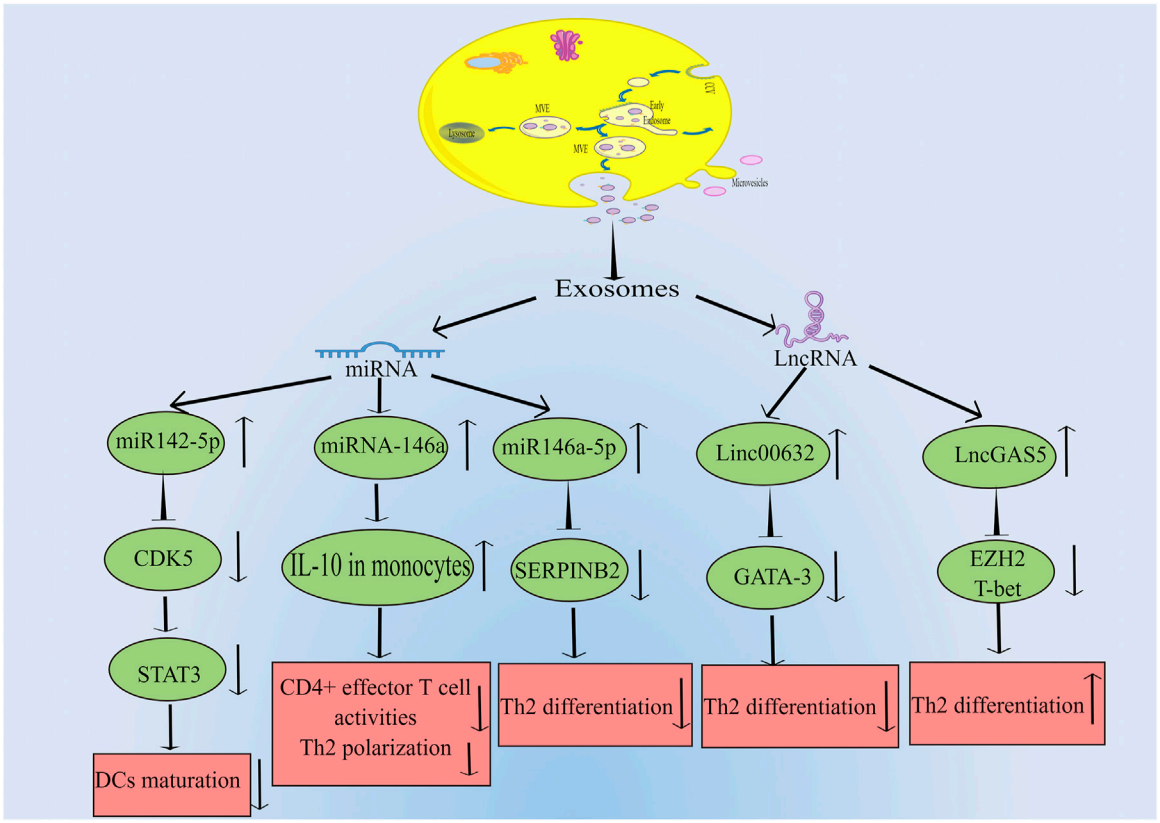

FIGURE 1
Exosomes can be produced by many kinds of cells, which can transmit intercellular signals through the release of miRNA and LncRNA, and affect the expression of related genes, thus leading to the occurrence and progression of allergic rhinitis. The main miRNAs released by exosomes are miR142-5p, miR146a and miR146-5p. MiR142-5p can inhibit the expression of CDK5, which leads to the decrease of STAT3 and ultimately inhibits DCs maturation. MiR146a can increase the level of IL-10 in monocytes, and then inhibit $CD4^+$ effector T cell activity and Th2 polarization. MiR146-5p can inhibit the expression of SERPINB2 and lead to the decrease of Th2 differentiation. LncRNAs mainly include Linc00632 and LncGAS5. Linc00632 can inhibit the expression of GATA-3 and lead to the decrease of Th2 differentiation. While LncGAS5 can inhibit the expression of EZH2 and T-bet, ultimately increases Th2 differentiation (By Figdraw).

central role in allergic rhinitis pathogenesis by regulating the miR-142-5p/CDK5/STAT3 signaling pathway axis (Teng et al., 2022). It has been discussed above how miRNA secreted by exosomes influences the pathogenesis of allergic rhinitis. Interestingly, exosomes can also release long noncoding RNA (LncRNA), thus affecting the occurrence and progression of allergic rhinitis. Zhu et al. (2020) found that the expression of LncGAS5 was up-regulated in exosomes secreted by nasal epithelial cells of patients with allergic rhinitis, while LncGAS5 can promote the differentiation of Th2 cells by inhibiting the expression of transcription factor T-bet and EZH2. Their results suggested that LncGAS5 in allergic rhinitis exosomes plays a critical role in Th1/Th2 differentiation, providing a potential therapeutic target. Moreover, Li et al. (2022) showed that there was a significant drop in Linc00632 expression in nasal mucosa of allergic rhinitis patients by four times. Exosomes derived from human umbilical cord mesenchymal stem cells showed dramatic inhibition of Th2 differentiation, inhibited GATA binding protein-3 (GATA-3) expression, and decreased IL-4 levels in $CD4^+$ T cells. Further research revealed that the interaction between Linc00632 and EZH2 inhibited the expression of GATA-3. As discussed above, current studies on exosome-mediated allergic rhinitis pathogenesis are mainly conducted through miRNA and LncRNA secreted by exosomes from different cell sources. The relevant signal regulation is shown in Figure 1.

Conclusion

It is acknowleged that allergy rhinitis is a pathological condition in which exosomes act as inflammatory mediators, promote or inhibit cell proliferation and differentiation, and present antigens. There is a possibility that further research could lead to the development of nasal sprays delivering therapeutic drugs or genes to the nasal mucosa in allergy

rhinitis using exosomes. For example, it may be possible to induce tolerance by nasal vaccines based on exosomes *via* intranasal administration. With allergy vaccines containing allergen-modified molecules, new delivery systems, and alternative routes of administration, allergy patients' daily lives will be improved as well as unraveling the immunological mechanisms that underlie immunotherapy in order to develop new therapeutic approaches (Villalba et al., 2014). However, there are currently few studies on the effect of exosomes in allergic rhinitis pathogenesis. In addition to other extracellular vesicles, it remains unclear whether exogenous drugs or genes will have additional undiscovered side effects. It is also important to support more relevant experiments and to simplify exosome preservation conditions. Extra studies are therefore indispensable to determine how exosomes are formed, released, and transported as well as their role in allergic rhinitis. A potential focus of allergic rhinitis research may be to understand the functions of exosomes in regulating mast cells and mucin-secreting epithelial tissues. Meanwhile, exosomes produced by mesenchymal stem cells (MSCs) may prove potent in treating allergic rhinitis for their immunosuppressive properties, tissue repair ability, and secretion of various biological factors. Actually, numerous clinical and preclinical studies have proven the efficacy of MSC-based therapy for a number of allergic diseases, and the mechanisms related to these interventions have been explored (Li et al., 2020). Overall, targeted exosomes is a very promising treatment for allergic rhinitis that is expected to require many participants in the future(Shen et al., 2018).

Author contributions

ZZ designed and wrote this manuscript, YY wrote and checked the manuscript.

Conflict of interest

The authors declare that the research was conducted in the absence of any commercial or financial relationships that could be construed as a potential conflict of interest.

Publisher's note

All claims expressed in this article are solely those of the authors and do not necessarily represent those of their affiliated organizations, or those of the publisher, the editors and the reviewers. Any product that may be evaluated in this article, or claim that may be made by its manufacturer, is not guaranteed or endorsed by the publisher.

References

Amritwar, A. U., Lowry, C. A., Brenner, L. A., Hoisington, A. J., Hamilton, R., Stiller, J. W., et al. (2017). Mental health in allergic rhinitis: Depression and suicidal behavior. *Curr. Treat. Options Allergy* 4 (1), 71–97. doi:10.1007/s40521-017-0110-z

Bernstein, D. I., Schwartz, G., and Bernstein, J. A. (2016). Allergic rhinitis: Mechanisms and treatment. *Immunol. Allergy Clin. North Am.* 36 (2), 261–278. doi:10.1016/j.iac.2015.12.004

Bousquet, J., Anto, J. M., Bachert, C., Baiardini, I., Bosnic-Anticevich, S., Walter Canonica, G., et al. (2020). Allergic rhinitis. *Nat. Rev. Dis. Prim.* 6 (1), 96. doi:10.1038/s41572-020-00237-y

Cheng, L., Zhang, K., Wu, S., Cui, M., and Xu, T. (2017). Focus on mesenchymal stem cell-derived exosomes: Opportunities and challenges in cell-free therapy. *Stem Cells Int.* 2017, 6305295. doi:10.1155/2017/6305295

Choi, H., Kim, Y., Mirzaaghasi, A., Heo, J., Kim, Y. N., Shin, J. H., et al. (2020). Exosome-based delivery of super-repressor IκBα relieves sepsis-associated organ damage and mortality. *Sci. Adv.* 6 (15), eaaz6980. doi:10.1126/sciadv.aaz6980

Cui, X. Y., Chen, X., Yu, C. J., Yang, J., Lin, Z. P., Yin, M., et al. (2015). Increased expression of toll-like receptors 2 and 4 and related cytokines in persistent allergic rhinitis. *Otolaryngol. Head. Neck Surg.* 152 (2), 233–238. doi:10.1177/0194599814562173

Drazdauskaite, G., Layhadi, J. A., and Shamji, M. H. (2020). Mechanisms of allergen immunotherapy in allergic rhinitis. *Curr. Allergy Asthma Rep.* 21 (1), 2. doi:10.1007/s11882-020-00977-7

Gao, K., Jin, J., Huang, C., Li, J., Luo, H., Li, L., et al. (2019). Exosomes derived from septic mouse serum modulate immune responses via exosome-associated cytokines. *Front. Immunol.* 10, 1560. doi:10.3389/fimmu.2019.01560

Gunawan, M., Venkatesan, N., Loh, J. T., Wong, J. F., Berger, H., Neo, W. H., et al. (2015). The methyltransferase Ezh2 controls cell adhesion and migration through direct methylation of the extranuclear regulatory protein talin. *Nat. Immunol.* 16 (5), 505–516. doi:10.1038/ni.3125

Harischandra, D. S., Rokad, D., Neal, M. L., Ghaisas, S., Manne, S., Sarkar, S., et al. (2019). Manganese promotes the aggregation and prion-like cell-to-cell exosomal transmission of alpha-synuclein. *Sci. Signal.* 12 (572), eaau4543. doi:10.1126/scisignal.aau4543

Harrell, C. R., Jovicic, N., Djonov, V., Arsenijevic, N., and Volarevic, V. (2019). Mesenchymal stem cell-derived exosomes and other extracellular vesicles as new remedies in the therapy of inflammatory diseases. *Cells* 8 (12), 1605. doi:10.3390/cells8121605

Harrell, C. R., Volarevic, A., Djonov, V., and Volarevic, V. (2021). Mesenchymal stem cell-derived exosomes as new remedy for the treatment of neurocognitive disorders. *Int. J. Mol. Sci.* 22 (3), 1433. doi:10.3390/ijms22031433

Haruna, T., Kariya, S., Fujiwara, T., Yuta, A., Higaki, T., Zhao, P., et al. (2019). Role of whole saliva in the efficacy of sublingual immunotherapy in seasonal allergic rhinitis. *Allergol. Int.* 68 (1), 82–89. doi:10.1016/j.alit.2018.07.008

He, C., Hua, W., Liu, J., Fan, L., Wang, H., and Sun, G. (2020). Exosomes derived from endoplasmic reticulum-stressed liver cancer cells enhance the expression of cytokines in macrophages via the STAT3 signaling pathway. *Oncol. Lett.* 20 (1), 589–600. doi:10.3892/ol.2020.11609

Izuhara, K., Nunomura, S., Nanri, Y., Ono, J., Takai, M., and Kawaguchi, A. (2019). Periostin: An emerging biomarker for allergic diseases. *Allergy* 74 (11), 2116–2128. doi:10.1111/all.13814

Izuhara, K., Ohta, S., and Ono, J. (2016). Using periostin as a biomarker in the treatment of asthma. *Allergy Asthma Immunol. Res.* 8 (6), 491–498. doi:10.4168/aair.2016.8.6.491

Jiang, L., Dong, H., Cao, H., Ji, X., Luan, S., and Liu, J. (2019). Exosomes in pathogenesis, diagnosis, and treatment of alzheimer's disease. *Med. Sci. Monit.* 25, 3329–3335. doi:10.12659/MSM.914027

Jiang, S., Xie, S., Fan, R., Tang, Q., Zhang, H., Wang, F., et al. (2022). Exosomes derived hsa-miR-4669 as a novel biomarker for early predicting the response of subcutaneous immunotherapy in pediatric allergic rhinitis. *J. Inflamm. Res.* 15, 5063–5074. doi:10.2147/JIR.S379414

Kalluri, R., and LeBleu, V. S. (2020). The biology, function, and biomedical applications of exosomes. *Science* 367 (6478), eaau6977. doi:10.1126/science.aau6977

Kim, M. J., Shim, D. H., Cha, H. R., Moon, K. Y., Yang, C. M., Hwang, S. J., et al. (2019). Chitinase 3-like 1 protein plays a critical role in respiratory syncytial virus-induced airway inflammation. *Allergy* 74 (4), 685–697. doi:10.1111/all.13661

Konala, V. B., Mamidi, M. K., Bhonde, R., Das, A. K., Pochampally, R., and Pal, R. (2016). The current landscape of the mesenchymal stromal cell secretome: A new paradigm for cell-free regeneration. *Cytotherapy* 18 (1), 13–24. doi:10.1016/j.jcyt.2015.10.008

Lauriello, M., Micera, A., Muzi, P., Di Rienzo Businco, L., and Bonini, S. (2012). TLR4 and TLR9 expression in different phenotypes of rhinitis. *Int. J. Otolaryngol.* 2012, 925164. doi:10.1155/2012/925164

Lee, J. Y., Park, J. K., Lee, E. Y., Lee, E. B., and Song, Y. W. (2016). Circulating exosomes from patients with systemic lupus erythematosus induce an proinflammatory immune response. *Arthritis Res. Ther.* 18 (1), 264. doi:10.1186/s13075-016-1159-y

Leth-Moller, K. B., Skaaby, T., and Linneberg, A. (2020). Allergic rhinitis and allergic sensitisation are still increasing among Danish adults. *Allergy* 75 (3), 660–668. doi:10.1111/all.14046

Li, F., Wang, Y., Lin, L., Wang, J., Xiao, H., Li, J., et al. (2016a). Mast cell-derived exosomes promote Th2 cell differentiation via ox40l-OX40 ligation. *J. Immunol. Res.* 2016, 3623898. doi:10.1155/2016/3623898

Li, H., Tian, Y., Xie, L., Liu, X., Huang, Z., and Su, W. (2020). Mesenchymal stem cells in allergic diseases: Current status. *Allergol. Int.* 69 (1), 35–45. doi:10.1016/j.alit.2019.08.001

Li, J. G., Du, Y. M., Yan, Z. D., Yan, J., Zhuansun, Y. X., Chen, R., et al. (2016b). CD80 and CD86 knockdown in dendritic cells regulates Th1/Th2 cytokine production in asthmatic mice. *Exp. Ther. Med.* 11 (3), 878–884. doi:10.3892/etm.2016.2989

Li, M. Y., Liu, L. Z., and Dong, M. (2021). Progress on pivotal role and application of exosome in lung cancer carcinogenesis, diagnosis, therapy and prognosis. *Mol. Cancer* 20 (1), 22. doi:10.1186/s12943-021-01312-y

Li, W., Cai, C. Y., and Zeng, J. J. (2022). Mesenchymal stem cell-derived exosome-containing Linc00632 regulates GATA binding protein-3 expression in allergic rhinitis by interacting with enhancer of zeste homolog 2 to inhibit T helper cell 2 differentiation. *Int. Arch. Allergy Immunol.* 183 (2), 235–245. doi:10.1159/000518950

Liu, Y., and Liu, Z. (2022). Epidemiology, prevention and clinical treatment of allergic rhinitis: More understanding, better patient care. *J. Clin. Med.* 11 (20), 6062. doi:10.3390/jcm11206062

Luo, X., Han, M., Liu, J., Wang, Y., Luo, X., Zheng, J., et al. (2015). Epithelial cell-derived micro RNA-146a generates interleukin-10-producing monocytes to inhibit nasal allergy. *Sci. Rep.* 5, 15937. doi:10.1038/srep15937

Mathieu, M., Martin-Jaular, L., Lavieu, G., and Thery, C. (2019). Specificities of secretion and uptake of exosomes and other extracellular vesicles for cell-to-cell communication. *Nat. Cell Biol.* 21 (1), 9–17. doi:10.1038/s41556-018-0250-9

Mims, J. W. (2014). Epidemiology of allergic rhinitis. *Int. Forum Allergy Rhinol.* 4 (2), S18–S20. doi:10.1002/alr.21385

Ocansey, D. K. W., Zhang, L., Wang, Y., Yan, Y., Qian, H., Zhang, X., et al. (2020). Exosome-mediated effects and applications in inflammatory bowel disease. *Biol. Rev. Camb. Philos. Soc.* 95 (5), 1287–1307. doi:10.1111/brv.12608

Park, S. J., Jun, Y. J., Kim, T. H., Jung, J. Y., Hwang, G. H., Jung, K. J., et al. (2013). Increased expression of YKL-40 in mild and moderate/severe persistent allergic rhinitis and its possible contribution to remodeling of nasal mucosa. *Am. J. Rhinol. Allergy* 27 (5), 372–380. doi:10.2500/ajra.2013.27.3941

Pegtel, D. M., and Gould, S. J. (2019). Exosomes. *Annu. Rev. Biochem.* 88, 487–514. doi:10.1146/annurev-biochem-013118-111902

Peng, Y. Q., Qin, Z. L., Fang, S. B., Xu, Z. B., Zhang, H. Y., Chen, D., et al. (2020). Effects of myeloid and plasmacytoid dendritic cells on ILC2s in patients with allergic rhinitis. *J. Allergy Clin. Immunol.* 145 (3), 855–867. doi:10.1016/j.jaci.2019.11.029

Pirayesh, A., Shahsavan, S., Zargari Samani, O., Shirzad, H., Amani, S., Bagheri, N., et al. (2020). Local expression of mucosal YKL-40; correlation of YKL-40 with clinical manifestations and immunopathogenesis of moderate/severe persistent allergic rhinitis patients. *Immunol. Invest.* 49 (1-2), 46–57. doi:10.1080/08820139.2019.1634096

Qiu, S., Du, Y., Duan, X., Geng, X., Xie, J., Gao, H., et al. (2011). Cytotoxic T lymphocytes mediate chronic inflammation of the nasal mucosa of patients with atypical allergic rhinitis. *N. Am. J. Med. Sci.* 3 (8), 378–383. doi:10.4297/najms.2011.3378

Qiu, S., Duan, X., Geng, X., Xie, J., and Gao, H. (2012). Antigen-specific activities of CD8+ T cells in the nasal mucosa of patients with nasal allergy. *Asian pac. J. Allergy Immunol.* 30 (2), 107–113.

Radman, M., Golshiri, A., Shamsizadeh, A., Zainodini, N., Bagheri, V., Arababadi, M. K., et al. (2015). Toll-like receptor 4 plays significant roles during allergic rhinitis. *Allergol. Immunopathol.* 43 (4), 416–420. doi:10.1016/j.aller.2014.04.006

Riazifar, M., Mohammadi, M. R., Pone, E. J., Yeri, A., Lasser, C., Segaliny, A. I., et al. (2019). Stem cell-derived exosomes as nanotherapeutics for autoimmune and neurodegenerative disorders. *ACS Nano* 13 (6), 6670–6688. doi:10.1021/acsnano.9b01004

Robak, E., Sysa-Jedrzejewska, A., Dziankowska, B., Torzecka, D., Chojnowski, K., and Robak, T. (1998). Association of interferon gamma, tumor necrosis factor alpha and interleukin 6 serum levels with systemic lupus erythematosus activity. *Arch. Immunol. Ther. Exp.* 46 (6), 375–380.

Sanai, A., Nagata, H., and Konno, A. (1999). Extensive interstitial collagen deposition on the basement membrane zone in allergic nasal mucosa. *Acta Otolaryngol.* 119 (4), 473–478. doi:10.1080/00016489950181026

Schuler Iv, C. F., and Montejo, J. M. (2019). Allergic rhinitis in children and adolescents. *Pediatr. Clin. North Am.* 66 (5), 981–993. doi:10.1016/j.pcl.2019.06.004

Schuler Iv, C. F., and Montejo, J. M. (2021). Allergic rhinitis in children and adolescents. *Immunol. Allergy Clin. North Am.* 41 (4), 613–625. doi:10.1016/j.iac.2021.07.010

Sha, Y., Zmijewski, J., Xu, Z., and Abraham, E. (2008). HMGB1 develops enhanced proinflammatory activity by binding to cytokines. *J. Immunol.* 180 (4), 2531–2537. doi:10.4049/jimmunol.180.4.2531

Sharma, A., and Johnson, A. (2020). Exosome DNA: Critical regulator of tumor immunity and a diagnostic biomarker. *J. Cell. Physiol.* 235 (3), 1921–1932. doi:10.1002/jcp.29153

Shekari, F., Nazari, A., Assar Kashani, S., Hajizadeh-Saffar, E., Lim, R., and Baharvand, H. (2021). Pre-clinical investigation of mesenchymal stromal cell-derived extracellular vesicles: A systematic review. *Cytotherapy* 23 (4), 277–284. doi:10.1016/j.jcyt.2020.12.009

Shen, J., Zhu, X., Fei, J., Shi, P., Yu, S., and Zhou, J. (2018). Advances of exosome in the development of ovarian cancer and its diagnostic and therapeutic prospect. *Onco. Targets. Ther.* 11, 2831–2841. doi:10.2147/OTT.S159829

Siles-Lucas, M., Morchon, R., Simon, F., and Manzano-Roman, R. (2015). Exosome-transported microRNAs of helminth origin: New tools for allergic and autoimmune diseases therapy? *Parasite Immunol.* 37 (4), 208–214. doi:10.1111/pim.12182

Steelant, B., Wawrzyniak, P., Martens, K., Jonckheere, A. C., Pugin, B., Schrijvers, R., et al. (2019). Blocking histone deacetylase activity as a novel target for epithelial barrier defects in patients with allergic rhinitis. *J. Allergy Clin. Immunol.* 144 (5), 1242–1253. doi:10.1016/j.jaci.2019.04.027

Sun, R., Yang, Y., Gu, Z., Tang, X., Zhang, C., Kou, W., et al. (2019). Silencing of CD86 in dendritic cells by small interfering RNA regulates cytokine production in T cells from patients with allergic rhinitis *in vitro*. *Mol. Med. Rep.* 20 (4), 3893–3900. doi:10.3892/mmr.2019.10638

Teng, Z. X., Zhou, X. C., Xu, R. T., Zhu, F. Y., Bing, X., Guo, N., et al. (2022). Tfh exosomes derived from allergic rhinitis promote DC maturation through miR-142-5p/CDK5/STAT3 pathway. *J. Inflamm. Res.* 15, 3187–3205. doi:10.2147/JIR.S365217

van Niel, G., D'Angelo, G., and Raposo, G. (2018). Shedding light on the cell biology of extracellular vesicles. *Nat. Rev. Mol. Cell Biol.* 19 (4), 213–228. doi:10.1038/nrm.2017.125

Villalba, M., Rodriguez, R., and Batanero, E. (2014). The spectrum of olive pollen allergens. From structures to diagnosis and treatment. *Methods* 66 (1), 44–54. doi:10.1016/j.ymeth.2013.07.038

Wang, X., Zhou, Y., Gao, Q., Ping, D., Wang, Y., Wu, W., et al. (2020). The role of exosomal microRNAs and oxidative stress in neurodegenerative diseases. *Oxid. Med. Cell. Longev.* 2020, 3232869. doi:10.1155/2020/3232869

Wu, G., Yang, G., Zhang, R., Xu, G., Zhang, L., Wen, W., et al. (2015). Altered microRNA expression profiles of extracellular vesicles in nasal mucus from patients with allergic rhinitis. *Allergy Asthma Immunol. Res.* 7 (5), 449–457. doi:10.4168/aair.2015.7.5.449

Zamani, P., Fereydouni, N., Butler, A. E., Navashenaq, J. G., and Sahebkar, A. (2019). The therapeutic and diagnostic role of exosomes in cardiovascular diseases. *Trends cardiovasc. Med.* 29 (6), 313–323. doi:10.1016/j.tcm.2018.10.010

Zhang, L., and Yu, D. (2019). Exosomes in cancer development, metastasis, and immunity. *Biochim. Biophys. Acta. Rev. Cancer* 1871 (2), 455–468. doi:10.1016/j.bbcan.2019.04.004

Zhang, Y., Bi, J., Huang, J., Tang, Y., Du, S., and Li, P. (2020). Exosome: A review of its classification, isolation techniques, storage, diagnostic and targeted therapy applications. *Int. J. Nanomedicine* 15, 6917–6934. doi:10.2147/IJN.S264498

Zhang, Y., Lan, F., and Zhang, L. (2021). Advances and highlights in allergic rhinitis. *Allergy* 76 (11), 3383–3389. doi:10.1111/all.15044

Zhang, Y., Lan, F., and Zhang, L. (2022). Update on pathomechanisms and treatments in allergic rhinitis. *Allergy* 77 (11), 3309–3319. doi:10.1111/all.15454

Zhao, J. M., and Luo, Q. (2019). The role and research progress of exosomes in chronic inflammatory diseases of airway. *Lin. Chung Er Bi Yan Hou Tou Jing Wai Ke Za Zhi* 33 (7), 681–684. doi:10.13201/j.issn.1001-1781.2019.07.027

Zhou, C., Chen, Y., He, X., Zheng, Z., and Xue, D. (2020). Functional implication of exosomal miR-217 and miR-23b-3p in the progression of prostate cancer. *Onco. Targets. Ther.* 13, 11595–11606. doi:10.2147/OTT.S272869

Zhou, J., Lu, Y., Wu, W., and Feng, Y. (2021). HMSC-derived exosome inhibited Th2 cell differentiation via regulating miR-146a-5p/SERPINB2 pathway. *J. Immunol. Res.* 2021, 6696525. doi:10.1155/2021/6696525

Zhu, X., Wang, X., Wang, Y., and Zhao, Y. (2020). Exosomal long non-coding RNA GAS5 suppresses Th1 differentiation and promotes Th2 differentiation via downregulating EZH2 and T-bet in allergic rhinitis. *Mol. Immunol.* 118, 30–39. doi:10.1016/j.molimm.2019.11.009

frontiers | Frontiers in Pharmacology

TYPE Review
PUBLISHED 22 December 2022
DOI 10.3389/fphar.2022.1103309

OPEN ACCESS

EDITED BY
Li Wu,
Nanjing University of Chinese Medicine, China

REVIEWED BY
Yingjie Zhao,
Second Hospital of Anhui Medical University, China
Yang Yang,
University of Texas Health Science Center at Houston, United States
Victor E. Laubach,
University of Virginia, United States

*CORRESPONDENCE
Yiwen Zhang,
zhyw0802@163.com
Yinghong Wang,
wyh518@ustc.edu.cn

SPECIALTY SECTION
This article was submitted to Inflammation Pharmacology, a section of the journal Frontiers in Pharmacology

RECEIVED 20 November 2022
ACCEPTED 07 December 2022
PUBLISHED 22 December 2022

CITATION
Zhu W, Zhang Y and Wang Y (2022), Immunotherapy strategies and prospects for acute lung injury: Focus on immune cells and cytokines. *Front. Pharmacol.* 13:1103309. doi: 10.3389/fphar.2022.1103309

Immunotherapy strategies and prospects for acute lung injury: Focus on immune cells and cytokines

Wenfang Zhu[1], Yiwen Zhang[1]* and Yinghong Wang[2]*

[1]Department of Respiratory Medicine, Anhui Chest Hospital, Hefei, China, [2]Department of Pharmacy, Anhui Provincial Cancer Hospital, The First Affiliated Hospital of USTC, Division of Life Sciences and Medicine, University of Science and Technology of China, Hefei, China

Acute lung injury/acute respiratory distress syndrome (ALI/ARDS) is a disastrous condition, which can be caused by a wide range of diseases, such as pneumonia, sepsis, traumas, and the most recent, COVID-19. Even though we have gained an improved understanding of acute lung injury/acute respiratory distress syndrome pathogenesis and treatment mechanism, there is still no effective treatment for acute lung injury/acute respiratory distress syndrome, which is partly responsible for the unacceptable mortality rate. In the pathogenesis of acute lung injury, the inflammatory storm is the main pathological feature. More and more evidences show that immune cells and cytokines secreted by immune cells play an irreplaceable role in the pathogenesis of acute lung injury. Therefore, here we mainly reviewed the role of various immune cells in acute lung injury from the perspective of immunotherapy, and elaborated the crosstalk of immune cells and cytokines, aiming to provide novel ideas and targets for the treatment of acute lung injury.

KEYWORDS

immunotherapy, acute lung injury, immune cells, cytokines, prospects

1 Introduction

Acute lung injury (ALI) is a clinical syndrome involved in inflammation and enhanced pulmonary capillary permeability, which can cause ARDS in severe cases. Its pathological characteristics are diffuse alveolar capillary membrane injury (Perl et al., 2011). Acute lung injury/acute respiratory distress syndrome (ALI/ARDS) encompasses a wide range of pathologic processes, including multiple organ dysfunction syndrome, which has a 40% mortality rate (Matthay et al., 2019). Currently, COVID-19 patients die primarily from ALI/ARDS. There are reports that about 1/3 of hospitalized COVID-19 patients suffered from ARDS, with a frightening 70% mortality rate in these cases (COVID-19/ARDS) (Tzotzos et al., 2020). So far, severe COVID-19 infection has brought millions of people deaths globally. More than 90% of death victims of COVID-19 died from ARDS, suggesting that the majority of deaths caused by COVID-19 are related to ARDS (Tzotzos et al., 2020).

Currently, major efforts are being made to discover mechanism for cognizing and ameliorating ALI, and there has been extensive coverage of these topics in recent reviews (Butt et al., 2016b; Liu et al., 2022; Vichare and Janjic, 2022). Here, however, we focus more on recent developments regarding the role of immunotherapy to ALI/ADRS. We succinctly recapitulate the current insights into ALI signaling, indicate the molecular mechanisms that contribute to immune pathway activation in a variety of pathophysiological situations, and discussed its role in disease-related preclinical models. In light of recent advances in understanding of the ALI pathology and treatment, we explore possible pharmacological intervention strategies focused on these immune cells and discuss their therapeutic potential in treating inflammation associated with ALI.

2 Etiology and pathology of ALI

ALI is presently recognized as an acute diffuse lung injury that can be caused directly through the airway (e.g., inhalation of human stomach contents or toxic substances) or indirectly through the bloodstream (e.g., sepsis or trauma) (Ware and Matthay, 2000). The etiology of ALI is quite numerous, and it can be caused by either internal or external pathogens, including severe infections, sepsis, trauma, shock, acute pancreatitis, iatrogenic lung damage caused by radiotherapy and chemotherapy, inhalation of harmful substances, etc., (Thompson et al., 2017). From the clinical point of view, it can be divided into 10 categories, such as shock, trauma, severe infection and sepsis, aspiration of harmful fluids, inhalation of damaging gases, drugs and metabolic diseases. No matter which etiology causes ALI, its pathogenesis is related to out-of-control inflammatory response. The most common reason of ALI is indirect lung injury, for instance sepsis, trauma and blood transfusion. These triggers can travel through the bloodstream to the lungs and throughout the body, causing systemic inflammatory responses (Castro, 2006; Butt et al., 2016a).

Diffuse alveolar injury is the dominant pathological feature of ALI (Castro, 2006). Moreover, pathological features of ALI also include uncontrolled inflammatory response during neutrophil movement, the production and secretion of proinflammatory cytokines, large numbers of lung epithelial cells apoptosis, loss of alveolar integrity, the damage of alveolar capillary membrane and barrier functions. The flow of protein edema fluid into the alveoli can lead to the inactivation of surfactants and the loss of the protective layer on the alveolar surface, thus destroying the surface cell structure (Mokrá, 2020). Moreover, an injured capillary endothelium attaches neutrophils, which pass through the interstitial cavity to the alveolar cavity filled with protein-rich edema fluid (Scozzi et al., 2022). ALI is also accompanied by local or distant inflammation, and the extent of lung damage depends on whether it is directly to the lungs or caused by external factors, such as lipopolysaccharides (LPS) or inflammatory mediators produced by other organs that circulate throughout the body to the lungs (Liu et al., 2015).

Inflammation in ALI can be triggered through both exogenous and endogenous pathways. Exogenous pathways like bacterial antigens rouse inflammatory responses by triggering toll-like receptors (TLR). Chemical damage can also induce cell membrane damage and oxidative stress, resulting in activation of various intracellular kinases (Arora et al., 2019). The endogenous pathways are mainly composed of hazard signal molecules, members of the damage-associated molecular pattern (DAMP) released by dead cells or local inflammatory cells, which engage and recruit immune cells by binding to various receptors, including TLRs and IL-1 receptors (IL-1R), as a result, the pro-inflammatory pathway is activated (Tolle and Standiford, 2013). At the early stage of ALI, the damage of alveolar-capillary barrier and the formation of pulmonary edema are the main pathological features of ALI. Studies have shown that the change of alveolar barrier function is closely related to inflammation, and pathological results show that when ALI patients suffer from the onset of disease, there may be a great deal of white blood cells in the lungs, alveolar edema, bleeding and other manifestations (Herold et al., 2013). Ultrastructural studies of the lungs in patients with sepsis secondary to ALI have shown significant increases in the number of intravascular and extravascular neutrophils (PMN), platelets, and fibrin, and endothelial and epithelial lesions, which are considered to be inflammatory edema of ALI (Maniatis et al., 2008).

3 Review of current treatment strategies for ALI

According to the pathogenesis of ALI/ARDS, the current drugs used to treat ALI/ARDS mainly include the following categories.

3.1 Vasodilator drugs

Nitric oxide (NO) can induce pulmonary vasodilation without systemic vasodilation through inhalation of NO. Although NO can improve oxygen levels in some extent, many studies have shown that it could not reduce the mortality of ALI/ARDS, and might also cause complications such as pulmonary edema and pumonary hypertension. Therefore, it is not routinely recommended for clinical use. Prostaglandin is another drug for vasodilating, which has the same effect as NO. It is convenient to administer by aerosol inhalation and can be used as a substitute for NO, but its disadvantage is that it is controversial and expensive (Adhikari et al., 2007; White et al., 2008; Afshari et al., 2010; Bosch et al., 2022).

3.2 Surfactant (pulmonary surfactant)

Surfactant is mainly composed of lipids and related proteins, can maintain the structural stability of alveoli by reducing the surface tension of alveoli, and can also prevent pulmonary edema and reduce inflammation (Lewis and Veldhuizen, 2006; Lan et al., 2021). However, due to the poor therapeutic effect of pulmonary surfactant, the dosage and usage are still controversial, so it should be used cautiously (Ali et al., 2021).

3.3 Antioxidants

Because immune cells produce a large number of free radicals during the inflammatory reaction of ALI, a therapeutic method that uses antioxidants to combat free radicals is developed (Sarma and Ward, 2011). Such as glutathione (Moradi et al., 2009), vitamin C (Fowler et al., 2019; Holford et al., 2020), and vitamin E (Wang Y. et al., 2022), but their effects are still to be studied.

3.4 β2 receptor agonist

It is controversial to use an agonist for the treatment of ALI and ARDS patients, in some studies and clinical datas, results showed that β2 agonists have no benefit in improving survival, but can increase morbidity. β2 agonists are not recommended for ALI/ARDS patients based on current evidence (Singh et al., 2014).

3.5 Anti-inflammatory drugs

Corticosteroids are mainly used, however, there are a number of studies that suggest that early use of high-dose corticosteroids can increase the death of ALI/ARDS patients, so the use is not recommended (Mokra et al., 2019; Bobot et al., 2022).

3.6 Stem cell therapy

ALI has been treated using mesenchymal stem cells (MSCs), which can modulate interconnected signal pathways including PI3K/AKT, Wnt, and NF-κB to alleviate inflammation. There are MSCs in various tissues that are capable of self-renewal and differentiation. Their activation is triggered by specific substances or environments, and they can be directed to damaged tissues, where they regenerate and repair the damage. It has been shown that exosomes, as well as cytokines involved in the paracrine pathway of MSCs, are effective in treating ALI (Fernández-Francos et al., 2021; Wang et al., 2022d).

We summarized the advantages and disadvantages of previous ALI treatment methods in the Table 1. According to the above treatment methods, it is currently impossible to find a gratifying drug that can effectively treat ALI/ARDS. In light of this, further research on the pathogenesis of ALI/ARDS is urgently needed, as well as the identification of more effective therapeutic methods and targets.

4 The immune cells in ALI/ARDS

4.1 Neutrophil

Neutrophils, as an immune system cell, can circulate freely inside blood vessels and can be recruited to inflammatory sites when a microbial infection occurs in the human body. It is thought that neutrophil activation and recruitment play a major role in ALI/ARDS progression. Among the first cells to be recruited to inflammation sites, neutrophils have powerful antimicrobial properties, including oxidants, proteinases and cationic peptides. As early immunologic effectors in ALI, neutrophils could stimulate the expression of NF-κB, IL-1β, macrophage inflammatory protein-2 (MIP-2), and tumor necrosis factor-a (TNF-a) (Abraham et al., 2000; Yang et al., 2003). Microbicidal compounds, however, can paradoxically damage host tissues under pathological circumstances (Grommes and Soehnlein, 2011). Neutrophils are known to bind to each other *via* neutrophil extracellular traps (NETs). This process is called netosis, and it is a specific type of cell death, different from necrosis and apoptosis (Zhu et al., 2022). The formation of NETs takes place when neutrophils are exposed to bacteria, fungi, activated platelets, or numerous inflammatory stimuli, and this process is affiliated with dramatic changes in the morphology of the cells (Meyers et al., 2022). It is DNA and granular antimicrobial proteins that determine NETs' antimicrobial properties. Both oxidative and non-oxidative mechanisms are used in the killing of pathogens trapped in NETs (Mamtimin et al., 2022). In addition, it has also been reported that chromatin and proteases released when NETs form can affect procoagulant and prothrombotic factors and participate in the formation of blood clots (Meyers et al., 2022).

There has also been evidence of NETs in patients with ALI/ARDS, where they appear to participate in chronic inflammation processes. Poor degradation and excessive NET formation, however, can exacerbate immune responses and tissue damage. Through the promotion of macrophage polarization to the M1 phenotype, NETs can facilitate ARDS inflammation in the process of the acute phase of the disease (Song et al., 2019). Furthermore, in mice with ALI induced by LPS, NETs formed, caused organ damage, and induced an inflammatory response. Degradation of NETs by DNase I contributed to NET protein clearance and protected against ALI (Liu et al., 2016). In addition, neutrophils are involved in the formation of blood clots.

TABLE 1 Advantages and disadvantages of existing acute lung injury (ALI) treatment strategies.

Strategies	Representative	Advantages	Disadvantages
Vasodilator drugs	NO	Convenient and Effective	Short duration. No reduction in case fatality
	Prostaglandin	Convenient	Expensive, Controversial
Surfactant	Pulmonary Surfactant	Effective	Controversy usage
Antioxidants	Glutathione, Vitamin C/E	Cheap	Low effective
β2 receptor agonist	Propranolol Metoprolol	Effective	Allergies. Arrhythmia, Heart failure
Anti-inflammatory drugs	Corticosteroids	Effective	Increase the mortality of late ARDS
Stem cell therapy	Mesenchymal stem cells	Effective	Expensive

Neutrophils adhered better to activated platelets due to increased ICAM-1 expression in the endothelial cells. As a result of inhibiting platelet-neutrophil aggregation, gas exchange was improved, neutrophil recruitment was reduced, and neutrophil permeability was reduced. These main outcomes were confirmed in a sepsis-induced model of ALI (Zarbock et al., 2006). Among those with sepsis-induced acute lower respiratory infection, Park et al. (2019) noted a rapid decline in the functional capillary ratio during the early stages. By capturing images intravitally, this decrease was attributed to the generation of dead space, caused by prolonged neutrophil entrapment in capillaries. Their results further indicated that neutrophils also displayed an arrest-like dynamic behavior and an extended sequestration time, which sparked neutrophil aggregates inside capillaries and arterioles. As a result of septic shock, osteopontin's neutralization could lessen neutrophil migration into the lungs (Hirano et al., 2015). In addition, p38δ and PKD1 oppositely modulate PTEN activity in neutrophils, therefore, they will be able to control their extravasation and chemotaxis. PKD1 phosphorylates p85δ to promote its relation with PTEN, resulting in polarized PTEN activity, consequently regulating neutrophil migration (Ittner et al., 2012).

4.2 Alveolar macrophages

Although it is well known that neutrophil influx and activation within the lungs participate in ALI pathogenesis, there is increasing evidence that alveolar macrophages (AM) are also involved in modulating inflammatory responses. Macrophages are classified into classical (M1) and alternative (M2) macrophages based on their roles in host defense, despite these distinct *in vitro* classifications, macrophage polarization probably exists in a continuum (Ruytinx et al., 2018; Orecchioni et al., 2019). M1 cells produce high levels of proinflammatory factors such as IL-1β, IL-12, TNF-α, and inducible nitric oxide synthase (iNOS), which are induced by Th1 cytokines. Th2 cytokines, such as IL-4 and IL-13, are known to induce the M2 phenotype, which is characterized by the production of anti-inflammatory molecules such as IL-10 (Mantovani et al., 2002; Mantovani et al., 2005). It is important to note that macrophages are unlike other discrete leukocyte populations in that they retain their plasticity and can be altered by various factors within the microenvironment, including cytokine milieus, among others (Johnston et al., 2012). This study suggested that reprogramming macrophages may contribute to ALI progression.

In ALI, there are a variety of factors that can induce macrophages to change to M1 type, such as LPS and ischemia-reperfusion injury (Zhao et al., 2006; Jiang et al., 2022). There is increasing evidence that inhibiting the transformation of macrophages in various ways can effectively alleviate ALI and even the disease course of COVID-19 (Wang et al., 2022c). Current studies have shown that macrophages are involved in ALI inflammation with two modes, one is that they are induced to secrete inflammatory factors. According to this study, recruited lung macrophages inhibit IL-1β–mediated ALI in gram-negative pneumonia by release of IL-1 receptor antagonist (Herold et al., 2011). Another mode of action is interaction with neutrophils. As is well known that early in ALI there is a penetration of neutrophil, upon intratracheal LPS administration, necrotic AM released pro-interleukin-1α(IL-1α), which activated endothelial cells (EC) to initiate vascular leakage by losing VE-cadherin. Ultimately, it can promote the infiltration of neutrophils and promote the development of ALI (Dagvadorj et al., 2015). In addition, by regulating NF-kB activity and inducing M1 macrophage polarization, exosomal miR-30d-5p from PMNs can influence sepsis-related ALI (Jiao et al., 2021). In conclusion, the crosstalk between AM and neutrophils deserves more research.

4.3 T cells

According to current theories, ARDS is caused by the destruction of alveolar endothelial and epithelial tissue by

platelet-derived products and innate immune cells. As of yet, it is unclear what role adaptive immune cells play in ARDS. In terms of immunological function, T cells can be divided into T helper cells (Th), Cytotoxic T cell and Regulatory T cell (Treg). $CD8^+$T cells are killer T cells, which can release cytokines and perforin to kill virus-infected cells or tumor cells when activated. There is evidence that a malaria-associated lung injury requires an overreaction of $CD8^+$T cells. Excited $CD8^+$T cells migrate to the lungs during infection, and immune-mediated anti-CD8 antibody treatment ameliorates pulmonary damage (Claser et al., 2019).

There is evidence that regulatory T-cells (Tregs) facilitate tissue repair and promote ARDS resolution. It has also been shown that Treg-depleted mice have impaired Th1 and Th17 immune responses, suggesting that Tregs are indispensable for tissue repair, modulating and promoting the Th immune response in LPS-induced pulmonary inflammation (Tan et al., 2019). Normally, T-regs are found in lymphoid tissues and peripheral blood, Leukotrienes B4 (LTB4) can recruit $CD4^+CD25^+$ $Foxp3^+$ Regulatory T Cells during ALI, which reduce the inflammation of the ALI (D'Alessio et al., 2009; Wang et al., 2012). In general, Treg cells communicate with other T cells by secreting anti-inflammatory factors. For example, the production of IL-10 by Treg cells and dendritic cells can protect the lungs from injury caused by transfusion (Kapur et al., 2017). In addition, it is noteworthy that Treg can also reduce the proliferation of ALI fibers by reducing fibrocyte recruitment (Garibaldi et al., 2013). It has also been reported that $CD39^+$ Treg cells reduce LPS induced ALI through autophagy and ERK/FOS pathways (Chen et al., 2020).

Recent studies have focused on the effect and function of Treg on ALI, but further studies on Th cells are needed. Compared with Treg, Th cells may have a more unique function, and it has been reported that CTLA4 plays a role in T cell pathways in ALI models (Nakajima et al., 2010). Importantly, a gradual understanding of Th17's function is emerging in ALI, Th17 cells are T helper cells that secrete a distinct subset of T cell cytokines, including IL-17A and F, IL-21 and IL-22. IL-17A and F, especially, are released in the setting of bacterial infections and have distinctive roles in reply to bacterial and fungal pathogens (Li et al., 2015; Sakaguchi et al., 2016).

4.4 Monocytes

Monocytes originate from hematopoietic stem cells in the bone marrow and develop in the bone marrow. When they enter the blood, they are still immature cells. Monocytes also take part in the immune response, after phagocytosis of antigen to carry the antigen epitope to the lymphocyte, inducing lymphocyte specific immune response (Merad and Martin, 2020).

Monocytes in the lung can be divided into mature and immature mononuclear cells. The plasticity of immature mononuclear cells in diseases is higher. Studies have indicated that immature monocytes promote cardiopulmonary bypass-induced ALI by generating inflammatory descendants (Xing et al., 2017). The reason is that immature $CD14^{low}$ CD16− monocytes have a limited ability to produce TNF-α and inhibit T cell proliferation mediated by T cell receptor signaling. However, these immature cells are highly proliferative and can differentiate into mature $CD14^{high}$ $CD16^+$ monocytes that produce TNF-α (Xing et al., 2017). Crosstalk between monocytes and other immune cells has always been the focus of research. It is believed that the communication between monocytes and immune cells is a key point. In ALI, monocytes are activated by LPS and can recruit neutrophils to the site of inflammation, thus achieving a synergistic effect (Dhaliwal et al., 2012). In addition, Plasmacytoid Dendritic Cells can recruit monocytes to activate inflammatory in mice lung injury (Venet et al., 2010). Interestingly, it is not only lung queued monocytes that have a direct effect. Chemokines secreted by monocytes in blood play a pivotal role in the progression and outcome of lung injury during ischemia-reperfusion ALI. The main reason is that chemokines in the blood can activate lung monocytes and induce inflammatory expression after reaching the lungs. Blocking this process can significantly reduce the extent of lung damage (McKenzie et al., 2014).

4.5 Other immune cells

In addition, there are some studies on NK cells and eosinophils in ALI. Eosinophils, like other granulocytes, are derived from blood-forming stem cells in the bone marrow. Eosinophils have the function of killing bacteria and parasites, and are very important cells in immune response and allergic reaction. Eosinophils can release the contents of the particles, causing tissue damage and promoting the progression of inflammation (Grisaru-Tal et al., 2022). Recent studies have shown that eosinophils have an excellent protective effect against ALI, while eosinopenia may increase mortality risks. Apart from pulmonary macrophages, homeostasis eosinophils are a newly discovered cell group, which play a key role in the ALI. The LPS challenge induces rapid agglomeration of eosinophils from the peripheral circulation into the lungs. Loss of eosinophils increases LPS-induced neutrophilic inflammation and eventual injury levels. Homeostasis $CD101^-$ but not allergic $CD101^+$ eosinophils play an anti-inflammatory role in ALI (Zhu et al., 2020). In addition, IL-33-induced eosinophilia is critical for preventing death induced by *staphylococcus aureus* (Krishack et al., 2021), which provides evidence for novel and potentially beneficial effects of eosinophils. As a powerful toxic cell, NK cells play a crucial role in a variety of diseases. As the first line of defense, NK cells are key players in innate immunity. However, its function in ALI is seriously underestimated. Activated lung NK cells overexpress activated receptors NKG2D and CD27, and become functional NK cells by producing large

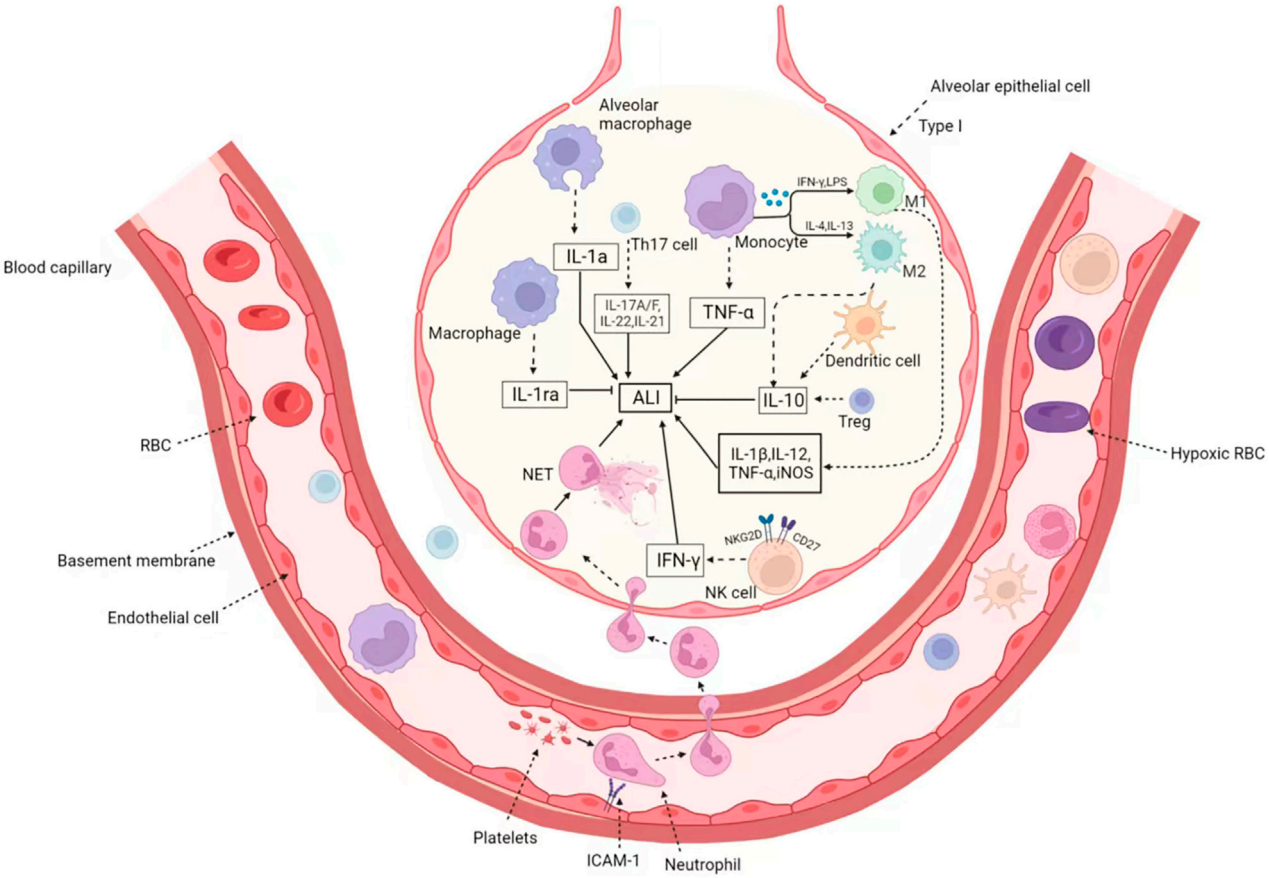

FIGURE 1
The immune cells in Acute lung injury/acute respiratory distress syndrome. When ALI occurs, various immune cells are recruited through the blood vessels to the inflammatory region and enter the alveoli through the swollen outer walls of the blood vessels. On the one hand, neutrophils recruit platelets to form microthrombus, endothelial cells expressed ICAM-1 and increased platelet adhesion. On the other hand, they form NET through capillaries to enlarge inflammatory lesions. The activated macrophages are divided into M1 type and M2 type. M1-type macrophages induced by IFN-γ and LPS secrete pro-inflammatory factors such as IL-1β, IL-12, TNF-α, and iNOS. While M1 macrophages induced by IL-4 and IL-13 have the opposite function, which product IL-10 and relief ALI. In addition, eosinophils, NK cells, dendritic cell and Treg cells were also recruited to play different roles. Treg and dendritic cells secrete IL-10 to inhibit inflammatory response, and activated NK cells overexpress NKG2D and CD27 receptors, release IFN-γ, and promote the occurrence of ALI.

amounts of interferon γ, which is the cause of acute lung immune injury. The decrease of NK cells significantly reduced lung immune damage, total inflammatory cell infiltration and IFN-γ production in bronchoalveolar lavage fluid (BALF) (Li et al., 2012). We have sorted out the role and mechanism of immune cells in ALI as shown in the Figure 1.

5 The immune-related factors in ALI/ARDS

5.1 Interleukin

There are several functions of interleukins in inflammation, including transmitting information, activating and regulating immune cells, and promoting proliferation and differentiation of T and B cells (Briukhovetska et al., 2021). In ALI, IL-1β is at the top of the list. As one of the most common pro-inflammatory factors, numerous studies have focused on the anti-IL-1β function. Recruitment of neutrophils is known to be critical in prophase ALI. Studies have reported that Il-1β is also involved in this process. In lung injury after lung transplantation, classical monocytes infiltrated by the graft produce myD88-dependent IL-1β, thus mediating neutrophil exosmosis (Hsiao et al., 2018). In addition, IL-1β in acid—induced and sepsis—induced ALI is also associated with the development of inflammation (Mizushina et al., 2019; Xiong et al., 2020). So, the source of IL-1β has been a focus of attention, on the one hand, IL-1β is produced by different immune cells, such as alveolar macrophages (Xu et al., 2022), monocytes (Hsiao et al., 2018). On the other

hand, NLRP3 inflammasome also mediates the shearing and maturation of IL-1β (Mizushina et al., 2019).

Another family of cytokines that play a pro-inflammatory role in ALI is IL-17. Studies have shown that IL-17 is primarily congenital lymphocyte production in ALI (Muir et al., 2016), in the case of LPS-induced airway epithelial cell injury, the interaction between IL-17A and endoplasmic reticulum stress is pivotal and exhibits positive feedback (Kim et al., 2015). In addition, the production of IL-17 by lung γδ T cells is also considered to be one of the important factors in the pathogenesis of ALI (Menoret et al., 2018).

In addition, several other interleukins are associated with the progression of ALI. For example, blocking IL-3 and IL-5 can significantly reduce the hyperinflammatory response in ARDS models (Wang H. et al., 2022). Of note is the self-sustaining IL-8 cycle driving the prethrombotic neutrophil phenotype in severe COVID-19 (Kaiser et al., 2021). Coincidentally, interleukin-36γ and IL-36 receptor signaling pathways reconcile damaged host immunity and lung damage in cytotoxic *Pseudomonas aeruginosa* lung infection (Aoyagi et al., 2017).

Conversely, some studies have reported on the anti-inflammatory interleukin. For example, IL-10 and IL-35 have a protective effect on ARDS by increasing CD4+Treg ratio in extrapulmonary ARDS (Kapur et al., 2017; Wang et al., 2019). ARDS also can be alleviated by IL-4 mediated reprogramming of lung macrophages (D'Alessio et al., 2016). In addition, IL-33-dependent regulatory T cell accumulation mediates lung epithelial regeneration at the end stage of ALI (Tan et al., 2021).

5.2 Interferon

Besides interleukin, interferon also plays an irreplaceable role in ALI. The function of interferon in ALI is two-sided. On the one hand, influenza-induced IFN-γ triggers the hyperreactivity of bone marrow cells to MRSA, resulting in excessive inflammatory responses and fatal lung injury during co-infection (Verma et al., 2022). On the other hand, IFN-β can restore the function of damaged alveolar macrophages by recruiting neutrophils to the alveoli, thus improving the survival rate (Hiruma et al., 2018; Sekheri et al., 2022).

5.3 NLRP3 inflammasome

In addition to membrane-bound Pattern Recognition Receptors (PRRs), cytoplasmic PRRs, such as the NLRP3 inflammasome, indirectly recognize PAMP and DAMP. This process can be called a molecular process that detects changes in homeostasis. The NLRP3 inflammasome consists of NLRP3, ASC and caspase-1. When NLRP3 inflammasome recognizes PAMP and DAMP, caspase-1 splits IL-1β and IL-18, producing active IL-1β and IL-18, which mediate multiple inflammatory responses (Harapas et al., 2022). The role of NLRP3 in ALI has been controversial. Studies have shown that macrophages are over-activated in LPS-induced ALI, activating NLRP3 inflammasome and triggering pyroptosis, a process that exacerbates the disease of ALI (Li et al., 2018; Hu et al., 2022). In addition, NLRP3-mediated pyroptosis may not be limited to macrophages, but may also be discovered in neutrophils (Feng et al., 2017). In brief, the role of the inflammasome represented by NLRP3 in ALI deserves continuous attention.

5.4 Other immune-related factors

The role of most immune-related factors is reflected in the understanding of immune cell function. The regulation of alveolar macrophages is particularly important in ALI. It is well known that macrophage activation is one of the important mechanisms of its action, and it has been reported that CD36 regulates LPS-induced ALI by enhancing macrophages M1 polarization (Sun et al., 2022). Similarly, Protein phosphatase 2A (PP2A) (He et al., 2019), sphingosine-1-phosphate (S1P) (Joshi et al., 2020), oxidative stress-induced FABP5-S glutathione acylation inhibits macrophage inflammation (Guo et al., 2021).

Neutrophils are crucial immune cells in ALI, and the regulation of neutrophils has been studied more and more. Targeted binding adhesion molecule c can improve ALI caused by sepsis by reducing $CXCR4^{+}$ neutrophils (Hirano et al., 2018). In addition, PDL1 and GM-CSF also alleviated the course of ALI by promoting the completion of neutrophil traps (De Alessandris et al., 2019; Zhu et al., 2022).

In other cells, for example, overexpression of cAMP response element modulator (CREM) in T cells exacerbates lipopolysaccharide-induced ALI (Verjans et al., 2013), and NKG2D-activated natural killer cells mediate lung ischemia-reperfusion injury (Calabrese et al., 2021). We summarized the role and mechanism of immune cytokines in ALI as shown in the Figure 2.

6 Prospects for future treatment strategies for ALI

As a disease with rapid onset and rapid course, there is no specific treatment strategy for ALI. Recently there has been a growing focus on the critical role of immune cells and immune-related factors in various diseases, including tumors. The progress has been enormous and valuable. As ALI is a disease with uncontrolled immune cells and inflammatory storms, the application of immunotherapy will have a high prospect. Just as a study by Xu et al. (2020) recently, they retrospectively studied 21 patients with severe and critical COVID-19 who were treated

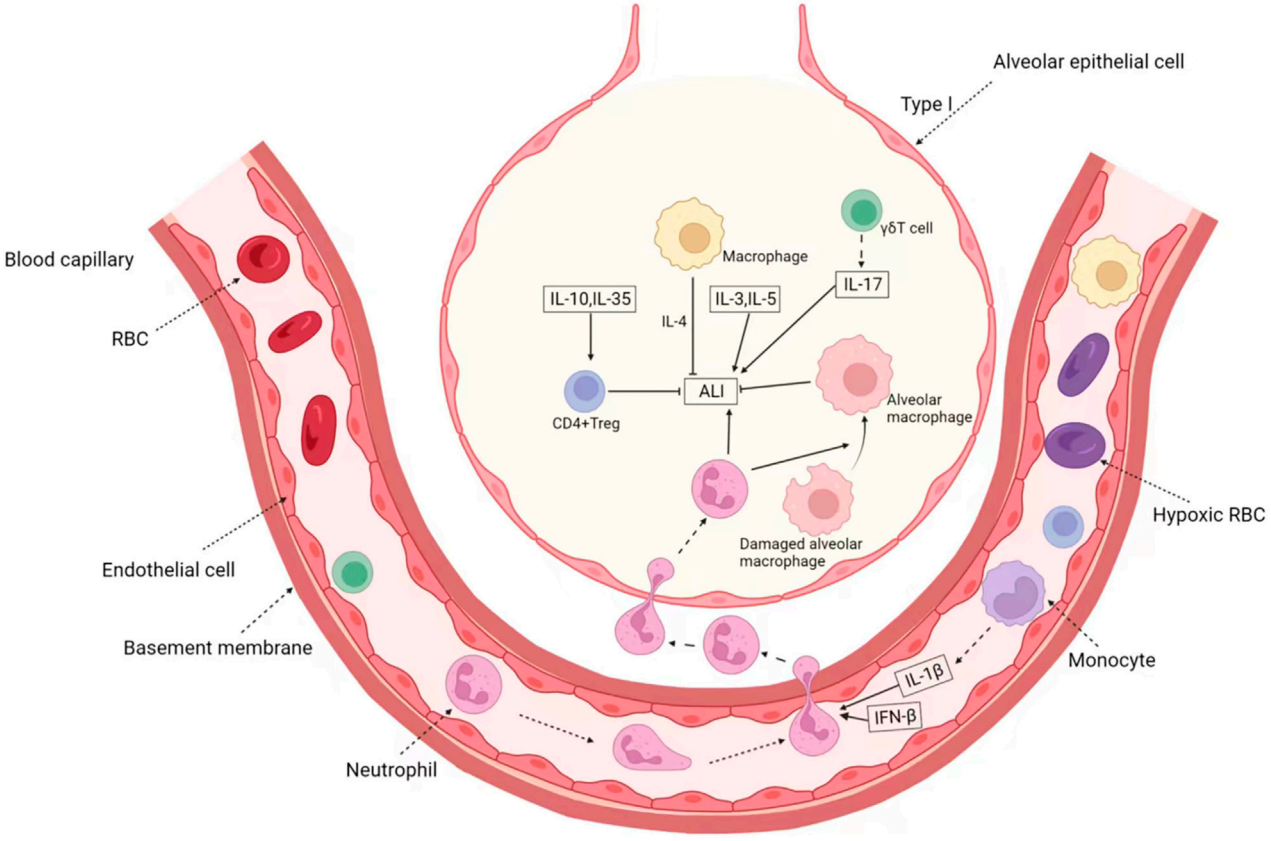

FIGURE 2
The Immune-related factors in ALI/ARDS. In ALI, immune cytokines mainly play the role of cell communication, which is represented by interleukin. Anti-inflammatory cytokines IL-10 and IL-35 can induce the activation of $CD4^+$ Treg and then inhibit ALI. IL-1β produced by monocyte and IFN-β can induce the activation of neutrophil, which aggravate ALI. Besides the factors secreted by recruited immune cell, IL-3 and IL-5 can directly promote ALI. On the other hand, activated γδT cells and macrophages can secrete IL-17, IL-5 and so on, forming positive feedback. In addition, immune cells represented by M2-type macrophages can also secrete IL-4 to alleviate the progression of inflammation.

with tocilizumab, an IL6 receptor inhibitor. Surprisingly, their results showed that a majority of patients with tocilizumab experienced an immediate improvement in both symptoms, hypoxygenemia, and CT opacity changes after treatment. As a result, they concluded that tocilizumab improves clinical symptoms and inhibits deterioration in severe COVID-19 patients, which is an effective treatment option for COVID-19 and can provide a therapeutic strategy for this deadly infectious disease. Furthermore, their team also identified a monocyte subpopulation that promotes the inflammatory cytokine storms by using single-cell mRNA sequencing in two severe-stage COVID-19 patients before and after tocilizumab treatment. In spite of the fact that tocilizumab treatment reduces inflammation, immune cells (including plasma B cells and $CD8^+$ T cells) still exert a robust antiviral response both humorally and cellularly. Therefore, they indicated that treatment with tocilizumab can not only reduce the damage caused by monocyte inflammatory factor storms, but also maintain the normal antiviral immune response of COVID-19 (Guo et al., 2020).

However, despite the promise of immunotherapy, few drugs are available for clinical use. The use of monoclonal antibodies or antagonists to neutralize cytokines such as TNF, IL-1, and IL-8 can significantly reduce lung injury in animal studies, but most clinical trials have negative results. The results of clinical trials showed that anti-TNF monoclonal antibody (Afelimomab) was used to treat severely infected ALI, among which the MONARCS study (n = 2,634) showed that the mortality of the Afelimomab treatment group was significantly reduced in severely infected patients with high or low levels of IL-6 (Panacek et al., 2004; Rondon and Venkataraman, 2005). But another study did not reduce the case fatality rate (Reinhart et al., 2001). There is a lack of clinical evidence on whether cytokine monoclonal antibodies or antagonists can be used in the treatment of ALI/ARDS. Moreover, whether Itolizumab, a novel anti-CD6 monoclonal antibody, can be used in ARDS caused by COVID-19 has also

attracted wide attention. On the one hand, previous clinical data showed that Itolizumab could significantly reduce IL-6 level in patients with psoriasis and internal rheumatoid arthritis (Budamakuntla et al., 2015; Aira et al., 2016); On the other hand, data also showed that patients with COVID-19 experienced severe second-degree heart block after infusion of Itolizumab (Kumar et al., 2021). Therefore, judging from the current research and clinical data, there is still a lot of work to be done on immunotherapy for ALI in the future. It is important to fully understand the immunological pathogenesis of ALI and regulate the immune balance, rather than simply regulate a certain inflammatory factor. Drugs that target a specific cytokine are only capable of inhibiting that cytokine, and may not limit the effects of other cytokines as well. As a consequence, selecting the correct time period for anti-inflammatory therapy and identifying those patients who would benefit from immunosuppression remains crucial (Mastitskaya et al., 2021).

Although we have encountered some setbacks in the process of applying immunotherapy to ALI, there is no denying that the initial exploration of immunotherapy has brought new hope to more patients. The immune mechanism of ALI is very complex. Multiple immune cells interact with each other and play different roles. Monoclonal antibody, as a key drug in immunotherapy, is always accompanied by serious side effects in the process of immunotherapy, which makes it unable to play its proper therapeutic role. On the one hand, this is due to our insufficient understanding of the immune pathogenesis of ALI, and on the other hand, it is also caused by the versatility of the drug targets of monoclonal antibody therapy. Perhaps, the screening and study of compounds that target the immune system is a meaningful therapeutic strategy, and the use of combination medication regimen to prevent side effects is also a viable approach.

In a word, for the immunotherapy of ALI, it is difficult but indispensable to maintain the dynamic balance of various immune cells. Perhaps a good strategy is to have a deeper understanding of the immune cytokines concerned with the development of disease, this opens up new therapeutic targets for ALI.

Author contributions

WZ designed and wrote this manuscript, YZ checked the manuscript. YW designed and checked this manuscript.

Conflict of interest

The authors declare that the research was conducted in the absence of any commercial or financial relationships that could be construed as a potential conflict of interest.

Publisher's note

All claims expressed in this article are solely those of the authors and do not necessarily represent those of their affiliated organizations, or those of the publisher, the editors and the reviewers. Any product that may be evaluated in this article, or claim that may be made by its manufacturer, is not guaranteed or endorsed by the publisher.

References

Abraham, E., Carmody, A., Shenkar, R., and Arcaroli, J. (2000). Neutrophils as early immunologic effectors in hemorrhage- or endotoxemia-induced acute lung injury. *Am. J. physiology Lung Cell. Mol. physiology* 279 (6), L1137–L1145. doi:10.1152/ajplung.2000.279.6.L1137

Adhikari, N., Burns, K., Friedrich, J., Granton, J., Cook, D., and Meade, M. (2007). Effect of nitric oxide on oxygenation and mortality in acute lung injury: Systematic review and meta-analysis. *BMJ Clin. Res. ed.)* 334 (7597), 779. doi:10.1136/bmj.39139.716794.55

Afshari, A., Brok, J., Møller, A., and Wetterslev, J. (2010). Aerosolized prostacyclin for acute lung injury (ALI) and acute respiratory distress syndrome (ARDS). *Cochrane database Syst. Rev.* 1 (8), CD007733. doi:10.1002/14651858.CD007733.pub2

Aira, L. E., Hernandez, P., Prada, D., Chico, A., Gomez, J. A., Gonzalez, Z., et al. (2016). Immunological evaluation of rheumatoid arthritis patients treated with itolizumab. *MAbs* 8 (1), 187–195. doi:10.1080/19420862.2015.1105416

Ali, A., Pettenuzzo, T., Ramadan, K., Farrell, A., Di Nardo, M., Liu, M., et al. (2021). Surfactant therapy in lung transplantation: A systematic review and meta-analysis. *Transplant. Rev. Orl. Fla* 35 (4), 100637. doi:10.1016/j.trre.2021.100637

Aoyagi, T., Newstead, M. W., Zeng, X., Nanjo, Y., Peters-Golden, M., Kaku, M., et al. (2017). Interleukin-36γ and IL-36 receptor signaling mediate impaired host immunity and lung injury in cytotoxic *Pseudomonas aeruginosa* pulmonary infection: Role of prostaglandin E2. *PLoS Pathog.* 13 (11), e1006737. doi:10.1371/journal.ppat.1006737

Arora, S., Ahmad, S., Irshad, R., Goyal, Y., Rafat, S., Siddiqui, N., et al. (2019). TLRs in pulmonary diseases. *Life Sci.* 233, 116671. doi:10.1016/j.lfs.2019.116671

Bobot, M., Tonon, D., Peres, N., Guervilly, C., Lefèvre, F., Max, H., et al. (2022). Impact of dexamethasone and inhaled nitric oxide on severe acute kidney injury in critically ill patients with COVID-19. *J. Clin. Med.* 11 (20), 6130. doi:10.3390/jcm11206130

Bosch, N., Law, A., Vail, E., Gillmeyer, K., Gershengorn, H., Wunsch, H., et al. (2022). Inhaled nitric oxide vs epoprostenol during acute respiratory failure: An observational target trial emulation. *Chest* 162, 1287–1296. doi:10.1016/j.chest.2022.08.001

Briukhovetska, D., Dörr, J., Endres, S., Libby, P., Dinarello, C., and Kobold, S. (2021). Interleukins in cancer: From biology to therapy. *Nat. Rev. Cancer* 21 (8), 481–499. doi:10.1038/s41568-021-00363-z

Budamakuntla, L., Madaiah, M., Sarvajnamurthy, S., and Kapanigowda, S. (2015). Itolizumab provides sustained remission in plaque psoriasis: A 5-year follow-up experience. *Clin. Exp. Dermatol* 40 (2), 152–155. doi:10.1111/ced.12509

Butt, Y., Kurdowska, A., and Allen, T. (2016a). Acute lung injury: A clinical and molecular review. *Archives pathology laboratory Med.* 140 (4), 345–350. doi:10.5858/arpa.2015-0519-RA

Butt, Y., Kurdowska, A., and Allen, T. C. (2016b). Acute lung injury: A clinical and molecular review. *Arch. Pathol. Lab. Med.* 140 (4), 345–350. doi:10.5858/arpa.2015-0519-RA

Calabrese, D. R., Aminian, E., Mallavia, B., Liu, F., Cleary, S. J., Aguilar, O. A., et al. (2021). Natural killer cells activated through NKG2D mediate lung ischemia-reperfusion injury. *J. Clin. Invest* 131 (3), e137047. doi:10.1172/JCI137047

Castro, C. (2006). ARDS and diffuse alveolar damage: A pathologist's perspective. *Seminars Thorac. Cardiovasc. Surg.* 18 (1), 13–19. doi:10.1053/j.semtcvs.2006.02.001

Chen, C., Li, X., Li, C., Jin, J., Wang, D., Zhao, Y., et al. (2020). CD39(+) regulatory T cells attenuate lipopolysaccharide-induced acute lung injury via autophagy and the ERK/FOS pathway. *Front. Immunol.* 11, 602605. doi:10.3389/fimmu.2020.602605

Claser, C., Nguee, S. Y. T., Balachander, A., Wu Howland, S., Becht, E., Gunasegaran, B., et al. (2019). Lung endothelial cell antigen cross-presentation to CD8(+)T cells drives malaria-associated lung injury. *Nat. Commun.* 10 (1), 4241. doi:10.1038/s41467-019-12017-8

D'Alessio, F. R., Craig, J. M., Singer, B. D., Files, D. C., Mock, J. R., Garibaldi, B. T., et al. (2016). Enhanced resolution of experimental ARDS through IL-4-mediated lung macrophage reprogramming. *Am. J. Physiol. Lung Cell Mol. Physiol.* 310 (8), L733–L746. doi:10.1152/ajplung.00419.2015

D'Alessio, F. R., Tsushima, K., Aggarwal, N. R., West, E. E., Willett, M. H., Britos, M. F., et al. (2009). CD4+CD25+Foxp3+ Tregs resolve experimental lung injury in mice and are present in humans with acute lung injury. *J. Clin. Invest* 119 (10), 2898–2913. doi:10.1172/JCI36498

Dagvadorj, J., Shimada, K., Chen, S., Jones, H., Tumurkhuu, G., Zhang, W., et al. (2015). Lipopolysaccharide induces alveolar macrophage necrosis via CD14 and the P2X7 receptor leading to interleukin-1α release. *Immunity* 42 (4), 640–653. doi:10.1016/j.immuni.2015.03.007

De Alessandris, S., Ferguson, G. J., Dodd, A. J., Juss, J. K., Devaprasad, A., Piper, S., et al. (2019). Neutrophil GM-CSF receptor dynamics in acute lung injury. *J. Leukoc. Biol.* 105 (6), 1183–1194. doi:10.1002/JLB.3MA0918-347R

Dhaliwal, K., Scholefield, E., Ferenbach, D., Gibbons, M., Duffin, R., Dorward, D. A., et al. (2012). Monocytes control second-phase neutrophil emigration in established lipopolysaccharide-induced murine lung injury. *Am. J. Respir. Crit. Care Med.* 186 (6), 514–524. doi:10.1164/rccm.201112-2132OC

Feng, Z., Qi, S., Zhang, Y., Qi, Z., Yan, L., Zhou, J., et al. (2017). Ly6G+ neutrophil-derived miR-223 inhibits the NLRP3 inflammasome in mitochondrial DAMP-induced acute lung injury. *Cell Death Dis.* 8 (11), e3170. doi:10.1038/cddis.2017.549

Fernández-Francos, S., Eiro, N., González-Galiano, N., and Vizoso, F. (2021). Mesenchymal stem cell-based therapy as an alternative to the treatment of acute respiratory distress syndrome: Current evidence and future perspectives. *Int. J. Mol. Sci.* 22 (15), 7850. doi:10.3390/ijms22157850

Fowler, A., Truwit, J., Hite, R., Morris, P., DeWilde, C., Priday, A., et al. (2019). Effect of vitamin C infusion on organ failure and biomarkers of inflammation and vascular injury in patients with sepsis and severe acute respiratory failure: The CITRIS-ALI randomized clinical trial. *JAMA* 322 (13), 1261–1270. doi:10.1001/jama.2019.11825

Garibaldi, B. T., D'Alessio, F. R., Mock, J. R., Files, D. C., Chau, E., Eto, Y., et al. (2013). Regulatory T cells reduce acute lung injury fibroproliferation by decreasing fibrocyte recruitment. *Am. J. Respir. Cell Mol. Biol.* 48 (1), 35–43. doi:10.1165/rcmb.2012-0198OC

Grisaru-Tal, S., Rothenberg, M., and Munitz, A. (2022). Eosinophil-lymphocyte interactions in the tumor microenvironment and cancer immunotherapy. *Nat. Immunol.* 23 (9), 1309–1316. doi:10.1038/s41590-022-01291-2

Grommes, J., and Soehnlein, O. (2011). Contribution of neutrophils to acute lung injury. *Mol. Med. Camb. Mass* 17, 293–307. doi:10.2119/molmed.2010.00138

Guo, C., Li, B., Ma, H., Wang, X., Cai, P., Yu, Q., et al. (2020). Single-cell analysis of two severe COVID-19 patients reveals a monocyte-associated and tocilizumab-responding cytokine storm. *Nat. Commun.* 11 (1), 3924. doi:10.1038/s41467-020-17834-w

Guo, Y., Liu, Y., Zhao, S., Xu, W., Li, Y., Zhao, P., et al. (2021). Oxidative stress-induced FABP5 S-glutathionylation protects against acute lung injury by suppressing inflammation in macrophages. *Nat. Commun.* 12 (1), 7094. doi:10.1038/s41467-021-27428-9

Harapas, C., Idiiatullina, E., Al-Azab, M., Hrovat-Schaale, K., Reygaerts, T., Steiner, A., et al. (2022). Organellar homeostasis and innate immune sensing. *Nat. Rev. Immunol.* 22 (9), 535–549. doi:10.1038/s41577-022-00682-8

He, Z., Du, L., Ke, Y., Wen, C., and Zhang, Y. (2019). PP2ACα of alveolar macrophages is a novel protective factor for LPS-induced acute respiratory distress syndrome. *Inflammation* 42 (3), 1004–1014. doi:10.1007/s10753-019-00962-x

Herold, S., Gabrielli, N., and Vadász, I. (2013). Novel concepts of acute lung injury and alveolar-capillary barrier dysfunction. *Am. J. physiology. Lung Cell. Mol. physiology* 305 (10), L665–L681. doi:10.1152/ajplung.00232.2013

Herold, S., Tabar, T., Janssen, H., Hoegner, K., Cabanski, M., Lewe-Schlosser, P., et al. (2011). Exudate macrophages attenuate lung injury by the release of IL-1 receptor antagonist in gram-negative pneumonia. *Am. J. Respir. Crit. care Med.* 183 (10), 1380–1390. doi:10.1164/rccm.201009-1431OC

Hirano, Y., Aziz, M., Yang, W., Wang, Z., Zhou, M., Ochani, M., et al. (2015). Neutralization of osteopontin attenuates neutrophil migration in sepsis-induced acute lung injury. *Crit. care (London, Engl.* 19, 53. doi:10.1186/s13054-015-0782-3

Hirano, Y., Ode, Y., Ochani, M., Wang, P., and Aziz, M. (2018). Targeting junctional adhesion molecule-C ameliorates sepsis-induced acute lung injury by decreasing CXCR4(+) aged neutrophils. *J. Leukoc. Biol.* 104 (6), 1159–1171. doi:10.1002/JLB.3A0218-050R

Hiruma, T., Tsuyuzaki, H., Uchida, K., Trapnell, B. C., Yamamura, Y., Kusakabe, Y., et al. (2018). IFN-Beta improves sepsis-related alveolar macrophage dysfunction and postseptic acute respiratory distress syndrome-related mortality. *Am. J. Respir. Cell Mol. Biol.* 59 (1), 45–55. doi:10.1165/rcmb.2017-0261OC

Holford, P., Carr, A., Jovic, T., Ali, S., Whitaker, I., Marik, P., et al. (2020). Vitamin C-an adjunctive therapy for respiratory infection, sepsis and COVID-19. *Nutrients* 12 (12), 3760. doi:10.3390/nu12123760

Hsiao, H. M., Fernandez, R., Tanaka, S., Li, W., Spahn, J. H., Chiu, S., et al. (2018). Spleen-derived classical monocytes mediate lung ischemia-reperfusion injury through IL-1β. *J. Clin. Invest* 128 (7), 2833–2847. doi:10.1172/JCI98436

Hu, L., Shao, C., Pan, L., and Jiang, Z. (2022). Lack of STAT6 enhances murine acute lung injury through NLRP3/p38 MAPK signaling pathway in macrophages. *BMC Immunol.* 23 (1), 25. doi:10.1186/s12865-022-00500-9

Ittner, A., Block, H., Reichel, C., Varjosalo, M., Gehart, H., Sumara, G., et al. (2012). Regulation of PTEN activity by p38δ-PKD1 signaling in neutrophils confers inflammatory responses in the lung. *J. Exp. Med.* 209 (12), 2229–2246. doi:10.1084/jem.20120677

Jiang, W., Ma, C., Bai, J., and Du, X. (2022). Macrophage SAMSN1 protects against sepsis-induced acute lung injury in mice. *Redox Biol.* 56, 102432. doi:10.1016/j.redox.2022.102432

Jiao, Y., Zhang, T., Zhang, C., Ji, H., Tong, X., Xia, R., et al. (2021). Exosomal miR-30d-5p of neutrophils induces M1 macrophage polarization and primes macrophage pyroptosis in sepsis-related acute lung injury. *Crit. care (London, Engl.* 25 (1), 356. doi:10.1186/s13054-021-03775-3

Johnston, L., Rims, C., Gill, S., McGuire, J., and Manicone, A. (2012). Pulmonary macrophage subpopulations in the induction and resolution of acute lung injury. *Am. J. Respir. cell Mol. Biol.* 47 (4), 417–426. doi:10.1165/rcmb.2012-0090OC

Joshi, J. C., Joshi, B., Rochford, I., Rayees, S., Akhter, M. Z., Baweja, S., et al. (2020). SPHK2-Generated S1P in CD11b(+) macrophages blocks STING to suppress the inflammatory function of alveolar macrophages. *Cell Rep.* 30 (12), 4096–4109. e4095. doi:10.1016/j.celrep.2020.02.112

Kaiser, R., Leunig, A., Pekayvaz, K., Popp, O., Joppich, M., Polewka, V., et al. (2021). Self-sustaining IL-8 loops drive a prothrombotic neutrophil phenotype in severe COVID-19. *JCI Insight* 6 (18), e150862. doi:10.1172/jci.insight.150862

Kapur, R., Kim, M., Aslam, R., McVey, M. J., Tabuchi, A., Luo, A., et al. (2017). T regulatory cells and dendritic cells protect against transfusion-related acute lung injury via IL-10. *Blood* 129 (18), 2557–2569. doi:10.1182/blood-2016-12-758185

Kim, S. R., Kim, H. J., Kim, D. I., Lee, K. B., Park, H. J., Jeong, J. S., et al. (2015). Blockade of interplay between IL-17a and endoplasmic reticulum stress attenuates LPS-induced lung injury. *Theranostics* 5 (12), 1343–1362. doi:10.7150/thno.11685

Krishack, P. A., Hollinger, M. K., Kuzel, T. G., Decker, T. S., Louviere, T. J., Hrusch, C. L., et al. (2021). IL-33-mediated eosinophilia protects against acute lung injury. *Am. J. Respir. Cell Mol. Biol.* 64 (5), 569–578. doi:10.1165/rcmb.2020-0166OC

Kumar, A., Kumar, N., Lenin, D., Kumar, A., and Ahmad, S. (2021). Second-degree heart block caused by itolizumab-induced infusion reaction in COVID-19. *Indian J. Crit. Care Med.* 25 (4), 474–475. doi:10.5005/jp-journals-10071-23794

Lan, C., Wu, Y., Peng, C., Huang, K., and Wu, C. (2021). Surfactant attenuates air embolism-induced lung injury by suppressing NKCC1 expression and NF-κB activation. *Inflammation* 44 (1), 57–67. doi:10.1007/s10753-020-01266-1

Lewis, J., and Veldhuizen, R. (2006). The future of surfactant therapy during ALI/ARDS. *Seminars Respir. Crit. care Med.* 27 (4), 377–388. doi:10.1055/s-2006-948291

Li, D., Ren, W., Jiang, Z., and Zhu, L. (2018). Regulation of the NLRP3 inflammasome and macrophage pyroptosis by the p38 MAPK signaling pathway in a mouse model of acute lung injury. *Mol. Med. Rep.* 18 (5), 4399–4409. doi:10.3892/mmr.2018.9427

Li, F., Zhu, H., Sun, R., Wei, H., and Tian, Z. (2012). Natural killer cells are involved in acute lung immune injury caused by respiratory syncytial virus infection. *J. Virol.* 86 (4), 2251–2258. doi:10.1128/JVI.06209-11

Li, J. T., Melton, A. C., Su, G., Hamm, D. E., LaFemina, M., Howard, J., et al. (2015). Unexpected role for adaptive αβTh17 cells in acute respiratory distress syndrome. *J. Immunol.* 195 (1), 87–95. doi:10.4049/jimmunol.1500054

Liu, C., Xiao, K., and Xie, L. (2022). Advances in the use of exosomes for the treatment of ALI/ARDS. *Front. Immunol.* 13, 971189. doi:10.3389/fimmu.2022.971189

Liu, H., Yu, X., Yu, S., and Kou, J. (2015). Molecular mechanisms in lipopolysaccharide-induced pulmonary endothelial barrier dysfunction. *Int. Immunopharmacol.* 29 (2), 937–946. doi:10.1016/j.intimp.2015.10.010

Liu, S., Su, X., Pan, P., Zhang, L., Hu, Y., Tan, H., et al. (2016). Neutrophil extracellular traps are indirectly triggered by lipopolysaccharide and contribute to acute lung injury. *Sci. Rep.* 6, 37252. doi:10.1038/srep37252

Mamtimin, M., Pinarci, A., Han, C., Braun, A., Anders, H., Gudermann, T., et al. (2022). Extracellular DNA traps: Origin, function and implications for anti-cancer therapies. *Front. Oncol.* 12, 869706. doi:10.3389/fonc.2022.869706

Maniatis, N., Kotanidou, A., Catravas, J., and Orfanos, S. (2008). Endothelial pathomechanisms in acute lung injury. *Vasc. Pharmacol.* 49, 119–133. doi:10.1016/j.vph.2008.06.009

Mantovani, A., Sica, A., and Locati, M. (2005). Macrophage polarization comes of age. *Immunity* 23 (4), 344–346. doi:10.1016/j.immuni.2005.10.001

Mantovani, A., Sozzani, S., Locati, M., Allavena, P., and Sica, A. (2002). Macrophage polarization: Tumor-associated macrophages as a paradigm for polarized M2 mononuclear phagocytes. *Trends Immunol.* 23 (11), 549–555. doi:10.1016/s1471-4906(02)02302-5

Mastitskaya, S., Thompson, N., and Holder, D. (2021). Selective vagus nerve stimulation as a therapeutic approach for the treatment of ARDS: A rationale for neuro-immunomodulation in COVID-19 disease. *Front. Neurosci.* 15, 667036. doi:10.3389/fnins.2021.667036

Matthay, M., Zemans, R., Zimmerman, G., Arabi, Y., Beitler, J., Mercat, A., et al. (2019). Acute respiratory distress syndrome. *Nat. Rev. Dis. Prim.* 5 (1), 18. doi:10.1038/s41572-019-0069-0

McKenzie, C. G., Kim, M., Singh, T. K., Milev, Y., Freedman, J., and Semple, J. W. (2014). Peripheral blood monocyte-derived chemokine blockade prevents murine transfusion-related acute lung injury (TRALI). *Blood* 123 (22), 3496–3503. doi:10.1182/blood-2013-11-536755

Menoret, A., Buturla, J. A., Xu, M. M., Svedova, J., Kumar, S., Rathinam, V. A. K., et al. (2018). T cell-directed IL-17 production by lung granular γδ T cells is coordinated by a novel IL-2 and IL-1β circuit. *Mucosal Immunol.* 11 (5), 1398–1407. doi:10.1038/s41385-018-0037-0

Merad, M., and Martin, J. (2020). Pathological inflammation in patients with COVID-19: A key role for monocytes and macrophages. *Nat. Rev. Immunol.* 20 (6), 355–362. doi:10.1038/s41577-020-0331-4

Meyers, S., Crescente, M., Verhamme, P., and Martinod, K. (2022). *Staphylococcus aureus* and neutrophil extracellular traps: The master manipulator meets its match in immunothrombosis. *Arteriosclerosis, thrombosis, Vasc. Biol.* 42 (3), 261–276. doi:10.1161/atvbaha.121.316930

Mizushina, Y., Karasawa, T., Aizawa, K., Kimura, H., Watanabe, S., Kamata, R., et al. (2019). Inflammasome-independent and atypical processing of IL-1β contributes to acid aspiration-induced acute lung injury. *J. Immunol.* 203 (1), 236–246. doi:10.4049/jimmunol.1900168

Mokrá, D. (2020). Acute lung injury - from pathophysiology to treatment. *Physiological Res.* 69, S353–S366. doi:10.33549/physiolres.934602

Mokra, D., Mikolka, P., Kosutova, P., and Mokry, J. (2019). Corticosteroids in acute lung injury: The dilemma continues. *Int. J. Mol. Sci.* 20 (19), 4765. doi:10.3390/ijms20194765

Moradi, M., Mojtahedzadeh, M., Mandegari, A., Soltan-Sharifi, M., Najafi, A., Khajavi, M., et al. (2009). The role of glutathione-S-transferase polymorphisms on clinical outcome of ALI/ARDS patient treated with N-acetylcysteine. *Respir. Med.* 103 (3), 434–441. doi:10.1016/j.rmed.2008.09.013

Muir, R., Osbourn, M., Dubois, A. V., Doran, E., Small, D. M., Monahan, A., et al. (2016). Innate lymphoid cells are the predominant source of IL-17a during the early pathogenesis of acute respiratory distress syndrome. *Am. J. Respir. Crit. Care Med.* 193 (4), 407–416. doi:10.1164/rccm.201410-1782OC

Nakajima, T., Suarez, C. J., Lin, K. W., Jen, K. Y., Schnitzer, J. E., Makani, S. S., et al. (2010). T cell pathways involving CTLA4 contribute to a model of acute lung injury. *J. Immunol.* 184 (10), 5835–5841. doi:10.4049/jimmunol.0903238

Orecchioni, M., Ghosheh, Y., Pramod, A., and Ley, K. (2019). Macrophage polarization: Different gene signatures in M1(LPS+) vs. Classically and M2(LPS-) vs. Alternatively activated macrophages. *Front. Immunol.* 10, 1084. doi:10.3389/fimmu.2019.01084

Panacek, E. A., Marshall, J. C., Albertson, T. E., Johnson, D. H., Johnson, S., MacArthur, R. D., et al. (2004). Efficacy and safety of the monoclonal anti-tumor necrosis factor antibody F(ab')2 fragment afelimomab in patients with severe sepsis and elevated interleukin-6 levels. *Crit. Care Med.* 32 (11), 2173–2182. doi:10.1097/01.ccm.0000145229.59014.6c

Park, I., Kim, M., Choe, K., Song, E., Seo, H., Hwang, Y., et al. (2019). Neutrophils disturb pulmonary microcirculation in sepsis-induced acute lung injury. *Eur. Respir. J.* 53 (3), 1800786. doi:10.1183/13993003.00786-2018

Perl, M., Lomas-Neira, J., Venet, F., Chung, C., and Ayala, A. (2011). Pathogenesis of indirect (secondary) acute lung injury. *Expert Rev. Respir. Med.* 5 (1), 115–126. doi:10.1586/ers.10.92

Reinhart, K., Menges, T., Gardlund, B., Harm Zwaveling, J., Smithes, M., Vincent, J. L., et al. (2001). Randomized, placebo-controlled trial of the anti-tumor necrosis factor antibody fragment afelimomab in hyperinflammatory response during severe sepsis: The RAMSES Study. *Crit. Care Med.* 29 (4), 765–769. doi:10.1097/00003246-200104000-00015

Rondon, E., and Venkataraman, R. (2005). Afelimomab led to a modest mortality benefit in patients with severe sepsis and elevated interleukin-6 levels. *Crit. Care* 9 (5), E20. doi:10.1186/cc3798

Ruytinx, P., Proost, P., Van Damme, J., and Struyf, S. (2018). Chemokine-induced macrophage polarization in inflammatory conditions. *Front. Immunol.* 9, 1930. doi:10.3389/fimmu.2018.01930

Sakaguchi, R., Chikuma, S., Shichita, T., Morita, R., Sekiya, T., Ouyang, W., et al. (2016). Innate-like function of memory Th17 cells for enhancing endotoxin-induced acute lung inflammation through IL-22. *Int. Immunol.* 28 (5), 233–243. doi:10.1093/intimm/dxv070

Sarma, J., and Ward, P. (2011). Oxidants and redox signaling in acute lung injury. *Compr. Physiol.* 1 (3), 1365–1381. doi:10.1002/cphy.c100068

Scozzi, D., Liao, F., Krupnick, A., Kreisel, D., and Gelman, A. (2022). The role of neutrophil extracellular traps in acute lung injury. *Front. Immunol.* 13, 953195. doi:10.3389/fimmu.2022.953195

Sekheri, M., Rizo-Tellez, S. A., Othman, A., El Kebir, D., and Filep, J. G. (2022). Interferon-beta regulates proresolving lipids to promote the resolution of acute airway inflammation. *Proc. Natl. Acad. Sci. U. S. A.* 119 (31), e2201146119. doi:10.1073/pnas.2201146119

Singh, B., Tiwari, A. K., Singh, K., Singh, S. K., Ahmed, A., Erwin, P. J., et al. (2014). β2 agonist for the treatment of acute lung injury: A systematic review and meta-analysis. *Respir. Care* 59 (2), 288–296. doi:10.4187/respcare.02571

Song, C., Li, H., Li, Y., Dai, M., Zhang, L., Liu, S., et al. (2019). NETs promote ALI/ARDS inflammation by regulating alveolar macrophage polarization. *Exp. cell Res.* 382 (2), 111486. doi:10.1016/j.yexcr.2019.06.031

Sun, S., Yao, Y., Huang, C., Xu, H., Zhao, Y., Wang, Y., et al. (2022). CD36 regulates LPS-induced acute lung injury by promoting macrophages M1 polarization. *Cell Immunol.* 372, 104475. doi:10.1016/j.cellimm.2021.104475

Tan, W., Zhang, B., Liu, X., Zhang, C., Liu, J., and Miao, Q. (2021). Interleukin-33-Dependent accumulation of regulatory T cells mediates pulmonary epithelial regeneration during acute respiratory distress syndrome. *Front. Immunol.* 12, 653803. doi:10.3389/fimmu.2021.653803

Tan, W., Zhang, C., Liu, J., and Miao, Q. (2019). Regulatory T-cells promote pulmonary repair by modulating T helper cell immune responses in lipopolysaccharide-induced acute respiratory distress syndrome. *Immunology* 157 (2), 151–162. doi:10.1111/imm.13060

Thompson, B., Chambers, R., and Liu, K. (2017). Acute respiratory distress syndrome. *N. Engl. J. Med.* 377 (6), 562–572. doi:10.1056/NEJMra1608077

Tolle, L., and Standiford, T. (2013). Danger-associated molecular patterns (DAMPs) in acute lung injury. *J. pathology* 229 (2), 145–156. doi:10.1002/path.4124

Tzotzos, S., Fischer, B., Fischer, H., and Zeitlinger, M. (2020). Incidence of ARDS and outcomes in hospitalized patients with COVID-19: A global literature survey. *Crit. care (London, Engl.* 24 (1), 516. doi:10.1186/s13054-020-03240-7

Venet, F., Huang, X., Chung, C. S., Chen, Y., and Ayala, A. (2010). Plasmacytoid dendritic cells control lung inflammation and monocyte recruitment in indirect acute lung injury in mice. *Am. J. Pathol.* 176 (2), 764–773. doi:10.2353/ajpath.2010.090765

Verjans, E., Ohl, K., Yu, Y., Lippe, R., Schippers, A., Wiener, A., et al. (2013). Overexpression of CREMα in T cells aggravates lipopolysaccharide-induced acute lung injury. *J. Immunol.* 191 (3), 1316–1323. doi:10.4049/jimmunol.1203147

Verma, A. K., McKelvey, M., Uddin, M. B., Palani, S., Niu, M., Bauer, C., et al. (2022). IFN-gamma transforms the transcriptomic landscape and triggers myeloid cell hyperresponsiveness to cause lethal lung injury. *Front. Immunol.* 13, 1011132. doi:10.3389/fimmu.2022.1011132

Vichare, R., and Janjic, J. M. (2022). Macrophage-targeted nanomedicines for ARDS/ALI: Promise and potential. *Inflammation* 45 (6), 2124–2141. doi:10.1007/s10753-022-01692-3

Wang, C. J., Zhang, M., Wu, H., Lin, S. H., and Xu, F. (2019). IL-35 interferes with splenic T cells in a clinical and experimental model of acute respiratory distress syndrome. *Int. Immunopharmacol.* 67, 386–395. doi:10.1016/j.intimp.2018.12.024

Wang, H., Tumes, D. J., Hercus, T. R., Yip, K. H., Aloe, C., Vlahos, R., et al. (2022a). Blocking the human common beta subunit of the GM-CSF, IL-5 and IL-3 receptors markedly reduces hyperinflammation in ARDS models. *Cell Death Dis.* 13 (2), 137. doi:10.1038/s41419-022-04589-z

Wang, L., Zhao, L., Lv, J., Yin, Q., Liang, X., Chu, Y., et al. (2012). BLT1-dependent alveolar recruitment of CD4(+)CD25(+) Foxp3(+) regulatory T cells is important for resolution of acute lung injury. *Am. J. Respir. Crit. Care Med.* 186 (10), 989–998. doi:10.1164/rccm.201202-0261OC

Wang, Y., Gong, F., Qi, X., Zheng, Y., Zheng, X., Chen, Y., et al. (2022b). βMucin 1 inhibits ferroptosis and sensitizes vitamin E to alleviate sepsis-induced acute lung injury through GSK3/keap1-nrf2-GPX4 pathway. *Oxidative Med. Cell. Longev.* 2022, 2405943. doi:10.1155/2022/2405943

Wang, Z., Li, S., and Huang, B. (2022c). Alveolar macrophages: Achilles' heel of SARS-CoV-2 infection. *Signal Transduct. Target. Ther.* 7 (1), 242. doi:10.1038/s41392-022-01106-8

Wang, Z., Yu, T., Hou, Y., Zhou, W., Ding, Y., and Nie, H. (2022d). Mesenchymal stem cell therapy for ALI/ARDS: Therapeutic potential and challenges. *Curr. Pharm. Des.* 28 (27), 2234–2240. doi:10.2174/1381612828666220707104356

Ware, L., and Matthay, M. (2000). The acute respiratory distress syndrome. *N. Engl. J. Med.* 342 (18), 1334–1349. doi:10.1056/nejm200005043421806

White, K., Ding, Q., Moore, B., Peters-Golden, M., Ware, L., Matthay, M., et al. (2008). Prostaglandin E2 mediates IL-1beta-related fibroblast mitogenic effects in acute lung injury through differential utilization of prostanoid receptors. *J. Immunol. Baltim. Md* 180 (1), 637–646. doi:10.4049/jimmunol.180.1.637

Xing, Z., Han, J., Hao, X., Wang, J., Jiang, C., Hao, Y., et al. (2017). Immature monocytes contribute to cardiopulmonary bypass-induced acute lung injury by generating inflammatory descendants. *Thorax* 72 (3), 245–255. doi:10.1136/thoraxjnl-2015-208023

Xiong, S., Hong, Z., Huang, L. S., Tsukasaki, Y., Nepal, S., Di, A., et al. (2020). IL-1β suppression of VE-cadherin transcription underlies sepsis-induced inflammatory lung injury. *J. Clin. Invest* 130 (7), 3684–3698. doi:10.1172/JCI136908

Xu, X., Han, M., Li, T., Sun, W., Wang, D., Fu, B., et al. (2020). Effective treatment of severe COVID-19 patients with tocilizumab. *Proc. Natl. Acad. Sci. U. S. A.* 117 (20), 10970–10975. doi:10.1073/pnas.2005615117

Xu, X., Liu, X., Dong, X., Qiu, H., Yang, Y., and Liu, L. (2022). Secretory autophagosomes from alveolar macrophages exacerbate acute respiratory distress syndrome by releasing IL-1β. *J. Inflamm. Res.* 15, 127–140. doi:10.2147/jir.S344857

Yang, K., Arcaroli, J., and Abraham, E. (2003). Early alterations in neutrophil activation are associated with outcome in acute lung injury. *Am. J. Respir. Crit. care Med.* 167 (11), 1567–1574. doi:10.1164/rccm.200207-664OC

Zarbock, A., Singbartl, K., and Ley, K. (2006). Complete reversal of acid-induced acute lung injury by blocking of platelet-neutrophil aggregation. *J. Clin. investigation* 116 (12), 3211–3219. doi:10.1172/jci29499

Zhao, M., Fernandez, L., Doctor, A., Sharma, A., Zarbock, A., Tribble, C., et al. (2006). Alveolar macrophage activation is a key initiation signal for acute lung ischemia-reperfusion injury. *Am. J. physiology Lung Cell. Mol. physiology* 291 (5), L1018–L1026. doi:10.1152/ajplung.00086.2006

Zhu, C., Weng, Q. Y., Zhou, L. R., Cao, C., Li, F., Wu, Y. F., et al. (2020). Homeostatic and early-recruited CD101(-) eosinophils suppress endotoxin-induced acute lung injury. *Eur. Respir. J.* 56 (5), 1902354. doi:10.1183/13993003.02354-2019

Zhu, C., Xie, J., Zhao, Z., Li, P., Liu, Q., Guo, Y., et al. (2022). PD-L1 maintains neutrophil extracellular traps release by inhibiting neutrophil autophagy in endotoxin-induced lung injury. *Front. Immunol.* 13, 949217. doi:10.3389/fimmu.2022.949217

frontiers | Frontiers in Pharmacology

TYPE Original Research
PUBLISHED 23 December 2022
DOI 10.3389/fphar.2022.1051344

OPEN ACCESS

EDITED BY
Feng Li,
Shanghai Jiao Tong University, China

REVIEWED BY
Hao Tang,
Shanghai Changzheng Hospital, China
Hangming Dong,
Southern Medical University, China
Fengying Zhang,
Putuo District Central Hospital, China

*CORRESPONDENCE
Qingling Zhang,
zqling@gzhmu.edu.cn
Riken Chen,
chenriken@126.com
Yu Zhang,
dr_zhangyu@163.com

†These authors have contributed equally to this work

SPECIALTY SECTION
This article was submitted to Inflammation Pharmacology, a section of the journal Frontiers in Pharmacology

RECEIVED 22 September 2022
ACCEPTED 05 December 2022
PUBLISHED 23 December 2022

CITATION
Deng Z, Zhang X, Wen J, Yang X, Xue L, Ou C, Ma J, Zhan H, Cen X, Cai X, Zhang Y, Chen R and Zhang Q (2022), Lonicerin attenuates house dust mite-induced eosinophilic asthma through targeting Src/EGFR signaling. *Front. Pharmacol.* 13:1051344. doi: 10.3389/fphar.2022.1051344

Lonicerin attenuates house dust mite-induced eosinophilic asthma through targeting Src/EGFR signaling

Zhenan Deng[1†], Xuefei Zhang[2†], Junjie Wen[1†], Xiaojing Yang[1†], Lingna Xue[1], Changxing Ou[1], Jianjuan Ma[3], Hongrui Zhan[4], Xiaomin Cen[1], Xuliang Cai[1], Yu Zhang[5*], Riken Chen[1*] and Qingling Zhang[1*]

[1]State Key Laboratory of Respiratory Diseases, Department of Pulmonary and Critical Care Medicine, Guangzhou Institute of Respiratory Health, National Clinical Research Center for Respiratory Disease, National Center for Respiratory Medicine, The First Affiliated Hospital of Guangzhou Medical University, Guangzhou, China, [2]Department of Rehabilitation Medicine, Zhujiang Hospital, Southern Medical University, Guangzhou, China, [3]Department of Pediatric Hematology, Affiliated Hospital of Guizhou Medical University, Guiyang, China, [4]Department of Rehabilitation, The Fifth Affiliated Hospital of Sun Yat-sen University, Zhuhai, China, [5]Department of Critical Care Medicine, First Affiliated Hospital of Guangzhou Medical University, Guangzhou, China

Eosinophilic asthma is the predominant phenotype of asthma, and although these patients are sensitive to glucocorticoid therapy, they also experience many side effects. Lonicerin is a kind of bioflavonoid isolated from the Chinese herb *Lonicera japonica* Thunb, which has anti-inflammatory and immunomodulatory effects. The aim of this study was to elucidate the effects of lonicerin on eosinophilic asthma and its potential mechanisms. Here, we established a house dust mite (house dust mite)-induced eosinophilic asthma model in BALB/c mouse, and evaluated the effects of lonicerin on it. Our results showed that lonicerin significantly reduced airway hyperresponsiveness the number of inflammatory cells (especially eosinophils) and the elevation of interleukin (IL)-4, IL-5, IL-13 and eotaxin in bronchoalveolar lavage fluid (BALF) supernatants of mice. Additionally, lonicerin also eminently blunted inflammatory infiltration and mucus secretion, as well as mRNA levels of Mucin 5AC (MUC5AC) in lung tissue. Furthermore, results of network pharmacology and molecular docking revealed that Src kinase and epidermal growth factor receptor may be the potential targets responsible for the effects of lonicerin. Finally, *in vivo* experiments confirmed that lonicerin inhibited activation of the Src/EGFR pathway by decreasing their phosphorylation. Taken together, the present study demonstrated that lonicerin could suppress HDM-induced eosinophilic asthma in mice through inhibiting the activation of Src/EGFR pathway, which also provides a basis for further research as a new potentially therapeutic agent for eosinophilic asthma and its underlying mechanisms in the future.

KEYWORDS

asthma, eosinophil, lonicerin, network pharmacology, molecular docking, src, EGFR

1 Introduction

Asthma is a well-known chronic respiratory disease that affects approximately 1%–18% of the population worldwide (GINA, 2022), and it is driven by airway inflammation, which triggers biological changes such as mucus production, airway wall remodeling and bronchial hyperresponsiveness (Papi et al., 2018). It was gradually discovered that asthma is highly heterogeneous and can be classified into various phenotypes or endotypes, such as type 2-high (mainly eosinophilic asthma) and type 2-low (mainly neutrophilic or paucigranulocytic asthma) (Hammad and Lambrecht, 2021). A recent study showed that the eosinophilic phenotype accounted for up to 76.8% of severe asthma patients in China (Zhang et al., 2022). Currently, Inhaled corticosteroids are widely considered to be the most basic treatment for asthma, effectively controlling symptoms and preventing exacerbations. However, long-term corticosteroid use may have certain side effects on general health (Costello and Cushen, 2020). Therefore, the quest for some safe and effective asthma treatment drugs is always on the way for researchers.

Traditional Chinese Medicine (TCM) has distinctive effects in the treatment of chronic diseases and has been widely recognized as a core component of complementary and alternative medicine (Newman and Cragg, 2020). *Lonicera japonica* Thunb (Called Jinyinhua in Chinese) is a medicine food homology herb with a wide range of pharmacological effects, such as anti-inflammatory, antibacterial, antiviral, antioxidant, etc. (Shang et al., 2011; Ge et al., 2022). Notably, *Lonicera japonica* extract was found to alleviate OVA-induced asthma or allergic rhinitis in mice (Hong et al., 2013; Lin et al., 2019; Li et al., 2021). Lonicerin is a kind of bioflavonoid isolated from the Chinese herb *Lonicera japonica* Thunb and has been shown to possesses anti-inflammatory and immunomodulatory functions in some studies (Lee et al., 1995; Lee and Han, 2011; Lee et al., 2022). However, there are no studies reporting whether lonicerin has a therapeutic effect on asthma.

Network pharmacology is the product of rapid developments in the combination of bioinformatics, systems biology and integrative pharmacology, which can explore the relationships between compound-gene-disease networks and predict the potential mechanism of TCM for the treatment of corresponding diseases (Li and Zhang, 2013; Zhang et al., 2019). In this study, based on the fact that house dust mite (HDM) as a common allergen can more closely mimic clinical asthma (Gorska, 2018), we first investigated the effect of lonicerin on HDM-induced eosinophilic asthmatic mice. Next, network pharmacology was applied to uncover the potential targets of lonicerin for asthma treatment. Finally, molecular docking analysis and experiments were applied to validate the reliability of the key targets.

2 Materials and methods

2.1 Chemicals and reagents

Lonicerin was purchased from Push Bio-Technology Co., Ltd (Chengdu, China) and the purity (>98%) was confirmed by high-performance liquid chromatography (HPLC) (Figure 1C). HDM was purchased from Greer Laboratories (Lenoir, NC, United States). Methacholine was purchased from Sigma-Aldrich (Sigma-Aldrich China, Shanghai, China). Enzyme-linked immunosorbent assay (ELISA) kits were purchased from MultiSciences Biotech, Co., LTD. (Hangzhou, China). Hematoxylin-eosin (HE), periodic acid Schiff (PAS) and Congo red staining kits were supplied from Servicebio Technology Co., Ltd. (Wuhan, China). The antibodies including anti-p-Src, anti-p-EGFR, anti-Src, anti-EGFR and anti-β-actin were obtained from Abcam (Cambridge, MA, United States).

2.2 Establishment of a mouse model of eosinophilic asthma and drug treatment

Female BALB/c mice aged 6–8 weeks and weighing approximately 20 g were purchased from Youda (Guangzhou) Biotechnology Co. Mice were housed in an SPF facility and treated as described in Figure 2A. Mice were randomly assigned to four groups (n = 6 for each group) (GINA, 2022): Normal control group (Papi et al., 2018); HDM-induced eosinophilic asthma model group (Hammad and Lambrecht, 2021); 10 mg/kg low dose lonicerin intervention group: HDM + Lonicerin (L) (Zhang et al., 2022); 30 mg/kg high dose lonicerin intervention group: HDM + Lonicerin (H). The dosage of lonicerin was referred to the previous study (Gu and Sun, 2020; Lv et al., 2021). All of the above groups were modeled by HDM, except for the control group. On days 0, 7, and 14, mice were sensitized with 50 μg HDM by intraperitoneal (i.p) injection and then were challenged intranasally (i.n.) with 25 μg HDM from day 21 to day 23 for three consecutive days. Lonicerin was administered intragastrically (i.g.) from day 17 to day 23. Lonicerin was dissolved with 5% DMSO. During the administration, the control and model groups were given equal amounts of 5% DMSO. Animal experimental procedures were approved by the Animal Care and Use Committee of the First Affiliated Hospital of Guangzhou Medical University.

2.3 Measurement of airway hyperresponsiveness

On day 24, Buxco's modular and invasive system (DSI-Buxco, St. Paul, MN, United States) was used to detect bronchial provocation test in mice, and the changes in

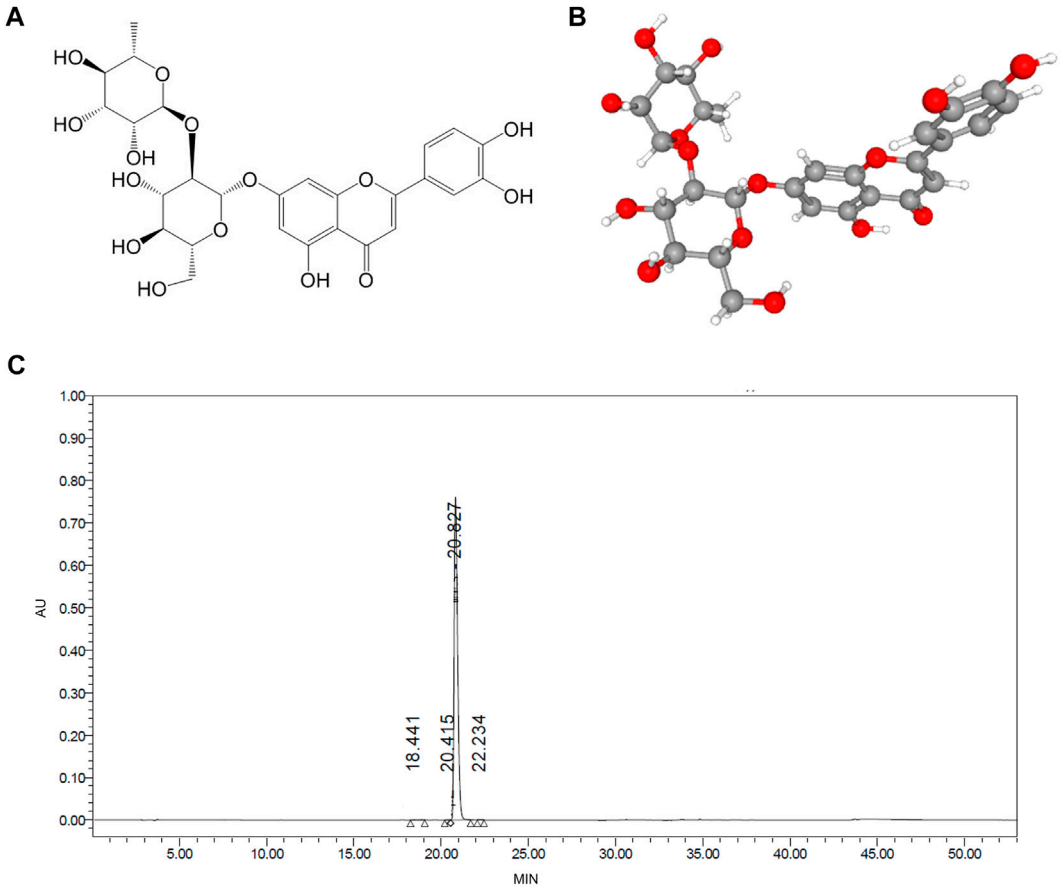

FIGURE 1
The molecular structure and purify of lonicerin. **(A,B)** 2D and 3D molecular structure were obtained from the PubChem database **(C)** The purify of lonicerin was detected by HPLC.

airway resistance (R_L) and lung dynamic compliance (Cdyn) were recorded to characterize airway hyperresponsiveness. Briefly, the anesthetized mice were tracheally intubated and exposed to methacholine (Mch) at sequentially increasing concentrations (0, 6.25, 12.5, 25 and 50 mg/ml) to evaluate lung function.

2.4 Serum collection and drug toxicity detection

Serum was extracted from a blood sample by centrifugation at 12,000 rpm for 15 min and stored at −80°C. Four indicators of liver and kidney function in serum: alanine aminotransferase (ALT), aspartate aminotransferase (AST), blood urea nitrogen (BUN) and serum creatinine (SCR), were detected by Chemray-120 Automatic Biochemistry Analyzer (Rayto Life and Analytical Sciences Co., Ltd., China).

2.5 Bronchoalveolar lavage fluid (BALF) analysis

After the trachea was dissected, a sterile tube was inserted and lavaged twice with 1 ml sterile phosphate buffered saline (PBS). The collected BALF were centrifuged at 4°C (500 g, 10 min). The total cell count in BALF was calculated and the number of different inflammatory cells was determined by cytospin stained with HE. The levels of IL-4, IL-5, IL-13 and eotaxin in BALF supernatants were determined by ELISA kits according to the manufacturer's protocol.

2.6 Lung histology

The right lung was fixed with 4% paraformaldehyde and embedded in paraffin, and then 4-μm tissue sections were prepared. Referring to previous criteria, HE and PAS staining was used to measure inflammatory infiltration and mucus secretion in the

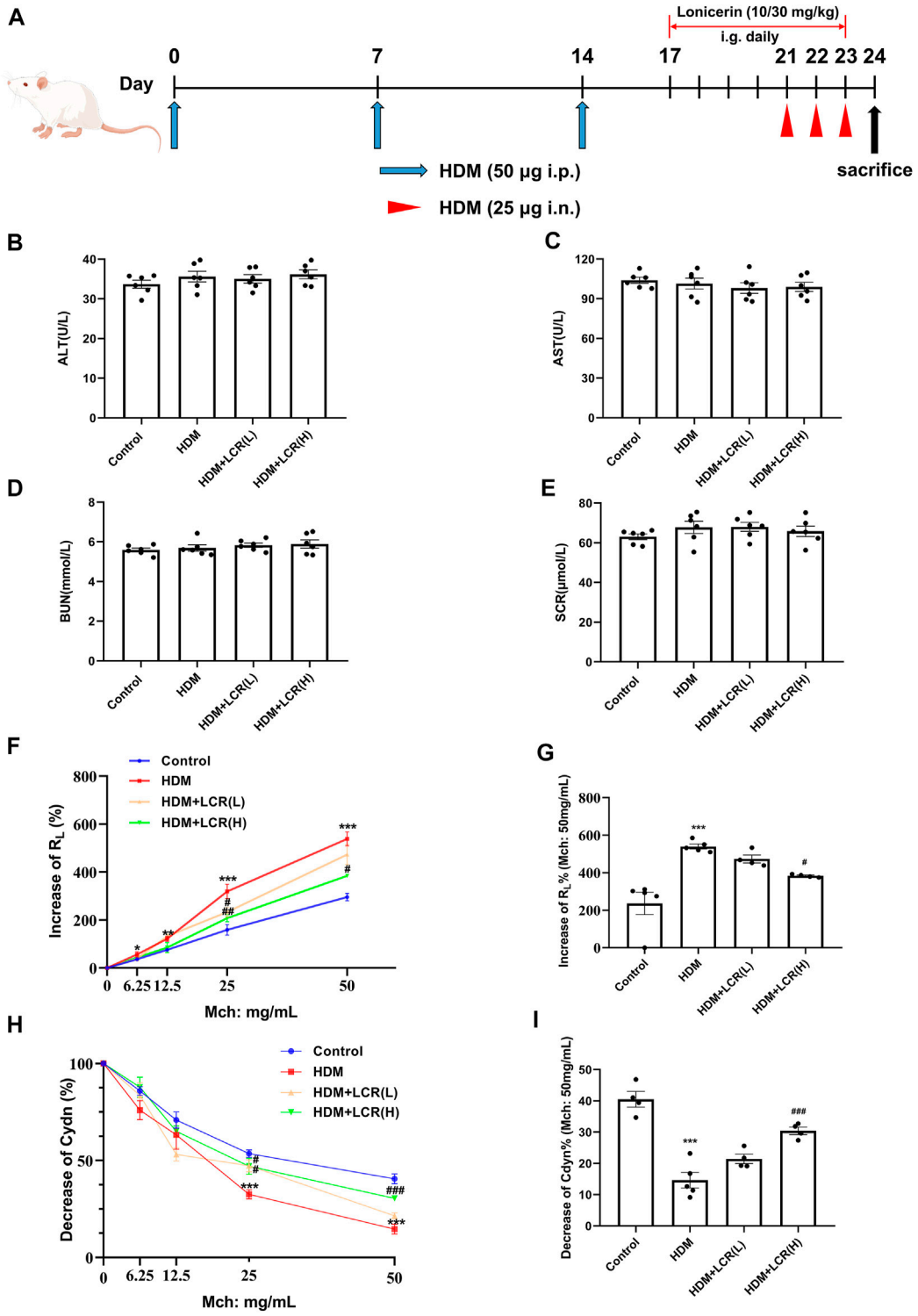

FIGURE 2
Effects of lonicerin on liver and kidney function and AHR in a mouse model of HDM-induced eosinophilic asthma. **(A)** Asthma model establishment and treatment protocol as described in *Materials and Methods*. **(B–E)** the levels of AST, ALT, BUN and SCR in serum detected by Automatic Biochemistry Analyzer. (n = 6). **(F)** Increase of R_L%. **(G)** Changes in R_L to 50 mg/ml of Mch dose. **(H)** Decrease of Cdyn%. **(I)** Changes in Cdyn to 50 mg/ml of Mch dose. (n = 4–5). Data are expressed as mean ± SEM. Differences between groups were determined with one-way ANOVA followed by the Tukey's *post hoc* test. *p < 0.05, **p < 0.01, ***p < 0.001 vs. Control group; #p < 0.05, ##p < 0.01, ###p < 0.001 vs. HDM group.

airways, and masson staining was utilized to assess collagen deposition. Since eosinophils are not easily distinguished from other inflammatory cells in mouse lungs, they were detected by Congo red staining. The statistics of these three staining results were as described in previous studies (Huang et al., 2017; Deng et al., 2020; Xue et al., 2021). Briefly, inflammation scores are as follows: 0, no inflammatory cells; 1, occasional inflammatory cells; 2, only one layer of inflammatory cells around most bronchi or blood vessels; 3, 2 layers of inflammatory cells around most bronchi and blood vessels; 4, more than 2 layers of inflammatory cells around most bronchi or blood vessels. In addition, PAS scores are based on the percentage of PAS-positive goblet cells: 0, <5%; 1, 5%–25%; 2, 25%–50%; 3, 50%–75%; 4, >75%.

2.7 Immunohistochemistry and immunofluorescence

For immunohistochemistry, the lung sections were blocked with 5% goat serum after antigen retrieval, and then immunostained with corresponding antibody (anti-p-Src or anti-p-EGFR) at 4°C overnight, followed by incubation with HRP-conjugated goat anti-rabbit IgG secondary antibody for 30 min at 37°C. At last, the signals detected using a 3, 3′-diaminobenzidine (DAB) peroxidase substrate kit (Servicebio) and then imaged by an Olympus microscope (Mantra, PerkinElmer). The results were analyzed by Image-Pro Plus software and quantified as average optical density (AOD) in the peribronchial area.

For immunofluorescence, the lung sections were blocked in 5% goat serum for 1 h and incubated overnight at 4°C with corresponding antibody (anti-p-Src or anti-p-EGFR). After washing with PBS, lung sections were incubated with Alexa 488 anti-rabbit secondary antibody or Alexa 594 anti-mouse secondary antibody at for 1 h at room temperature. Nuclei were stained with DAPI (4,6-diamidino-2-phenylindole). Photographs were taken by a fluorescence inverted/laser scanning confocal microscope (Leica Imaging Systems). The results were analyzed by Image-Pro Plus software and quantified as fluorescence intensity.

2.8 Quantitative real-time PCR

Total RNA was extracted from lung tissues using TRIzol reagent (Invitrogen). Next, RNA was reverse transcribed into cDNA by HiScript®II Q RT SuperMix for qPCR (Vazyme Biotechnology Co., LTD., Nanjing, China), and then quantification was performed with ChamQ Universal SYBR qPCR Master Mix (Vazyme) on a LightCycler 480 II system (Roche, Switzerland). All procedures refer to the manufacturer's manual. The levels of GAPDH mRNA were served as an internal reference. Data are expressed as the fold change over the control group by the $2^{-\triangle\triangle Ct}$ method. The primers (Sangon Biotech, Shanghai, China) are listed in Table 1.

TABLE 1 Primer sequences for genes used for qRT-PCR.

Gene		Sequences (5′–3′)
EGFR	Forward	GCCATCTGGGCCAAAGATACC
	Reverse	GTCTTCGCATGAATAGGCCAAT
MUC5AC	Forward	CAGGACTCTCTGAAATCGTACCA
	Reverse	GAAGGCTCGTACCACAGGG
P53	Forward	CCCCTGTCATCTTTTGTCCCT
	Reverse	AGCTGGCAGAATAGCTTATTGAG
Src	Forward	GAACCCGAGAGGGACCTTC
	Reverse	GAGGCAGTAGGCACCTTTTGT
TNF-α	Forward	CAGGCGGTGCCTATGTCTC
	Reverse	CGATCACCCCGAAGTTCAGTAG
KDR	Forward	TTTGGCAAATACAACCCTTCAGA
	Reverse	GCTCAGTATCATTTCCAACCA
GAPDH	Forward	GGCAAATTCAACGGCACAGTCAAG
	Reverse	TCGCTCCTGGAAGATGGTGATGG

2.9 Western blot

Mouse lung tissue samples were lysed with radioimmunoprecipitation assay (RIPA) buffer containing protease and phosphatase inhibitors. The BCA Protein Assay Kit (Fudebiotech) was used for protein concentration quantification. Proteins were electrophoresed on 10% or 12% SDS-polyacrylamide gels and transferred to PVDF membranes (EMD Millipore). Membranes were blocked with 5% skim milk at room temperature for 1 h and then incubated overnight at 4°C with specific primary antibodies. The membranes were washed three times with Tris-Buffered Saline Tween-20 (TBST) and then incubated with secondary antibodies conjugated with HRP (Abcam) for 1 h at room temperature. At last, the signal was scanned using the Tanon-5200 infrared scanning system (anon Science & Technology Co., Ltd., Shanghai, China) after three washes again and quantified using ImageJ software.

2.10 Network pharmacology analysis

2.10.1 Potential targets prediction

The 2D and 3D structures of lonicerin (Figures 1A, B) were obtained from the PubChem (https://pubchem.ncbi.nlm.nih.gov/) and the targets were collected through the SwissTargetPrediction (http://www.swisstargetprediction.ch/).

2.10.2 Disease-related targets screening

The disease-related genes were searched in the GeneCards (https://www.genecards.org/), OMIM (https://www.omim.org/), PharmGKB (https://www.pharmgkb.org)/, TTD (http://db.idrblab.net/ttd/) and DrugBank (https://go.drugbank.com/), with "bronchial asthma" as the key word. The disease-related targets were obtained by combining with results from the above 5 databases followed by elimination of redundant genes.

2.10.3 Protein-protein interaction (PPI) network construction

The targets were imported into the STRING database (https://string-db.org/) to obtain the PPI network, and the Cytoscape (V3.9.1) was used for network visualization. Finally, the top 10 core targets were constructed through the CytoHubba plug-in.

2.10.4 Gene ontology (GO) and kyoto encyclopedia genes and genomes (KEGG) enrichment analysis

R language software (v4.1.3) was used to analyze the role of the asthma-related targets of lonicerin in gene function and signaling pathways.

2.11 Molecular docking analysis

SWISS-MODEL was used to construct the tertiary structure of the top 5 core targets. The 3D structure and free energy surface were created, and the receptor protein was dehydrated using PyMOL software. Hydrogenation and charge calculations were performed using AutoDock software, and AutoDockVina was used for docking to find the optimal conformation.

2.12 Statistical analysis

All values are presented as mean ± SEMM. Differences between groups were determined with one-way ANOVA followed by the Tukey's *post hoc* test. Statistical comparisons were performed in Prism 8 software (GraphPad, La Jolla, California, United States). Values of $p < 0.05$ were considered statistically significant.

3 Results

3.1 Effects of lonicerin on liver and kidney function in mice

Firstly, to test whether two concentrations of lonicerin were toxic to mice, the levels of AST, ALT, BUN and SCR in serum were detected, and the results showed that there was no significant difference between four groups (Figures 2B–E), indicating that lonicerin was almost non-toxic.

3.2 Lonicerin alleviated AHR in a mouse model of HDM-induced eosinophilic asthma

Compared with the control group, the HDM group showed increases in R_L at four concentrations of Mch provocation, and decreases in Cdyn were observed at Mch = 25 and 50 mg/ml, indicating that we successfully established an asthma model with AHR. In addition, both the HDM + LCR L) group (Mch = 25 mg/ml) and the HDM + LCR H) group (Mch = 25 and 50 mg/ml) showed significant decreases in R_L as well as increases in Cdyn compared to the HDM group (Figures 2F–I).

3.3 Lonicerin reduced the inflammatory cells and type 2-associated cytokines and chemokines in BALF

As shown in Figures 3A–C, HDM caused an increase in inflammatory cells (mainly eosinophils) in BALF of mice. Compared with the HDM group, the counts of total inflammatory cells, eosinophils, macrophages and neutrophils in the two doses of lonicerin intervention group, especially in the HDM + LCR H) group, were significantly decreased. Next, ELISA was used to detect Type 2-associated cytokines, represented by IL-4, IL-5 and IL-13, and the chemokine eotaxin in the BALF supernatant. The results showed that lonicerin could effectively reduce the elevation of above inflammatory factors induced by HDM (Figures 3D–G).

3.4 Lonicerin alleviated inflammatory cell infiltration and mucus hypersecretion in the lungs of asthmatic mice

As shown in Figure 4, the results of HE and Congo red staining showed that HDM induced abundant infiltration of peritracheal and perivascular inflammatory cells (especially Congo red-stained eosinophils) and mucosal oedema, which were mitigated by intervention with both concentrations of lonicerin. Similarly, PAS staining score and mRNA expression of MUC5AC, reflecting mucus secretion, were significantly increased in the HDM group, while lonicerin treatment also significantly reduced mucus hypersecretion compared to the HDM group.

In addition, masson staining was used to observe the deposition of collagen fibers in the lungs. Interestingly, our results showed that two concentrations of lonicerin did not

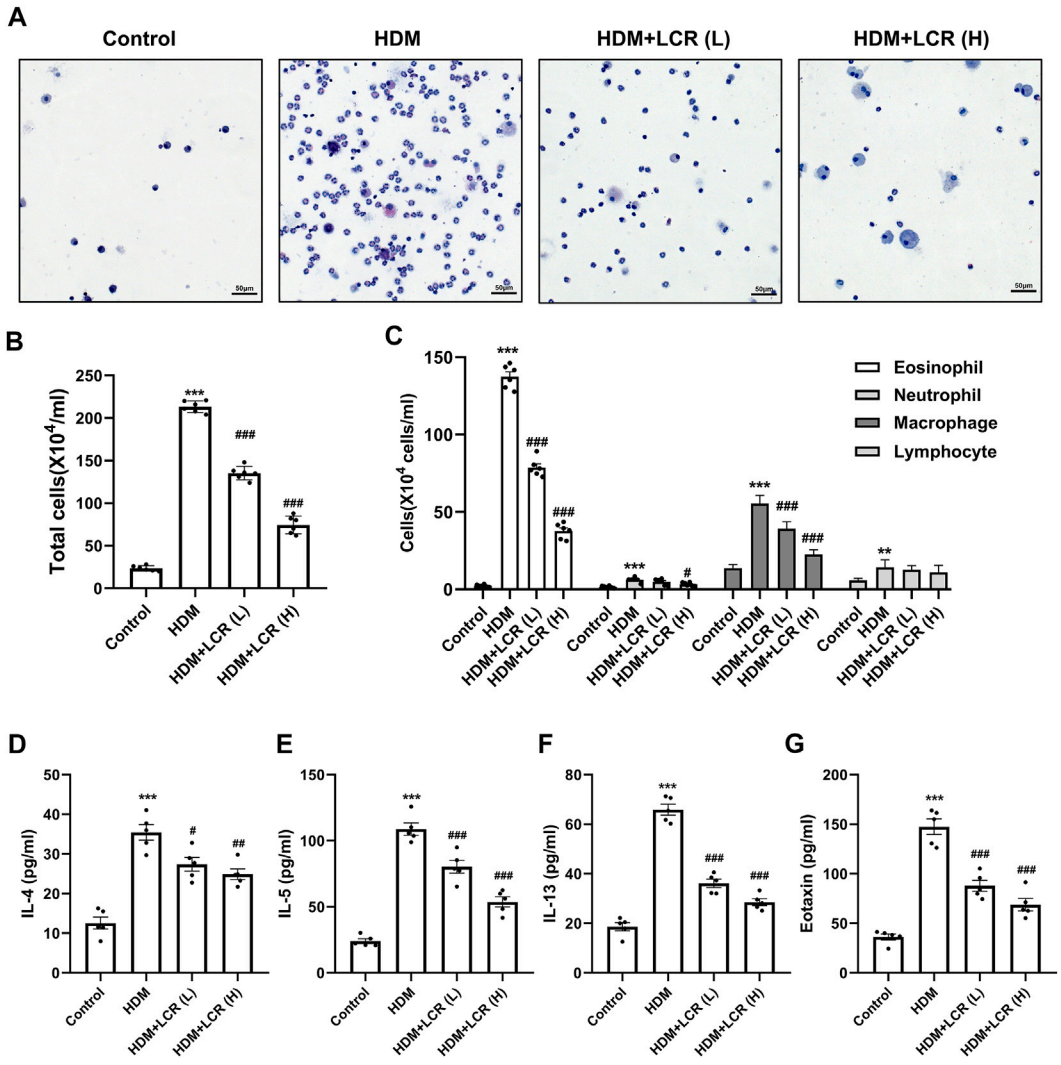

FIGURE 3
Lonicerin reduced the inflammatory cells and type 2-associated cytokines and chemokines in BALF. **(A)** HE staining was performed to count the cells in the BALF (scale bar, 50 μm). **(B,C)** Total and differentiated inflammatory cells in the BALFs of mice. (n = 6). **(D–G)** Levels of IL-4, IL-5, IL-13, and eotaxin in the BALFs supernatant measured by ELISA (n = 5). Data are expressed as mean ± SEM. Differences between groups were determined with one-way ANOVA followed by the Tukey's *post hoc* test. *p < 0.05, **p < 0.01, ***p < 0.001 vs. Control group; #p < 0.05, ##p < 0.01, ###p < 0.001 vs. HDM group.

significantly reverse HDM-induced collagen fiber production (Supplementary Figure S1).

3.5 Identification of the possible targets of lonicerin in the treatment of asthma by network pharmacology and molecular docking analysis

A total of 1786 asthma-related genes and 100 target genes of lonicerin were obtained after merging and de-duplication by searching in GeneCards, OMIM, PharmGKB, TTD and DrugBank databases (Figure 5A; Supplementary Tables S1, S2). Next, the target genes of lonicerin and asthma-related genes were intersected to obtain a total of 44 lonicerin-asthma related genes (Figure 5B; Supplementary Table S3), which may be potential targets of lonicerin for asthma treatment.

GO enrichment analysis showed that the predicted targets of lonicerin for asthma treatment were involved in biological processes such as cellular responses to chemical stress, wound healing, regulation of body fluid levels, and regulation of inflammatory responses, etc. (Figure 5C). KEGG pathway analysis demonstrated that the predicted targets were enriched

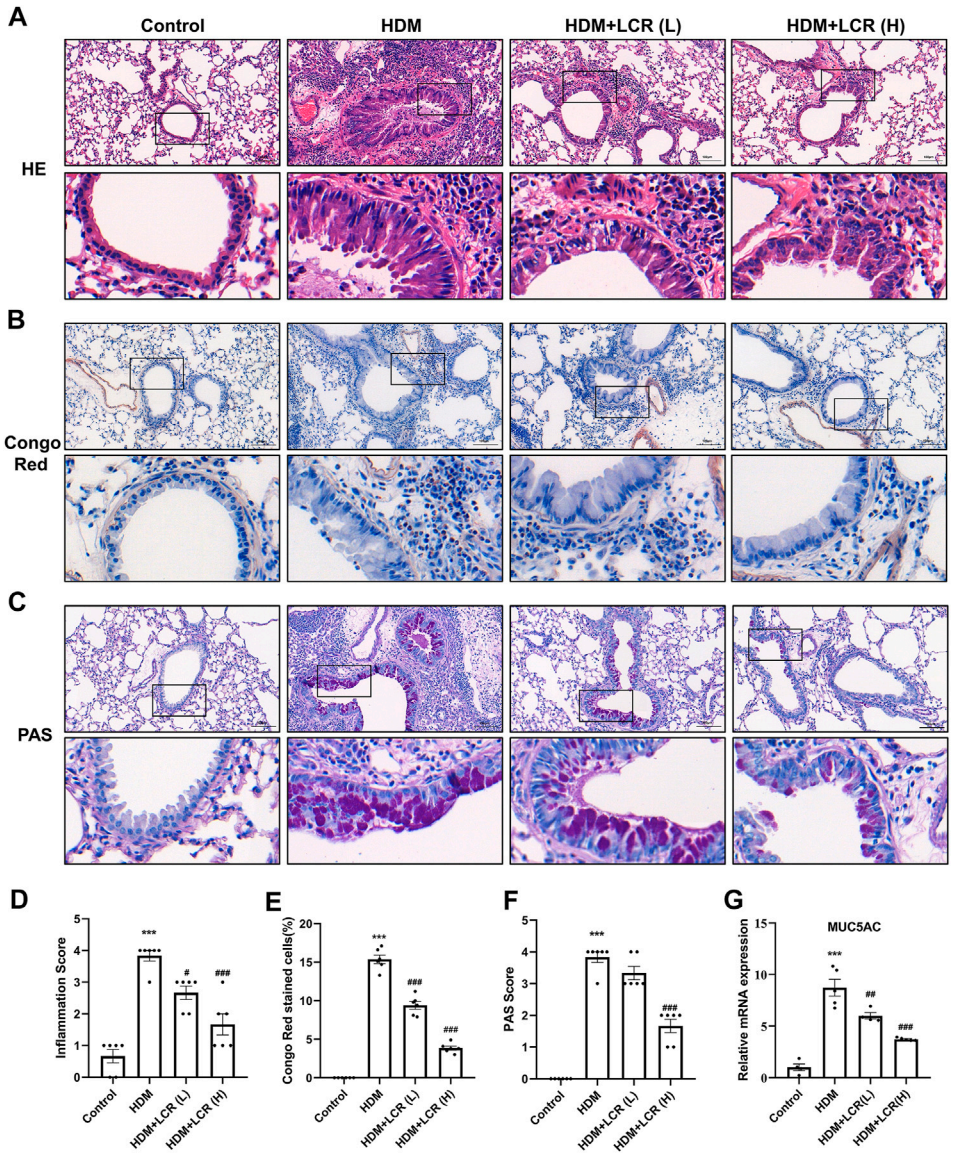

FIGURE 4
Lonicerin alleviated inflammatory cell infiltration and mucus hypersecretion in the lungs of asthmatic mice. **(A)** HE staining was performed to evaluate airway inflammatory infiltration. **(B)** Lung eosinophils detected by Congo red staining. **(C)** PAS staining was performed to show mucus production (scale bar, 100 μm). **(D–F)** The corresponding quantification histograms of **(A–C)**, respectively. (n = 6). **(G)** Detection of MUC5AC mRNA expression in lung tissues of different groups of mice by qPCR. (n = 4–5). Data are expressed as mean ± SEM. Differences between groups were determined with one-way ANOVA followed by the Tukey's *post hoc* test. *p < 0.05, **p < 0.01, ***p < 0.001 vs. Control group; #p < 0.05, ##p < 0.01, ###p < 0.001 vs. HDM group.

in AGE-RAGE pathway, Rap1 pathway, PI3K-Akt pathway, MAPK pathway, EGFR pathway, etc (Figure 5D).

To identify the hub genes and their interactions, we constructed the PPI networks from the 44 targets obtained above in the STRING network platform (Figure 5E). Then, the PPI network was downloaded and imported into Cytoscape software, and the top 10 core targets were sorted and output, including TP53, TNF, SRC, EGFR, KDR, MMP9, BCL2L1, IL2, PTGS2 and MMP2 (Figure 5F).

The results of molecular docking showed that the binding free energy of the top 5 targets obtained above were all less than -5 kcal/mol (Table 2). The visualization of molecular docking was then performed (Figure 6). These results suggested that lonicerin binds well to all of the top 5 targets.

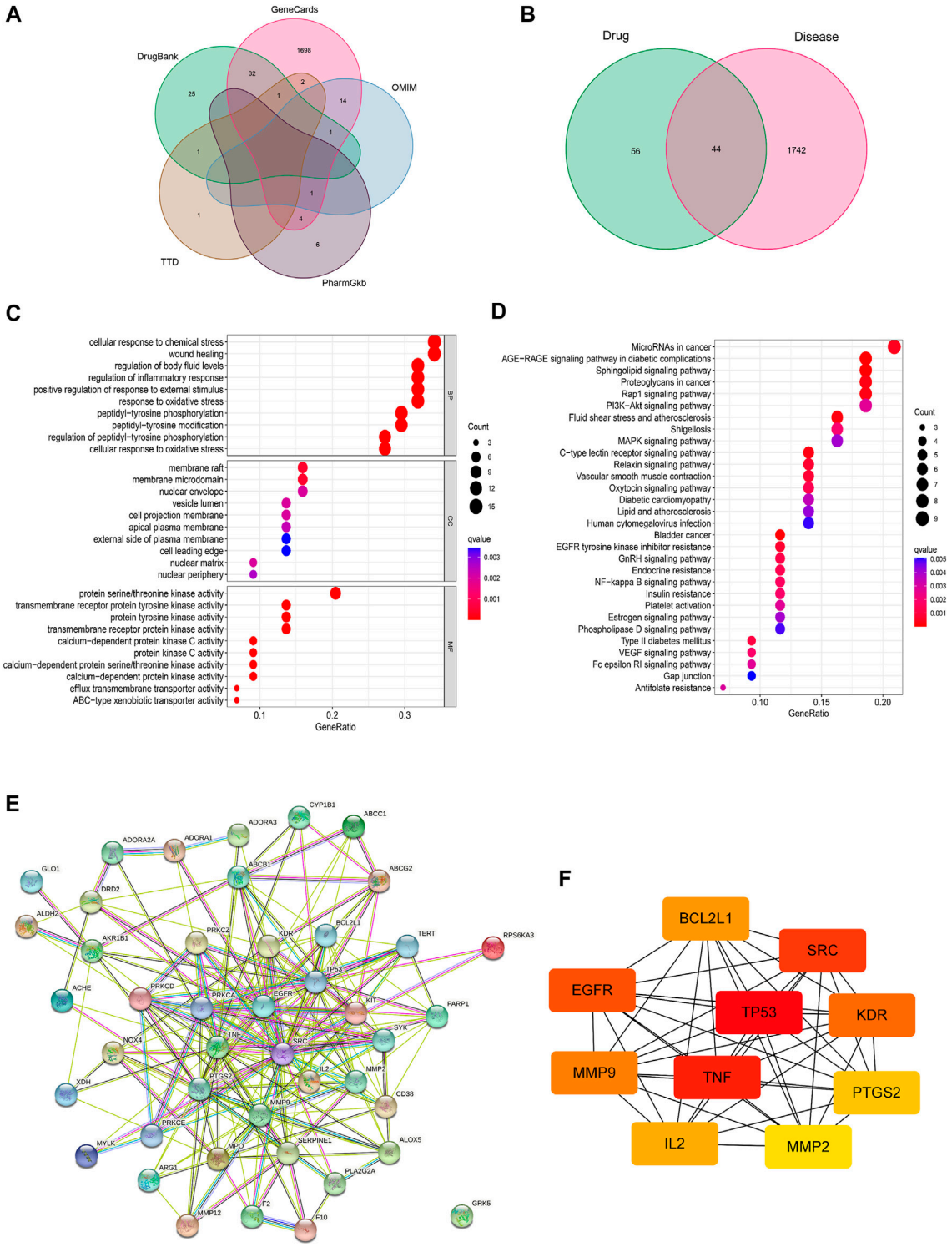

FIGURE 5
Screening of lonicerin-asthma related target genes. **(A)** Venn diagram of asthma-related genes obtained from various databases. **(B)** Venn diagram of the predicted target genes of lonicerin and asthma-related genes. **(C)** Bubble diagram of GO functional enrichment analysis. **(D)** Bubble diagram of KEGG pathway enrichment analysis. **(E)** PPI network of 44 lonicerin-asthma related target genes. **(F)** Top 10 hub gene analysis.

TABLE 2 The binding free energy of lonicerin docking with core target molecules.

Gene	Binding free energy (kcal/mol)
SRC	−10.7
EGFR	−8.3
TP53	−7.9
TNF	−7.5
KDR	−7.1

3.6 *In vivo* validation of lonicerin for the treatment of asthma by inhibiting the Src/EGFR pathway

To verify the reliability of the predicted top 5 target genes, we first measured their mRNA expression by qPCR in different groups of lung tissues, the results showed that the mRNA levels of four genes other than p53 were upregulated in the HDM group compared with the control group. Compared to the HDM group, two concentrations of lonicerin treatment reduced the mRNA levels of Src and EGFR (Figures 7A–E). In addition, Western blot results showed that HDM increased the expression of p-EGFR and p-Src, but had no significant changes in EGFR and Src. The expression of both p-EGFR and p-Src in lonicerin group decreased significantly compared with HDM group (Figures 7F–H).

Further, we detected the localization and expression of p-Src and p-EGFR in lung sections by immunohistochemistry and immunofluorescence. As shown in Figure 8, the results indicated that both p-Src and p-EGFR were predominantly expressed in the airway epithelium. Besides, HDM modeling caused significant upregulation of the AOD values and fluorescence intensity of p-Src and p-EGFR, but these trends were effectively reversed with the use of lonicerin.

Consequently, combined with the enrichment of the EGFR signaling pathway in the KEGG pathway analysis above, we speculate that the possible target suggesting lonicerin for asthma treatment may be Src/EGFR pathway.

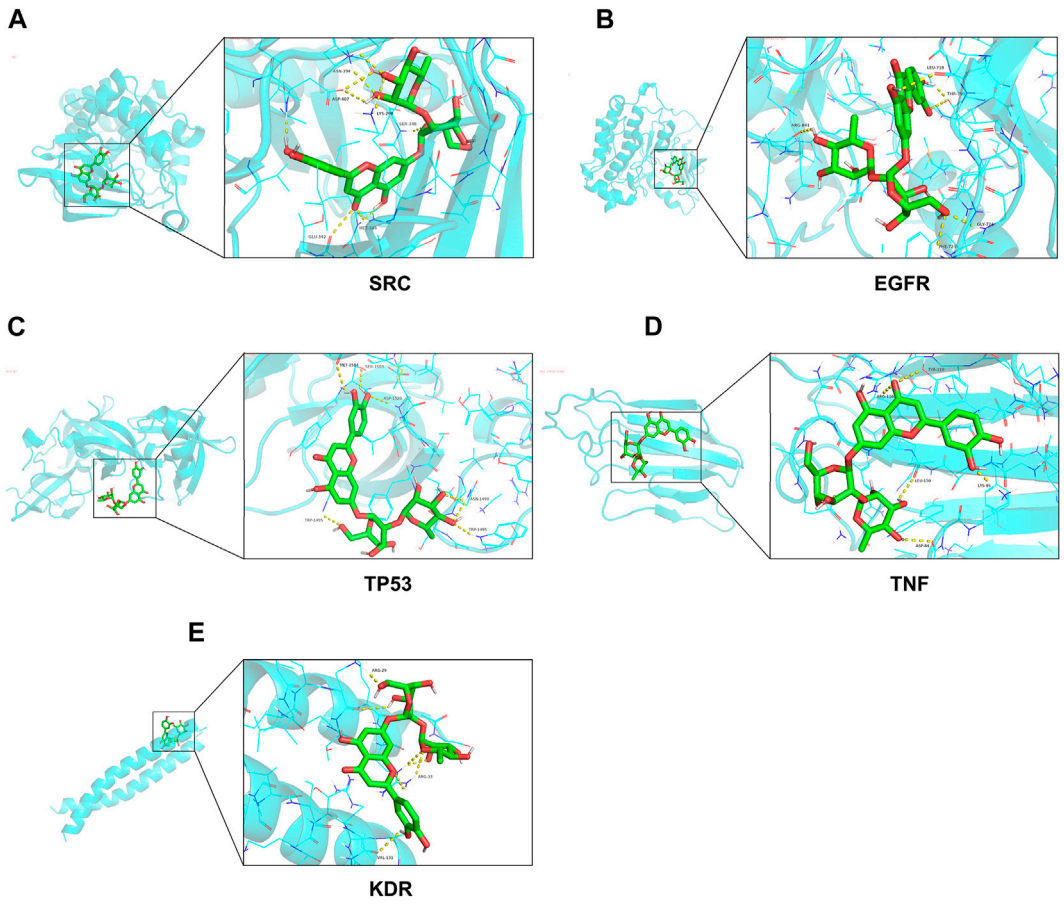

FIGURE 6
Molecular docking diagrams of lonicerin and top 5 hub genes. **(A–E) (A)** SRC, **(B)** EGFR, **(C)** TP53, **(D)** TNF and **(E)** KDR are shown interacting with a lonicerin molecule.

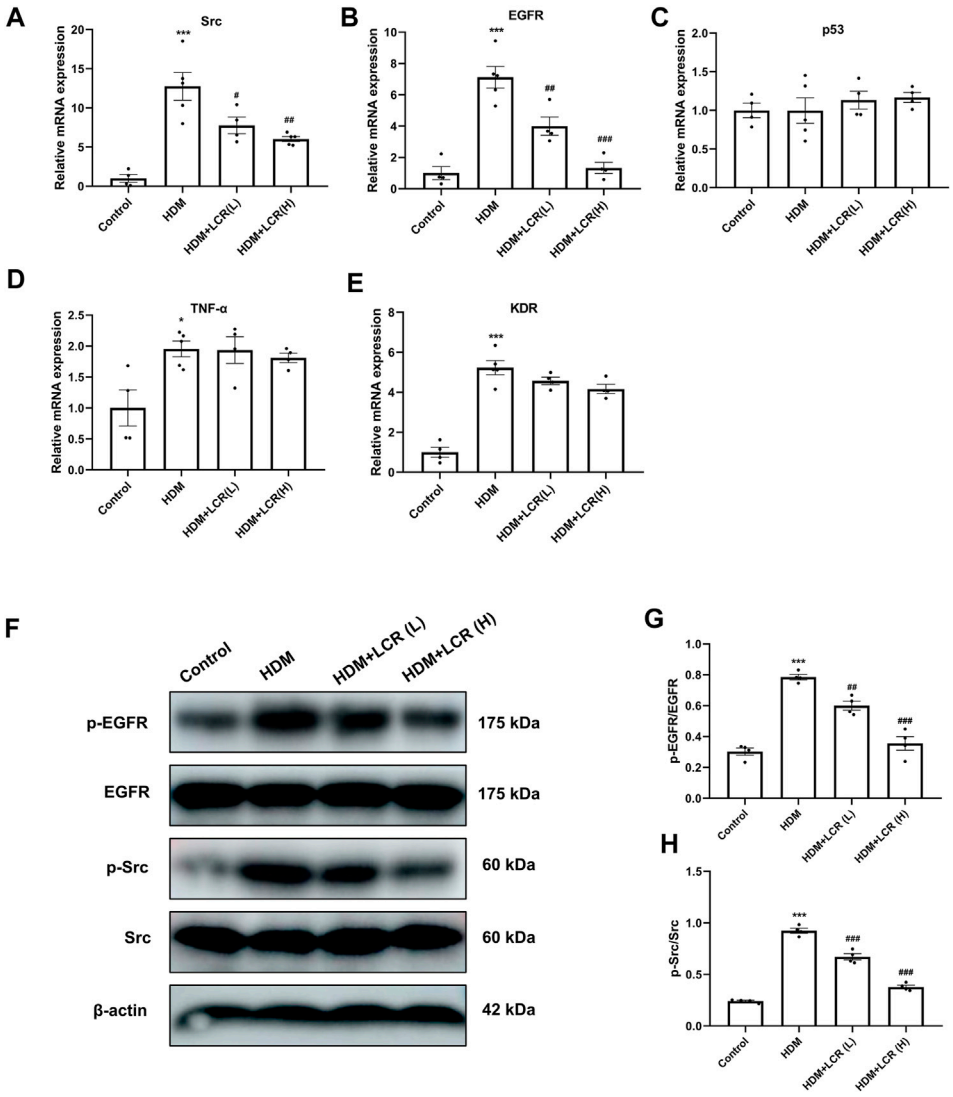

FIGURE 7
In vivo validation of lonicerin for the treatment of asthma by inhibiting the Src/EGFR pathway. **(A–E)** Detection of mRNA expression of Src, EGFR, p53, TNF-α and KDR in lung tissues of different groups of mice by qPCR. (n = 4–5). **(F)** Lung tissues from each group were extracted for Western blot to analyse the protein levels of p-EGFR, EGFR, p-Src and Src. **(G,H)** The corresponding quantification histograms of **(F)**. (n = 4). Data are expressed as mean ± SEM. Differences between groups were determined with one-way ANOVA followed by the Tukey's *post hoc* test. *p < 0.05, **p < 0.01, ***p < 0.001 vs. Control group; #p < 0.05, ##p < 0.01, ###p < 0.001 vs. HDM group.

4 Disscusion

Eosinophilic asthma is the dominant phenotype of asthma, and it was reported that the higher the blood eosinophil count, the worse the prognosis for asthma patients. Patients with eosinophilic asthma are sensitive to glucocorticoid therapy, which is effective in controlling symptoms and suppressing eosinophil levels. However, the side effects of glucocorticoids such as obesity, hypertension, and osteoporosis are of increasing concern (Price et al., 2015; Heaney et al., 2021). Therefore, it is necessary to find safe and effective treatment options for asthma.

Previous studies have found that *Lonicera japonica* extract can treat OVA-induced asthma/allergic rhinitis animal models through the activation of Th1 and Treg cells and inhibition of Th2 and Th17 cells (Hong et al., 2013; Lin et al., 2019; Li et al., 2021). In addition, *Lonicera japonica* extract was found to exert the concentration-dependent bronchial relaxation (Kim et al., 2021). However, the specific components of *Lonicera japonica* that may exert anti-asthmatic effects and the role as well as molecular mechanisms in the HDM-induced asthma model, which could better mimic clinical asthma, have not been investigated. In this study, we found that lonicerin effectively

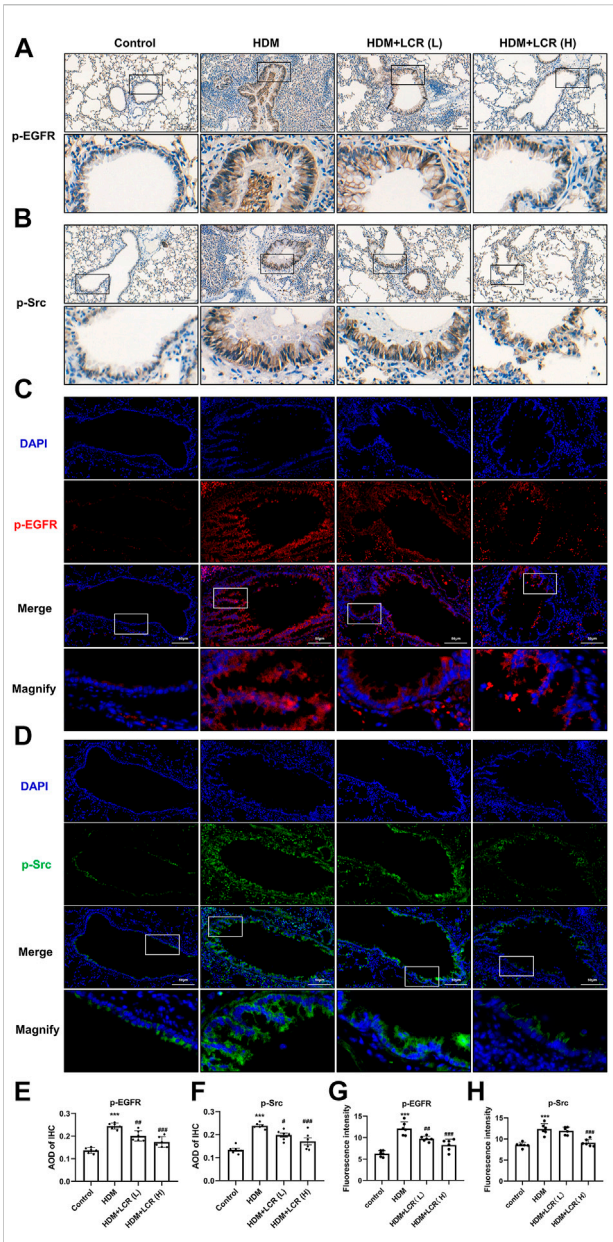

FIGURE 8
Effects of lonicerin on the immunohistochemistry and immunofluorescence staining of p-EGFR and p-Src. **(A,B)** Immunohistochemical staining of mice lungs for p-Src and p-EGFR. (scale bar, 100 μm). **(C,D)** Immunofluorescent detection of p-Src and p-EGFR in lung sections, p-EGFR was visualized in red, p-Src was visualized in green, and DAPI-stained nuclei was in blue. (scale bar, 50 μm). **(E,F)** Quantitative analysis of immunohistochemical staining for p-Src and p-EGFR by AOD. **(G,H)** Quantitative analysis of immunofluorescence staining for p-Src and p-EGFR by fluorescence intensity. (n = 6). Data are expressed as mean ± SEM. Differences between groups were determined with one-way ANOVA followed by the Tukey's *post hoc* test. *p < 0.05, **p < 0.01, ***p < 0.001 vs. Control group; #p < 0.05, ##p < 0.01, ###p < 0.001 vs. HDM group.

attenuated airway hyperresponsiveness, type 2 inflammatory factor expression, inflammatory cell (especially eosinophil) infiltration, and mucus hypersecretion in HDM-induced eosinophilic asthmatic mice. Airway remodeling has always been a major contradiction in refractory asthma, and it has been reported that biologics and some traditional Chinese medicines could alleviate airway remodeling, but there are still many controversies and lack of long-term clinical observation (Varricchi et al., 2022; Zhou et al., 2022). Our results showed that lonicerin reduced mucus hypersecretion, but cannot reverse collagen fiber deposition, which needs to be further observed with a longer course of medication in future studies.

Network pharmacology analysis was utilized to further explore the potential molecular mechanisms of lonicerin for the treatment of asthma. PPI network analysis identified 10 most strongly interacting hub gene targets: TP53, TNF, SRC, EGFR, KDR, MMP9, BCL2L1, IL2, PTGS2 and MMP2. Interestingly, KEGG pathway enrichment analysis found that the EGFR signaling cascade was one of the most enriched pathways. Therefore, we speculate that lonicerin may exert anti-asthma effects by affecting the EGFR signaling cascade. Further molecular docking analysis revealed that lonicerin had a high binding free energy with EGFR, showing a good binding ability between them. Finally, qPCR and immunohistochemistry verified that EGFR expression and phosphorylation were elevated in the lungs of HDM-induced asthmatic mice, while lonicera significantly reversed these trends.

EGFR is a glycoprotein with a transmembrane tyrosine kinase receptor that is activated by phosphorylation of its ligand binding (Chen et al., 2016). EGFR expression was found to be increased in airway epithelial cells of asthmatic patients, especially those with severe asthma (Amishima et al., 1998). *In vitro* experiments also showed that histamine enhanced EGFR phosphorylation in airway epithelial cells (Hirota et al., 2012). In addition, EGFR expression was upregulated in the lungs of both OVA and HDM-induced asthmatic animals, and treatment with EGFR inhibitors (gefitinib or erlotinib) improved eosinophilic airway inflammation, epithelial barrier function, goblet cell hyperplasia, and AHR (Hur et al., 2007; Jia et al., 2021). These studies implicated that EGFR may be a potential therapeutic target for asthma (Inoue et al., 2020).

Our results also showed that lonicerin not only binded extremely well to Src kinase, but also reversed HDM-induced Src upregulation and phosphorylation. It has been found that Src expression is elevated in asthma animal models and that activation of Src leads to HDM-induced IL-33 secretion as well as activation of type 2 inflammation (Dustin et al., 2021). Knockdown of Src or using the Src inhibitor SU6656 can alleviate airway inflammation in asthmatic animals (El-Hashim et al.,

2019; Wu et al., 2022). It is worth mentioning that Src mediates EGFR trans-activation in allergic asthmatic mice, demonstrating that Src is an upstream regulatory molecule of EGFR (Danyal et al., 2016; El-Hashim et al., 2017). Thus, our results suggest that lonicerin may exert anti-asthmatic effects by upregulating the Src/EGFR signaling pathway.

This study has some limitations. Firstly, the databases of network pharmacology are dynamically updated, which may affect the screening of drug targets, and the application of high-throughput omics technology may improve the accuracy. Secondly, it is necessary to explore the downstream regulatory mechanisms of Src/EGFR, the target of lonicerin, in future studies.

In conclusion, this study demonstrated for the first time that lonicerin, a flavonoid natural product derived from *Lonicera japonica*, can reduce airway inflammation, mucus hypersecretion and airway hyperresponsiveness in HDM-induced eosinophilic asthma model. In addition, network pharmacology, molecular docking analysis and experimental validation revealed that the potential target of lonicerin could be the Src/EGFR signaling pathway. Our findings provide a possible avenue for further investigation of the therapeutic role of lonicerin in patients with eosinophilic asthma.

Data availability statement

The datasets presented in this study can be found in online repositories. The names of the repository/repositories and accession number(s) can be found in the article/Supplementary Material.

Ethics statement

The animal study was reviewed and approved by the Animal Care and Use Committee of the First Affiliated Hospital of Guangzhou Medical University. Written informed consent was obtained from the owners for the participation of their animals in this study.

Author contributions

ZD, XZ, JW, and XY are the guarantor of the manuscript and take responsibility for the content of this manuscript. ZD, YZ, RC, and QZ contributed to the design of the study. LX, CO, JM, HZ, XiC, and XuC participated in the experiments and data analysis. ZD wrote the initial draft of the manuscript. YZ, RC, and QZ contributed significantly to the revision of the manuscript. All authors have read and approved the manuscript.

Funding

This study was supported by National Natural Science Foundation of China (82070026), Zhongnanshan Medical Foundation of Guangdong Province (ZNSA-2020013), Zhongnanshan Medical Foundation of Guangdong Province (ZNSA-2020003), and Construction Project of Guangzhou Chinese and Western Medicine Integrated Treatment for Critical and Refractory Diseases Demonstration Unit.

Conflict of interest

The authors declare that the research was conducted in the absence of any commercial or financial relationships that could be construed as a potential conflict of interest.

The reviewer HD declared a shared affiliation, with no collaboration, with one of the authors XZ to the handling editor at the time of the review.

Publisher's note

Supplementary material

The Supplementary Material for this article can be found online at: https://www.frontiersin.org/articles/10.3389/fphar.2022.1051344/full#supplementary-material

SUPPLEMENTARY FIGURE S1
Effects of lonicerin on HDM-induced deposition of collagen fibers in the lungs. Masson staining was performed to determined collagen deposition. **(B)** The corresponding quantification histograms of **(A)**, respectively. (n = 6). Data are expressed as mean ± SEM. Differences between groups were determined with one-way ANOVA followed by the Tukey's post-hoc test. ***p < 0.001 vs. Control group.

References

Amishima, M., Munakata, M., Nasuhara, Y., Sato, A., Takahashi, T., Homma, Y., et al. (1998). Expression of epidermal growth factor and epidermal growth factor receptor immunoreactivity in the asthmatic human airway. *Am. J. Respir. Crit. Care Med.* 157 (6), 1907–1912. doi:10.1164/ajrccm.157.6.9609040

Chen, J., Zeng, F., Forrester, S. J., Eguchi, S., Zhang, M. Z., and Harris, R. C. (2016). Expression and function of the epidermal growth factor receptor in physiology and disease. *Physiol. Rev.* 96 (3), 1025–1069. doi:10.1152/physrev.00030.2015

Costello, R. W., and Cushen, B. (2020). Looking back to go forward: Adherence to inhaled therapy before biologic therapy in severe asthma. *Eur. Respir. J.* 55 (5), 2000954. doi:10.1183/13993003.00954-2020

Danyal, K., de Jong, W., O'Brien, E., Bauer, R. A., Heppner, D. E., Little, A. C., et al. (2016). Acrolein and thiol-reactive electrophiles suppress allergen-induced innate airway epithelial responses by inhibition of DUOX1 and EGFR. *Am. J. Physiol. Lung Cell. Mol. Physiol.* 311 (5), L913–L923. doi:10.1152/ajplung.00276.2016

Deng, Z., Xie, H., Cheng, W., Zhang, M., Liu, J., Huo, Y., et al. (2020). Dabigatran ameliorates airway smooth muscle remodeling in asthma by modulating Yes-associated protein. *J. Cell. Mol. Med.* 24 (14), 8179–8193. doi:10.1111/jcmm.15485

Dustin, C. M., Habibovic, A., Hristova, M., Schiffers, C., Morris, C. R., Lin, M. C. J., et al. (2021). Oxidation-dependent activation of Src kinase mediates epithelial IL-33 production and signaling during acute airway allergen challenge. *J. Immunol.* 206 (12), 2989–2999. doi:10.4049/jimmunol.2000995

El-Hashim, A. Z., Khajah, M. A., Babyson, R. S., Renno, W. M., Ezeamuzie, C. I., Benter, I. F., et al. (2019). Ang-(1-7)/MAS1 receptor axis inhibits allergic airway inflammation via blockade of Src-mediated EGFR transactivation in a murine model of asthma. *PLoS One* 14 (11), e0224163. doi:10.1371/journal.pone.0224163

El-Hashim, A. Z., Khajah, M. A., Renno, W. M., Babyson, R. S., Uddin, M., Benter, I. F., et al. (2017). Src-dependent EGFR transactivation regulates lung inflammation via downstream signaling involving ERK1/2, PI3Kδ/Akt and NFκB induction in a murine asthma model. *Sci. Rep.* 7 (1), 9919. doi:10.1038/s41598-017-09349-0

Ge, L., Xie, Q., Jiang, Y., Xiao, L., Wan, H., Zhou, B., et al. (2022). Genus Lonicera: New drug discovery from traditional usage to modern chemical and pharmacological research. *Phytomedicine.* 96, 153889. doi:10.1016/j.phymed.2021.153889

GINA (2022). 2022 GINA main report - global initiative for asthma - GINA. Available at: https://ginasthma.org/gina-reports/.

Gorska, M. M. (2018). Mouse models of asthma. *Methods Mol. Biol.* 1809, 351–362. doi:10.1007/978-1-4939-8570-8_23

Gu, L. Z., and Sun, H. (2020). Lonicerin prevents inflammation and apoptosis in LPS-induced acute lung injury. *Front. Biosci.* 25 (3), 480–497. doi:10.2741/4815

Hammad, H., and Lambrecht, B. N. (2021). The basic immunology of asthma. *Cell* 184 (9), 2521–2522. doi:10.1016/j.cell.2021.04.019

Heaney, L. G., Perez de Llano, L., Al-Ahmad, M., Backer, V., Busby, J., Canonica, G. W., et al. (2021). Eosinophilic and noneosinophilic asthma: An expert consensus framework to characterize phenotypes in a global real-life severe asthma cohort. *Chest* 160 (3), 814–830. doi:10.1016/j.chest.2021.04.013

Hirota, N., Risse, P. A., Novali, M., McGovern, T., Al-Alwan, L., McCuaig, S., et al. (2012). Histamine may induce airway remodeling through release of epidermal growth factor receptor ligands from bronchial epithelial cells. *FASEB J.* 26 (4), 1704–1716. doi:10.1096/fj.11-197061

Hong, S. H., Kwon, J. T., Shin, J. Y., Kim, J. E., Minai-Tehrani, A., Yu, K. N., et al. (2013). Therapeutic effect of Broussonetia papyrifera and *Lonicera japonica* in ovalbumin-induced murine asthma model. *Nat. Prod. Commun.* 8 (11), 1934578X1300801–14. doi:10.1177/1934578x1300801127

Huang, P., Li, Y., Lv, Z., Wang, J., Zhang, Q., Yao, X., et al. (2017). Comprehensive attenuation of IL-25-induced airway hyperresponsiveness, inflammation and remodelling by the PI3K inhibitor LY294002. *Respirology* 22 (1), 78–85. doi:10.1111/resp.12880

Hur, G. Y., Lee, S. Y., Lee, S. H., Kim, S. J., Lee, K. J., Jung, J. Y., et al. (2007). Potential use of an anticancer drug gefinitib, an EGFR inhibitor, on allergic airway inflammation. *Exp. Mol. Med.* 39 (3), 367–375. doi:10.1038/emm.2007.41

Inoue, H., Akimoto, K., Homma, T., Tanaka, A., and Sagara, H. (2020). Airway epithelial dysfunction in asthma: Relevant to epidermal growth factor receptors and airway epithelial cells. *J. Clin. Med.* 9 (11), E3698. doi:10.3390/jcm9113698

Jia, Z., Bao, K., Wei, P., Yu, X., Zhang, Y., Wang, X., et al. (2021). EGFR activation-induced decreases in claudin1 promote MUC5AC expression and exacerbate asthma in mice. *Mucosal Immunol.* 14 (1), 125–134. doi:10.1038/s41385-020-0272-z

Kim, H. Y., Yoon, J. J., Kim, D. S., Kang, D. G., and Lee, H. S. (2021). YG-1 extract improves acute pulmonary inflammation by inducing bronchodilation and inhibiting inflammatory cytokines. *Nutrients* 13 (10), 3414. doi:10.3390/nu13103414

Lee, J. H., and Han, Y. (2011). Antiarthritic effect of lonicerin on Candida albicans arthritis in mice. *Arch. Pharm. Res.* 34 (5), 853–859. doi:10.1007/s12272-011-0520-6

Lee, S. J., Shin, E. J., Son, K. H., Chang, H. W., Kang, S. S., and Kim, H. P. (2022). Anti-inflammatory activity of the major constituents ofLonicera japonica. *Archives Pharmacal Res.* 18, 133–135. doi:10.1007/BF02979147

Lee, S. J., Choi, J. H., Son, K. H., Chang, H. W., Kang, S. S., and Kim, H. P. (1995). Suppression of mouse lymphocyte proliferation *in vitro* by naturally-occurring biflavonoids. *Life Sci.* 57 (6), 551–558. doi:10.1016/0024-3205(95)00305-p

Li, P., Tsang, M. S. M., Kan, L. L. Y., Hou, T., Hon, S. S. M., Chan, B. C. L., et al. (2021). The immuno-modulatory activities of pentaherbs formula on ovalbumin-induced allergic rhinitis mice via the activation of Th1 and Treg cells and inhibition of Th2 and Th17 cells. *Molecules* 27 (1), 239. doi:10.3390/molecules27010239

Li, S., and Zhang, B. (2013). Traditional Chinese medicine network pharmacology: Theory, methodology and application. *Chin. J. Nat. Med.* 11 (2), 110–120. doi:10.1016/S1875-5364(13)60037-0

Lin, B., Cai, B., and Wang, H. (2019). Honeysuckle extract relieves ovalbumin-induced allergic rhinitis by inhibiting AR-induced inflammation and autoimmunity. *Biosci. Rep.* 39 (7), BSR20190673. doi:10.1042/BSR20190673

Lv, Q., Xing, Y., Liu, J., Dong, D., Liu, Y., Qiao, H., et al. (2021). Lonicerin targets EZH2 to alleviate ulcerative colitis by autophagy-mediated NLRP3 inflammasome inactivation. *Acta Pharm. Sin. B* 11 (9), 2880–2899. doi:10.1016/j.apsb.2021.03.011

Newman, D. J., and Cragg, G. M. (2020). Natural products as sources of new drugs over the nearly four decades from 01/1981 to 09/2019. *J. Nat. Prod.* 83 (3), 770–803. doi:10.1021/acs.jnatprod.9b01285

Papi, A., Brightling, C., Pedersen, S. E., and Reddel, H. K. (2018). Asthma. *Lancet* 391 (10122), 783–800. doi:10.1016/S0140-6736(17)33311-1

Price, D. B., Rigazio, A., Campbell, J. D., Bleecker, E. R., Corrigan, C. J., Thomas, M., et al. (2015). Blood eosinophil count and prospective annual asthma disease burden: A UK cohort study. *Lancet. Respir. Med.* 3 (11), 849–858. doi:10.1016/S2213-2600(15)00367-7

Shang, X., Pan, H., Li, M., Miao, X., and Ding, H. (2011). *Lonicera japonica* Thunb.: Ethnopharmacology, phytochemistry and pharmacology of an important traditional Chinese medicine. *J. Ethnopharmacol.* 138 (1), 1–21. doi:10.1016/j.jep.2011.08.016

Varricchi, G., Ferri, S., Pepys, J., Poto, R., Spadaro, G., Nappi, E., et al. (2022). Biologics and airway remodeling in severe asthma. *Allergy* 77, 3538–3552. doi:10.1111/all.15473

Wu, M., Yang, J., Liu, T., Xuan, P., Bu, B., Xu, X., et al. (2022). Effect of Src tyrosine kinase on a rat model of asthma. *Exp. Ther. Med.* 23 (2), 172. doi:10.3892/etm.2021.11095

Xue, L., Li, C., Ge, G., Zhang, S., Tian, L., Wang, Y., et al. (2021). Jia-wei-yu-ping-feng-san attenuates group 2 innate lymphoid cell-mediated airway inflammation in allergic asthma. *Front. Pharmacol.* 12, 703724. doi:10.3389/fphar.2021.703724

Zhang, Q., Fu, X., Wang, C., Shen, H., Zhu, L., Shi, G., et al. (2022). Severe eosinophilic asthma in Chinese C-BIOPRED asthma cohort. *Clin. Transl. Med.* 12 (2), e710. doi:10.1002/ctm2.710

Zhang, R., Zhu, X., Bai, H., and Ning, K. (2019). Network pharmacology databases for traditional Chinese medicine: Review and assessment. *Front. Pharmacol.* 10, 123. doi:10.3389/fphar.2019.00123

Zhou, B. W., Liu, H. M., and Jia, X. H. (2022). The role and mechanisms of traditional Chinese medicine for airway inflammation and remodeling in asthma: Overview and progress. *Front. Pharmacol.* 13, 917256. doi:10.3389/fphar.2022.917256

frontiers | Frontiers in Pharmacology

TYPE Original Research
PUBLISHED 10 January 2023
DOI 10.3389/fphar.2022.1076116

OPEN ACCESS

EDITED BY
Yan Huang,
Anhui Medical University, China

REVIEWED BY
James S. K. Sham,
Johns Hopkins Medicine, United States
Yoshikazu Nakaoka,
National Cerebral and Cardiovascular Center, Japan

*CORRESPONDENCE
Koichi Inoue,
ino-k@umin.ac.jp

SPECIALTY SECTION
This article was submitted to Inflammation Pharmacology, a section of the journal Frontiers in Pharmacology

RECEIVED 21 October 2022
ACCEPTED 23 December 2022
PUBLISHED 10 January 2023

CITATION
Yamanaka T, Ueki T, Mase M and Inoue K (2023), Arbitrary Ca^{2+} regulation for endothelial nitric oxide, NFAT and NF-κB activities by an optogenetic approach. *Front. Pharmacol.* 13:1076116. doi: 10.3389/fphar.2022.1076116

Arbitrary Ca^{2+} regulation for endothelial nitric oxide, NFAT and NF-κB activities by an optogenetic approach

Tomoyasu Yamanaka[1], Takatoshi Ueki[2], Mitsuhito Mase[1] and Koichi Inoue[2]*

[1]Department of Neurosurgery, Nagoya City University Graduate School of Medical Sciences, Nagoya, Japan, [2]Department of Integrative Anatomy, Nagoya City University Graduate School of Medical Sciences, Nagoya, Japan

Modern western dietary habits and low physical activity cause metabolic abnormalities and abnormally elevated levels of metabolites such as low-density lipoprotein, which can lead to immune cell activation, and inflammatory reactions, and atherosclerosis. Appropriate stimulation of vascular endothelial cells can confer protective responses against inflammatory reactions and atherosclerotic conditions. This study aims to determine whether a designed optogenetic approach is capable of affecting functional changes in vascular endothelial cells and to evaluate its potential for therapeutic regulation of vascular inflammatory responses *in vitro*. We employed a genetically engineered, blue light-activated Ca^{2+} channel switch molecule that utilizes an endogenous store-operated calcium entry system and induces intracellular Ca^{2+} influx through blue light irradiation and observed an increase in intracellular Ca^{2+} in vascular endothelial cells. Ca^{2+}-dependent activation of the nuclear factor of activated T cells and nitric oxide production were also detected. Microarray analysis of Ca^{2+}-induced changes in vascular endothelial cells explored several genes involved in cellular contractility and inflammatory responses. Indeed, there was an increase in the gene expression of molecules related to anti-inflammatory and vasorelaxant effects. Thus, a combination of human blue light-activated Ca^{2+} channel switch 2 (hBACCS2) and blue light possibly attenuates TNFα-induced inflammatory NF-κB activity. We propose that extrinsic cellular Ca^{2+} regulation could be a novel approach against vascular inflammation.

KEYWORDS

optogenetics, vascular endothelial cells, calcium, nitric oxide, microarray, inflammation

1 Introduction

Vascular endothelial cells form the vascular endothelium, a monolayer of cells lining the lumen of blood vessels, and contribute to blood circulation throughout the body by preventing blockages through anticoagulation. In addition to supporting blood circulation, vascular endothelial cells also release many bioactive molecules that regulate vasoconstriction and dilation (Bauer and Sotnikova, 2010; Zhao et al., 2015; Kruger-Genge et al., 2019). One of these molecules is nitric oxide (NO), a small gaseous molecule that is produced in vascular endothelial cells and then diffuses to and permeates the cell membranes of surrounding cells. Activation of soluble guanylate cyclase by NO in vascular smooth muscle leads to an increase in cyclic guanosine 3′,5′-cyclic monophosphate (cGMP). cGMP then promotes actin-myosin chain relaxation by decreasing Ca^{2+} influx in vascular

smooth muscle cells, thus maintaining vascular function (Bauer and Sotnikova, 2010; Zhao et al., 2015; Kruger-Genge et al., 2019).

NO is usually synthesized in vascular endothelial cells by endothelial NO synthase (eNOS). eNOS is constitutively present in vascular endothelial cells, and its activity is regulated by the intracellular Ca^{2+}-calmodulin system (Forstermann et al., 1991; Pollock et al., 1991). In this system, specific stimulation of vascular endothelial cells leads to Ca^{2+} influx, resulting in the formation of the Ca^{2+}-calmodulin complex that then binds to eNOS, followed by migration of the complex into the cellular caveola, which promotes NO production. Additionally, phosphorylation of eNOS also modulates its activity. Alternatively, some stimuli result in increased eNOS protein expression levels, which facilitates increased NO production (Inoue and Xiong, 2009; Bauer and Sotnikova, 2010; Rafikov et al., 2011). The mechanisms involved in NO production hint at the clinical importance of NO. When vascular endothelial dysfunction occurs in the early stages of cardiac ischemia, NO production can become insufficient. Reflecting this, during angina pectoris or myocardial infarction, treatment with acute sublingual administration of nitroglycerin increases blood NO levels, possibly resulting in coronary vasodilation and enhanced cardiac blood supply. In addition, the test for coronary artery spasm involves cardiac catheterization-administered acetylcholine, which induces NO production, predominantly in the functional vascular endothelial cells over vascular smooth muscle cells, resulting in vascular dilation. On the other hand, acetylcholine-induced production of NO is not sufficient in dysfunctional endothelial cells; therefore, acetylcholine-induced contractions occur predominantly in vascular smooth muscle cells, leading to vasospasm (Ong et al., 2012; Ong et al., 2014). Thus, decreased NO production due to endothelial dysfunction minimizes vasodilatory capacity, resulting in arterial stiffness and a tendency for thrombosis development, which may further contribute to development of diseases, such as cerebral infarction, myocardial infarction, and peripheral arterial occlusion (Daiber et al., 2019).

In addition to NO production, an increase in intracellular Ca^{2+} in vascular endothelial cells facilitates prostaglandin production, which acts on vascular smooth muscle cells to induce vasodilation and binds to its receptors on platelets to activate adenylate cyclase, inhibiting platelet activation and promoting anti-thrombotic effects (Weksler et al., 1978; Braune et al., 2020). Elevation of Ca^{2+} in vascular endothelial cells also plays important roles in the immune response, including contributing to the regulation of E-selectin and VCAM-1 gene expression, or regulating immune cell adhesion and tissue infiltration, which is implicated in the development of atherosclerosis (Kielbassa-Schnepp et al., 2001; Erdogan et al., 2007; Moccia et al., 2014).

To date, we have focused our studies of vascular function on molecules involved in Ca^{2+} dynamics and inflammation (Inoue et al., 2004; Inoue and Xiong, 2009; Sun et al., 2013; Zeng et al., 2015; Inoue et al., 2020) and have found that suppression of TRPM7, one of TRP family members, augments eNOS protein levels, resulting in increased NO production (Inoue and Xiong, 2009). Moreover, under high glucose conditions, TRPM7 is upregulated in vascular endothelial cells, resulting in decreased eNOS expression and NO production, and inhibition of TRPM7 restores these levels (Sun et al., 2013). Regardless of these adverse effects, TRPM7 plays a role in cardiovascular Mg^{2+} homeostasis, and inhibition of immune responses (Rios et al., 2020), which demonstrates the difficulty in targeting suppression of a single endogenous molecule as a therapeutic approach. As inhibition of TRPM7 enhances NO production, we have focused on other target molecules that regulate NO production and expression of related genes. If their activities can be controlled, extrinsic regulation of production of NO and other molecules may be possible, ultimately leading to the regulation of vascular tone and function. However, isolation of endogenous molecule-dependent targets could require extensive research on identification and validation of the target molecule, followed by discovery of specific interacting molecules through drug library screening, with further optimization of the molecular structure using *in silico* techniques (Hughes et al., 2011; Esch et al., 2015; Schneider, 2018). Indeed, because of the difficulties involved previously in developing therapeutic agents through this process, it may be useful to introduce exogenous molecules into vascular endothelial cells to actively modulate their functional activity, for example, by promoting Ca^{2+} influx.

Recently, a lot of research has been conducted in exploiting molecules that are not endogenously present in higher organisms, including human beings. Channelrhodopsin, an algal protein that acts as a cation channel, is one such molecule and is activated by specific wavelengths of light. Photoactivation of channelrhodopsin results in passive diffusion of ions according to their equilibrium potentials, leading to changes in membrane potential; in neuronal cells, this generates action potentials, often resulting in neuronal discharges. Targeting genes that confer channels such as channelrhodopsin has enabled external control of neuronal activity by light manipulation; this technique is known as optogenetics (Deisseroth, 2011; Deisseroth, 2015). Different types of optogenetic tools, including anion channels, have already been discovered and developed for biomedical usage, with one of the most common channels being channelrhodopsin-2 (ChR2). ChR2 is a non-specific cation channel, conducting multiple cations such as Na^{+} and Ca^{2+} (Lorenz-Fonfria and Heberle, 2014). Previously, whilst analyzing channel activity modified by redox status (Wu et al., 2017), we considered that Ca^{2+} influx controlled by means of an optogenetic strategy and consequent activation of the downstream pathways could stimulate NO production and other activities in vascular endothelial cells, facilitating beneficial vascular processes. Photoactivation of vascular endothelial cells using light sensors could dilate vessels and release hormones, which control blood flow, at certain regions of vasculature in the body. In this study, we attempt to employ a relatively new optogenetic tool to facilitate an increase in intracellular Ca^{2+} by blue light irradiation and provoke NO production and gene expression in vascular endothelial cells, to explore the possibility of regulating vascular inflammatory responses.

2 Materials and methods

2.1 Reagents and antibodies

The following reagents and antibodies were used: Fluo-8/AM (ABD21081, AAT Bioquest, Sunnyvale, CA, United States); DAF-FM/DA (SK1004-01, Goryo Kagaku, Sapporo, Japan); NucreoSpin RNA Plus (U0984B, Takara, Kusatsu, Japan); Lipofectamine 3000 (L3000001, Thermo Fisher, Waltham, MA, United States); O,O′-Bis(2-aminoethyl) ethyleneglycol-N,N,N′,N′-tetraacetic acid (EGTA; 348-01311, Dojindo, Kumamoto, Japan); N^{G}-nitro-L-arginine methyl ester (L-NAME; 80210, Fuji Film, Tokyo, Japan); BAPTA/AM (T2845, TCI, Tokyo, Japan); protease inhibitor cocktail (S8820, Sigma-Aldrich, St. Louis, MO, United States); Dual-Luciferase Reporter System (E1910, Promega, Madison, WI, United States); mouse monoclonal antibodies against Flag (F1804, Sigma-Aldrich) and GAPDH (60004-1-Ig, Proteintech, Rosemont,

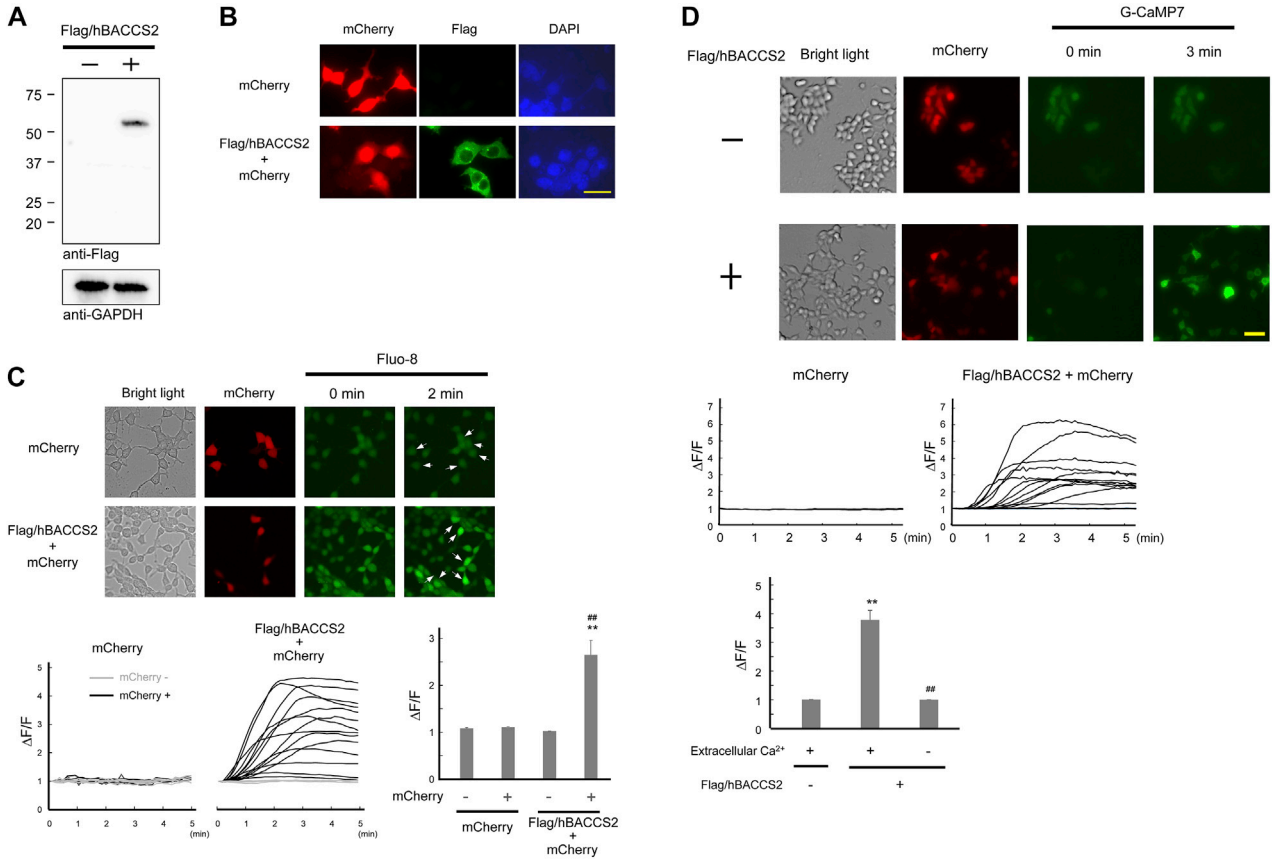

FIGURE 1
Flag/hBACCS2 leads to blue light-mediated Ca^{2+} increase in HEK293 cells. **(A,B)** Either Flag/hBACCS2-mCherry- or mCherry-expressing plasmid was transfected into HEK293 cells and incubated for 2 days. Cells were collected, followed by immunoblotting analysis **(A)** or fixed and Flag/hBACCS2 protein was visualized using an antibody to Flag **(B)**. The scale bar represents 20 μm. **(C)** Cells transfected with either Flag/hBACCS2-mCherry or mCherry were stained with Fluo-8/AM. Blue light was then applied (.2 Hz) and Fluo-8 signals were monitored. Arrows indicate mCherry-positive cells. Each trace represents fluorescence intensity from randomly selected cells. Bar graph shows the normalized fluorescence intensity of maximal values within 5 min in the different conditions as indicated. n = 11–24 from 3 independent experiments. $^{**}p < .01$ vs. Flag/hBACCS2-negative cells, $^{\#\#}p < .01$ vs. mCherry-transfected cells, Student's t-test. **(D)** Cells were transfected with G-CaMP7 and either Flag/hBACCS2-mCherry or mCherry, and photoactivated with blue light (.2 Hz). Each trace represents fluorescence intensity from randomly selected cells. Bar graph shows the normalized fluorescence intensity of maximal values within 5 min in the different conditions as indicated. The scale bar represents 50 μm n = 12–54 from 3 to 4 independent experiments. $^{**}p < .01$ vs. Flag/hBACCS2-negative cells, $^{\#\#}p < .01$ vs. extracellular Ca^{2+}-including condition, Student's t-test.

IL, United States), rabbit monoclonal antibody against NF-κB p65 (#8242P, CST, Danvers, MA, United States), TNFα (HZ-1014, Proteintech).

2.2 Cell culture

HEK293 cells, a murine vascular endothelial cell line F2 (RCB 1994, Riken BRC, Tsukuba, Japan) (Toda et al., 1990) and a murine brain derived endothelial cell line b.End3 (CRL-2299, ATCC, Manassas, VA, United States) (Montesano et al., 1990) were grown in Dulbecco's modified eagle medium with 10% fetal bovine serum and antibiotics.

2.3 Plasmid transfection and photostimulation

A plasmid expressing human blue light-activated Ca^{2+} channel switch 2 (hBACCS2) with bicistronic expression of mCherry was provided by Dr. Takao Nakata, Tokyo Medical and Dental University, Tokyo, Japan; (Ishii et al., 2015) through Addgene (Watertown, MA, United States).

A fragment of mCherry or hBAACCS2-IRES-mCherry was inserted into a pCAG-GS vector provided by Dr. Junichi Miyazaki, Osaka University, Osaka, Japan; (Niwa et al., 1991) with Flag-tag on hBACCS2 (pCAG-hBACCS2-mCherry). G-CaMP7 [provided by Dr. Junichi Nakai, Saitama University, Saitama, Japan through Riken BRC; (Ohkura et al., 2012)] was subcloned into the pCAG-GS vector.

For transfection, Lipofectamine 3000 (Thermo Fisher) was used according to the manufacturer's instructions. Transfection efficiencies, as determined by mCherry-positive cells, were ~50% in HEK293 and F2 cells, and ~5% in b.End3 cells.

For photostimulation, the fluorescence microscopic system described below was used for fluorescence (~.4 mW/mm^2, for Figures 1, 2, 4, see below) and blue light LED (~.4 mW/mm^2, for Figures 3, 5, 6; LIU470A, ThorLabs, Newton, NJ, United States) were used.

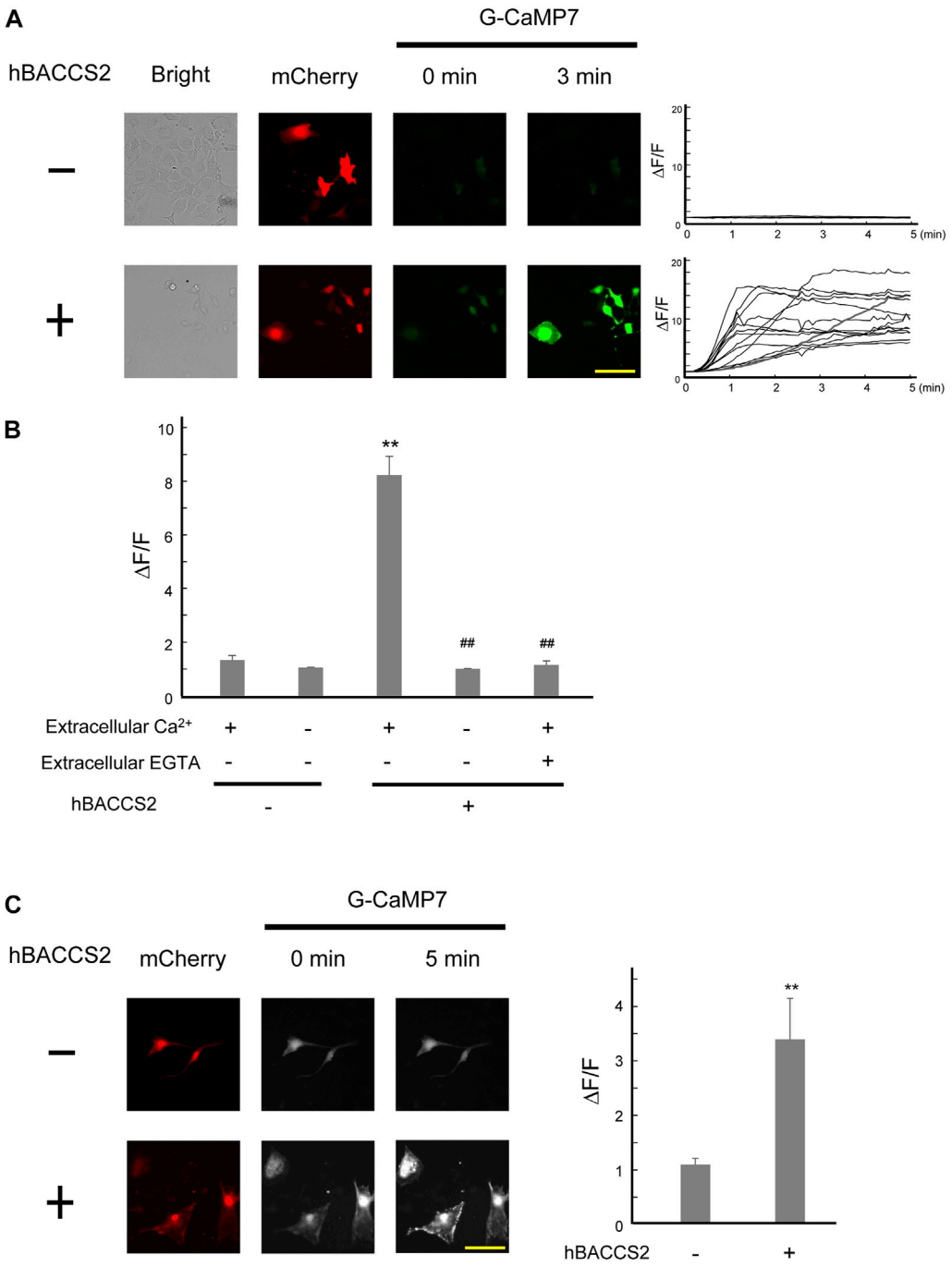

FIGURE 2
hBACCS2 leads to blue light-mediated Ca^{2+} increase in murine vascular endothelial cells. **(A)** Vascular endothelial F2 cells were transfected with G-CaMP7 and either hBACCS2-mCherry or mCherry, photoactivated with blue light (.2 Hz). Each trace represents fluorescence intensity from randomly selected cells. The scale bar represents 50 μm. **(B)** Bar graph shows the normalized fluorescence intensity of maximal values within 5 min in the different conditions as indicated. n = 13–58 from 3 to 6 independent experiments. $^{**}p < .01$ vs. hBACCS2-negative cells, $^{\#\#}p < .01$ vs. extracellular Ca^{2+} +/EGTA - condition, one-way ANOVA with Fisher's LSD post hoc test. **(C)** Brain microvascular b.End3 cells were transfected with G-CaMP7 and either hBACCS2-mCherry or mCherry and photoactivated with blue light (.2 Hz). Bar graph shows the normalized fluorescence intensity of maximal values within 5 min in the different conditions as indicated. The scale bar represents 100 μm n = 13–17 from 3 independent experiments. $^{**}p < .01$ vs. hBACCS2-negative cells, Student's t-test.

2.4 Fluorescence Ca^{2+} and NO imaging

Cells, spread on poly-L-lysine-coated coverslips were incubated with 5 μM Fluo-8/AM in standard extracellular fluid (ECF), which contained: 140 mM NaCl, 5.4 mM KCl, 2 mM $CaCl_2$, 1 mM $MgCl_2$, 10 mM glucose, and 20 mM HEPES (pH 7.4 with NaOH), for 30 min at 37°C, followed by de-esterification of the dye for another 30 min at room temperature (22°C–25°C). The coverslips containing dye-loaded cells were held in a recording chamber placed on the stage of an inverted microscope (U-RFL-T mercury lamp, U-FBNA mirror unit, XL73, Olympus,

Tokyo, Japan). Blue light (470–495 nm, 500 msec exposure, .2 Hz) for Fluo-8 excitation works by activating hBACCS2-mediated Ca^{2+} increase, and emitted light was culled with a 500–550 nm band pass filter. The fluorescence was detected with a ×20 objective lens (Olympus) and a CMOS camera (ORCA-Flash 2.8, Hamamatsu Photonics, Hamamatsu, Japan), using HCImage software 4.3.5 (Hamamatsu Photonics). Fluorescence intensities (ΔF) were normalized to the initial values (t = 0). Cells were not stained and incubated with ECF when G-CaMP7 was time-lapse monitored.

For NO imaging, cells were prepared as above and incubated with 5 μM DAF-FM/DA (Itoh et al., 2000) in standard ECF including 1 mM L-arginine, in the absence or presence of 1 mM N^G-nitro-L-arginine methyl ester (L-NAME) for 30 min at 37°C, followed by de-esterification of the dye for another 30 min at room temperature. Thereafter, the procedure was the same as for Ca^{2+} imaging.

2.5 Reverse transcription and quantitative real-time PCR

Total RNAs of F2 cells were extracted with NucleoSpin RNA Plus (Takara). cDNAs were synthesized from 500 ng total RNA in 20 μl reactions using oligo $(dT)_{15}$ and reverse transcriptase (Toyobo, Osaka, Japan).

Quantitative real-time PCR was performed to validate the expression levels of selected genes using SYBR® Premix Ex Taq (Takara) and the Thermal Cycler Dice Real Time System (Takara) in accordance with the manufacturer's protocols. The PCR amplification cycles consisted of denaturation at 95°C for 30 s, 40 cycles of denaturation at 95°C for 5 s, and annealing/extension at 60°C to for 60 s, followed by the detection of melt curve, 65°C–95°C. Real-time PCR reactions were carried out in duplicate for each sample, and the average values were applied to the ΔΔCt method for data analysis. Primer sets are described in "Supplementary Table S1".

2.6 Microarray analysis

RNA samples (one from each condition) were used for global gene expression profiling. Microarray analysis was performed by Filgen Inc. (Nagoya, Japan) using the Clariom S array for mice (Thermo Fisher), for ~22,000 genes, and GeneChip Scanner 3000 7G System (Thermo Fisher). The Microarray Data Analysis Tool version 3.2 (Filgen Inc.) was used for data normalization and subsequent processing. Differentially expressed mRNAs were identified using a set cutoff (signal intensities > 24, which is close to the median of negative control values, and fold change > 2 or < .5). Selected genes were processed for pathway analysis and those involved were classified based on gene ontology (GO) terms. A statistically ranked list of GO terms was then generated in terms of the z-score, which is a statistical measure of the relative amounts of gene expression changes in a given GO term (Doniger et al., 2003). A z-score of more than 3 is considered a statistically significant association between the differentially expressed genes and their corresponding GO terms. GO terms describing fewer than two genes that met the user-defined criteria were not considered in this study because of difficulty in ruling out coincidence.

Microarray data has been deposited in the Gene Expression Omnibus (GEO) at the National Center for Biotechnology Information (NCBI) (accession number GSE214156).

2.7 Reporter gene assays

Cells grown on 24-well plates were transfected with either pGL4.30 [luc2P/NFAT-RE/Hygro] or pGL4.32[luc2P/NF-κB-RE/Hygro] (Promega) together with pRL-TK (Promega) to compensate for transfection efficiency. Expression plasmids were transfected in the following amounts per well: .2 μg of mCherry-containing vector, .15 μg of pGL4.30[luc2P/NFAT-RE/Hygro], .05 μg of pRL-TK for F2 cells. Luciferase assays were performed using the Dual-Luciferase Reporter System (Promega) with microplate luminometer (Molecular Devices, San Jose, CA, United States) according to the manufacturer's instruction. For chelation of intracellular Ca^{2+}, cells were pretreated with either BAPTA/AM (25 μM) or vehicle (dimethyl sulfoxide) for 30 min, after which blue light was applied.

2.8 Immunoblotting

Immunoblotting was performed as described (Inoue et al., 2010; Inoue et al., 2012). Cells cultured on 35 mm dishes were lysed in lysis buffer [50 mM Tris-HCl, pH 7.5, 100 mM NaCl, 1% Triton X-100, and protease inhibitor (Sigma-Aldrich)]. The lysates were collected after centrifugation at 14,000 × *g* and 4°C for 30 min. The aliquots were thereafter mixed with Laemmli sample buffer and boiled at 95°C for 10 min. The samples were resolved in 4%–20% SDS-PAGE, followed by electrotransfer to polyvinylidene difluoride membranes. For visualization, blots were probed with antibodies against Flag (1:1000) or GAPDH (1:3000), and detected using horseradish peroxidase-conjugated secondary antibodies (1:2000; Promega) and an ECL kit (Bio-Rad, Hercules, CA, United States).

2.9 Immunofluorescence staining

Cells were fixed with 4% paraformaldehyde in phosphate-buffered saline (PBS), followed by permeabilization in PBS containing .2% Triton X-100. The cells were first incubated with antibodies against Flag (1:1000) or NF-κB (1:500), and then with the Alexa 488-conjugated secondary antibodies (Thermo Fisher). For DNA staining, coverslips were incubated with 4′,6′-diamidino-2-phenylindole (DAPI). Fluorescent images were analyzed using a fluorescence microscopy (XL73, Olympus, Tokyo, Japan).

2.10 Statistical analysis

Data are presented as means ± SEM. Kaleidagraph 4.0 (Synergy Software, Reading, PA, United States) was used for statistical analysis. Differences between two groups were compared using an unpaired Student's *t*-test. Comparisons among three or more groups were performed by one-way ANOVA, followed by Fisher's least significant difference (LSD) *post hoc* test where applicable. $p < .05$ was regarded as statistically significant.

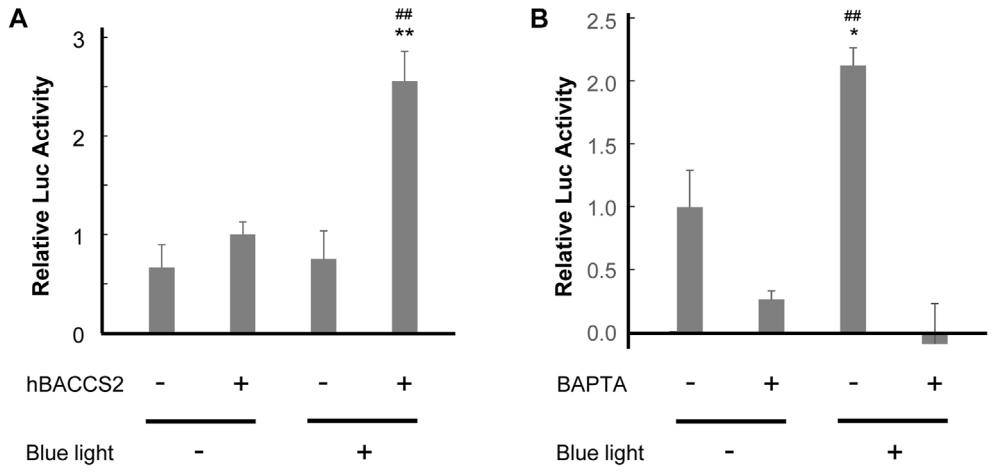

FIGURE 3
hBACCS2 leads to blue light-mediated NFAT activation in vascular endothelial cells. **(A)** F2 cells were transfected with pGL4.30[luc2P/NFAT-RE/Hygro], a firefly luciferase reporter plasmid containing an NFAT response element, pRL-TK, a control Renilla luciferase reporter plasmid, and either hBACCS2-mCherry or mCherry. Next day, 4 h after photoactivation (repletion of 2 min light irradiation and 18 min interval), the ratio of firefly luciferase activity to Renilla luciferase activity was calculated (n = 5). $^{**}p < .01$ vs. hBACCS2 –, $^{\#\#}p < .01$ vs. blue light –, one-way ANOVA with Fisher's LSD *post hoc* test. **(B)** F2 cells were transfected with pGL4.30[luc2P/NFAT-RE/Hygro], pRL-TK, and pCAG-hBACCS2-mCherry. On the following day after transfection, cells were pretreated with either 25 μM BAPTA/AM or vehicle for 30 min and photoactivation was then carried out for 4 h before being harvested. For each condition, the ratio of firefly luciferase activity to Renilla luciferase activity was calculated (n = 3). $^{*}p < .05$ vs. blue light –, $^{\#\#}p < .01$ vs. BAPTA +, one-way ANOVA with Fisher's LSD *post hoc* test.

3 Results

3.1 Detection of Flag/hBACCS2-mediated G-CaMP activation by blue light irradiation

Numerous literature have been published on light-sensitive intracellular Ca^{2+} modulators (Fukuda et al., 2014; Ma et al., 2017a). Among them, as reported by Ishii et al. (2015) is a plasmid that bicistronically expresses mCherry and hBACCS2, which causes an intracellular Ca^{2+} increase when exposed to blue light. hBACCS2 is a fusion protein of phototropin 1, a light sensor, and STIM1, which binds to the Ca^{2+} channel ORAI1. Exposure to blue light irradiation facilitates a conformational change in the fusion protein, leading to binding and opening of ORAI1 and subsequent Ca^{2+} influx, sufficient for stimulation of downstream cellular processes (Ishii et al., 2015). To obtain enhanced expression levels in a variety of cells, we constructed a plasmid expressing Flag-tagged hBACCS2 and mCherry under a CAG promoter, which is often used for intensive and *in vivo* expression (Niwa et al., 1991; Araki et al., 1997). As shown in Figures 1A,B, a band with the expected molecular size (~55 kDa) was detected using anti-Flag antibodies and the molecule was localized in the cytoplasmic region in HEK293 cells (Figures 1A,B). Blue light-induced Ca^{2+} increase was also observed in HEK293 cells containing the newly constructed Flag/hBACCS2-mCherry-expressing plasmid when cells were stained with a fluorescence Ca^{2+} indicator Fluo-8, while no change in fluorescence intensities were observed in either non-transfected or mCherry-positive (Flag/hBACCS2-negative) cells (Figure 1C).

For further convenience, we attempted to use G-CaMP7, an intracellularly expressed artificial Ca^{2+} sensor molecule, as opposed to staining with fluorescence indicators. G-CaMP7 is a derivative of GFP and its fluorescence intensity is Ca^{2+} concentration-dependent (Ohkura et al., 2012). Blue light application induced an elevation of fluorescence intensities in HEK293 cells expressing G-CaMP7 and Flag/hBACCS2-mCherry, whereas an elevation did not occur in the absence of Flag/hBACCS2 (Figure 1D). Removal of extracellular Ca^{2+} prevented increases in the fluorescence intensities, even in the presence of Flag/hBACCS2 (Figure 1D). These results suggest that photoactivation of Flag/hBACCS2 by blue light is detectable using G-CaMP7 fluorescence intensity. "Flag/hBACCS2" is hereafter simply represented as "hBACCS2".

3.2 Ca^{2+} increase in the presence of hBACCS2 and blue light application in vascular endothelial cells

We examined whether the blue light/hBACCS2 system works in vascular endothelial cells, where the ORAI1-STIM1 system is present (Abdullaev et al., 2008; Li et al., 2011). In murine vascular endothelial F2 cells (Toda et al., 1990), fluorescence intensities of G-CaMP7 were elevated by blue light irradiation when hBACCS2 was present (Figures 2A,B). In contrast, hBACCS2-negative cells did not show a blue light-induced increase in G-CaMP7 fluorescence intensity. Under similar procedures, removal of extracellular Ca^{2+} prevented an increase in G-CaMP7 fluorescence intensities in hBCAACS2-positive cells (Figure 2B). An addition of EGTA, a Ca^{2+} chelator, also weakened the fluorescence (Figure 2B).

To obtain further insight into the availability of hBACCS2-dependent Ca^{2+} influx in vascular endothelial cells, we employed the b.End3 vascular endothelial cell line derived from brain vasculature. Similar to the case of F2 cells, fluorescence intensities of G-CaMP7 were elevated by blue light irradiation in hBACCS2-positive, but not hBACCS2-negative b.End3 cells (Figure 2C).

10.3389/fphar.2022.1076116

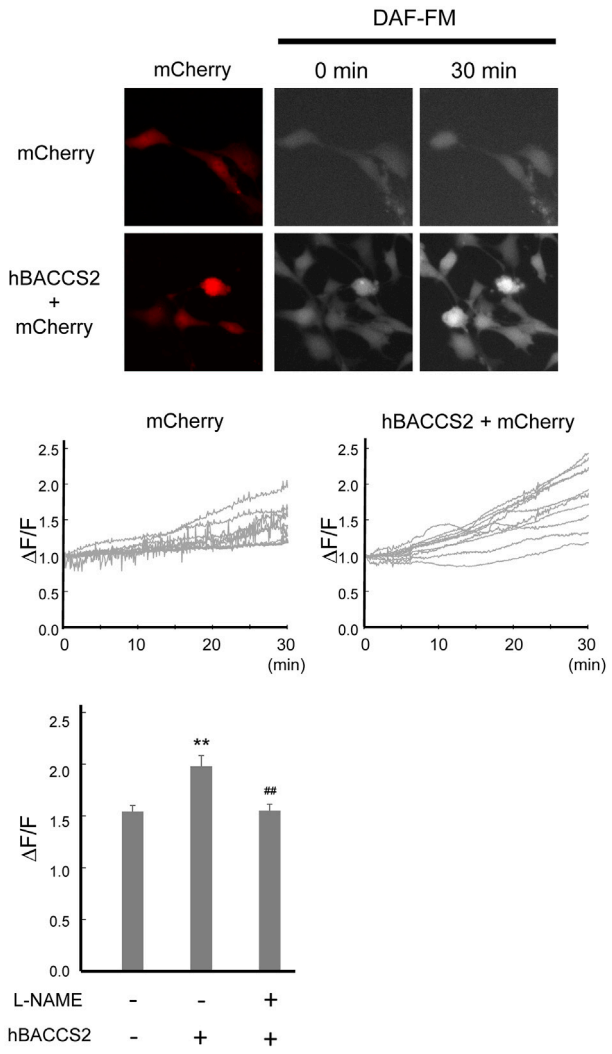

FIGURE 4
hBACCS2 leads to blue light-mediated NO production in vascular endothelial cells. F2 cells transfected with either hBACCS2-mCherry or mCherry were stained with DAF-FM/DA. Blue light was then applied (.2 Hz) and DAF-FM signals were monitored. Each trace represents fluorescence intensity from randomly selected mCherry-positive cells. Bar graph shows the normalized fluorescence intensity of maximal values within 30 min in the different conditions as indicated. n = 33–46 from 3–5 independent experiments. $^{**}p < .01$ vs. hBACCS2-negative cells, $^{\#\#}p < .01$ vs. L-NAME - condition, one-way ANOVA with Fisher's LSD *post hoc* test.

3.3 Intracellular Ca^{2+} signaling activation with hBACCS2 and blue light irradiation

Following observations of Ca^{2+} increase, we examined whether intracellular Ca^{2+}-dependent signaling activity is influenced under our approach in vascular endothelial cells. Ishii et al. (2015) indicated that Ca^{2+}-dependent activation of a transcription factor, nuclear factor of activated T cell (NFAT), was detected in HEK293 cells (Ishii et al., 2015). Consequently, we performed a reporter gene assay of NFAT in F2 cells. In this process, we challenged different conditions for 4 h in total, and cells that underwent 2 min/18 min cycles (repletion of 2 min irradiation and 18 min interval) showed the highest activity of NFAT reporter in the presence of hBACCS2 and blue light irradiation (Figure 3A). The photoactivation was eradicated when cells were pretreated with BAPTA/AM, a Ca^{2+} chelator (Figure 3B). Thus, a combination of blue light irradiation and presence of hBACCS2 can induce the activation of intracellular Ca^{2+} signaling.

3.4 NO production with hBACCS2 and blue light irradiation in vascular endothelial cells

NO production and release is an important function of vascular endothelial cells. Intracellular Ca^{2+} increase, such as by acetylcholine, activates eNOS, leading to enhanced NO production. We investigated whether NO production is facilitated by hBACCS2 and blue light irradiation. Transfected F2 cells were incubated with DAF-FM/DA, an NO-sensitive fluorescence indicator, and photostimulation was conducted. As shown in Figure 4, while hBACCS2-negative cells still displayed a slight increase in DAF-FM fluorescence intensities, hBACCS2-positive cells showed higher elevation (Figure 4). L-NAME, an NOS inhibitor, attenuated this increase (Figure 4). This indicated that photoactivation by the combination of blue light and hBACCS2 facilitates NO production.

3.5 Gene expression profiling of blue light-induced hBACCS2-positive vascular endothelial cells

Ca^{2+} signaling can also affect gene expression, as demonstrated by the altered activity of the transcription factor NFAT, as shown in Figure 3. To understand the global effect of Ca^{2+} elevation on gene expression in hBACCS2-transfected vascular endothelial cells, Clariom S microarray assay (Thermo Fisher) was used for analysis of RNA samples treated as in Figure 3 (2 min/18 min for 4 h). The scatter plot analysis in Figure 5A demonstrates that blue light irradiation resulted in up- and downregulated gene expression of 105 and 144 genes, respectively (Supplementary Tables S2, S3). To elucidate the possible molecular mechanisms associated with these differentially expressed genes, MAPP pathway analysis identified several pathways regulated by blue light irradiation, including apoptosis, myometrial relation/contraction, and inflammatory responses (Tables 1, 2). To validate the changes in gene expression of blue light-irradiated cells observed in microarray analysis, we performed quantitative real-time PCR for several target genes whose expressions were upregulated in hBACCS2-transfected F2 cells. As a result, blue light photoactivation upregulated the expression of genes indicated in Figure 5A in hBACCS2-positive cells [in contrast, the increase in ATF4 expression was non-significant (p = .058)], but not in hBACCS2-negative cells (Figure 5B). Although it was curious to us that the expression of E-selectin and ICAM-1, which are supposed to be expressed in a Ca^{2+}-dependent manner, were not upregulated in this analysis (Chen et al., 2002), quantitative PCR also showed that Ca^{2+} increase alone is insufficient for its upregulation (Figure 5B, ICAM-1 was not detectable in our study, not shown). This may correspond with the results of a recent study that showed that extrinsic Ca^{2+} elevation by means of TRPV4 agonist does not increase E-selectin level (Chen et al., 2002; Beddek et al., 2021). Thus, consistent with microarray data, blue light mediated Ca^{2+} influx is possibly associated with vascular contractility and inflammation in the presence of hBACCS2.

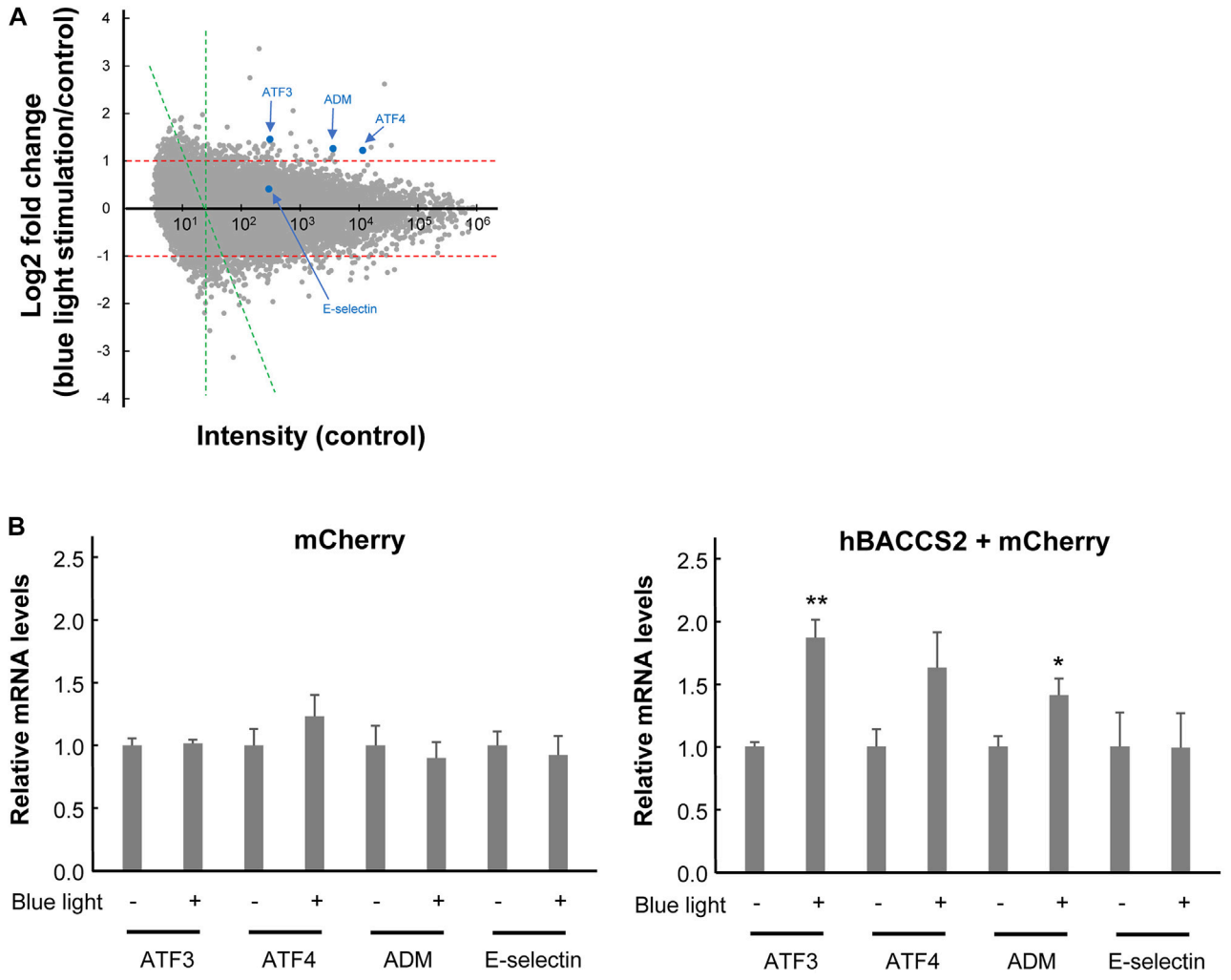

FIGURE 5
Gene expression profiling of hBACCS2-transfected F2 cells in the absence or presence of photoactivation. **(A)** Microarray analysis was performed comparing the gene expression profiles of hBACCS2-transfected F2 cells with or without blue light irradiation. A single dot is plotted for each gene. Some of representative genes were plotted with blue. Scatterplot comparing control intensities (x-axis) and their fold changes (log2-fold change, y-axis) was shown. A cut off intensity (x = 24) applied for pathway analysis (see methods) was indicated with green lines. **(B)** Quantitative real-time PCR was performed to validate mRNA levels of the indicated genes in F2 cells treated as described in **(A)**. n = 5–12. *p < .05, **p < .01 vs. blue light -, Student's t-test.

3.6 Possible attenuation of NF-κB activity by blue light activation in hBACCS2-transfected vascular endothelial cells

Ca^{2+} elevation often evokes an attenuation of inflammatory responses in vascular endothelial cells (de Martin et al., 2000; Munaron, 2006; Bair et al., 2009; Li et al., 2017). In order to gain insight into this pathway during vascular inflammation, we examined whether inflammatory NF-κB activity is influenced by blue light and hBACCS2. It is well known that inflammatory mediators such as lipopolysaccharide and TNFα elicit vascular inflammatory activation. First, to inspect NF-κB activity, cells were treated with TNFα in the absence or presence of hBACCS2 and/or blue light irradiation, and a reporter system containing the NK-κB consensus sequence was challenged. While hBACCS2 simply enhanced basal reporter activities, TNFα induced NF-κB reporter activity in hBACCS2-transfected cells. The increased activity was significantly attenuated with blue light irradiation (Figure 6A). We then probed levels of nuclear translocation of NK-κB with TNFα treatment. Blue light-induced cytoplasmic retention of NF-κB was significantly greater in hBACCS2-positive cells than in hBACCS2-negative cells when stimulated with TNFα (Figure 6B). Taken together, although the functional effect of hBACCS2-dependent Ca^{2+} increase on TNFα-induced inflammatory responses was not significantly detectable, NF-κB translocation is likely to be influenced by the combination of hBACCS2 and blue light irradiation. This suggests that TNFα-induced inflammatory responses could possibly be attenuated with the combination of hBACCS2 and blue light with optimal photostimulatory doses.

4 Discussion

In blood vessels, vascular endothelial cells generate NO, an anti-coagulant that acts on platelets, and exhibit vasodilatory effects *via* vascular smooth muscles (Bauer and Sotnikova, 2010; Smolenski,

TABLE 1 Up-regulated pathway by pathway analysis.

MAPP name	Number changed	Number measured	Z-score	*p*-value
Mm_Apoptosis_modulation_by_HSP70	2	17	6.67	.0037
Mm_Myometrialrelaxation_andcontraction_pathways	4	151	3.81	.0060
Mm_Mapk_signaling_pathway	4	158	3.69	.0070
Mm Oxidative stress response	2	27	5.16	.0084
Mm Inflammatory response_pathway	2	30	4.86	.0102
Mm Exercise-induced circadian_regulation	2	48	3.66	.0240
Mm_Lung fibrosis	2	61	3.13	.0368

TABLE 2 Down-regulated pathway by pathway analysis.

MAPP name	Number changed	Number measured	Z-score	*p*-value
Mm White fat cell differentiation	2	32	3.40	.0307
Mm Fatty acid beta-oxidation	2	33	3.34	.0324

2012). The lack of NO production due to metabolic diseases such as hypertension and hypercholesterolemia can lead to atherosclerosis (Forstermann et al., 2017). Thus, regulation of NO production plays a critical role in vascular function. We attempted to manipulate cellular Ca^{2+} levels in cultured vascular endothelial cells, and consequently NO production and changes in gene expression by means of an optogenetic technique, which is widely available in neurobiological fields. Recently, studies using this technique for the cardiovascular system, have mainly focused on cardiac or vascular smooth muscle cells (Lee et al., 2021; Tong et al., 2021); to our knowledge, there is no literature focusing on vascular endothelial cells. As some optogenetic tools that can regulate Ca^{2+} levels are known, we employed a BACCS system which utilizes store-operated calcium entry, the ORAI1-STIM1 machinery, that is present endogenously in vascular endothelial cells. Among the currently used techniques that manipulate cellular function, the chemogenomic technique involves a designer receptor exclusively activated by designer drugs (DREADDs) which activates artificial G protein-coupled receptors through certain reagents (Urban and Roth, 2015; Aldrin-Kirk et al., 2016). However, the problems with DREADDs are: 1) introduction of artificial molecules into cells or tissues, 2) artificial drugs must be administered into the body, and 3) follow-up observation should be done, proving them harmless to the body (Keifer et al., 2020). Comparing the optogenetic approaches, some optogenetic tools also require introduction of artificial molecules into the body, and DREADDs may offer an advantage as their effects reach deeply in the body where light irradiation does not penetrate. Nonetheless, as optogenetics require less consideration of the impact of artificial drugs potentially involved in generation of the side effects, they can be considered more appropriate as a therapeutic strategy. This study initially aimed to examine whether our approach works in vascular endothelial cells; thus, we employed two vascular endothelial cell lines, F2 and b.End3 cells. As a result, we found that blue light irradiation induces an hBACCS2-dependent Ca^{2+} increase in both cells lines. Transfection efficiency and fold changes in fluorescence intensities of b.End3 cells were lower compared to those of F2 cells; therefore, we focused on F2 cells thereafter. Increase in intracellular Ca^{2+} levels induces calmodulin binding to eNOS, resulting in NOS enzymatic activity (Abu-Soud et al., 1994; McCabe et al., 2000). Consistent with this, we found that a combination of blue light and hBACCS2 induces Ca^{2+} influx and subsequent NO production. Thus, with incorporation of hBACCS2 into the vascular endothelium *in vivo*, it may be possible to control vascular function.

Apart from regulating cytoplasmic NO production, Ca^{2+} is regarded as a secondary messenger for intracellular signaling and plays a role in gene expression. NFAT activity, a known Ca^{2+}-dependent factor, is also induced by the combination of hBACCS2 and blue light irradiation, and is eliminated in their absence. Moreover, intracellular chelation of Ca^{2+} with BAPTA eradicates NFAT activity, confirming that intracellular Ca^{2+} regulates NFAT transcriptional activity. As intracellular Ca^{2+} elevation is also known to alter gene expression *via* other transcription factors such as AP-1 (Salnikow et al., 2002; Liu et al., 2004), microarray analysis was carried out to depict a more comprehensive view of the cellular functions of Ca^{2+}. The upregulation in adrenomedullin (ADM) expression, along with others, by hBACCS2/blue light was observed using microarray analysis in this study; however, the mechanism by which ADM responds to Ca^{2+} elevation was not pursued, along with potential AP-1 sites implicated in the human ADM promoter region (Ishimitsu et al., 2003), and this needs to be addressed for better understanding. ATF3 and ATF4 were also upregulated, and a recent study revealed that both of these genes expressed in vascular endothelial cells are critical for metabolic oxidative stress-induced angiogenesis (Fan et al., 2021), suggesting the possibility that optogenetic Ca^{2+} entry could support angiogenic potential. The benefit of this method of Ca^{2+} influx induction is that the expression of multiple beneficial molecules may be upregulated simultaneously. Although some detrimental genes could also be upregulated, it can be successful if an overall vascular or systemic improvement is observed.

Pathway analysis identified some pathways that are influenced by blue light irradiation. Regarding vascular endothelial roles, pathways for contractility and inflammatory responses were identified. Since inflammation dysregulates vascular contractility, resulting in vascular stiffness and atherosclerosis, we examined whether blue light

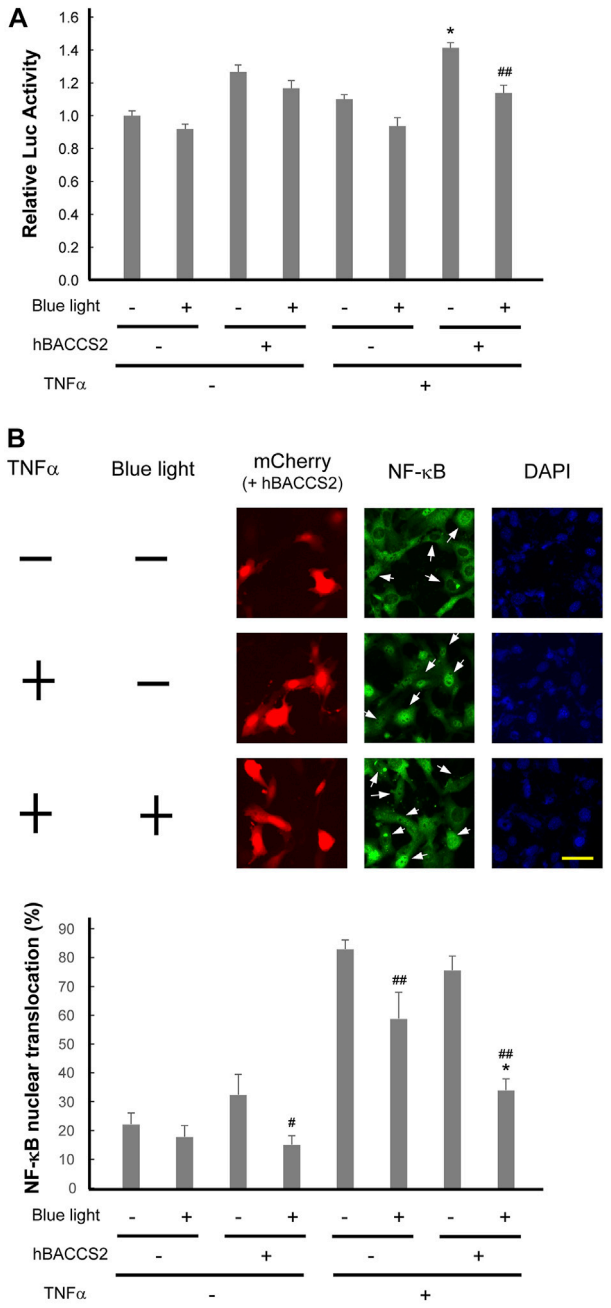

FIGURE 6
Photoactivation using hBACCS2 possibly attenuates TNFα-induced NF-κB activation in vascular endothelial cells. **(A)** F2 cells were transfected with pGL4.32[luc2P/NF-κB-RE/Hygro], a firefly luciferase reporter plasmid containing an NF-κB response element, pRL-TK, and either hBACCS2-mCherry or mCherry. Two h after photoactivation, they were either untreated or treated with 20 ng/ml TNFα for 2 h, followed by manipulation for reporter assay. (n = 6–7). TNFα-induced NF-κB activity was significantly attenuated with blue light irradiation in hBACCS2-transfected cells. *p < .05 vs. TNFα -, $^{\#\#}p$ < .01 vs. blue light -, one-way ANOVA with Fisher's LSD *post hoc* test. The effect of hBACCS2 was always significant (p < .01); this is not indicated in the panel. **(B)** F2 cells were transfected with either hBACCS2-mCherry or mCherry. In the absence or presence of 2 h after photoactivation, cells were either untreated or treated with 20 ng/ml TNFα for 30 min, and then fixed. NF-κB p65 protein was visualized by indirect immunofluorescence staining using an antibody for p65. Arrows indicate mCherry-positive cells. The scale bar represents 50 μm. Bar graph shows quantitative analysis of NK-κB-translocated cells. Cells, in which nuclear NF-κB staining was visible as clearly as the merge of the nucleus

(*Continued*)

FIGURE 6 (Continued)
was detectable, were regarded as NF-κB-translocated cells, and their percentage was calculated. 11–52 transfected cells were counted in each field. (n = 4). hBACCS2 enhanced cytosolic retention of NF-κB significantly in TNFα-cells. *p < .05 vs. hBACCS2 -, $^{\#}p$ < .05, $^{\#\#}p$ < .01 vs. blue light -, one-way ANOVA with Fisher's LSD *post hoc* test. The effect of TNFα was always significant (p < .05); this is not indicated in the panel.

irradiation affects inflammatory responses. In line with their relationship between arbitrary Ca^{2+} levels and inflammation, TNFα-induced NF-κB changes were monitored, and photostimulation of hBACCS2 attenuated its nuclear translocation and perhaps consequently its transcriptional activity. We provide a direction for future indications for the regulation of vascular function by arbitrary Ca^{2+} induction. Certain stimuli that potentially facilitate intracellular Ca^{2+} elevation can precondition vascular endothelial cells to detrimental stresses (Zahler et al., 2000; Jabs et al., 2010; Leonard et al., 2014), and the attenuation of inflammatory responses by Ca^{2+} increase in this study may induce this preconditioning. Surprisingly, arbitrary Ca^{2+} increase by blue light and hBACCS2 did not potentiate NF-κB, and thus the simple Ca^{2+} increase may not always be sufficient for NF-κB activation, as it sometimes needs other stimulation in addition to Ca^{2+} increase in other cells (Casolaro et al., 1995; Brignall et al., 2017). Of interest, as shown in Figure 6B, blue light irradiation alone may diminish the capacity of the inflammatory responses, as longer wavelengths have been indicated to have anti-inflammatory effects (Hamblin, 2017; Hamblin, 2018). Studies on optimization of light doses are required to move forward to *in vivo* studies.

Thus, although we found that hBACCS2 combined with blue light irradiation can activate vascular endothelial cellular functions, one of the limitations of this study is that we could not evaluate the optimal degree (e.g., intensity and frequency) of blue light stimulation. As performed by Ishii et al. (2015), we also performed an NFAT reporter assay under several conditions (data not shown) to obtain the optimum condition, and applied the most significant condition as found for microarray analysis. However, there might be more optimal conditions, that may result in greater improved functional changes. However, even if optimal stimulatory conditions are discovered in cultured cells, such stimulation may not always be transferrable *in vivo*; therefore, it would be better to start the search for optimal photostimulatory doses for *in vivo* studies. Also, in line with *in vivo* applications, a strong CAG promoter-containing expression plasmid was introduced in this study, which may cause vascular contraction when it is involved in neighboring vascular smooth muscle cells.

Ultimately, we hope to apply this method in a non-transgenic manner to treat human patients with conditions such as arteriosclerosis obliterans. However, testing the introduction of hBACCS2 into blood vessels by various methods in experimental animal models (Martin et al., 2000; Rutanen et al., 2002; Ouma et al., 2014; Young and Dean, 2015; Ma et al., 2017b; Goudy et al., 2019; Rasanen et al., 2021) should ideally precede any application in human. While introducing plasmid or viral vectors, it will be necessary to contain the effects of blue light in vascular endothelial cells, without affecting vascular smooth muscle cells (Wynne et al., 2009). Thus, this study presents the initial findings and a basis for further investigations on safe use of this approach *in vivo*. Further research is essential to allow this method to be promoted with *in vivo* applications in mind.

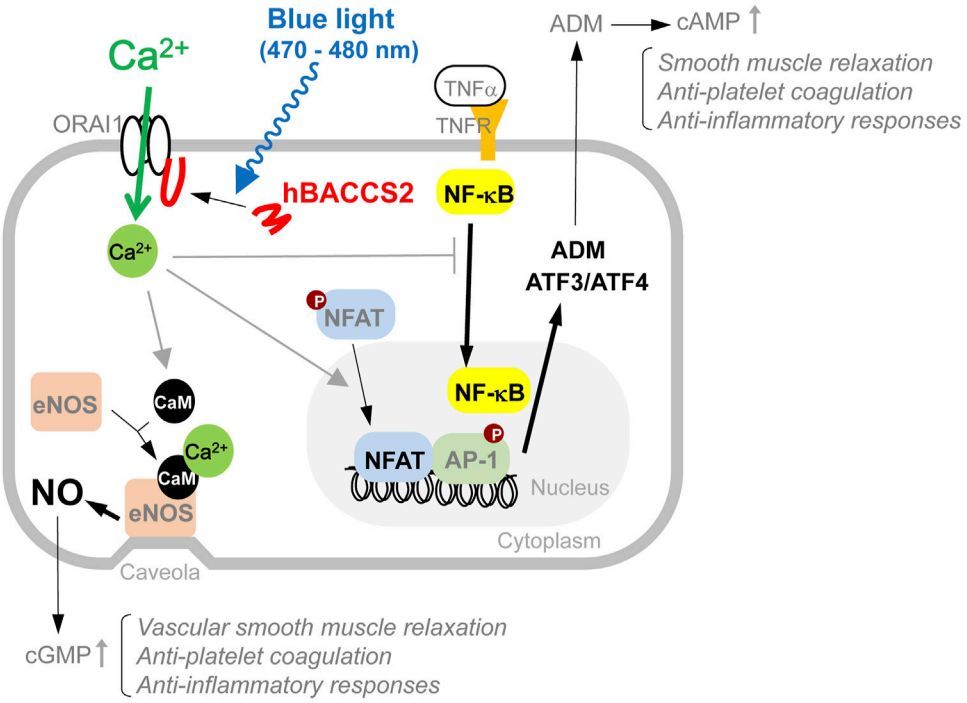

FIGURE 7
Model of intracellular events involved in blue light/hBACCS2-dependent Ca^{2+} regulation in vascular endothelial cells. Results from this study show that arbitrary increase in intracellular Ca^{2+} alters a variety of cellular events such as NO production and gene expression, resulting in changes in cellular function in vascular endothelial cells. Molecules observed in this study are indicated with bold and black letters, and the related changes are shown by thicker arrows.

A model of the arbitrary Ca^{2+}-dependent cellular actions and their involvement in downstream possible anti-inflammatory signaling used in this study is depicted in Figure 7.

5 Conclusion

In this study, we employed a recently described optogenetic technique and found that blue light irradiation, along with hBACCS2 introduction, induces an arbitrary increase in Ca^{2+} in vascular endothelial cells, followed by a subsequent increase in intracellular Ca^{2+}, NFAT activity and NO production. A comprehensive analysis of gene expression changes induced by blue light-dependent Ca^{2+} elevation using DNA microarrays revealed potential changes in the expression of genes related to smooth muscle contractility and inflammatory responses. The blue light-dependent Ca^{2+} increase also appeared to influence NF-κB activity induced by TNFα, an inflammatory mediator. These findings suggest that successful Ca^{2+} regulation of vascular endothelial cells may improve vascular function or regulate inflammatory responses. Further optimization of the stimulatory features and system, and its application *in vivo* are expected in the future.

Data availability statement

The datasets presented in this study can be found in online repositories. The names of the repository/repositories and accession number(s) can be found below: https://www.ncbi.nlm.nih.gov/, GSE214156.

Author contributions

Material preparation, data collection and analysis were performed by TY and KI. The first draft of the manuscript was written by KI, and all authors commented on previous versions of the manuscript. All authors read and approved the final manuscript.

Funding

This work was supported by the Mishima Kaiun Memorial Foundation, and Grant-in-Aid for Scientific Research No. 21K09133 from the Japan Society for the Promotion of Science, Japan (KI).

Acknowledgments

We thank Daiya Ohashi (Clinical Research Management Center, Nagoya City University Hospital) for assistance with the statistical analysis, J. Miyazaki for providing pCAG-GS, T. Nakata for providing hBACCS2-IRES-mCherry cDNA, J. Nakai for providing G-CaMP7 cDNA, and Editage (www.editage.com) for English language editing.

Conflict of interest

The authors declare that the research was conducted in the absence of any commercial or financial relationships that could be construed as a potential conflict of interest.

Publisher's note

All claims expressed in this article are solely those of the authors and do not necessarily represent those of their affiliated organizations, or those of the publisher, the editors and the reviewers. Any product that may be evaluated in this article, or claim that may be made by its manufacturer, is not guaranteed or endorsed by the publisher.

Supplementary material

The Supplementary Material for this article can be found online at: https://www.frontiersin.org/articles/10.3389/fphar.2022.1076116/full#supplementary-material

References

Abdullaev, I. F., Bisaillon, J. M., Potier, M., Gonzalez, J. C., Motiani, R. K., and Trebak, M. (2008). Stim1 and Orai1 mediate CRAC currents and store-operated calcium entry important for endothelial cell proliferation. *Circ. Res.* 103, 1289–1299. doi:10.1161/01.RES.0000338496.95579.56

Abu-Soud, H. M., Yoho, L. L., and Stuehr, D. J. (1994). Calmodulin controls neuronal nitric-oxide synthase by a dual mechanism. Activation of intra- and interdomain electron transfer. *J. Biol. Chem.* 269, 32047–32050. doi:10.1016/s0021-9258(18)31597-7

Aldrin-Kirk, P., Heuer, A., Wang, G., Mattsson, B., Lundblad, M., Parmar, M., et al. (2016). DREADD modulation of transplanted DA neurons reveals a novel Parkinsonian dyskinesia mechanism mediated by the serotonin 5-HT6 receptor. *Neuron* 90, 955–968. doi:10.1016/j.neuron.2016.04.017

Araki, K., Imaizumi, T., Okuyama, K., Oike, Y., and Yamamura, K. (1997). Efficiency of recombination by cre transient expression in embryonic stem cells: comparison of various promoters. *J. Biochem.* 122, 977–982. doi:10.1093/oxfordjournals.jbchem.a021860

Bair, A. M., Thippegowda, P. B., Freichel, M., Cheng, N., Ye, R. D., Vogel, S. M., et al. (2009). Ca^{2+} entry via TRPC channels is necessary for thrombin-induced NF-κB activation in endothelial cells through AMP-activated protein kinase and protein kinase Cδ. *J. Biol. Chem.* 284, 563–574. doi:10.1074/jbc.M803984200

Bauer, V., and Sotnikova, R. (2010). Nitric oxide--the endothelium-derived relaxing factor and its role in endothelial functions. *Gen. Physiol. Biophys.* 29, 319–340. doi:10.4149/gpb_2010_04_319

Beddek, K., Raffin, F., Borgel, D., Saller, F., Riccobono, D., Bobe, R., et al. (2021). TRPV4 channel activation induces the transition of venous and arterial endothelial cells toward a pro-inflammatory phenotype. *Physiol. Rep.* 9, e14613. doi:10.14814/phy2.14613

Braune, S., Kupper, J. H., and Jung, F. (2020). Effect of prostanoids on human platelet function: an overview. *Int. J. Mol. Sci.* 21 (23), 9020. doi:10.3390/ijms21239020

Brignall, R., Cauchy, P., Bevington, S. L., Gorman, B., Pisco, A. O., Bagnall, J., et al. (2017). Integration of kinase and calcium signaling at the level of chromatin underlies inducible gene activation in T cells. *J. Immunol.* 199, 2652–2667. doi:10.4049/jimmunol.1602033

Casolaro, V., Georas, S. N., Song, Z., Zubkoff, I. D., Abdulkadir, S. A., Thanos, D., et al. (1995). Inhibition of NF-AT-dependent transcription by NF-κB: implications for differential gene expression in T helper cell subsets. *Proc. Natl. Acad. Sci. U. S. A.* 92, 11623–11627. doi:10.1073/pnas.92.25.11623

Chen, K. H., Chang, B. H., Younan, P., Shlykov, S. G., Sanborn, B. M., and Chan, L. (2002). Increased intracellular calcium transients by calmodulin antagonists differentially modulate tumor necrosis factor-α-induced E-selectin and ICAM-1 expression. *Atherosclerosis* 165, 5–13. doi:10.1016/s0021-9150(01)00768-7

Daiber, A., Xia, N., Steven, S., Oelze, M., Hanf, A., Kroller-Schon, S., et al. (2019). New therapeutic implications of endothelial nitric oxide synthase (eNOS) function/dysfunction in cardiovascular disease. *Int. J. Mol. Sci.* 20 (1), 187. doi:10.3390/ijms20010187

de Martin, R., Hoeth, M., Hofer-Warbinek, R., and Schmid, J. A. (2000). The transcription factor NF-κB and the regulation of vascular cell function. *Arterioscler. Thromb. Vasc. Biol.* 20, E83–E88. doi:10.1161/01.atv.20.11.e83

Deisseroth, K. (2011). Optogenetics. *Nat. Methods* 8, 26–29. doi:10.1038/nmeth.f.324

Deisseroth, K. (2015). Optogenetics: 10 years of microbial opsins in neuroscience. *Nat. Neurosci.* 18, 1213–1225. doi:10.1038/nn.4091

Doniger, S. W., Salomonis, N., Dahlquist, K. D., Vranizan, K., Lawlor, S. C., and Conklin, B. R. (2003). MAPPFinder: using gene ontology and GenMAPP to create a global gene-expression profile from microarray data. *Genome Biol.* 4, R7. doi:10.1186/gb-2003-4-1-r7

Erdogan, A., Schaefer, M. B., Kuhlmann, C. R., Most, A., Hartmann, M., Mayer, K., et al. (2007). Activation of Ca^{2+} -activated potassium channels is involved in lysophosphatidylcholine-induced monocyte adhesion to endothelial cells. *Atherosclerosis* 190, 100–105. doi:10.1016/j.atherosclerosis.2006.02.035

Esch, E. W., Bahinski, A., and Huh, D. (2015). Organs-on-chips at the frontiers of drug discovery. *Nat. Rev. Drug Discov.* 14, 248–260. doi:10.1038/nrd4539

Fan, Z., Turiel, G., Ardicoglu, R., Ghobrial, M., Masschelein, E., Kocijan, T., et al. (2021). Exercise-induced angiogenesis is dependent on metabolically primed ATF3/4^{+} endothelial cells. *Cell Metab.* 33, 1793–1807.e9. doi:10.1016/j.cmet.2021.07.015

Forstermann, U., Pollock, J. S., Schmidt, H. H., Heller, M., and Murad, F. (1991). Calmodulin-dependent endothelium-derived relaxing factor/nitric oxide synthase activity is present in the particulate and cytosolic fractions of bovine aortic endothelial cells. *Proc. Natl. Acad. Sci. U. S. A.* 88, 1788–1792. doi:10.1073/pnas.88.5.1788

Forstermann, U., Xia, N., and Li, H. (2017). Roles of vascular oxidative stress and nitric oxide in the pathogenesis of atherosclerosis. *Circ. Res.* 120, 713–735. doi:10.1161/CIRCRESAHA.116.309326

Fukuda, N., Matsuda, T., and Nagai, T. (2014). Optical control of the Ca^{2+} concentration in a live specimen with a genetically encoded Ca^{2+}-releasing molecular tool. *ACS Chem. Biol.* 9, 1197–1203. doi:10.1021/cb400849n

Goudy, J., Henley, T., Mendez, H. G., and Bressan, M. (2019). Simplified platform for mosaic *in vivo* analysis of cellular maturation in the developing heart. *Sci. Rep.* 9, 10716. doi:10.1038/s41598-019-47009-7

Hamblin, M. R. (2017). Mechanisms and applications of the anti-inflammatory effects of photobiomodulation. *AIMS Biophys.* 4, 337–361. doi:10.3934/biophy.2017.3.337

Hamblin, M. R. (2018). Mechanisms and mitochondrial redox signaling in photobiomodulation. *Photochem Photobiol.* 94, 199–212. doi:10.1111/php.12864

Hughes, J. P., Rees, S., Kalindjian, S. B., and Philpott, K. L. (2011). Principles of early drug discovery. *Br. J. Pharmacol.* 162, 1239–1249. doi:10.1111/j.1476-5381.2010.01127.x

Inoue, K., and Xiong, Z. G. (2009). Silencing TRPM7 promotes growth/proliferation and nitric oxide production of vascular endothelial cells via the ERK pathway. *Cardiovasc Res.* 83, 547–557. doi:10.1093/cvr/cvp153

Inoue, K., Zama, T., Kamimoto, T., Aoki, R., Ikeda, Y., Kimura, H., et al. (2004). TNFalpha-induced ATF3 expression is bidirectionally regulated by the JNK and ERK pathways in vascular endothelial cells. *Genes Cells* 9, 59–70. doi:10.1111/j.1356-9597.2004.00707.x

Inoue, K., Branigan, D., and Xiong, Z. G. (2010). Zinc-induced neurotoxicity mediated by transient receptor potential melastatin 7 channels. *J. Biol. Chem.* 285, 7430–7439. doi:10.1074/jbc.M109.040485

Inoue, K., Furukawa, T., Kumada, T., Yamada, J., Wang, T., Inoue, R., et al. (2012). Taurine inhibits K^{+}-Cl^{-} cotransporter KCC2 to regulate embryonic Cl^{-} homeostasis via with-no-lysine (WNK) protein kinase signaling pathway. *J. Biol. Chem.* 287, 20839–20850. doi:10.1074/jbc.M111.319418

Inoue, K., Xiong, Z. G., and Ueki, T. (2020). The TRPM7 channel in the nervous and cardiovascular systems. *Curr. Protein Pept. Sci.* 21, 985–992. doi:10.2174/1389203721666200605170938

Ishii, T., Sato, K., Kakumoto, T., Miura, S., Touhara, K., Takeuchi, S., et al. (2015). Light generation of intracellular Ca^{2+} signals by a genetically encoded protein BACCS. *Nat. Commun.* 6, 8021. doi:10.1038/ncomms9021

Ishimitsu, T., Tsukada, K., Minami, J., Ono, H., and Matsuoka, H. (2003). Variations of human adrenomedullin gene and its relation to cardiovascular diseases. *Hypertens. Res.* 26, S129–S134. doi:10.1291/hypres.26.s129

Itoh, Y., Ma, F. H., Hoshi, H., Oka, M., Noda, K., Ukai, Y., et al. (2000). Determination and bioimaging method for nitric oxide in biological specimens by diaminofluorescein fluorometry. *Anal. Biochem.* 287, 203–209. doi:10.1006/abio.2000.4859

Jabs, A., Fasola, F., Muxel, S., Munzel, T., and Gori, T. (2010). Ischemic and non-ischemic preconditioning: Endothelium-focused translation into clinical practice. *Clin. Hemorheol. Microcirc.* 45, 185–191. doi:10.3233/CH-2010-1297

Keifer, O., Kambara, K., Lau, A., Makinson, S., and Bertrand, D. (2020). Chemogenetics a robust approach to pharmacology and gene therapy. *Biochem. Pharmacol.* 175, 113889. doi:10.1016/j.bcp.2020.113889

Kielbassa-Schnepp, K., Strey, A., Janning, A., Missiaen, L., Nilius, B., and Gerke, V. (2001). Endothelial intracellular Ca^{2+} release following monocyte adhesion is required for the transendothelial migration of monocytes. *Cell Calcium* 30, 29–40. doi:10.1054/ceca.2001.0210

Kruger-Genge, A., Blocki, A., Franke, R. P., and Jung, F. (2019). Vascular endothelial cell biology: an update. *Int. J. Mol. Sci.* 20 (4411), 4411. doi:10.3390/ijms20184411

Lee, F. K., Lee, J. C., Shui, B., Reining, S., Jibilian, M., Small, D. M., et al. (2021). Genetically engineered mice for combinatorial cardiovascular optobiology. *eLife* 10, e67858. doi:10.7554/eLife.67858

Leonard, A., Paton, A. W., El-Quadi, M., Paton, J. C., and Fazal, F. (2014). Preconditioning with endoplasmic reticulum stress ameliorates endothelial cell inflammation. *PLoS One* 9, e110949. doi:10.1371/journal.pone.0110949

Li, J., Cubbon, R. M., Wilson, L. A., Amer, M. S., McKeown, L., Hou, B., et al. (2011). Orai1 and CRAC channel dependence of VEGF-activated Ca^{2+} entry and endothelial tube formation. *Circ. Res.* 108, 1190–1198. doi:10.1161/CIRCRESAHA.111.243352

Li, S., Ning, H., Ye, Y., Wei, W., Guo, R., Song, Q., et al. (2017). Increasing extracellular Ca^{2+} sensitizes TNF-alpha-induced vascular cell adhesion molecule-1 (VCAM-1) via a TRPC1/ERK1/2/NFκB-dependent pathway in human vascular endothelial cells. *Biochim. Biophys. Acta Mol. Cell Res.* 1864, 1566–1577. doi:10.1016/j.bbamcr.2017.06.001

Liu, Q., Moller, U., Flugel, D., and Kietzmann, T. (2004). Induction of plasminogen activator inhibitor I gene expression by intracellular calcium via hypoxia-inducible factor-1. *Blood* 104, 3993–4001. doi:10.1182/blood-2004-03-1017

Lorenz-Fonfria, V. A., and Heberle, J. (2014). Channelrhodopsin unchained: Structure and mechanism of a light-gated cation channel. *Biochim. Biophys. Acta* 1837, 626–642. doi:10.1016/j.bbabio.2013.10.014

Ma, G., Wen, S., He, L., Huang, Y., Wang, Y., and Zhou, Y. (2017). Optogenetic toolkit for precise control of calcium signaling. *Cell Calcium* 64, 36–46. doi:10.1016/j.ceca.2017.01.004

Ma, J., Pichavant, C., du Bois, H., Bhakta, M., and Calos, M. P. (2017). DNA-mediated gene therapy in a mouse model of limb girdle muscular dystrophy 2B. *Mol. Ther. Methods Clin. Dev.* 7, 123–131. doi:10.1016/j.omtm.2017.10.005

Martin, J. B., Young, J. L., Benoit, J. N., and Dean, D. A. (2000). Gene transfer to intact mesenteric arteries by electroporation. *J. Vasc. Res.* 37, 372–380. doi:10.1159/000025753

McCabe, T. J., Fulton, D., Roman, L. J., and Sessa, W. C. (2000). Enhanced electron flux and reduced calmodulin dissociation may explain "calcium-independent" eNOS activation by phosphorylation. *J. Biol. Chem.* 275, 6123–6128. doi:10.1074/jbc.275.9.6123

Moccia, F., Tanzi, F., and Munaron, L. (2014). Endothelial remodelling and intracellular calcium machinery. *Curr. Mol. Med.* 14, 457–480. doi:10.2174/1566524013666131118113410

Montesano, R., Pepper, M. S., Mohle-Steinlein, U., Risau, W., Wagner, E. F., and Orci, L. (1990). Increased proteolytic activity is responsible for the aberrant morphogenetic behavior of endothelial cells expressing the middle T oncogene. *Cell* 62, 435–445. doi:10.1016/0092-8674(90)90009-4

Munaron, L. (2006). Intracellular calcium, endothelial cells and angiogenesis. *Recent Pat. Anticancer Drug Discov.* 1, 105–119. doi:10.2174/157489206775246502

Niwa, H., Yamamura, K., and Miyazaki, J. (1991). Efficient selection for high-expression transfectants with a novel eukaryotic vector. *Gene* 108, 193–199. doi:10.1016/0378-1119(91)90434-d

Ohkura, M., Sasaki, T., Sadakari, J., Gengyo-Ando, K., Kagawa-Nagamura, Y., Kobayashi, C., et al. (2012). Genetically encoded green fluorescent Ca^{2+} indicators with improved detectability for neuronal Ca^{2+} signals. *PLoS One* 7, e51286. doi:10.1371/journal.pone.0051286

Ong, P., Athanasiadis, A., Borgulya, G., Mahrholdt, H., Kaski, J. C., and Sechtem, U. (2012). High prevalence of a pathological response to acetylcholine testing in patients with stable angina pectoris and unobstructed coronary arteries. The ACOVA Study (Abnormal COronary VAsomotion in patients with stable angina and unobstructed coronary arteries). *J. Am. Coll. Cardiol.* 59, 655–662. doi:10.1016/j.jacc.2011.11.015

Ong, P., Athanasiadis, A., Borgulya, G., Vokshi, I., Bastiaenen, R., Kubik, S., et al. (2014). Clinical usefulness, angiographic characteristics, and safety evaluation of intracoronary acetylcholine provocation testing among 921 consecutive white patients with unobstructed coronary arteries. *Circulation* 129, 1723–1730. doi:10.1161/CIRCULATIONAHA.113.004096

Ouma, G. O., Rodriguez, E., Muthumani, K., Weiner, D. B., Wilensky, R. L., and Mohler, E. R., 3rd (2014). *In vivo* electroporation of constitutively expressed HIF-1α plasmid DNA improves neovascularization in a mouse model of limb ischemia. *J. Vasc. Surg.* 59, 786–793. doi:10.1016/j.jvs.2013.04.043

Pollock, J. S., Forstermann, U., Mitchell, J. A., Warner, T. D., Schmidt, H. H., Nakane, M., et al. (1991). Purification and characterization of particulate endothelium-derived relaxing factor synthase from cultured and native bovine aortic endothelial cells. *Proc. Natl. Acad. Sci. U. S. A.* 88, 10480–10484. doi:10.1073/pnas.88.23.10480

Rafikov, R., Fonseca, F. V., Kumar, S., Pardo, D., Darragh, C., Elms, S., et al. (2011). eNOS activation and NO function: structural motifs responsible for the posttranslational control of endothelial nitric oxide synthase activity. *J. Endocrinol.* 210, 271–284. doi:10.1530/JOE-11-0083

Rasanen, M., Sultan, I., Paech, J., Hemanthakumar, K. A., Yu, W., He, L., et al. (2021). VEGF-B promotes endocardium-derived coronary vessel development and cardiac regeneration. *Circulation* 143, 65–77. doi:10.1161/CIRCULATIONAHA.120.050635

Rios, F. J., Zou, Z. G., Harvey, A. P., Harvey, K. Y., Nosalski, R., Anyfanti, P., et al. (2020). Chanzyme TRPM7 protects against cardiovascular inflammation and fibrosis. *Cardiovasc Res.* 116, 721–735. doi:10.1093/cvr/cvz164

Rutanen, J., Puhakka, H., and Yla-Herttuala, S. (2002). Post-intervention vessel remodeling. *Gene Ther.* 9, 1487–1491. doi:10.1038/sj.gt.3301866

Salnikow, K., Kluz, T., Costa, M., Piquemal, D., Demidenko, Z. N., Xie, K., et al. (2002). The regulation of hypoxic genes by calcium involves c-Jun/AP-1, which cooperates with hypoxia-inducible factor 1 in response to hypoxia. *Mol. Cell Biol.* 22, 1734–1741. doi:10.1128/MCB.22.6.1734-1741.2002

Schneider, G. (2018). Automating drug discovery. *Nat. Rev. Drug Discov.* 17, 97–113. doi:10.1038/nrd.2017.232

Smolenski, A. (2012). Novel roles of cAMP/cGMP-dependent signaling in platelets. *J. Thromb. Haemost.* 10, 167–176. doi:10.1111/j.1538-7836.2011.04576.x

Sun, H., Leng, T., Zeng, Z., Gao, X., Inoue, K., and Xiong, Z. G. (2013). Role of TRPM7 channels in hyperglycemia-mediated Injury of vascular endothelial cells. *PLoS One* 8, e79540. doi:10.1371/journal.pone.0079540

Toda, K., Tsujioka, K., Maruguchi, Y., Ishii, K., Miyachi, Y., Kuribayashi, K., et al. (1990). Establishment and characterization of a tumorigenic murine vascular endothelial cell line (F-2). *Cancer Res.* 50, 5526–5530.

Tong, L., Hill, R. A., Damisah, E. C., Murray, K. N., Yuan, P., Bordey, A., et al. (2021). Imaging and optogenetic modulation of vascular mural cells in the live brain. *Nat. Protoc.* 16, 472–496. doi:10.1038/s41596-020-00425-w

Urban, D. J., and Roth, B. L. (2015). DREADDs (designer receptors exclusively activated by designer drugs): chemogenetic tools with therapeutic utility. *Annu. Rev. Pharmacol. Toxicol.* 55, 399–417. doi:10.1146/annurev-pharmtox-010814-124803

Weksler, B. B., Ley, C. W., and Jaffe, E. A. (1978). Stimulation of endothelial cell prostacyclin production by thrombin, trypsin, and the ionophore A23187. *J. Clin. Invest.* 62, 923–930. doi:10.1172/JCI109220

Wu, B. M., Leng, T. D., Inoue, K., Li, J., and Xiong, Z. G. (2017). Effect of redox-modifying agents on the activity of Channelrhodopsin-2. *CNS Neurosci. Ther.* 23, 216–221. doi:10.1111/cns.12662

Wynne, B. M., Chiao, C. W., and Webb, R. C. (2009). Vascular smooth muscle cell signaling mechanisms for contraction to Angiotensin II and Endothelin-1. *J. Am. Soc. Hypertens.* 3, 84–95. doi:10.1016/j.jash.2008.09.002

Young, J. L., and Dean, D. A. (2015). Electroporation-mediated gene delivery. *Adv. Genet.* 89, 49–88. doi:10.1016/bs.adgen.2014.10.003

Zahler, S., Kupatt, C., and Becker, B. F. (2000). Endothelial preconditioning by transient oxidative stress reduces inflammatory responses of cultured endothelial cells to TNF-alpha. *FASEB J.* 14, 555–564. doi:10.1096/fasebj.14.3.555

Zeng, Z., Inoue, K., Sun, H., Leng, T., Feng, X., Zhu, L., et al. (2015). TRPM7 regulates vascular endothelial cell adhesion and tube formation. *Am. J. Physiol. Cell Physiol.* 308, C308–C318. doi:10.1152/ajpcell.00275.2013

Zhao, Y., Vanhoutte, P. M., and Leung, S. W. (2015). Vascular nitric oxide: Beyond eNOS. *J. Pharmacol. Sci.* 129, 83–94. doi:10.1016/j.jphs.2015.09.002

frontiers | Frontiers in Pharmacology

TYPE Original Research
PUBLISHED 29 March 2023
DOI 10.3389/fphar.2023.1146276

OPEN ACCESS

EDITED BY
Yan Huang,
Anhui Medical University, China

REVIEWED BY
Xuan Qin,
Baylor College of Medicine, United States
Soon Yew Tang,
University of Pennsylvania, United States

*CORRESPONDENCE
Meijuan Fang,
fangmj@xmu.edu.cn

†These authors have contributed equally to this work

SPECIALTY SECTION
This article was submitted to Inflammation Pharmacology, a section of the journal Frontiers in Pharmacology

RECEIVED 17 January 2023
ACCEPTED 15 March 2023
PUBLISHED 29 March 2023

CITATION
Fang H, Cao Y, Zhang J, Wang X, Li M, Hong Z, Wu Z and Fang M (2023), Lipidome remodeling activities of DPA-EA in palmitic acid-stimulated HepG2 cells and the *in vivo* anti-obesity effect of the DPA-EA and DHA-EA mixture prepared from algae oil. *Front. Pharmacol.* 14:1146276. doi: 10.3389/fphar.2023.1146276

Lipidome remodeling activities of DPA-EA in palmitic acid-stimulated HepG2 cells and the *in vivo* anti-obesity effect of the DPA-EA and DHA-EA mixture prepared from algae oil

Hua Fang[1†], Yin Cao[2†], Jianyu Zhang[2], Xiumei Wang[2], Mengyu Li[1,3], Zhuan Hong[1], Zhen Wu[2] and Meijuan Fang[2*]

[1]Technical Innovation Center for Utilization of Marine Biological Resources, Third Institute of Oceanography, Ministry of Natural Resources, Xiamen, China, [2]Fujian Provincial Key Laboratory of Innovative Drug Target Research and State Key Laboratory of Cellular Stress Biology, School of Pharmaceutical Sciences, Xiamen University, Xiamen, China, [3]College of Ocean Food and Biological Engineering, Jimei University, Xiamen, China

Background: The nuclear receptor Nur77 has been demonstrated to play a vital role in the inflammatory response and cellular metabolisms, and its ligands exhibit efficacy in the treatment of inflammation-related diseases (e.g., improving mouse acute lung injury (ALI) and obesity. Recently, ω-3 polyunsaturated fatty acid-ethanolamine derivatives (ω-3 PUFA-EAs), including DPA-EA and DHA-EA, have been reported as new Nur77-targeting anti-inflammatory agents. However, the lipid-lowering effect of ω-3 PUFA-EAs is still unknown, and lipid profile changes induced by Nur77-targeting anti-inflammatory agents also remain unclear.

Objective: This study aimed to evaluate the lipid-lowering effect and the underlying mechanism of DPA-EA acting as Nur77-targeting anti-inflammatory agents. It also aimed to investigate the *in vitro* and *in vivo* lipid-lowering effects of the DPA-EA and DHA-EA mixture prepared from algae oil.

Methods: The *in vitro* lipid-lowing effect of DPA-EA and its mixture with DHA-EA was first evaluated in palmitic acid-stimulated HepG2 Cells. To confirm the lipid-lowering effect and explore the underlying mechanism, we performed untargeted lipidomic analysis using ultra-performance liquid chromatography/triple quadrupole-time-of-flight (TOF) mass spectrometry coupled with multivariate statistical analysis, with another Nur77-targeting anti-inflammatory compound Celastrol (Cel) as a reference. Finally, we examined the anti-obesity effect of the DPA-EA and DHA-EA mixture synthesized from algae oil in a high-fat diet (HFD)-fed mice model.

Results: DPA-EA significantly alleviated lipid accumulation with lower toxicity than Celastrol. Nur77-targeting compounds DPA-EA and Celastrol could simultaneously reduce 14 lipids (9 TGs, 2 PCs, 1 PA, 1 SM, and 1 LacCer) and increase 13 lipids (4 DGs, 6 LPEs, 2 PEs, and 1PC) in Pal-stimulated HepG2 cells. However, Cer lipids were more sensitive to DPA-EA, while the over-downregulation of SM lipids might be associated with the off-target toxicity of Celastrol. The mixture of DPA-EA and DHA-EA synthesized from algae oil could significantly decrease TG, TC, and LDL levels and increase HDL levels in HFD-fed mice, exerting an excellent anti-obesity effect.

Conclusion: Nur77-targeting anti-inflammatory compound DAP-EA could promote the hydrolysis of PEs and TGs to ameliorate lipid accumulation. The DPA-EA and DHA-EA mixture prepared from algae oil might be a potential therapeutic agent for obesity and other inflammation-related diseases.

KEYWORDS

DPA-EA, lipidomics, anti-inflammation, anti-obesity, biomarker

1 Introduction

Obesity is a complex disease involving abnormal or excessive fat accumulation in subcutaneous and/or organs. Increasing evidence suggests that obesity is a causative factor in developing many chronic inflammation-related diseases (Wang et al., 2018), including non-alcoholic fatty liver disease (NAFLD), cardiovascular disease, type 2 diabetes, colitis, cancer, *etc.* Nowadays, obesity and its complications have become a social health problem affecting the quality of life and even threatening life (Rana et al., 2007). It is demonstrated that excess macronutrients in adipose tissue can stimulate the release of inflammatory mediators such as tumor necrosis factor-alpha (TNF-α) and interleukin 6 (IL-6) (Ellulu et al., 2017). In the high-fat diet (HFD)-induced liver disease, high liver enzyme levels in the blood and liver fat accumulation indicate that prolonged mild inflammation is always associated with obesity (Kim et al., 2012). Overall, obesity is characterized as a state of chronic inflammation in adipose tissue mediated by the secretion of a range of inflammatory cytokines. On the other hand, extracts or compounds from plants with potent anti-inflammatory activity also have significant anti-obesity effects. For instance, fermented lemon peel exhibited an anti-obesity effect on HFD-induced obese mice by modulating the inflammatory response (Pan et al., 2022). Maize extract rich in ferulic acid and anthocyanins prevents HFD-induced obesity in mice by modulating Sirtuin 1 (SIRT1)/AMP-activated protein kinase (AMPK)/IL-6 associated metabolic and inflammatory pathways (Luna-Vital et al., 2020). Hakka stir-fried tea produces anti-obesity and anti-inflammation effects on HFD-induced obese mice model *via* activating the AMPK/acetyl-CoA carboxylase (ACC)/carnitine palmitoyltransferase 1 (CPT1) pathway (Li Q. et al., 2020). All these studies suggest that anti-inflammatory substances have significant lipid-lowering effects and can effectively prevent or improve obesity.

Nur77 is a member of the nuclear receptor subfamily 4A (NR4A) subfamily, which can negatively regulate inflammation and has been identified as a promising therapeutic target for treating inflammation-related diseases (Li et al., 2015). Recently, Nur77 has been demonstrated to play a vital role in cellular metabolisms such as lipid metabolism and glucose metabolism (Deng et al., 2022). For instance, adenovirus-mediated liver-specific Nur77 overexpression accounts for the decrease of triglyceride (TG) and high-density lipoprotein (HDL) levels and the increase of low-density lipoprotein (LDL) levels. Additionally, Nur77 overexpression inhibits the lipogenic transcription factor, sterol regulatory element-binding transcription factor 1c (SREBF-1c) (Pols et al., 2008). Increased expression of Nur77 also reduces macrophage-derived foam cell formation and hepatic lipid deposition, accompanied by downregulation of gene levels of inflammatory molecules, adhesion molecules, and intestinal lipid absorption (Hu et al., 2014). In contrast, Nur77 knockdown increases susceptibility to HFD-induced obesity (Chen et al., 2015). Besides, the liver tissue of Nur77-null mice can accumulate more TGs than wild-type mice (Chao et al., 2009). In particular, Celastrol, a previously reported Nur77 modulator, can not only inhibit acute liver inflammation and chronic inflammation in obese animals (Hu et al., 2017) but also ameliorate NAFLD by decreasing lipid synthesis and improving the anti-oxidative and anti-inflammatory status *via* SIRT1(Zhang et al., 2017). Together, Nur77 serves as a vital therapeutic target in inflammation-related diseases, and its protective effect on improving obesity has been confirmed. Nur77-targeting anti-inflammatory agents may be an effective strategy for improving obesity and its related diseases. However, lipid profile changes induced by anti-inflammatory compounds targeting Nur77 in the lipid-lowering process remain unclear.

Unsaturated fatty acids (UFAs) have broad and critical biological functions (Calder, 2017), (Menegaut et al., 2019). Among them, polyunsaturated fatty acids (PUFA), which can only get from food, are healthy fatty acids that the body needs for brain function and cell growth. Nowadays, much attention has been given to the ω-3 polyunsaturated fatty acids (ω-3 PUFAs), a series of representative natural products with anti-inflammatory and anti-obesity activities. ω-3 PUFAs can affect intracellular signal transduction by elevating the ratio of eicosapentaenoic acid (EPA) and docosahexaenoic acid (DHA) in the cell membrane and inhibiting the transcriptional activity of the inflammation-related transcription factor NF-κB, thereby reducing the pro-inflammatory cytokine TNF-α, IL-6, and interleukin 8 (IL-8) expression (Schumann and Fuhrmann, 2010). Also, ω-3 PUFA can stimulate neutrophils and macrophages to secrete anti-inflammatory cytokines such as interleukin 10 (IL-10), interleukin 4 (IL-4), and interleukin 13 (IL-13) to reduce the inflammatory response (de Bus et al., 2019). Besides,ω-3 PUFAs have been demonstrated to alleviate HFD-induced obesity in mice by reducing adipose tissue cellularity (Ruzickova et al., 2005). Importantly, DHA, an ω-3 PUFA, has been identified as an endogenous lipid reported to bind to Nur77 (Fang et al., 2020). In our recent work, ω-3 polyunsaturated fatty acid-ethanolamine (PUFA-EA) derivatives such as docosahexaenoic acid-ethanolamine (DHA-EA), eicosapentaenoic acid-ethanolamine (EPA-EA), and docosapentaenoic acid-ethanolamine (DPA-EA) were identified as excellent anti-inflammatory agents targeting Nur77 (Fang et al., 2020). Notably, the representative compound DPA-EA (4 k) was demonstrated to bind to Nur77 (TR3) and exerted a Nur77-dependent anti-inflammatory effect through the NF-κB pathway (Fang et al., 2020). To explore the lipid profile changes induced by the anti-inflammatory compounds targeting Nur77, DPA-EA was selected to assess the lipid-lowering effect and

underlying mechanism, with Celastrol as a reference compound. Furthermore, given that PUFA-EAs exhibited excellent anti-inflammatory activity and algae oil was a plant-based source of ω-3 PUFA widely used as a dietary supplement, the ω-3 PUFA-EA mixture was synthesized by the reaction of algae oil with ethanolamine under free-solvent condition and evaluated for the potential anti-obesity effect on the HFD-induced obese mice model and the acute toxicity in mice.

2 Materials and methods

2.1 Reagents and chemicals

DPA-EA was obtained as our previously reported (Fang et al., 2020). Algae oil, composed of 16.23% DHA and 5.22% DPA, was purchased from Xiamen Kingdomway Group Company (Fujian, China). High-performance liquid chromatography (HPLC) grade methanol was purchased from Sigma Aldrich (St. Louis, MO, United States). The HFD was obtained from Nanjing University of Chinese Medical Animal Center, with the composition of 40.56% corn starch, 7.78% wheat meal, 20.23% fish meal, 14.56% oil, 2.33% bone meal, 1.79% yeast powder, 1.39% salt, 0.16% vitamin, 10% egg yolk powder, and 1.2% cholesterol. The mouse IL-6 enzyme-linked immunosorbent assay (ELISA) kit and TNF-α ELISA kit were purchased from DAKEWE (DAKEWE, China). Interleukin-1β (IL-1β) and TNF-α antibodies were purchased from Abcam (Abcam, Cambridge, UK). The kits of TG, TC, LDL cholesterol (LDL-C), and HDL cholesterol (HDL-C) were purchased from Beijing North Kangtai clinical Reagent Co., Ltd., Beijing, China. Saline was prepared as a 0.9% NaCl solution. Griess reagent was purchased from Beyotime (Beyotime, Shanghai, China). MTT (3-(4,5-dimethylthiazol-2-yl)-2,5-diphenyltetrazolium bromide) was purchased from Beyotime (Beyotime, Shanghai, China). Lipopolysaccharide (LPS) was purchased from Sigma (Sigma, St. Louis, MO, United States). Other reagents used in this study were purchased from the domestic market and were all analytically pure and used without further purification.

2.2 MTT assay

HepG2 cells were obtained from the American Type Culture Collection (United States) and were cultured in Dulbecco's Modified Eagle Medium (DMEM) (Hyclone, Logan, Utah, United States) supplemented with 10% FBS, 100 U/mL penicillin, and 100 mg/mL streptomycin at 37°C with 5% CO_2. MTT assay was performed according to the previously described (Fang et al., 2020). HepG2 cells were seeded at 4.5×10^3 cells per well into 96-well plates and incubated overnight; celastrol or DPA-EA with indicated concentrations was prepared and added to each well, respectively. Following drug treatment for 24 h, 20 μL of MTT solution (5 mg/mL) was added to each well, and the cells were incubated for 4 h at 37°C. Then, the solution containing MTT was removed, and 150 μL of dimethyl sulfoxide was added per well to dissolve the formazan. Finally, the absorbance of the solution was measured at 490 nm (OD490) using a UV spectrophotometer (Model 3555, Thermo). Cell viability was calculated from three independent experiments. The average density of the control group (1‰ DMSO) was set as 100% of viability. Cell viability (%) = compound (OD490)/blank (OD490)×100%. Finally, the IC_{50} value was obtained with Graphpad Prism 8.0.

2.3 Lipid accumulation observation

HepG2 cells were inoculated into the 12-well plate at a cell density of 3.0×10^5/well, and small slides were pre-placed in the bottom of each well in the 12-well plate before inoculating the cells for cell crawling. Cells were adhered overnight, pretreated with 1‰ DMSO or selected compounds at different concentrations for 2 h, and then stimulated with 200 μM palmitic acid (Pal). After 24 h treatment, the supernatant medium was discarded, and the cells were stained with Oil Red O. We detected Pal-induced lipid accumulation in HepG2 cells using the Oil Red O stain kit (ACMEC, AG1262-4).

2.4 Lipidomics analysis in HepG2 cell model

2.4.1 Cell sample collection

HepG2 cells were inoculated at ~10^6 cells per well in a 10 cm plate and cultured in DMEM for 20 h. The cells in control groups were only treated with 1‰ DMSO. The cells in Pal, Pal+DPA-EA, and Pal+Cel groups were pretreated with 1‰ DMSO, 10 mM DPA-EA, and 2 mM Celastrol for 2h, respectively, then stimulated with 200 μM Pal. After 24 h treatment, the supernatant medium was discarded, and the cells were quickly washed with ice-cold PBS three times, digested with trypsin (HyClone, United States), and performed cell count. After the supernatant was discarded, the pretreat HepG2 cell samples for Control, Pal, Pal + DPA-EA, and Pal + Cel groups (n = 7) were quenched with the following buffer (8.5 g/L NH_4HCO_3, 60% MeOH, pH = 7.4). Next, the quenched cell samples were collected by centrifugation (12,000 rpm, 5 min, 4°C) and stored at −80°C before lipid extraction.

2.4.2 Lipid extraction

The extract buffer (methyl tert-butyl ether (MTBE) : methanol = 5: 1, 480 μL) containing internal standard was added to the samples, then frozen and thawed with liquid nitrogen for 3 times. Next, the cell samples were sonicated for 10 min in an ice-water bath, incubated at −40°C for 1 h, and centrifuged at 3000 rpm for 15 min at 4°C. Approximately 350 μL of supernatant was transferred to a fresh tube and dried in a vacuum concentrator at 37°C. Subsequently, the dried samples were reconstituted in 100 μL of 50% methanol in dichloromethane by sonication for 10 min in the ice-water bath. The constitution was then centrifuged at 13,000 rpm for 15 min at 4°C, and 80 μL of supernatant was transferred to a fresh glass vial for LC/MS analysis. The quality control (QC) sample was prepared by mixing an equal aliquot of the supernatants from all of the samples and was used to evaluate the stability and reproducibility of the analytes detected in the analytical run. The lipid extraction experiment was done by Biotree Biotech Co., Ltd (Shanghai, China).

2.4.3 Lipid detection by UPLC-HRMS/MS

The UPLC separation was conducted using a 1290 Infinity series UPLC System (Agilent Technologies), equipped with a Kinetex C18 column (2.1 * 100 mm, 1.7 μm, Phenomen). The mobile phase

was a combination of solvent A (40% water, 60% acetonitrile supplemented with 10 mmol/L ammonium formate) and solvent B (10% acetonitrile, 90% isopropanol added with 5% 10 mmol/L ammonium formate). The analysis was carried out with a linear gradient as follows: 0–12.0 min, 40%–100% B; 12.0–13.5 min, 100% B; 13.5–13.7 min, 100%–40% B; 13.7–18.0 min, 40% B. The column temperature was 45°C. The auto-sampler temperature was 4°C, and the injection volume was 0.5 μL in positive mode or 2 μL in negative mode. The Triple TOF mass spectrometer (Triple TOF 6600, ABsciex) was used for its ability to acquire MS/MS spectra on an information-dependent basis (IDA) during an LC/MS experiment. In each cycle, 12 precursor ions with the strongest intensities above 100 were chosen for MS/MS at collision energy of 45 eV. ESI source conditions were set as follows: Gas 1: 60 psi, Gas 2: 60 psi, Curtain Gas: 30 psi, Source Temperature as 600°C, Declustering potential as 100 V, Ion Spray Voltage Floating (ISVF) as 5,000 V or −4,500 V in positive or negative modes, respectively. Full scan was conducted along with the MS/MS and the *m/z* scan range was set as 200–2,000. The UPLC-HRMS/MS analysis was assisted by Biotree Biotech Co., Ltd (Shanghai, China).

2.4.4 Data preprocessing and annotation

The raw data files (.wiff format) were converted to files in mzXML format with ProteoWizard. XCMS was applied for retention time correction, peak identification, peak extraction, peak integration, and peak alignment with minfrac set to 0.5 and cutoff set to 0.6. Lipid identification was performed using XCMS-based software, a self-written R package, and a self-built lipid secondary database. Furthermore, all processed peak areas of lipid substances (see Supplementary Data S1) were imported into SIMCA-P14.1 software (Umetrics) for multivariate statistical analysis, including principal component analyses (PCA), orthogonal projections to latent structures discriminate analysis (OPLS-DA), and permutation tests. Lipid substances with a VIP value > 1.0 in the OPLS-DA model and a *p*-value <0.05 in the Student's t-test were considered important differential biomarkers for discriminating each group.

2.5 The preparation of the PUFA-EA mixture from algae oil

The DPA-EA and DHA-EA mixture was prepared as described in Supplementary Scheme S1. Algae oil (100.0 g) and ethanolamine (15.0 g) were added to a round bottom flask (250 mL) without any solvent. The reaction mixture was stirred for 24 h at 80°C, which was purified by silica gel column chromatography (petroleum ether/ethyl acetate 1:1) to give PUFA-EA mixture as pale yellow oil (14.1 g). The reverse phase HPLC (C18, methanol/H_2O = 90:10) analysis indicated that the mixture contained 67.54% of DHA-EA (tR = 6.58 min) and 27.96% of DPA-EA (tR = 7.65 min), respectively (Supplementary Scheme S1 and Supplementary Figure S1).

2.6 Anti-inflammatory evaluation in RAW264.7 cells

Mouse RAW 264.7 macrophages were obtained from the American Type Culture Collection (United States). Cells were treated with DPA-EA, DHA-EA and EPA-EA with the concentration of 10 μM and PUFA-EA with gradient dose from 20 to 2.5 μM. The experiments, including NO production assay, Real-Time Quantitative PCR, and Western blot Analysis, were performed as described previously (Fang et al., 2020).

2.7 Determination of anti-obesity activity *in vivo*

In total, 40 ICR (male/female = 1:1, 18–22 g) mice were obtained from Nanjing University of Chinese Medical Animal Center. The animal room was maintained at 22°C ± 2°C and humidity-controlled 55% ± 5% with a 12-h light and 12-h dark cycle. After a 3-day acclimatization period, feeding with a standard rat diet, forty mice were divided randomly into four groups (male/female = 1:1): The normal diet (ND) group was the normal control in which mice were fed with a standard rat diet. The HFD group was the model group in which mice were fed with an HFD. The HFD + ORL group was the positive control group in which mice were fed an HFD and intragastric administration with Orlistat (ORL) at 0.468 g/kg daily. The HFD + PUFA-EA group was a treatment group in which mice were fed with an HFD and intragastric administration with algae oil-derived PUFA-EA mixture at 0.167 g/kg daily. Drugs were intragastrically administered as a suspension in 0.5% carboxymethyl cellulose for 36 consecutive days. The ND and HFD groups were administered only the 0.5% carboxymethyl cellulose vehicle. The food and water were available *ad libitum* during the 6-week administration. This experiment was performed in compliance with the Chinese legislation on the use and care of laboratory animals and was approved by the Experimental Animals Ethics Committee of Nanjing University of Chinese Medicine (No. 201906A012).

2.8 Determination of serum biomarkers

The serum levels of TG, TC, LDL-C, and HDL-C were measured enzymatically with commercial assay kits. TC content was determined with the total cholestenone content assay kit (Solarbio, BC 1985), and TG was measured with a triglyceride content detection kit (Solarbio, BC0625). The assay kits of LDL-C and HDL-C were BC5335 and BC5325 from Solarbio, respectively. The results were expressed as mmol/L. All analytical procedures follow the essay kit's instructions and are replicated at least three times.

2.9 Morphological analysis of hepatic tissue

Liver samples removed from mice were fixed overnight with 4% paraformaldehyde. Fixed tissues were embedded in paraffin, sliced into 3 μm pieces, and stained with hematoxylin and eosin (H&E). The stained areas were viewed using an optical microscope (Olympus CX31, Tokyo, Japan) with a magnifying power of ×200.

2.10 Acute toxicity study in mice

Acute toxicity studies were carried out according to OECD Test Guidelines. The C57BL/6 mice used (8–10 weeks old and 18–20 g) were provided by the Animal Experiment Center of Xiamen University,

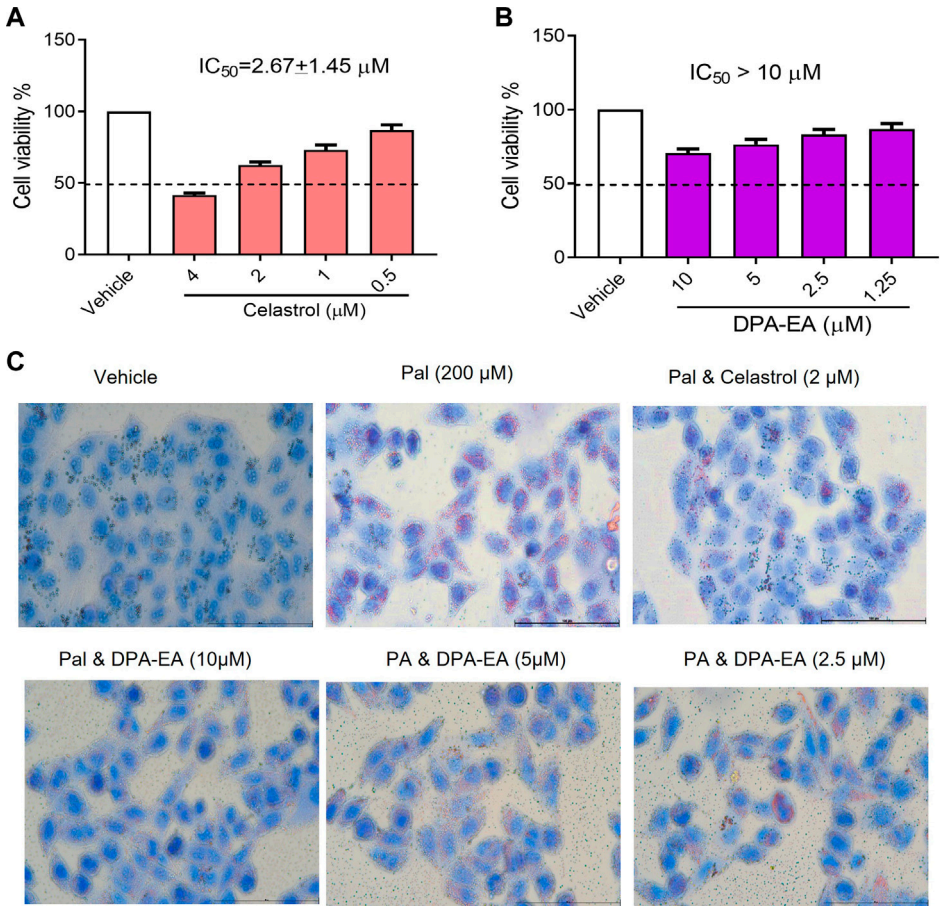

FIGURE 1
Effects of Celastrol and DPA-EA on cell viability and lipid droplets in HepG2 cells. **(A)** Effects of Celastrol at different concentrations (0.5, 1, 2, and 4 μM) on the cell growth of HepG2. **(B)** Effects of DPA-EA at different concentrations (1.25, 2.5, 5, and 10 μM) on the cell growth of HepG2 cells. **(C)** Effects of DPA-EA and Celastrol at indicating concentrations on formation of lipid droplets in Pal-induced (200 μM) HepG2 cells with Oil red staining assay. Images were captured with a microscope (200×).

Fujian, China. After the mice were adaptively reared in the animal room for 5 days, the mice (20 males and 20 females) were randomly divided into four groups (control mice: male (10), female (10). Mice treated by PUFA-EA: male (10) and female (10)). The 0.6 mL (540 mg) PUFA-EA was intragastrically administrated as suspension in 0.5% carboxymethyl cellulose twice a day for 14 days consecutively in the treatment group, and the control group was intragastrically administrated with 0.6 mL saline. The maximum tolerated dose is calculated as 540 × 2/0.02 = 54,000 mg/kg. Mice had free access to distilled water and commercial standard diets. Feeding behaviors such as food intake and drinking water were measured daily. General appearances (spirit, skin, fur, eyes, nose, respiration, urine, feces, and locomotor) were observed daily. This experiment was performed in compliance with Chinese legislation on the use and care of laboratory animals. This animal experiment was approved by the animal care and use committee of Xiamen University (XmuLAC 20200029).

2.11 Statistical analysis

All assays were performed in triplicate. The result's data were expressed as mean ± SD (standard deviation). Other data were analyzed by the SPSS statistical software, version 18.0 (SPSS Inc., United States). Student's t-test was used as specified in the figure legends. $P < 0.05$ was considered statistically significant (*), $p < 0.01$ as highly significant (**), $p < 0.001$ as extremely significant (***), and ns as not significant.

3 Results

3.1 Evaluation of the lipid-lowering activity of Nur77 modulators in Pal-stimulated HepG2 cells

NAFLD is a common inflammation-related disease. Its occurrence is mainly due to the body's metabolic disorders, along with the accumulation of liver fat in the body. Nur77 plays diverse and vital roles in regulating lipid metabolism and emerges as a hot therapeutic target for metabolic diseases (Chao et al., 2009). Celastrol has been reported to be a modulator of Nur77 and exerts anti-inflammation, lipidome remodeling, and weight-losing function (Zhang et al., 2017; Wang et al., 2021). Interestingly, we have demonstrated that PUFA-EAs such as DPA-EA and DHA-EA

exert excellent anti-inflammation activities in a Nur77-dependent manner (Fang et al., 2020). Herein, we constructed an adipose hepatocyte model by Pal-induced HepG2 lipid accumulation to detect the lipid-lowering activity of DPA-EA, with Celastrol as a reference compound. The cytotoxicity of DPA-EA and Celastrol against HepG2 cells was first tested using the MTT assay. DPA-EA at 10 μM reduced cell growth to 71.7% (Figure 1A), exhibiting low cell growth inhibition toward HepG2 (IC_{50} > 10 μM). Celastrol displayed noticeable cytotoxic activity with an IC_{50} value of 2.67 μM (Figure 1B). Then, the effect of DPA-EA and Celastrol on lipid accumulation was observed under a microscope using an oil-red O staining experiment. The results are shown in Figure 1C and Supplementary Figure S2. Pal significantly caused lipid accumulation in HepG2 because an apparent increase of red oil droplets was observed under the microscope. Celastrol treatment decreased red oil droplets, confirming the lipid-lowering effects of Celastrol (Liu et al., 2015). Also, DPA-EA attenuated Pal-induced lipid accumulation in HepG2, with a dose-dependent reduction in red lipid droplets. In contrast, DPA-EA at 10 and 5 μM showed better lipid-lowering effects than celastrol at 4 μM, with considerably lower cytotoxicity (Figure 1 and Supplementary Figure S2). These results suggested that DPA-EA might be an effective lipid-lowering compound with lower cytotoxicity than Celastrol.

3.2 Perturbation of DPA-EA and celastrol on the lipid profile of pal-induced HepG2 cells

3.2.1 Raw mass spectrometry data preprocessing

The experimental groups were set as followings: untreated hepatocyte group (Ctrl group); Pal-stimulated HepG2 group (Pal group); Pal-stimulated HepG2 cells with DPA-EA intervention (Pal + DPA-EA group); and Pal-stimulated HepG2 cells with Celastrol administration (Pal + Cel group). The lipid metabolites in each group were examined using UHPLC-QTOF-MS technology. After baseline filtering, peak recognition and integration, retention time correction, peak alignment, and normalization to an internal standard (IS), we detected a total of 21 major lipids, including TG, diacylglycerol (DG), monoglyceride (MG), cholesteryl ester (CE), phosphatidylcholine (PC), phosphatidylethanolamine (PE), phosphatidic acid (PA), phosphatidylinositol (PI), phosphatidylserine (PS), phosphatidylglycerol (PG), lysophosphatidylcholine (LPC), Lysophosphatidylethanolamines (LPE), lysophosphatidylinositol (LPI), lysophosphatidylserine (LysoPS), lysophosphatidic acid (LPA), lysophosphatidylglycerol (LPG), ceramide (Cer), glucosylceramide (GlcCer), lactosylceramide (LacCer), sphingomyelin (SM), and sphingosine (Sph) in HepG2 cells. Besides, 990 and 711 lipids were detected in the positive and negative ion patterns, respectively. The QC procedures showed good reproducibility of the collected data in the positive and negative ion modes (Supplementary Figures S3A, B). Besides, PCA models demonstrated the excellent aggregation of QC samples (Supplementary Figures S3C, D), suggesting the stable instrument state and high reliability of the experimental data.

3.2.2 The differential lipid metabolite profile of HepG2 cells under Pal stimulation

The processed MS data were imported into SIMCA 14.0 software (Umetrics) for multivariate pattern recognition analysis. The PCA analysis showed that all samples were within the 95% confidence interval in both positive and negative ion modes, and significant existed differences between the Ctrl and the Pal groups (Supplementary Table S1 and Supplementary Figures S4A, B). To maximize the distinction between the Ctrl and Pal groups, OPLS-DA analysis was also executed for the collected data in positive and negative ion modes, respectively. It can be observed that there was a significant lipid metabolism change between the Ctrl and Pal groups (Supplementary Figures S5A, B), and the corresponding model parameters were in the effective range (Table 1). These results indicated that Pal stimulation caused significant alterations in the lipid profile of HepG2 hepatocytes. According to $p < 0.05$ and VIP >1, we first picked out 571 and 363 differential-expressed lipids (DELs) in the positive and negative ion modes, respectively (Supplementary Table S2). Totally, Pal stimulation in HepG2 cells led to 865 DELs. Most of them (563) were upregulated. Using the fold change (FC) value of >2 as a cutoff, we found that Pal significantly upregulated the expression of 310 lipids, including TG (103), PC (34), Cer (32), PE (20), *etc* (Supplementary Table S4, Figures 2A, B). Notably, TG (12:0/16:0/14:1), TG (12:0/14:0/14:1), TG (12:0/16:1/14:1), Cer(d18:1)/18:0) and SM (d14:1/20:0) were significantly elevated in Pal-stimulated HepG2 cells (Figures 2A, B), with the fold change indices (Pal/Ctrl) of 61.13, 56.33, 37.54, 28.75, and 19.46, respectively. These results were consistent with lipid droplet accumulation in Pal-stimulated HepG2 cells. Additionally, we found 302 Pal-downregulated DELs. Using the FC value of <1/2 as a cutoff, we observed that Pal could significantly downregulate the expression of 71 lipids involved in 21 lipid species of six classes, in which glycerophospholipids (GPs) were identified as the most species (58), such as PC (36) and PS (13) (Supplementary Table S3 and Figures 2C, D). Especially, PC (O-20:2/17:0), PC (2:0/15:0), PS (4:0/26:0), and PS (18:1/24:1) expressions were significantly downregulated (Figures 2A, B), with the FC values of 0.20, 0.26, 0.22 and 0.28, respectively. Interestingly, several DGs were also observed with a robust reduction, especially DG (26:1/18:1/0:0) and DG (24:1/18:1/0:0) with corresponding FC indices of 0.24 and 0.28 (Figures 2A, B).

3.2.3 Lipid profile's perturbation by Nur77 modulators in Pal-induced fatty liver HepG2 cells

3.2.3.1 Celastrol-induced lipidomics changes in Pal-stimulated HepG2 cells

Celastrol is a well-known Nur77 modulator with an excellent weight-loss effect in HFD-fed mice (Hu et al., 2017). Also, our oil-red O staining experiment showed that Celastrol decreased Pal-induced lipid accumulation in HepG2 cells. Therefore, we treated Pal-stimulated HepG2 cells with Celastrol for 24 h and then performed lipidomics analysis to explore whether Celastrol could reprogram the hepatic lipidome. PCA score plots indicated significant differences in lipid profiles between the Pal + Cel and Pal groups in the positive and negative ion modes (Supplementary Table S2, Supplementary Figures S4C, D), suggesting that Celastrol intervention could significantly alter the lipid profile of Pal-stimulated HepG2 cells. Next, we performed an OPLS-DA analysis to gain further insight into global lipid alterations (Supplementary Figures S5C, D). Two separate multivariate

TABLE 1 Corresponding values of R^2X, R^2Y, and Q^2 of OPLS-DA models.

No.	Description	Ion mode	N	R^2X (cum)	R^2Y (cum)	Q^2 (cum)	R^2Y - Q^2
1	Ctrl, Pal, Pal + DPA-EA, and Pal + Cel	(+)	28	0.774	0.988	0.972	0.016
		(−)	28	0.783	0.980	0.961	0.019
2	Pal vs. Ctrl	(+)	14	0.683	0.994	0.980	0.014
		(−)	14	0.741	0.980	0.968	0.012
3	Pal + Cel vs. Pal	(+)	14	0.672	0.992	0.969	0.023
		(−)	14	0.689	0.987	0.963	0.024
4	Pal + DPA-EA vs. Pal	(+)	14	0.630	0.996	0.977	0.019
		(−)	14	0.659	0.989	0.963	0.026

Ctrl, Control group; Pal: Pal-induced HepG2 group; Pal + Cel: Pal-stimulated HepG2 cells with Celastrol administration; Pal + DPA-EA: Pal-stimulated HepG2 cells with DPA-EA, intervention. *Vs, versus*.

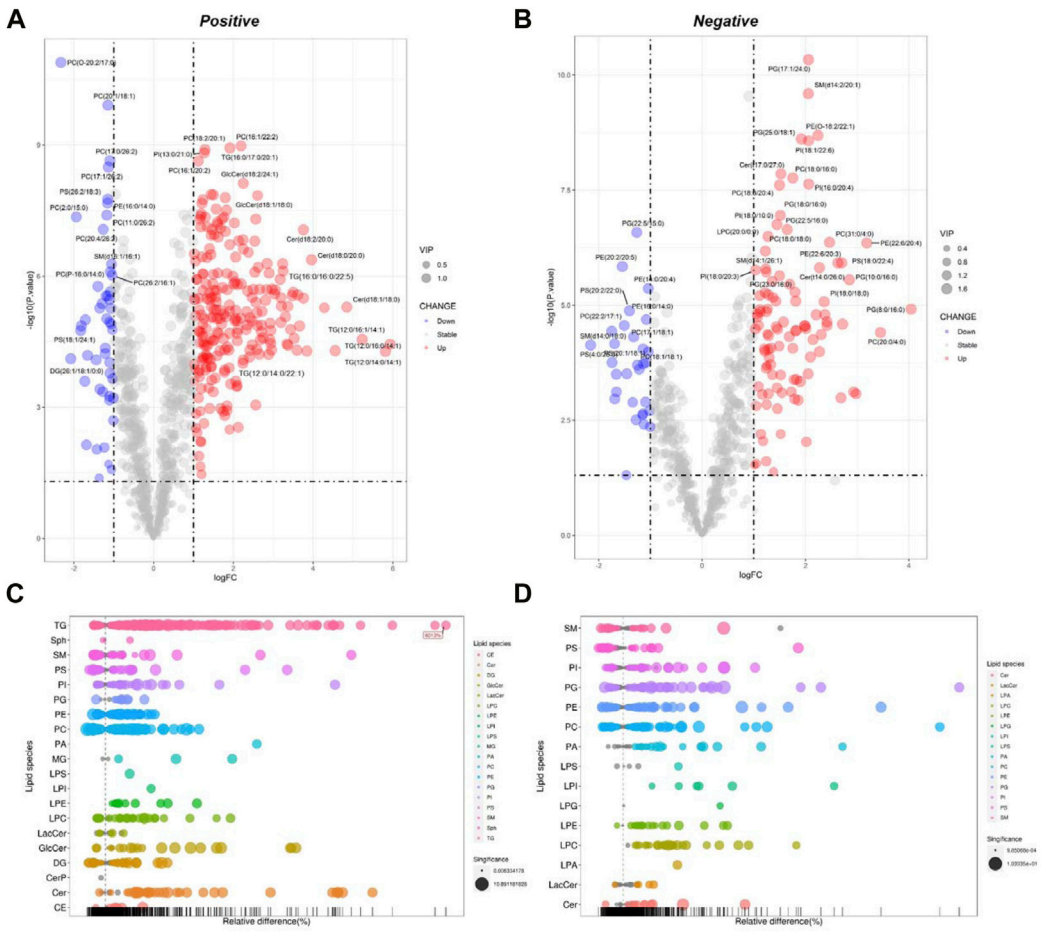

FIGURE 2
Analysis of significantly differential lipid substances in the Pal group *versus* the Ctrl group. Volcano plots **(A,B)** and lipid plots **(C,D)** in both positive and negative ion modes, respectively. In the volcano plot, lipid species were screened out based on the criteria of $p < 0.05$, VIP≥1, and fold change <0.5 or >2.

OPLS-DA models of Pal + Cel and Pal groups were generated for the positive and negative ion patterns. Their relevant validation parameters all satisfied $R^2Y > 0.9$, $Q^2 > 0.9$, and $R^2Y - Q^2 < 0.2$, indicating a faithful representation of the data and a good predictive ability of the models (Table 1). The good separations of the Pal and Pal + Cel groups in both models implied that Celastrol could alleviate lipid metabolism disorders to a certain extent. According to $p < 0.05$ and VIP >1, we picked out 469 and 326 DELs between the

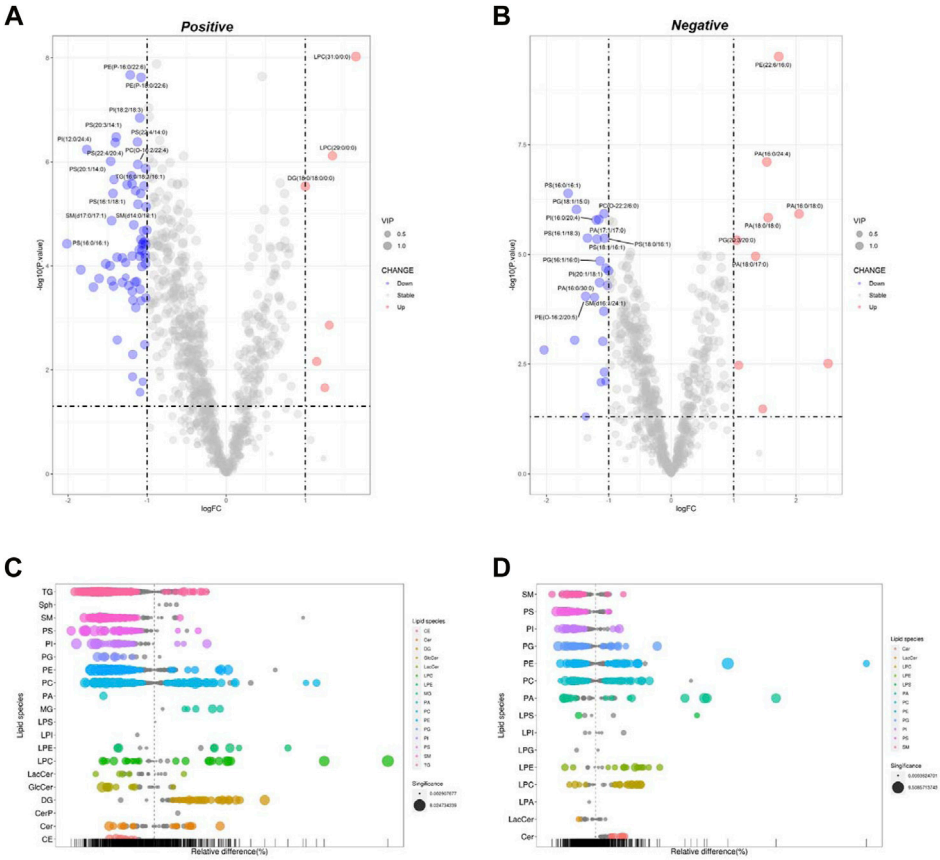

FIGURE 3
Analysis of significantly differential lipid substances in the Pal + Cel group *versus* the Pal group. Volcano plots **(A,B)** and lipid plots **(C,D)** in both positive and negative ion modes, respectively. In the volcano plot, lipid species were screened out based on the criteria of $p < 0.05$, VIP≥1, and fold change <0.5 or >2.

Pal + Cel and Pal groups in the positive and negative ion modes, respectively (Supplementary Table S2). In total, Celastrol administration in Pal-stimulated HepG2 cells led to 722 DELs. Notably, Celastrol could significantly decrease 78 lipids (FC < 1/2) in Pal-stimulated HepG2 cells, mainly including TG (23), PC (11), PI (11), SM (11), PS (9), et al. (Supplementary Table S3, Figures 3A–D). Typically, Celastrol downregulated PS(16:0/16:1), TG (16:1/16:1/16:1), PI(12:0/24:4), TG (12:0/14:0/14:1), and TG (14:0/16:1/16:1) with the FC indices of 0.24, 0.27, 0.29, 0.31 and 0.32, respectively. Meanwhile, the expression levels of 15 lipids significantly increased (FC > 2) in the Pal + Cel group compared to the Pal group (Supplementary Table S3, Figures 3A, B). Significantly, Celastrol administration elevated the contents of LPC(31:0/0:0), LPC(29:0/0:0), PE (5:0/18:0), and PA (16:0/18:0) with the FC indices of 3.11, 2.54, 5.71, and 4.14, respectively.

3.2.3.2 DPA-EA-induced lipidomics changes in Pal-stimulated HepG2 cells

DPA-EA is a potent anti-inflammatory compound targeting Nur77 that we previously reported (Fang et al., 2020). Furthermore, we also demonstrated that DPA-EA could alleviate Pal-induced lipid accumulation in HepG2 cells. Therefore, we treated Pal-stimulated HepG2 cells with DPA-EA for 24 h and analyzed the interference of DPA-EA on lipidomics profiling of Pal-stimulated HepG2 cells to understand the lipid-lowering mechanism of DPA-EA comprehensively. First, two separate sample clusters, which corresponded to the Pal and Pal + DPA-EA groups, were observed in PCA score plots of positive and negative modes (Supplementary Table S1, Supplementary Figures S4E, F). It signified that DPA-EA might have a significant improvement effect on Pal-induced HepG2 cells at the lipid level. Then, the supervised OPLS-DA models were further constructed to capture the distinctive metabolic phenotypes and to maximize the discrimination between the Pal and Pal + DPA-EA groups. As shown in Table 1 and Supplementary Figures S5E, F, the Pal + DPA-EA group was discriminated from the Pal group with $R^2Y > 0.9$, $Q^2 > 0.9$, and $R^2Y\text{-}Q^2 < 0.2$ in both OPLS-DA models of positive and negative modes. It suggested that DPA-EA could reprogram the lipid profile in Pal-stimulated HepG2 cells. Based on VIP >1.0 and $p < 0.05$, 705 DELs were identified between the Pal + DPA-EA and Pal groups (Supplementary Table S2). Compared with the Pal group, 45 lipids were significantly decreased (FC < 1/2), and 61 lipids were significantly elevated (FC > 2) in the Pal + DPA-EA group (Supplementary Table S4, Figures 4A–D). For example, DPA-EA

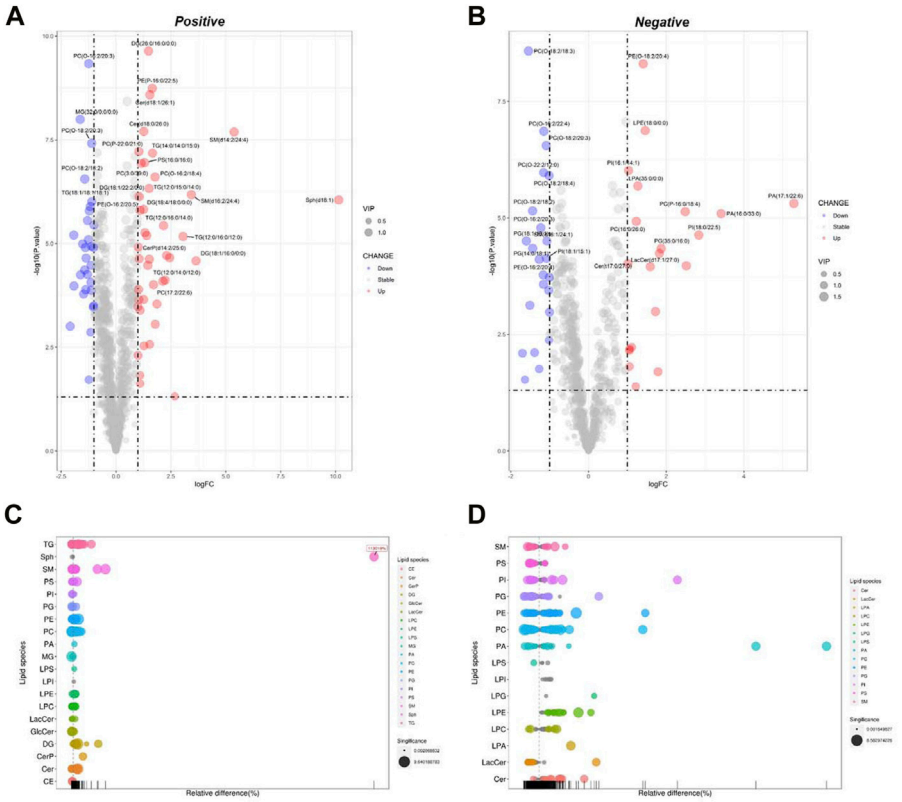

FIGURE 4
Analysis of significantly differential lipid substances in the Pal + DPA-EA group *versus* the Pal group. Volcano plots **(A,B)** and lipid plots **(C,D)** in both positive and negative ion modes, respectively. In the volcano plot, lipid species were screened out based on the criteria of $p < 0.05$, VIP≥1, and fold change <0.5 or >2.

could significantly reduce the levels of PC(O-18:2/18:3), GlcCer(d18:1/18:0), TG (16:1/16:1/16:1), and TG (16:1/16:1/18:1), with the FC indices of 0.23, 0.26, 0.26, and 0.32, respectively. Meanwhile, DPA-EA robustly increased some lipids such as Sph (d18:1), SM(d14:2/24:4), SM(d16:2/24:4), and PA (17:1/22:6), with the FC indices of 1131.19, 41.59, 10.79, and 39.03, respectively.

3.2.4 Comparison of lipidomics prfile changes caused by DPA-EA and celastrol on Pal-induced fatty liver HepG2 cells

DPA-EA and Celastrol are two Nur77-targeting anti-inflammatory compounds with prominent lipid-lowering activities (Fang et al., 2020). However, DPA-EA showed lower toxicity, while Celastrol had apparent off-target toxicity (Wang et al., 2011). Celastrol and DPA-EA might activate other targets besides Nur77. Therefore, we performed PCA and OPLS-DA analysis among four groups. The Pal + DPA-EA and Pal + Cel groups partially overlapped in PCA analysis (Supplementary Figures S4G, H), hinting that lipid profiles reprogrammed by DPA-EA and Celastrol were part in common. However, the sample clusters of the Pal + DPA-EA group and Pal + Cel group were significantly separated in both positive and negative OPLS-DA score plots (Figures 5A, B). The same DELs caused by DPA-EA and Celastrol interventions may be associated with their Nur77-targeting lipid-lowering effect. In contrast, the different DELs may be caused due to their targeting of other proteins.

3.2.4.1 The same DELs caused by DPA-EA and Celastrol interventions

Between the two multivariate OPLS-DA models (Pal + Cel group vs. Pal group and Pal + DPA-EA group vs. Pal group), there were a total of 443 same DELs ($p < 0.05$ and VIP >1) (Supplementary Table S4). Among them, 272 lipids were simultaneously decreased by DPA-EA and Celastrol administrations (Supplementary Table S4). Notably, the levels of 14 lipids (9 TGs, 2 PCs, 1 PA, 1 SM, and 1 LacCer) were significantly reduced (compared with the PA group, FC < 0.5) both in the Pal + DPA-EA and Pal + Cel groups (Figures 5C, D). These 14 lipids were significantly increased in the Pal group (compared with the Ctrl group); these increases were markedly diminished by supplementation with DPA-EA and Celastrol. Most of these 14 lipids were TGs such as TG (16:1/16:1/16:1) and TG (16:0/16:1/16:1), implying that DPA-EA and Celastrol had the effect of improving lipid metabolism. Besides, DPA-EA and Celastrol could simultaneously upregulate 104 lipids in Pal-stimulated HepG2 cells, mainly concentrated in Cer, DG, PE and PC classes (Supplementary Table S4). Among them, 13 lipids (6 LPEs, 4 DGs, 2 PEs, and 1 PC) were remarkably increased (compared with the Pal

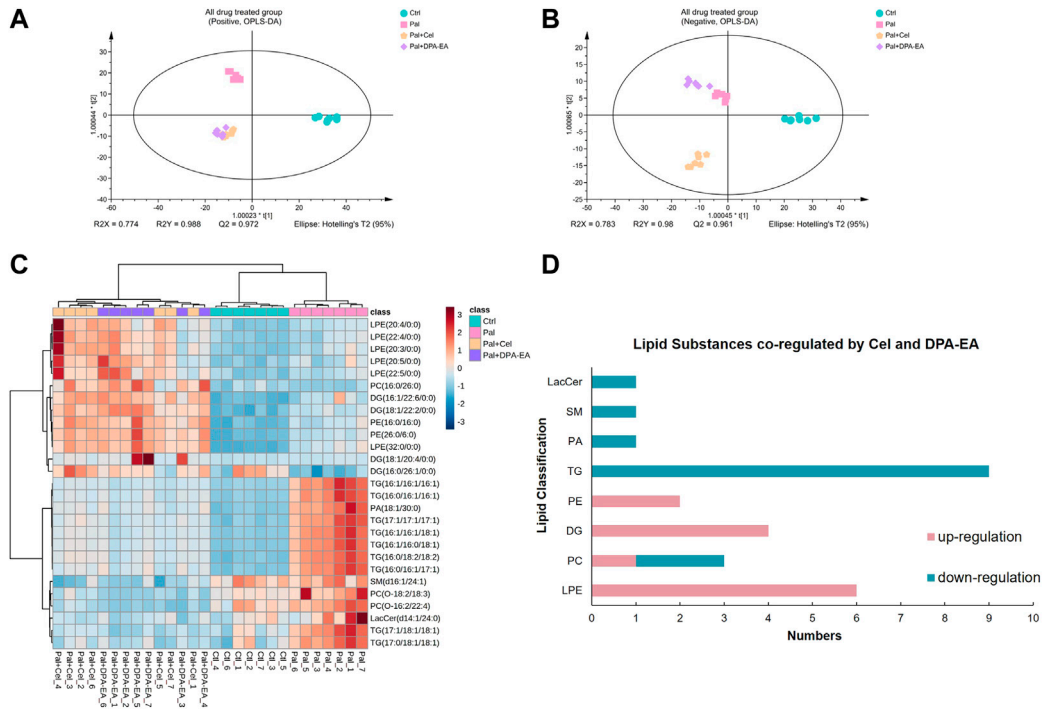

FIGURE 5
Analysis of significantly differential lipids in Ctrl, Pal, Pal + Cel, and Pal + DPA-EA groups. OPLS-DA score plots **(A,B)** in positive and negative ion modes, respectively. **(C)** Heatmap of common DELs in the Pal + Cel vs. Pal and Pal + DPA-EA vs. Pal models, selected with the fold change cutoff of FC > 1.5 or FC < 0.5 as upregulated and downregulated, respectively. Red and blue indicate increased and decreased lipids, respectively. **(D)** Classifications of the regulated lipid species.

group, FC > 1.6) in the Pal + DPA-EA and Pal + Cel groups (Figures 5C, D). Most of these 13 upregulated lipids were LPEs (*e.g.*, LPE (22:5/0:0) and LPE (32:0/0:0)) and DGs (*e.g.*, DG (18:1/20:4/0:0) and DG (16:1/26:1/0:0)). LPEs and DGs are the downstream hydrolysis products of PEs and TGs, respectively. Thus, our results indicated that the common lipid-lowering mechanism of DPA-EA and Celastrol might be by promoting the hydrolysis of esters, thereby reducing the level of esters and alleviating lipid accumulation.

3.2.4.2 The specific DELs caused by Celastrol intervention

A total of 722 DELs (VIP >1.0 and $p < 0.05$) were identified for the Pal + Cel group vs. Pal group model, in which 279 DELs could be attained only in the Pal + Cel group vs. Pal model but not in the Pal + DPA-EA vs. Pal model. Interestingly, 200 lipids were downregulated, and 79 lipids were on the contrary (Supplementary Table S5). Notably, 20 lipids were significantly decreased (compared with the Pal group, FC < 0.5), and 22 lipids were significantly increased (compared with the Pal group, FC > 1.6) in the Pal + Cel group (Figure 6). Most of these up- or downregulated DELs belonged to GP class such as PC, LPC, and PE (Figure 6). The first six downregulated lipids with the most significant differences (Pal + Cel group vs. Pal group model) were PI(16:0/20:3), PC(22:6/23:0), TG (14:0/16:0/16:1), PI(14:1/24:4), PC(15:0/16:0) and PC(14:1/28:0), and their average contents in the Pal + Cel group were similar to those in the Ctrl group. At the same time, PA (16:0/24:4), PA (18:0/17:0), LPC (22:5/0:0), PC(6:0/26:2), PC(2:0/16:1), and PG (20:3/20:0) levels were still significantly increased (compared with the Pal group) in the Pal + Cel group and well above those in the Ctrl group.

3.2.4.3 The specific DELs caused by DPA-EA intervention

A total of 705 DELs (VIP >1.0 and $p < 0.05$) were identified for the Pal + DPA-EA vs. Pal model. Besides the 443 co-regulated DELs, DPA-EA also individually upregulated 108 lipids (51 lipids with FC value > 1.6) and downregulated 154 lipids (13 lipids with FC value <0.5) (Supplementary Table S6). The 64 lipids with FC > 1.6 or FC < 0.5 were involved in 18 lipid types, including Cer, SM, TG, PE, PC, PG, PI, LPC *et al.* (Figure 7). The types of lipids specificly modulated by DPA-EA were much more than those only modulated by Celastrol (Figures 6, 7). The first six downregulated lipids (the Pal + DPA-EA group vs. Pal group model) were PC(17:1/20:5), PA (16:0/34:0), PC(O-16:2/22:2), PG (19:0/22:4), GlcCer(d18:1/22:1) and GlcCer(d18:1/22:0). Among them, the average contents of GlcCer(d18:1/22:1), PA (16:0/34:0), and PC(O-16:2/22:2) in the DPA-EA group were similar to those in the Ctrl group. However, the levels of most upregulated metabolites in the Pal + DPA-EA group were remarkably higher than in the Pal and Ctrl groups. Interestingly, DPA-EA administration significantly increased another six SMs and 9 TGs, while Celastrol significantly decreased another 4 SMs and 2 TGs. Different types of DELs and various change trends of the same DELs induced by Celastrol and

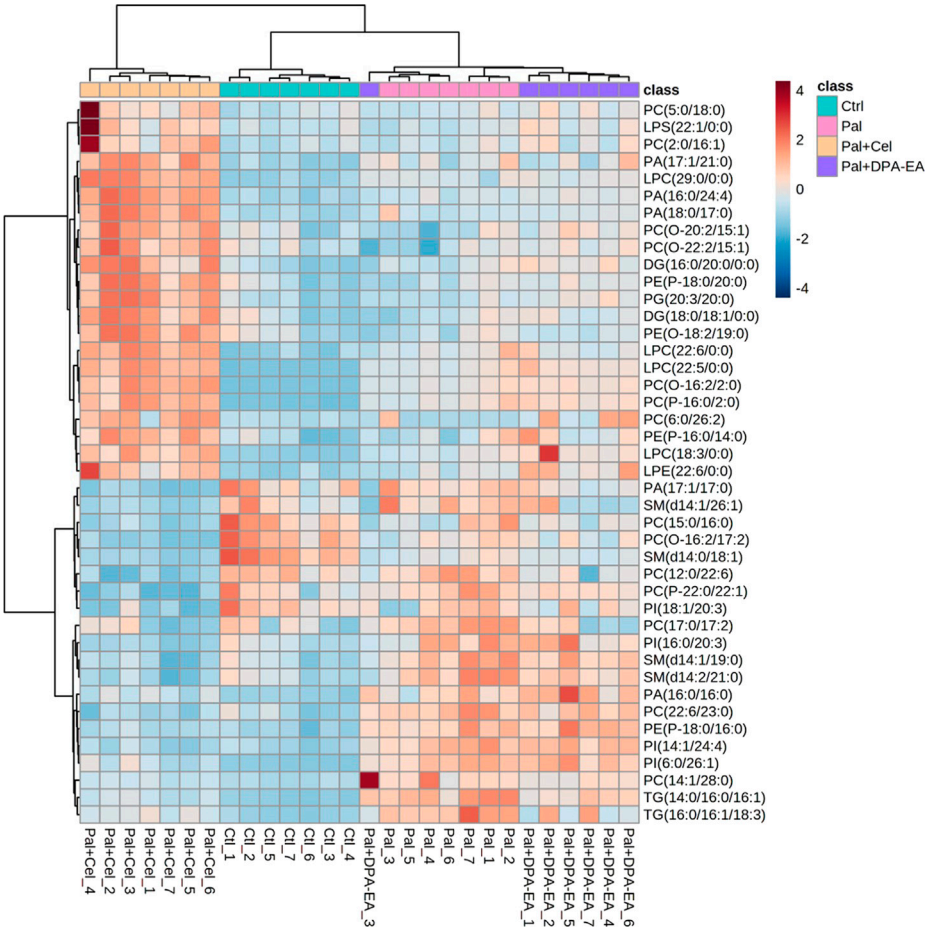

FIGURE 6
Heatmap of DELs only in the Pal + Cel vs. Pal model, not in the Pal + DPA-EA vs. Pal model, selected with the fold change cutoff of FC > 1.6 or FC < 0.5 as upregulated and downregulated, respectively. Red and blue indicate increased and decreased lipids, respectively.

DPA-EA suggested that they had different other potential mechanisms of action (Figures 6, 7).

Finally, several typical lipid metabolites were selected for further investigation. As depicted in Figure 8, trend clusters of eight significantly changed lipids were noted for comparative analysis. DPA-EA and Celastrol mainly reversed the Pal-induced upregulation of TG lipids, in which TG (16:1/16:1/16:1), TG (16:1/16:0/18:1), and TG (16:1/16:1/18:1) ranked as the three most significant lipid metabolites. Meanwhile, as for Pal-induced downregulated lipid metabolites, both DPA-EA and Celastrol significantly upregulated PCs, in which PC (26:1/16:1) and PC (16:0/26:2) were the two representative metabolites. These overlapped metabolites might be associated with their common target, Nur77. It was worth noting that DPA-EA and Celastrol also had different effects on lipidomics profile in Pal-induced fatty liver HepG2 cells. For example, DPA-EA significantly downregulated the expression of Cer (d18:1/18:0), but Celastrol had no significant effect on it. Also, we found that DPA-EA remarkably elevated sphingomyelin expressions such as Sph (d18:1) and SM (d16:2/24:4). However, Celastrol did not affect the levels of these two lipid metabolites. It might be attributed to their different additional targets.

3.3 The DPA-EA and DHA-EA mixture has a significant anti-inflammatory and anti-obesity effects with excellent safety properties

Our previous work demonstrated that ω-3 PUFA-EA derivatives such as DPA-EA, DHA-EA, and EPA-EA had excellent anti-inflammatory effects acting as Nur77 modulators (Fang et al., 2020). In the pre-part of this work, we further confirmed that the represented compound DPA-EA exhibited excellent lipid-lowering activities with lower toxicity than Celastrol. Moreover, lipidomics analysis revealed that DPA-EA could remodel lipid profile and improve lipid metabolism in the Pal-simulated HepG2 cell model. It suggested that anti-inflammatory Nur77-targeting compounds, DPA-EA and Celastrol, alleviated lipid accumulation by promoting the hydrolysis of PEs and TGs. Based on these

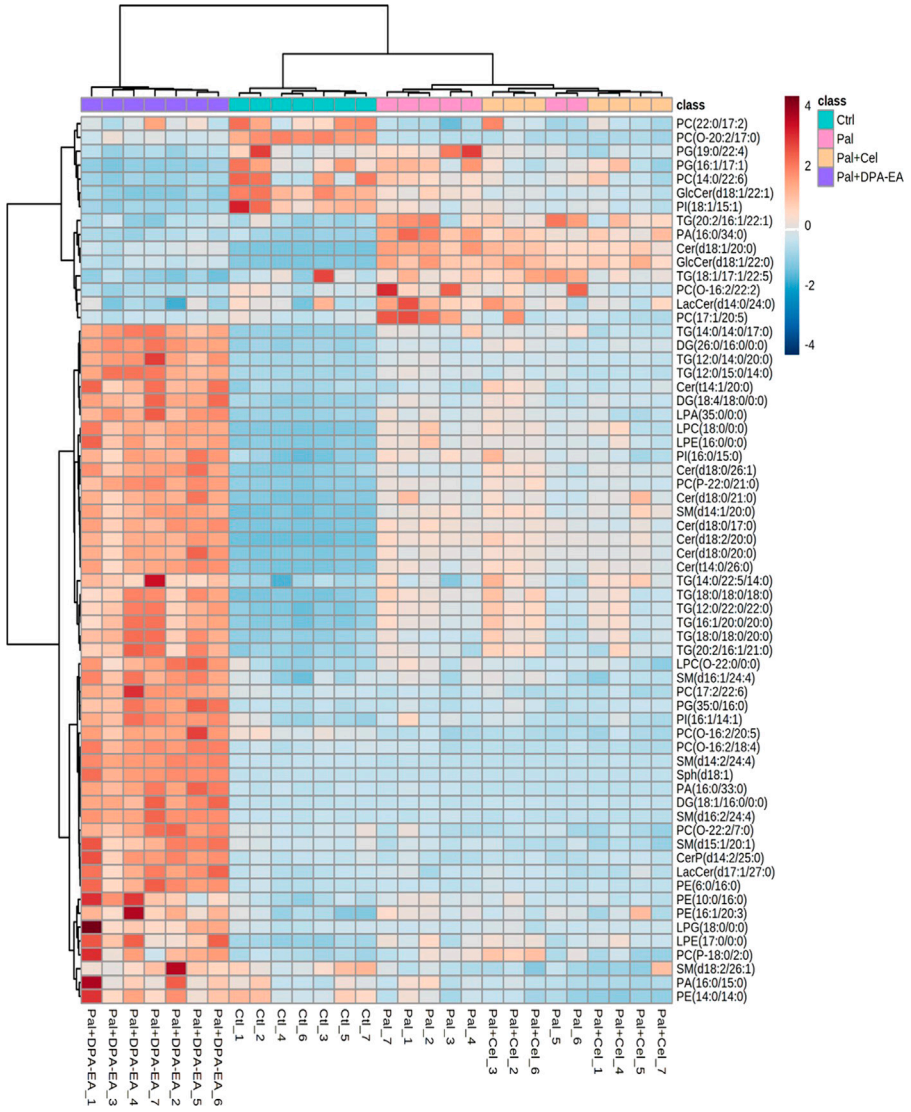

FIGURE 7
Heatmap of DELs only in the Pal + DPA-EA vs. Pal model, not in the Pal + Cel vs. Pal model, selected with the fold change cutoff of FC > 1.6 or FC < 0.5 as upregulated and downregulated, respectively. Red and blue indicate increased and decreased lipids in each group, respectively.

findings, we hypothesized the algae oil-derived PUFA-EA mixture (the DPA-EA and DHA-EA mixture) might also exert excellent anti-obesity effects like Celastrol but with low toxicity. Therefore, algal oil containing DHA (16.23%) and DPA (5.22%) was first reacted with ethanolamine without any solvents at 80°C for 24 h and then purified on a silica gel column to obtain the PUFA-EA mixture of DHA-EA (67.54%) and DPA-EA (27.96%) (Supplementary Scheme S1 and Supplementary Figure S1).

3.3.1 The anti-inflammatory activity of the PUFA-EA mixture

First, the synthesized PUFA-EA mixture was further evaluated for *in vitro* anti-inflammatory activity. As shown in Figures 9A–D, LPS treatment caused a dramatic increase in NO release and the expressions of pro-inflammatory cytokines IL-1β and IL-6 compared to control, while DPA-EA, DHA-EA, and the PUFA-EA mixture could significantly alleviate LPS-induced NO release and pro-inflammatory cytokine expressions at the concentration of 10 μM (Figures 9A–C). Also, the PUFA-EA mixture significantly reduced the protein expression of TNF-α and IL-1β induced by LPS in a dose-dependent manner (Supplementary Figure S6). These results implied that the PUFA-EA mixture exhibited anti-inflammatory activity like their monomer molecules (Figures 9A–C and Supplementary Figure S6). In addition, Oil red O staining further demonstrated that PUFA-EA had similar lipid-lowering

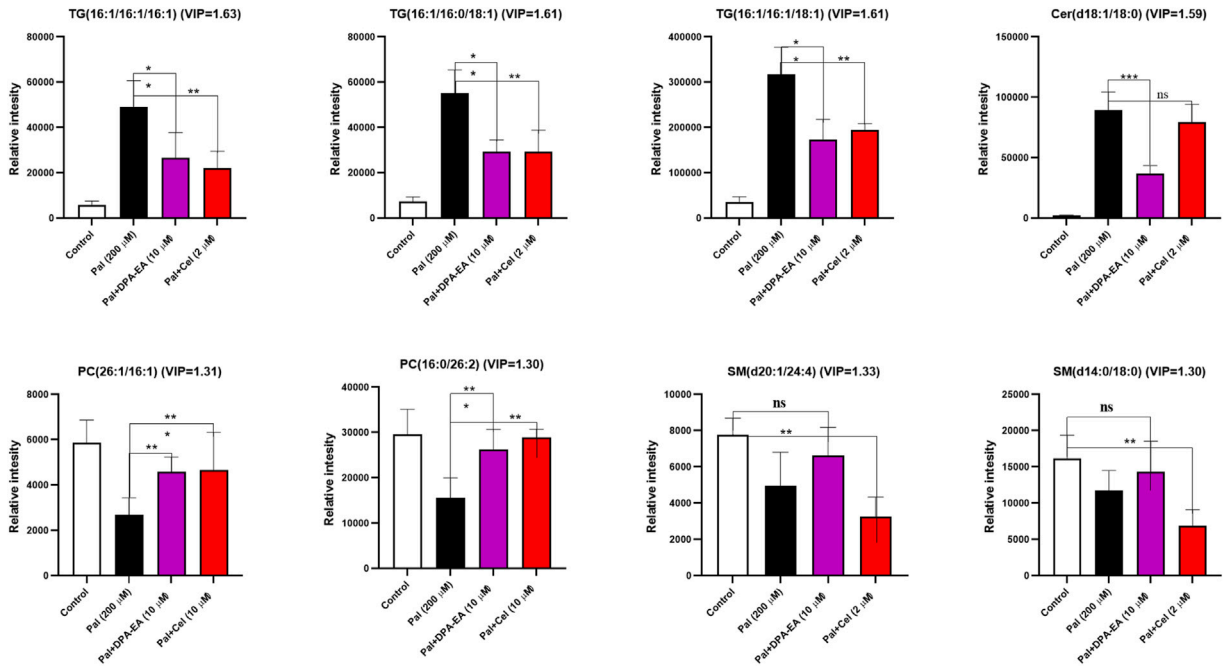

FIGURE 8
Several potential lipid biomarkers (FC ≥ 2 or ≤0.5; VIP ≥1) in response to the effects of DPA-EA and Celastrol on lipid metabolism. All data in the figure are shown as mean ± SD (n ≥ 3). Bars represent the standard deviation from triplicate determinations. Student's t-test was used for the statistical analysis, *$p < 0.05$ and **$p < 0.01$.

activity with DHA-EA and DPA-EA (Figure 9D and Supplementary Figure S7).

3.3.2 The anti-obesity activity of PUFA-EAs in HFD-fed obesity mice model

Next, the algae oil-derived PUFA-EA mixture was considered for the *in vivo* anti-obesity activity in the HFD-fed obesity mice model, with a well-known anti-obesity drug, Orlistat, as the positive control. The experiment results are summarized in Table 2 and Figure 10A–C.

3.3.2.1 The effects of PUFA-EA mixture on the body weight, food intake, liver weight, and white adipose tissue

As shown in Table 2, The initial body weights of experimental mice were similar ($p > 0.05$), and the body weight increased significantly at the end of the obesity-modeling period (6 weeks). Compared to the initial body weight, the final body weight of the ND, HFD, HFD + ORL, and HFD + PUFA-EAs groups increased by 9.78 ± 3.17 g (44.54%), 12.76 ± 3.44 g (58.21%), 7.80 ± 4.42 g (36.30%), and 7.57 ± 3.09 g (34.84%), respectively. The net body-weight gain, total food intake, liver index, and fat coefficient of the HFD group were significantly higher than those of the ND group ($p < 0.01$), indicating that HFD intake promoted the development of obesity in ICR mice. However, compared to the HFD group, The HFD + ORL group showed significantly lower values of final body weight, PER, Lee's index, liver index, and WAT weight. It indicated that the Orlistat administration could reverse these changes upon the HFD challenge. A similar inhibitory effect was also observed in the PUFA-EAs group. For example, the final body weights of the HFD + ORL and HFD + PUFA-EAs groups were significantly lower than those of the HFD group ($p < 0.01$). The fat coefficient of the HFD + ORL and HFD + PUFA-EA groups were also significantly lower than those of the HFD group ($p < 0.05$). Besides, the inhibitory effect of Orlistat and PUFA-EAs on food intake was no significant difference. These results implied that PUFA-EAs had good fat-reducing potential in obese mice, equivalent to Orlistat ($p > 0.05$).

3.3.2.2 The effects of PUFA-EAs on the pathology of the liver in mice

The morphological structure of the experimental mice's liver tissues was observed using a microscope. The maximum size of adipocytes and the calculated number of liver cells in the full view captured with the microscope (200×) were shown in Figure 10A. Compared with the ND group, fewer cells in the full view were calculated in the HFD group, while cell numbers could be increased after the treatment of Orlistat and the PUFA-EA mixture. Therefore, larger adipocytes were observed in the HFD group, which could be inhibited by the supplementations of Orlistat and the PUFA-EA mixture; Figure 10B shows the H&E staining pathology of mice's liver tissue. The hepatic tissue sections in the ND group showed normal hepatocytes arranged neatly. However, apparent lipid droplets diffusely appeared in the livers of HFD-fed mice, and the boundary between individual liver cells is blurred compared with that of the ND group. The results are similar as reported previously (Tsuru et al., 2020). The PUFA-EA mixture, like Orlistat, effectively reduced the number and volume of lipid droplets induced by the HFD and clarified the cell boundaries. These findings

10.3389/fphar.2023.1146276

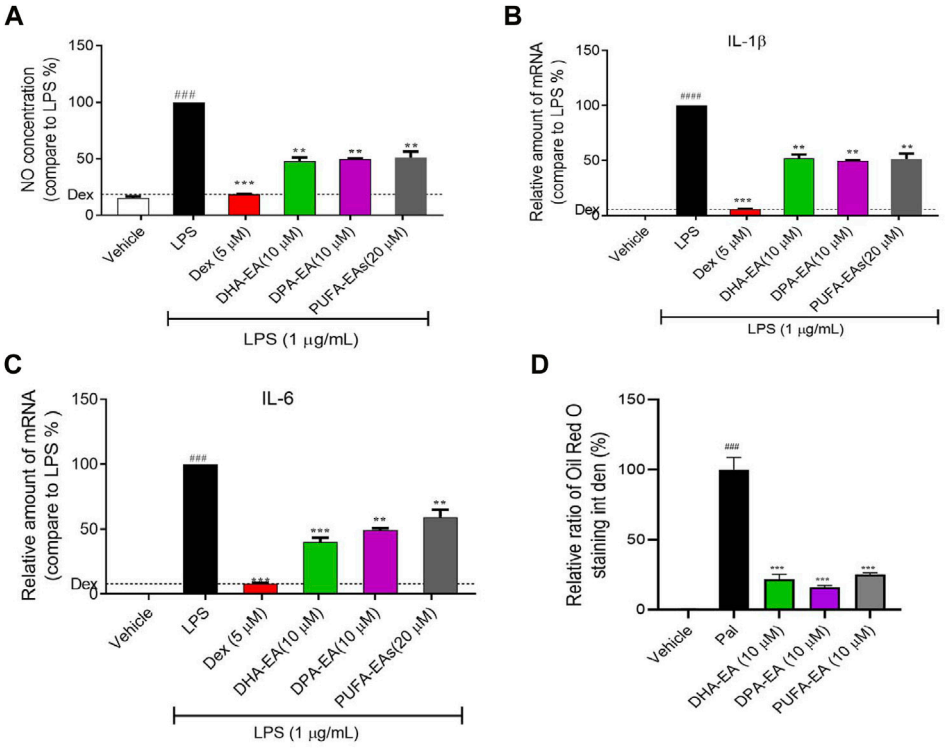

FIGURE 9
The PUFA-EA mixture showed excellent anti-inflammation activities in LPS-stimulated RAW264.7 cells. **(A)** The NO levels in the medium. **(B,C)** The mRNA levels of IL-1β and IL-6. **(D)** Quantification analysis of Oil Red O staining in Supplementary Figure S7. Int den stands for integrated density. All data in the figure are shown as mean ± SD (n ≥ 3). Bars represent the standard deviation from triplicate determinations. Student's t-test was used for the statistical analysis, #$p < 0.05$, ##$p < 0.01$, and ###$p < 0.001$, compared with the control group; *$p < 0.05$ and **$p < 0.01$, ***$p < 0.001$, compared with the LPS alone-stimulated group.

TABLE 2 The effects of Orlistat and the PUFA-EA mixture on body weight gain, food intake, and tissue weights in HFD-fed obese mice at the end of 6-week feeding (n = 10)[a].

	ND	HFD	HFD + ORL	HFD + PUFA-EA
Body weight				
*Initial body weight (g)	21.96 ± 1.34	21.92 ± 1.14	21.49 ± 1.49	21.73 ± 1.04
*Final body weight (g)	31.74 ± 4.06	34.68 ± 3.58	29.29 ± 4.26**	29.30 ± 2.39**
*Net weight gain (g)	9.78 ± 3.17	12.76 ± 3.44	7.80 ± 4.42*	7.57 ± 3.09**
Total food intake (g/d)	7.31 ± 0.87**	8.35 ± 1.16	7.55 ± 1.04**	7.27 ± 0.97**
PER[b]	3.72 ± 1.20*	4.24 ± 1.14	2.87 ± 1.63**	2.89 ± 1.18**
Body length				
*Initial body length (cm)	7.85 ± 0.20	7.77 ± 0.18	7.81 ± 0.19	7.87 ± 0.20
*Final body length (cm)	9.68 ± 0.56	10.02 ± 0.58	9.32 ± 0.62*	9.52 ± 0.25*
Lee's index[c]	14.83 ± 0.43	15.11 ± 0.28	14.62 ± 0.59*	14.54 ± 0.36**
Liver weight (g)	1.52 ± 0.29**	1.92 ± 0.21	1.48 ± 0.18**	1.46 ± 0.18**
Liver index (%)[d]	4.79 ± 0.58**	5.55 ± 0.57	5.11 ± 0.60**	4.97 ± 0.29**
White adipose tissues (WAT)				
*Epididymal fat (g)	0.52 ± 0.11**	0.84 ± 0.21	0.50 ± 0.18**	0.47 ± 0.10**
*Perirenal fat (g)	0.31 ± 0.09 **	0.55 ± 0.10	0.31 ± 0.15*	0.35 ± 0.12**
Fat coefficient (%)[e]	2.62 ± 0.27**	4.02 ± 1.20	2.70 ± 0.87*	2.80 ± 0.29**

[a]All data in the table are shown as mean ± SD. *$p < 0.05$, **$p < 0.01$ vs. the HFD, group.
[b]PER, food efficiency ratio (%) = [body weight gain (g)/diet consumed (g)] × 100.
[c]Lee's index = [body weight (g) × 1000/body length (cm)]$^{1/3}$.
[d]Liver index (%) = liver weight (g)/body weight (g) × 100.
[e]Fat coefficient (%) = [epididymal fat (g) + perirenal fat (g)]/body weight (g) × 100.

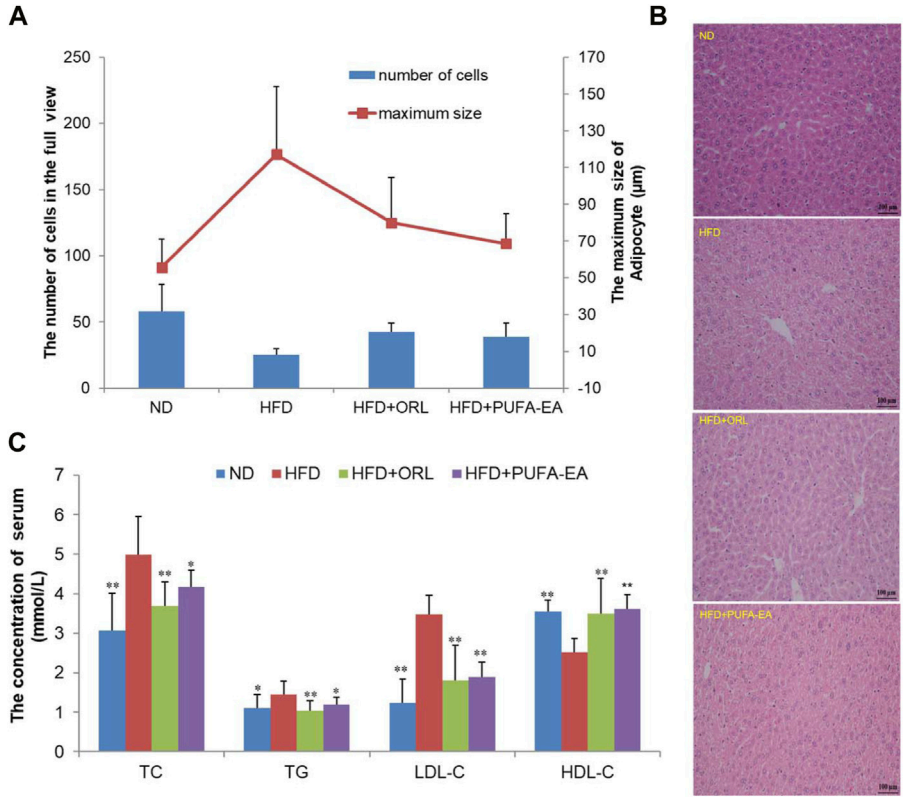

FIGURE 10
The PUFA-EA mixture showed *in vivo* anti-obesity effects in HFD mouse models. **(A)** The maximum size of adipocyte and the number of cells of the experimental mice's liver tissue in the full view captured with the microscope (200×). All data in the figure are shown as mean ± SD. Bars represent the standard deviation from duplicate determinations. **(B)** H&E staining of the liver after PUFA-EA supplementation. **(C)** Effects of PUFA-EA on plasma biochemical indicators (TC, TG, HDL-C, and LDL-C) in different groups at the end of 6-week feeding (n = 10). All data in the figure are shown as mean ± SD. Bars represent the standard deviation from duplicate determinations. *$p < 0.05$ and **$p < 0.01$.

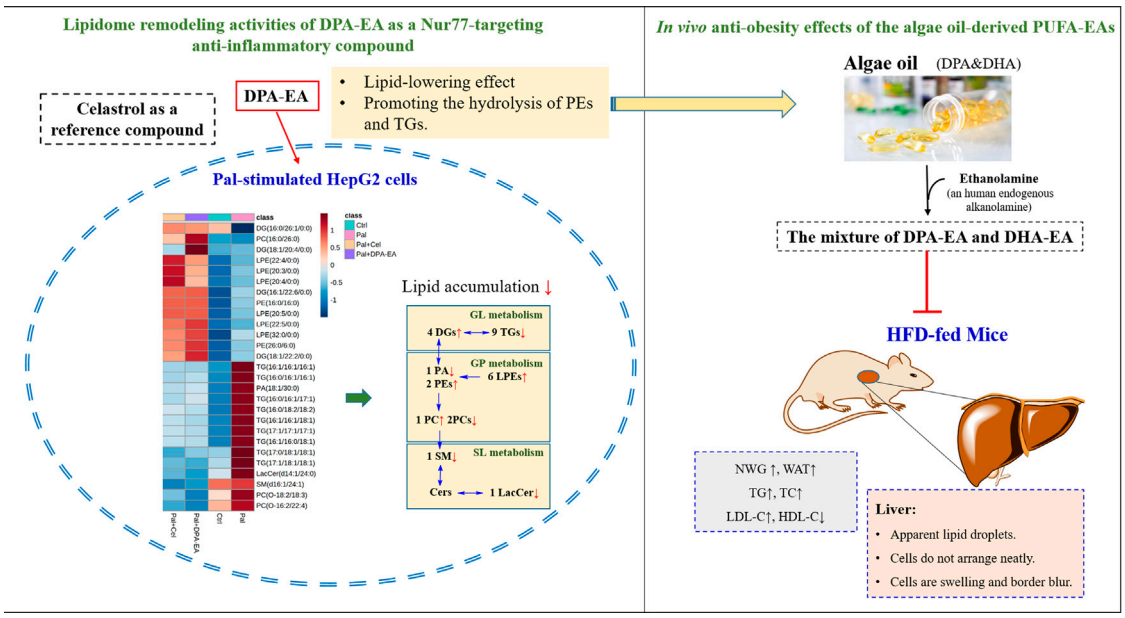

FIGURE 11
Lipidome remodeling activities of DPA-EA by targeting Nur77 and in vivo anti-obesity effects of the algae oil-derived PUFA-EAs.

suggested that the administration of the algae oil-derived PUFA-EA mixture produced an excellent inhibitory effect on obesity caused by an HFD.

3.3.2.3 Determination of the blood lipid-related indices (HDL- C, LDL- C, TC, and TG)

Feeding an HFD for 6 weeks could cause obesity, hyperlipidemia, and hyperglycemia in ICR mice (Li J. L. et al., 2020). It is a good model for studying diet-induced obesity. To further confirm the *in vivo* lipid-lowering effects of algae oil-derived PUFA-EA mixture, we measured the changes of crucial blood biochemical indexes upon HFD challenge and drug administration. Values of lipid parameters at the end of the experiment were presented in Figure 10C. The serum TC, TG, and LDL-C levels in the HFD group were significantly increased by 63.07%, 30.63%, and 182.93%, respectively, compared to those of the control group ($p < 0.01$). Meanwhile, HDL-C levels decreased by 40.87% in the HFD group compared to the control group ($p < 0.01$). However, the treatment of the PUFA-EA mixture could significantly inhibit the increased levels of TG, TC, and LDL-C induced by HFD, with inhibition rates of 21.85%, 19.38%, and 84.12%, respectively. At the same time, the treatment of the PUFA-EA mixture significantly increased the HDL-C level (upon (%), 43.65) relative to HFD-fed mice. A reduced ratio of LDL-C/HDL-C was also observed in the PUFA-EA and Orlistat groups' mice. The effect of the PUFA-EA mixture on the blood lipid-related indices is similar to that of Orlistat treatment, implying the potent anti-obesity activity *in vivo*.

3.3.3 The acute toxicity study of the PUFA-EA mixture in mice

To verify the *in vivo* safety of the algae oil-derived PUFA-EA mixture, we evaluated the acute toxicity in mice. The daily dose of 54,000 mg/kg of PUFA-EA mixture did not lead to any mortality throughout the study period of 14 days. All parameters observed were normal even when the limit dose was maintained at 54,000 mg/kg body weight (Supplementary Table S7). The autopsy results of all mice at the end of the experimental period (14 days) also revealed that no apparent changes were observed in any mice organs. These results indicated that the algae oil-derived PUFA-EA mixture had no acute toxicity in mice at a dose of 54,000 mg/kg (significantly exceeding the limit dose of 5,000 mg/kg/day), and the PUFA-EA mixture at a higher dose is unnecessary. The algae oil-derived PUFA-EAs was practically non-toxic *in vivo*, indicating the great therapeutic and safety potential for further development as an anti-obesity agent.

4 Discussion

Nur77 plays a crucial role in the inflammation process and lipid metabolism. Moreover, Nur77-targeting anti-inflammatory compounds are a potential therapeutic strategy for treating inflammation-related diseases such as obesity. However, the lipid-lowering mechanism of anti-inflammatory compounds targeting Nur77 remains unclear and has not been investigated. Understanding lipid profile changes induced by specific Nur77 modulators in the lipid-lowering process is crucial to exploring the underlying mechanism of their anti-obesity effects. The reference compound, Celastrol, has been proven to Nur77-dependently inhibit chronic inflammation and play a role in weight loss in obese animals (Wang et al., 2011). DHA, an essential ω-3 PUFA with anti-inflammatory and anti-obesity activities (Wei et al., 2021), is recently found to be an endogenous lipid reported to bind to Nur77[21]. Additionally, our previous work demonstrated that ω-3 PUFA-EA derivatives such as DPA-EA displayed excellent anti-inflammatory effects in a Nur77-dependent manner[21]. NAFLD is the most common liver disease associated directly with obesity. The present work also demonstrated that DPA-EA and Celastrol had excellent lipid-lowering lipid profile-remodeling activities in the liver HepG2 Cell Model (Figure 11).

Pal is a saturated fatty acid that has been reported to induce pro-inflammatory production in hepatocytes. The overload treatment of Pal causes triglyceride accumulation into specialized organelles termed lipid droplets. When rendering lipid droplets and hepatic lipotoxicity, Pal can cause glucotoxicity, oxidative stress, apoptosis, and endoplasmic reticulum (ER) and mitochondrial dysfunction in HepG2 cells (Zang et al., 2018; Eynaudi et al., 2021). The present work also demonstrated that Pal administration caused lipid accumulation in HepG2 cells, with a significant elevation of lipid droplets. Besides, several lipidomics studies have noted that Pal can influence the overall lipid metabolism (Shih et al., 2018; Cabezas et al., 2022). For example, Pal insult could affect lipid metabolites such as PE, PS, PC, and glycerophosphocholine (GPC) (Cabezas et al., 2022). The stable isotope-labeled lipidomics on Pal-stimulated HepG2 cells revealed that Pal significantly altered the levels of many lipids (*e.g.,* PL, Cer, GL, *et al.*), which were involved in biosynthetic pathways of DG, TG, PI, dihydroceramide (dHCer), Cer, SM, PC, PE, LPA, and LPE (Shih et al., 2018). Our lipidomics study also showed Pal-induced a significantly dysregulated lipid profile in HepG2 cells. We found 17 types of DELs between the control and Pal groups, mainly Cer, PC, TG, PE, Sph, SM, *etc.* Among them, most metabolites of glycerides (GLs), GPs, and sphingomyelin were significantly upregulated by Pal, implying that Pal treatment led to severe lipid gathering in HepG2 cells.

TGs are the primary storage and transport form of fatty acids in cells and plasma (Alves-Bezerra and Cohen, 2017). Lipid accumulation (*e.g.*, TG accumulation) in NAFLD has been reported to be one of the causes of insulin resistance in the liver (Gaggini et al., 2013). Moreover, the progressive increases in TG content are associated with progressive impairment of insulin action in the liver, skeletal muscle, and adipose tissue in non-diabetic obese subjects (Korenblat et al., 2008). Reducing triglyceride content *via* triglyceride synthase DAGT2 inhibition can improve hepatic steatosis in obese mice with non-alcoholic steatohepatitis (Yamaguchi et al., 2007). In our data, TGs involved in the insulin resistance transduction pathway, such as TAG (C57:1), TAG (C48:1), and TAG (C54:5) (Al-Sulaiti et al., 2018), were also identified as differential metabolites between the Ctrl and Pal groups, presented as TG (12:0/14:0/22:1) and TG (16:0/16:0/22:5). Additionally, DPA-EA and Celastrol could reverse the Pal-induced elevation of TGs in HepG2 cells, especially TG (16:1/16:1/16:1), TG (16:0/16:1/16:1), TG (17:1/17:1/17:1) *et al.* On the other hand, MGs and DGs are precursor molecules for the synthesis of TG. Diglycerides (DGs), with essential functions in lowering blood lipids, reducing visceral fat, and inhibiting weight gain (Hue et al., 2009), are mainly produced by blocking the accumulation of TG in the body. In Pal-stimulated HepG2 cells, both DPA-EA and

Celastrol markedly upregulated the contents of several DGs, particularly DG (16:1/22:6/0:0), DG (18:1/22:2/0:0), DG (18:1/20:4/0:0) and DG (16:0/26:1/0:0). Thus, DPA-EA and Celastrol might alleviate lipid accumulation by promoting the hydrolysis of triglycerides or lower triglyceride expression. In all, DPA-EA and Celastrol robustly affected GL metabolism and metabolites of GL species (TG and DG) in Pal-induced HepG2 cells.

GPs (*e.g.*, PC, PE, PG, *et al.*) regulate lipid metabolism, lipoprotein, and whole-body energy metabolism, too (van der Veen et al., 2017). PCs are the most abundant phospholipids in all mammalian cell membranes (van der Veen et al., 2017). In the present study, GP metabolism was significantly altered by DPA-EA and Celastrol in Pal-induced HepG2 cells. It is reported that PC therapy can relieve HFD-induced obesity and obesity-related complications by reducing TG and TC levels in serum (Lee et al., 2014). Buang *et al.* also reported that dietary PC could attenuate orotate-induced fatty liver in Sprague-Dawley rats by increasing CPT1 activity and preventing TG accumulation (Kumar et al., 2021). However, it was also found that some PCs were increased in the LPS-stimulated zebrafish model and acute TNFα-treated HepG2 cells (Chico et al., 2019; Luo et al., 2019). These data suggests various PCs may have different functions in the progress of inflammation and NAFLD. Interestingly, our results showed that in Pal-stimulated HepG2 cells, DPA-EA and Celastrol could significantly decrease PC(O-16:2/22:4) and PC(O-18:2/18:3) and elevated PC (16:0/26:0) or other PCs (8 for Celastrol and seven for DPA-EA). PEs are the second most abundant GPs in eukaryotic cells. Clinical research shows that a standard PC/PE ratio (~1.5–1.8) is relevant to liver health and a large proportion of NAFLD patients have abnormally low cellular PC/PE ratios (van der Veen et al., 2017). Besides, it is reported that PEs are significantly lower in human fatty livers (Puri et al., 2007). Notably, our present work exhibited that DPA-EA and Celastrol administrations caused a steady increase of two typical PEs, PE (16:0/16:0) and PE (26:0/6:0), in Pal-induced HepG2 cells. Celastrol also elevated PE (P-16:0/14:0) (P-18:0/20:0), and PE (O-18:2/19:0), while DPA-EA increased PE (6:0/16:0) (10:0/16:0), PE (16:1/20:3), and PE (14:0/14:0). However, Celastrol downregulated most of the other PEs but DPA-EA did not. Together, different classes of GPs displayed various alterations due to DPA-EA and Celastrol perturbation. PCs and PEs might not be the lipid markers to illustrate the underlying anti-inflammation and anti-obesity mechanism that Nur77-targeting anti-inflammatory compounds mediated.

Lysophospholipids (*e.g.*, LPCs and LPEs) are signaling molecules that play an essential role in inflammation, insulin resistance, and fatty liver disease (Zu and Cham, 2008). The interconversion between phospholipids and lysophospholipids is catalyzed by phospholipase A2 (D'Arrigo and Servi, 2010). Many studies show that LPC and LPE are reduced due to obesity or obesity-associated insulin resistance (Barber et al., 2012; Weir et al., 2013; Heimerl et al., 2014). For example, the circulating concentrations of some plasma LPEs (*e.g.*, LPE (14:1), LPE (18:1), and LPE (18:2)) are lower in obese subjects than in normal-weight subjects (Del Bas et al., 2016). Interestingly, our results showed that both DPA-EA and Celastrol could slightly increase the content of LPEs, including LPE (20:4/0:0), LPE (22:4/0:0), LPE (20:3/0:0), LPE (20:5/0:0), LPE (22:5/0:0), and LPE (32:0/0:0). It is consistent with the proposal that LPE plays a vital role in obesity and inflammation. Additionally, MN Barber *et al.* reported that levels of LPCs in the plasma of HFD-fed mice were stably decreased (Barber et al., 2012; Heimerl et al., 2014). As expected, both DPA-EA and Celastrol could upregulate the levels of LPCs in Pal-induced HepG2 cells. However, Celastrol upregulated LPC more significantly than DPA-EA. Celastrol increased another nine LPCs, such as LPC (22:6/0:0), LPC (20:5/0:0), and LPC (22:2/0:0). In comparison, DPA-EA enhanced the expression of another three LPCs including LPC (20:0/0:0), LPC (18:0/0:0), and LPC (O-22:0/0:0). Whatever, both DPA-EA and Celastrol significantly upregulated the expressions of LPE and LPC species.

Sphingolipids such as Cer and SM are also associated with the progression of obesity and insulin resistance (Haus et al., 2009; Sokolowska and Blachnio-Zabielska, 2019). Cer levels are increased in insulin-resistant individuals (Adams et al., 2004). The inhibition of Cer synthesis can improve glucocorticoid, saturated fat, and obesity-induced insulin resistance (Holland et al., 2007). An unbalanced ratio between ceramides and terminal metabolic products in the liver and plasma promotes weight gain, inflammation, and insulin resistance (Regnier et al., 2019). Similarly, we found that Pal could increase Cer in HepG2 cells. Both DPA-EA and Celastrol significantly reversed the Pal-induced increase of LacCer(d14:1/24:0). Especially, DPA-EA also diminished the Pal-induced increase of several other Cers, including GlcCer(d18:1/22:1), GlcCer(d18:1/22:0), Cer(d18:1/20:0), and LacCer(d14:0/24:0), but Celastrol did not. At the same time, in Pal-induced HepG2 cells, DPA-EA markedly upregulated another 11 Cers, but Celastrol significantly increased no Cer. Additionally, Jorge Simon *et al.* reported that the levels of sphingomyelin and ceramide were elevated during steatosis and non-alcoholic steatohepatitis (NASH) (Simon et al., 2019). Our present study showed that DPA-EA and Celastrol could significantly co-decrease the Pal-upregulated expression of SM (d16:1/24:1). Celastrol also downregulated the expression levels of SM (d14:2/21:0) and SM (d14:1/19:0) but upregulated no other SM. DPA-EA could not downregulate other SMs but significantly upregulate the contents of SM (d14:1/20:0), SM (d14:2/24:4), SM (d16:2/24:4), SM (d16:1/24:4), SM (d15:1/20:1), SM (d15:1/27:0), SM (d18:2/26:1), and Sph (d18:1). Based on those above-mentioned, it was concluded that DPA-EA is more sensitive to Cer than Celastrol, but Celastrol might cause over-downregulation of SM. Interestingly, it was reported that Celastrol decreased the levels of SM and Sph in the blood when inducing liver injury in mice (Zhang et al., 2019). Thus, the over-downregulation of SM may be associated with the off-target toxicity of Celastrol.

Nur77 is a crucial physiological modulator of lipid metabolism in adipose tissue. Female Nur77-deficiency mice show decreased lipolysis in white adipose tissue and increased hepatic fat storage (Perez-Sieira et al., 2013). The liver tissue of Nur77-null mice can accumulate more TGs than wild-type mice (Chao et al., 2009). However, adenovirus-mediated Nur77 overexpression reduces hepatic triglyceride levels while increasing plasma LDL-C and decreasing HDL-C (Hu et al., 2014). In live HepG2 cells, Pal can induce the downregulation of Nur77 and lipid accumulation, while Nur77 overexpression can improve the phenomenon of lipotoxicity (Zhao et al., 2018). Additionally, Celastrol can Nur77-dependently inhibit chronic inflammation in obese mice, thereby protecting them against HFD-induced obesity (decreasing body weight, adipose tissue mass, and the size of adipocytes and ameliorating HFD-caused fatty liver). Excitedly, the present work demonstrated that both DPA-EA and Celastrol displayed lipid-lowering activities in Pal-stimulated HepG2 cells. Using lipidomics analysis, we found that DPA-EA and Celastrol could co-downregulate

the TG expressions but upregulate DG expressions in Pal-stimulated HepG2 cells. It is consistent with the effects of Nur77 overexpression (Zhao et al., 2018). In particular, 27 lipid metabolites with statistically significant changes were identified as critical factors responding to the lipid-lowering process of DPA-EA and Celastrol (Figure 11).

In summary, the present study demonstrates that anti-inflammatory Nur77 modulators can decrease lipid accumulation by promoting lipolysis. Moreover, a total of 27 lipids were identified as potential biomarkers that responded to the anti-obesity effect of Nur77-targeting anti-inflammatory compounds. These biomarkers have important implications for developing anti-obesity agents targeting Nur77 and predicting the recovery of aberrant lipid metabolism in obesity-related metabolic disorders. Notably, the algae oil-derived PUFA-EA mixture showed excellent anti-obesity effects on HFD-fed mice (Figure 11) with practically no toxicity *in vivo*. Overall, we provide new insights into the intervention mechanism of Nur77-targeting anti-inflammatory compounds on lipid metabolism. In particular, the algae oil-derived PUFA-EA mixture may be a promising therapeutic agent of obesity and NAFLD worthy of further development.

Data availability statement

The original contributions presented in the study are included in the article/Supplementary Material, further inquiries can be directed to the corresponding author.

Ethics statement

The animal study was reviewed and approved by The Experimental Animals Ethics Committee of Nanjing University of Chinese Medicine (No. 201906A012) and the Animal Care and Use Committee of Xiamen University (XmuLAC 20200029).

Author contributions

MF, HF, and YC designed the study and interpreted data; HF, JZ, XW, and ML performed the experiments; YC, HF, JZ, XW, and ML analyzed and visualized the data; HZ and ZW supported the experiment resources; MF and HF supervised the research; YC and JZ wrote the original draft; MF and YC reviewed and edited the paper. All authors agree to be accountable for all aspects of work, ensuring integrity and accuracy.

Funding

This work was supported by grants from the Natural Science Foundation of Fujian Province of China (No. 2021N0029 and 2019N0032), the Fundamental Research Funds for the Central Universities (No. 20720180051), and Science and Technology Project of Xiamen (No. 3502Z20221036).

Acknowledgments

We thank the editor for careful review.

Conflict of interest

The authors declare that the research was conducted in the absence of any commercial or financial relationships that could be construed as a potential conflict of interest.

Publisher's note

Supplementary material

The Supplementary Material for this article can be found online at: https://www.frontiersin.org/articles/10.3389/fphar.2023.1146276/full#supplementary-material

References

Adams, J. M., 2nd, Pratipanawatr, T., Berria, R., Wang, E., DeFronzo, R. A., Sullards, M. C., et al. (2004). Ceramide content is increased in skeletal muscle from obese insulin-resistant humans. *Diabetes* 53 (1), 25–31. doi:10.2337/diabetes.53.1.25

Al-Sulaiti, H., Diboun, I., Banu, S., Al-Emadi, M., Amani, P., Harvey, T. M., et al. (2018). Triglyceride profiling in adipose tissues from obese insulin sensitive, insulin resistant and type 2 diabetes mellitus individuals. *J. Transl. Med.* 16 (1), 175. doi:10.1186/s12967-018-1548-x

Alves-Bezerra, M., and Cohen, D. E. (2017). Triglyceride metabolism in the liver. *Compr. Physiol.* 8 (1), 1–8. doi:10.1002/cphy.c170012

Barber, M. N., Risis, S., Yang, C., Meikle, P. J., Staples, M., Febbraio, M. A., et al. (2012). Plasma lysophosphatidylcholine levels are reduced in obesity and type 2 diabetes. *PLoS One* 7 (7), e41456. doi:10.1371/journal.pone.0041456

Cabezas, R., Martin-Jimenez, C., Zuluaga, M., Pinzon, A., Barreto, G. E., and Gonzalez, J. (2022). Integrated metabolomics and lipidomics reveal high accumulation of glycerophospholipids in human astrocytes under the lipotoxic effect of palmitic acid and tibolone protection. *Int. J. Mol. Sci.* 23 (5), 2474. doi:10.3390/ijms23052474

Calder, P. C. (2017). Omega-3 fatty acids and inflammatory processes: From molecules to man. *Biochem. Soc. Trans.* 45 (5), 1105–1115. doi:10.1042/BST20160474

Chao, L. C., Wroblewski, K., Zhang, Z., Pei, L., Vergnes, L., Ilkayeva, O. R., et al. (2009). Insulin resistance and altered systemic glucose metabolism in mice lacking Nur77. *Diabetes* 58 (12), 2788–2796. doi:10.2337/db09-0763

Chen, Y., Wu, R., Chen, H. Z., Xiao, Q., Wang, W. J., He, J. P., et al. (2015). Enhancement of hypothalamic STAT3 acetylation by nuclear receptor Nur77 dictates leptin sensitivity. *Diabetes* 64 (6), 2069–2081. doi:10.2337/db14-1206

Chico, Y., Abad-Garcia, B., Ochoa, B., and Martinez, M. J. (2019). Lipidomic data uncover extensive heterogeneity in phosphatidylcholine structural variants in HepG2 cells. *Data Brief.* 27, 104608. doi:10.1016/j.dib.2019.104608

D'Arrigo, P., and Servi, S. (2010). Synthesis of lysophospholipids. *Molecules* 15 (3), 1354–1377. doi:10.3390/molecules15031354

de Bus, I., Witkamp, R., Zuilhof, H., Albada, B., and Balvers, M. (2019). The role of n-3 PUFA-derived fatty acid derivatives and their oxygenated metabolites in the modulation of inflammation. *Prostagl. Other Lipid Mediat* 144, 106351. doi:10.1016/j.prostaglandins.2019.106351

Del Bas, J. M., Caimari, A., Rodriguez-Naranjo, M. I., Childs, C. E., Paras Chavez, C., West, A. L., et al. (2016). Impairment of lysophospholipid metabolism in obesity: Altered plasma profile and desensitization to the modulatory properties of n-3 polyunsaturated fatty acids in a randomized controlled trial. *Am. J. Clin. Nutr.* 104 (2), 266–279. doi:10.3945/ajcn.116.130872

Deng, S., Chen, B., Huo, J., and Liu, X. (2022). Therapeutic potential of NR4A1 in cancer: Focus on metabolism. *Front. Oncol.* 12, 972984. doi:10.3389/fonc.2022.972984

Ellulu, M. S., Patimah, I., Khaza'ai, H., Rahmat, A., and Abed, Y. (2017). Obesity and inflammation: The linking mechanism and the complications. *Arch. Med. Sci.* 13 (4), 851–863. doi:10.5114/aoms.2016.58928

Eynaudi, A., Diaz-Castro, F., Borquez, J. C., Bravo-Sagua, R., Parra, V., and Troncoso, R. (2021). Differential effects of oleic and palmitic acids on lipid droplet-mitochondria interaction in the hepatic cell line HepG2. *Front. Nutr.* 8, 775382. doi:10.3389/fnut.2021.775382

Fang, H., Zhang, J., Ao, M., He, F., Chen, W., Qian, Y., et al. (2020). Synthesis and discovery of omega-3 polyunsaturated fatty acid-alkanolamine (PUFA-AA) derivatives as anti-inflammatory agents targeting Nur77. *Bioorg Chem.* 105, 104456. doi:10.1016/j.bioorg.2020.104456

Gaggini, M., Morelli, M., Buzzigoli, E., DeFronzo, R. A., Bugianesi, E., and Gastaldelli, A. (2013). Non-alcoholic fatty liver disease (NAFLD) and its connection with insulin resistance, dyslipidemia, atherosclerosis and coronary heart disease. *Nutrients* 5 (5), 1544–1560. doi:10.3390/nu5051544

Haus, J. M., Kashyap, S. R., Kasumov, T., Zhang, R., Kelly, K. R., Defronzo, R. A., et al. (2009). Plasma ceramides are elevated in obese subjects with type 2 diabetes and correlate with the severity of insulin resistance. *Diabetes* 58 (2), 337–343. doi:10.2337/db08-1228

Heimerl, S., Fischer, M., Baessler, A., Liebisch, G., Sigruener, A., Wallner, S., et al. (2014). Alterations of plasma lysophosphatidylcholine species in obesity and weight loss. *PLoS One* 9 (10), e111348. doi:10.1371/journal.pone.0111348

Holland, W. L., Brozinick, J. T., Wang, L. P., Hawkins, E. D., Sargent, K. M., Liu, Y., et al. (2007). Inhibition of ceramide synthesis ameliorates glucocorticoid-saturated-fat-and obesity-induced insulin resistance. *Cell Metab.* 5 (3), 167–179. doi:10.1016/j.cmet.2007.01.002

Hu, M., Luo, Q., Alitongbieke, G., Chong, S., Xu, C., Xie, L., et al. (2017). Celastrol-induced Nur77 interaction with TRAF2 alleviates inflammation by promoting mitochondrial ubiquitination and autophagy. *Mol. Cell* 66 (1), 141–153.e6. doi:10.1016/j.molcel.2017.03.008

Hu, Y. W., Zhang, P., Yang, J. Y., Huang, J. L., Ma, X., Li, S. F., et al. (2014). Nur77 decreases atherosclerosis progression in apoE(-/-) mice fed a high-fat/high-cholesterol diet. *Plos One* 9 (1), e87313. ARTN e87313. doi:10.1371/journal.pone.0087313

Hue, J. J., Lee, K. N., Jeong, J. H., Lee, S. H., Lee, Y. H., Jeong, S. W., et al. (2009). Anti-obesity activity of diglyceride containing conjugated linoleic acid in C57BL/6J ob/ob mice. *J. Vet. Sci.* 10 (3), 189–195. doi:10.4142/jvs.2009.10.3.189

Kim, K. A., Gu, W., Lee, I. A., Joh, E. H., and Kim, D. H. (2012). High fat diet-induced gut microbiota exacerbates inflammation and obesity in mice via the TLR4 signaling pathway. *PLoS One* 7 (10), e47713. doi:10.1371/journal.pone.0047713

Korenblat, K. M., Fabbrini, E., Mohammed, B. S., and Klein, S. (2008). Liver, muscle, and adipose tissue insulin action is directly related to intrahepatic triglyceride content in obese subjects. *Gastroenterology* 134 (5), 1369–1375. doi:10.1053/j.gastro.2008.01.075

Kumar, A., Sundaram, K., Mu, J., Dryden, G. W., Sriwastva, M. K., Lei, C., et al. (2021). High-fat diet-induced upregulation of exosomal phosphatidylcholine contributes to insulin resistance. *Nat. Commun.* 12 (1), 213. doi:10.1038/s41467-020-20500-w

Lee, H. S., Nam, Y., Chung, Y. H., Kim, H. R., Park, E. S., Chung, S. J., et al. (2014). Beneficial effects of phosphatidylcholine on high-fat diet-induced obesity, hyperlipidemia and fatty liver in mice. *Life Sci.* 118 (1), 7–14. doi:10.1016/j.lfs.2014.09.027

Li, J. L., Wu, H. S., Liu, Y. T., and Yang, L. (2020). High fat diet induced obesity model using four strains of mice: Kunming, C57BL/6, BALB/c and ICR. *Exp. Anim.* 69 (3), 326–335. doi:10.1538/expanim.19-0148

Li, Q., Lai, X., Sun, L., Cao, J., Ling, C., Zhang, W., et al. (2020). Antiobesity and anti-inflammation effects of Hakka stir-fried tea of different storage years on high-fat diet-induced obese mice model via activating the AMPK/ACC/CPT1 pathway. *Food Nutr. Res.* 64. doi:10.29219/fnr.v64.1681

Li, X. M., Lu, X. X., Xu, Q., Wang, J. R., Zhang, S., Guo, P. D., et al. (2015). Nur77 deficiency leads to systemic inflammation in elderly mice. *J. Inflamm. (Lond)* 12, 40. doi:10.1186/s12950-015-0085-0

Liu, J., Lee, J., Salazar Hernandez, M. A., Mazitschek, R., and Ozcan, U. (2015). Treatment of obesity with celastrol. *Cell* 161 (5), 999–1011. doi:10.1016/j.cell.2015.05.011

Luna-Vital, D., Luzardo-Ocampo, I., Cuellar-Nunez, M. L., Loarca-Pina, G., and Gonzalez de Mejia, E. (2020). Maize extract rich in ferulic acid and anthocyanins prevents high-fat-induced obesity in mice by modulating SIRT1, AMPK and IL-6 associated metabolic and inflammatory pathways. *J. Nutr. Biochem.* 79, 108343. doi:10.1016/j.jnutbio.2020.108343

Luo, L., Zhou, J., Zhao, H., Fan, M., and Gao, W. (2019). The anti-inflammatory effects of formononetin and ononin on lipopolysaccharide-induced zebrafish models based on lipidomics and targeted transcriptomics. *Metabolomics* 15 (12), 153. doi:10.1007/s11306-019-1614-2

Menegaut, L., Jalil, A., Thomas, C., and Masson, D. (2019). Macrophage fatty acid metabolism and atherosclerosis: The rise of PUFAs. *Atherosclerosis* 291, 52–61. doi:10.1016/j.atherosclerosis.2019.10.002

Pan, Y., Tan, J., Long, X., Yi, R., Zhao, X., and Park, K. Y. (2022). Anti-obesity effect of fermented lemon peel on high-fat diet-induced obese mice by modulating the inflammatory response. *J. Food Biochem.* 46 (8), e14200. doi:10.1111/jfbc.14200

Perez-Sieira, S., Martinez, G., Porteiro, B., Lopez, M., Vidal, A., Nogueiras, R., et al. (2013). Female nur77-deficient mice show increased susceptibility to diet-induced obesity. *Plos One* 8 (1), e53836. ARTN e53836. doi:10.1371/journal.pone.0053836

Pols, T. W. H., Ottenhoff, R., Vos, M., Levels, J. H. M., Quax, P. H. A., Meijers, J. C. M., et al. (2008). Nur77 modulates hepatic lipid metabolism through suppression of SREBP1c activity. *Biochem. Biophysical Res. Commun.* 366 (4), 910–916. doi:10.1016/j.bbrc.2007.12.039

Puri, P., Baillie, R. A., Wiest, M. M., Mirshahi, F., Choudhury, J., Cheung, O., et al. (2007). A lipidomic analysis of nonalcoholic fatty liver disease. *Hepatology* 46 (4), 1081–1090. doi:10.1002/hep.21763

Rana, J. S., Nieuwdorp, M., Jukema, J. W., and Kastelein, J. J. (2007). Cardiovascular metabolic syndrome - an interplay of, obesity, inflammation, diabetes and coronary heart disease. *Diabetes Obes. Metab.* 9 (3), 218–232. doi:10.1111/j.1463-1326.2006.00594.x

Regnier, M., Polizzi, A., Guillou, H., and Loiseau, N. (2019). Sphingolipid metabolism in non-alcoholic fatty liver diseases. *Biochimie* 159, 9–22. doi:10.1016/j.biochi.2018.07.021

Ruzickova, J., Rossmeisl, M., Prazak, T., Flachs, P., Sponarova, J., Vecka, M., et al. (2005). Omega-3 PUFA of marine origin limit diet-induced obesity in mice by reducing cellularity of adipose tissue (vol 39, pg 1177, 2004). *Lipids* 40 (1), 115.

Schumann, J., and Fuhrmann, H. (2010). Impairment of NFkappaB activity by unsaturated fatty acids. *Int. Immunopharmacol.* 10 (8), 978–984. doi:10.1016/j.intimp.2010.05.011

Shih, L. M., Tang, H. Y., Lynn, K. S., Huang, C. Y., Ho, H. Y., and Cheng, M. L. (2018). Stable isotope-labeled lipidomics to unravel the heterogeneous development lipotoxicity. *Molecules* 23 (11), 2862. doi:10.3390/molecules23112862

Simon, J., Ouro, A., Ala-Ibanibo, L., Presa, N., Delgado, T. C., and Martinez-Chantar, M. L. (2019). Sphingolipids in non-alcoholic fatty liver disease and hepatocellular carcinoma: Ceramide turnover. *Int. J. Mol. Sci.* 21 (1), 40. doi:10.3390/ijms21010040

Sokolowska, E., and Blachnio-Zabielska, A. (2019). The role of ceramides in insulin resistance. *Front. Endocrinol. (Lausanne)* 10, 577. doi:10.3389/fendo.2019.00577

Tsuru, H., Osaka, M., Hiraoka, Y., and Yoshida, M. (2020). HFD-induced hepatic lipid accumulation and inflammation are decreased in Factor D deficient mouse. *Sci. Rep.* 10 (1), 17593. doi:10.1038/s41598-020-74617-5

van der Veen, J. N., Kennelly, J. P., Wan, S., Vance, J. E., Vance, D. E., and Jacobs, R. L. (2017). The critical role of phosphatidylcholine and phosphatidylethanolamine metabolism in health and disease. *Biochim. Biophys. Acta Biomembr.* 1859, 1558–1572. doi:10.1016/j.bbamem.2017.04.006

Wang, B., Yang, X., Zhao, M., Su, Z., Hu, Z., Zhang, C., et al. (2021). Celastrol prevents high-fat diet-induced obesity by promoting white adipose tissue browning. *Clin. Transl. Med.* 11 (12), e641. doi:10.1002/ctm2.641

Wang, S., Liu, K., Wang, X., He, Q., and Chen, X. (2011). Toxic effects of celastrol on embryonic development of zebrafish (*Danio rerio*). *Drug Chem. Toxicol.* 34 (1), 61–65. doi:10.3109/01480545.2010.494664

Wang, W., Yang, J., Zhang, J., Wang, Y., Hwang, S. H., Qi, W., et al. (2018). Lipidomic profiling reveals soluble epoxide hydrolase as a therapeutic target of obesity-induced colonic inflammation. *Proc. Natl. Acad. Sci. U. S. A.* 115 (20), 5283–5288. doi:10.1073/pnas.1721711115

Wei, W. T., Hu, M. J., Huang, J., Yu, S. Y., Li, X. D., Li, Y. H., et al. (2021). Anti-obesity effects of DHA and EPA in high fat-induced insulin resistant mice. *Food and Funct.* 12 (4), 1614–1625. doi:10.1039/d0fo02448a

Weir, J. M., Wong, G., Barlow, C. K., Greeve, M. A., Kowalczyk, A., Almasy, L., et al. (2013). Plasma lipid profiling in a large population-based cohort. *J. Lipid Res.* 54 (10), 2898–2908. doi:10.1194/jlr.P035808

Yamaguchi, K., Yang, L., McCall, S., Huang, J. W., Yu, X. X., Pandey, S. K., et al. (2007). Inhibiting triglyceride synthesis improves hepatic steatosis but exacerbates liver damage and fibrosis in obese mice with nonalcoholic steatohepatitis. *Hepatology* 45 (6), 1366–1374. doi:10.1002/hep.21655

Zang, Y., Fan, L., Chen, J., Huang, R., and Qin, H. (2018). Improvement of lipid and glucose metabolism by capsiate in palmitic acid-treated HepG2 cells via activation of the AMPK/SIRT1 signaling pathway. *J. Agric. Food Chem.* 66 (26), 6772–6781. doi:10.1021/acs.jafc.8b01831

Zhang, T., Zhao, Q., Xiao, X., Yang, R., Hu, D., Zhu, X., et al. (2019). Modulation of lipid metabolism by celastrol. *J. Proteome Res.* 18 (3), 1133–1144. doi:10.1021/acs.jproteome.8b00797

Zhang, Y., Geng, C., Liu, X., Li, M., Gao, M., Liu, X., et al. (2017). Celastrol ameliorates liver metabolic damage caused by a high-fat diet through Sirt1. *Mol. Metab.* 6 (1), 138–147. doi:10.1016/j.molmet.2016.11.002

Zhao, N., Li, X., Feng, Y., Han, J., Feng, Z., Li, X., et al. (2018). The nuclear orphan receptor Nur77 alleviates palmitate-induced fat accumulation by down-regulating G0S2 in HepG2 cells. *Sci. Rep.* 8 (1), 4809. doi:10.1038/s41598-018-23141-8

Zu, H., and Cham, D. J. (2008). Lysophospholipids.

frontiers | Frontiers in Pharmacology

TYPE Original Research
PUBLISHED 12 May 2023
DOI 10.3389/fphar.2023.1124633

OPEN ACCESS

EDITED BY
Yan Huang,
Anhui Medical University, China

REVIEWED BY
Shuainan Liu,
Chinese Academy of Medical Sciences and Peking Union Medical College, China
Gabriele Christine Saretzki,
Newcastle University, United Kingdom

*CORRESPONDENCE
Cheng Zhang,
zhangc@sdu.edu.cn
Ming Zhong,
zhongming2sdu@163.com

RECEIVED 15 December 2022
ACCEPTED 19 April 2023
PUBLISHED 12 May 2023

CITATION
Liu Y, Han L, Zhu P, Song M, Zhang Y, Meng L, Zhang W, Zhang C and Zhong M (2023), PTPN2 targets TAK1 for dephosphorylation to improve cellular senescence and promote adipose tissue browning in T2DM.
Front. Pharmacol. 14:1124633.
doi: 10.3389/fphar.2023.1124633

PTPN2 targets TAK1 for dephosphorylation to improve cellular senescence and promote adipose tissue browning in T2DM

Yapeng Liu[1], Lu Han[1,2], Ping Zhu[1], Ming Song[1], Yaoyuan Zhang[1], Linlin Meng[1], Wei Zhang[1], Cheng Zhang[1]* and Ming Zhong[1]*

[1]The Key Laboratory of Cardiovascular Remodeling and Function Research, Chinese Ministry of Education, Chinese National Health Commission and Chinese Academy of Medical Sciences, The State and Shandong Province Joint Key Laboratory of Translational Cardiovascular Medicine, Department of Cardiology, Qilu Hospital, Cheeloo College of Medicine, Shandong University, Jinan, Shandong, China, [2]Department of General Practice, Qilu Hospital, Cheeloo College of Medicine, Shandong University, Jinan, Shandong, China

Introduction: The energy imbalance when energy intake exceeds expenditure acts as an essential factor in the development of insulin resistance (IR). The activity of brown adipose tissue, which is involved in the dissipation of energy via heat expenditure decreases under type 2 diabetic mellitus (T2DM) state when the number of pathological aging adipocytes increases. Protein tyrosine phosphatase non-receptor type 2 (PTPN2) regulates several biological processes by dephosphorylating several cellular substrates; however, whether PTPN2 regulates cellular senescence in adipocytes and the underlying mechanism has not been reported.

Methods: We constructed a model of type 2 diabetic mice with PTPN2 overexpression to explore the role of PTPN2 in T2DM.

Results: We revealed that PTPN2 facilitated adipose tissue browning by alleviating pathological senescence, thus improving glucose tolerance and IR in T2DM. Mechanistically, we are the first to report that PTPN2 could bind with transforming growth factor-activated kinase 1 (TAK1) directly for dephosphorylation to inhibit the downstream MAPK/NF-κB pathway in adipocytes and regulate cellular senescence and the browning process subsequently.

Discussion: Our study revealed a critical mechanism of adipocytes browning progression and provided a potential target for the treatment of related diseases.

KEYWORDS

PTPN2, TAK1, adipocytes, senescence, adipose tissue browning

Introduction

Type 2 diabetes mellitus (T2DM) is rising to a global epidemic over the last few decades (Hildebrand et al., 2019). As a determining factor of T2DM, insulin resistance (IR) gains acceptance as the target of treatment (Sampath et al., 2019). Adipose tissue is a central regulator of systemic glucose homeostasis (Czech, 2020) and it can be subdivided into white adipose tissue (WAT), brown adipose tissue (BAT) and beige adipose tissue (Ying et al., 2017; Shimobayashi et al., 2018). WAT, including subcutaneous adipose tissue (SAT) and

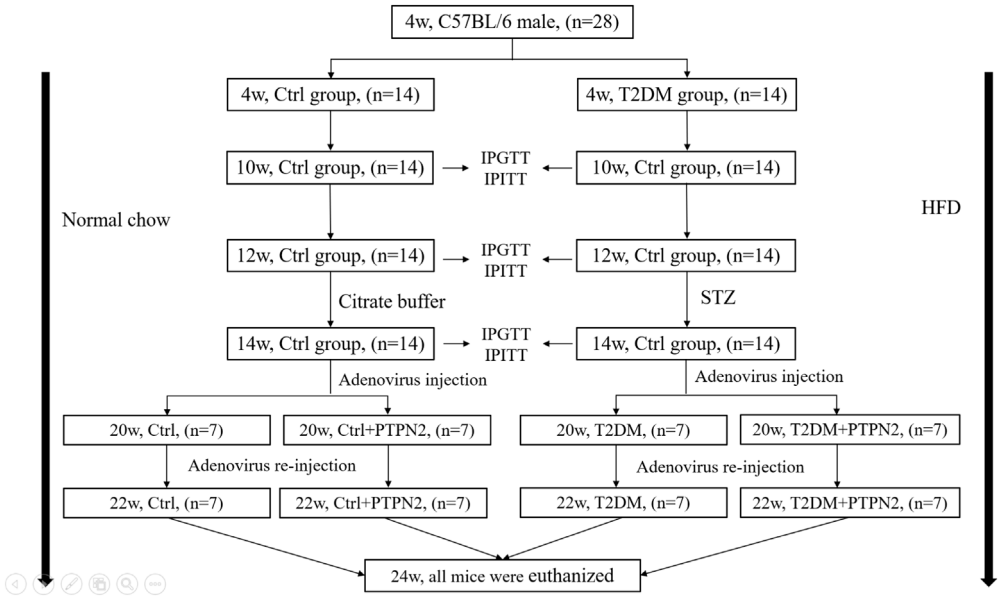

GRAPHICAL ABSTRACT
The timeline design of animal models.

visceral adipose tissue (VAT), stores energy in the form of triglycerides while BAT drives thermogenesis by consuming fatty acids (Janssen et al., 2020; Krisko et al., 2020). Beige adipocytes are a kind of brown-like cells that have been identified in WAT. Both beige adipose tissue and BAT express high levels of uncoupled protein 1(UCP1) and are involved in the dissipation of energy via heat generation (Keipert et al., 2020; Xu et al., 2020). In T2DM, free fatty acids and pro-inflammatory mediators are highly released due to the imbalance between energy intake and output, eventually leading to the chronic low-grade inflammation and IR (Ljubkovic et al., 2019; Randeria et al., 2019). Thus, white adipose tissue browning ameliorates IR via the increase of energy output (Chen et al., 2021; Maliszewska and Kretowski, 2021). White adipose tissue browning is characterized by the gene expression of classical browning markers including UCP1, PRDM16, Dio2, PGC1α, and PPARα and when most of these markers are decreased, adipose tissue browning is inhibited (Miao et al., 2021). Adipose tissue browning can increase energy expenditure in humans and contribute to the control of adiposity in humans, as has been established in mice (Yoneshiro et al., 2011). Studies have shown that adipose tissue browning is inhibited in T2DM (Rogers et al., 2012; Moreno-Santos et al., 2016) and the corresponding mechanism needs to be further elucidated.

The role of senescence of adipose tissue in T2DM is well established (Börgeson et al., 2015; Gómez-Serrano et al., 2017). In tissues including BAT and WAT with senescence, free oxygen radical reactions are able to result in progressive accumulation of oxidative damage to DNA and lipids in addition to shortened telomeres, so may promote several pathological features (Jankovic et al., 2015; Wang and Hai, 2015). Mitochondrial dysfunction has been discussed in senescing brown adipocytes, where the release of reactive oxygen species (ROS) from dysfunctional mitochondria in senescing adipocytes results in lipid accumulation and chronic inflammation (Jankovic et al., 2015), and thus contributes the development of IR. Beige adipose tissue can reduce metabolic defects of WAT and is also influenced by aging (Xu et al., 2020; Cohen and Kajimura, 2021). Beige adipocytes are known to proliferate and differentiate from a sub-population of progenitors resident in white adipose tissue (Zoico et al., 2019). Besides, when metabolic changes are induced (e.g., nitrate-mediated activation), adipocyte browning can also occur in already differentiating WAT cells (Roberts, 2015). However, the defective ability of CD137/TMEM26 progenitor cells with strong differentiation potential has been proposed when trophic factors associated with regulating progenitor cell proliferation and differentiation in the adipose tissue microenvironment change during aging (Zoico et al., 2019), preventing the formation of beige adipose tissue. Adipose senescence in T2DM might be an important mechanism involved in the inhibition of adipose tissue browning.

The mitogen-activated protein kinase (MAPK) and nuclear factor-kappa B (NF-κB) pathway control cellular senescence traits by phosphorylating senescence-related proteins inorder to regulate their activity (Tian et al., 2019; Anerillas et al., 2020). In response to senescence stimulation, the MAPK/NF-κB pathway activates the P21/P53 axis, the P16 axis and the occurrence of senescence-associated secretory phenotype (SASP). The activated P38/MAPK-P16 pathway can induce senescence of progenitor cells and thereby inhibit adipose tissue browning (Berry et al., 2017). Transforming growth factor-activated kinase 1 (TAK1) is a critical upstream activator of the MAPK/NF-κB pathway (Dai et al., 2020; Zhao et al., 2021), which also triggers cellular senescence programs (Rajagopalan et al., 2014; Zhang et al., 2018a). However, whether TAK1 promotes cellular senescence and inhibits browning via the MAPK/NF-κB pathway in adipocytes remains unclear.

The protein tyrosine phosphatase non-receptor type 2 (PTPN2, gene ID: 19255) has extensive biological activity and acts as a crucial

regulator of T2DM with its complications (Zhang et al., 2018b; Zheng et al., 2018). Our previous study has demonstrated that PTPN2 could improve diabetic nephropathy (Li et al., 2019). Nowadays, most studies about the effect of PTPN2 on adipose tissue are restricted to tissue level while the role of PTPN2 in regulating adipocytes browning directly needs to be further explained. PTPN2 has been demonstrated to be an inhibitor of P38/MAPK (Berry et al., 2017), however, whether PTPN2 improves adipocyte senescence by regulating TAK1/MAPK/NF-κB has not been reported.

In this study, we constructed a model of T2DM mice and demonstrated that PTPN2 could mediate adipose tissue browning by preventing adipose tissue from senescence, thereby improving IR. Mechanistically, we explored that PTPN2 targeted TAK1 directly for dephosphorylation to inhibit MAPK/NF-κB-mediated senescence for the first time.

Materials and methods

Animal models

We enrolled 28 C57BL/6 male mice aged 3 weeks weighting 14 (median)±2 g, purchased from experimental animal center of Shandong University, Ji'nan, China. All procedures were approved by Animal Care and Use Committee of Shandong University. Animals group-housed 3 per cage under standard laboratory conditions (25°C, 60%–70% relative humidity and 12 h of light and dark circulation) were tested for intraperitoneal glucose tolerance tests (IPGTT) after 1 week of adaptation.

After IPGTT, 28 mice were randomly assigned to the control group (Ctrl, n =14) and type 2 diabetes group (T2DM, n =14). The control group were fed a normal chow while the T2DM group received a high-fat diet (HFD, 34.5% fat, 17.5% protein, and 48% carbohydrate; Beijing HFK Bio-Technology, China). After 6 weeks, insulin tolerance was evaluated by intraperitoneal insulin tolerance tests (IPITT). After 8 weeks, IPITT and IPGTT were performed again to confirm the induction of IR. Mice exhibiting IR were given once low-dose of streptozotocin (STZ) injection intraperitoneally (Sigma, St. Louis, MO; 75–80 mg/kg i. p. in 0.1 mol/L citrate buffer, pH 4.5); the control group was administered with citrate buffer intraperitoneally only. IPGTT was measured again 2 weeks after injection of STZ. Most HFD/STZ-treated mice exhibited hyperglycemia (random blood glucose >11.1 mmol/L), IR and abnormal glucose tolerance.

At the age of 14 week, mice with similar degrees of hyperglycemia and body weight were randomly divided into the vehicle group (T2DM, n = 7) and PTPN2-overexpression group (T2DM + PTPN2, n = 7). Mice fed on a normal diet were classified as the non-diabetic control group, divided into the vehicle group (Ctrl, n = 7) and PTPN2-overexpression group (Ctrl + PTPN2, n = 7).

After food intervention, body weight was recorded every week and blood glucose level was examined every 2 weeks. The fasting glucose level was measured by OneTouch Glucometer (LifeScan, Milpitas, CA) following 6 h of fasting. IPGTT and IPITT were conducted according to the previously reported method (Li et al., 2019; Fukumura et al., 2021).

A recombinant pAdxsi adenovirus constitutively expressing PTPN2 systemically was constructed using the pAdxsi adenovirus system (SinoGenoMax, Beijing, China). Mouse-derived PTPN2 cDNAs were inserted into the pShuttle-CMV-EGFP vector and the pAdxsi vector adenovirus was used as a control vector. At 20 weeks mice were treated with 5×10^9 plaque-forming units of virus by caudal intravenous injection. Adenovirus re-transferred at 22 weeks and the control group was injected with control virus (vehicle). All mice were euthanized at 24 weeks of age for further study as below.

Histological and morphometric analysis of adipose tissue

Samples were taken from epididymal, subcutaneous and brown adipose tissue (SAT, VAT, and BAT) and each sample was cut into 2 parts on average, one of which was fixed with 4% paraformaldehyde, embedded with paraffin and sliced into 5um-thick sections. The morphology of adipocytes was analyzed from sections staining with hematoxylin and eosin (H&E). Adipocyte areas were assessed under X400 magnification within adipose tissue, and the number of adipocytes per area was obtained by quantitative morphometry with automated image analysis (Image-Pro Plus, Version 5.0; Media Cybernatics, Houston, TX) to assess the size of adipocytes.

Immunohistochemical staining

Paraffin sections were treated with immunohistochemistry using microwave-based antigen retrieval method. These sections were incubated with primary rabbit polyclonal antibodies at 4°C overnight, and then with a matching biotinylated secondary antibody for 20 min at 37°C. The stained sections were developed with diaminobenzidin (DAB) and restained with hematoxylin. The staining results were observed under a confocal FV 1000 SPD laser scanning microscope (Olympus, Japan) and the integrated optical density values (IOD)/total IOD were evaluated by quantitative morphometry with automated image analysis (Image-Pro Plus, Version 5.0; Media Cybernatics, Houston, TX).

Total protein extraction

Total protein of adipose tissue and cells was extracted using Cell Lysis (C2978, Sigma-Aldrich, USA) added with a protease inhibitor cocktail (1: 100, CW2200S, CWBIO in Beijing, China). After centrifuging at 13,000×g, 4°C for 15 min, supernatant was collected and protein concentration was measured using BCA Protein Assay Kit (23227; ThermoFisher Scientific, United States). Then loading buffer was added, followed by incubating at 99°C for 5 min and subject to Western blotting analysis.

Western blotting analysis

Proteins extracted from tissues or cells were separated by 10% as well as 12% SDS-PAGE and transferred on PVDF membrane. After

TABLE 1 Antibodies and manufacturers.

Target antigen	Company	Catalog no.	Working concentration
PTPN2	Cell Signaling Technology	58935S	Western blotting: 1:1000
Normal rabbit IgG	Cell Signaling Technology	2729S	
β-actin	Abcam	ab8226	Western blotting: 1:1000
Myc	Cell Signaling Technology	2278S	Western blotting: 1:1000
			IF: 1:50
Flag	Sigma-Aldrich	F1804	Western blotting: 1:1000
			IF: 1:50
HA	ORIGENE	TA180128	Western blotting: 1:1000
Erk	Cell Signaling Technology	4695S	Western blotting: 1:1000
p-Erk	Cell Signaling Technology	4370S	Western blotting: 1:1000
JNK	Cell Signaling Technology	9252S	Western blotting: 1:1000
p-JNK	Cell Signaling Technology	4668S	Western blotting: 1:1000
P38	Cell Signaling Technology	9212S	Western blotting: 1:1000
p-P38	Cell Signaling Technology	4511S	Western blotting: 1:1000
P65	Cell Signaling Technology	8242S	Western blotting: 1:1000
p-P65	Cell Signaling Technology	3033S	Western blotting: 1:1000
IκB	Cell Signaling Technology	4812S	Western blotting: 1:1000
p- IκB	Cell Signaling Technology	2859S	Western blotting: 1:1000
P53	Cell Signaling Technology	2524S	Western blotting: 1:1000
			IHC:1:100
P16	Abcam	ab270058	Western blotting: 1:1000
			IHC:1:100
P21	Abcam	ab109199	Western blotting: 1:1000
P27	Abcam	ab32034	Western blotting: 1:1000
TAK1	Cell Signaling Technology	5206S	Western blotting: 1:1000
p-TAK1	Cell Signaling Technology	9339S	Western blotting: 1:1000
UCP1	Cell Signaling Technology	72298S	Western blotting: 1:1000
			IHC:1:100
PGC1α	Cell Signaling Technology	2178S	Western blotting: 1:1000
FABP4	Abcam	ab92501	Western blotting: 1:1000
INSR	Abcam	ab283689	Western blotting: 1:1000
Acox1	Abcam	ab2184032	Western blotting: 1:1000
PPARγ	Abcam	ab272718	Western blotting: 1:1000
SIRT3	Abcam	ab246522	Western blotting: 1:1000
SLC27A1	Abclonal	A12847	Western blotting: 1:1000
ATGL	Abcam	ab207799	Western blotting: 1:1000
			IHC:1:100
HSL	Abcam	ab45422	Western blotting: 1:1000

(Continued on following page)

TABLE 1 (*Continued*) Antibodies and manufacturers.

Target antigen	Company	Catalog no.	Working concentration
			IHC:1:100
LPL	Abcam	ab91606	Western blotting: 1:1000

TABLE 2 Primer sequences.

Gene name	Sequence 5′-3′
mouse β-*actin* forward	CCACACCCGCCACCAGTTCG
mouse β-*actin* reverse	TACAGCCCGGGGAGCATCGT
mouse *Ptpn2* forward	AGCAGTGAGAGCATTCTACGG
mouse *Ptpn2* reverse	GTGCAGAAAGGTGCTGGGTA
mouse *Ucp1* forward	TCACCACCCTGGCAAAAACA
mouse *Ucp1* reverse	GCAGGTGTTTCTCTCCCTGAA
mouse *Fabp4* forward	CGACAGGAAGGTGAAGAGCATCATA
mouse *Fabp4* reverse	CATAAACTCTTGTGGAAGTCACGCCT
mouse *Insr* forward	GATCCGCGCCGCCTTTT
mouse *Insr* reverse	GGGACTGTCTCTCGGCTCTC
mouse *Pgc1α* forward	ACCATGACTACTGTCAGTCACTC
mouse *Pgc1α* reverse	GTCACAGGAGGCATGTTTGAAG
mouse *Atgl* forward	TGACCATCTGCCTTCCAGA
mouse *Atgl* reverse	GAGAGGTTGTTTCGTACCCA
mouse *Hsl* forward	GCACTGTGACCTGCTTGGT
mouse *Hsl* reverse	CTGGCACCCTCACTCCATA
mouse *Lpl* forward	ACTCTGTGTCTAACTGCCACTTCAA
mouse *Lpl* reverse	ATACATTCCCGTTACCGTCCAT

TABLE 3 Plasmids and manufacturers.

Gene name	Tag	Vector name	Manufacturer
Vector only	C-Flag	pReceiver-M35	GeneCopoeia
Vector only	N-3xHA	pReceiver-M06	GeneCopoeia
Vector only	C-Myc	pReceiver-M09	GeneCopoeia
PTPN2	C-Flag	pReceiver-M35	GeneCopoeia
PTPN2	C-Myc	pReceiver-M09	GeneCopoeia
TRAF6	C-Flag	pReceiver-M35	GeneCopoeia
TAK1	C-Flag	pReceiver-M35	GeneCopoeia
TAK1	C-Myc	pReceiver-M09	GeneCopoeia
TAB1	N-3xHA	pReceiver-M06	GeneCopoeia
TAB2	C-Flag	pReceiver-M35	GeneCopoeia

incubation with 5% BSA (Albumin from bovine serum), transferred blots were incubated with primary antibodies (listed in Table 1) overnight at 4°C. On the next day, the PVDF membrane was added with anti-IgG horseradish peroxidase-conjugated secondary antibody at room temperature for 2 h. Blot images were detected by chemiluminescent reagent (WBKLS0500, Millipore, United States) via a luminescent image instrument (Amersham Imager 680, GE, United States). Total protein levels were normalized to β-actin levels.

Total RNA extraction and quantitative RT-PCR assay

Total RNA was extracted from adipocytes using the Total RNA Extraction Kit (220011, Fastagen in Shanghai, China) based on protocols. The PrimeScript RT reagent kit was used for reversed-transcribtion including gDNA Eraser (RR047A, TaKaRa, Japan). The cDNA samples were subject to quantitative PCR process for indicators detection using the LightCycler® 480 SYBR® Green I Master (04887352001, Roche, Switzerland) by Roche LightCycler480 according to protocols. The level of β-actin was used for data normalization and the $2^{-\Delta\Delta CT}$ method was used for calculation. Primer sequences are listed in Table 2.

Elisa assay

The concentrations of IL6 (SM6000B, R&D) and IL1β (MHSLB00, R&D) of adipocyte supernatant was measured using Enzyme-linked immunosorbent assay (ELISA) kits according to instructions.

Cell culture

Primary preadipocytes were isolated from SAT according to a standard protocol (Macotela et al., 2012). Then cells differentiated into mature adipocytes (hereafter primary adipocytes) exposed to serum-containing media supplemented with insulin, 1-methyl-3-isobutylxanthine (IBMX), indomethacin, dexamethasone, triiodothyronine (T3) and rosiglitazone and then switched to insulin, T3 and rosiglitazone for maintenance (Armani et al., 2014). Mouse 3T3-L1 cell line were purchased from the cellbank of Chinese Academy of Sciences. The mouse 3T3-L1 cell line is immortalised and does not undergo senescence as primary adipocytes. Then, cells were cultured and induced to differentiate (hereafter 3T3-L1-derived adipocytes) as previously reported (Molinari et al., 2021). After differentiation, Adipocytes were treated with tumor necrosis factor-alpha (TNFα) stimulation.

Human HEK293T cells and Hela cells were obtained from KeyGene BioTech (China) and cultured in complete Dulbecco's Modified Eagle's Medium (DMEM; C11995500BT, Gibco, United States) medium.

Plasmids and siRNA transfection

Plasmids were transiently transfected into cells with the help of lipofectamine 3000 reagent (100022052, Invitrogen, USA) based on manufacturer's protocols. The lipofectamine RNAiMAX reagent (56532, Invitrogen) was used for siRNA transfection. After plasmid or siRNA transfection for 24 h, cells could be treated for further processing, then lysed for protein collection. For adipocytes, siRNA and plasmids were transfected during initial plating and grown to confluence, and transfected once again after 48 h. After transfection, primary adipocytes and the 3T3-L1 cell line were differentiated into mature adipocytes. Plasmids are listed in Table 3.

Co-immunoprecipitation (Co-IP) analysis

For exogenous Co-IP analysis, plasmids expressing PTPN2 and other indicators were transfected into HEK293T cells. After transfection with 24 h, cells were lysed with 1 mL Cell Lysis for protein extraction. After centrifugation for 15 min at 13,000g, 4°C, 100ul supernatant was removed as "Input" and the rest was incubated with agarose immunoprecipitation beads for tag combination with 4 °C incubation overnight on a rotary mixer. Beads were then washed for 5 times using Radio Immunoprecipitation Assay (RIPA) buffer (P0013c, Beyotime Biotechnology, China). Precipitated proteins were separated from beads after incubation at 99°C for 5min with 2x loading buffer. Before the incubation at 99°C, c-Myc peptide (M2435, sigma) or 3X-Flag peptide (F4799, sigma) was added to compete out the binding of c-Myc or 3X-Flag for necessary.

The protocol of endogenous Co-IP in 3T3-L1-derived adipocytes was similar to exogenous analysis described above. After supernatant preparation, corresponding antibodies were added for endogenous protein combination at 4°C for 1 h. Then protein A/G Plus Agarose (sc-2003, Santa Cruz Biotechnology, United States) was used for antibody-combination at 4°C overnight with gentle mixture. Notably, normal rabbit IgG (2729S, Cell Signaling Technology, United States) was used as a negative control (Ida et al., 2021).

Laser confocal photography of cells

Hela cells were seeded on climbing slices for staining. Plasmids expressing PTPN2 and TAK1 were co-transfected into Hela cells for 24 h. After fixation, 0.1% Triton X-100 was used for cell membranes permeabilization for 5 min, and then 10% goat serum was used for blocking. Then cells were incubated using primary antibodies at 4°C overnight. On the next day, corresponding fluoresce secondary antibodies were used to multiple signaling cascades. DAPI was used for nuclei stain and mounting. Samples incubated with IgG and secondary antibody were used as negative control. Images were captured via laser confocal microscope or electric upright microscope.

Senescence-associated β-galactosidase (SA-β-gal) staining

SA-β-gal staining was performed with Senescence β-Galactosidase Staining Kit (Beyotime, China) according to the manufacturer's instruction. Primary adipocytes were fixed with β-Galactosidase fixing solution for 15 min after washed with PBS, and then maintained with the staining solution. The blue areas were recognized to be SA-β-gal-positive.

Statistical analysis

All data were statistically analyzed using GraphPad Prism 8 (GraphPad, San Diego, CA) and expressed as mean ± standard deviation (SD). The number of replicates was indicated in figure legends (n-numbers) and we did independent biological repeats for each experiment. The Shapiro-wilk test was used to evaluate the normality assumption of the data distribution. For normally distribution, the statistical difference was determined by unpaired two-tailed Student's t-tests, one-way ANOVA test or two-way ANOVA accordingly. If *p*-value was less than 0.05, the comparison was considered to be statistically significant. $^{*}P < 0.05$, $^{**}P < 0.01$, $^{***}P < 0.001$; $^{\#}P < 0.05$, $^{\#\#}P < 0.01$, $^{\#\#\#}P < 0.001$.

Results

PTPN2 ameliorates cellular senescence in adipocytes

The expression level of PTPN2 in the serum is downregulated in T2DM patients (Zheng et al., 2018). As TNFα is a triggering factor in IR (Pedersen, 2017) and involved in several pathogenesis programs, we chose TNFα as the stimulation factor for adipocytes. 3T3-L1 cells were used to differentiate into mature adipocytes. Then, 3T3-L1-derived adipocytes were incubated with TNFα (40 ng/mL) for different time points (0, 4, 8, 12, 24, and 36 h) and we found that the mRNA and protein level of PTPN2 by TNFα stimulation was decreased in a time-dependent manner, especially significant after 24 h stimulation (Figures 1A, B). The mRNA and protein levels of PTPN2 also declined in a concentration-dependent manner in response to TNFα (Figures 1C, D) in 3T3-L1-derived adipocytes. Furthermore, the time-dependent downregulation was confirmed in mouse primary adipocytes (Figures 1E, F).

To further investigate the role of PTPN2 in adipocytes, a whole genome RNA-sequence analysis was performed using primary adipocytes with or without PTPN2 knockdown. Kyoto Encyclopedia of Genes and Genomes (KEGG) enrichment analysis in cellular processes revealed a strong association between PTPN2 and cellular senescence (Figure 1G). Therefore, we silenced the PTPN2 gene in primary adipocytes from mice using small interfering RNA (siRNA). PTPN2-deficient (siPTPN2) primary adipocytes exhibited an increase in senescence-associated β-galactosidase (SA-β-gal) activity compared with the control group (siCtrl) as demonstrated with SA-β-gal staining (Figure 1H). Interleukin-6 (IL6) and Interleukin-1β (IL1β) are two key components of SASP (Gorgoulis et al., 2019). Excessive IL6 and

10.3389/fphar.2023.1124633

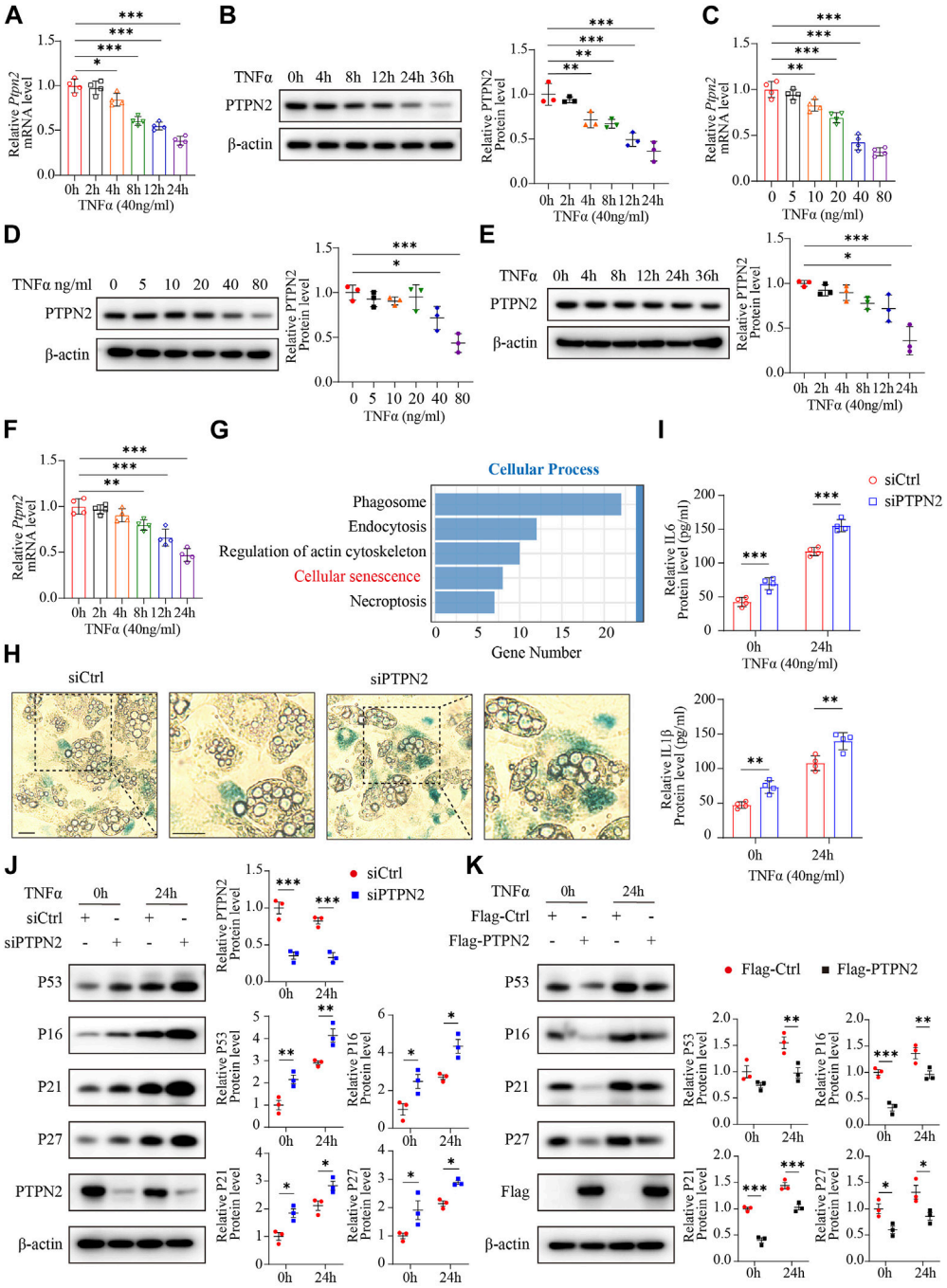

FIGURE 1
PTPN2 ameliorates cellular senescence in adipocytes. **(A)** Quantitative PCR (n = 4) of PTPN2 mRNA level in 3T3-L1-derived adipocytes treated with TNFα (40 ng/mL) for different time points. **(B)**, Western blotting of 3T3-L1-derived adipocytes treated with TNFα (40 ng/mL) for different time points (left) and data analysis (right, n = 3). β-actin was used for normalization. **(C),** Quantitative PCR (n = 4) of PTPN2 mRNA level in 3T3-L1-derived adipocytes treated with a concentration gradient of TNFα for 24 h. **(D)**, Western blotting of 3T3-L1-derived adipocytes treated with a concentration gradient of TNFα for 24 h (left) and data analysis (right, n = 3). **(E)**, Western blotting of primary preadipocyte-derived mature adipocytes treated with TNFα (40 ng/mL) for different time points (left) and data analysis (right, n = 3). **(F)**, Quantitative PCR (n = 4) of PTPN2 mRNA level in primary adipocytes treated with TNFα (40 ng/mL) for different time points. **(G)**, Primary preadipocytes were transfected with negative control siRNA (siCtrl) or PTPN2-siRNA (siPTPN2) and then induced to differentiate into mature primary adipocytes before TNFα stimulation for 24 h. The whole genome RNA-sequence analysis was performed and Kyoto Encyclopedia of Genes and Genomes (KEGG) enrichment analysis in cellular process between the two groups was shown (n = 3). **(H)**, The senescence-associated β-galactosidase (SA-β-gal) staining of primary adipocytes transfected with siCtrl or siPTPN2. Scale bar:50 μm. **(I)**, Elisa assay of interleukin-6 (IL6) and Interleukin-1β (IL1β) secreted from 3T3-L1-derived adipocytes with or without PTPN2 knockdown. Cells were pre-incubated with TNFα for 24 h before supernatant collection (n = 4). **(J)**, Western blotting images of indicated proteins in 3T3-L1-derived adipocytes transfected with negative control or PTPN2-siRNA in response to TNFα (40 ng/mL hereafter) and its quantitative analysis (n = 3). **(K)**, Western blotting images of indicated proteins in 3T3-L1-derived adipocytes transfected with or without Flag-tagged PTPN2 plasmid (Flag-PTPN2) overexpression in response to TNFα (n = 3). *P < 0.05, **P < 0.01, ***P < 0.001.

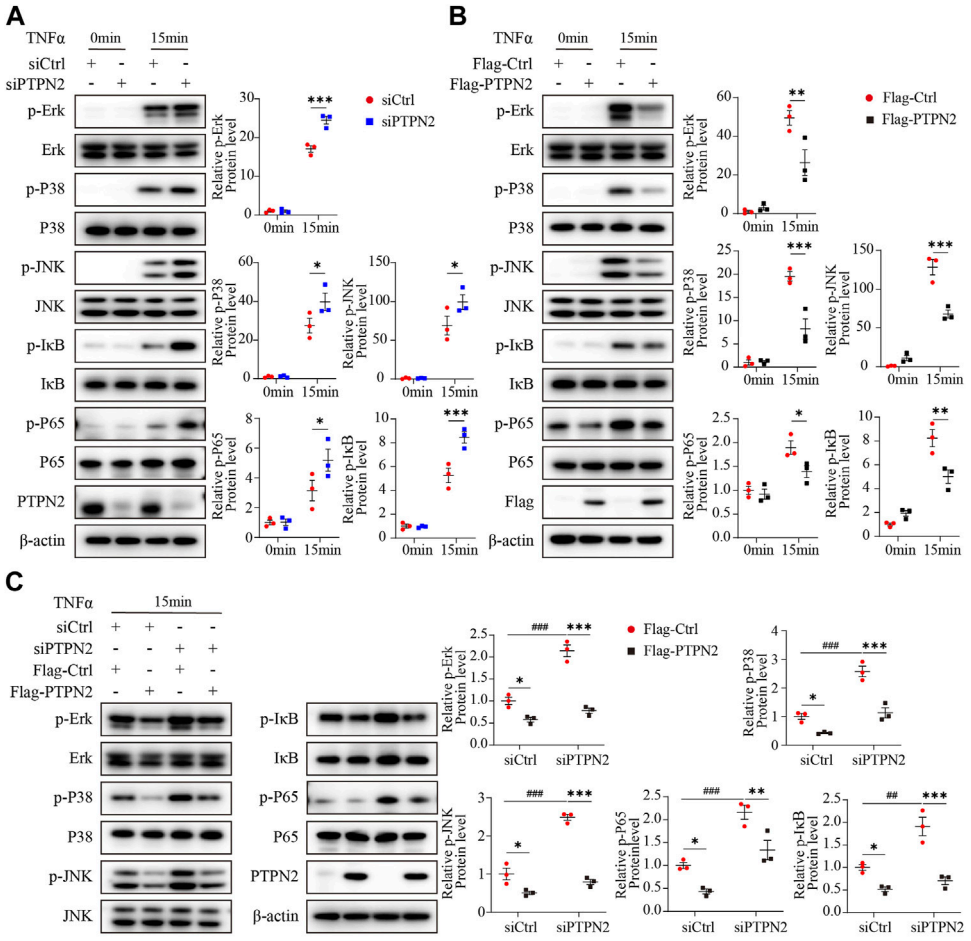

FIGURE 2
PTPN2 inhibits phosphorylation of MAPK/NF-κB in adipocytes induced by TNFα. **(A)**, Representative Western blotting images and data analysis of indicated proteins in 3T3-L1-derived adipocytes transfected with siCtrl or siPTPN2 with TNFα stimulation within 15 min (n = 3). **(B)**, Western blotting analysis of indicated proteins in 3T3-L1-derived adipocytes with or without Flag-PTPN2 overexpression in response to TNFα (n = 3). **(C)**, In 3T3-L1-derived adipocytes, PTPN2 protein level was silenced via siPTPN2 followed by overexpression with or without Flag-PTPN2 for rescue. Western blotting analysis of indicated proteins in response to TNFα was shown (n = 3). *P < 0.05, **P < 0.01, ***P < 0.001; #P < 0.05, ##P < 0.01, ###P < 0.001.

IL1β were secreted from 3T3-L1-derived adipocytes after TNFα stimulation and increased in siPTPN2 group (Figure 1I). Then, we tested the protein level of P53, P16, P27 and P21, which often gradually increase during cellular senescence. PTPN2 deficiency increased the level of senescence-related proteins (Figure 1J), and 3T3-L1-derived adipocytes with overexpressed PTPN2 confirmed these findings (Figure 1K). Thus, PTPN2 might alleviate senescent phenotype in adipocytes.

PTPN2 inhibits phosphorylation of MAPK/NF-κB in adipocytes induced by TNFα

As the MAPK/NF-κB pathway implements key traits of cellular senescence (Anerillas et al., 2020), we investigated the role of PTPN2 in the regulation of the MAPK/NF-κB pathway. We treated 3T3-L1-derived adipocytes with TNFα as an inducer and the phosphorylation level of Erk (p-Erk), P38 (p-P38), JNK (p-JNK), IκB (p- IκB) and P65 (p-P65) was upregulated in siRNA-mediated PTPN2-silent 3T3-L1-derived adipocytes after TNFα treatment (Figure 2A). Consistently, when 3T3-L1-derived adipocytes were transfected with Flag-tagged PTPN2 plasmid (Flag-PTPN2) for PTPN2 overexpression, the phosphorylation level of Erk, P38, JNK, IκB, and P65 was decreased significantly in response to TNFα (Figure 2B). To further confirm the effect of PTPN2 on MAPK/NF-κB pathway, we first silenced PTPN2 expression via siRNA, where the phosphorylation level was upregulated, and then rescued PTPN2 protein level by overexpression so that the phosphorylation level was inhibited subsequently (Figure 2C).

PTPN2 interacts with TAK1 directly

To identify exact molecules regulated by PTPN2, we co-transfected HEK293T cells with Myc-tagged PTPN2 plasmid and other plasmids encoding upstream regulators of MAPK/NF-κB pathway for the co-immunoprecipitation (Co-IP) experiment.

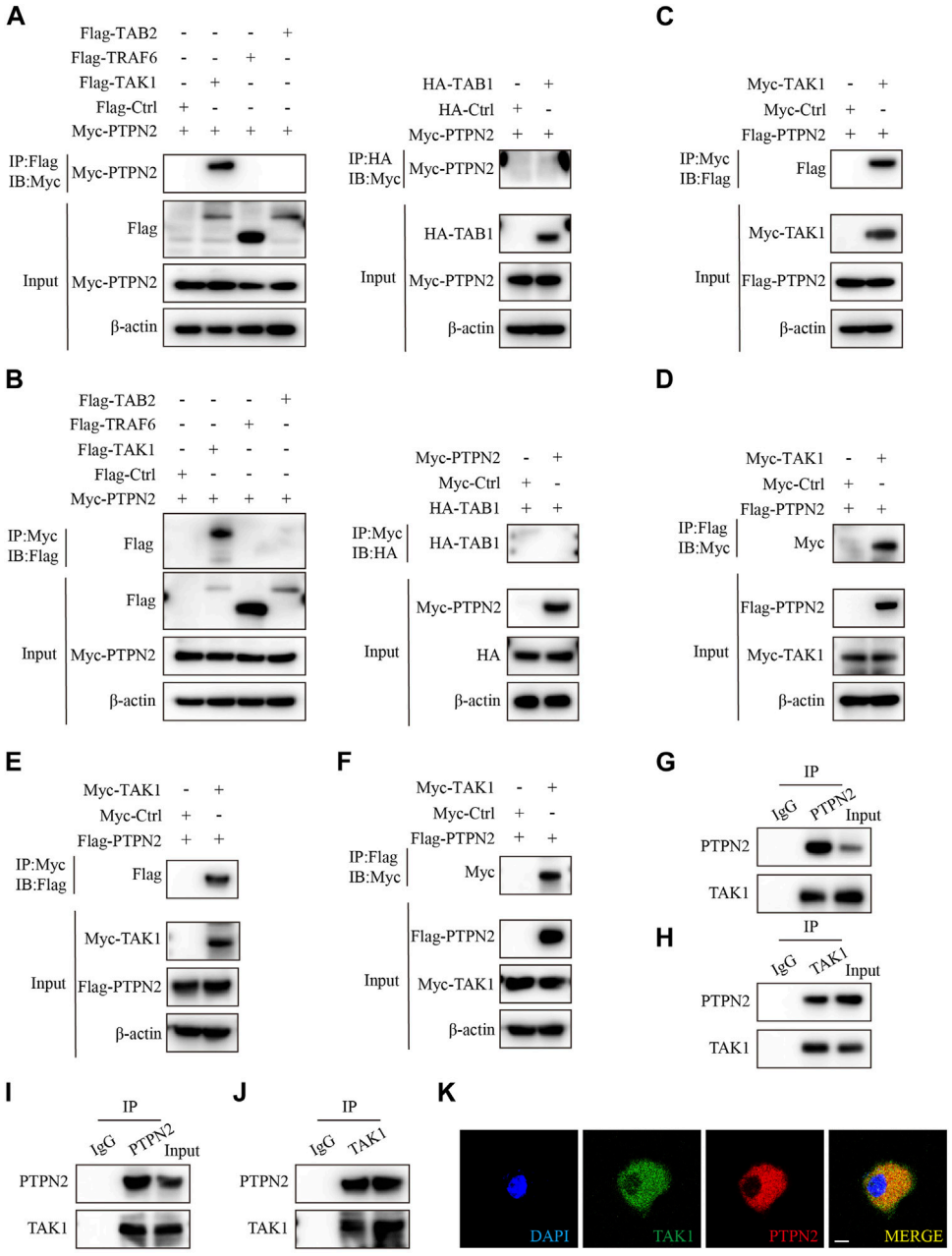

FIGURE 3
PTPN2 interacts with TAK1. **(A)**, Co-immunoprecipitation (Co-IP) analysis of HEK293T cells co-transfected with Myc-tagged PTPN2 and Flag-tagged TAK1, TRAF6, TAB2 to examine the interactors of PTPN2. Co-IP of whole cell lysates was immunoprecipitated using Flag beads (left). HEK293T cells were co-transfected with Myc-tagged PTPN2 and HA-tagged TAB1 and Co-IP of whole cell lysates was immunoprecipitated using HA beads (right). **(B)**, HEK293T cells were co-transfected with Myc-tagged PTPN2 and Flag-tagged TAK1, TRAF6, TAB2 and HA-tagged TAB1. Co-IP of whole cell lysates was immunoprecipitated using Myc beads. **(C, D)**, Co-IP assay of HEK293T cells co-transfected with Myc-TAK1 and Flag-PTPN2. Co-IP was performed using Myc beads **(C)** and Flag beads **(D)** respectively. **(E, F)**, Co-IP assay of Hela cells co-transfected with Myc-TAK1 and Flag-PTPN2. Co-IP was performed using Myc beads **(E)** and Flag beads **(F)** respectively. **(G, H)**, Western blotting images of indicated proteins of endogenous Co-IP in 3T3-L1-derived adipocytes immunoprecipitated with anti-PTPN2 **(G)**, anti-TAK1 **(H)** or with rabbit IgG control under TNFα stimulation. **(I, J)**, Western blotting images of indicated proteins of endogenous Co-IP in primary adipocytes immunoprecipitated with anti-PTPN2 **(I)**, anti-TAK1 **(J)** or with rabbit IgG control under TNFα stimulation. **(K)**, Representative confocal microscopic images of colocalization between PTPN2 and TAK1 in Hela cells co-transfected with Flag-tagged PTPN2 and Myc-tagged TAK1. Scale bar: 10 μm.

PTPN2 interacted with TAK1 directly, but not with TRAF6, TAB2 and TAB1 (Figures 3A, B). Then, we confirmed the interaction between PTPN2 and TAK1 using tag-altered plasmids in HEK293T cells (Figures 3C, D) and Hela cells (Figures 3E, F), respectively. Endogenous Co-IP experiments in 3T3-L1-derived adipocytes (Figures 3G, H) and primary adipocytes (Figures 3I, J) confirmed the interaction between endogenous PTPN2 and TAK1. Moreover, we co-transfected PTPN2 and TAK1 plasmids into HeLa

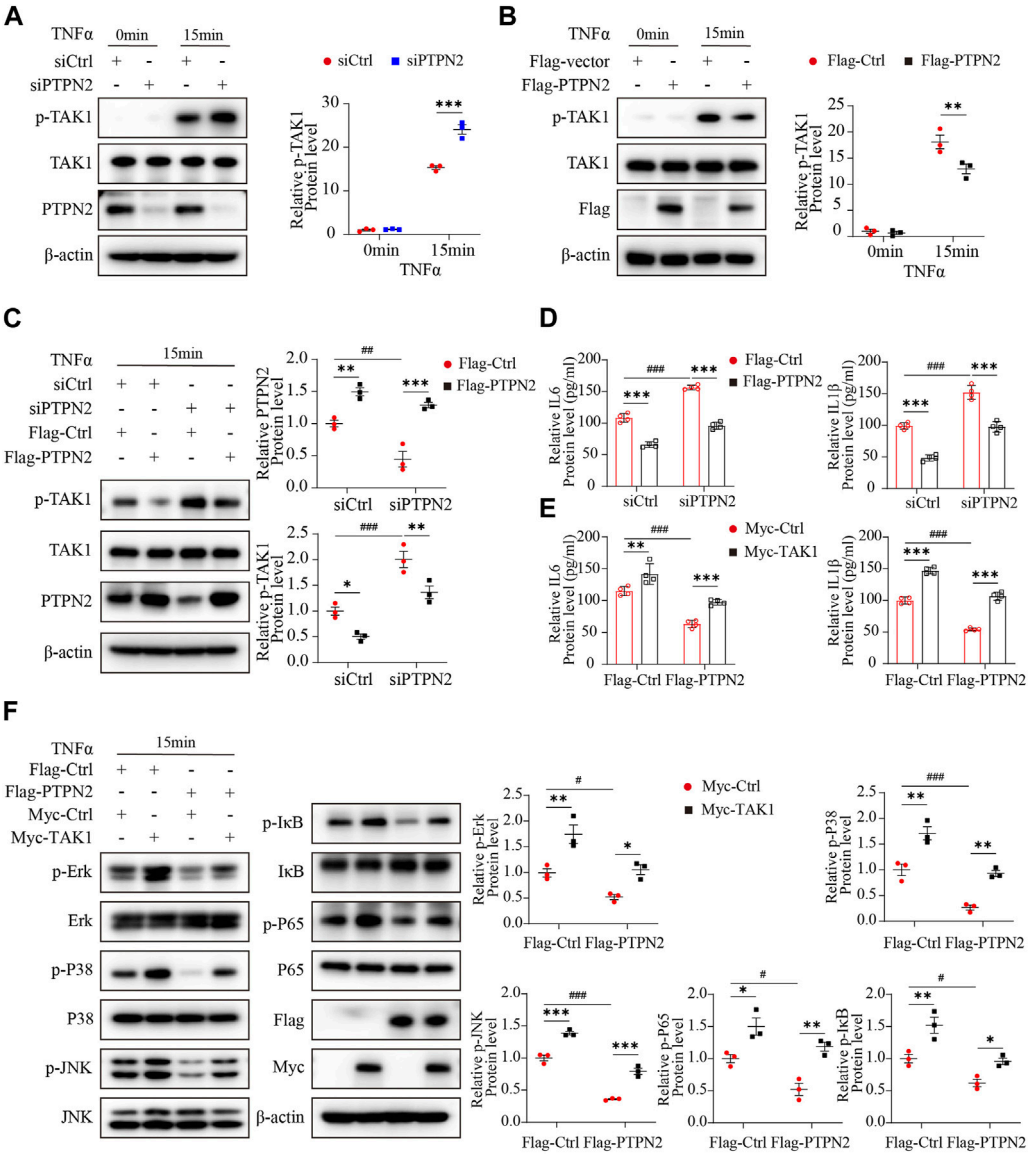

FIGURE 4
PTPN2 inhibits MAPK/NF-κB pathway via targeting TAK1 for dephosphorylation. **(A),** Western blotting images of indicated proteins in 3T3-L1-derived adipocytes transfected with siCtrl or siPTPN2 in response to TNFα (n = 3). **(B),** Western blotting analysis of indicated proteins in 3T3-L1-derived adipocytes transfected with control vector or Flag-PTPN2 with TNFα stimulation (n = 3). **(C, D),** In 3T3-L1-derived adipocytes, PTPN2 protein level was silenced via siPTPN2 firstly followed by overexpression with or without Flag-PTPN2 for rescue. Western blotting analysis of indicated proteins **(C),** (n = 3) and elisa assay of IL6 and IL1β secreted from 3T3-L1-derived adipocytes **(D),** (n = 4) in response to TNFα was shown. **(E, F),** In 3T3-L1-derived adipocytes, PTPN2 was overexpressed via Flag-PTPN2 transfection followed by overexpression with or without Myc-TAK1. Elisa assay of IL6 and IL1β secreted from 3T3-L1-derived adipocytes **(E),** (n = 4) and Western blotting analysis of indicated proteins **(F)**, (n = 3) in response to TNFα was shown. *P < 0.05, **P < 0.01, ***P < 0.001; $^{\#}$P < 0.05, $^{\#\#}$P < 0.01, $^{\#\#\#}$P < 0.001.

cells and confocal microscopy revealed that PTPN2 was colocalized with TAK1 (Figure 3K). Therefore, PTPN2 could bind to TAK1.

PTPN2 inhibits the MAPK/NF-κB pathway via targeting TAK1 for dephosphorylation

To explore the effect of PTPN2 on TAK1, we silenced PTPN2 in 3T3-L1-derived adipocytes using siRNA to test the phosphorylation level of TAK1. After the stimulation of TNFα, the level of phosphorylated TAK1 was upregulated in the PTPN2-deficient group compared with the control group (Figure 4A). Consistently, the phosphorylation level of TAK1 was significantly downregulated when PTPN2 was overexpressed in 3T3-L1-derived adipocytes (Figure 4B). Furthermore, we transfected Flag-tagged PTPN2 plasmid in 3T3-L1-derived adipocytes after PTPN2 silencing for rescue, and the result revealed that PTPN2-silence promoted the phosphorylation level of TAK1 while its phosphorylation was inhibited after PTPN2 overexpression (Figure 4C). A similar trend was also observed for the level of

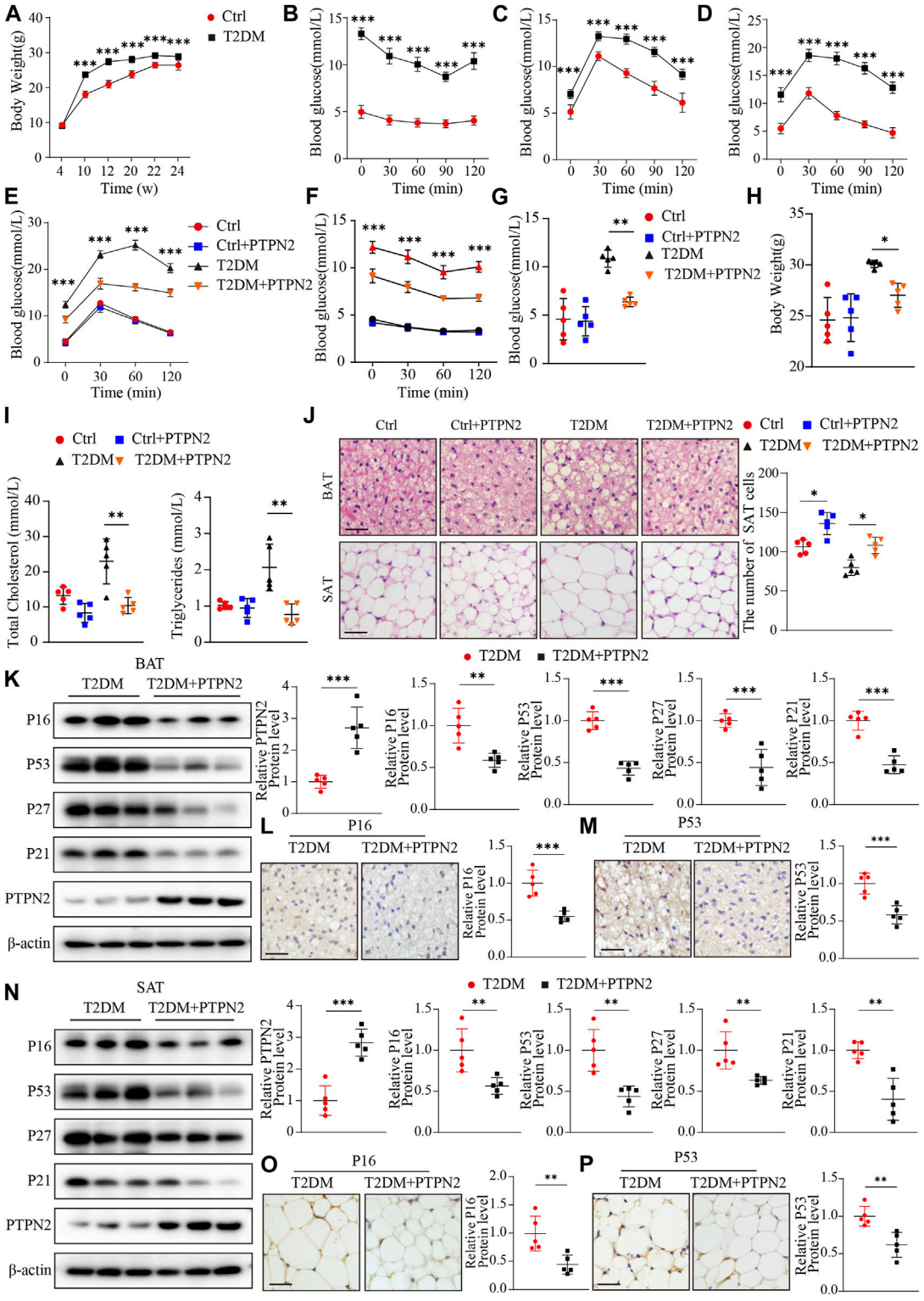

FIGURE 5
Overexpression of PTPN2 alleviates senescence in adipose tissue in T2DM mice. **(A),** Body weight of mice at the age of 4, 10, 12, 20, 22 and 24 weeks (n = 10). **(B),** Blood glucose level of IPITT at the age of 12 weeks (n = 10). **(C, D),** Blood glucose level of IPGTT at the age of 10 and 12 weeks (n = 10). **(E),** Blood glucose level of IPGTT in mice at the age of 24 weeks (***P < 0.001 vs. T2DM + PTPN2, n = 5). **(F),** Blood glucose level of IPITT in mice at the age of 24 weeks (***P < 0.001 vs. T2DM + PTPN2, n = 5). **(G)**, Fasting blood glucose level in mice at the age of 24 weeks (n = 5). **(H)**, Body weight of mice at the age of 24 weeks. **(I)**, Total Cholesterol level (left) and Triglycerides level (right) of mice at the age of 24 weeks. **(J),** BAT, SAT were stained with H&E (left) and the count of 3T3-L1-derived adipocytes in SAT within the field of the same size (right) was shown (n = 5, scale bar: 20 μm). **(K),** Representative Western blotting of indicated proteins in BAT of T2DM and T2DM + PTPN2 mice
(*Continued*)

FIGURE 5 (Continued)
with data analysis (n = 5). **(L, M)**, Immunohistochemical staining of P16 (**L**) and P53 (**M**) protein in BAT, respectively (brown staining considered to be positive; scale bar: 20 μm). **(N),** Representative Western blotting of indicated proteins in SAT of T2DM and T2DM + PTPN2 mice with data analysis (n = 5). **(O, P)**, Immunohistochemical staining of P16 (**O**) and P53 (**P**) protein in SAT, respectively. scale bar: 20 μm. *P < 0.05, **P < 0.01, ***P < 0.001.

IL6 and IL1β secreted into the supernatant from cultured 3T3-L1-derived adipocytes (Figure 4D).

Finally, to investigate whether TAK1 has a role in the regulation of PTPN2 for the MAPK/NF-κB pathway, a recovery experiment was performed where TAK1 protein level was rescued in PTPN2-deficient 3T3-L1-derived adipocytes. Obviously, when stimulated with TNFα, the diminished SASP protein level of the PTPN2-overexpressed group was rescued by TAK1 overexpression (Figure 4E) and similar results were observed from the phosphorylation level detection of proteins of the MAPK/NF-κB pathway (Erk, P38, JNK, IκB and P65) (Figure 4F). Therefore, TAK1 acts as an essential regulator mediating the dephosphorylation effect of PTPN2 on the MAPK/NF-κB pathway.

PTPN2 overexpression improves IR and lipid retention of adipose tissue in T2DM mice

The results above suggested that PTPN2 ameliorated adipocyte senescence and as adipocytes are the major cell type in adipose tissue, we proposed that PTPN2 could improve senescence in adipose tissue.

A non-genetic rodent model closely resembling human T2DM was generated by giving male C57BL/6 mice HFD as well as the STZ treatment (referred to as T2DM hereafter) while normal-diet fed mice served as controls (Ctrl hereafter). Multiple metabolic parameters of mice were examined to confirm the model generation. The body weight gain in the T2DM group was significantly increased compared with that in the control group after week-10 as expected (Figure 5A). IR in mice was verified by IPITT which showed that the blood glucose levels of T2DM group were higher than that of the control group at week-12 (Figure 5B). IPGTT was also tested at the age of 10 and 12 weeks, showing that blood glucose levels in the T2DM group were significantly elevated compared to the control group at all of the 5 time points (Figures 5C, D). Therefore, the T2DM model induced by HFD and STZ showed typical features of IR, hyperglycaemia and obesity, resembling the state of human T2DM.

For the T2DM model, IPGTT and IPITT demonstrated that compared with the control group, blood glucose levels in T2DM group were higher at all of the points tested at the age of 24 weeks, while levels in the PTPN2-overexpression group (T2DM + PTPN2) were lower than those in T2DM mice, indicating an improvement role of PTPN2 in IR and hyperglycaemia (Figures 5E, F). The fasting blood glucose level also showed that PTPN2 overexpression improved hyperglycaemia in T2DM mice (Figure 5G). We also discovered that the body weight, total cholesterol level and triglycerides level were decreased in the PTPN2-overexpression group compared with that in the T2DM group (Figures 5H, I). As adipose tissue plays a pivotal role in the development of insulin resistance, we isolated BAT, SAT and VAT respectively for subsequent experiments. The H&E staining demonstrated that the number of adipocytes in SAT counted in the T2DM group was lower than that of the control group in a field of identical size, indicating the bigger size and more lipid content of adipocytes in T2DM group. However, after Ad-PTPN2 treatment, the adipocyte number of SAT in the T2DM + PTPN2 group was significantly higher than that in T2DM group and a similar trend was also observed in VAT (data not shown). For BAT, we found that there were unilocular adipocytes akin to white adipocytes in T2DM mice while after PTPN2 intervention, there was a switch from unilocular to multilocular morphology in the T2DM + PTPN2 group (Figure 5J).

Overexpression of PTPN2 alleviates senescence in adipose tissue in T2DM mice

We have demonstrated that PTPN2 ameliorated cellular senescence in adipocytes *in vitro*, then we assessed the effects of PTPN2 on adipose tissue *in vivo* and proteins related to senescence were analyzed in T2DM mice. Western blotting showed that the protein levels of P16, P53, P27 and P21 was downregulated in BAT of the PTPN2-overexpressing mice compared with the T2DM group without PTPN2-overexpression (Figure 5K). Furthermore, two main indicators, P16 and P53, were characterized by immunohistochemical staining in adipose tissue which showed that the protein level of p16 and P53 in the T2DM + PTPN2 group after PTPN2 intervention was significantly decreased compared with the T2DM group (Figures 5L, M). Similar results were also obtained from SAT of T2DM mice, indicating the role of PTPN2 in improving senescence in adipose tissue (Figures 5N–P).

PTPN2 promotes the browning process of adipocytes in adipose tissue

As aging aggravates the loss of brown adipocytes (Rogers et al., 2012) and PTPN2 was demonstrated to regulate senescence in adipose tissue, we evaluated regulatory genes that promoted adipocyte browning. Firstly, PTPN2 was silenced in 3T3-L1-derived adipocytes and then stimulated with TNFα. The expression of specific markers including UCP1, PGC1α [proliferator-activated receptor gamma coactivator-1-alpha, which regulates mitochondrial biogenesis and fatty acid oxidation (Yan et al., 2016)], FABP4 [fatty acid-binding protein-4, which regulates adipocyte differentiation and β-oxidation of fatty acids (Walenna et al., 2018)] and INSR (insulin receptor, relating to adipocyte differentiation and function) were assessed at both of the protein (Figure 6A) and mRNA (Figure 6B) levels. The results revealed that PTPN2 knockdown inhibited the browning process of adipocytes. White adipocyte browning develops predominantly in response to cold exposure and adrenergic stress, and it has become a therapeutic target for weight gain and metabolic dysfunction (Sidossis et al., 2015; Sakers et al., 2022).

Then we assessed the influence of PTPN2 on adipose tissue browning activity *in vivo*. The protein levels of Acox1 (acyl-coenzyme A oxidase 1, which regulates β-oxidation of adipose tissue (De Carvalho et al., 2021)), INSR, PGC1α, PPARγ [peroxisome-proliferator-activated receptor-gamma, which activates the thermogenic brown fat gene program (Ohno et al., 2012)], SIRT3 [Sirtuin 3, a NAD-dependent deacetylase which regulates mitochondrial fatty-acid oxidation

10.3389/fphar.2023.1124633

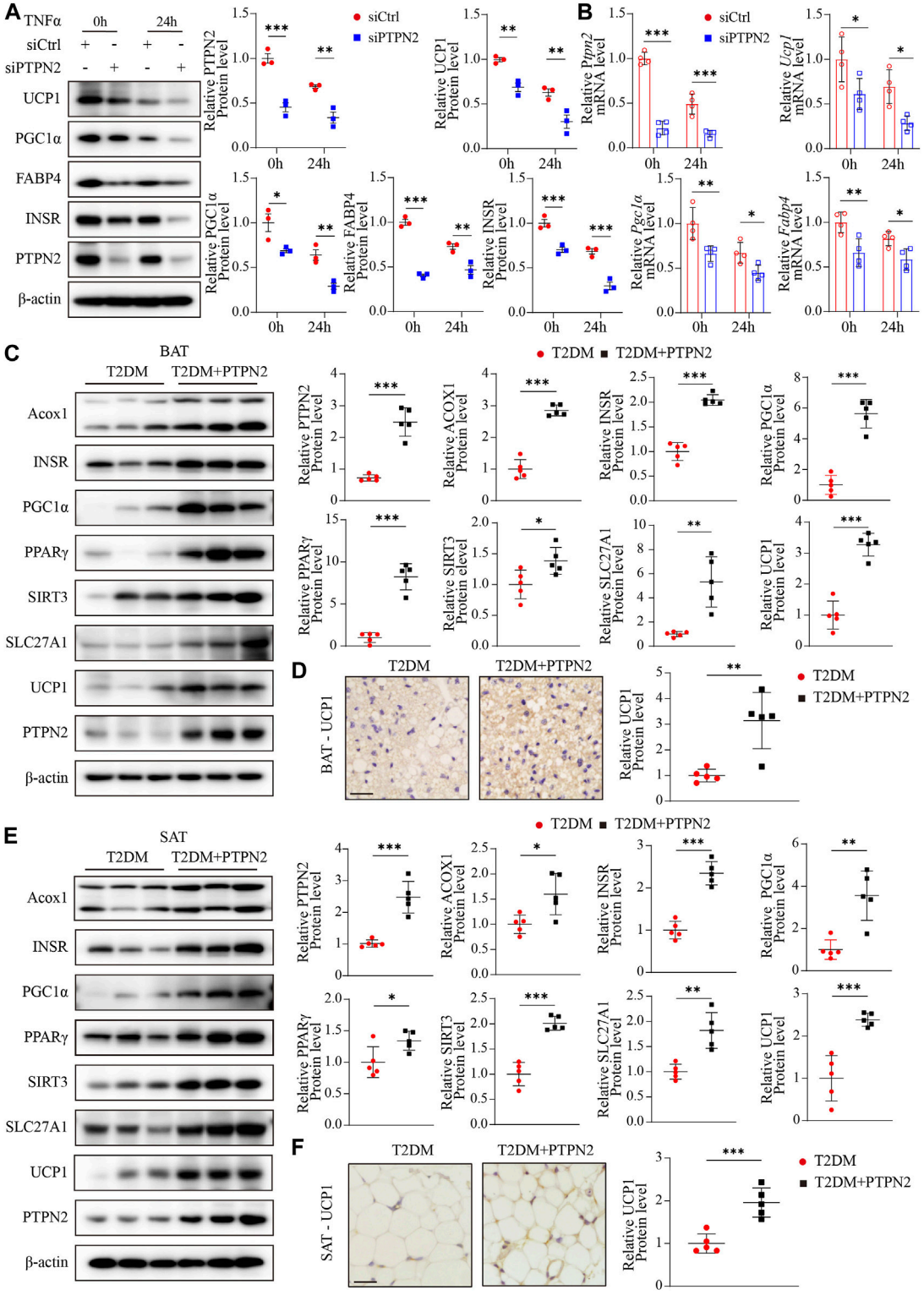

FIGURE 6
PTPN2 promotes the browning process of adipocytes in adipose tissue. **(A),** Western blotting analysis of indicated proteins in 3T3-L1-derived adipocytes transfected with siCtrl or siPTPN2 in response to TNFα (n = 3). **(B),** Quantitative PCR analysis of indicated mRNA levels in 3T3-L1-derived adipocytes transfected with siCtrl or siPTPN2 in response to TNFα (n = 4). **(C),** Representative Western blotting images of indicated proteins in BAT (left) and corresponding quantitative analysis (right, n = 5). **(D),** Immunohistochemical staining of UCP1 in BAT (n = 5, scale bar: 20 μm). **(E),** Western blotting analysis of indicated proteins in SAT (n = 5). **(F),** Immunohistochemical staining of UCP1 in SAT (n = 5, scale bar: 20 μm). *P < 0.05, **P < 0.01, ***P < 0.001.

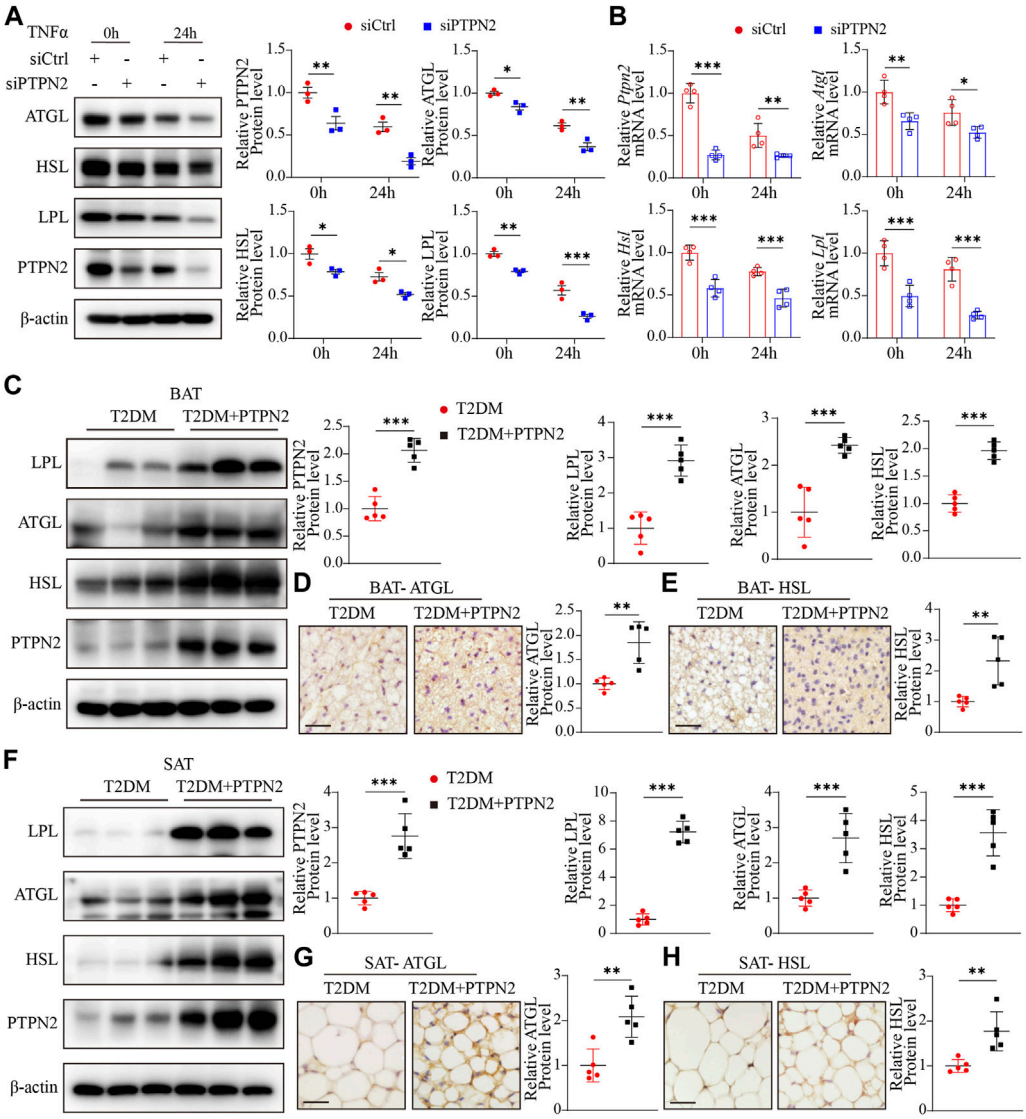

FIGURE 7
PTPN2 overexpression ameliorates adipose tissue functional remodeling in T2DM mice. **(A),** Western blotting analysis of indicated proteins in 3T3-L1-derived adipocytes transfected with siCtrl or siPTPN2 in response to TNFα (n = 3). **(B),** Quantitative PCR analysis of indicated mRNA levels in 3T3-L1-derived adipocytes transfected with siCtrl or siPTPN2 with TNFα stimulation (n = 4). **(C),** Representative Western blotting images of indicated proteins in BAT (left) and corresponding quantitative analysis (right, n = 5). **(D, E),** Immunohistochemical staining of ATGL **(D)** and HSL **(E)** in BAT, respectively (n = 5, scale bar: 20 μm). **(F),** Western blotting analysis of indicated proteins in SAT (n = 5). **(G, H),** Immunohistochemical staining of ATGL **(G)** and HSL **(H)** in SAT (n = 5, scale bar: 20 μm). *P < 0.05, **P < 0.01, ***P < 0.001.

(Hirschey et al., 2010)], SLC27A1 [fatty acid transport protein 1, which promotes the WAT-browning process (Guo et al., 2022)] and UCP1 in adipose tissue were detected by Western blotting. Both mice and humans have thermogenic BAT. A major murine BAT depot is located in the interscapular region and is also found in cervical, axillary, perivascular, and perirenal regions. Human infants also possess BAT depot in the interscapular region, however, it later regresses and is absent in adults. Adult humans possess variable BAT and beige adipose tissue in the paravertebral junctions, cervical/axillary regions and in perirenal/adrenal locations (Sakers et al., 2022).

For BAT, our results showed that overexpressed PTPN2 promoted the protein levels of these browning-related regulators (Figure 6C). Moreover, the protein level of the best characterized thermogenic effector, UCP1, was re-confirmed by immunohistochemical staining, which indicated that overexpressed PTPN2 in T2DM + PTPN2 group facilitated the protein level of UCP1 compared with the T2DM group (Figure 6D). The same analysis was performed in SAT and the protein level of Acox1, INSR, PGC1α, PPARγ, SIRT3, SLC27A1 and UCP1 was upregulated by PTPN2 overexpression (Figures 6E, F), illustrating the role of PTPN2 in promoting the WAT-browning process.

PTPN2 overexpression ameliorates adipose tissue functional remodeling in T2DM mice

Adipose tissue remodeling is a complex process and is regulated by various metabolic challenges. Adipocytes have the ability to act

rapidly in response to excess caloric intake and hypertrophy and hyperplasia are the main mechanisms of adipocyte plasticity (Zhu et al., 2022). Adipose tissue remodeling can be pathologically accelerated in the obese state, featuring reduced angiogenic remodeling, a heightened state of immune cell infiltration and subsequent proinflammatory responses (Sun et al., 2011). Disturbance of lipid metabolism contributes to the progression of IR in T2DM, so we investigated the role of PTPN2 in controlling lipid metabolism. Experiments *in vitro* were performed using 3T3-L1-derived adipocytes transfected with PTPN2-siRNA, and lipid metabolic gene expression was analyzed at the protein and mRNA levels. The results of Western blotting demonstrated that the levels of ATGL (adipose triglyceride lipase, which hydrolyzes intracellular triglyceride), HSL (hormone-sensitive lipase, which is involved in lipid catabolism (Jocken et al., 2016)) and LPL (lipoprotein lipase, which catalyzes the hydrolysis of triglyceride-rich lipoproteins (Jocken et al., 2016)) was reduced in PTPN2-silent 3T3-L1-derived adipocytes compared with the control group (Figures 7A, B).

Then we assessed the effect of PTPN2 on lipid homeostasis in adipose tissue *in vivo*. Compared with the T2DM group, the protein levels of LPL, ATGL and HSL was significantly higher in BAT in T2DM + PTPN2 group (Figures 7C–E). Consistently, these regulators hydrolyzing triglycerides and promoting thermogenesis were upregulated with PTPN2 overexpression in SAT (Figures 7F–H), confirming the function of PTPN2 on preventing lipid retention in adipocytes.

Discussion

As a crucial metabolic organ for energy homeostasis, adipose tissue is critical in regulating IR through its lipid storage capacity, thermogenic role and endocrine functions. Energy imbalance due to excess lipid retention results in adipocyte hypertrophy (an increase in adipocyte size) and WAT remodeling, especially for SAT (Bays, 2014). As a key thermogenic protein in BAT, UCP1 plays an essential role in energy expenditure, which can be regulated by many environmental factors like diet (Okla et al., 2017). Our study observed that in a model of T2DM, adipocyte hypertrophy with more lipids was significant in SAT and BAT, which was reversed by PTPN2 overexpression. Besides, the protein levels of UCP1 and other indicators promoting energy consumption was also upregulated by PTPN2. Therefore, IR could be improved by PTPN2 via shrinking white adipocyte size, reducing lipid retention and enhancing energy expenditure. Free fatty acids, which were derived from hydrolysis of triglycerides, act as fuel substrate for thermogenesis (Schreiber et al., 2017). Furthermore, we observed that proteins facilitating hydrolysis of triglycerides including ATGL and HSL were upregulated by PTPN2 overexpression, which confirmed the role of PTPN2 in promoting lipid decomposition and energy expenditure. Although PTPN2 has been previously reported to be involved in adipose tissue browning indirectly, our study elucidated its role in regulating the browning process of adipocytes directly for the first time.

Senescent cells have been found in adipose tissue of a T2DM state and aging has been reported to promote IR (Lee et al., 2022). Adipose tissue browning is inhibited during aging (Berry et al., 2017), with a functional decline of mitochondria and UCP1 activation. Meanwhile, the potential of progenitor cells for beige adipogenesis declines due to senescence, therefore, the reduction of UCP1 protein level in WAT and impaired lipid mobilization were induced in T2DM (Koenen et al., 2021). Our study suggested that PTPN2 overexpression lowered senescence-related factors like P16 and P53 in adipose tissue under a T2DM state. As PTPN2 expression is downregulated in T2DM (Zheng et al., 2018), we proposed that PTPN2 at the crossroad of adipose tissue browning, lipid disturbance and IR might be involved in senescence of adipocytes in T2DM. Adipocytes are the primary cell type in adipose tissue exhibiting the role of energy reservoir and endocrine function (Lee et al., 2022). However, adipocyte senescence still needs to be further studied. Our study *in vitro* emphasized that senescence in adipocytes might impede the browning process of adipocytes and we first demonstrated that PTPN2 improved adipocyte senescence from the state of preadipocytes, thus promoting the browning process.

The MAPK/NF-κB pathway mediates signaling to various biological processes including cell senescence. Berry et al. (Berry et al., 2017) showed that phosphorylation of p38/MAPK contributed to p16 expression while dephosphorylation improved senescence of adipocytes. The activation of TAK1 is involved in the activation of downstream kinases including MAPK/NF-κB identified in cellular senescence (Rajagopalan et al., 2014). Our study is the first to investigate that PTPN2 could interact with TAK1 directly and catalyze dephosphorylation of TAK1 in adipocytes, resulting in dephosphorylation of the downstream proteins (Erk, P38, JNK, IκB, and P65) subsequently. Thus, TAK1 exhibited a role by which PTPN2 ameliorated cellular senescence and facilitated the browning process of adipocytes.

In summary, our study revealed that PTPN2 gene overexpression promoted adipose tissue browning by attenuating senescence, thus improving glucose tolerance and IR in T2DM mice. Mechanistically, we are the first to demonstrate that PTPN2 targeted TAK1 directly for dephosphorylation to inhibit the downstream MAPK/NF-κB pathway and ameliorated cellular senescence in adipocytes consequently. Therefore, PTPN2 in adipocytes may be a potential therapeutic target for T2DM.

Limitation

The recombinant pAdxsi adenovirus system we used in this study is not specifically expressed on adipose tissue so the non-specific expression in other tissues may influence the regulation of glucose and lipid metabolism. Further studies need to be conducted in the future to determine the function of PTPN2 in adipocytes *in vivo* using gene conditional knockout mice or recombinant pAdxsi adenovirus specifically expressed.

Data availability statement

The original contributions presented in the study are included in the article/Supplementary Material, further inquiries can be directed to the corresponding authors.

Ethics statement

The animal study was reviewed and approved by the Animal Care and Use Committee of Shandong University.

Author contributions

MZ, CZ, and WZ designed the study. YL, LH, PZ, and MS performed experiments and analyzed results. YZ and LM drafted the manuscript. All authors read and approved the final paper. All authors listed have made a substantial, direct, and intellectual contribution to the work and approved it for publication. All authors contributed to the article and approved the submitted version.

Funding

This work was supported by the research grants from the National Natural Science Foundation of China (82070392, 81570400).

Conflict of interest

The authors declare that the research was conducted in the absence of any commercial or financial relationships that could be construed as a potential conflict of interest.

Publisher's note

All claims expressed in this article are solely those of the authors and do not necessarily represent those of their affiliated organizations, or those of the publisher, the editors and the reviewers. Any product that may be evaluated in this article, or claim that may be made by its manufacturer, is not guaranteed or endorsed by the publisher.

Supplementary material

The Supplementary Material for this article can be found online at: https://www.frontiersin.org/articles/10.3389/fphar.2023.1124633/full#supplementary-material

References

Anerillas, C., Abdelmohsen, K., and Gorospe, M. (2020). Regulation of senescence traits by MAPKs. *Geroscience* 42 (2), 397–408. doi:10.1007/s11357-020-00183-3

Armani, A., Cinti, F., Marzolla, V., Morgan, J., Cranston, G. A., Antelmi, A., et al. (2014). Mineralocorticoid receptor antagonism induces browning of white adipose tissue through impairment of autophagy and prevents adipocyte dysfunction in high-fat-diet-fed mice. *FASEB J.* 28 (8), 3745–3757. doi:10.1096/fj.13-245415

Bays, H. (2014). Central obesity as a clinical marker of adiposopathy; increased visceral adiposity as a surrogate marker for global fat dysfunction. *Curr. Opin. Endocrinol. Diabetes Obes.* 21 (5), 345–351. doi:10.1097/MED.0000000000000093

Berry, D. C., Jiang, Y., Arpke, R. W., Close, E. L., Uchida, A., Reading, D., et al. (2017). Cellular aging contributes to failure of cold-induced beige adipocyte formation in old mice and humans. *Cell Metab.* 25 (1), 166–181. doi:10.1016/j.cmet.2016.10.023

Börgeson, E., Johnson, A. M., Lee, Y. S., Till, A., Syed, G. H., Ali-Shah, S. T., et al. (2015). Lipoxin A4 attenuates obesity-induced adipose inflammation and associated liver and kidney disease. *Cell Metab.* 22 (1), 125–137. doi:10.1016/j.cmet.2015.05.003

Chen, C. C., Kuo, C. H., Leu, Y. L., and Wang, S. H. (2021). Corylin reduces obesity and insulin resistance and promotes adipose tissue browning through SIRT-1 and β3-AR activation. *Pharmacol. Res.* 164, 105291. doi:10.1016/j.phrs.2020.105291

Cohen, P., and Kajimura, S. (2021). The cellular and functional complexity of thermogenic fat. *Nat. Rev. Mol. Cell Biol.* 22 (6), 393–409. doi:10.1038/s41580-021-00350-0

Czech, M. P. (2020). Mechanisms of insulin resistance related to white, beige, and Brown adipocytes. *Mol. Metab.* 34, 27–42. doi:10.1016/j.molmet.2019.12.014

Dai, W. L., Yan, B., Bao, Y. N., Fan, J. F., and Liu, J. H. (2020). Suppression of peripheral NGF attenuates neuropathic pain induced by chronic constriction injury through the TAK1-MAPK/NF-κB signaling pathways. *Cell Commun. Signal* 18 (1), 66. doi:10.1186/s12964-020-00556-3

De Carvalho, F. G., Brandao, C. F. C., Batitucci, G., Souza, A. O., Ferrari, G. D., Alberici, L. C., et al. (2021). Taurine supplementation associated with exercise increases mitochondrial activity and fatty acid oxidation gene expression in the subcutaneous white adipose tissue of obese women. *Clin. Nutr.* 40 (4), 2180–2187. doi:10.1016/j.clnu.2020.09.044

Fukumura, K., Narimatsu, Y., Moriwaki, S., Iwakoshi-Ukena, E., Furumitsu, M., and Ukena, K. (2021). Effects of overexpression of neurosecretory protein GL-precursor gene on glucose homeostasis and insulin sensitivity in mice. *Int. J. Mol. Sci.* 22 (9), 4681. doi:10.3390/ijms22094681

Gómez-Serrano, M., Camafeita, E., López, J. A., Rubio, M. A., Bretón, I., García-Consuegra, I., et al. (2017). Differential proteomic and oxidative profiles unveil dysfunctional protein import to adipocyte mitochondria in obesity-associated aging and diabetes. *Redox Biol.* 11, 415–428. doi:10.1016/j.redox.2016.12.013

Gorgoulis, V., Adams, P. D., Alimonti, A., Bennett, D. C., Bischof, O., Bishop, C., et al. (2019). Cellular senescence: Defining a path forward. *Cell. Senescence Defin. a Path Forw.* 179 (4), 813–827. doi:10.1016/j.cell.2019.10.005

Guo, B., Liu, J., Wang, B., Zhang, C., Su, Z., Zhao, M., et al. (2022). Withaferin A promotes white adipose browning and prevents obesity through sympathetic nerve-activated prdm16-FATP1 Axis. *Diabetes* 71 (2), 249–263. doi:10.2337/db21-0470

Hildebrand, J., Thakar, S., Watts, T. L., Banfield, L., Thabane, L., Macri, J., et al. (2019). The impact of environmental cadmium exposure on type 2 diabetes risk: A protocol for an overview of systematic reviews. *Syst. Rev.* 8 (1), 309. doi:10.1186/s13643-019-1246-7

Hirschey, M. D., Shimazu, T., Goetzman, E., Jing, E., Schwer, B., Lombard, D. B., et al. (2010). SIRT3 regulates mitochondrial fatty-acid oxidation by reversible enzyme deacetylation. *Nature* 464 (7285), 121–125. doi:10.1038/nature08778

Ida, Y., Hikage, F., and Ohguro, H. (2021). ROCK inhibitors enhance the production of large lipid-enriched 3D organoids of 3T3-L1 cells. *Sci. Rep.* 11 (1), 5479. doi:10.1038/s41598-021-84955-7

Jankovic, A., Korac, A., Buzadzic, B., Otasevic, V., Stancic, A., Daiber, A., et al. (2015). Redox implications in adipose tissue (dys)function--A new look at old acquaintances. *Redox Biol.* 6, 19–32. doi:10.1016/j.redox.2015.06.018

Janssen, L. G. M., Nahon, K. J., Bracké, K. F. M., van den Broek, D., Smit, R., Sardjoe Mishre, A. S. D., et al. (2020). Twelve weeks of exenatide treatment increases $^{[18F]}$fluorodeoxyglucose uptake by Brown adipose tissue without affecting oxidative resting energy expenditure in nondiabetic males. *Metabolism* 106, 154167. doi:10.1016/j.metabol.2020.154167

Jocken, J. W., Goossens, G. H., Popeijus, H., Essers, Y., Hoebers, N., and Blaak, E. E. (2016). Contribution of lipase deficiency to mitochondrial dysfunction and insulin resistance in hMADS adipocytes. *Int. J. Obes. (Lond).* 40 (3), 507–513. doi:10.1038/ijo.2015.211

Keipert, S., Lutter, D., Schroeder, B. O., Brandt, D., Ståhlman, M., Schwarzmayr, T., et al. (2020). Endogenous FGF21-signaling controls paradoxical obesity resistance of UCP1-deficient mice. *Nat. Commun.* 11 (1), 624. doi:10.1038/s41467-019-14069-2

Koenen, M., Hill, M. A., Cohen, P., and Sowers, J. R. (2021). Obesity, adipose tissue and vascular dysfunction. *Circ. Res.* 128 (7), 951–968. doi:10.1161/CIRCRESAHA.121.318093

Krisko, T. I., Nicholls, H. T., Bare, C. J., Holman, C. D., Putzel, G. G., Jansen, R. S., et al. (2020). Dissociation of adaptive thermogenesis from glucose homeostasis in microbiome-deficient mice. *Cell Metab.* 31 (3), 592–604. doi:10.1016/j.cmet.2020.01.012

Lee, G., Kim, Y. Y., Jang, H., Han, J. S., Nahmgoong, H., Park, Y. J., et al. (2022). SREBP1c-PARP1 axis tunes anti-senescence activity of adipocytes and ameliorates metabolic imbalance in obesity. *Cell Metab.* 34 (5), 702–718.e5. doi:10.1016/j.cmet.2022.03.010

Li, Y., Zhou, H., Li, Y., Han, L., Song, M., Chen, F., et al. (2019). PTPN2 improved renal injury and fibrosis by suppressing STAT-induced inflammation in early diabetic nephropathy. *J. Cell Mol. Med.* 23 (6), 4179–4195. doi:10.1111/jcmm.14304

Ljubkovic, M., Gressette, M., Bulat, C., Cavar, M., Bakovic, D., Fabijanic, D., et al. (2019). Disturbed fatty acid oxidation, endoplasmic reticulum stress, and apoptosis in

left ventricle of patients with type 2 diabetes. *Diabetes* 68 (10), 1924–1933. doi:10.2337/db19-0423

Macotela, Y., Emanuelli, B., Mori, M. A., Gesta, S., Schulz, T. J., Tseng, Y. H., et al. (2012). Intrinsic differences in adipocyte precursor cells from different white fat depots. *Diabetes* 61 (7), 1691–1699. doi:10.2337/db11-1753

Maliszewska, K., and Kretowski, A. (2021). Brown adipose tissue and its role in insulin and glucose homeostasis. *Int. J. Mol. Sci.* 22 (4), 1530. doi:10.3390/ijms22041530

Miao, Y., Qin, H., Zhong, Y., Huang, K., and Rao, C. (2021). Novel adipokine asprosin modulates browning and adipogenesis in white adipose tissue. *J. Endocrinol.* 249 (2), 83–93. doi:10.1530/JOE-20-0503

Molinari, F., Feraco, A., Mirabilii, S., Saladini, S., Sansone, L., Vernucci, E., et al. (2021). SIRT5 inhibition induces Brown fat-like phenotype in 3T3-L1 preadipocytes. *Cells* 10 (5), 1126. doi:10.3390/cells10051126

Moreno-Santos, I., Pérez-Belmonte, L. M., Macías-González, M., Mataró, M. J., Castellano, D., López-Garrido, M., et al. (2016). Type 2 diabetes is associated with decreased PGC1α expression in epicardial adipose tissue of patients with coronary artery disease. *J. Transl. Med.* 14 (1), 243. doi:10.1186/s12967-016-0999-1

Ohno, H., Shinoda, K., Spiegelman, B. M., and Kajimura, S. (2012). PPARγ agonists induce a white-to-Brown fat conversion through stabilization of PRDM16 protein. *Cell Metab.* 15 (3), 395–404. doi:10.1016/j.cmet.2012.01.019

Okla, M., Kim, J., Koehler, K., and Chung, S. (2017). Dietary factors promoting Brown and beige fat development and thermogenesis. *Adv. Nutr.* 8 (3), 473–483. doi:10.3945/an.116.014332

Pedersen, B. K. (2017). Anti-inflammatory effects of exercise: Role in diabetes and cardiovascular disease. *Eur. J. Clin. Invest.* 47 (8), 600–611. doi:10.1111/eci.12781

Rajagopalan, S., Lee, E. C., DuPrie, M. L., and Long, E. O. (2014). TNFR-associated factor 6 and TGF-β-activated kinase 1 control signals for a senescence response by an endosomal NK cell receptor. *J. Immunol.* 192 (2), 714–721. doi:10.4049/jimmunol.1302384

Randeria, S. N., Thomson, G. J. A., Nell, T. A., Roberts, T., and Pretorius, E. (2019). Inflammatory cytokines in type 2 diabetes mellitus as facilitators of hypercoagulation and abnormal clot formation. *Cardiovasc Diabetol.* 18 (1), 72. doi:10.1186/s12933-019-0870-9

Roberts, L. .D. (2015). Does inorganic nitrate say NO to obesity by browning white adipose tissue? *Adipocyte* 4 (4), 311–314. doi:10.1080/21623945.2015.1005525

Rogers, N. H., Landa, A., Park, S., and Smith, R. G. (2012). Aging leads to a programmed loss of Brown adipocytes in murine subcutaneous white adipose tissue. *Aging Cell* 11 (6), 1074–1083. doi:10.1111/acel.12010

Sakers, A., De, S. M. .K., Seale, P., and Villanueva, C. .J. (2022). Adipose-tissue plasticity in health and disease. *Cell* 185 (3), 419–446. doi:10.1016/j.cell.2021.12.016

Sampath, K. A., Maiya, A. G., Shastry, B. A., Vaishali, K., Ravishankar, N., Hazari, A., et al. (2019). Exercise and insulin resistance in type 2 diabetes mellitus: A systematic review and meta-analysis. *Ann. Phys. Rehabil. Med.* 62 (2), 98–103. doi:10.1016/j.rehab.2018.11.001

Schreiber, R., Diwoky, C., Schoiswohl, G., Feiler, U., Wongsiriroj, N., Abdellatif, M., et al. (2017). Cold-induced thermogenesis depends on ATGL-mediated lipolysis in cardiac muscle, but not Brown adipose tissue. *Cell Metab.* 26 (5), 753–763. doi:10.1016/j.cmet.2017.09.004

Shimobayashi, M., Albert, V., Woelnerhanssen, B., Frei, I. C., Weissenberger, D., Meyer-Gerspach, A. C., et al. (2018). Insulin resistance causes inflammation in adipose tissue. *J. Clin. Invest.* 128 (4), 1538–1550. doi:10.1172/JCI96139

Sidossis, L. .S., Porter, C., Saraf, M. .K., Børsheim, E., Radhakrishnan, R. .S., Chao, T., et al. (2015). Browning of subcutaneous white adipose tissue in humans after severe adrenergic stress. *Cell Metab.* 22 (2), 219–227. doi:10.1016/j.cmet.2015.06.022

Sun, K., Kusminski, C. .M., and Scherer, P. .E. (2011). Adipose tissue remodeling and obesity. *J. Clin. Invest.* 121 (6), 2094–2101. doi:10.1172/JCI45887

Tian, Y., Li, H., Qiu, T., Dai, J., Zhang, Y., Chen, J., et al. (2019). Loss of PTEN induces lung fibrosis via alveolar epithelial cell senescence depending on NF-κB activation. *Aging Cell* 18 (1), e12858. doi:10.1111/acel.12858

Walenna, N. F., Kurihara, Y., Chou, B., Ishii, K., Soejima, T., Itoh, R., et al. (2018). Chlamydia pneumoniae exploits adipocyte lipid chaperone FABP4 to facilitate fat mobilization and intracellular growth in murine adipocytes. *Biochem. Biophys. Res. Commun.* 495 (1), 353–359. doi:10.1016/j.bbrc.2017.11.005

Wang, X., and Hai, C. (2015). Redox modulation of adipocyte differentiation: Hypothesis of "redox chain" and novel insights into intervention of adipogenesis and obesity. *Free Radic. Biol. Med.* 89, 99–125. doi:10.1016/j.freeradbiomed.2015.07.012

Xu, Z., You, W., Liu, J., Wang, Y., and Shan, T. (2020). Elucidating the regulatory role of melatonin in Brown, white, and beige adipocytes. *Adv. Nutr.* 11 (2), 447–460. doi:10.1093/advances/nmz070

Yan, M., Audet-Walsh, É., Manteghi, S., Dufour, C. R., Walker, B., Baba, M., et al. (2016). Chronic AMPK activation via loss of FLCN induces functional beige adipose tissue through PGC-1α/ERRα. *Genes Dev.* 30 (9), 1034–1046. doi:10.1101/gad.281410.116

Ying, W., Riopel, M., Bandyopadhyay, G., Dong, Y., Birmingham, A., Seo, J. B., et al. (2017). Adipose tissue macrophage-derived exosomal miRNAs can modulate *in vivo* and *in vitro* insulin sensitivity. *Cell* 171 (2), 372–384. doi:10.1016/j.cell.2017.08.035

Yoneshiro, T., Aita, S., Matsushita, M., Okamatsu-Ogura, Y., Kameya, T., Kawai, Y., et al. (2011). Age-related decrease in cold-activated Brown adipose tissue and accumulation of body fat in healthy humans. *Obes. (Silver Spring)* 19 (9), 1755–1760. doi:10.1038/oby.2011.125

Zhang, B., Fu, D., Xu, Q., Cong, X., Wu, C., Zhong, X., et al. (2018). The senescence-associated secretory phenotype is potentiated by feedforward regulatory mechanisms involving Zscan4 and TAK1. *Nat. Commun.* 9 (1), 1723. doi:10.1038/s41467-018-04010-4

Zhang, P., Zhang, W., Zhang, D., Wang, M., Aprecio, R., Ji, N., et al. (2018). 25-Hydroxyvitamin D3 -enhanced PTPN2 positively regulates periodontal inflammation through the JAK/STAT pathway in human oral keratinocytes and a mouse model of type 2 diabetes mellitus. *J. Periodontal Res.* 53 (3), 467–477. doi:10.1111/jre.12535

Zhao, J., Cai, B., Shao, Z., Zhang, L., Zheng, Y., Ma, C., et al. (2021). TRIM26 positively regulates the inflammatory immune response through K11-linked ubiquitination of TAB1. *Cell Death Differ.* 28 (11), 3077–3091. doi:10.1038/s41418-021-00803-1

Zheng, L., Zhang, W., Li, A., Liu, Y., Yi, B., Nakhoul, F., et al. (2018). PTPN2 downregulation is associated with albuminuria and vitamin D receptor deficiency in type 2 diabetes mellitus. *J. Diabetes Res.* 2018, 3984797. doi:10.1155/2018/3984797

Zhu, Q., An, Y. .A., and Scherer, P. .E. (2022). Mitochondrial regulation and white adipose tissue homeostasis. *Trends Cell Biol.* 32 (4), 351–364. doi:10.1016/j.tcb.2021.10.008

Zoico, E., Rubele, S., De Caro, A., Nori, N., Mazzali, G., Fantin, F., et al. (2019). Brown and beige adipose tissue and aging. *Front. Endocrinol. (Lausanne).* 10, 368. doi:10.3389/fendo.2019.00368

Frontiers in Pharmacology

Explores the interactions between chemicals and living beings

The most cited journal in its field, which advances access to pharmacological discoveries to prevent and treat human disease.

Discover the latest Research Topics

See more →

Frontiers

Avenue du Tribunal-Fédéral 34
1005 Lausanne, Switzerland
frontiersin.org

Contact us

+41 (0)21 510 17 00
frontiersin.org/about/contact